TECHNISCHE UNIVERSITÄT DRESDEN

HØGSKOLEN I AGDER

Berechnung einer zweigleisigen Eisenbahn-Netzwerkbogenbrücke unter Einsatz des europäischen Normenkonzepts

Calculation of a double track railway network arch bridge applying the European standards

Benjamin Brunn

Frank Schanack

Technische Universität Dresden
Fakultät Bauingenieurwesen
Institut für Tragwerke und Baustoffe
Lehrstuhl für Stahlbau

Dresden University of Technology
Department of Civil Engineering
Institute for Structures and Materials
Chair of Steel Structures

Betreuer

Tutors

Prof. Dr.-Ing habil. W. Graβe
Doz. em. Dr.-Ing. P. Tveit
Dipl.-Ing. S. Teich

Grimstad, August 2003

The authors hereby declare that this diploma thesis is entirely the result of their own work. Information derived from the published and unpublished work of others has been acknowledged in the text and a list of references given.

Hiermit erklären die Autoren, dass die vorliegende Diplomarbeit vollständig Resultat ihrer selbstständigen Arbeit ist. Informationen die aus der veröffentlichten und unveröffentlichten Arbeit Dritter stammen sind im Text gekennzeichnet und im Literaturverzeichnis nachgewiesen.

Benjamin Brunn   Frank Schanack

Grimstad, 18 August 2003

Abstract

In this work the results of investigations into how to optimise a network arch for the special demands of railway traffic are presented. Network arch bridges have inclined hangers that cross each other at least twice. The beneficial structural behaviour leads to slender bridge members mainly subjected to axial forces. Structural parts above the bridge deck are therefore more likely to be tolerated. Furthermore, the high stiffness and therefore small deflections favour the application of network arches for railway bridges. Stress ranges caused by the load character of railway bridges require special considerations for the design. Adequate solutions are elaborated considering as an example a double track railway bridge spanning 100 meters.

The arrangement of the hangers has considerable influence on the structural behaviour. It decides on the forces and force variations within the network arch depending on many parameters, as for example span, rise, number of hangers, loading or arch curvature. A new introduced type of hanger arrangement is involved in an optimisation process with regard to the mentioned parameters. This improved hanger arrangement provides a simple method of designing network arches with small hanger forces and small bending moments in the chords.

The hanger connection details call for special attention to fatigue strains. The fatigue design check is decisive for the hanger cross section. Various designs of hanger connection details for circular hangers are tested by numeric analysis. A hanger connection detail is derived from the results satisfying the special demands of slender arches as they are found in network arches.

The structural behaviour of a network arch favours a lower chord consisting of a concrete slab. Its vertical deflections are limited to ensure passenger comfort and track stability. Alternatives with and without transverse prestressing are compared considering the deformation behaviour and economic differences. Several other construction details such as arch root point, bearings or drainage are elaborated on and the solutions are presented. An erection method using a temporary lower chord is assessed and described in detail.

The investigations confirm the suitability of network arches for railway bridges. Economic advantages due to significant savings of steel compared to other arch bridges contribute to the overall convincing performance.

Zusammenfassung

In dieser Arbeit werden die Ergebnisse von Untersuchungen zur Optimierung von Netzwerkbogenbrücken entsprechend den speziellen Ansprüchen aus Eisenbahnverkehr vorgestellt. Netzwerkbogenbrücken sind Bogenbrücken mit geneigten Hängern die sich wenigstens zweimal überkreuzen. Da ihr vorteilhaftes Tragverhalten schlanke Bauteile ermöglicht, die hauptsächlich durch Normalkräfte beansprucht werden, sind tragende Bauwerkselemente über der Brückennutzfläche eher tolerierbar. Die hohe Steifigkeit und demzufolge kleinen Verformungen von Netzwerkbögen tragen zusätzlich zu deren Anwendbarkeit als Eisenbahnbrücken bei. Der Lastcharakter von Eisenbahnbrücken verursacht große Spannungsschwingbreiten deren besondere Berücksichtigung beim Entwurf gefordert ist. Am Beispiel einer zweigleisigen Eisenbahnbrücke mit 100 Metern Spannweite werden passende Lösungen erarbeitet.

Die Anordnung der Hänger hat einen erheblichen Einfluss auf das Tragverhalten. In Abhängigkeit vieler Parameter, wie zum Beispiel Spannweite, Bogenstich, Hängeranzahl, Lasten oder Bogenkrümmung, entscheidet sie über die Schnittkräfte und das Spannungsspiel innerhalb des Netzwerkbogens. Eine neue Art der Hängeranordnung wird eingeführt und unter Berücksichtigung der genannten Parameter einem Optimierungsprozess unterzogen. Diese verbesserte Hängeranordnung stellt eine einfache Methode für den Entwurf von Netzwerkbogenbrücken mit kleinen Hängerkräften und kleinen Biegemomenten in den Gurten zur Verfügung.

Die Hängeranschlüsse unterliegen in besonderem Maße Ermüdungsbeanspruchungen, so dass der Querschnitt der Hänger vom Ermüdungsfestigkeitsnachweis seines Anschlusses bestimmt wird. Mit Hilfe von FEM-Berechnungen werden unterschiedliche Hängeranschlüsse hinsichtlich ihrer Ermüdungsfestigkeit untersucht. Aus den Ergebnissen wird eine verbesserte Anschlussgeometrie abgeleitet, die den speziellen Anforderungen von schlanken Bögen, wie sie bei Netzwerkbögen vorkommen, gerecht werden.

Das Tragverhalten von Netzwerkbogenbrücken begünstigt die Verwendung einer einfachen Betonplatte als Untergurt, dessen Durchbiegung für den Fahrgastkomfort und zur Sicherstellung der Stabilität der Gleise beschränkt ist. Alternativen mit und ohne Quervorspannung werden hinsichtlich des Verformungsverhaltens und wirtschaftlicher Unterschiede verglichen. Für weitere Konstruktionsdetails, wie Bogenfußpunkt, Lagerarten oder Brückenentwässerung werden Lösungsvorschläge vorgestellt. Als eine Möglichkeit der Bauausführung werden Montagezustände unter Verwendung eines temporären Untergurtes sorgfältig berechnet und detailliert beschrieben.

Die durchgeführten Untersuchungen bestätigen die Eignung von Netzwerkbögen für den Einsatz als Eisenbahnbrücken. Die Kosteneinsparungen gegenüber anderen Bogenbrücken durch das bedeutend geringere Stahlgewicht tragen zu dem überzeugenden Gesamteindruck bei.

Resumen

En este trabajo se presentan los resultados de las investigaciones realizadas sobre la optimización de arcos network, con respecto a las exigencias especiales del tráfico de ferrocarriles. El puente en arco tipo network es un puente en arco, en el cual algunos tirantes se interceptan al menos 2 veces entre sí. El buen comportamiento estructural de este tipo de arco, nos lleva a utilizar elementos esbeltos en los puentes, los cuales toman principalmente fuerzas axiales, por esta razón los elementos estructurales sobre el tablero pueden ser tolerados de mejor forma. Además, la rigidez alta y por ende las deflexiones pequeñas, favorecen la aplicación de arcos network para puentes de ferrocarril. El carácter de cargas de puentes de ferrocarril causa altas variaciones de fuerzas interiores lo cual requiere consideraciones especiales para el diseño, para esto se elaboran soluciones adecuadas utilizando como ejemplo un puente de ferrocarril con dos vías y una luz de 100 metros.

La colocación de los tirantes influye cuantiosamente en el comportamiento estructural. Las fuerzas y la variación de fuerzas en el arco network, dependen de muchos parámetros como por ejemplo: la luz, la altura del arco, el número de tirantes, las cargas y la curvatura del arco. Un nuevo tipo de colocación de tirantes es introducido y incluido en un proceso de optimización con respecto a dichos parámetros. Esta colocación de tirantes mejorada pone a disposición un método fácil de diseñar arcos network con fuerzas axiales pequeñas en los tirantes y momentos flectores pequeños en los cordones.

Los detalles de la conexión de los tirantes necesitan atención especial referente a exigencias de fatiga. Las pruebas del estado límite de fatiga son decisivas para la sección transversal de los tirantes. Usando FEM-calculaciones, son estudiados distintos detalles de la conexión de tirantes con sección transversal circular, de los resultados es derivada una geometría del detalle, la cual satisface las exigencias especiales de arcos esbeltos, como usualmente ocurren en los arcos tipo network.

El comportamiento estructural de un arco network favorece a un tablero inferior construido en hormigón. Las deflexiones verticales de estos están limitadas para asegurar el confort de los pasajeros y la estabilidad de las vías. Alternativas con y sin cables postensados transversales son comparadas con respecto al comportamiento de deformación y las diferencias económicas. Soluciones para otros detalles del diseño como los extremos del arco, los portes o el desaguado, son elaborados y presentados. Como un método posible de la erección del puente los estados de construcción utilizando un cordón inferior temporero son calculados y trazados detalladamente.

Las investigaciones comprueban la aptitud y el buen comportamiento de arcos tipo network para puentes de ferrocarril, así como también las ventajas económicas que se tienen por los ahorros notables de acero en comparación con otros puentes en arco, todo esto en conjunto contribuye a la convincente impresión general.

Contents

Preface

The present work was done by the authors at the end of their 5-year studies. It has been submitted to the Faculty of Civil engineering of Dresden Technical University in order to obtain the degree of a *Diplom-Ingenieur*.

The topic, ‘Calculation of a double track railway network arch bridge applying the European standards’, deals with a very efficient structure. Its inventor and the most vigorous researcher in this field is Dr.-Ing. Docent Emeritus PER TVEIT. The authors were fortunate to be offered the opportunity to carry out their investigations and to write this thesis from May to August 2003 at the office of this engineer. From the conversations with him and his answers to questions several suggestions arose, which are separately marked.

Serving as a basis for the calculated network arch bridge was the one designed in the Diploma thesis of UWE STEIMANN, also done with TVEIT’S collaboration, in Grimstad, Norway. It is mentioned in the text when STEIMANN’S ideas are adopted.

B. Brunn
F. Schanack
Grimstad, Norway
August, 2003

Acknowledgements

Not only while working on this Diploma thesis, but also during the years of studying there are many persons and institutions to which the authors owe deep thanks. Without a surely incomplete list, our gratefulness should be expressed hereby.

Special thanks go to Per Tveit, for his permanent disposition to answer our questions, for his constructive criticism of our results which encouraged us to further investigate and review, and last but not least for his willingness to share his office with three students.

Task for the diploma thesis

TECHNISCHE UNIVERSITÄT DRESDEN

Fakultät Bauingenieurwesen

Aufgabenstellung für die Diplomarbeit

in der Studienrichtung: Konstruktiver Ingenieurbau

Namen der Diplomanden: Benjamin Brunn
Frank Schanack

Thema:

Berechnung einer zweigleisigen Eisenbahn-Netzwerkbogenbrücke unter Einsatz des Europäischen Normenkonzepts

Zielsetzung:

Die Diplomanden erhalten die Aufgabe, anhand eines konkreten Beispiels einer zweigleisigen Eisenbahnbrücke eine Vergleichsbemessung unter ausschließlicher Verwendung des Eurocodes durchzuführen.

Nach einer Aufstellung der relevanten Lasten sind anhand des Beispieltragwerkes überschlägige Bauteilabmessungen zu ermitteln. Mit diesen Werten soll eine dreidimensionale Berechnung der Brücke erfolgen.

Mit Hilfe der erforderlichen Nachweise im Grenzzustand der Tragfähigkeit und im Grenzzustand der Gebrauchstauglichkeit sind die Abmessungen der Stahlbauteile zu optimieren. Die Bögen sollen dabei aus Profilen der Serie Universal-Column oder aus American-Wide-Flange-Profilen gefertigt werden. Die Pfeilhöhe des Bogens soll zwischen 0.15 und 0.17 der Spannweite liegen. Weiterhin soll die Auswirkung der Hängeranordnung (Abstände und Neigung) auf die Rückstellkräfte der Netzwerkhänger beim Ausweichen rechtwinklig zur Bogenebene untersucht werden.

Zur Aufnahme der Windlasten soll eine geeignete Aussteifung gewählt werden. Eine eventuelle Ausführung des Brückenbauwerkes ohne oberen Windverband ist ebenfalls in Betracht zu ziehen.

Unter Berücksichtigung des Ermüdungsverhaltens ist eine vorteilhafte Hängerkonstruktion zu entwerfen und zu bemessen. Dabei ist besonders die Anordnung des Hängernetzes aber auch die Ausführung der Hängeranschlussdetails zu betrachten. Es soll eine Aussage über die Auswirkungen der Hängerneigung auf die auftretenden Spannungsschwingbreiten getroffen werden. Bei der Wahl eines geeigneten Hängeranschlusses sollen die in den Diplomarbeiten von Herrn Steimann sowie Herrn Wendelin und Herrn Teich verwendeten Anschlüsse sowie die in den Richtzeichnungen der Deutschen Bahn enthaltenen Details als Grundlage dienen.

Die Biegetragfähigkeit des Betonuntergurtes soll nachgewiesen und die zur Aufnahme der Zugkräfte aus Bogenschub erforderlichen Spannglieder dimensioniert werden. Zusätzlich ist auch eine Variante mit schlaffer Bewehrung zu untersuchen.

Die erforderlichen Materialmengen sind zu berechnen.

Die Aufgaben der Studenten sind folgendermaßen verteilt:

Benjamin Brunn	Frank Schanack
• Ermittlung der relevanten Lasten und Berechnungsvorschriften unter Verwendung des Eurocodes • Bestimmung vorläufiger Abmessungen • Durchführung einer dreidimensionalen Computerberechnung	
• Suche nach einer optimalen Hängeranordnung in Bezug auf die Hängerkräfte und die Spannungsschwingbreiten • Ermüdungsuntersuchung der Hänger • Bemessung des Betonquerschnitts einschließlich Endquerträgers • Ermittlung der erforderlichen Spannkraft.	• Stabilitätsuntersuchungen des Bogens unter Volllast, Halblast und außergewöhnlichen Beanspruchungen • Untersuchungen der Hängerrückstellkräfte • Bemessung der Windaussteifung • Konstruktive Durchbildung des Bogenfußpunktes. • Lagerbemessung (Untersuchung verschiedener Lagerarten)
• Sorgfältige Berechnung der Montagezustände unter Verwendung eines temporären Untergurts	

Betreuer: Prof. Dr.-Ing. habil. W. Graße
Doz. em. Dr.-Ing. Per Tveit
Dipl.-Ing. S. Teich

Ausgehändigt am: 22.05.2003

Einzureichen am: 22.08.2003

Verantwortlicher Hochschullehrer

Theses

The following theses list relevant problems and results of the diploma thesis. Hopefully they willl inspire scientific discussion.

1. Two intersecting hangers with adjacent nodes at the arch can be assumed to act as a pair at the arch. A line can be drawn between the middle of their upper hanger nodes and their intersection which shall be called ‘direction of action’.

2. Small hanger forces in one hanger pair are obtained if their ‘direction of action’ is aligned to the deflection of the arch at the centre point between the adjacent nodes.

3. Each hanger pair causes a resulting force at the arch. Small bending moments about the horizontal axis in the arch are obtained if these resulting forces cause a line of thrust along the centre line of the arch.

4. The following simplification to the first three points can be assumed:

   1a. On an average the hanger forces are equal, i. e. their resulting force is collinear to their ‘direction of action’.

   2a. Small deflections in the centre range of a circular arch are radial for uniform loading, i. e. for this load case the ‘direction of action’ is to align to the radii of the arch circle to obtain small hanger forces.

   3a. The centre range of a clamped arch behaves like the centre range of a simply supported arch, i. e. uniform forces acting radially on a circular arch will cause a line of thrust along the centre line of the arch.

5. On the basis of these assumptions a hanger arrangement for circular arches can be derived from 1., 2. and 3. giving small bending in the arch and small hanger forces. It can be described as follows:

   All hangers in the centre range of the arch cross the arch with the same angle; the upper hanger nodes are equidistant.

6. The clamping at the ends of the arch causes other conditions. In order to obtain small bending in the arch and small hanger forces the hanger pairs must be oriented differently as along the radii of the arch circle.

7. The variable in such a hanger arrangement is the cross angle between the hanger and the arch, found to influence the forces and force variations in the structural members of the bridge. This cross angle is to be optimised regarding desired attributes. A cross angle of 45° gives smallest variation of bending moments in the arch.

8. The application of the derived hanger arrangement caused a significant decrease of bending in the arch and hanger forces compared to hanger arrangements which used to be considered as near optimal.

9. Hanger connections along the especially slender arches of network arch bridges are considerably restricted in their dimensions. This implies that details which are appropriate for arch bridges with vertical hangers might not be advantageous in respect of fatigue for network arches.

10. All transitions in hanger connection details must be made continuous and smooth in order to reduce stress concentrations.

11. For the fatigue assessment of details such as hanger connections it might be essential to include finite element analysis in order to determine stress concentrations. Dangerous stress peaks arise at geometrical discontinuities; their magnitude depends on the shape of the member at that location and the nominal stress level. Either factor alone is not meaningful in order to judge the fatigue performance.

12. There is a tendency that about 10 m wide non-prestressed bridge decks are more economical than their counterparts with prestressing. Prestressed slabs stand out because of small deformations and higher durability.

13. The adaptation of roller bearings by eliminating the parts of the roll that never have contact with the top or bottom member allows large radii without having a giant roll. This bearing alternative is suitable for narrow and straight bridges, where a large construction height of the bearing can be tolerated.

14. The decisive loads for the longitudinal beams of the temporary lower chord are self-weight of formwork, reinforcement, prestressing tendons and end cross girder (see Figure E.8).

15. The sequence of casting the bridge deck during erection of the bridge using a temporary lower chord has to be determined for each project to avoid extensive hanger relaxation.

Introduction

Bridges are considered to be masterstrokes of engineering. Light, wide spanning structures especially attract attention. The world's most slender and lightest arch bridge was erected over Bolstadstraumen 60 km northeast of Bergen, Norway (TVEIT *[45]*, page 7). Using the benefits of a network arch, PER TVEIT designed this bridge in the early 1960s. Since then, surprisingly few network arch bridges have been built.

The authors are convinced that this is not due to any weak points, but rather due to little familiarity with and maybe doubt about the benefits of such a structure. In light of this, the authors have written this diploma thesis in English so that many persons will have easy access to this information. Furthermore, the application of the European standards (Eurocode) for assessment provides a comparison basis within the European Union and may simplify relating the results to other standards.

Working together, the authors acquired sufficient time for intensive research, besides the assessment of the network arch bridge.

The fields of this research shall be presented briefly:

Force distribution in structural parts of a network arch bridge, especially in hangers and arches, depends on the slope and arrangement of the inclined hangers. Since the structure is sensitive to changes in the hanger arrangement, this topic calls for special attention. The authors searched for predictions on best hanger arrangements by an optimisation process.

Railway bridges, like the one calculated in this work, are subject to fatigue strains. Hangers and their connection details are especially at risk of failure. Known design solutions for tied arches are not optimal for the more slender structural members of network arches. Investigations were carried out to find how to best adapt the known connection details.

Erection is always an important topic when designing bridges. PER TVEIT suggested an erection method using a temporary lower steel chord. Its applicability to the bridge, the object of this work, was verified in detail.

As alternative designs a concrete tie without transverse prestressing and the possibility of a "stilt bearing" (see Section 5.9) were investigated. Special attention was also given to the constructive design of the arch root point.

Carrying out the investigations and discussing the results with PER TVEIT, the authors gained knowledge about the structural behaviour of network arch bridges. Utilising this behaviour correctly leads to very efficient structures. The authors would be delighted to see more network arch bridges built using all the advantages they offer.

What is a network arch?

The structure named 'network arch bridge' was invented by PER TVEIT. He defines it as an arch bridge in which some hangers intersect at least twice (TVEIT *[46]*, page 3). A short description of this type of bridge will be given. An extended manuscript containing 100 pages about network arches can be found on the homepage of PER TVEIT *[45]*. On the front page, in Figure 5.29 and on the cover page of the Annexes the network arch bridge calculated in this work is shown.

Characteristics

To achieve great efficiency with this type of structure the following characteristics should be applied. The arch should be part of a circle as this makes fabrication easy and contributes to a more constant axial force in the middle portion of the arch and even maximum bending moments along the tie. The hangers should be spaced equidistantly along the arch and not merged in nodal points. This decreases bending due to local curvature and gives more efficient support to the arch in buckling. The lower chord is a concrete slab between small concrete edge beams. Longitudinal prestressing of the edge beams takes the horizontal forces of the arch. Furthermore, the prestressing increases durability of the concrete. For a width between the arches of more than about 10 meters transverse prestressing is suggested as this gives a more slender tie. The number of hangers is usually much higher than for tied arch bridges with vertical hangers. Their arrangement is a central question, which we have attempted to answer in this work.

Advantages in the structural behaviour

Compared with tied arches with vertical hangers the network arch bridges feature the fact that the chords are only subjected to very little bending. The bridge acts more like a simple beam and shows therefore a high stiffness and small deflections. Figures 4.1 and 4.2 will help to explain the reason.

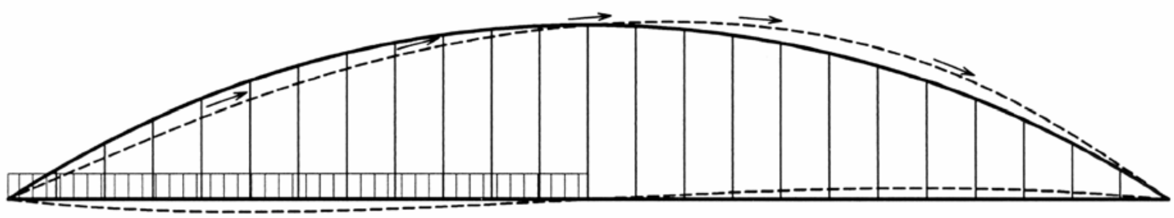

Fig. 4.1. Tied arch with vertical hangers, structural behaviour with partial loading (TVEIT *[39]*, page 16)

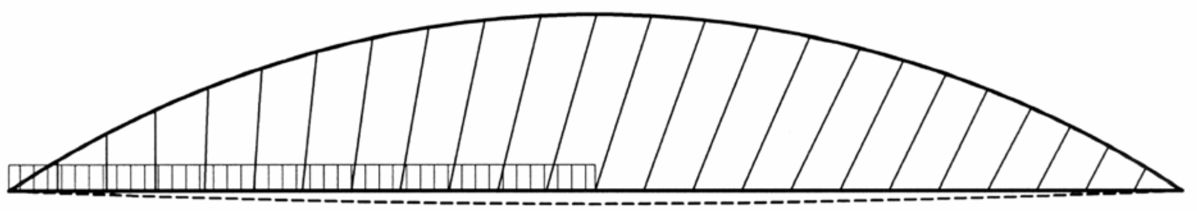

Fig. 4.2. Tied arch with one set of inclined hangers, structural behaviour with partial loading (TVEIT *[39]*, page 16)

Partial loading of the span leads to a deflection of the upper and lower chord in the arch with vertical hangers. This causes bending which is to be taken by big cross-sections of the arch and the tie. In network arches the inclined hangers restrict these deflections, and so bending only occurs as a result of local loading and the arch and tie are mainly subjected to axial force. Figure 4.3 shows the comparison of the influence lines for bending moments in the chords between an arch with vertical hangers and a network arch.

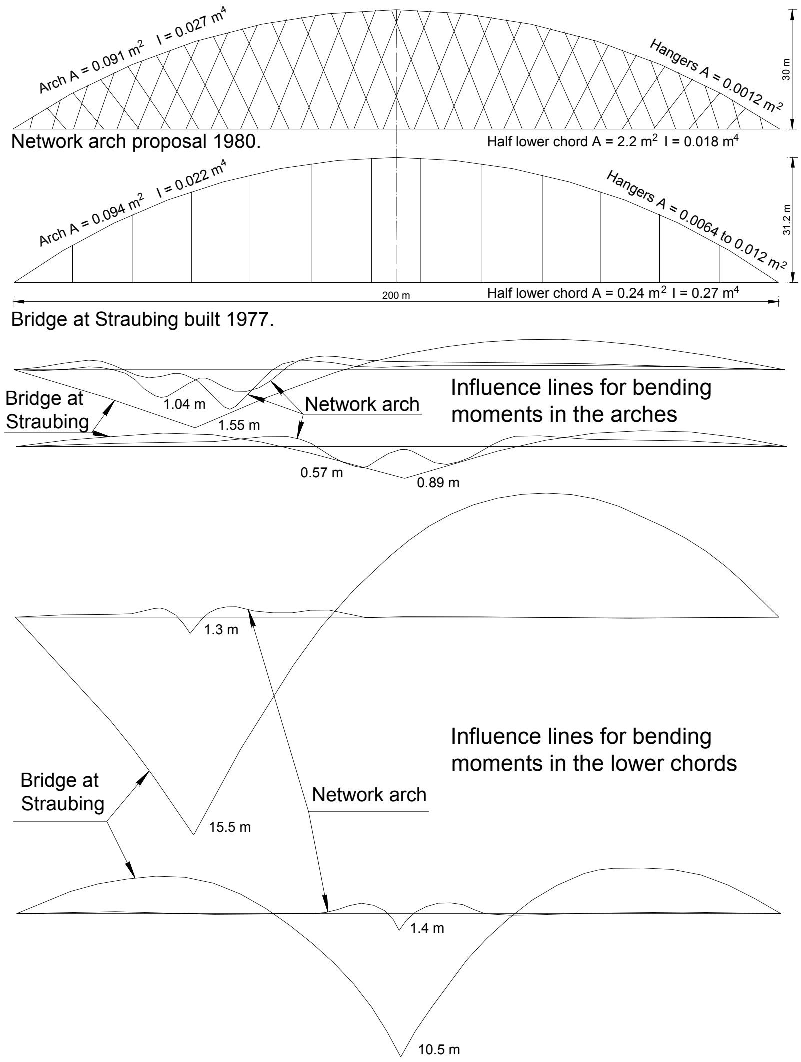

Fig. 4.3. Areas, stiffnesses and influence lines for the lower and upper chord of two tied arches (TVEIT *[45]*, page 14)

Due to the stiffness of the hanger web, the bridge deck spans between the planes of the arches and does not have to take much longitudinal bending, therefore it can be slender. As a result of the larger number of hangers their cross-section can be very small.

As a conclusion, the structural members of the network arch mainly take axial forces and the compression member, the arch, is more supported in buckling. The cross-sections can be very compact, which contributes to a more efficient use of material, to less steel weight and a better design due to higher transparency of the structure, SEIDEL *[34]*.

The bridge design

5.1 The arches

Each arch consists of six segments, which are connected by butt-welding on the construction site. The two lower segments are American Wide flange profiles W360x410x900, have a constant curvature radius of 66.86 metres and a bow length of 17.44 metres. The four upper segments are W360x410x634 and have a constant curvature radius of 83.58 metres. Their bow length is 18.06 metres. This gives the arch a rise of 17 metres. The smaller radius of the arch ends leads to a smaller length of the wind portal frame, which decreases bending moments. The weak axis of the profiles is horizontal. The distance between the arch planes is 10.15 metres. As material S 460 ML is used. ARCELOR LONG COMMERCIAL S.A. *[4]* provides such profiles with a constant curvature.

5.2 The hangers and hanger connections

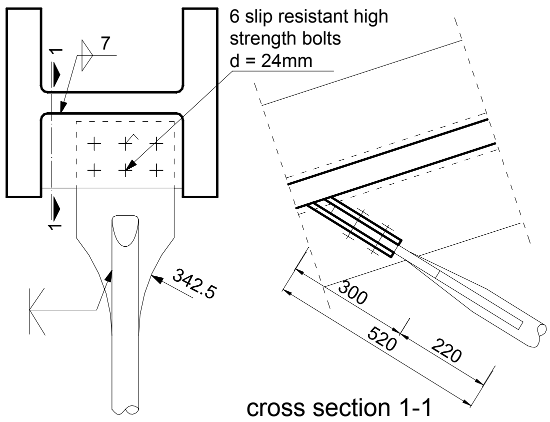

Fig. 5.1. Upper hanger connection detail

The bridge has 48 hangers per arch plane. The geometry of their arrangement follows the improvements found in Section 6, hence all hangers cross the arch with an angle of 49°. At the ends of the spans a special arrangement according to Section 6.7.5 was applied. For the upper and lower hanger connection details the solutions found to be best in Section 7 were chosen (see Figure 5.1). Each set of hangers is shifted half the diameter of the hangers out of the arch plane. This allows them to cross without deflections. The eccentricity causes torsional moments in the arch profiles, which are partially taken by the wind bracing. The direction of the eccentricity changes from each hanger connection to the next, so the torsional moments counteract each other. In the event of hanger relaxation several hangers in a line cause torsional moments in the same direction, which will give decisive forces. In the bridge calculated in this work no relaxing hangers occurred.

At their intersections the hangers are protected by a sheathing of slit open plastic tubes and tied together with elastic rubber bands. This couples the deflections out of the arch plane and therefore increases damping. All hangers consist of a smooth bar with a circular cross-section and a diameter of 60 mm. As material S 460 ML is used.

5.3 The wind bracing

The truss of the wind bracing is shown in Figure 5.2. Instead of a bending resistant top cross bar the wind portal frame is completed by a truss. Diagonal struts below this truss allow a shorter length of the portal frame columns, because the truss can be drawn down alongside the clearance gauge. For aesthetic reasons the rest of the wind bracing was chosen to be a K-truss. The distance between the Ks along the arch is 6.95 metres. The diagonal members have a system length of 8.60 metres. For all members the circular hollow section CHS 219.1x8 was chosen. At the nodes II and VIII extra bending moments occur because the connected members do not lie in one plane, but on a cylindrical sphere. Therefore the straight members at nodes II and VIII need to be CHS 219.1x10. The joints within the wind bracing are welded joints between hollow sections. The truss members are connected to the arch profile by welded endplates bolted to the flanges on the construction site. S 355 is used as material. CORUS TUBES STRUCTURAL & CONVEYANCE BUSINESS *[7]* provides such profiles.

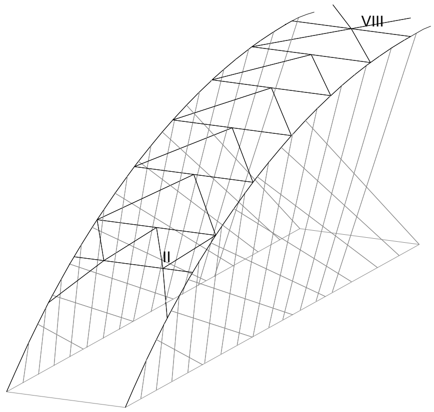

Fig. 5.2. System lines of the wind bracing, half bridge

5.4 The bridge deck

5.4.1 Main design

The tie of the bridge consists of a concrete slab (C50/60) spanning 10.15 metres between the hangers. It is prestressed in transverse direction to prevent cracking in serviceability limit state and decrease vertical deflections. Additionally this increases durability and leads to a slender cross-section. An alternative without transverse prestressing can be found in Section 5.4.2. The prestressing in longitudinal direction mainly counteracts the horizontal thrust of the arches. It is increased to compress the concrete for the same reasons as before.

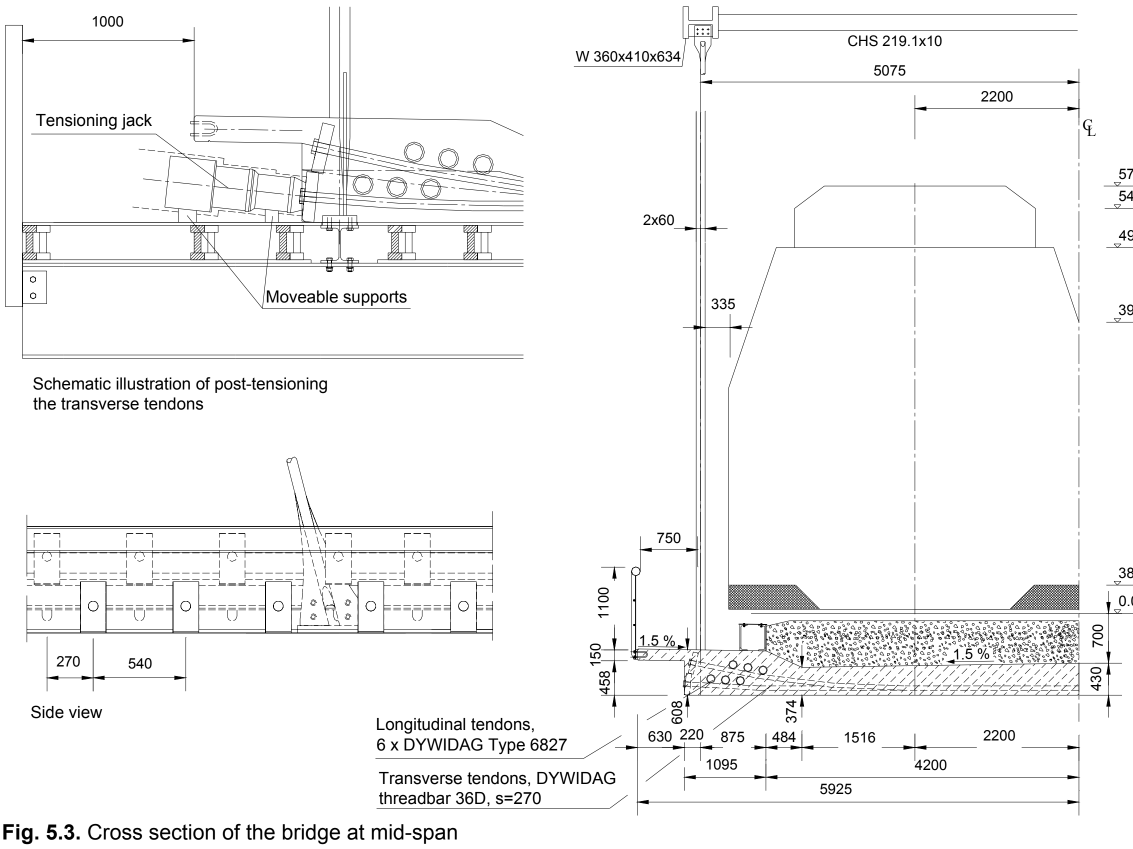

Fig. 5.3. Cross section of the bridge at mid-span

The formwork of the bridge deck receives a camber, sized according to the vertical deflections due to dead load. The additional reinforcement is shown in Figure 5.4. For transverse prestressing 370 DYWIDAG thread bars type 36D are placed every 27 cm along the tie. One side is dead anchored and the other prestressed (see Figure 5.3). Afterwards the prestressed anchorage is covered by a cap and protected by anti-corrosion agent. The tendons are put into place so that every second one has the dead anchorage on the same side. The longitudinal tendons are six DYWIDAG Type 6827 on each side of the bridge.

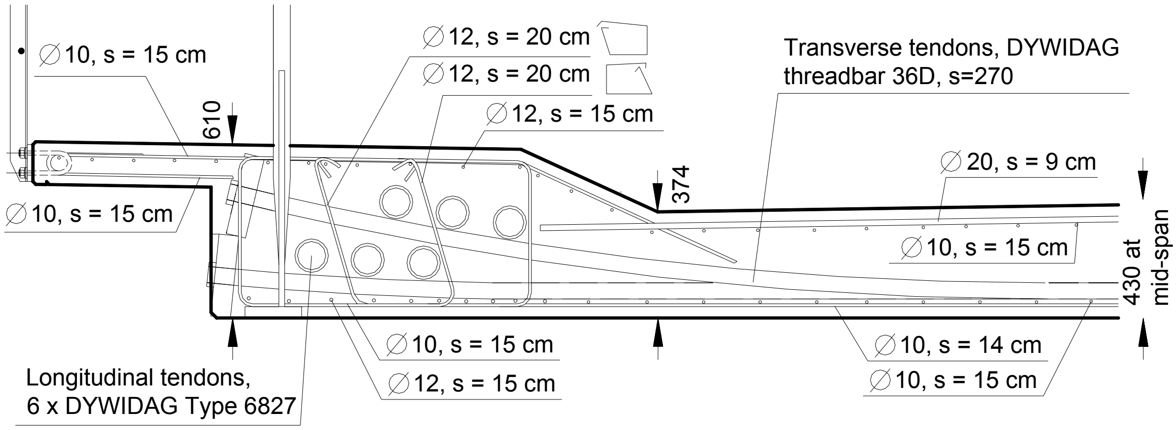

Fig. 5.4. Reinforcement of bridge deck with transverse prestressing

The main design has the disadvantage of requiring a large amount of compression reinforcement. This is caused by the small depth of the slab and the prestressing force which increases the height of the compressive zone in the concrete section. According to SCHNEIDER *[26],* page 5.126, DAfStb-Heft 425 suggests that the compression zone depth to effective depth ratio (x/d) shall not exceed the value 0.35 for concrete classes C 40/50 and higher. Otherwise compression reinforcement is required. In the bridge calculated in this work, the x/d ratio of 0.601 at the decisive section exceeds the limiting value significantly (Annex D. Section 5.2.1.1) making compression reinforcement of 35.6 cm^2/m necessary (re-bars: Ø 20, s = 9).

It might therefore be advisable to use a bridge deck of greater depth. Certainly, the increased dead load increases the bending moment. But the higher effective depth and the increased lever arm of the tendon counteracts the negative effect of the higher dead load. Therefore the required additional depth will be moderate and the compression reinforcement can be made redundant. Approximate calculations showed that a thickness of about 53 cm at the slab's mid-span would be enough to eliminate compression reinforcement. Besides, a thicker tie improves the stability and continuity of the track.

However, if desired, a thinner slab without compression reinforcement can still be achieved with higher concrete strength. The concrete class used, C 50/60, is the highest class regulated in EC 2.

5.4.2 Alternative design proposals (without transverse prestressing)

We wanted to investigate the alternative of a bridge deck without transverse prestressing. For long spans in transverse direction prestressing is essential, especially for railway bridges which are subjected to high loads. Shorter spans may be more economical without prestressing, but require a larger amount of reinforcement.

The double track railway bridge calculated in this work has a transverse span of 10.15 m, which lies in the range where both prestressed and non-prestressed solutions may be equally efficient. For example, the railway bridge calculated in STEIMANN *[37]* uses transverse prestressing at a span of 11.45 m. The distance between the arches of the bridge which is the object of attention in TVEIT *[42]* measures 9.65 m and uses transverse prestressing as well. TEICH & WENDELIN *[38]* calculated a network arch without transverse prestressing. Even though this bridge was designed for road traffic and not for railway traffic, it still indicates the possibility and feasibility of a non-prestressed solution.

Introduction of alternative design proposals

The required reinforcement and deflections are determined for two different variants:

For the first proposal a maximum reinforcing bar diameter of 25 mm with a minimum spacing of 9 cm was assumed, which is regarded as a lower boundary due to construction. Further assuming a single layer of reinforcement leads to a structural depth at the mid-span of 610 mm, which is equal to the depth of the edge beam. Compression reinforcement is not required.

The second proposal is based on a maximum ratio between compressive zone and effective depth x/d of 0.35, which is the upper boundary for a member using C50/60 concrete without compression reinforcement, SCHNEIDER *[29]*, page 5.126. In this case, a structural depth of 470 mm can be obtained. However, the reinforcement (Ø25) has to be applied in two layers, since otherwise the spacing would fall under the predetermined 9 cm. The spacing for the double layer reinforcement measures 14 cm.

Alternative design proposals

1. Slab depth at mid-span: 610 mm (Figure 5.5)
2. Slab depth at mid-span: 470 mm (Figure 5.6)

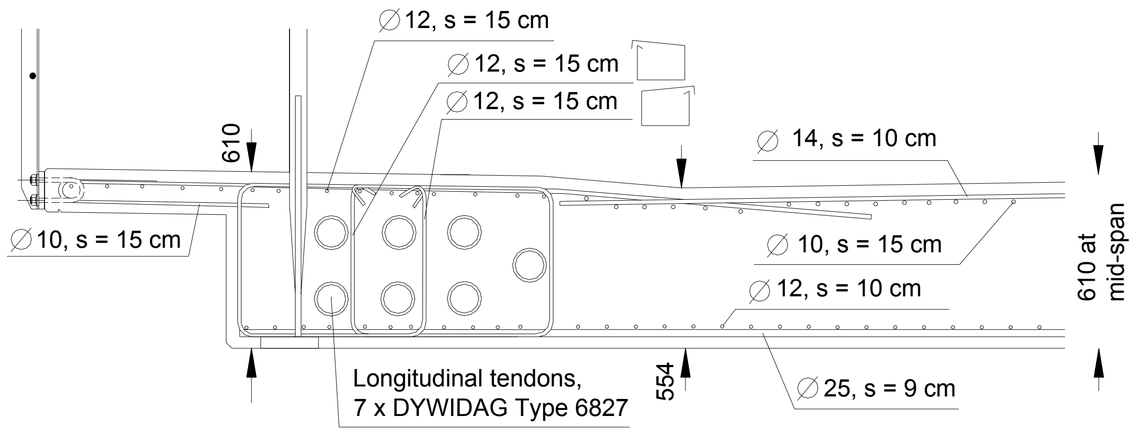

Fig. 5.5. Cross section with reinforcement of alternative design 1

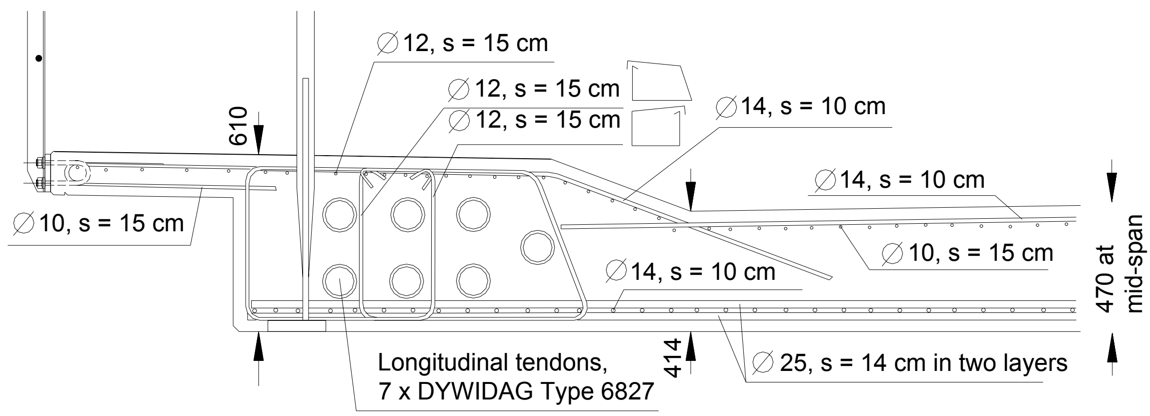

Fig. 5.6. Cross section with reinforcement of alternative design 2

Effects on the edge beams

The increased thickness of the bridge deck demands more longitudinal prestressing, because the higher dead load increases the horizontal thrust in the arch and therefore the axial tensile force in the tie. Furthermore the enlarged cross section area of the deck requires more prestressing to limit concrete tensile stresses.

The number of additionally required tendons was approximated by using the calculations for the preliminary design (Annex B, Figure B.9 and Figure B.12) with respectively increased cross sections and dead loads. To achieve at least the same concrete compressive stress, one more tendon per edge beam is necessary for both alternative designs. However, it might be possible to use only 6 tendons per edge beam for alternative design 2 with an only slightly increased concrete depth. Since this would have to be proven by a detailed assessment, 7 required tendons per edge beam will be presumed.

The edge beam dimensions of both alternative designs are sufficiently large enough to accommodate the additional tendon.

Effects on other structural elements

An increased depth of the bridge deck influences all other structural elements of the bridge. Hangers, arch profiles, bearings etc. receive higher internal forces due to the increased dead load. For example, the additional dead load of alternative design 1 leads to about 6% higher axial forces in the hangers and the arch, compared to the main design. Alternative 2 causes about 1% higher forces. Assuming that the clearance below the bridge is critical, the increased depth shifts the clearance gauge above the deck upwards which increases the length of the portal frame. Thus, transverse bending moments in the portal frame are also increased.

Deflections

The deflections of the alternative designs proved to be bigger than the deflections of the main design with transverse prestressing. The maximum deflection of the main design occurs at one edge beam, since only one track is loaded and the relative deflection of the slab is small. The deflection requirement of the main design is satisfied. The non-prestressed solutions show higher edge beam deflections (increased dead load), which however do not constitute locations of maximum deflections. The locations of the total maximum deflection lie between the edge beams, which is due to the large deflection of the deck relative to the edge beam.

Considering both alternative design proposals, design 1 gives a higher edge beam deflection, but the relative deck deflection is smaller. The latter is the decisive factor and results therefore in a smaller maximum deflection than for alternative design 2. Both designs satisfy the vertical deflection requirement of the Eurocode (Annex D, Section D.10, in this work).

5.4.3 Comparison

The following comparison between the main bridge deck design with transverse prestressing and the alternative design proposals without prestressing is based on approximate costs for tendons, reinforcement and concrete including material and labour, taken from VERCH *[50].*

In Figure 5.7, the amount of structural elements and materials of the three different bridge deck designs is listed together with respective costs. The main design with transverse prestressing appears to be the most costly solution at a cost of 350,640 €. Design proposal 1 shows hardly any difference. The costs for the eliminated transverse prestressing are countervailed by the additional reinforcement and concrete as well as the additional longitudinal tendons.

Design proposal 2 is the most economical solution at a cost of 339,837 €. It shows that costs due to the increased amount of reinforcement are less than costs saved by the reduced amount of concrete. The longitudinal tendons contribute considerably to the total costs and savings will have significant impact. As mentioned earlier, proposal 2 might work well with 6 tendons per edge beam, which would have to be checked for in detail. A reduction of 1 tendon per edge beam will then lead to a total sum of 323,271 €, which is approximately 10% cheaper than the main design with transverse prestressing.

Comparison of costs for different bridge deck designs					
		Weight/Volume		**Cost/Unit**	**Costs**
		[t]	**[m³]**	**[€/t] or [€/m³]**	**[€]**
Main design: Transverse prestressing					
Longitudinal prestressing	12 tendons [1)]	38,23		2600	99398
Transverse prestressing	373 thread bars [2)]	32,45		2600	84370
Reinforcement	500 S	62,028		800	49622,4
Concrete	C50/60		469	250	117250
				Total:	**350640**
Proposal 1: h[3)] = 0.61 m, no transverse prestressing					
Longitudinal prestressing	14 tendons [1)]	44,61		2600	115986
Reinforcement	500 S	95,527		800	76421,6
Concrete	C50/60		640	250	160000
				Total:	**352408**
				Difference to main design:	**1767**
Proposal 2: h[3)] = 0.47 m, no transverse prestressing					
Longitudinal prestressing	14 tendons [1)]	44,61		2600	115986
Reinforcement	500 S	114,81		800	91851,2
Concrete	C50/60		528	250	132000
				Total:	**339837**
				Difference to main design:	**-10803**
Notes:			additional reinforcement in end cross girders is neglected		
[1)] DYWIDAG Post-tensioning system, tendon type 6827					
[2)] DYWIDAG Post-tensioning system, thread bars, type 36 D					
[3)] h: structural depth at mid-span					

Fig. 5.7. Comparison of costs for different bridge deck designs

Immense compression reinforcement also contributes to the high cost of the main design. Approximations showed that a concrete slab about 10 cm deeper would make the compression reinforcement redundant. The application of only minimum reinforcement saves 27,647 €, whereas the additional concrete causes costs of about 20,000 €. However, additional longitudinal tendons would be necessary in order to countervail the increased dead load and cross section area. Thus, the design with transverse prestressing seems to constitute the most costly solution, regardless of whether compression reinforcement is used or not.

Design proposal 2 appears to be the most economical solution. However, the difference to the prestressed solution is still slight and it is necessary to consider the disadvantages of a non-prestressed bridge deck. The requirements for railway bridges regarding vibrations and deflections are high and often decisive. It might be possible that a non-prestressed deck does not satisfy such demands and therefore does not constitute a feasible solution. However, network arch bridges are stiffer than for example arch bridges with vertical hangers; deflections are smaller.

Nonetheless, durability reasons might necessitate prestressing in order to reduce or even avoid cracking. When deciding between prestressed and non-prestressed solution, it is therefore necessary to consider all aspects. Economical considerations cannot be the only criterion.

5.5 The end cross girder

The 1.75 metre wide end cross girders are formed by increasing the tie by 35 cm at the bottom. They transfer forces between the bearings, decrease the vertical deflection at the expansion joints and complete the wind portal frame. More details about this part of the structure can be found in Section 5.6.5.

5.6 Constructive design of the arch root point

The detail which deserves special attention is the point of the bridge which combines the bearing, the root of the arch, the end cross girder and the anchorages of the transversal and longitudinal tendons. In this section the design of this important detail will be explained, considering as an example the bridge calculated in this work.

5.6.1 Anchorage of the arch

The profile of the arch reaches the end of the bridge at an angle of 39° between the horizontal and the arch centreline. It transfers axial force, shear forces, and bending moments about 3 axes.

Axial force

The axial force is split into a vertical and a horizontal force acting in the plane of the arch. The vertical force is taken by the bearing with its centre underneath plate **B** and the horizontal part is taken by the longitudinal prestressing tendons. For this purpose the root of the arch profile is full penetration butt-welded to a vertical end plate **B** which is supported by the horizontal plate **C** above the bearing and serves as an anchorage for the prestressed cables, as well. Since railway bridges are subjected to large stress variations, the flanges of the profile have to be broadened to increase the length of the welds to plate **B** and lower shear stresses. The assessment of this connection detail showed that this is still insufficient to satisfy the fatigue check (Detail category 56). Consequently the enlargement of the flanges was extended, so that they are supported directly by **C**, as well. The enlargement was realized by plates **D**, full penetration butt-welded to the flanges of the profile, which gives a reasonable detail category (80) for the fatigue check. Additionally the perpendicular position of this weld prevents too large shear stresses.

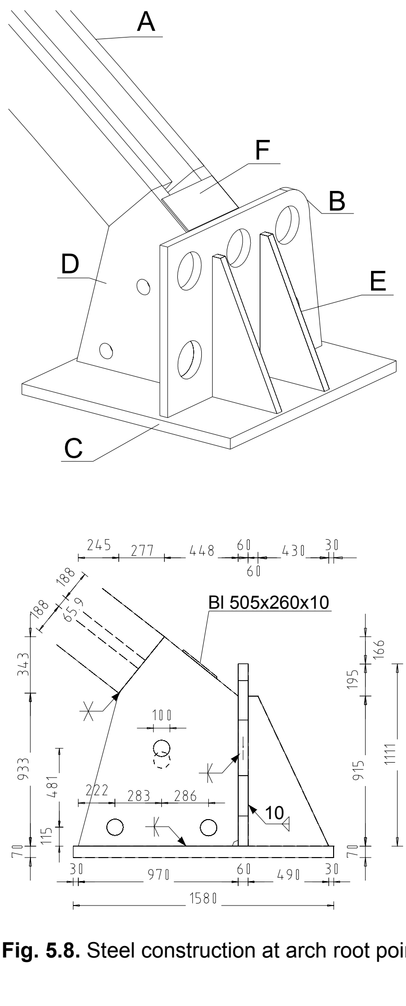

Fig. 5.8. Steel construction at arch root point

Shear forces

The occurring shear forces in the arch are small and converted into horizontal and vertical forces acting in the plane of the arch. They are borne like the axial force. Additionally a horizontal force exists, acting perpendicularly to the plane of the arch which is taken by the concrete pressure around the steel construction of the arch root and then taken by the bearings. The transverse prestressing takes the produced tensile stresses in the concrete and prevents cracking.

Bending moments

To take all acting bending moments, couples of forces in three axes are needed. In the transverse direction a large part of the bending moment about the longitudinal axis of the bridge is taken by the pair of pot bearings directly below the arch. The rest is transferred through the end cross girder and taken by the couple consisting of the bearings on each side of the bridge. This bending moment will be transferred by concrete pressure around the steel construction. The bending moment about the transverse axis of the bridge is taken by a clamping action of the plates **D** and **C**. It causes an angular rotation of the bridge end and is borne by the couple consisting of the bearings at each end of the bridge.

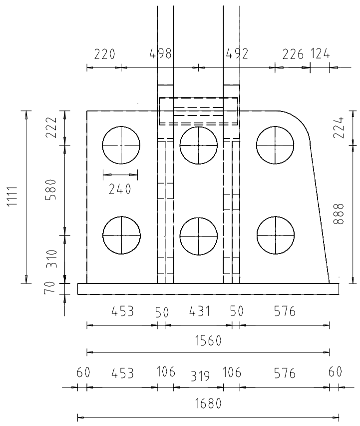

Fig. 5.8. Steel construction at arch root point

The bending moment about the vertical axis has to be taken by the concrete pressure around the steel construction, as well. It will be transferred by the shear-stiff bridge deck to the bearings. Compressive stress in the concrete around the steel structure cannot transfer the forces alone. As before, transverse and longitudinal prestressing form the counterpart, taking the tensile forces and preventing cracks around the steel structure.

5.6.2 Anchorage of the longitudinal tendons

The longitudinal tendons are anchored to the end plate **B**. The limits for centre and edge distances are given by the manufacturer DYWIDAG *[10]*. The minimum distances are larger at the anchorages than in the bridge deck. Additionally the neutral axis of the tendons should meet the neutral axis of the arch to avoid bending moments due to eccentricity. Therefore the prestressed strands have to be diverted with regard to the minimum radii. Their compressive forces are transferred by **B** to the concrete towards the middle of the span. Parts of the forces are directly taken by the arch flanges **D** which cause bending moments in plate **B**. Since there is always concrete pressure behind **B** when the tendons are prestressed, the bending moments do not demand additional vertical stiffening plates.

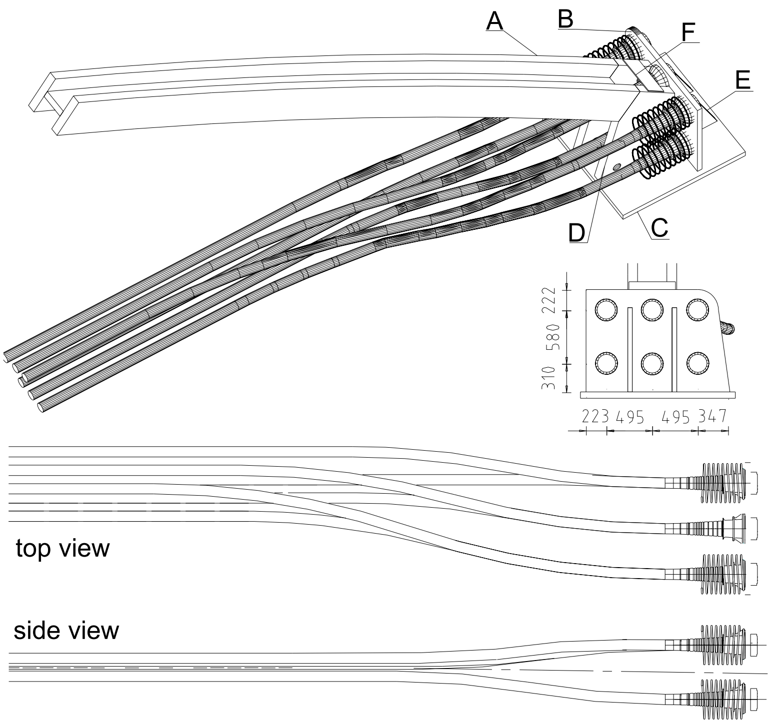

Fig. 5.9. Anchorage of the longitudinal prestressing strands

The primary tensile splitting forces of the four outer tendons are taken by helixes according to the permission certificate of the post-tensioned strands. The two inner tendons distribute their primary tensile splitting forces to the plates **D** and **C**. To enclose them completely the top plate **F** is needed. The web of **A** has to be cut out to let the inner tendons pass.

Since a significant part of the horizontal forces of the tendons are taken by the arch and the rest is already distributed to a larger area by plate **B,** it might be possible to eliminate the helixes to reduce the space required for the anchorages. This must be clarified with the manufacturer DYWIDAG.

Secondary tensile splitting forces and the lateral forces caused by the diversion of the tendons are taken by the transverse prestressing tendons.

5.6.3 Bearings

For this first draft two pot bearings were applied at each support of the bridge. An alternative is described in Section 5.6.6.

The pot bearings require a steel plate **C** above them to receive the vertical load. To achieve proper load distribution this plate must be levelled carefully. To avoid eccentricity of the vertical load the centre of the pot bearings is placed underneath plate **B**. The horizontal forces do not exceed the permitted limits set up by the manufacturer MAURER SÖHNE GmbH & Co. KG *[20]*. Therefore additional cams, tracks or bolts are not needed. The concrete behind plate **B**, towards the bridge ends, is cast at a later point during construction, to leave space for the tensioning jacks of the longitudinal tendons. Because of that, vertical stiffening plates **E** are needed to support plate **C** in transferring the vertical loads to the bearings.

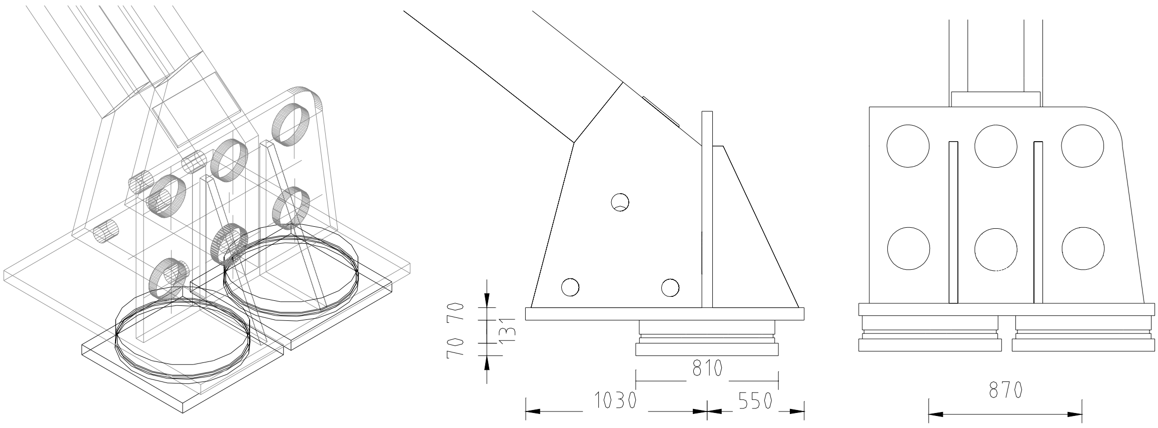

Fig 5.10. Pot bearings

5.6.4 Transverse prestressing

The transverse prestressing bars at the arch root point are arranged in the same manner as in the rest of the bridge deck. With the increasing depth of the concrete deck towards the end cross girder the tendons can be situated “lower” and the effective depth increases, as well. Therefore fewer tendons are needed. The width of the concrete deck also increases, which requires longer tendons. Where the tendons cross the arch root point holes have to be made in plates **D** to let them pass (Fig. 5.8). The last transverse prestressed bar behind plate **B** is placed after prestressing the longitudinal tendons. If the additional length of the bridge deck behind the bearings is reduced, it is possible to eliminate this tranverse tendon.

The longer transverse bars cross the plane of the arch where the concrete deck is supported by the hangers. On the cantilever side the neutral axis of the tendons lies above the neutral axis of the concrete section so that the bending moment caused by the prestressing counteracts the bending moments caused by the loading.

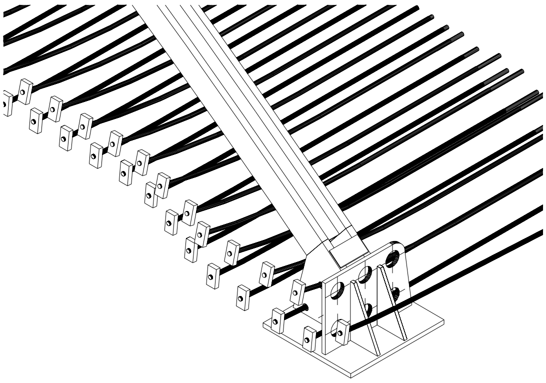

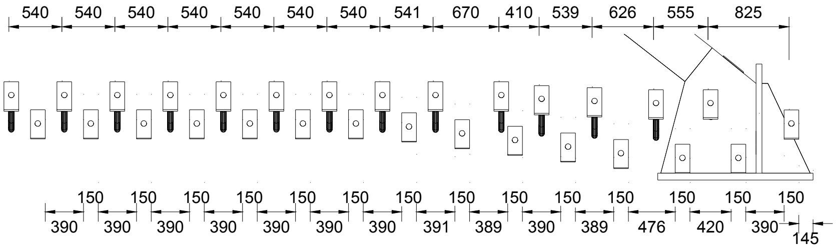

Fig. 5.11. Position of the transverse tendons at the end of the bridge

5.6.5 Lower hanger connection

The detail of the lower hanger connection is shaped as described in Section 7.8. Here, it will be shown how this detail fits into the transverse tendons. Where lower bars cross the hanger connection detail they can be put through the cut-out at the bottom of the hanger connection. The upper tendon bars have to be moved slightly sideways, which hardly influences the even distribution of their compression force. There is no influence on the design of the arch root construction detail.

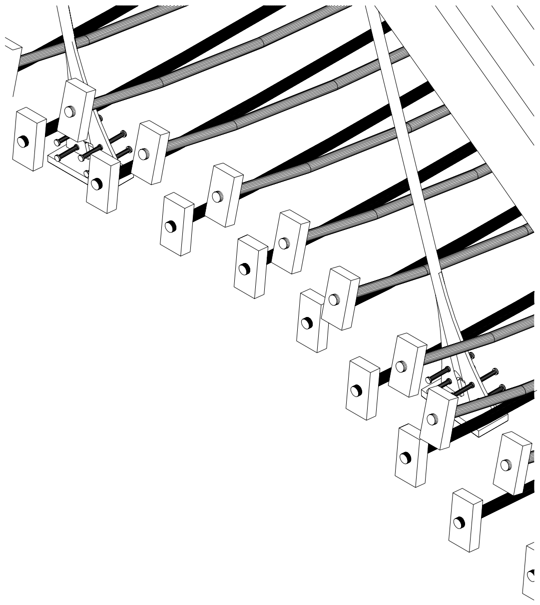

Fig. 5.12. Lower hanger connection with transverse tendons

5.6.6 End cross girder and concrete shape

The task of the end cross girder is to form a stiff beam between the two bearings at the end of the bridge. It distributes eccentric vertical forces, bending moments about the longitudinal axis of the bridge, reduces deflections, and supports the edge of the plate-like bridge deck.

The depth of the bridge deck was therefore increased at the lower surface from 430 mm to 780 mm in the middle of the bridge over 1.742 m of the bridge length. This additional space is also needed by the anchorages of the longitudinal tendons. The gradual diversion of the tendons requires a gradually increased depth of the bridge deck at the lower surface. For aesthetic and economic reasons this smooth transition is applied over the whole bridge width.

On the upper surface more space is also necessary to fit the anchorages of the longitudinal tendons into the bridge deck. However, only the edge beams were enlarged. This means there is an inclination of 9% for the footpath, which is accepted because it is non-public and if necessary the inclination can be reduced.

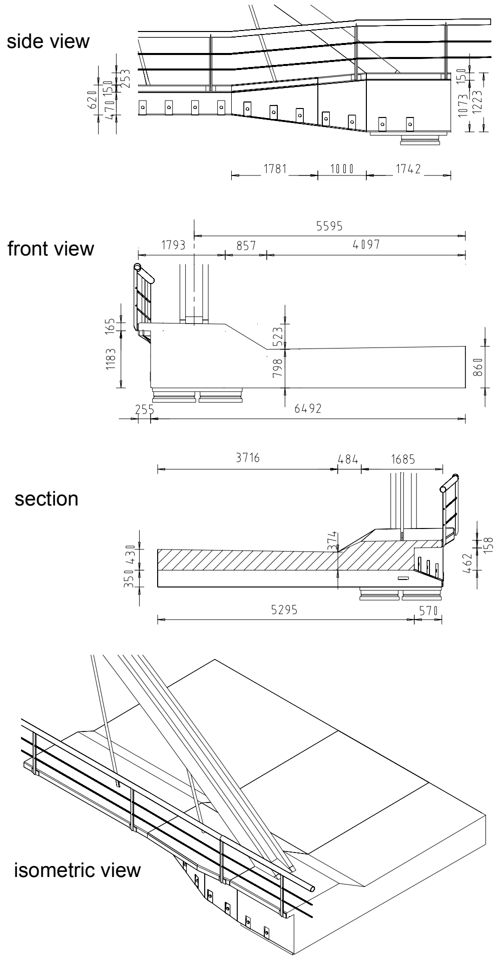

Fig. 5.13. Outer shape of the end of the bridge

The width of the footpath should be 0.75 m. To save self-weight the cantilevers have a width that allows 0.75 m clearance between the hangers and the handrail. To pass by the arches on the footpath, it was necessary to enlarge its width too. Due to the overall enlargement of the bridge deck in this area, the broadened footpath does not affect aesthetics.

At the inner corners of the arch profile there is a slight elevation of concrete, so that rain water and dirt do not collect close to the steel.

The large vertical forces acting on plate **C** cause large punching shear forces in the ends of the cross girder. The necessary reinforcement was calculated in Section D.6.2.3, but is not shown in the figures.

5.6.7 Alternative – stilt bearing

P. TVEIT proposes a stilt bearing as an alternative to the two pot bearings. It is described in Section 5.9. The changes to the construction of the arch root point to match the new conditions are:

1. The vertical loads will only be transferred by the vertical plate **B** to the bearing, because plate **C** cannot be used anymore for distribution of vertical forces. This raises again the problem with fatigue checks in the vertical weld between plates **D** and **B**. To increase the cross section area of the welds, plate **B** was slit and plates **D** receive full penetration butt welds on both sides. Additionally plates **D** have claws which rest on plate **B** (see Figure 5.14).

2. Although plate **C** is not capable of transferring vertical forces, it is still necessary to ensure that primary tensile splitting forces of the inner longitudinal tendons do not cause damage. But its dimensions can be decreased.

3. Without the load distribution of plate **C** the area provided to resist punching shear is decreased. Therefore more reinforcement is necessary. Furthermore, an interconnection between the loaded bearing plates **D** and **B** and the concrete, for example with shear studs, has to be ensured. Their assessment was omitted and therefore not shown in the figures.

4. The bearing takes place through the cylindrical bottom surface of plate **B**. In Section D.7.2 the necessary length was calculated. The thickness had to be adapted for the stilt bearing too. So plate **B** is twice as thick as for the pot bearings.

5. Additional vertical stiffening plates **E** are not necessary for construction phases.

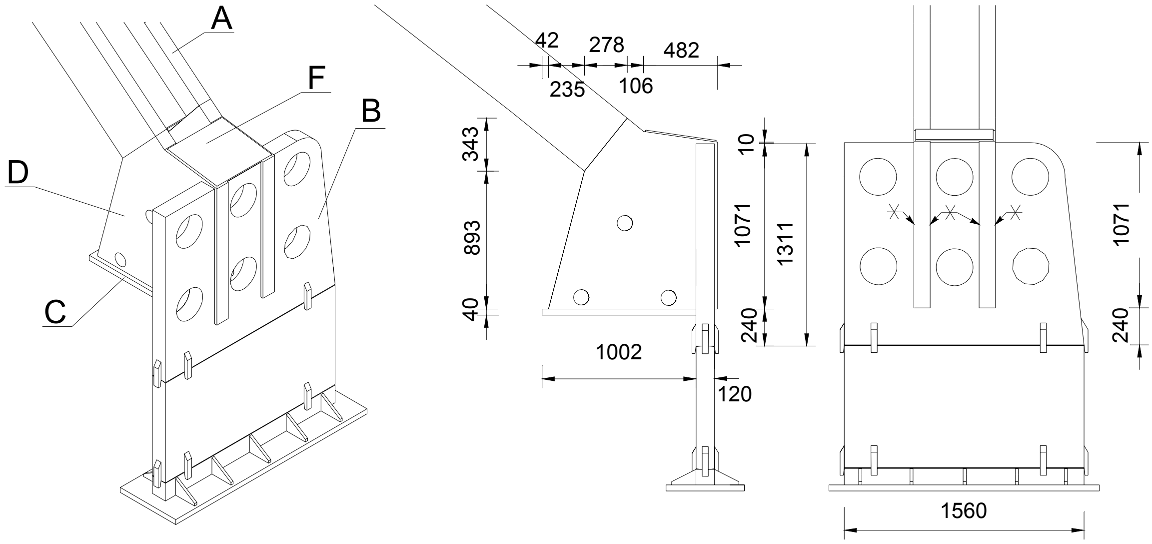

Fig. 5.14. Adapted design of the steel structure at the arch root point

5.7 The handrails

To protect pedestrians on the non-public footpaths a 1.10 metre high handrail is applied on both sides of the bridge. Figure 5.3 shows the construction details. The posts have a distance of 3 metres. The double hook concrete anchor provides 4 threads to connect the anchor plate with nuts. Structural steel S 275 is used.

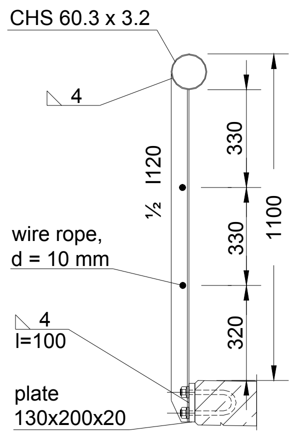

Fig. 5.15. Handrail

5.8 The drainage

The drainage is an important point when designing a network arch bridge. Since the lower chord is so slender despite the long spans, it is difficult to obtain the additional longitudinal incline for hidden drainage pipes. Nevertheless, it is possible to solve this problem. It just has to be kept in mind when designing the cross section of the tie. In the following some suggestions are given.

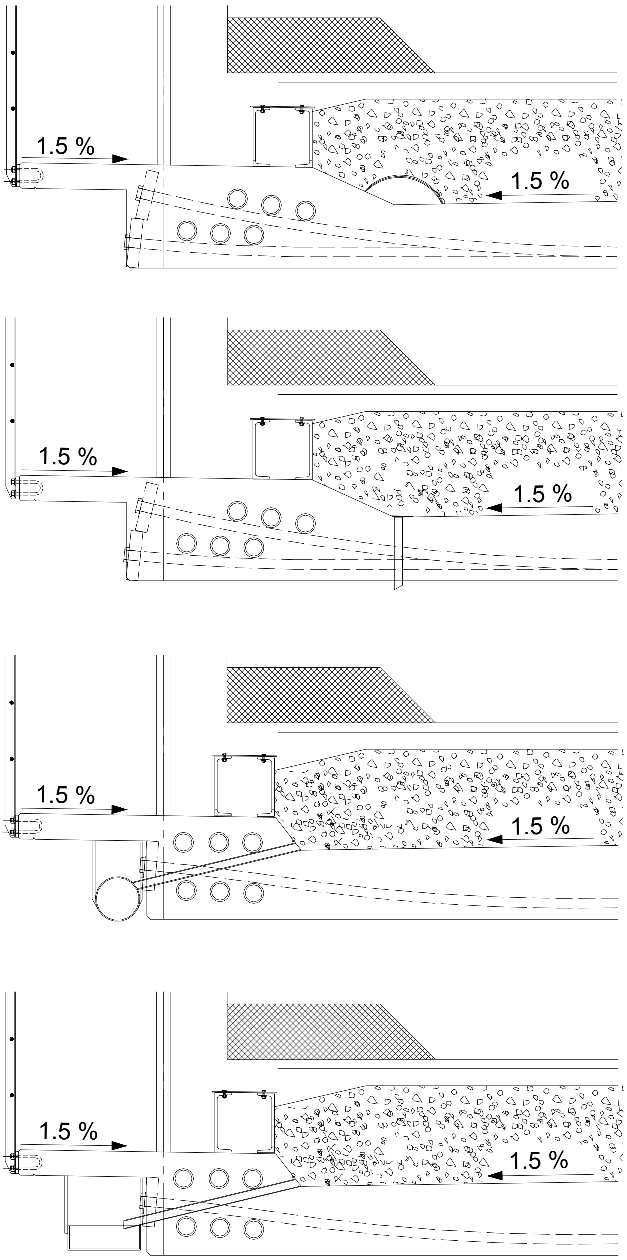

Fig. 5.16. Drainage options

If the gradient of the track provides a sufficient incline it is easiest to drain the bridge deck directly within the ballast. Then it might be a good idea to keep a clearance free at the lowest point so that water can flow faster. This can be protected by a perforated steel box, which is capable of bearing the railway loads.

Without an existing incline the easiest option is the application of spouts with inlets at the lowest points of the bridge that provide drainage by free falling water. The authors decided on that option. One spout with a diameter of 50 mm was arranged for the 100 m^2 bridge deck.

In some cases free falling water cannot be tolerated, and the incline of the bridge does not allow drainage of the whole length directly. Then pipes can be arranged underneath the cantilevers, which drain towards both ends of the bridge. This requires the consideration of a spout through the edge beam, already while designing the cross-section of the tie. Such pipes require a minimum incline due to the danger of sedimentation. For an example of the assessment of the longitudinal pipe see Annex D, Section D.8.

If such an incline cannot be provided an alternative would be an open canal which can be cleaned from time to time.

Another alternative for increasing the incline is to apply a camber to the bridge deck in the longitudinal direction. This would favour drainage to both sides of the bridge. Such a camber might be employed anyway, because a horizontal lower surface seems, to the human eye, to sag.

5.9 Investigation of two different types of bearings

5.9.1 General

The bridge is supported at the four corners of the bridge deck. Due to creep and shrinkage of the concrete tie and expansion and contraction caused by changes in temperature these supports must allow a horizontal movement. The maximum longitudinal horizontal deflection is 102 mm (Section C.7). Additionally the occurring horizontal forces have to be borne. Therefore moving and fixed bearings were combined as shown in Figure 5.17.

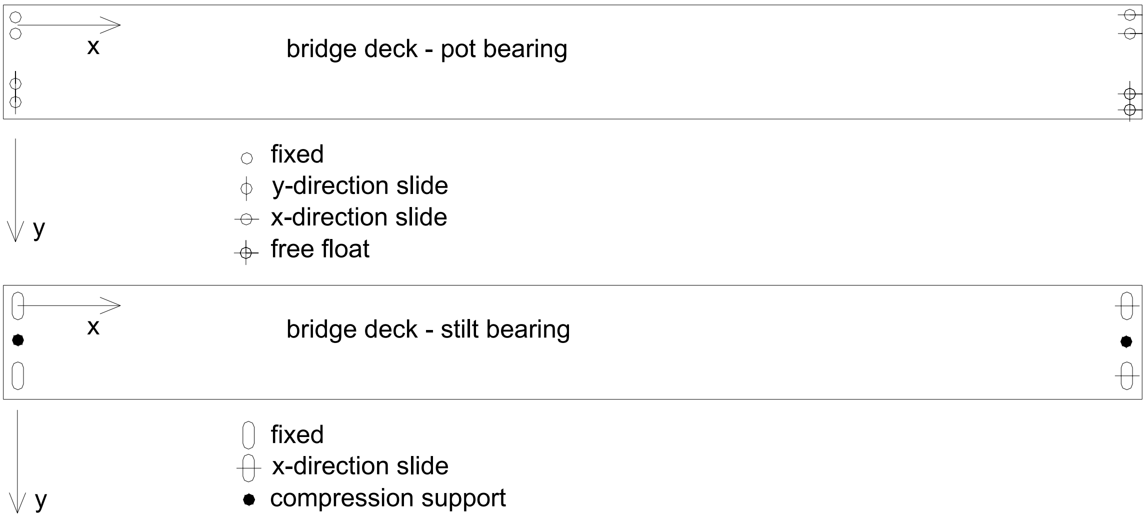

Fig. 5.17. Arrangement of bearings

The two different types of bearings investigated are 1. pot bearings and 2. stilt bearings.

The choice of pot bearings was influenced by STEIMANN *[37]*, whose bridge corresponds essentially with the bridge calculated in the present work. This bearing type represents a present-day standard method. The second type follows the idea of PER TVEIT and was applied in the network arches at Steinkjer and over Bolstadstraumen, both in Norway. In the following the two different types are described and then a comparison is drawn.

5.9.2 Pot bearings

Fig. 5.18. Pot bearing in situ

This type of bearing is designed to sustain large vertical loads and still allow tilt/angular rotation. It consists of metallic piston elements that contain an elastomeric disc. The free float type bearings have a PTFE (poly-tetra-fluoro-ethylene) insert sliding against a polished stainless steel plate, which provides translational movement in any direction from the neutral position. The addition of a "guide" steel bar to the polished steel plate and a flute to the counterpart transforms this bearing into the guide/slide type. Both guide and free float bearings provide for simultaneous rotation and translational movement. Shear keys are provided to bottom members to achieve retention within the abutment. The upper member will be welded to the horizontal plate of the arch root.

For this work pot bearings from MAURER SÖHNE GMBH & CO. KG *[20]* were used. For fixed bearings type TF-10, free floating bearings type TGa-10 and for guide/slide bearings type TGe-10 were used. The maximum diameter is 770 mm and for the sliding bearings the upper member has a length of 1110 mm.

The large bending moments reaching the bridge supports from the arch should be borne directly by the bearings and not distributed by the end cross girder. Therefore, a pair of pot bearings was applied at each support with a centre distance of 870 mm. Furthermore the neutral axis of the arch and the neutral axis of the bearings have a systematic offset of 62 mm. The bending moment caused by this eccentricity counteracts the bending moment from the arch and the end cross girder. This results in lower maximum vertical forces on the bearings.

The horizontal forces due to friction in the bearings while temperature changes should be decreased. The PTFE insert has a coefficient of friction μ = 0.032. With the vertical loads of approximately 10,000 kN on each bearing this gives a horizontal force of 1280 kN for four bearings. This is about 31 % of the maximum horizontal force occurring due to the other different actions on the bridge. The permitted horizontal force on the pot bearings is 10 % of the maximum vertical force, which means 4000 kN for four bearings. Therefore, it is not necessary to apply additional cams, tracks or bolts bearing the horizontal force.

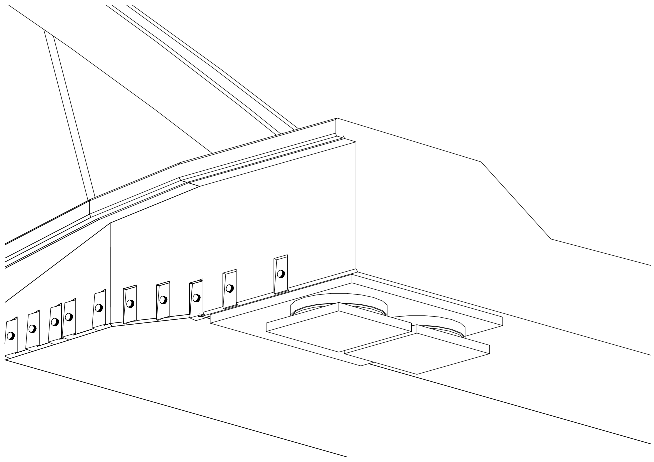

Fig. 5.19. Pot bearings at the bridge in this work

5.9.3 Stilt bearing with compression support in the middle of the end cross girder

This type is very similar to roller bearings, with the difference that the parts of the roll which never have contact to the top or bottom member are eliminated. This allows for large radii of the roller bearing without having a giant roll. In the fixed bearings the load is directly transferred to a plate with a cylindrical upper surface which is attached to the abutment. This allows angular rotations of the end of the bridge deck but constrains horizontal deflections. Horizontal deflections transverse to the bridge cannot be provided by this type of bearing.

The stilt bearing used in this work consists of the lower face of plate **A** (as shown in Figure 5.20), the “stilt” plate **B** and the elements **C**. It is all made of the same steel as used for the arches and the hangers, S 460 ML, but will be examined ultrasonically for evidence of laminations. The stilt plate has cylindrical upper and lower surfaces. The height of this plate must be twice the radius of these surfaces to allow proper roll-off properties. The required

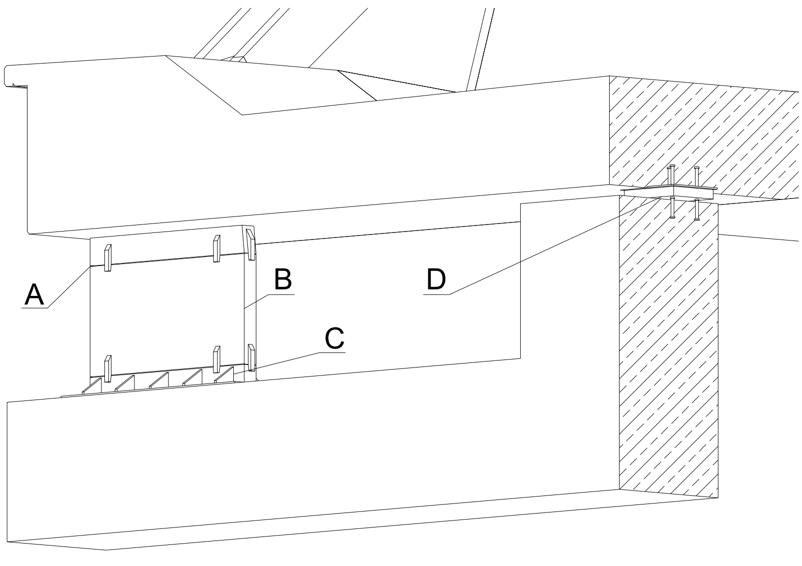

Fig. 5.20. Isometric view of stilt bearing and compression support

bow length is the maximum horizontal deflection of the bridge deck plus the diameter of the contact surfaces according to Hertz pressing plus the eccentricity due to angular rotation of the bridge deck end, Annex D.9.2.1. With regard to the stress distribution below the contact surface an additional safety length should be added. In this work a bow length of 103.3 mm was necessary.

The required radius and the width of the stilt plate can be calculated from the maximal actions and the permitted Hertz pressing. In this work the width was taken as 1560 mm corresponding to the pot bearings. The required radius is then 400 mm. The radius and the bow length lead to the required thickness of the stilt plate. This was taken as 120 mm. Using Hertz pressing for the assessment leads to non-conservative results as the “stilt” plate does not correspond to the full cylinder presumed for the formulas according to *Hertz,* see Section 10.

With this geometry the occurring nominal stress in the stilt plate is far below the yield strength, and a sufficient buckling resistance is provided. The distribution of the large vertical forces concentrated in a plate to the concrete of the abutment demands a stiffened steel plate **C** with a width of 510 mm.

As a locking feature the bearing receives cams.

The excellent behaviour of the stilt plate for longitudinal horizontal movements and rotations faces the impossibility of rotations transverse to the bridge. To avoid strong eccentric strains, the bending moments about the longitudinal axis of the bridge should be reduced. Therefore PER TVEIT suggested a compression support **D** (Figure 5.20) in the middle of the end cross girder, which is not connected to the bridge deck. For dead load only, the clearance between the bridge deck and the compression support should be 3 mm. This means the compression support will only act when live loads cause deflections larger than 3 mm and only take compression forces. The advantage is that this kind of bearing can consist of a simple fixed bearing, because in the short time of contact no horizontal deflections of the bridge will occur.

For **D** the elastomeric deformation bearing *MAURER Verformungslager Typ 1/2* was used, *[19]*. It consists of a reinforced elastomeric cuboid with one steel anchorage plate at the bottom, which is attached to the concrete of the abutment. The bottom side of the bridge deck is strengthened by another steel plate anchored with shear studs.

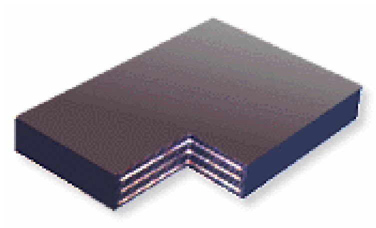

Fig. 5.21. Elastomeric reinforced deformation bearing

The maximum bending moments could be reduced from 2345 kNm to 930 kNm before contact and 934 kNm with contact, which is still considerable. As a further reduction the same eccentricity as for the pot bearings between the neutral axis of the bearing and the neutral axis of the arch was used. The eccentricity of the loads on the stilt plate was then sufficiently small.

Bearing **D** receives a maximum static vertical load of 1337 kN. Since, the bridge deck receives considerable acceleration while a train is passing, the static part of the force will be increased by impact. PER TVEIT suggested increasing the static part by 20 %.

Special attention is required for the design of the end cross girder. In this thesis it was only designed for the pot bearings. Nevertheless problematic points will be mentioned. For dead load the structural behaviour is much like that of a simply supported beam. On the other hand when the compression support acts, the end cross girder is a continuous beam and bending moments above the compression support change their direction. Transverse prestressing and reinforcement have to be assessed for both cases. PER TVEIT suggested reducing this problem by the use of compression bearings underneath each track.

The coefficient of friction for roller bearings made of structural steel is given as μ = 0.03, PETERSEN *[24]*, page 1156. Since this value is given for rolls with diameters of 100 to 200 mm, it is believed that due to an increase of the lever arm with a diameter of 800 mm the coefficient of friction can be reduced. It is assumed to be $\mu = 0.0075$. With the same vertical loads as for the pot bearings the maximum horizontal force due to friction in the bearings while temperature changes is 300 kN. That is 15 % of the rest of the horizontal forces.

5.9.4 Conclusion

Both types of bearings have advantages and disadvantages. For an evaluation the following comparison will help.

Pot bearing	Stilt bearing
Horizontal force due to friction: 1280 kN	Horizontal force due to friction: 300 kN
Overall height: 175 mm	Overall height: 1120 mm
Overall width: 1560 mm	Overall width: 1560 mm
Overall length: 1110 mm	Overall length: 510 mm
Free floating possible	Only one direction sliding possible
Free tilt/angular rotation	Tilt about transverse axis / no rotation about longitudinal axis allowed
Expensive	low cost material / expensive manufacturing
	Additional bearing in the middle of the end cross girder needed
	Danger of skew roll off
Assessment of end cross girder for one structural behaviour	Assessment of end cross girder for two structural behaviours
Usual static/dynamic internal forces	Impact forces due to shock on compression support
Difficulties for replacement	Easy replacement of stilt plate, difficult replacement of members
No extra construction for bearing of horizontal forces needed	Extra construction for bearing of horizontal forces needed

The general performance of the pot bearing shows a clear transfer of forces, no restraining loadings and easy handling. This bearing type is preferred by the authors.

The application of the stilt bearing is limited to narrow and straight bridges, where not disturbed by a large construction height of the bearing. The advantage over the pot bearings might be less expense if manufacturing costs are reduced by hiring qualified steel factories in developing countries.

5.10 Summary of materials used

In figures 5.24 to 5.27 on the following pages the weights of the materials calculated in the assessment can be found. The alternatives “stilt bearing” and bridge deck without transverse prestressing are included there, as well. The overall steel weight of the network arch calculated in this work is 376 tons. The temporary lower chord adds another 60 tons, but is not considered as steel weight of the bridge. As a comparison to other bridges already built, Figure 5.22 shows several railway bridges in a diagram depending on their spans and steel weight per track/span. It is still obvious that a network arch is an efficient and competitive structure.

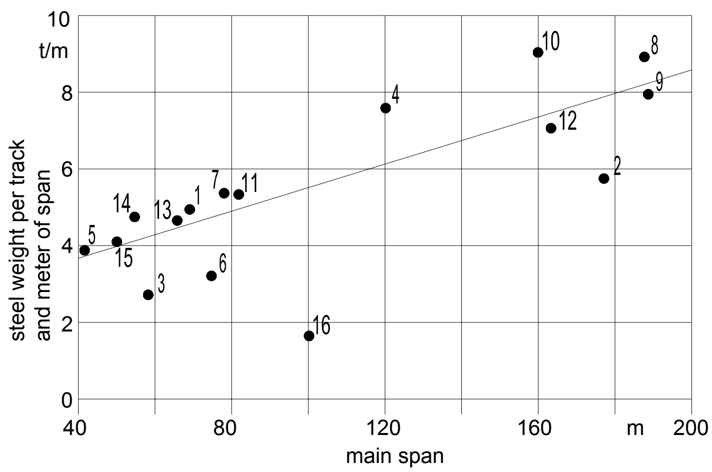

Fig. 5.22. Steel weight of railway bridges with ballast

	Location	Bridge type	Steel weight [t]	Span [m]	Number of tracks	Year of construction	Steel weight per track per meter span [t/m]
1	Data from [redacted] [17]	Tied arch		48		before 1975	5
2		Truss		175			5.8
3		Tied arch		58			2.8
4		Tied arch		120			7.5
5		Tied arch		43			3.7
6		Tied arch		75			3.2
7		Tied arch with orthotropic steel deck		77			5.4
8		Tied arch with truss		186			9
9		Tied arch with truss		187			7
10	River Main at Steinheim	Tied arch	1450	160	1	unknown	7.9
11	River Elbe at Torgau, track Halle/S.-Guben	Tied arch with orthotropic steel deck	440	80	1	1996	5.5
12	River Rhein	Two-hinge arch bridge	5350	165/368	2	1908-10	7.27
13	Oder-Havel-canal at Zerpenschleuse	Tied arch	300	65	1	1999	4.62
14	Spreebrücke Station Friedrichstrasse, Berlin	Two-hinge truss bridge	1600	55	6	1997-1998	4.84
15	Bridge over the Sachsendamm, Berlin	Continuous beam	510	50.55/ 41/34	1	1984	4.06
16	Bridge in this work	Network arch	376	100	2	none	1.88

Fig. 5.23. Bridges used for comparison

Steel weights									
		Weight per unit	Total number/length	Weight [t]					
Arches				S460 ML	S355	S275	St 1080/1230	St 1500/1770	S 500
Lower segments	W 360x410x900	900 kg/m	-/69.76 m	62.78					
Middle segments	W 360x410x634	634 kg/m	-/144.48 m	91.6					
Hangers									
Smooth bar d=60 mm	A = 0.00283 m²	22.2 kg/m	-/1650.24 m	36.63					
Wind bracing									
Bending members	CHS 219x10	51.55 kg/m	28.908 m		1.49				
Truss members	CHS 219x8	41.67 kg/m	316.59 m		13.19				
Arch root point									
Enlargment flanges	V = 0.09417 m³	739.23 kg	8/-	5.91					
Vertical plate	V = 0.08228 m³	645.9 kg	4/-	2.58					
Horizontal plate	V = 0.186 m³	1460.1 kg	4/-	5.84					
Vertical stiffeners	V = 0.0126 m³	98.75 kg	8/-	0.79					
Cover plate	V = 0.00133 m³	10.44 kg	4/-	0.042					
Handrail									
Top holm	CHS 60.3x3.2	4.5 kg/m	-/200 m			0.9			
Posts	½ I 120	5.57 kg/m	-/83.33 m			0.46			
Smooth bar d=10 mm	A = 0.785 cm²	0.62 kg/m	-/400 m			0.25			
Anchor plate	V = 0.00052 m³	4.09 kg	68/-			0.28			
Transverse prestress									
Transverse tendons	DYWIDAG threadbar 36D	8.27 kg/m	-/3923.96 m				32.45		
Anchor plates	V = 0.00305 m³	23.94 kg	746/-			17.9			
Longitudinal prestress									
Longitudinal tendons	DYWIDAG Type 6827	31.86 kg/m	-/1200 m					38.23	
Reinforcement									
Re-bars	Ø10	0.617 kg/m	-/21190.95 m						13.07
	Ø12	0.888 kg/m	-/3466.67 m						3.08
	Ø20	2.47 kg/m	-/13166.67 m						32.52
Stirrups	Ø10	0.617 kg/m	-/1333.33 m						0.82
sum of re-bars+stirrups	Ø12	0.888 kg/m	-/5000 m						4.44
increased by 15 %	Ø20	2.47 kg/m	-/952 m						2.35
Sum of each material				206.2	14.68	19.8	32.45	38.23	64.72
Sum prestress steel							70.68		
Sum reinforcement							135.402		
Sum structural steel				240.602					
Sum of all persistent steel				376.004					
Temporary lower chord									
Longitudinal beams	HEB 220	71.44 kg/m	-/198 m		14.14				
Transversal beams	IPEa 550	91.85 kg/m	-/407.1 m		37.39				
Wind bracing	L 120x10	18.21 kg/m	-/399 m		7.27				
Connection part	HEB 200	61.31 kg/m	-/1.2 m		0.074				
Bracing at transition point	V = 0.0039 m³	30.62 kg/m	8/-		0.24				
Sum of temporary lower chord					59.11				
Total sum				435.118					

Fig. 5.24. Steel weight of the bridge, calculated in this work

Material for formwork				
		Weight per unit	Amount	Weight [t]
Formwork sheets	Plywood t = 18 mm	12.6 kg/m²	1357 m²	17.1
Formwork timber beams	Doka formwork beam H 20 P	5.1 kg/m	4704 m	24

Concrete for bridge deck				
C50/60	V = 251.9 m³	2.5 t/m³	-	1259.4

Fig. 5.25. Formwork material needed for the erection

Steel weights of alternative "stilt bearing"									
		Weight per unit	Total number/length	Weight [t]					
				S460 ML	S355	S275	St 1080/1230	St 1500/1770	S 500
As in Figure 5.24 but:									
Arch root point									
Enlargment flanges	V = 0.11038 m^3	866.48 kg	8/-	6.93					
Horizontal plate	V = 0.026 m^3	204.1 kg	4/-	0.82					
Vertical plate	V = 0.173 m^3	1358.1 kg	4/-	5.43					
Stilt bearing									
Vertical bearing plate	V = 0.149 m^3	1169.7 kg	2/-	2.34					
Sum of each material				207.36	14.68	19.75	32.45	38.23	29.47
Sum prestress steel							70.68		
Sum reinforcement							100.15		
Sum structural steel				241.79					
Sum of all persistent steel				341.94					

Fig. 5.26. Changes in the steel weight due to the application of the stilt bearings

Steel weights of alternative without transverse prestressing, proposal 1; h = 0.61 m at mid-span									
		Weight per unit	Total number/length	Weight [t]					
				S460 ML	S355	S275	St 1080/1230	St 1500/1770	S 500
As in Figure 5.24 but:									
Transverse prestressing									
Transverse tendons			-/0 m						
Anchor plates			0/-						
Longitudinal prestressing									
Longitudinal tendons	DYWIDAG Type 6827	31.86 kg/m	-/1400 m					44.604	
Reinforcement									
Re-bars	Ø10	0.617 kg/m	-/7433.33 m						4.59
	Ø12	0.888 kg/m	-/13623.33 m						12.1
	Ø14	1.21 kg/m	-/11850.0 m						14.34
	Ø25	3.85 kg/m	-/11766.67 m						45.3
Stirrups	Ø10	0.617 kg/m	-/1333.33 m						0.82
sum of re-bars+stirrups increased by 15 %	Ø12	0.888 kg/m	-/6666.67 m						5.92
	Ø20	2.47 kg/m	-/952 m						2.35
Sum of each material				207.4	14.68	1.89	0	44.604	98.23
Sum prestress steel							44.604		
Sum reinforcement							142.837		
Sum structural steel				223.93					
Sum of all persistent steel				366.767					

Fig. 5.27. Changes in the steel weight for alternative bridge deck, proposal 1

Steel weights of alternative without transverse prestressing, proposal 2; h = 0.47 m at mid-span									
		Weight per unit	Total number/length	Weight [t]					
				S460 ML	S355	S275	St 1080/1230	St 1500/1770	S 500
As in Figure 5.24 but:									
Transverse prestressing									
Transverse tendons			-/0 m						
Anchor plates			0/-						
Longitudinal prestressing									
Longitudinal tendons	DYWIDAG Type 6827	31.86 kg/m	-/1400 m					44.604	
Reinforcement									
Re-bars	Ø10	0.617 kg/m	-/7433.33 m						4.59
	Ø12	0.888 kg/m	-/1733.33 m						1.54
	Ø14	1.21 kg/m	-/23740.0 m						28.73
	Ø25	3.85 kg/m	-/15128.57 m						58.25
Stirrups	Ø10	0.617 kg/m	-/1333.33 m						0.82
sum of re-bars+stirrups increased by 15 %	Ø12	0.888 kg/m	-/6666.67 m						5.92
	Ø20	2.47 kg/m	-/952 m						2.35
Sum of each material				207.4	14.68	1.89	0	44.604	117.5
Sum prestress steel							44.604		
Sum reinforcement							162.134		
Sum structural steel				223.93					
Sum of all persistent steel				386.064					

Fig. 5.28. Changes in the steel weight for alternative bridge deck, proposal 2

Fig. 5.29. Photo composition of the bridge calculated in this work

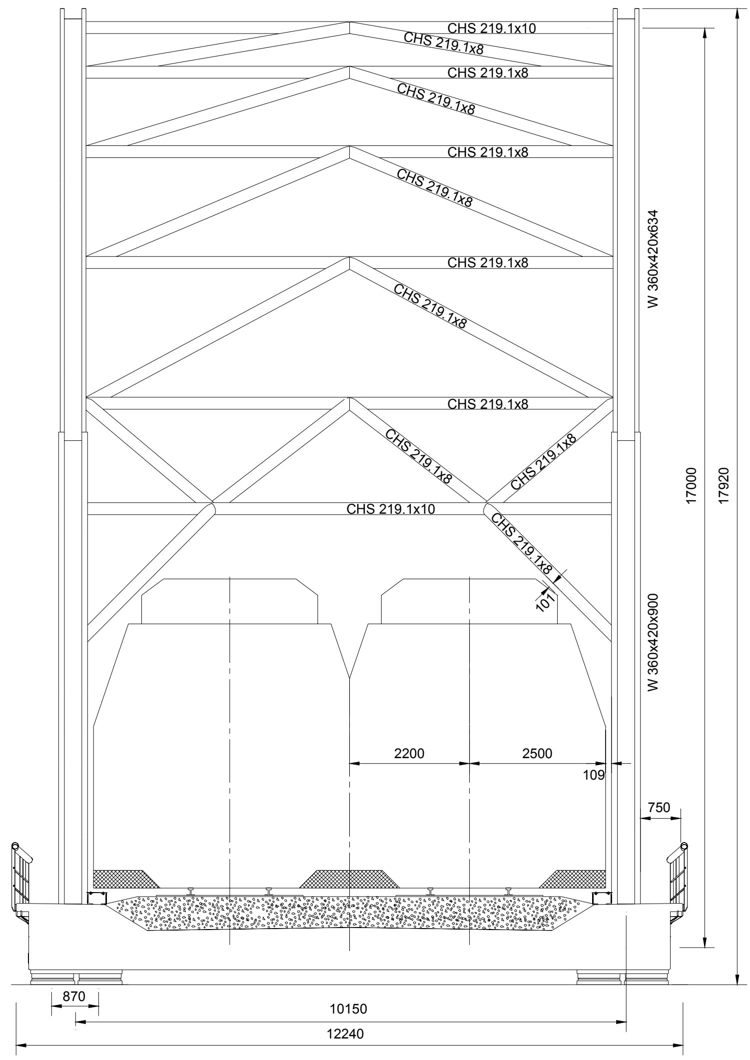

Fig. 5.30. Front view

Double track railway network arch bridge assessed for the European standards.

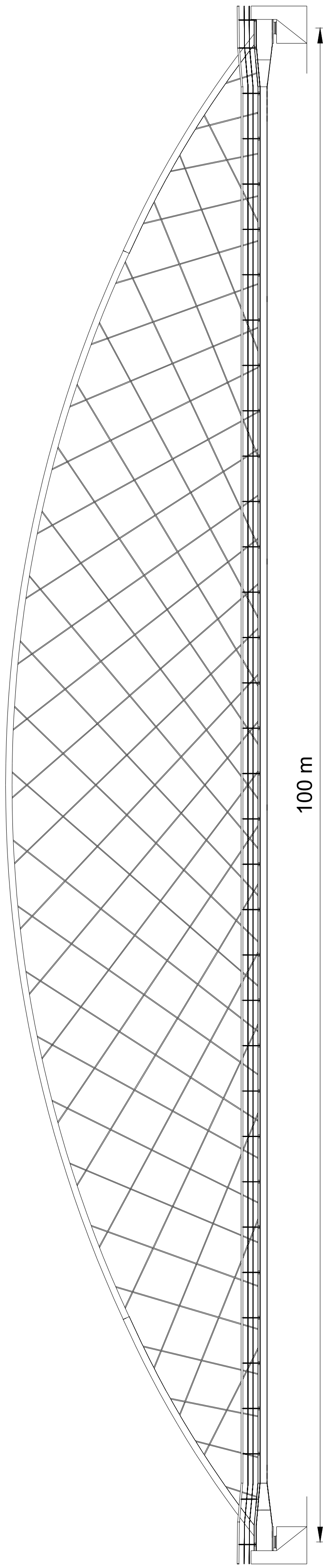

Fig. 5.31. Side view

Section 6

Optimisation of the hanger arrangement

6.1 Scope

Section 6 constitutes one of the main fields of research in this work. It was to optimise the number and arrangement of hangers regarding maximal hanger forces and stress ranges. In a preliminary investigation two algebraic descriptions were introduced for hanger arrangements similar to the ones considered as near optimal by former studies. Thereupon, it was possible to vary the geometry within these descriptions and analyse the influence lines of the structure using a 3D-FEM-model by means of SOFiSTiK structural analysis software. The results of 850 different hanger arrangements were compared searching for minimum internal forces.

Delving into this topic and studying theories of the optimisation of structures, the authors had an idea of a new description of the hanger arrangement. This was also converted into a 3D-FEM-model, and the numeric analysis of another 80 bridges showed considerably improved results.

With the new type of hanger arrangement, about 100 bridges more were calculated varying other geometry parameters, such as span, arch rise, number of hangers and curvature of arch, to develop further improvements.

The knowledge about the structural behaviour of network arches obtained from the investigations is discussed and explanations are suggested. As a summary a preliminary scheme is given which allows designing a network arch railway bridge according to the results found.

6.2 What is an optimal hanger arrangement?

According to GRAF/STRANSKY *[13]*, page 1/1, an optimal structure is characterised by the following attributes:

-safe/durable
-economic/inexpensive
-fast/easy to build
-functional, aesthetic, ecological…

The complexity of these demands would cause extensive work to satisfy them, so the number of attributes considered was reduced. Therefore, in the following the more appropriate word “improve” is used instead of “optimise”. The adapted attributes are:

-Minimal maximum hanger forces
-Minimal maximum bending moments in the arch about the horizontal axis

-Minimal variation in hanger forces
-Minimal variation in bending moments in the arch about the horizontal axis

The bending moments in the arch about the horizontal axis correspond in a certain way to those in the tie, so minimal bending moments in the arch will consequently give small bending moments in the tie. Railway bridges, like the one calculated in this work, are subjected to fatigue strains, so the force variation should always be considered. Fulfilling these demands saves material for hangers and arches, which can mean a less expensive structure and easier erection due to less weight. Furthermore it leads to more slender arches and hangers, which might be a criterion for aesthetics. So the limitation to the mentioned demands should still lead to important improvements in the structure.

6.3 The parameters

The parameters considered in this work to influence the internal forces are:

1. Location of hanger nodes along the arch
2. Location of hanger nodes on the lower chord
3. Number of hangers and span of the bridge
4. Rise of the arch
5. Loading
6. Curvature of the arch

Due to the number of parameters and the complexity of their influences, it was decided to use experimental improvement. As a further limitation of the extent the following simplifications were assumed:

To 1. According to the proposals by TVEIT *[45]*, page 26, the hangers were placed equidistantly along the arch for all hanger arrangements, and only the hanger nodes at each arch end were considered to be variable (see Section 6.7.5).

To 2. The location of the lower hanger nodes was obtained by algebraic/geometric descriptions as explained in Sections 6.5.1, 6.5.2 and 6.6.3. Only the first few lower hanger nodes were shifted manually (see Section 6.7.5).

To 3. For the calculations the number of hangers was chosen to be 44 and the span was 100 metres, as it was in STEIMANN *[37]*. Additional investigations were carried out varying the span and the number of hangers (see Section 6.7.1).

To 4. A rise of the arch of 17 meters was assumed, which gives a rise/span-ratio of 0.17. In Section 6.7.2 ratios between 0.14 and 0.18 were tested.

To 5. The bridges were loaded by prestressing and dead load. Furthermore, one load model 71 with a partial safety factor of 1.5 was applied on each track. For dead load a partial safety factor of 1.35 was used. This causes loads that are close to the decisive design forces for the ultimate limit state design checks.

The application of these partial safety factors gives too high stress ranges regarding fatigue checks. Since it only influences the absolute value, the results still describe correctly the tendency within the improvement process.

To 6. In TVEIT *[43]*, page 2195, it is suggested that the arch is a part of a circle. This was assumed for all investigations. The radius of curvature near the ends of the arch was decreased in Section 6.7.4, because it gives benefits for the wind portal (TVEIT *[48]*, page 4).

6.4 Evaluation of the results

The calculations were performed with the help of a 3D-model in SOFiSTiK (see Annex C.1). Resulting from the analysis of the hangers' influence lines, the maximum and minimum hanger forces were recorded by this software. So were the bending moments in the arch about the horizontal axis. The following names are used in the following sections.

MaxN = maximum hanger force
the maximum axial hanger force occurring in the calculation of one bridge

AveN = average hanger forces
the arithmetic average of the maximum axial hanger forces reported for one bridge

ΔN = maximum variation of hanger force
Variation means the difference between minimum and maximum axial hanger forces of each hanger of one bridge. The maximum of these values is recorded.

AveΔN = average variation of hanger force
the arithmetic average of the axial hanger force variations

The same is valid for the bending moments in the arch about the horizontal axis along the whole bow length:

MaxM, **AveM**, **ΔM**, **AveΔM**

The average values were of interest because the arch root point forms a clamping; therefore, hanger arrangements best for the middle of the span may cause unfavourable results for the ends. The occurring maverick axial hanger forces deviated significantly from the rest. The maximum bending moments in the arch are subject to deviations caused by these maverick hanger forces, so the average bending moments will also be involved into the evaluation. It is known that the bending moments are not uniformly distributed along the arch, especially not in arches with vertical hangers. So the relevance of the average bending moments in respect of minimisation of the maximal bending moments might be small. But it is believed that a hanger arrangement which causes small average bending moments also leads to small maximum bending moments.

An improved hanger arrangement can be expected if all values are minimums. Since this did not occur for one and the same hanger arrangement, a certain weighting of the results had to be made. The maximum forces shall satisfy the ultimate limit state and the stress range the fatigue limit state. The target would be to find a solution satisfying both limit states in a way that the utilisation rate of all checks is at about the same level, ideally 100%.

Therefore, not only the internal forces, but also the design checks would be needed in the improvement process providing indications about the weighting to be used. In turn, this would also mean that all design-relevant load combinations have to be included. Their consideration would extend the process drastically due to the very time-consuming data processing. Furthermore, the evaluation of that data would go beyond the scope of this work. So, the following evaluations based on intuition were used:

1. A search was conducted for the minimum of each data series (**MaxN**, **AveN**, **ΔN**, etc.) of one investigation, for example varying the span. Then each value of the data series was divided by this minimum. That means the data series were scaled, so that the minimum of each equals 1.
2. Then the scaled data series were summed up.

SummaxN = **MaxN** + **ΔN**
SumaveN = **AveN** + **AveΔN**
Summax = **AveN** + (0.5 **AveM** + **MaxM**)
Sumvariation = **AveΔN** + (0.5 **AveΔM**+**ΔM**) Terms in brackets scaled another time

Sumall = **Summax** + **Sumvariation**

The hanger arrangement leading to the minimum value of **Sumall** is considered to be the best.

Regrettably, from the investigations carried out in Section 6.5.1 and 6.5.2 no values of the bending moments in the arch were considered. It was not expected that considering only the axial hanger forces would lead to results that are not desired.

In Annex F, diagrams with all data series can be found, so that one can search for an improvement applying its own weightings.

6.5 Preliminary investigations

To obtain a first insight into the problems of the hanger arrangement, two algebraic descriptions of the geometry were set up. They are suitable for obtaining hanger arrangements similar to the ones considered as near optimal by former studies.

6.5.1 Variation of the lower hanger nodes by the node distances

The mathematical model

In TVEIT *[45]*, page 8, and TEICH & WENDELIN *[38]*, page 16, it is suggested to have equally spaced hanger nodes along the middle of the tie. Towards the bridge ends the distances of the nodal points of one set of hangers increase while the ones of the other decrease. So, for one set of hangers the node distances are arranged as shown in Figure 6.1 along the tie. The other set of hangers is the mirrored equivalent. That is why in the following only one set of hangers is considered.

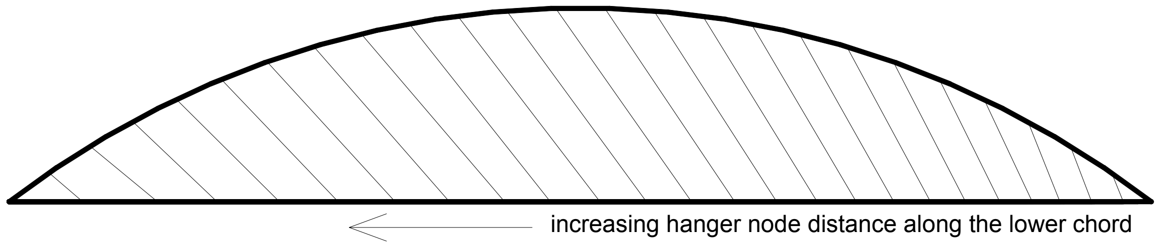

Fig. 6.1. One set of hangers

Starting from the right, the node distances increase with a certain increment. There is hardly a change of the distances in the mid range, and further to the left end the distances increase again with the same increment as on the right side.

The authors intended to calculate many different hanger arrangements which all follow this scheme. For this purpose an algebraic description of the mentioned geometry was needed. The same behaviour was then found in the curvature of an ellipse. The left part of Figure 6.2 shows the necessary adaptations, so that one can find the node distances by the help of an ellipse.

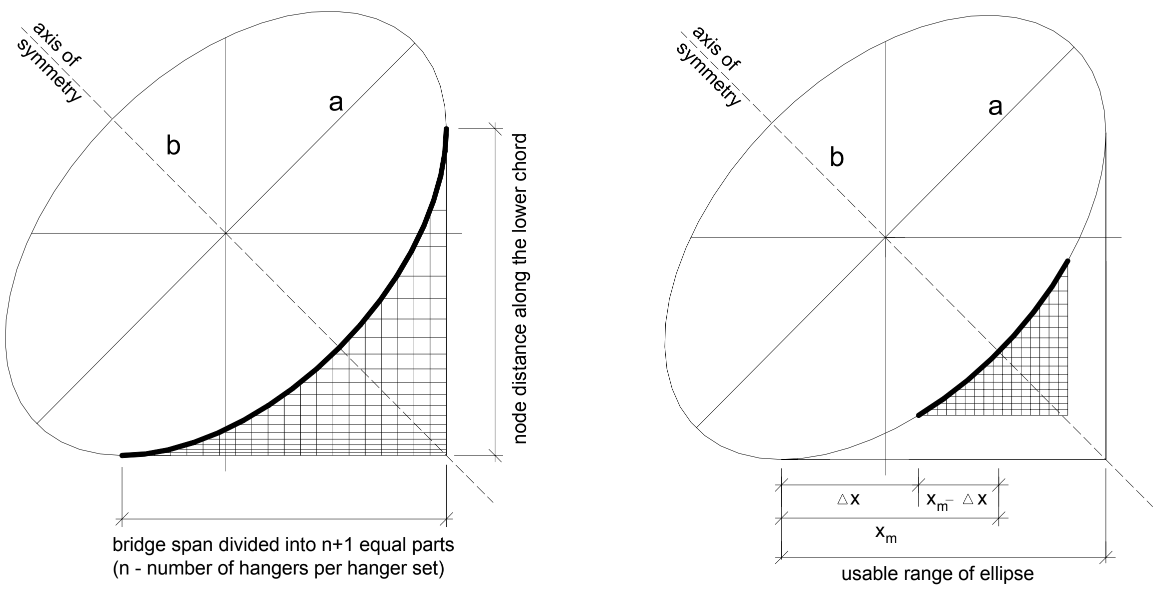

Fig. 6.2. Node distance spaced by the help of an ellipse (schematic illustration)

Two variables make it possible to change the hanger arrangement. The first is the ratio between semiminor axis b and semimajor axis a. The second is found, if not the whole usable bow length of the ellipse is deployed (see right part of Figure 6.2). The ratio between the unused range and the usable range will be the second variable.

$\lambda_{ellip} = \frac{b}{a}$ ratio between semiminor and semimajor axis, λ_{ellip} = [0..1]

$\lambda_{range} = \frac{\Delta x}{x_m}$ utilisation of the ellipse, λ_{range} = [0..1]

Parameter λ_{ellip} allows a variation between equidistant spacing (λ_{ellip} = 0) and an extreme increase from one distance to the next (λ_{ellip} = 1). Parameter λ_{range} can be used to exclude the larger curvature changes at the beginning and the end of the usable range and obtain more even node distances.

The analysis

As mentioned in Section 6.3 for this calculation the following fixed parameters were used.

Span of the bridge:	s = 100m
Arch rise:	f = 17m
Number of hangers per set:	n = 22

The results from the calculation of 450 different arrangements are presented in figures 6.3 to 6.7. In Annex F, Section F.2 large size illustrations of these diagrams are provided.

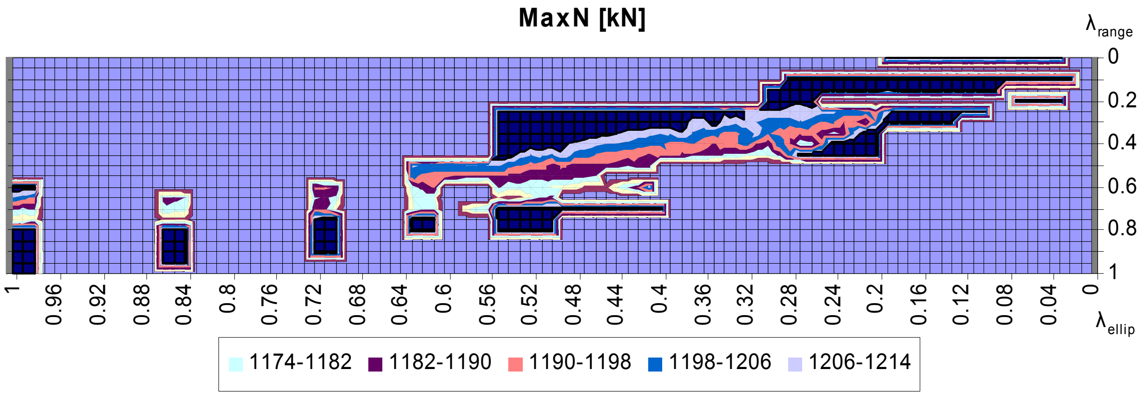

Fig. 6.3. Results for the maximum axial force of all hangers

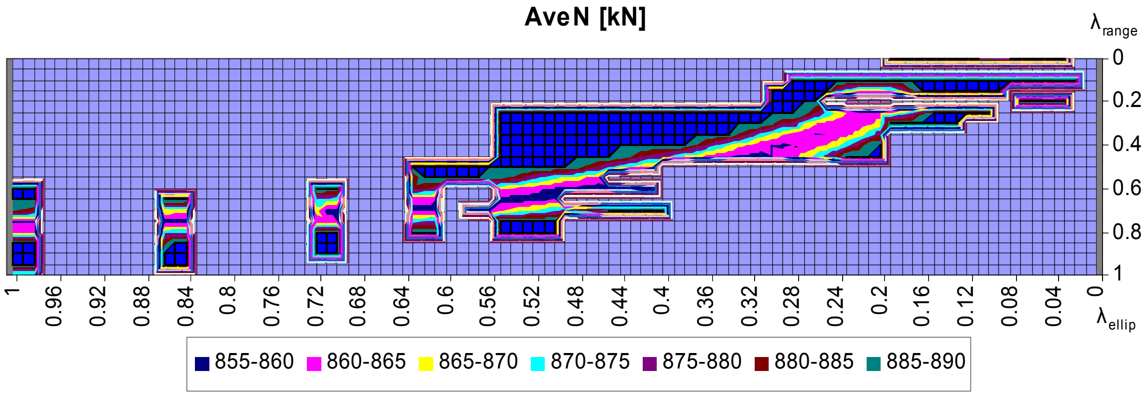

Fig. 6.4. Results for the average axial force of all hangers

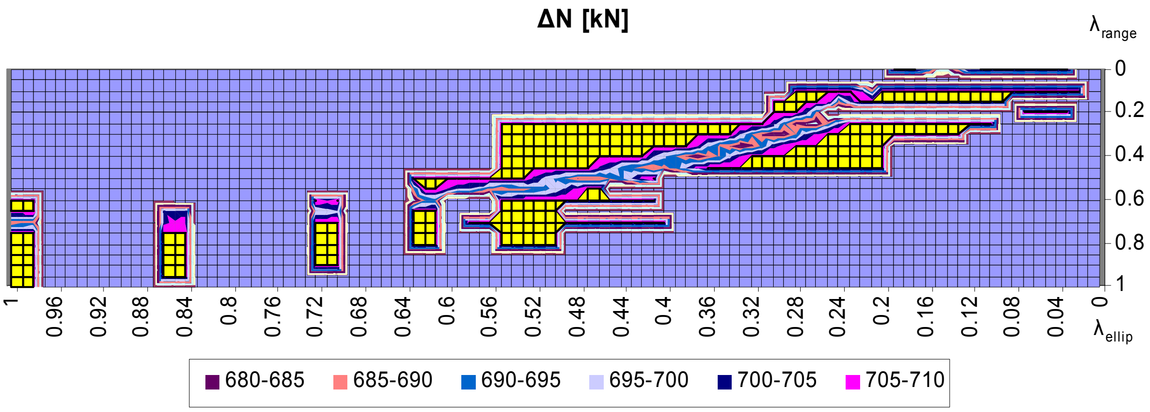

Fig. 6.5. Results for the maximum variation of axial forces of all hangers

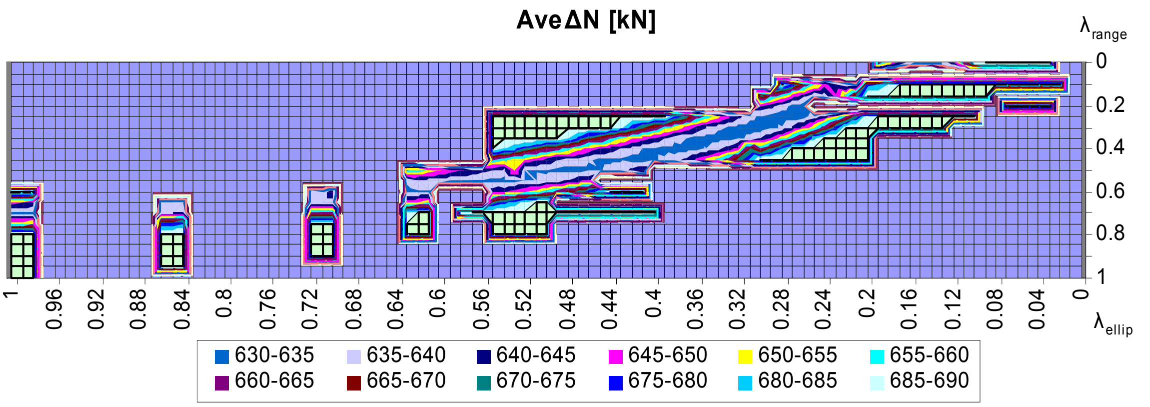

Fig. 6.6. Results for the average variation of axial forces of all hangers

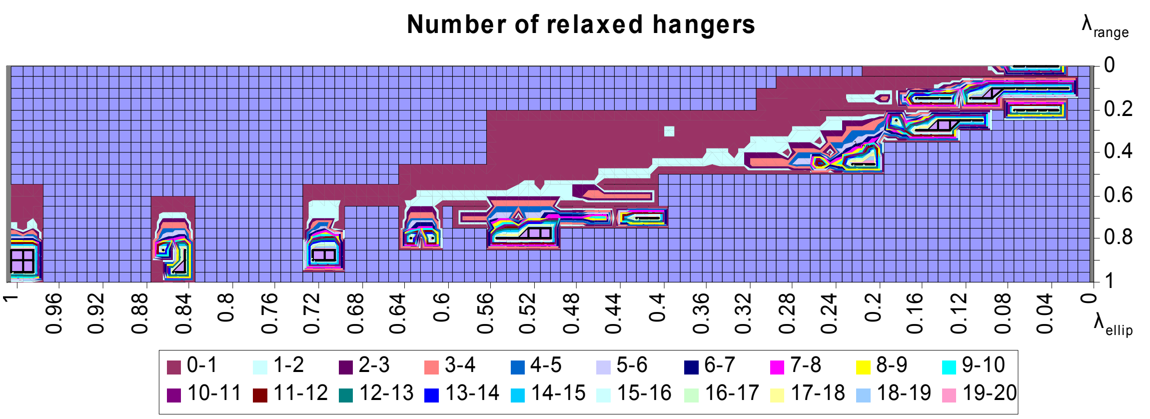

Fig. 6.7. Number of relaxed hangers

If we look at figures 6.3 to 6.7, the results appear to be very sensitive in respect of small variations in the parameters λ_{ellip} and λ_{range}. Minimum values of all considered forces accumulate along a curve, which ends in the vicinity of λ_{ellip} = 0.2 and λ_{range} = 0.2. Towards either side next to this curve, values increase significantly, which represents the high sensitivity of the system. In other words, the grid chosen for investigation is too coarse to make it possible to read sensible results from the diagrams. However, the coarse diagram is sufficient enough to give reasonable evidence about the existence of curves on which minima are found for each attribute of the optimisation. They will be called 'curves of minima'.

The curves of minima of each data series lie close together and the envelope will be called 'valley of minima'. Taking two different parameter combinations of λ_{ellip} and λ_{range} from the curve of minima of **maxN** and plotting the respective hanger arrangement shows their similarity (figures 6.8, 6.9). These two hanger arrangements are virtually equal. Consequently, they result in virtually equal values of **maxN**, which can be seen in the diagram again.

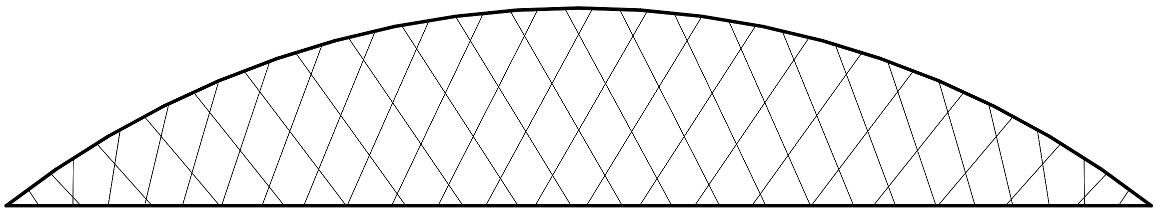

Fig. 6.8. Hanger arrangement with parameters λ_{ellip} = 0.54 and λ_{range} = 0.65, span: 100m, arch rise 17 m, number of hangers per arch plane: 44

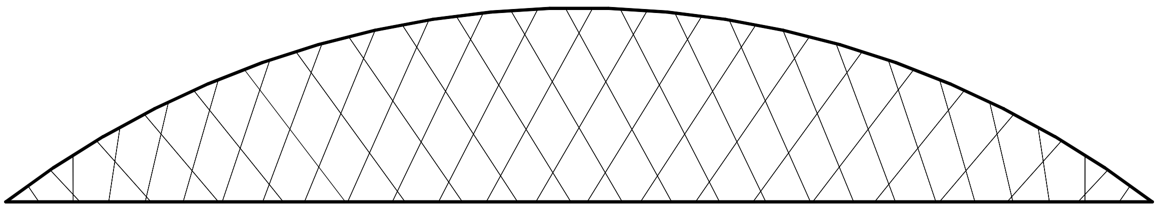

Fig. 6.9. Hanger arrangement with parameters λ_{ellip} = 0.84 and λ_{range} = 0.75, span: 100m, arch rise 17 m, number of hangers per arch plane: 44

However, a slight variation still exists along the ‘curves of minima’. The results increase towards the upper right corner in Figure 6.10. Except for that range, one and the same minimum value can be assumed to lie everywhere on each respective curve.

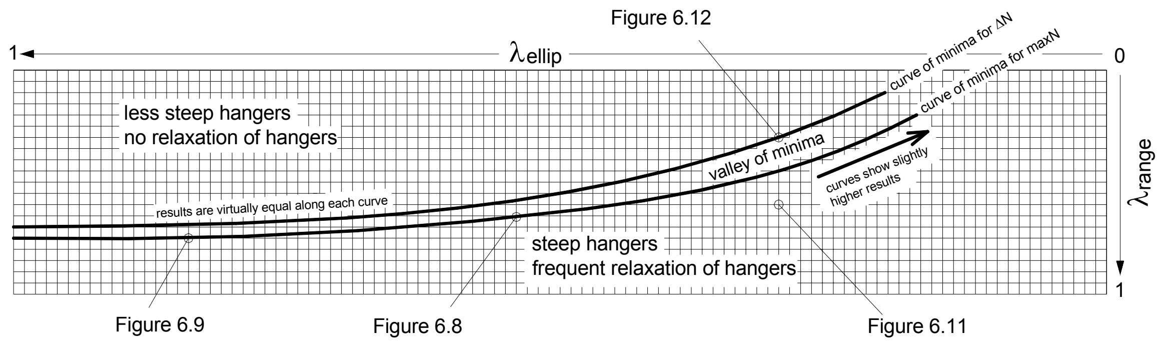

Fig. 6.10. Minimum curves within the data range

The arrangement in Figure 6.11 is taken from the curve of minima of **ΔN**. Again, as with **maxN**, all parameter combinations lying on that curve result in virtually one and the same arrangement.

When looking at Figure 6.10, below the ‘valley of minima’, parameter combinations lead to arrangements with fewer hanger crossings and steeper hangers. Further up in the diagram, hangers become less steep, which leads to more hanger crossings. That means hanger arrangements resulting from the curve of minima of **maxN** show steeper hangers than in the case of **ΔN**. Also, hanger relaxation appears not to happen above, but below the ‘valley of minima’, which can also be found in TVEIT *[45]*, page 27: ‘Too steep hangers lead to too much relaxation of hangers’.

Figure 6.11 shows an example of an arrangement resulting in many relaxed hangers and Figure 6.12 a hanger arrangement giving minimal stress ranges.

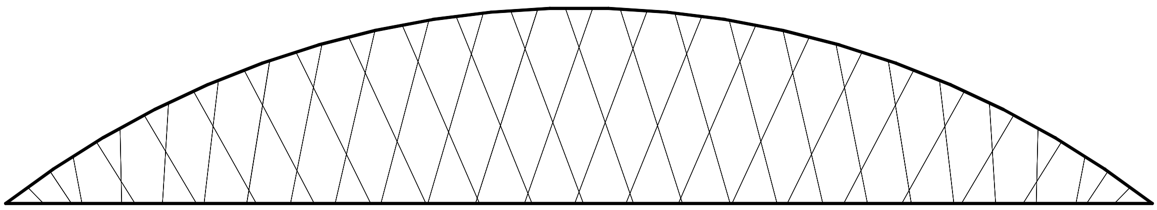

Fig. 6.11. Hanger arrangement with parameters λ_{ellip} = 0.3 and λ_{range} = 0.6, span: 100m, arch rise 17 m, number of hangers per arch plane: 44

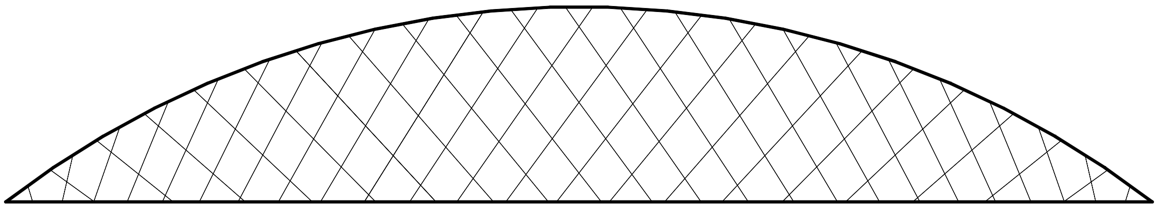

Fig. 6.12. Hanger arrangement with parameters λ_{ellip} = 0.3 and λ_{range} = 0.3, span: 100m, arch rise 17 m, number of hangers per arch plane: 44

Since there seems to be a certain dependence between the parameters λ_{ellip} and λ_{range} and the 'valley of minima' exists, it is sensible to make further investigations along a fixed parameter λ_{ellip}, hence along a section through the 'valley of minima'. This is necessary due to the coarse grid used so far. Obviously the two 'curves of minima' shown in Figure 6.10 represent improvements of the respective goals, but for final conclusions refinement is needed. The fixed parameter for further investigation will be λ_{ellip} = 0.5.

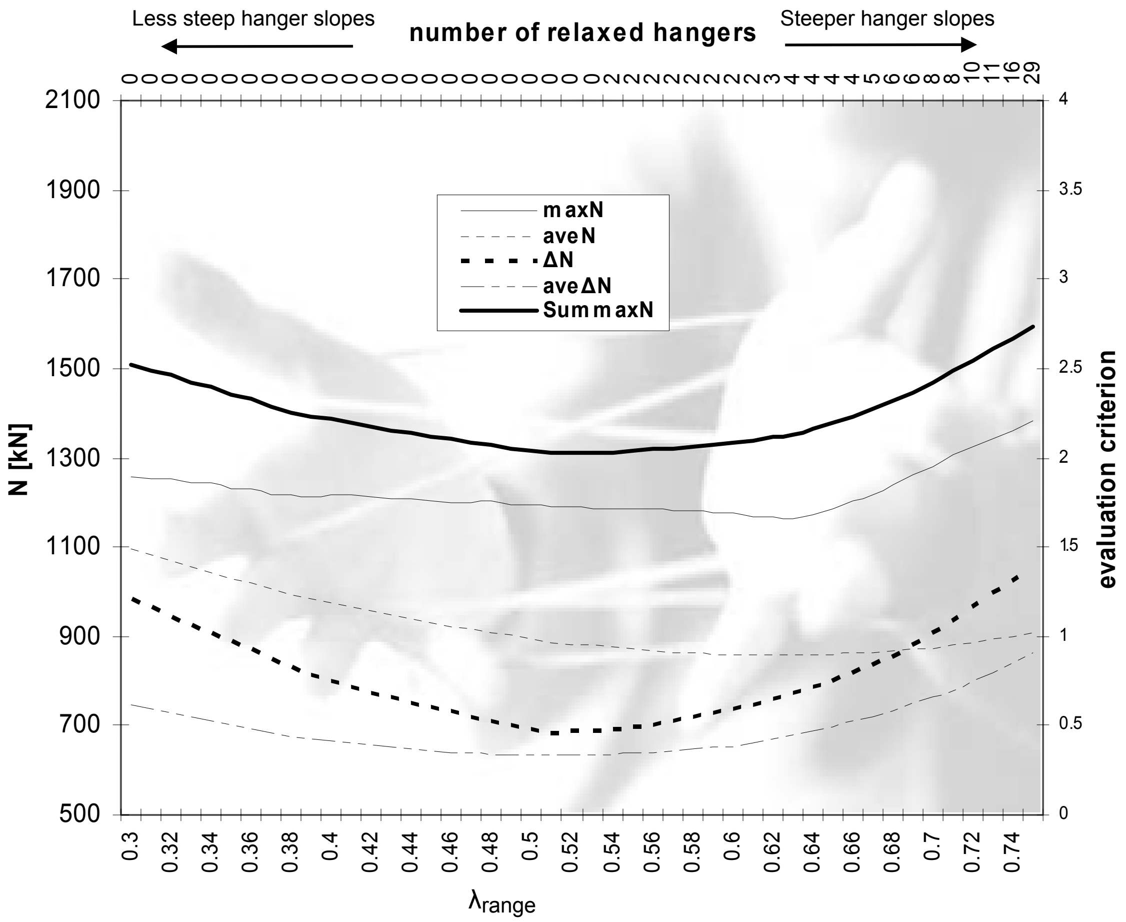

Fig. 6.13. Results of a refined variation of parameter λ_{range}, while λ_{ellip} = 0.5

Figure 6.13 shows that the minima of **maxN** and **ΔN** do not coincide, as already seen in Figure 6.10. Note the fact that hanger relaxation occurs very close to the minima of **ΔN**. For **maxN**, hanger relaxation even happens at the minimum. However, results with hanger relaxation have to be looked at critically, as the computing of influence lines is carried out in linear fashion where actual relaxed hangers take compression. This causes falsified internal forces for other structural elements. Since influence on the tendency of the curve shape is slight and otherwise the majority of the bridges calculated show none or only a few relaxed hangers, it is nevertheless assumed that the results are comparable.

The global minimum of the maximum hanger forces found in Figure 6.13 is at 1162 kN, whereas the global minimum of the maximum variation of the axial hanger force is found to be 685 kN.

SummaxN was calculated as described in Section 6.4 to make conclusions about an improvement satisfying both goals, the minima of **maxN** and **ΔN**. The minimum of the obtained data series can be taken from Figure 6.13. Having chosen the refined investigation along λ_{ellip} = 0.5, the best hanger arrangement is found at λ_{range} = 0.51.

The respective forces are as follows:

Maximum axial hanger force:	**maxN** = 1189 kN
Maximum variation of axial hanger force:	**ΔN** = 685 kN
	(at the end of Section 6.6.3 the best results of all examined descriptions of hanger arrangements are listed)

Remarkable is the fact that the hanger arrangement giving the minimum value for **maxN** also gives the minimum of the **SummaxN**. This indicates that deviation from the best hanger arrangement increases stress ranges more than maximal hanger forces.

The investigation shows that less steep hangers cause smaller stress ranges. Therefore less steep hangers are preferable in respect of fatigue design checks. On the other hand, the hangers must be steeper if smaller maximum hanger forces are desired.

In figures 6.8, 6.9, 6.11 and 6.12 the first and the last hangers do not fit in a regular pattern. It needs to be mentioned that their geometry is not a mistake, but also the result of the mathematical model providing node coordinates along the lower chord.

6.5.2. Variation of the lower hanger nodes by the slope of the hangers

This hanger arrangement is based on equidistant nodes along the arch from which the hangers slope down with a certain inclination until they reach the tie. It was derived from the diagrams in TVEIT *[45]*, page 27, dealing with the connection between slope of hangers and relaxation of the first hanger. Furthermore, in TVEIT *[42]*, page 6, a network arch is presented which is characterised by a constant angle change between two adjacent hangers.

The variables describing the arrangement are the start angle and the change of the inclination from one hanger to the next.

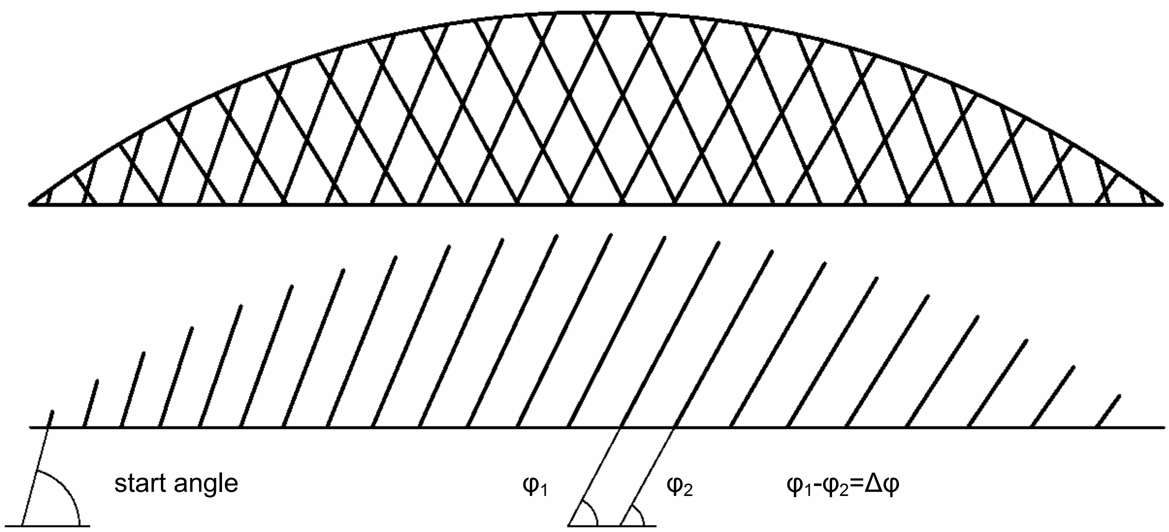

Fig. 6.14. Definition of start angle and angle change

The angle change, $\Delta\varphi$, can be described by any mathematical function. For simplicity the linear function $\Delta\varphi(x) = a \cdot x+b$ was chosen, where x is the number of the hanger; a and b are parameters varying the hanger arrangement. This turned out to be sufficient and sufficiently extensive to vary mainly the constant part of the angle change to achieve an improvement for this kind of hanger arrangement description.

To gain an insight into the behaviour of forces with this hanger arrangement, 400 different bridges were calculated. With this algebraic description it is possible to obtain extreme hanger arrangements. Thus, only start angles and angle changes that give reasonable geometries were investigated (start angles from 50° to 84° and constant angle change from -0.3° to 3.5°).

Results of the analysis

The results are shown in the diagrams of figures 6.15, 6.17, 6.19, 6.21, 6.22 and 6.23. The ordinate visualizes one value for each bridge.

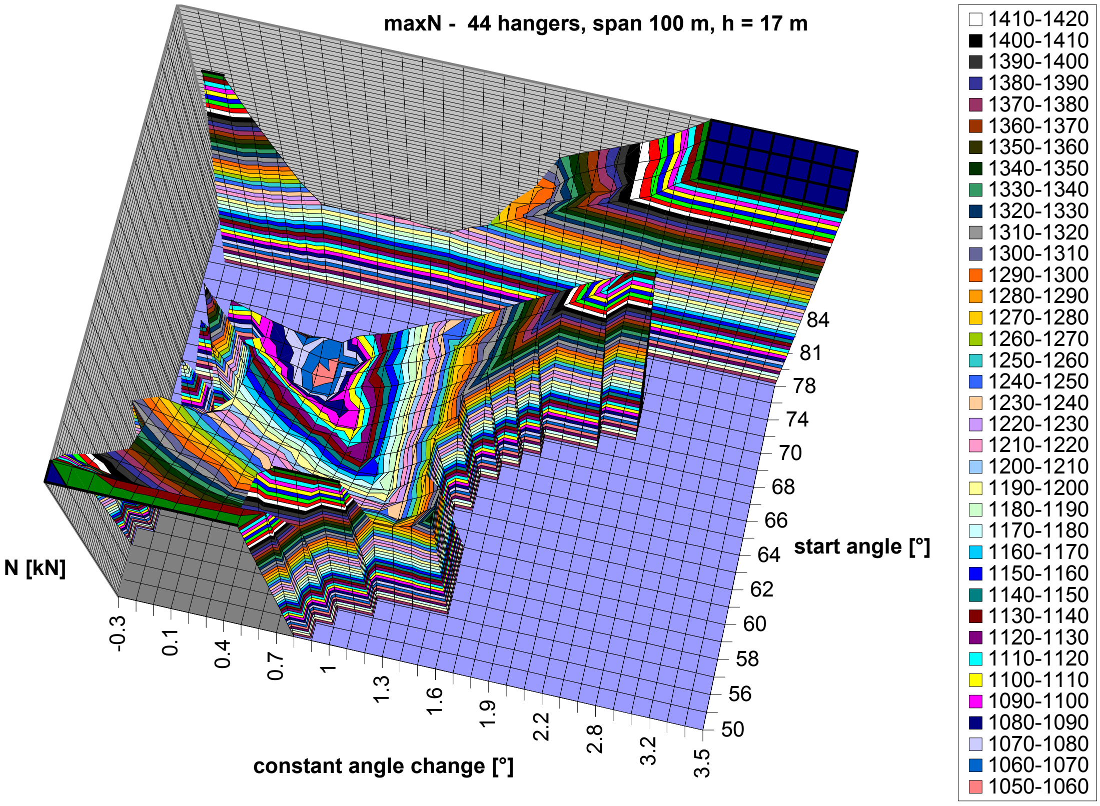

Fig. 6.15. Results for **maxN**

Figure 6.15 shows the maximal hanger force occurring in each of the 400 bridges. They have their minimum at a start angle of about 68° and a constant angle change of 0.6°. The minimum value is 1055 kN. Assuming an equal cross section for every hanger, this would be the force the hangers are designed for.

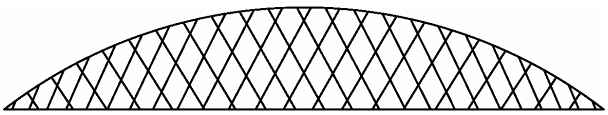

Fig. 6.16. Hanger arrangement with a start angle of 68° and constant angle change of 0.6°

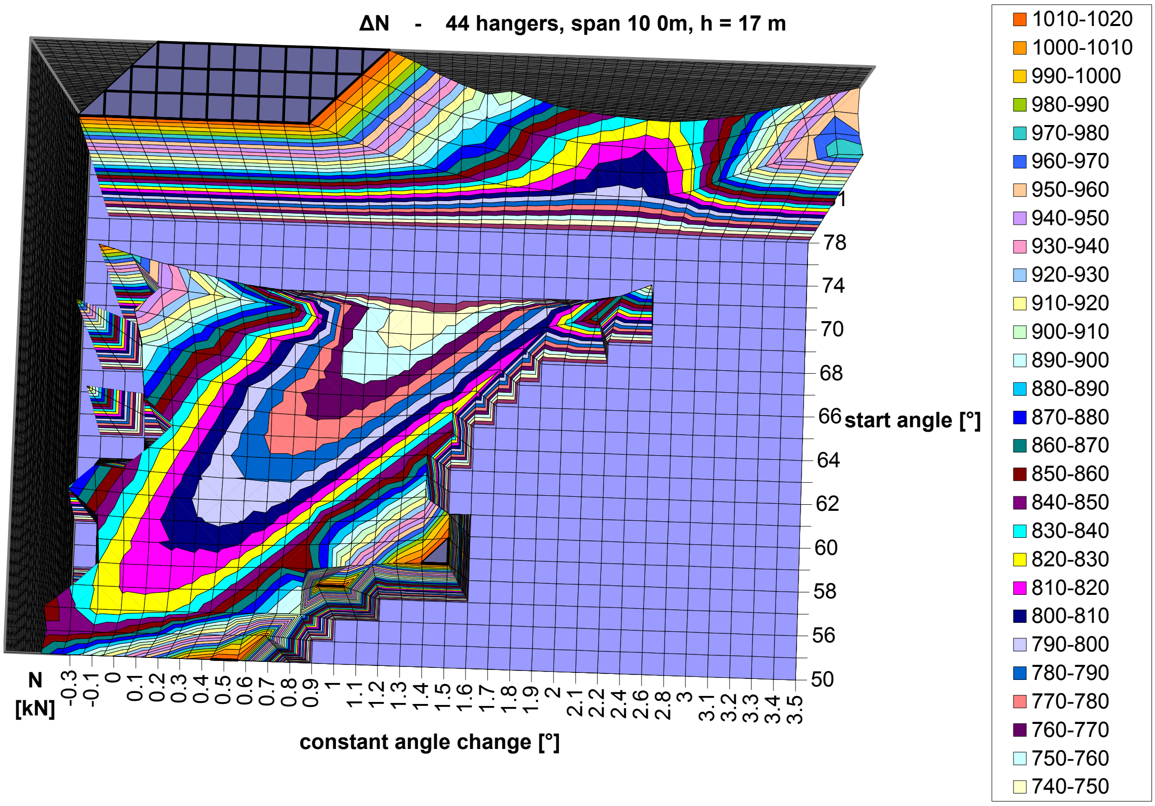

Fig. 6.17. Results for **ΔN**

Figure 6.17 shows the maximal difference between the maximal and the corresponding minimal hanger force. Assuming equal cross - sections for all hangers, this value indicates the stress range for fatigue checks. The minimum is 741 kN at a start angle of 70° and a constant angle change of 1.4°.

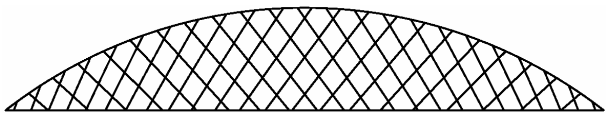

Fig. 6.18. Hanger arrangement with a start angle of 70° and a constant angle change of 1.4°

In order to draw conclusions about an improvement, the claims of the maximal forces and the maximal force variation will be combined. To achieve this, **SummaxN** was calculated according to Section 6.4 and shown in Figure 6.19.

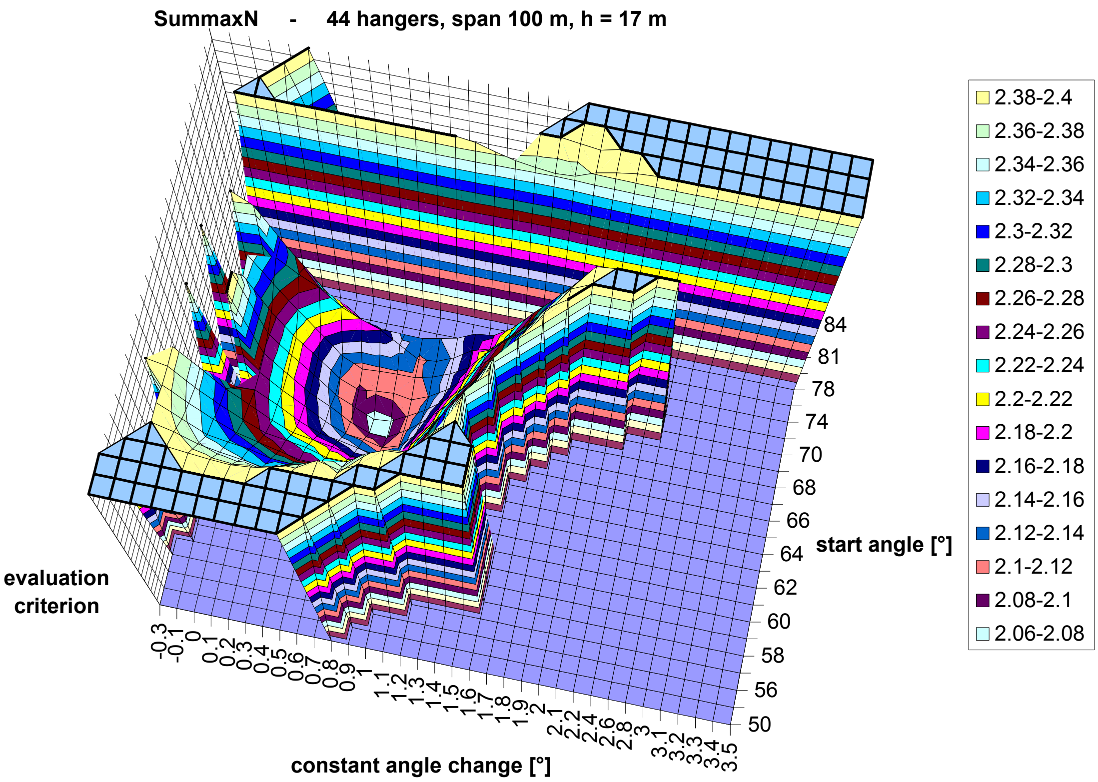

Fig. 6.19. Results for **SummaxN**

Here a new minimum is formed at a start angle of 66° and a constant angle change of 0.9°. The maximal hanger force is 1099.1 kN and the maximal force difference is 765.1 kN.

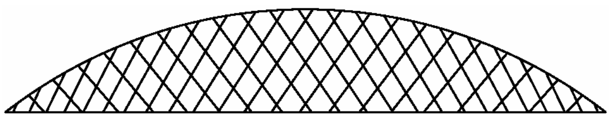

Fig. 6.20. Hanger arrangement with a start angle of 66° and a constant angle change of 0.9°

When we analyse the results from the calculation, it is seen that several hanger forces, especially of the hangers at the ends of the bridge, seriously deviate from the rest due to a disturbance range caused by the clamping of the arch to the tie. It is believed that these mavericks can be adapted at a later point of the improvement process. So it is regarded as more meaningful to look at the average values. Explanations for how to adapt the hanger arrangements to improve the hanger forces near the ends of the arch are given in Section 6.7.5.

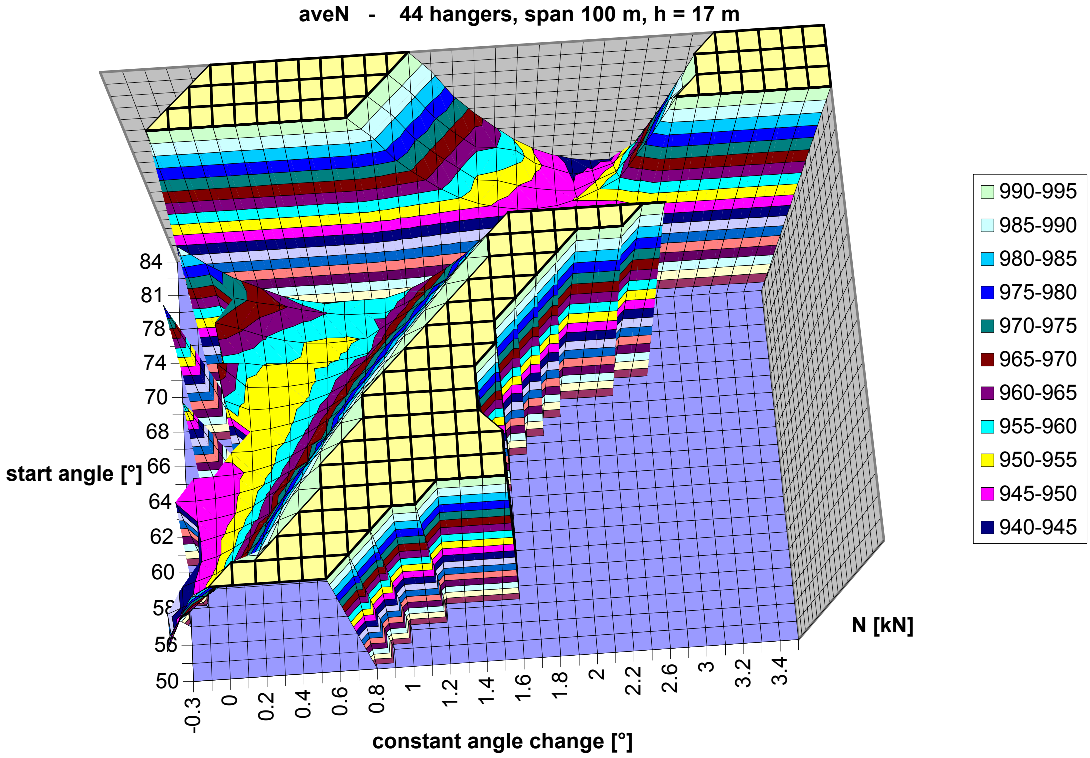

Fig. 6.21. Results for **aveN**

Figure 6.21 shows the average of all maximum hanger forces of each bridge. It is now apparent that, on average, the minimum is not found at one concentrated point, but rather in an expanded concave area with further decline at the end of the area examined.

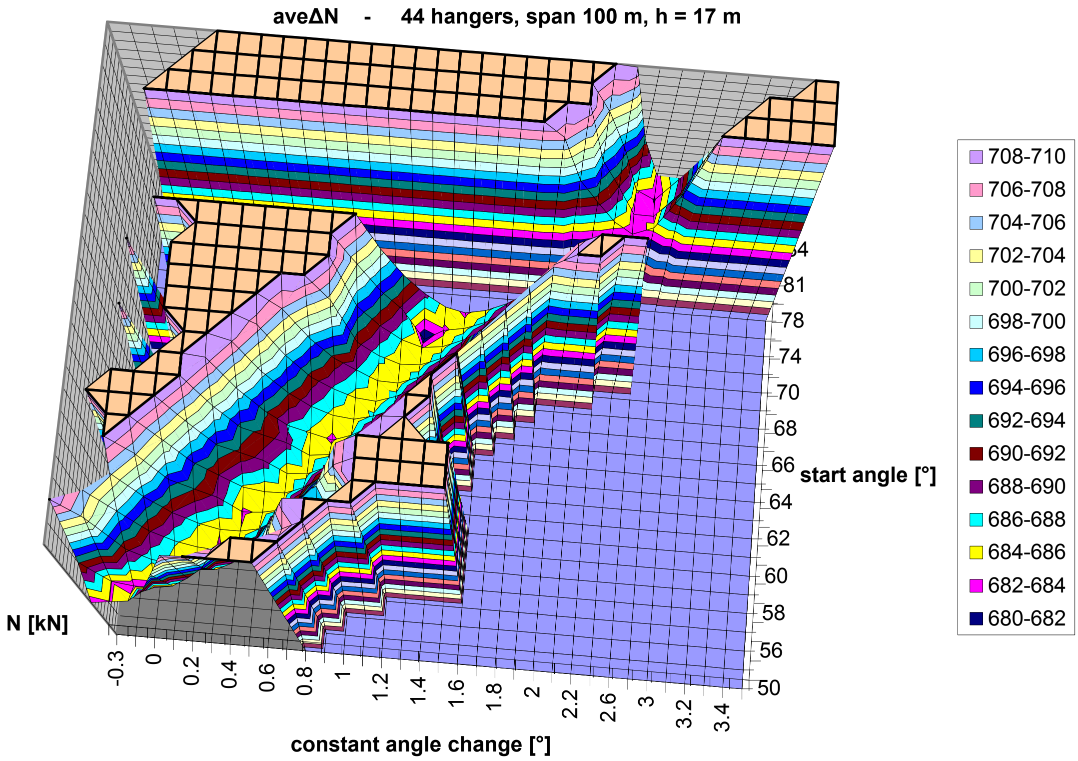

Fig. 6.22. Results for **aveΔN**

By considering the average difference between the maximal and the corresponding minimal hanger force we arrive at a similar expanded range of minimal values as in Figure 6.22. A slight decline at the ends of the diagram can also be reported.

Again, to combine the demands of the design check for maximal stresses and the fatigue check, **SumaveN** was calculated and shown in Figure 6.23.

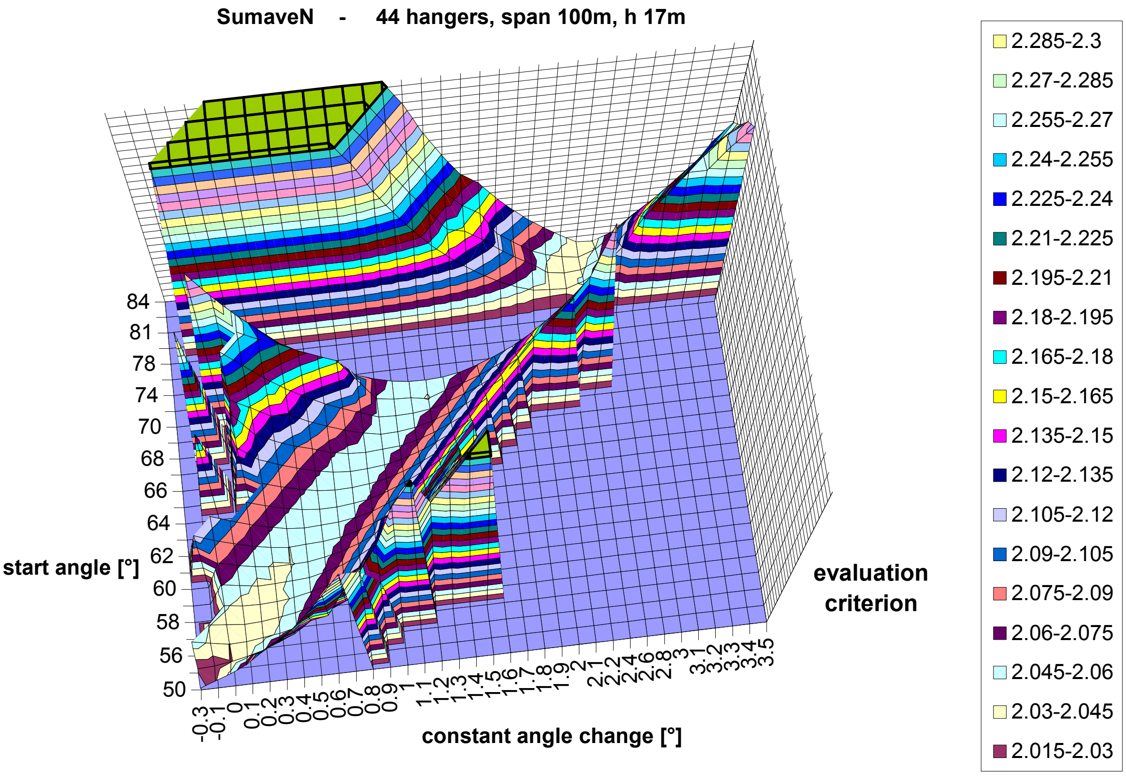

Fig. 6.23. Results for **SumaveN**

This diagram is found to be the most meaningful and shows that within the examined type of hanger arrangements a wide range of geometries exists, that cause similar minimal forces and force changes in the hangers. The minimum is found at a start angle of 50° and a constant angle change of -0.3°.

The results for this hanger arrangement are:

aveN: 937 kN
aveΔN: 682 kN

Optimal arrangement considering the hanger forces only

The decline at the ends of the concave minimum area in Figure 6.23 encouraged further examination of hanger arrangements that are not similar to the common ones. It was figured out that the best hanger arrangement considering minimal hanger forces and low change in hanger forces due to live load is the one shown in Figure 6.24.

The results for this arrangement are: **aveN**: 577 kN
aveΔN: 220 kN
(at the end of Section 6.6.3 the best results of all examined descriptions of hanger arrangements are listed)

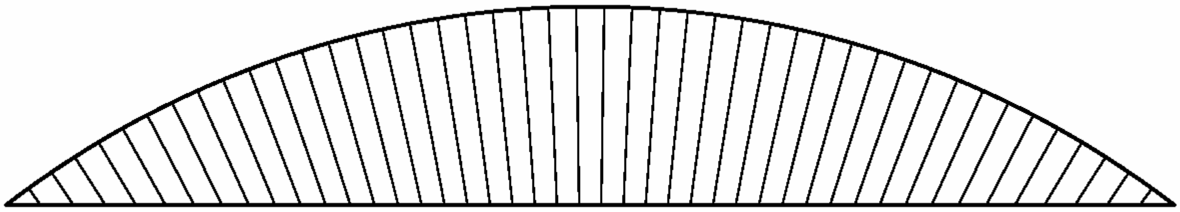

Fig. 6.24. Spoked wheel, span 100 m, rise of the arch 17 m, number of hangers: 44

The hangers are placed along the radii of the arch circle and spaced equidistantly along the arch. By chance the authors became aware that PHILIPPE VAN BOGAERT, Ghent University, had already built a tramway bridge and a high-speed railway bridge with this type of hanger arrangement but with fewer hangers. Furthermore, in January 2002 the Spanish architect and bridge designer SANTIAGO CALATRAVA was contracted by the City Council of Dallas, Texas for the Trinity River Corridor Project. Among several bridges that are going to be built there are two arch bridges planned with radial hangers *[40]*. There was another arch bridge built with radial hangers in Hannover, Germany *[35]*. It spans 58 meters and uses 7 hangers per arch plane.

Regrettably, the structural behaviour of such an arch bridge is similar to that of arch bridges with vertical hangers. These hangers lead to large bending moments about the horizontal axis in the arch and the tie. Thus, the bending moments in the arch and the tie will also be involved as attributes in the improvement process continued in Section 6.6.

6.6. Advanced model to describe the hanger arrangement

In this Section the hanger arrangement believed to be best is presented.

6.6.1 The idea

Bending in the arch about the horizontal axis is minimised if the line of thrust deviates very little from the centreline of the arch TVEIT *[43]*, page 2190. This can be achieved if uniformly distributed loads act ideally in the radial direction on the arch, as it is known from the structural behaviour of circular arches. The authors suggest imagining the resulting force of the hanger forces directed along the connecting line of their intersections (Figure 6.25). This would be true if all hangers had the same axial force. However, the axial forces are not the same, as they change due to moving live loads. Nevertheless, as a good approximation the authors adhere to their suggestion.

Then it is self-evident that the resulting forces should be aimed radially towards the arch to decrease its bending moments. This also leads to small hanger forces (see Section 6.6.2). One example of the suggested hanger arrangement is shown in Figure 6.25.

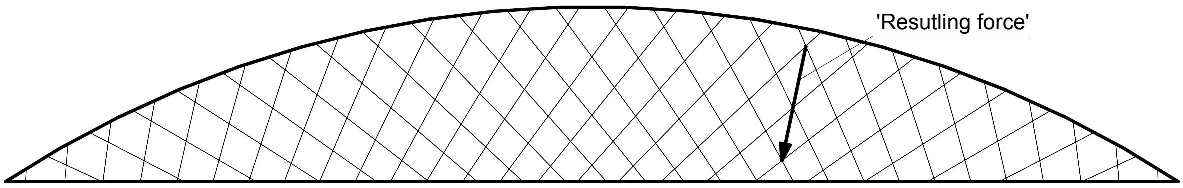

Fig. 6.25. Schematic illustration of the suggested hanger arrangement

Many publications about optimisation of structures indicate that the claim is true. The authors would like to give some examples.

The Australian mathematician JOHN HENRY MICHELL introduced a method for the optimisation of structures. He proposed to align structural members with the principal stress trajectories. He considered the resistance of the members to tension and compression as equal. This optimisation is only applicable to one load case. Despite these restrictions, the *Michell structures* are still used to evaluate optimisation software (SCHWARZ *[31]*, page 2). Two of them are shown in Figure 6.26. Similarities to the geometry proposed in Figure 6.25 cannot be denied.

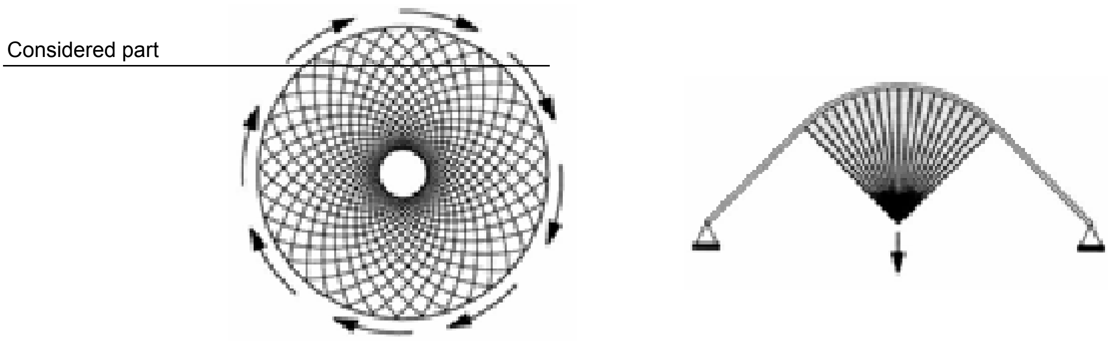

Fig. 6.26. Two *Michell structures*, found in BECKER *[5]*, page 7

An optimal network of cables for bearing loads underneath a parabolic arch is proposed in MCCULLOUGH *[21]*. It is shown in (c) of Figure 6.27. It can be seen that the cables connected to the arch are oriented vertically. Almost all intersections of the cables lie on the centrelines of these vertical cables. For a parabolic arch the thrust line is along the centreline of the arch if the loads are ideally vertical, as achieved in (c) of Figure 6.27. If transferred to a circular arch assuming that the line of thrust still coincides with the centreline of the arch, a network would be obtained that is similar to the one in Figure 6.25.

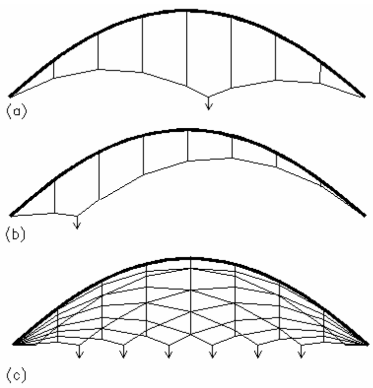

Fig. 6.27. An optimal load bearing network of cables underneath a parabolic arch, McCullough *[21]*

A network arch is considered to have a structural behaviour similar to a truss. In turn, optimised trusses can be examined to gain knowledge about network arches. In the demonstrations of the optimisation software *FrameGA [28]* several trusses with a circular upper chord can be found. Two of them are shown in Figure 6.28

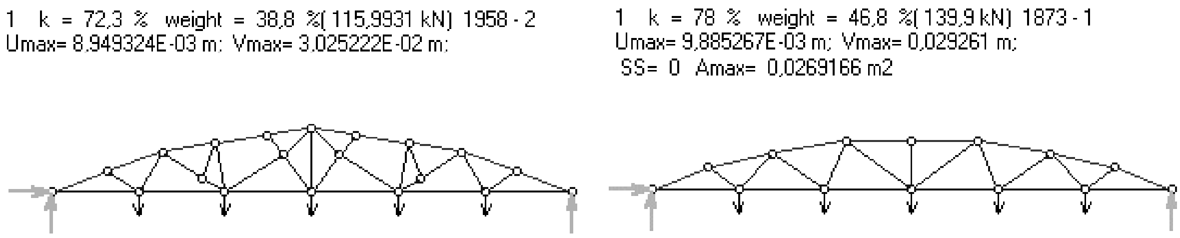

Fig. 6.28. Two optimised trusses with circular upper chord, found on the Internet *[28]*

For the optimisation a maximal cross-sectional area of the truss members was given. Both trusses are optima for the loads and constraints indicated in the picture. It can be seen that the diagonal truss members tend to connect the lower and upper chord with radial resulting forces.

The truss bridge in Figure 6.29 was found with graphical methods (ZALEWSKI ET AL. *[51]*). The loads B-G are equal. The axial force in the arch is constant along the span. The tension forces of the interior members are found to differ only slightly, as do the forces within the lower chord. If three fixed member sizes are standardized, one each for the top chord, the interior members, and lower chord, all the material in the truss is working at or near capacity. Thus, this is a very efficient form for a truss. Again, this confirms the suggestion to improve the network arch by applying the loads to the arch as near as possible in a radial direction.

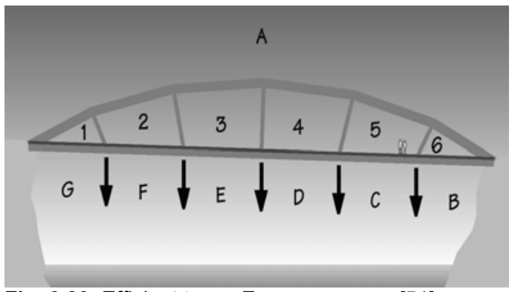

Fig. 6.29. Efficient truss, ZALEWSKI ET AL. *[51]*

An example of an already built bridge where diagonal members are radial to the circular arch is shown in Figure 6.30.

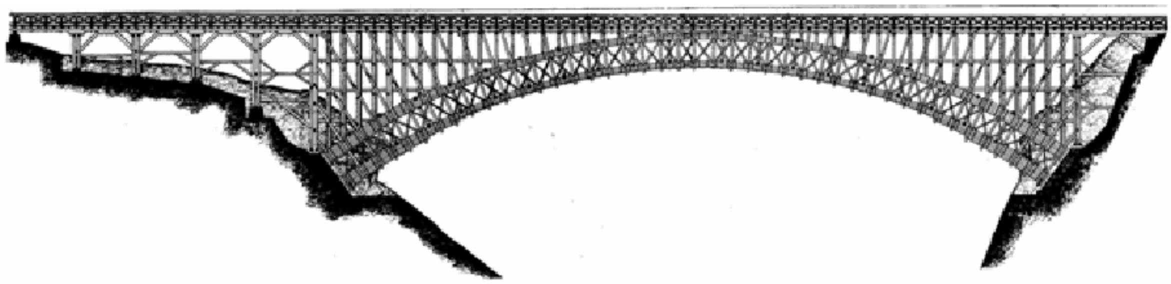

Fig. 6.30. Cascade bridge of the Erie Railway, USA around 1845, PETRASCHKA *[25]*

With all these examples of optimal or near optimal structures and the similarities with the authors' proposal, it should be worth applying the idea to the hanger arrangement of network arches and examining the changes, even though this idea has never been mentioned before in the sources about network arches known to the authors. In Section 6.6.2 the authors present their ideas, why their proposal should lead to improved results.

6.6.2 Derivation of the proposed hanger arrangement

With the help of the following figures it will be pointed out why the introduced hanger arrangement causes small bending moments in the arch and small hanger forces. For the derivation symmetrical loading and a simply supported arch are assumed.

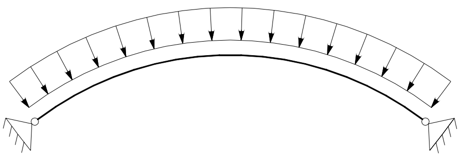

Figure 6.31.

For circular arches a uniformly distributed load that is directed along the radii of the arch circle causes no bending moments in the arch.

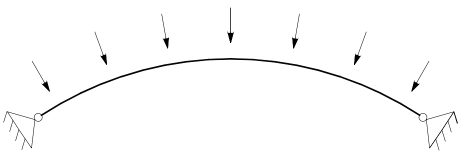

Figure 6.32.

The hangers transfer forces at their nodal points to the arch. Therefore, the uniformly distributed load is substituted by single loads. They have to be equidistant and their direction has to stay radial. With an infinite number of single loads the line of thrust follows the centre line of the arch.

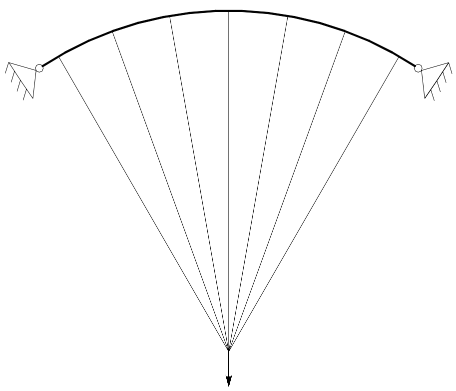

Figure 6.33.

In arch bridges with the lane under the arch the loads do not act on top of the arch but underneath. Vertical loads can be transferred to the arch in a radial direction by using radial hangers, Figure 6.33. The hanger forces are all of the same size because of the constant curvature and the equidistant hanger nodes. This is proven in Figure 6.34.

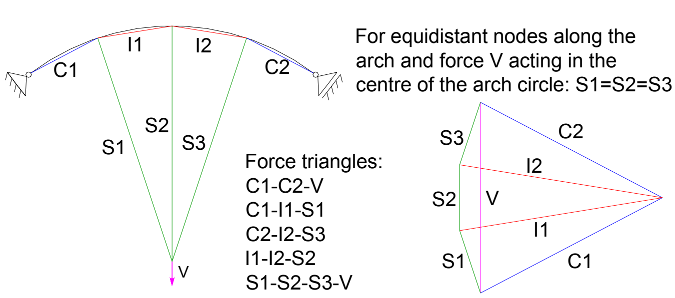

Figure 6.34.

The same structure as in Figure 6.33 with fewer hangers is subjected to a vertical load in the centre of the arch circle. The force transfer between the upper hanger nodes is straight. The hanger forces are equal. It is easy to imagine that this is true for a larger number of hangers as well.

This hanger arrangement represents the same loading as the single loads obtained by discretisation of the uniformly distributed load into the hanger nodes (Figure 6.32). Thus, with such arrangement of hangers the bending moments of the arch are smallest. With an infinite number of hangers no bending moments would occur at all.

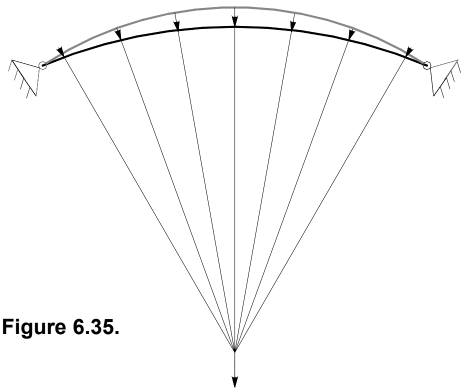

Figure 6.35.

Considering small deformations of such a structure it can be seen that each point of the arch moves almost in a radial direction (Figure 6.35). If the arch receives no bending moments, other deflections are impossible.

Another example where deflections are only possible in one direction is shown in Figure 6.36. The force required to cause deflection is minimal if it acts horizontally, hence along the direction of motion not restricted.

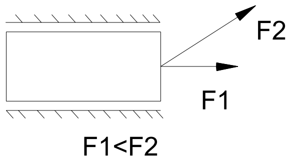

Figure 6.36.

It is obvious then, that smallest hanger forces are achieved if the hangers are directed along the possible deflections of the arch circle. Otherwise their force would be increased due to the diversion between the centreline of the hanger and the direction of deflection. Maybe a slight outwards deviation of the hanger’s direction is favourable.

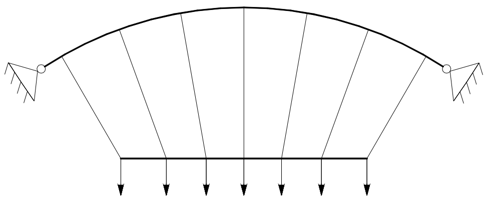

Figure 6.37.

The next step towards an arch bridge is shifting the point of action of the vertical force upwards. The stiff horizontal beam in Figure 6.37 distributes the single load in Figure 6.35 evenly to all hangers. The structural behaviour of the arch is not changed.

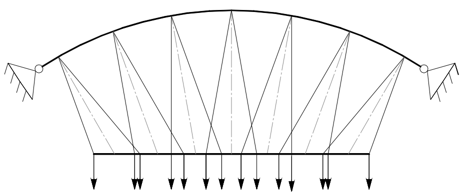

Figure 6.38.

As stated at the end of Section 6.5.2, the structural behaviour of an arch bridge with radial hangers leads to large bending moments in the chords with partial loading. To achieve the benefits of a network arch, in the next step the radial hangers are split into pairs, symmetrically to the radii. This increases the hanger forces, but this increase will be the smallest possible as long as their resulting forces stay along the radii.

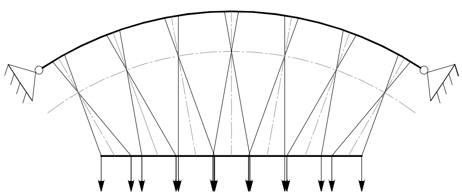

Figure 6.39.

In the following step the hanger crossings are placed below the arch, since two hangers in one node at the arch are not desired. Until now, bending moments in the arch and hanger forces seem the smallest possible for inclined hangers in a circular arch.

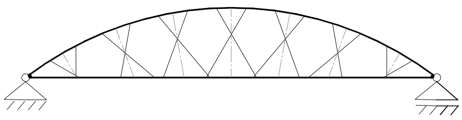

Figure 6.40.

Further towards a network arch bridge it is necessary to introduce changes in the structural system. The constraint conditions of the arch are changed due to a clamping at the lower chord. With this change a radial loading will cause bending moments in the ends of the arch. However, for the main part of the span the structural behaviour will almost be the same as before. A task for future research would be to investigate the direction of loading which causes a line of thrust still following the centreline of the arch. Then the hangers have to be aligned to this direction.

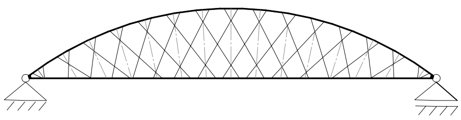

Figure 6.41.

The final design of the network arch is obtained by increasing the number of hangers following the introduced geometry (Figure 6.41). Such hanger arrangement transfers the vertical loads as far as possible in a radial direction, which leads to small bending moments in the arch. Furthermore, the hangers are almost aligned to the deflections of the arch. This results in small hanger forces.

On the basis of this reasoning it has been indicated that this hanger arrangement gives smallest bending moments in the arch and small hanger forces for uniform and symmetrical loading. The load characteristic of railway bridges leads to many different partial loadings. It is hard to say which load case should decide the hanger arrangement.

The load direction at the ends of the arch causing a line of thrust along the arch has to be calculated for every single bridge project again, but applying the radial direction is likely to always give good results for the main part of the span.

The variable in this kind of hanger arrangement is the cross angle between the hangers and the radii. If this angle is about 1° all hangers are radial to the arch circle; for increasing cross angles the structure becomes a network arch. Thus, to obtain improved results for different load cases, this cross angle can be used to vary the arrangement (see Section 6.6.3).

PER TVEIT suggested comparing the authors' kind of hanger arrangement with one of the network arches designed by him. It was decided on the Åkviksound network arch because many influence lines have been calculated for it, JAY *[18]*. The authors applied a radial oriented hanger web to the Åkviksound bridge; all other geometry, cross-sections and materials were retained unchanged. On an average the values of the influence lines of the proposed hanger arrangement were:

98 % (axial force in arch)
79 % (hanger force)
81 % (bending moments in the arch)

of the values of the Åkviksound network arch. Additionally internal forces and deflections were compared for live load on the whole and on 54% of the span. Similar improvements were found there as well.

The comparison can be found in Annex F, figures F.1 to F.10.

6.6.3 Variation of the lower hanger nodes using the advanced model

According to the idea mentioned in 6.6.1 another description for the geometry was used and analysed including the bending moments in the arch about the horizontal axis as a further attribute. As before equidistantly spaced upper hanger nodes were assumed. The hanger intersections lie on radii of the arch circle. The only variable is the angle with which the hangers cross each other. Due to the properties of the new hanger arrangement, corresponding hanger crossings lie on circles concentric to the arch circle. All hanger crossings on one circle have the same cross angle.

For the investigations the variable parameter will be defined as the angle between the hanger and the radius at the first hanger crossing below the arch (see Figure 6.42).

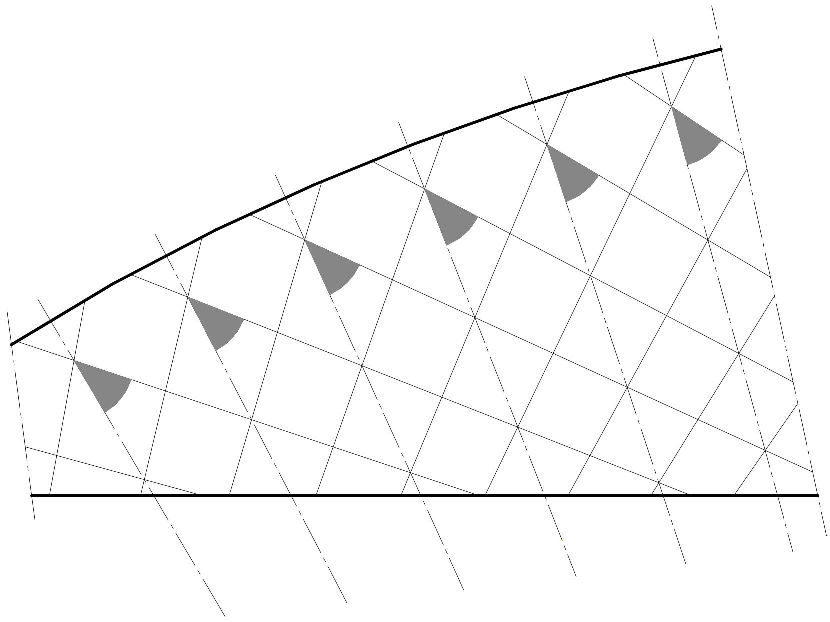

Fig. 6.42. The hangers cross symmetrically the radii with the same angle, the cross angle defined as being the variable is marked grey

To visualize the connection between the cross angle and the hanger arrangement, some examples are shown in Figure 6.43.

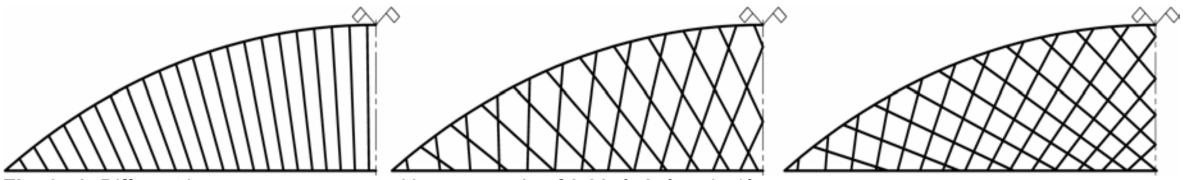

Fig. 6.43. Different hanger arrangement with cross angle of 0.835°, 25° and 41°

The introduced type of hanger arrangement gives reasonable results with cross angles between 0° and 50° for the bridge calculated in this work (span 100 m, rise of arch 17 m, number of hangers 44). 80 different bridges were calculated with angles varying from 0.835° to 50° and a shorter graduation between 38° and 45°, where the best result was believed to be found.

Results of the analysis

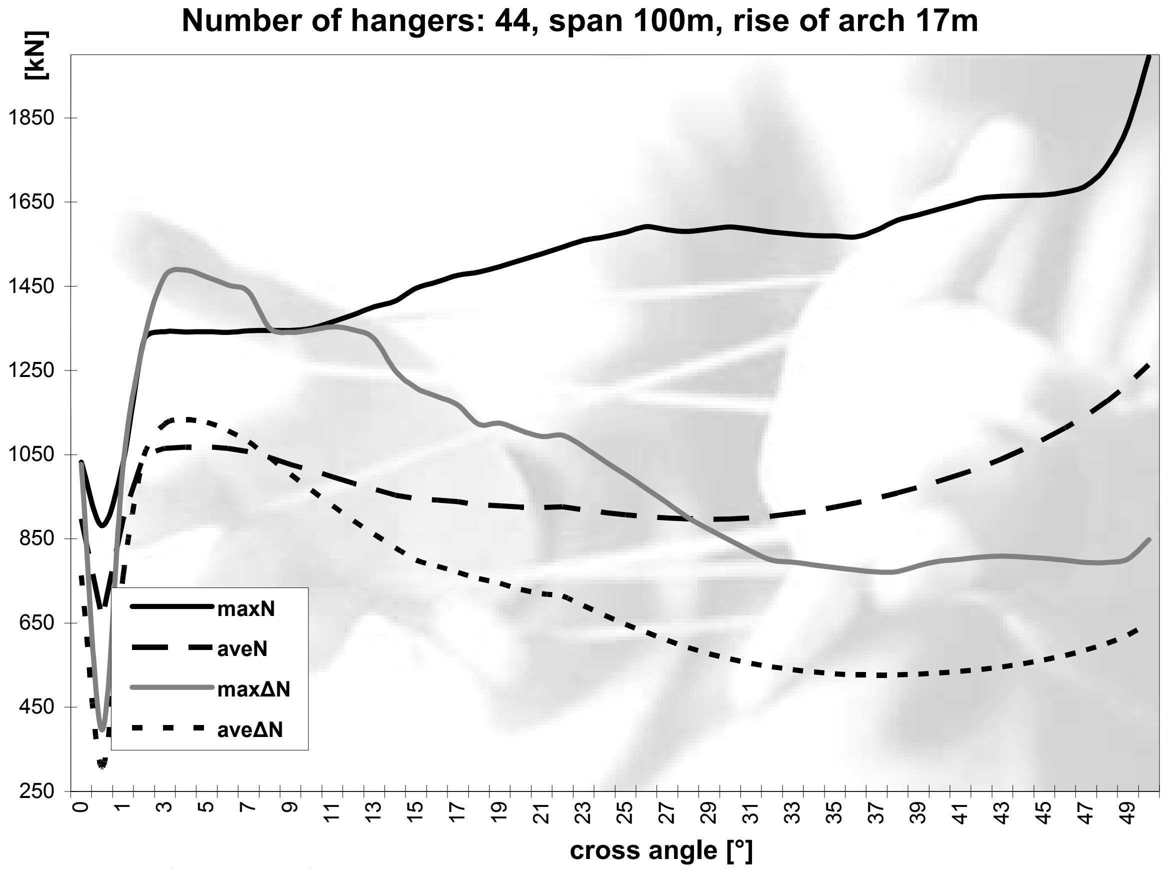

Fig. 6.44. Results for the hanger forces

As it can be seen in Figure 6.44 the global minimum of the hanger forces occurs at a cross angle of 0.8345°. The appendant geometry complies with the spoked wheel shown in Figure 6.24, which also gave best results for the type of arrangement of Section 6.5.2. But there is another local minimum in the range from 30° to 45°. To obtain the value of **SumaveN** in this range, the data series for the average values are scaled with their minimums to 1 and then added with an importance of 1:1, as explained in Section 6.4. The local minimum of **SumaveN** can be found at a cross angle of 35°.

The results are: **aveN**: 925 kN

aveΔN: 529 kN

(at the end of Section 6.6.3 the best results of all examined descriptions of hanger arrangements are listed)

To extend the criteria of the optimisation the bending moments in the arch will be examined now.

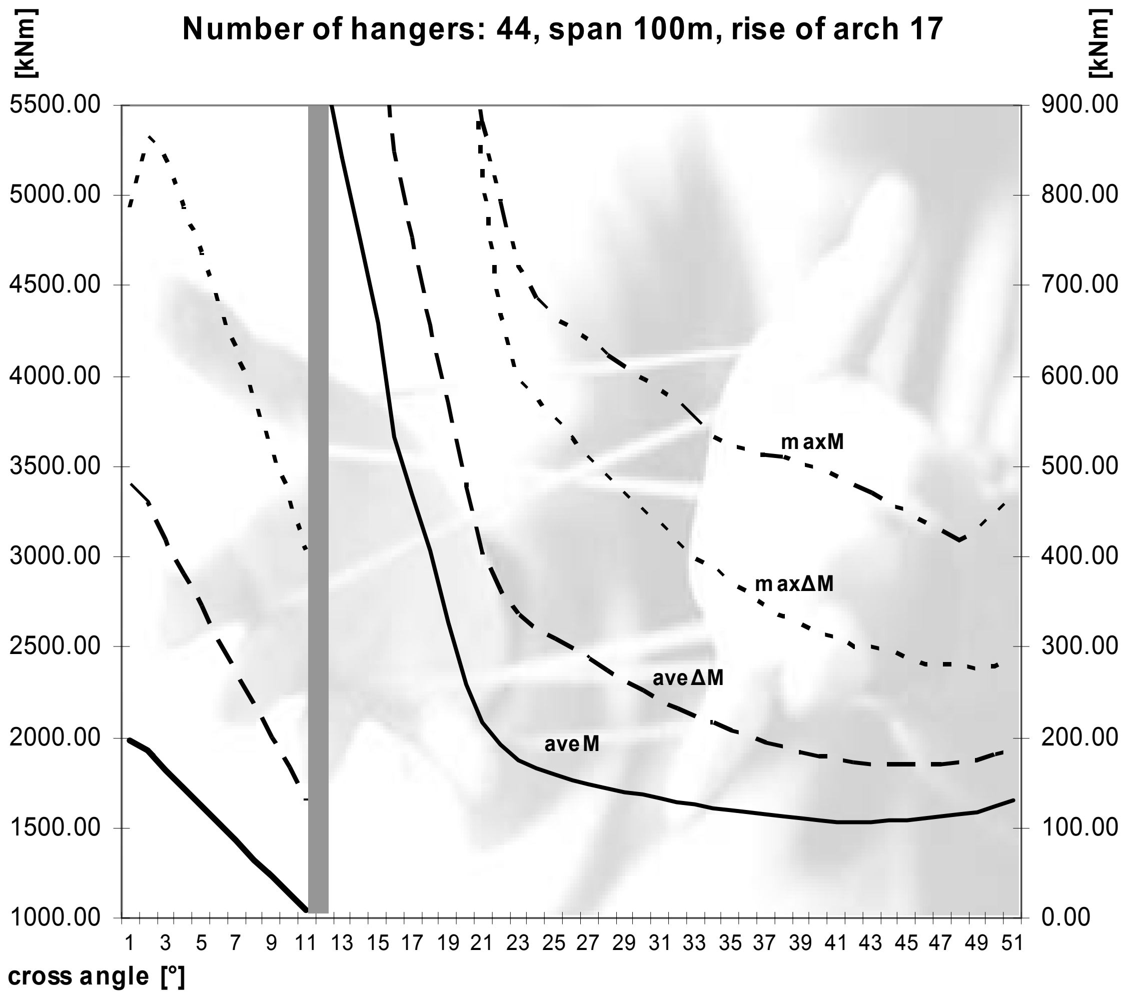

Fig. 6.45. Results for bending moments in the arch about the horizontal axis

As can be seen in Figure 6.45 the bending moments in the arch for small cross angles, which means hanger arrangements similar to vertical hangers are about 4 to 10 times larger than for hanger arrangements in accordance with the theory of network arch bridges (see Section 4). The stiffening effect of inclined crossing hangers deploys its impact at cross angles over approximately 25°. Best results only considering bending moments are achieved with a cross angle of about 48°:

maxM:	428 kNm
maxΔM:	280 kNm

In order to draw conclusions about an improvement satisfying both goals minimum hanger forces and minimum bending moments, the values of **Summax**, **Sumvariation** and **Sumall** were calculated out of the data series as described in Section 6.4. These three data series are shown in Figure 6.46.

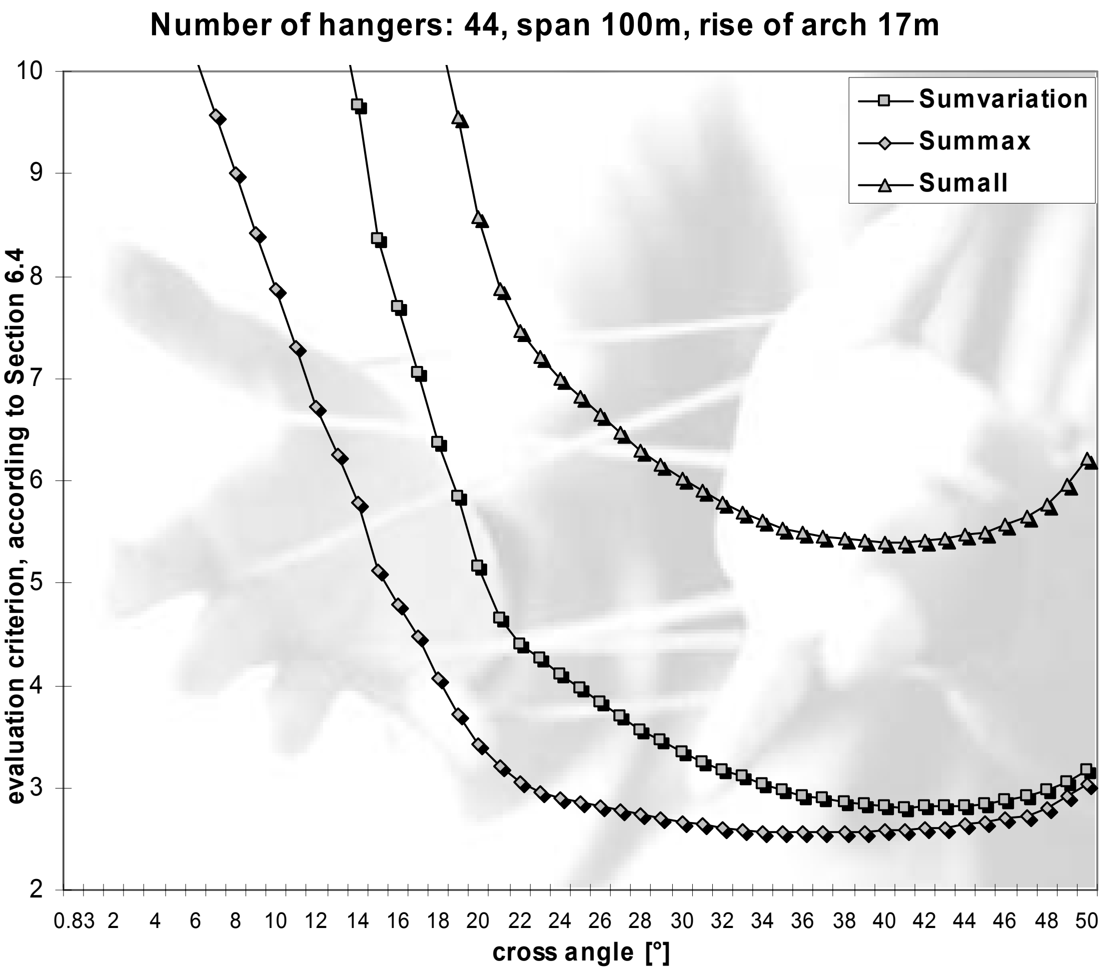

Fig. 6.46. Sums of scaled values, result of improvement process

As can be seen in Figure 6.46 best results considering small maximal forces are found at a cross angle of 35°.

In Figure 6.47 the results of the refined investigation are shown. The best results for minimal stress ranges are found at a cross angle of 41°. The combination with equal weighting for both leads to an improved hanger arrangement at a cross angle of 41°, as well.

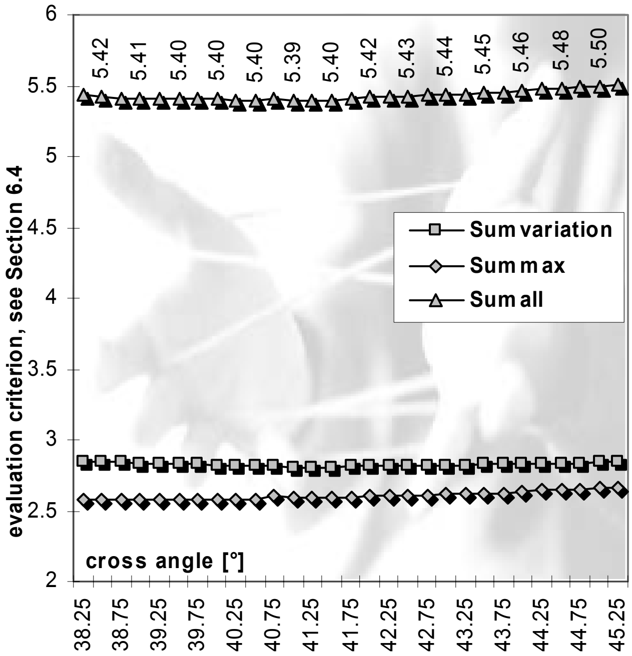

Fig. 6.47. Results of the refined analysis

For the cross angle 41° the results are:

aveN: 986 kN
aveΔN: 531 kN

maxM: 489 kNm
maxΔM: 310 kNm

In Figure 6.48 the best results of the three different hanger arrangements are compared.

	Hanger arrangement from Section:				
	6.5.1 "ellipse"	6.5.2 "slope"	6.6.3 "radial"		
			"spoked wheel"	overall best	minimal hanger force
Average maximum hanger force	885.3 kN	937.3 kN	577 kN	986.5 kN	896.5 kN
Average variation of hanger force	633.05 kN	682.4 kN	220 kN	531.7 kN	576.8 kN
Maximal bending moment	-	-	4900 kNm	489.5 kNm	610 kNm
Max variation of bending moments	-	-	4850 kNm	310.8 kNm	450 kNm

Fig. 6.48. Comparison of the results

As can be seen in Figure 6.48, the biggest advantage of the new type of hanger arrangement is found in a lower stress range. Due to the weighting and the inclusion of the bending moments as criteria, the maximum hanger forces are higher for “overall best” than for “ellipse” and “slope”. Therefore, the values for the hanger arrangement of the “radial” type with the minimal hanger forces are also shown. It is obvious that the introduced hanger arrangement is a noteworthy improvement.

Hanger relaxation

Relaxing hangers is an important topic for network arch bridges. For the kind of hanger arrangement dealt with in Section 6.6, there are no relaxing hangers reported at cross angles larger than 39°. The “spoked wheel” does not lead to hanger relaxation either. Much hanger relaxation occurs at cross angles from 1° to 25°, which additionally enlarges the bending moments in the arch due to the multiplication of the distance between points of supports and the changing of the structural behaviour. The chords in the area of relaxed hangers are only connected to each other by one set of hangers in tension. This part of a bridge functions similarly to a tied arch with one set of hangers. The equilibrium of the bridge in this area is dependent on shear and bending in the chords, and this can lead to large bending moments (TVEIT *[43]*, page 2191).

It should be added here, that the relaxed hangers for cross angles from 35° to 39° occurred at the ends of the span. In Section 6.7.5 it was found that this can be prevented by small changes in their geometry. After accurately recalculating the bridge, the object of this work, there were no relaxed hangers at all. The new type of hanger arrangement was also applied to the network arch calculated in RÄCK *[27]*, using a cross angle of 35°. His calculations did not show relaxed hangers, either.

Erection phases constitute an exception; see Section 8 and Annex E.

6.7 Investigation of other parameters

For all investigations in the following sections the type hanger arrangement found to be best is used.

6.7.1 Influence of the number of hangers and the span

To examine the influence of the number of hangers and the possibilities to transfer the cognitions found with the 100 m span bridge to bridges with different spans, another 80 bridges were calculated varying the span and the number of hangers.

The spans 75 m, 100 m, 150 m and 200 m with the scaled arch rise of 12.75 m, 17 m, 22.5 m and 34 m were chosen. This keeps the ratio of the span to the rise of the arch at 0.17. The number of hangers was also scaled and varied around the achieved value. Additionally different cross angles were applied to see if the results are near the optimum for each span. They were 38°, 39°, 40°, 41° and 42°.

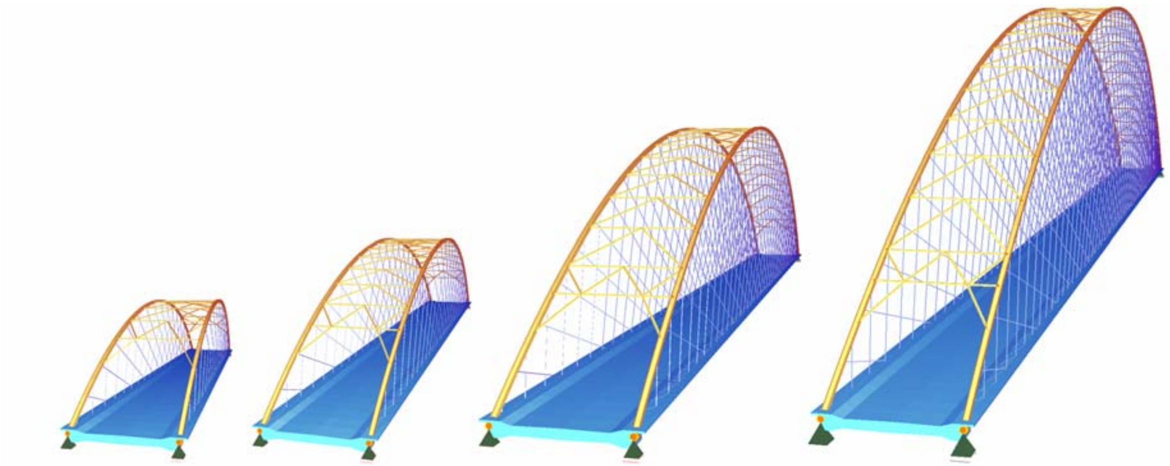

Fig. 6.49. Bridges with spans of 75 m, 100 m, 150 m and 200 m

In reality it would not be so easy to increase the span just by scaling the geometry. Different cross-sections of the structural members would have to be chosen. The problem is a changed stiffness. The increased thickness of the tie hardly influences its stiffness. But the necessary increase of the arch cross-section quickly leads to a multiplied moment of inertia. In later tests the authors found that this significantly influences the choice of the optimal cross angle. Regrettably this was not considered in the investigations. Indicating a tendency, the results of Section 6.7.1 are still considered as meaningful.

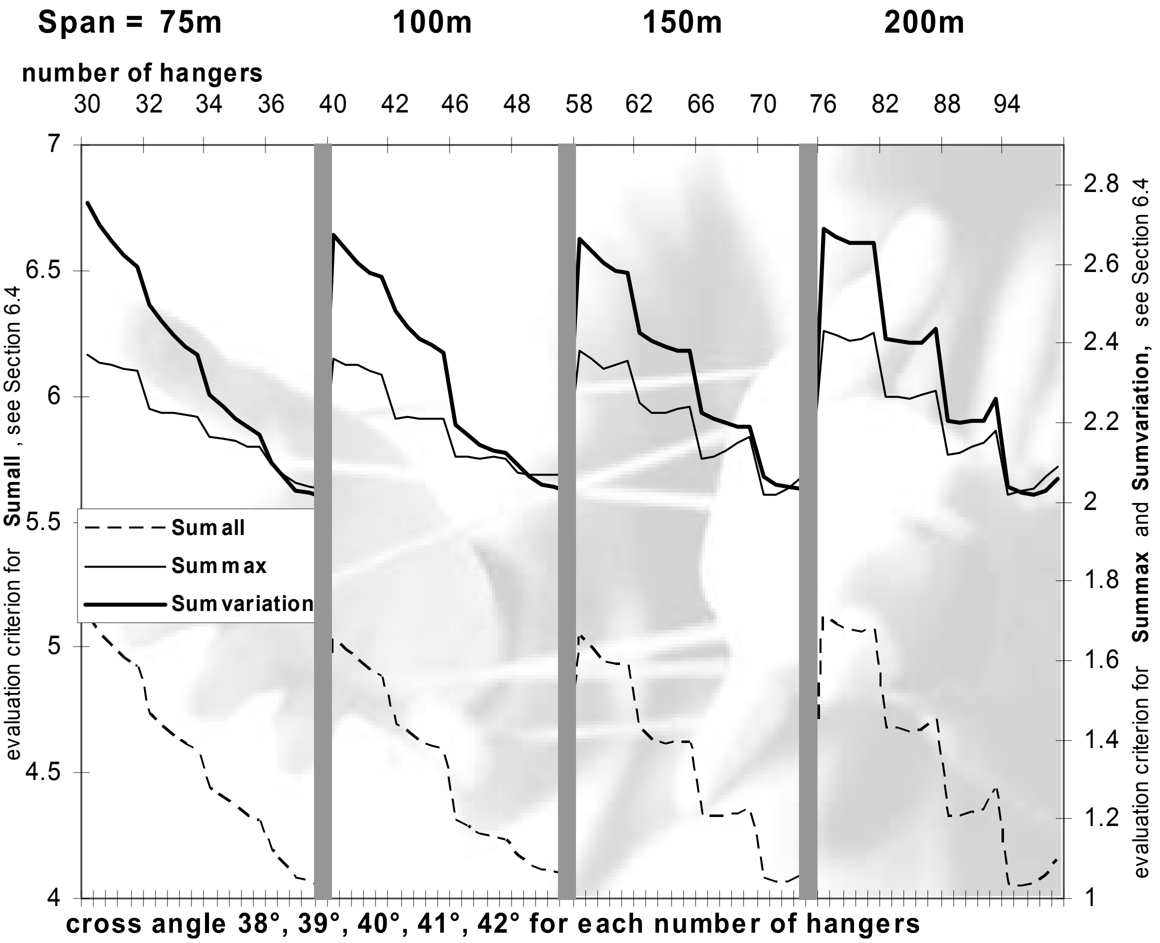

Fig. 6.50. Diagram with scaled and added values for determination of improved results

For larger spans with scaled arch rise and scaled number of hangers, best results are achieved with a similar cross angle as with a span of 100 meters. But a slight tendency can be seen towards smaller angles, which means steeper hangers. This is not right for a smaller span. Obviously an improved hanger arrangement concerning low hanger forces and bending moments in the arch is achieved in this case with larger cross angles. That means less steep hangers.

It can also be seen that fewer hangers demand a larger cross angle to obtain improved values, which means less steep hangers.

Figure 6.50 shows that an increased number of hangers reduces the forces in the hangers as well as the bending moments in the arch. This behaviour does not seem to have a global extreme. To conclude which number of hangers should be used, another data series was calculated using the 100 m span bridge.

The results were again scaled and added as described in Section 6.4 to find best results out of a combination of the hanger forces and bending moments in the arch.

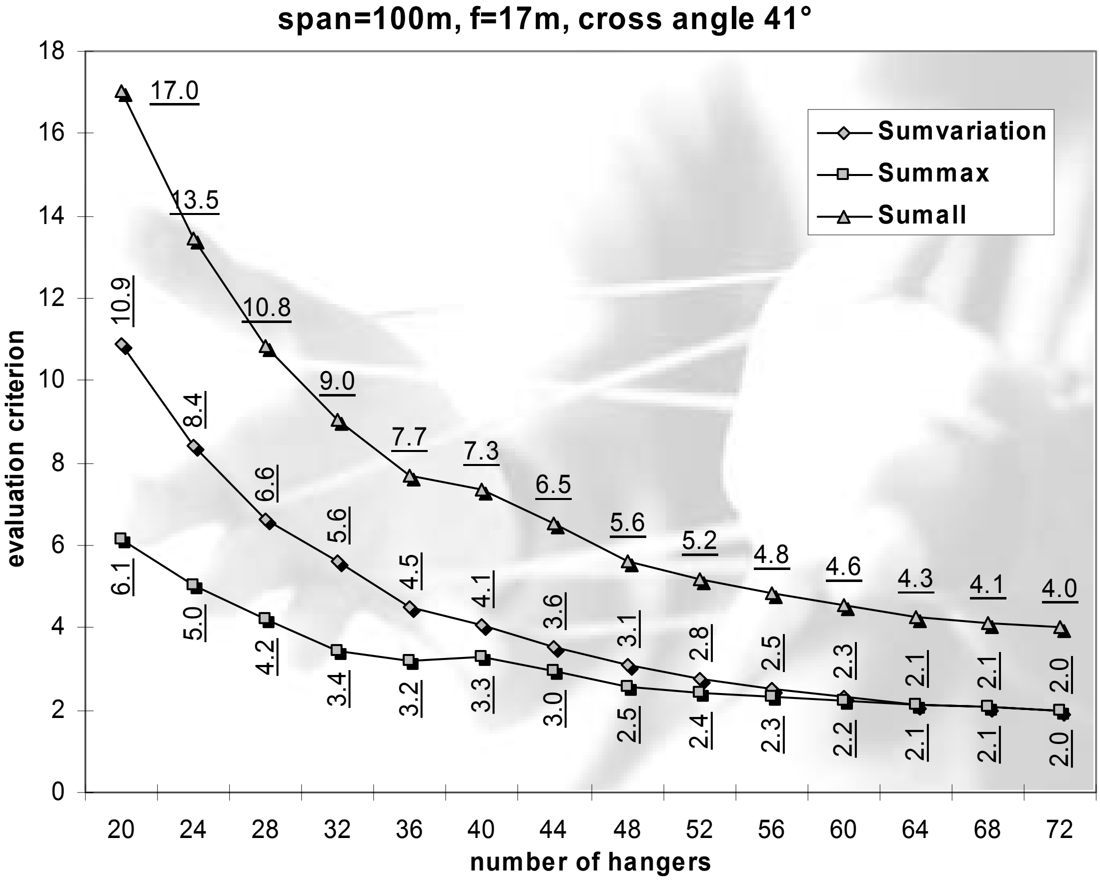

Fig. 6.51. Variation of the number of hangers, results scaled with their minimum to 1 and then added

As can be seen in Figure 6.51 the forces and bending moments become smaller with an increasing number of hangers. But the decrease is not constant, and in this case it does not significantly progress with more than 48 hangers. Maybe, considering aesthetic and economic matters, more than 48 hangers should not be used in a bridge with a 100 meter span. 48 hangers correspond to a distance of approximately 2.15 m between the hanger nodes along the arch and an average support distance of about 2 meters for the lower chord.

6.7.2 Influence of the rise of the arch

This section examines the effect of different arch rises. The arch rise of already built arch bridges lies mainly between 14% and 17% of the span, NAKAI *[22]*, page 129. This is primarily due to the appearance of the bridge, as rises above these values look rather ungraceful. The hanger arrangement of Section 6.6 and the 100 m span bridge with 44 hangers were used for calculations. The cross angle was 41°. The results are presented in figures 6.52 and 6.53.

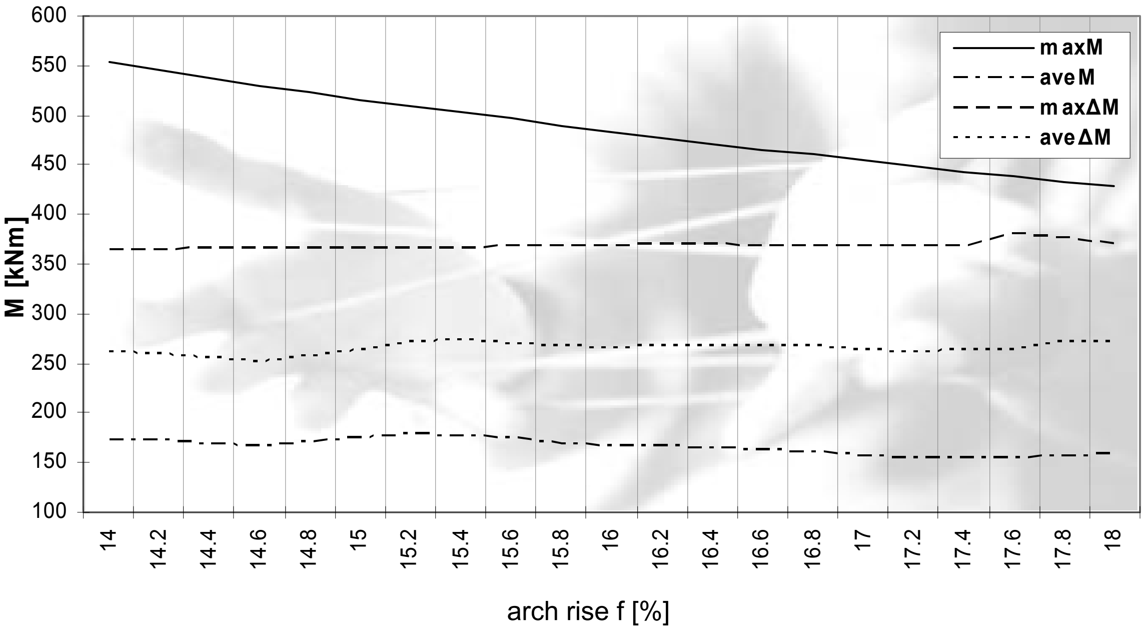

Fig. 6.52. Results for bending moments in the arch about the horizontal axis for different arch rises

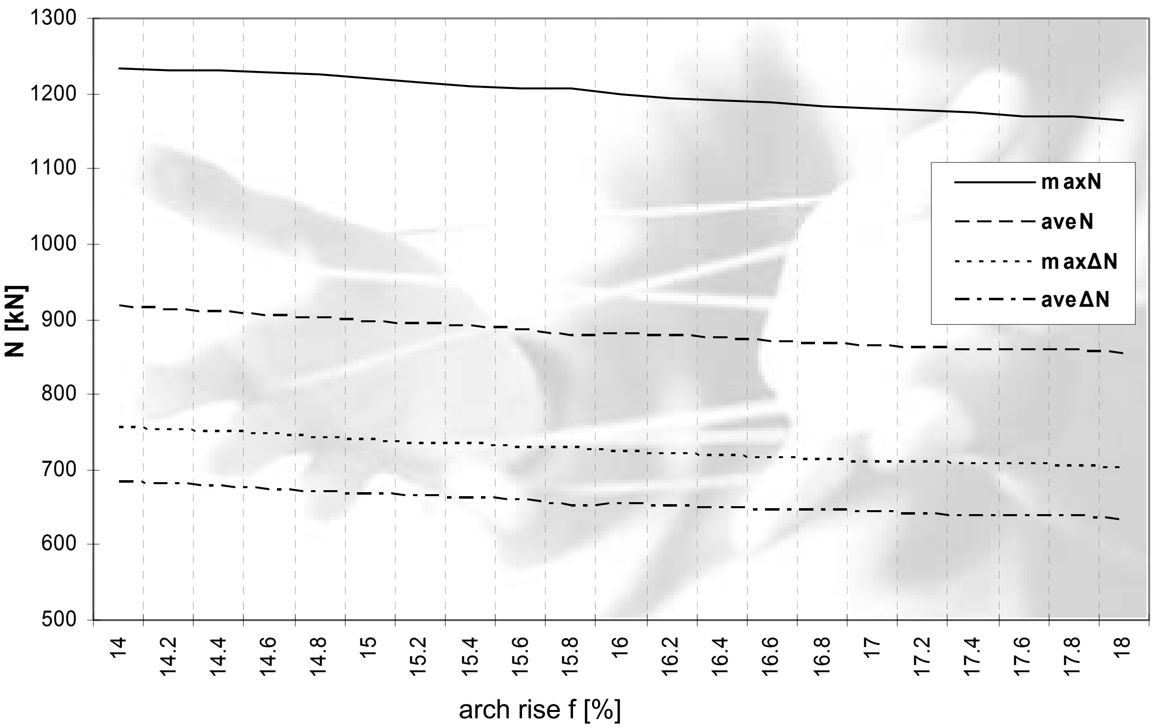

Fig. 6.53. Results for hanger forces for different arch rises

The larger the arch rise, the smaller the bending moments as well as the maximum axial hanger force. Therefore, larger rises should always be considered and balanced against aesthetic reasons.

6.7.3 Influence of the ratio between live load and dead load

Considering this parameter is necessary because the ratio between live loads and permanent loads changes from bridge to bridge. Even within the calculation of one bridge the ratio varies due to different load combination factors and partial safety factors for different design checks.

The self-weight of the arch and the hangers were not considered. Then the load used for the other calculations in Section 6 was 223.1 kN/m for permanent loads. The single loads of load model 71 are in conformity with 156.25 kN/m and the uniformly distributed part is 80 kN/m. For the permanent loads the partial safety factor of 1.35 and for the live load of 1.5 were used. There was one LM 71 applied on each of the two tracks. This leads to the ratios:

LL: 1.5·2·156.25 kN/m = 468.8 kN/m and
DL: 1.35·223.1 kN/m = 301.2 kN/m ratio single live load/dead load = 1.55

LL: 1.5·2·80 kN/m = 240 kN/m and
DL: 1.35·223.1 kN/m = 301.2 kN/m ratio uni. distr. live load/dead load = 0.8

Boundary conditions

For load model 71 the ratio between the single live load and the uniformly distributed load is fixed at 1.95. So it is only necessary to vary one ratio. It was decided on the ratio between the single live load and dead load and varied from 2 to 0.4. A bridge with a span of 100 m, arch rise of 17 m and number of hangers 44 was used for the calculations. The arrangement geometry found in Section 6.6 was applied with a cross angle of 41°.

Additionally loads common for road bridges were applied.

Results of the analysis

The results were scaled and added as described in 6.4 to find the best results out of a combination of the hanger forces and the bending moments in the arch.

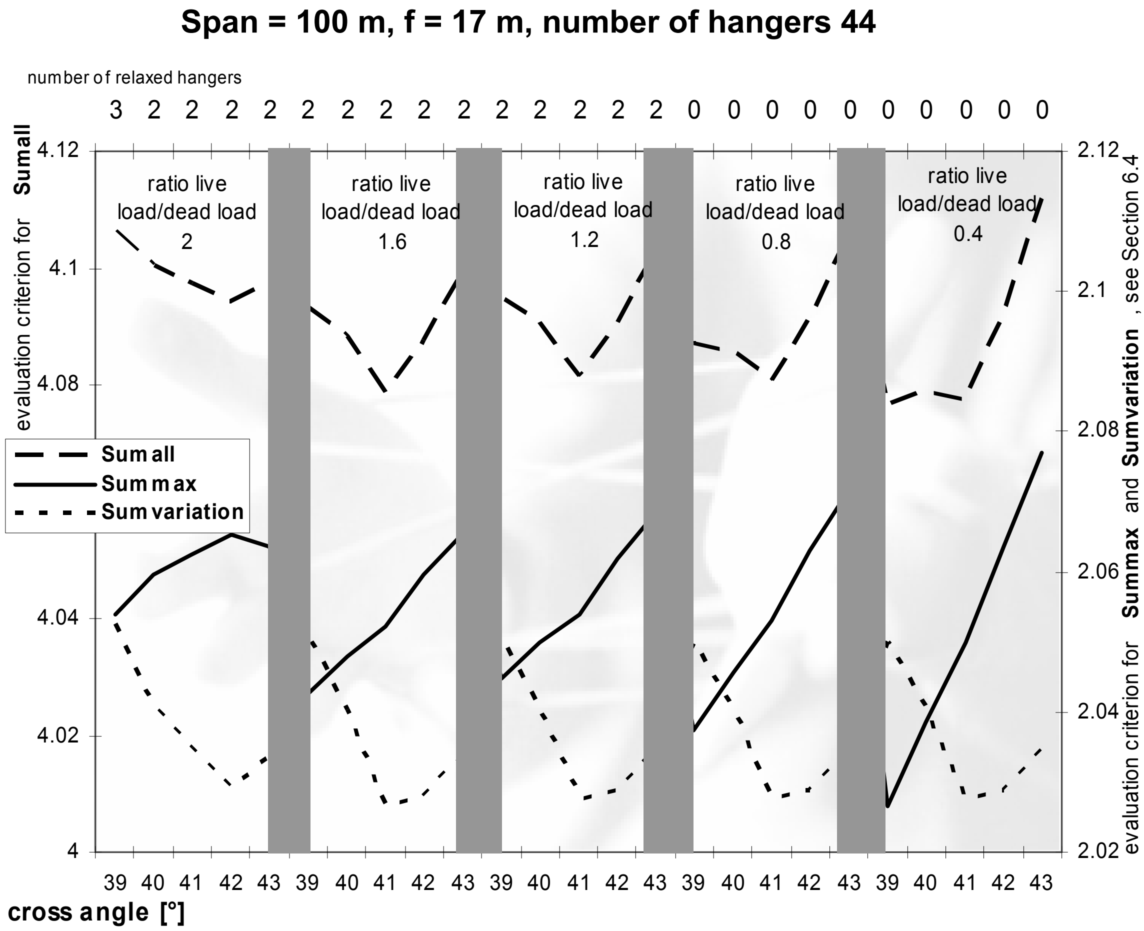

Fig. 6.54. Influence of the ratio between live load and dead load on the hanger arrangement

As can be seen in the diagram the ratio of live load to dead load hardly influences the hanger arrangement considering fatigue checks. A slight tendency to larger angles that means less steep hangers for higher live loads can be seen.

In contrast, for higher live load the inclination of the hangers must be steeper considering low maximum forces. It can also be seen that considering only this attribute would lead to significantly different hanger arrangements for different ratios.

In the combination best results are to be found at about the same cross angle (41°-42°) for all load ratios. Higher ratios need a slightly larger cross angle than lower ratios.

The enlargement of the number of relaxing hangers with likewise increasing load ratio shows an increase of the “compression” forces in the hangers caused by the live load. The only two relaxed hangers out of 44 are found at the end of the bridge which constitutes a disturbance range due to the clamping of the arch. In examinations presented in Section 6.7.5 it was found how the geometry of the first several hangers can be adapted to improve the results. After that no hanger relaxations occurred, except in construction phases (see Section 8 and Annex E).

Special examination: Road bridge loads

To imitate the actions occurring on road bridges, two lanes were applied to the bridge. According to *ENV 1991-3:1995 Section 4.3.2* the first lane was loaded by four wheel loads of 150 kN each and a uniformly distributed load of 9 kN/m. The second lane was loaded with another four wheel loads of 100 kN each and a uniformly distributed load of 2.5 kN/m. In addition the loads from rails, sleepers and ballast were removed. Live loads were multiplied by a partial safety factor of 1.5 and self weight by 1.35. The obtained results are presented, scaled and added as described in Section 6.4.

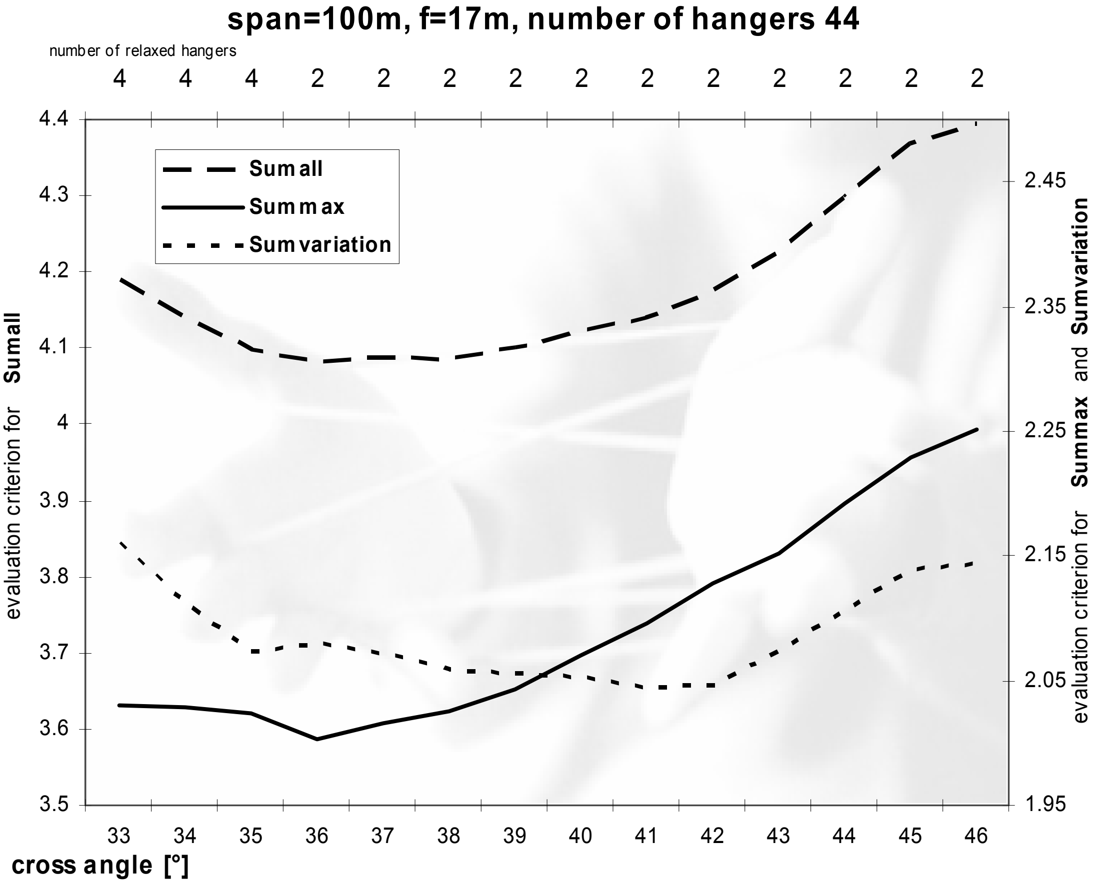

Fig. 6.55. Results for the calculation with loads similar to road bridge loads

For loads typical for road bridges, the optimal cross angle determined for railway bridges is not appropriate. Obviously the ratio between live load and dead load is much smaller for road bridges than for railway bridges. Therefore best results concerning small maximal forces are found at lower cross angles, which means steeper hangers. However, the best result considering a small stress range for a favourable fatigue check is found again at a cross angle of about 41° to 42°.

The combination of both demands leads to a cross angle of 36° and thus, to steeper hangers. The reduced self-weight and the necessary steeper hangers cause more relaxing hangers than for railway bridges. But as before, they are only in the disturbance range of the arch clamping. In Section 6.7.5 it is explained how these mavericks can be adapted for a special bridge project.

6.7.4 Influence of the ratio between the radii of ends and the middle of the arch

The hanger arrangement from Section 6.6 with a cross angle of 41° was used for this examination. The span was 100 meters and the number of hangers 44.

It is desired to examine the effect of a slightly smaller curvature at the ends of the arch, as this reduces the length of the columns of the wind portal frame and the transverse bending moments in it. Due to fabrication reasons, only circular curvatures are used, so that ΔR will be the ratio between the smaller radius R_1 of the end section and the larger radius R_2 of the mid section. The transition point depends on the segment lengths in which the arch is delivered. A smaller curvature radius is restricted to the first segment near the arch end. In this calculation the height of the transition point measures 8.8m, which means a length of the first arch segment of about 17.5 m.

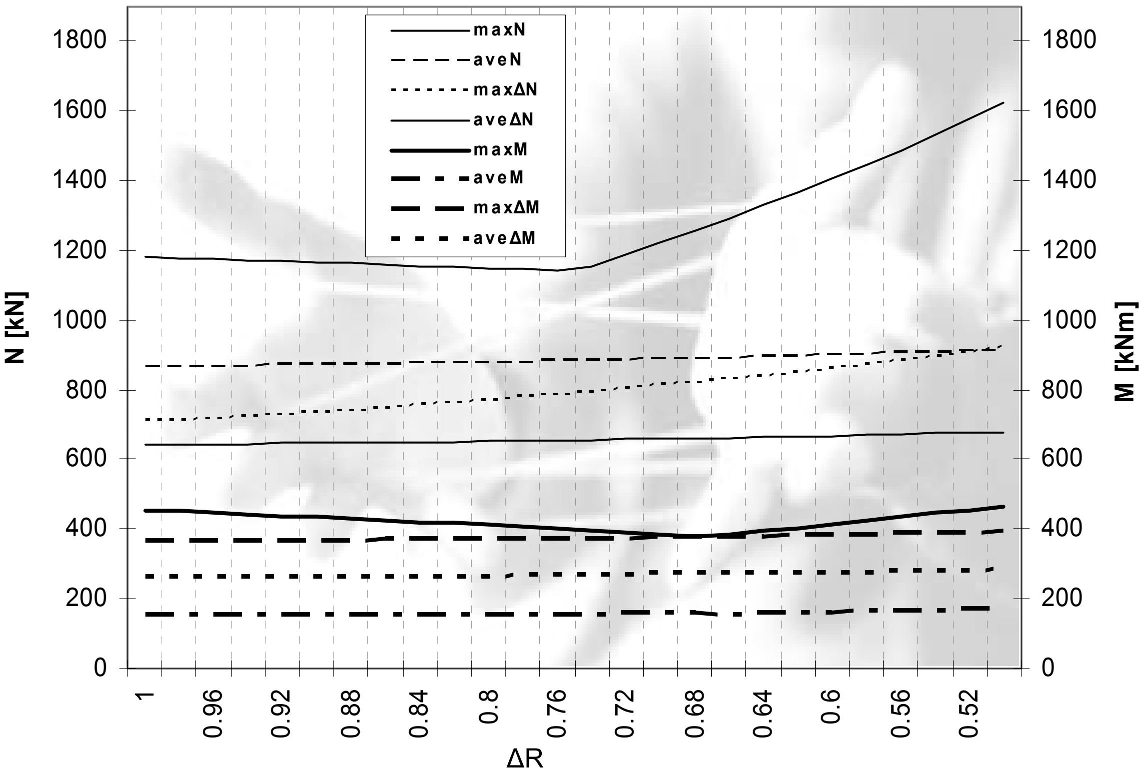

Fig. 6.56. Results from the calculation

Figure 6.56 shows that reducing ΔR to 0.76 hardly affects the hanger forces nor the bending moments in the arch. The axial force in the arch near the bearings decreases due to the steeper angle of the arch. A reduction of ΔR beyond 0.76 increases the bending moments in the arch about the horizontal axis. This is caused by the diversion of the axial force in the arch at the transition point.

As a result it can be said that reducing the radius at the ends of the arch until a ratio of the radii of about 0.8 is positive for the wind portal, but has no negative effects on hanger forces and bending moments in the arch.

6.7.5 Further considerations regarding the hanger arrangement

Hanger node distances along the lower chord

The hanger node distances along the lower chord, which are used in this work, result from mathematical or geometrical expressions. Therefore, some hanger nodes appear to be so close together that they have virtually the same coordinates. They should be merged, due to the fact that the size of the hanger connection detail requires minimum distances.

If a temporary lower chord is used for erection the distances between the hanger nodes and the temporary transverse beams should not be too large, because this increases bending in the temporary longitudinal beams. As far as possible the nodes should be shifted to gain benefits for this point.

Due to the greater thickness of the end cross girder, the temporary longitudinal beam has a kink at about 5 meters from the bearings. It would save cost if one hanger can be connected to this kink to take the vertical forces caused by the diversion of the axial tension forces.

Disturbance area

The hanger arrangement suggested in this work leads to larger maximum forces in the hangers nearest to the ends of the arch, compared to the rest. Naturally, the end of the arch constitutes a disturbance range, which has to be treated separately. For each single project there are special adaptations needed.

While calculating the bridge which is the object of this work and applying the improved hanger arrangement to the bridge calculated in RÄCK *[27]*, it was possible to improve the distribution of the hanger forces in the disturbance range. The different methods are presented here.

The analysis of the deflection line in the bridge of this work showed a point of contraflexure and a convex deflection directly above it at the bridge end (Figure 6.57). The hangers with upper nodes in the convex area receive above average maximum forces. Therefore, hangers within and around this zone should be spaced closer together, so that the higher forces to be transferred are distributed into more hangers. That means shifting upper and lower hanger nodes towards the convex deflection range (see Figures 6.63 and 6.65). As a result, the previous maverick hanger forces are reduced to the average value.

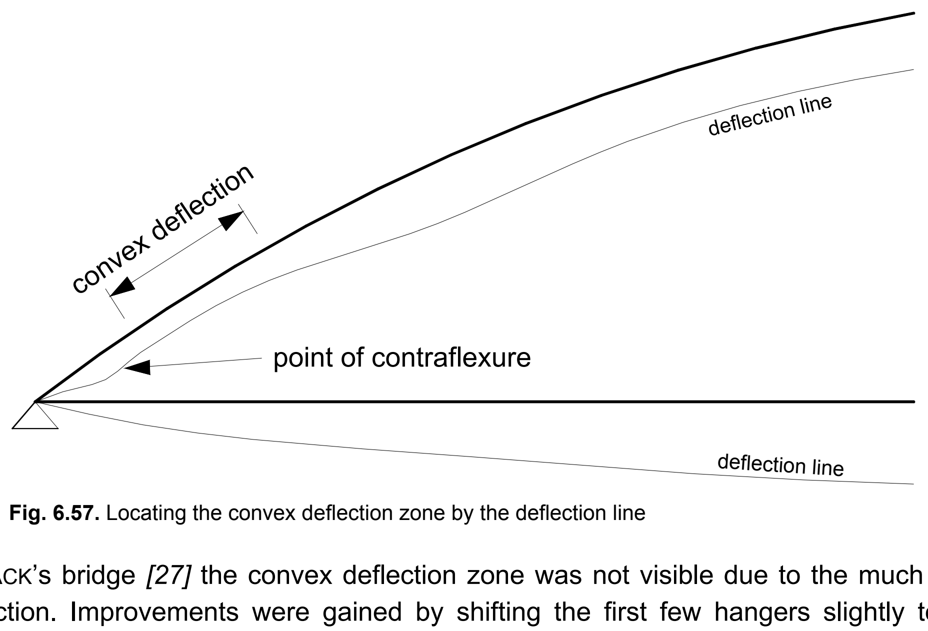

Fig. 6.57. Locating the convex deflection zone by the deflection line

In RÄCK's bridge *[27]* the convex deflection zone was not visible due to the much stiffer arch cross section. Improvements were gained by shifting the first few hangers slightly towards the middle of the bridge. Still hanger forces in the disturbance range showed deviations. Then the hangers with above average forces were made steeper and hangers with below average forces vice versa. This gave almost satisfying results. The final elimination of maverick hanger forces was achieved by changing the slope direction of the first hanger.

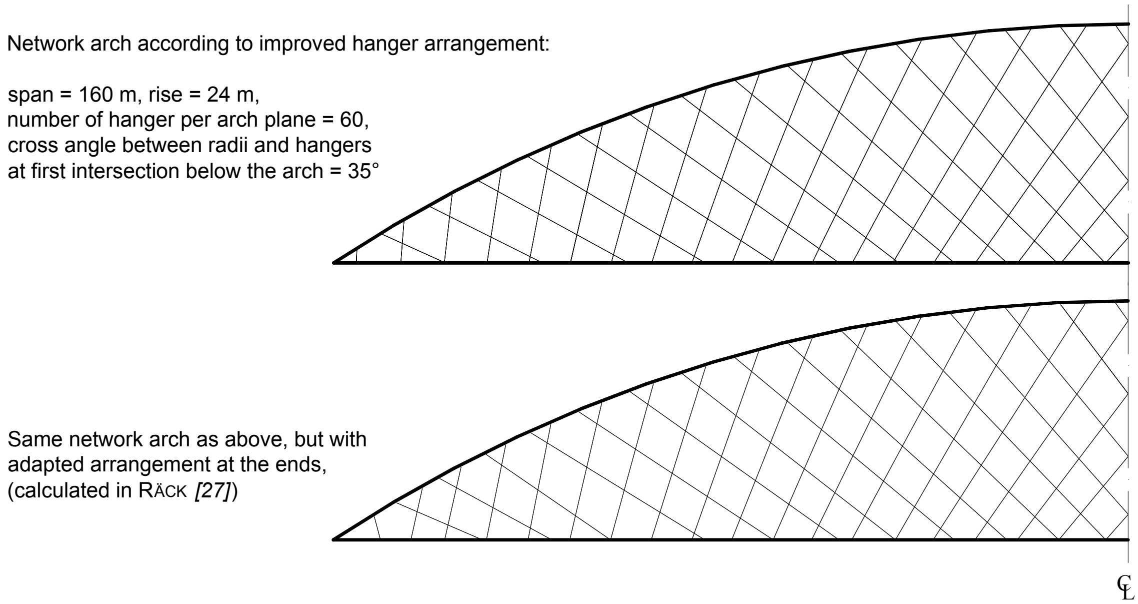

Fig. 6.58. Hanger arrangement used in RÄCK *[27]* for a network arch bridge with combined road and railway traffic and four arch planes

As described, finding the arrangement of the first several hangers is an iterative process.

The necessity of this measurement leads to the conclusion that neglecting different node distances along the arch may impede finding a satisfying hanger arrangement. This means for future work, that geometrical or mathematical models have to be found considering the variability of upper node locations, as well.

6.8 Discussion of results

On the structural behaviour

It is apparent that the ideal way of applying forces on a circular arch is if they act in a radial direction. That is why in the "spoked wheel" in Figure 6.24 smallest hanger forces among all hanger arrangements occur. The disadvantages of such a hanger arrangement are the large bending moments in the arch and the lower chord. The authors assume that they are result of the low stiffening effect of nearly vertical hangers and the small shear resistance of the area between the upper and the lower chord ("web"). Consequently the sections of the arch and the lower chord have to take additional bending moments and shear forces. An increase of the stiffness and consequently a better use of the "web" is obtained by using the hangers to constrict deflections between the arch and the bridge deck. This can be achieved by arranging pairs of hangers with opposite slopes that form a triangle, which is known to be immobile (Figure 6.59 on next page).

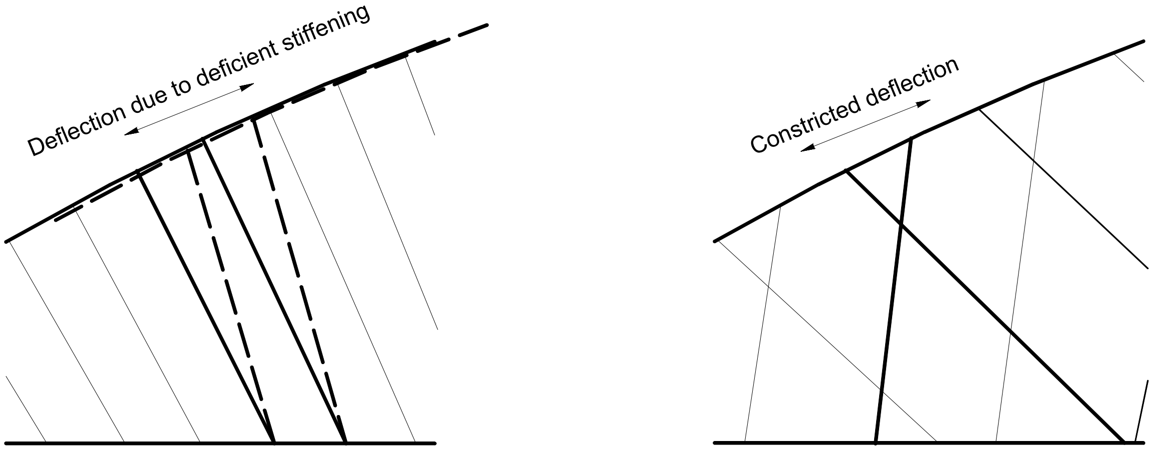

Fig. 6.59. Stiffening effect of pairs of crossing hangers

For an improved network arch not only small bending moments are of interest, but inter alia also small hanger forces. So, the idea was to combine the two effect principles. Thereto the forces transferred by the hangers should act on the arch in a radial way. Keeping in mind the idea of hangers acting as pairs the resulting force of each hanger pair should aim towards the centre point of the arch circle. Assuming equal average hanger forces this is achieved best by crossing the hangers on a radius, which intersects the arch in the middle between their upper nodes (see Figures 6.42). Then, an unknown angle in the triangle formed by each hanger pair is best for reducing the bending moments. With a certain angle all hangers will lie on the radii as in the "spoked wheel".

Out of these two principles, "spoked wheel" and triangular pair of hangers, there is a solution found if the demands of both aspects are combined and weighted as desired from case to case. The variable to determine is the cross angle of the hangers to the radius, defined in this work as the cross angle between the radii and the hangers in the first hanger crossing below the arch.

On fatigue

In the type of hanger arrangement introduced all hanger crossings lie on the same radii. The cross angle increases downwards. Independently of the cross angle at the first crossing below the arch, the cross angles within the web vary with different hanger numbers and arch rises. It was found that, only considering best results for fatigue, a range exists where the hangers cross the radii with an angle of 45°. Surprisingly this does not depend on the ratio between live load and dead load.

This means that the cross angle at the first node below the arch has to be smaller for a larger number of hangers, because with closer hangers the downward increase of the cross angle is larger. This was proven in Section 6.7.1. The location of the 45°-range is shown in Figure 6.60.

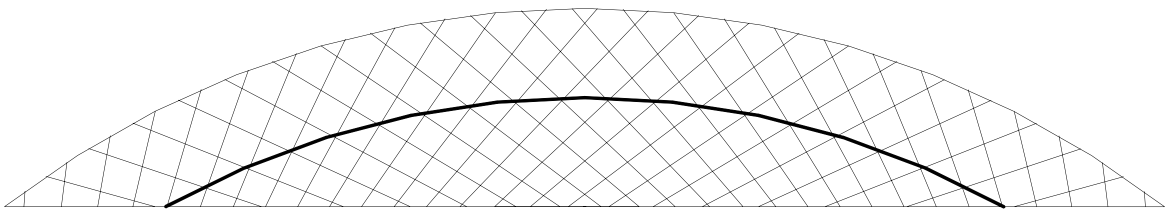

Fig. 6.60. Range where the hangers cross the radii at an angle of 45°

It seems, that the range in Figure 6.60 divides the hanger web evenly in some way. So maybe in order to obtain the smallest stress range, it would be best if all hangers cross each other perpendicularly. Regrettably this is not possible if the resulting force should still aim towards the centre of the arch circle.

It has to be mentioned that this range is the result of the combination of the demands of the hanger force variation and the bending moment variation weighted 1:1. Only considering the bending moments best results are obtained if all hangers cross the <u>arch</u> at an angle of about 45°, which means they distribute their force tangentially and radially in equal parts. This confirms the theory of all hangers crossing each other at an angle of 90° to obtain best results only considering fatigue checks.

On the number of hangers

Increasing the number of hangers reduces all internal forces. Since this reduction is not linearly dependent on the number of hangers, it is not reasonable to increase the number of hangers limitlessly. It has to be considered, that the saving of material due to the reduction of internal forces front the higher costs due to more hangers, hanger connections and labour hours for erection. For a span of 100 m it was found that the ratio between the number of hangers and the span [in meters] should not exceed 0.48. For longer spans a lower ratio and for shorter spans a higher one will give reasonable results.

On the span

For the bridges calculated in Section 6.6, different spans were applied with a scaled arch rise and number of hangers. Therefore, the largest difference between them was a changed ratio between the length of the bridge and the form of the live load. The load model 71 acts in longer spans much more like a single load. The results say that the cross angle has to be smaller for longer spans, which means steeper hangers for more concentrated loads. This conforms to TVEIT *[39]*, page 16.

On the rise of the arch

The variations of the arch rise showed the known results: With an enlarged arch rise the distance between the upper and the lower chord increases, which lowers the axial force in the arch and the hanger forces. Furthermore, the angle of the arch at the root point becomes steeper, which results in a decreased axial force and clamping moment in the arch.

Since the distances between the upper hanger nodes and the curvature of the arch become larger, local bending moments along the arch increase.

It shall be mentioned here that less steep hangers increase the axial force in the chords. This can be explained by the bigger number of hanger cross sections in a vertical section through the arch plane. The hangers contribute tension forces to the horizontal equilibrium in the vertical section, which results in increased axial forces in the chords. Nevertheless, this enlargement is small compared to the maximum axial arch force. With regard to the values of the internal forces, the benefits of less steep hangers outweigh the disadvantages.

On the ratio of live load to dead load

For a smaller ratio of live load to dead load as it occurs with heavier bridge decks or road instead of railway loads, the internal forces caused by the live load become proportionally smaller. If the importance of small stress ranges and low maximal forces is kept up by 1:1, the best combination results are shifted towards the best results for ultimate design checks, which means low maximal internal forces. The hangers must be steeper to satisfy the demand for minimal forces than for minimal variation of forces. That is why in this work it was found that the cross angle for a smaller ratio of live load to dead load has to be smaller and vice versa.

6.9 Summary of Section 6

6.9.1 In words

1. The target of the improvement process was to find the best hanger arrangement in respect of low maximum hanger forces and arch bending moments as well as low variations in both. Each attribute was considered with the same weighting.
2. Considering only small hanger forces and small stress variations in the hangers, the “spoked wheel” leads to best results.
3. The best hanger arrangements were achieved when hanger intersections lie on the radii of the arch circle. The cross angle is variable and depends on the weighting of the optimisation attributes and the characteristics of the loads and the geometry of the bridge.
4. A high arch rise is advantageous. It must be limited for aesthetical concerns.
5. A higher number of hangers leads to smaller internal forces. From a certain number of hangers, the savings do not countervail the extra expenses.
6. For railway bridges, the load ratio hardly affects hanger slopes. Road bridges call for steeper hangers.
7. Smaller curvatures of the arch near the ends are advantageous in respect of bending moments in the wind portal. For a ratio of 0.8 between the arch radius at the ends and the middle best results are expected.
8. The disturbance range near the ends of the arch leads to above average hanger forces. This can be eliminated by shifting the upper and lower node of the first several hangers in an iterative process.
9. Despite all statics, it is necessary to bear in mind boundary conditions, e.g. temporary lower chord or hanger connection details, which demand special locations of the lower hanger nodes especially at the ends of the span.
10. If small stress variations are more important than small hanger forces, hangers must be less steep.
11. The smallest variation in arch bending moments has been found if all hangers cross the arch at an angle of about 45º. For the smallest variation in hanger forces, hangers have to be steeper. For a combination of both, hangers cross a smaller circle than the arch circle at an angle of 45º.

The scheme in Figure 6.61 has been composed to give assistance on how to find an appropriate hanger arrangement according to the results obtained in Section 6. An example of use is given in Section 6.9.3.

Preliminary suggestion for finding an appropriate hanger arrangement for single and double track railway network arch bridges

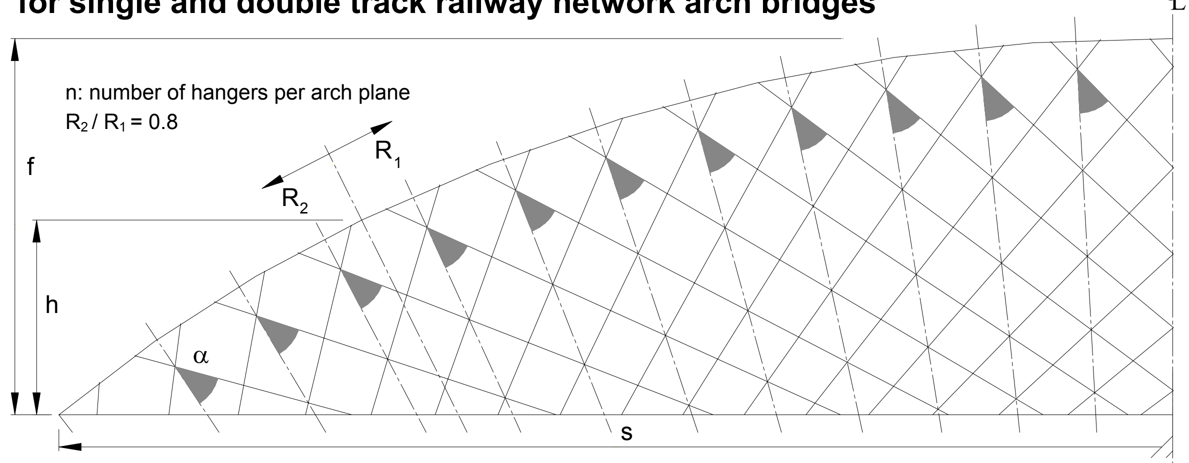

Fig. 1. Geometry and definition of variables

1. Decide on the rise of the arch: f = 14..17% of span
2. Determine number of hangers n from Fig.2.
3. Determine cross angle α from Fig.3.
4. Determine dead load g in kN/m
   Number of railway tracks: t

   Calculate factor L: $L = \dfrac{1.5 \cdot t \cdot 156.25\,\text{kN/m}}{1.35 \cdot g}$

   For L < 0.8, subtract 1° from α
   For L > 1.6, add 1° to α

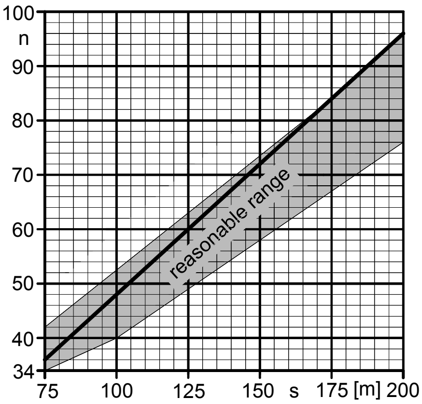

Fig. 2. Number of hangers

5. With $R_2 / R_1 = 0.8$ and equidistant upper hanger nodes acquire coordinates of nodes by drawing:
   - Hanger intersections lie on radii going through CP (Fig.1).
   - α: angle between radius and hanger at first intersections below the arch.
6. Run analysis of influence lines. Determine internal forces and deflection line

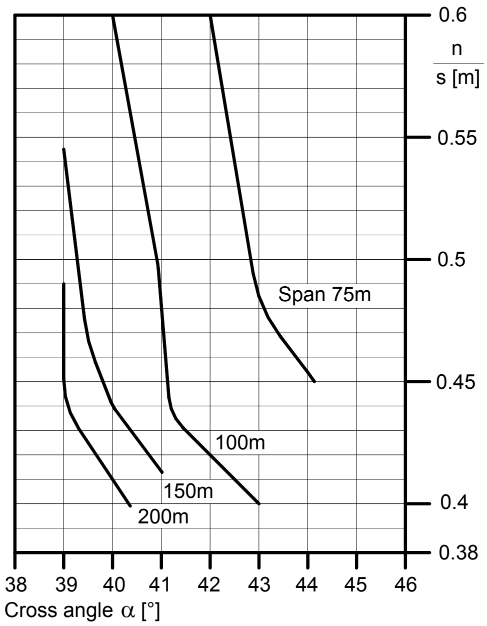

Fig. 3. Cross angle

7. Adapt maverick hanger forces at the ends of the span. Examples given in Section 6.7.5.
   Check results.
8. Adapt lower hanger nodes to other boundary conditions (e.g. temporary lower chord).

Note: This scheme is to be regarded as a summary of the results so far. Especially for spans different to 100 meters, further investigation is needed.

CP

BRUNN&SCHANACK

Fig 6.61. Section 6.9.2: Summary in a scheme

6.9 Summary of Section 6

6.9.1 In words

1. The target of the improvement process was to find the best hanger arrangement in respect of low maximum hanger forces and arch bending moments as well as low variations in both. Each attribute was considered with the same weighting.
2. Considering only small hanger forces and small stress variations in the hangers, the “spoked wheel” leads to best results.
3. The best hanger arrangements were achieved when hanger intersections lie on the radii of the arch circle. The cross angle is variable and depends on the weighting of the optimisation attributes and the characteristics of the loads and the geometry of the bridge.
4. A high arch rise is advantageous. It must be limited for aesthetical concerns.
5. A higher number of hangers leads to smaller internal forces. From a certain number of hangers, the savings do not countervail the extra expenses.
6. For railway bridges, the load ratio hardly affects hanger slopes. Road bridges call for steeper hangers.
7. Smaller curvatures of the arch near the ends are advantageous in respect of bending moments in the wind portal. For a ratio of 0.8 between the arch radius at the ends and the middle best results are expected.
8. The disturbance range near the ends of the arch leads to above average hanger forces. This can be eliminated by shifting the upper and lower node of the first several hangers in an iterative process.
9. Despite all statics, it is necessary to bear in mind boundary conditions, e.g. temporary lower chord or hanger connection details, which demand special locations of the lower hanger nodes especially at the ends of the span.
10. If small stress variations are more important than small hanger forces, hangers must be less steep.
11. The smallest variation in arch bending moments has been found if all hangers cross the arch at an angle of about 45º. For the smallest variation in hanger forces, hangers have to be steeper. For a combination of both, hangers cross a smaller circle than the arch circle at an angle of 45º.

The scheme in Figure 6.61 has been composed to give assistance on how to find an appropriate hanger arrangement according to the results obtained in Section 6. An example of use is given in Section 6.9.3.

6.9.3 Example of use

As an example, the scheme in Figure 6.61 will now be applied to the bridge which is the focus of this work. It is a double track railway bridge with a span of 100 m. The result is the design used for all sections apart from Section 6.

1. Decide on the rise of the arch:
   Small internal forces were more important than better aesthetics, so the arch rise was chosen to 0.17% of the span. $f = 17$ m

2. Number of hangers per arch:
   From Figure 2 in the scheme (Figure 6.61). It was decided on the best number of hangers
   $n = 48$

3. Cross angle:
   From Figure 3 in the scheme (Figure 6.61) with h = 48/100[m] = 0.48 and s = 100 m
   $\alpha = 41°$

4. Ratio live load to dead load:
   In a preliminary design a uniformly distributed load of 223.1 kN/m was determined as the self-weight of the lower chord including rails, ballast and sleepers. The bridge is a double track railway bridge. The factor to determine the load ratio is:

   $$L = \frac{1.5 \cdot 2 \cdot 156.25 kN/m}{1.35 \cdot 223.1N/m} = \underline{1.55}$$

   With factor L = 1.55, the cross angle does not have to be changed.

5. With the fixed ratio R_2 and R_1 of 0.8 and equidistant locations of the upper hanger nodes along the arch, the coordinates of the lower hanger nodes were acquired by drawing (Figure 6.62).

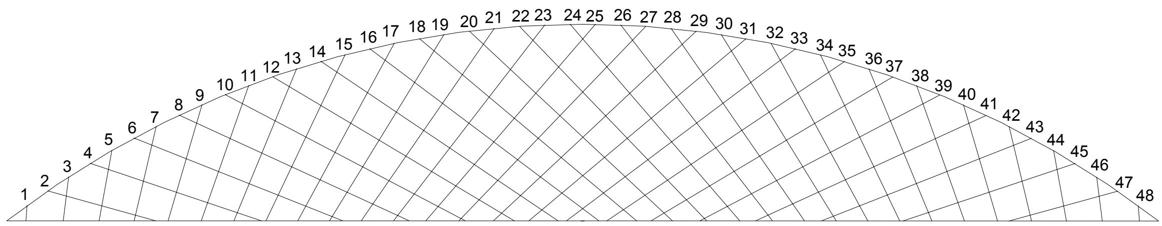

Fig. 6.62. Hanger arrangement found by the geometric description, labelling of the hangers

6. This first approach was calculated with one load model 71 on each track and the partial safety factors of γ_G=1.35 and γ_Q=1.5. The analysis of the influence lines gave maximal and minimal hanger forces as well as bending moments in the arch as can be seen in Figures 6.63 and 6.64.

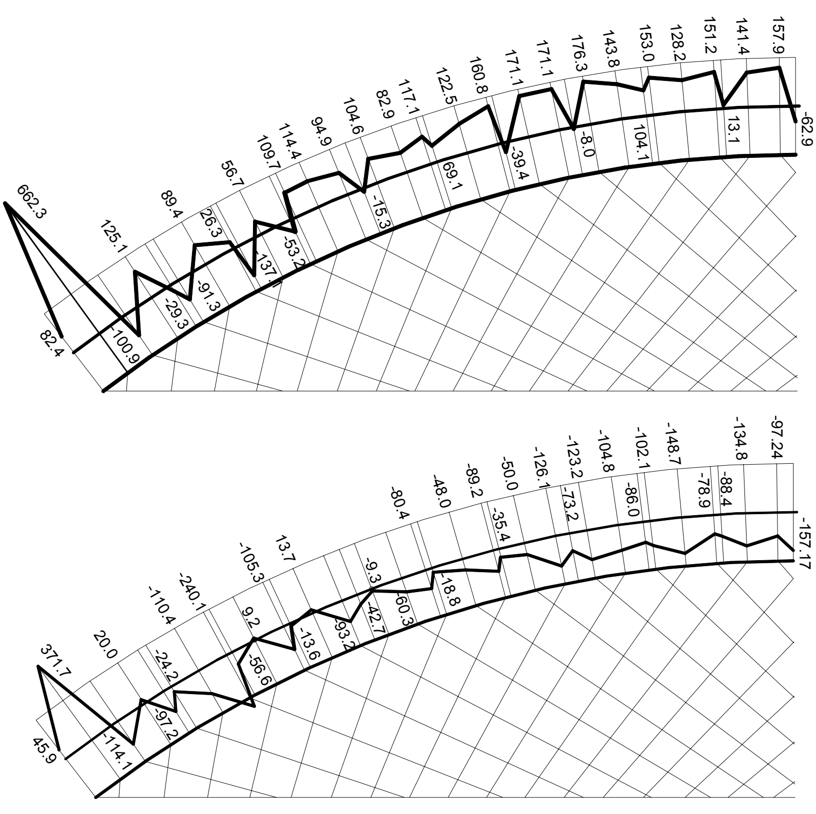

Fig. 6.63. Envelope of maximal and minimal bending moments in the arch

	max N	min N	ΔN
1	0,0	0,0	0,0
2	479,5	182,3	297,2
3	1277,4	821,6	455,8
4	893,5	406,2	487,3
5	1152,4	686,4	466,0
6	961,7	482,1	479,6
7	1001,3	540,9	460,4
8	878,5	466,4	412,1
9	837,0	427,9	409,1
10	848,4	451,7	396,7
11	830,1	415,6	414,5
12	892,2	453,6	438,6
13	855,5	397,5	458,0
14	947,4	457,0	490,4
15	915,4	378,6	536,8
16	962,9	445,6	517,3
17	950,1	348,3	601,8
18	936,3	396,2	540,1
19	947,7	327,4	620,3
20	892,7	369,2	523,5
21	932,3	331,1	601,2
22	896,3	367,2	529,1
23	924,6	343,5	581,1
24	914,8	363,6	551,2

Fig. 6.64. Hanger forces

7. Adapting maverick hanger forces

The maximal hanger forces of some hangers close to the end of the arch deviate from the rest. Since the maximal hanger force in the mid section of the arch is about 965 kN, it is desired to decrease the maverick hanger forces below this value. Thereto the deflection line of the arch was consulted to find the disturbance range in the arch caused by the clamping (see Section 6.7.5). In this area the upper nodes of the first 7 hangers were shifted upwards along the arch, so that they concentrate their impact in the disturbance range. After that the lower nodes of these hangers were shifted horizontally for aesthetic reasons, as well. Figures 6.65 and 6.66 show the results.

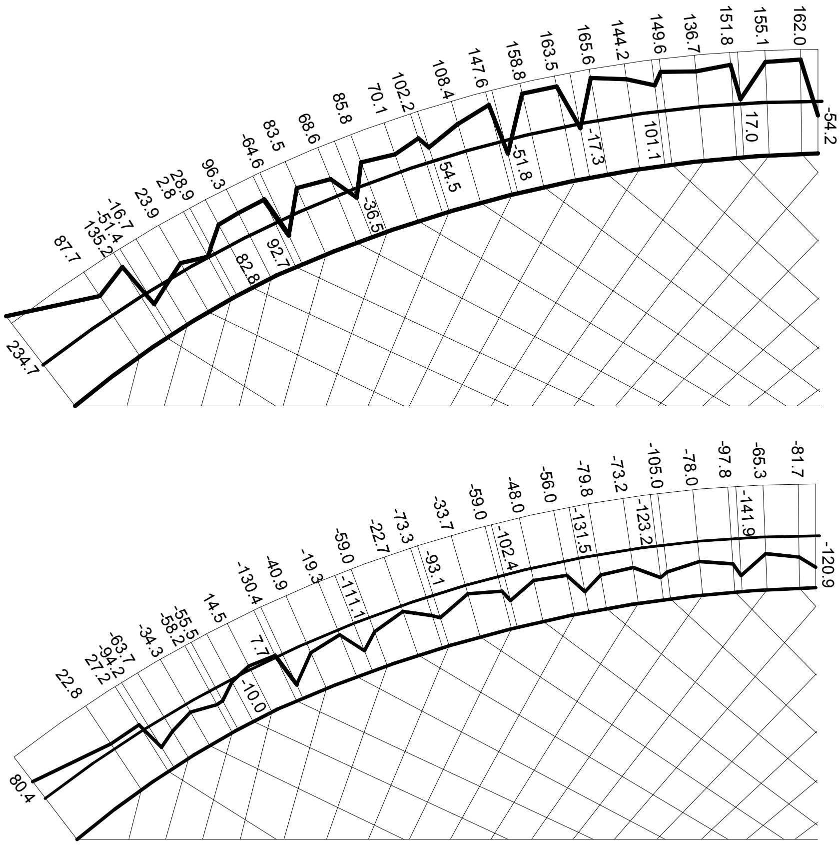

Fig. 6.65. Envelope of maximal and minimal bending moments in the arch, adapted hanger arrangement

	max N	min N	ΔN
1	174,8	128,1	46,7
2	912,4	420,7	491,7
3	666,8	390,1	276,7
4	829,2	383,8	445,4
5	779,9	396,3	383,6
6	774,1	389,8	384,3
7	826,9	405,9	421,0
8	790,1	423,3	366,8
9	813,1	406,9	406,2
10	857,8	458,0	399,8
11	814,9	402,6	412,3
12	903,4	453,6	449,8
13	835,3	380,8	454,5
14	943,6	446,5	497,1
15	903,5	370,5	533,0
16	949,4	432,8	516,6
17	944,3	347,7	596,6
18	917,0	381,8	535,2
19	945,2	330,7	614,5
20	871,1	353,4	517,7
21	931,9	336,4	595,5
22	871,9	346,9	525,0
23	924,2	349,1	575,1
24	889,8	343,2	546,6

Fig. 6.66. Hanger forces

Adjusting the hangers in the disturbance range is an empiric operation. Additionally, slight changes have considerable influences on the internal forces and may influence hangers in the mid section of the span. It is suggested to stopping the minimisation of the hanger forces when the forces are lower than the maximum forces in the mid section.

8. Adapting lower hanger nodes to other boundary conditions

For construction it is best if lower hanger nodes lying close together are merged into one hanger connection. Depending on the method of erection of the bridge there might be other conditions where to locate the lower hanger nodes on the lower chord. In this particular case a temporary lower chord will be used for erection. Therefore it is favourable not to have too large unsupported distances at the lower chord. These demands were applied and the effects on the internal forces shown in Figures 6.67 and 6.68

Investigation of hanger connection details regarding fatigue

7.1 General

Railway bridges are subjected to dynamic loading, which makes the consideration of the fatigue behaviour necessary. This is especially important for hangers and hanger connections, since they receive larger force variations than other bridge members. Subjected also to horizontal loading, hangers and their connections are therefore significantly prone to fatigue failure.

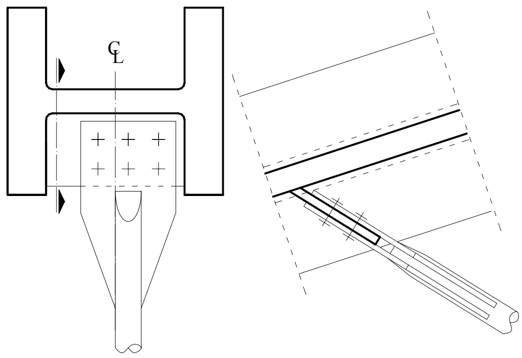

Fig. 7.1. Example of hanger connection

This section aims to investigate causes of dynamic loading and their effects on network arch bridges. A fatigue assessment is carried out for various types of hanger connections, resulting in a feasible design proposal, which is then adopted for the network arch calculated in this work. Two possibilities for the fatigue assessment provided in the Eurocode were applied:

1. Fatigue assessment based on nominal stress ranges (Section 7.4.1)
2. Fatigue assessment based on geometric stress ranges (Section 7.4.2)

The second method of assessment is necessary because the hanger connection details are more complex than the test specimen with which the detail categories and fatigue strength curves, such as in the Eurocode 3, were created. If the geometry and the loading differ significantly from the listed detail categories, the nominal stress is not meaningful, and its application would lead to wrong results. Therefore, local stress concentrations at geometric discontinuities were investigated.

This investigation is based on the specifics of network arch bridges, which makes the short introduction of relevant characteristics necessary. In network arches hangers cross each other at least twice. At their intersections, hangers are covered with plastic tubes and tied together by means of elastic rubber bands. This couples the horizontal movement of the hangers and therefore increases damping of the whole hanger web. Circular hanger sections are favourable due to their slender appearance regardless of the view angle. Smooth circular steel hangers will be basis for the design of the investigated hanger connection types.

7.2 Loading

7.2.1 Axial loads

Hangers are mainly subjected to axial loads, as they carry the bridge deck as well as the traffic loads. The maximum hanger force in the ultimate limit states in this work was determined to be F_{max} = 1062 kN. For fatigue considerations, the maximum force variation for two load models 71 acting on the bridge was obtained with $\Delta F_{p.1+2}$ = 440 kN, whereas the respective number for one load model was found to be $\Delta F_{p.1}$ = 295 kN. Effects due to the variation of axial loads are investigated in Section 7.4.

The damage equivalence factor λ was calculated to (Annex D, Section D.3.3):
See also: *ENV 1993-2: 1997 Section 9.5.3*

λ_1 = 0.6 EC Mix L = 100 m

λ_2 = 1.04 Traffic per year: $30 \cdot 10^6$ t/track

λ_3 = 1.0 Design life: 100 years

λ_4 = 0.77 $\dfrac{\Delta F_{p.1}}{\Delta F_{p.1+2}} = \dfrac{295\text{kN}}{440\text{kN}} = 0.67$

$$\underline{\lambda = 0.6 \cdot 1.04 \cdot 1.0 \cdot 0.77 = 0.48}$$

7.2.2 Horizontal loads

In the recent past a considerable number of vertical hangers in arch bridges, for example in Germany, had to be repaired because of serious fatigue damage. This damage was mainly caused by rain-wind-induced vibrations, GÜNTHER ET AL. *[15]*. Thus, it is important to examine how the hanger web in a network arch behaves under wind loading.

The gusset plate of the hanger connection detail is perpendicular to the plane of the arch. The resistance against movement of the hanger within the arch plane is therefore small, and large bending moments in the hanger connection do not occur. Furthermore, the hangers are tied together at their intersections reducing the deflections within the arch plane. In a network arch horizontal deflections of interest are therefore not the ones in the plane of the arch, but perpendicularly to it.

'Static' wind loads certainly cause the hanger web to deflect. The amplitude depends on the axial hanger force, since the virtual bending resistance of hangers increases with higher hanger forces. The maximum static deflection caused by wind loading in ultimate limit state and the absence of other live loads was determined to be 1.18 mm at a distance of 1 meter from the hanger node (Annex C, Figure C.22).

Regarding fatigue, it is to be examined apart from static deflection, if the possibility of a dynamic excitation of the hanger web exists. The analysis of the dynamic behaviour of rope-net-structures has to be performed considering the whole net, because the deformed shape is a result of a state of equilibrium of a rope-net, BRUGER *[6]*. Otherwise, considering each hanger alone, the fastening of the hangers at their crossings would have to be ignored in order to be on the safe side and the favourable influence on the dynamic behaviour of the hanger web would be lost.

For dynamic investigations the mode shapes are of interest. The first mode shapes are shown in Annex C, Figure C.24. As mentioned above, oscillation amplitudes are larger for less loaded hangers. It is likely that wind excited oscillations occur for long periods of time while no train is on the bridge, so the mode shapes were calculated without additional live load.

The following paragraphs give an introduction to various types of wind excitations relevant for slender structures, such as hangers of arch bridges. The authors will try to examine which types might occur in network arches.

7.2.2.1 Gust excitation – wind direction perpendicular to hanger web

This type of wind excitation is a 'separate excitation'.

Gust excitation is caused by varying wind velocity resulting from ellipsoid- globe- or boomerang-shaped areas of various velocities in the wind stream, PEIL *[23]*. The first mode shape of the hanger web (Figure 7.2) leads to the largest amplitudes and would therefore be decisive for gust wind response.
DIN 4131 09.1991 - "Antennentragwerke aus Stahl" suggests loading more than 10 m wide structures partly with only 60% of the wind load. To obtain maximum deflections, it is therefore necessary to apply full wind load to the centre range of the web and reduced wind load to the outer areas.

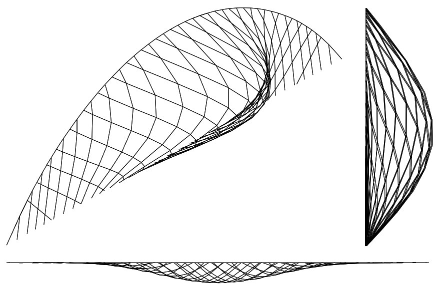

Fig. 7.2. First mode shape of hanger web, f = 0.97 Hz

Annex B of *ENV 1991-2-4* provides the dynamic factor c_d taking gusts into account as an increase of the static wind pressure. Regrettably the given calculation methods are not appropriate for the present structure. Besides, it is not stated if the forces calculated by these methods are relevant for fatigue assessment. The Eurocode refers to specialist advice.

7.2.2.2 Vortex excitation – wind along the hanger web

Wind flow around a slender structure leads to vortices inducing alternating lateral pressure. This transverse excitation is a combination of 'separate excitation' and 'self-excitation'. Especially slender structures with small stiffness and damping, such as cables, are prone to be affected.

This excitation can and probably will occur in the hanger webs of network arches, as well. But each hanger will oscillate with a different frequency and amplitude, since they have different lengths, slopes and axial forces. The advantage is that these hangers with different oscillations are tied together. A dangerous excitation will only occur if the dynamic wind forces cause an oscillation according to the mode shapes of the whole hanger web. Otherwise the hangers' vibrations damp each other. An excitation according to one of the mode shapes is considered as improbable.

In GÜNTHER *[15]*, page 908, it is stated that vortex vibrations are not critical. That article refers to single hangers, where this excitation is believed to happen more easily. Thus, it is not regarded as critical in network arches.

7.2.2.3 Aeroelastic instabilities and interference effects

These types of effects are based on self-induced excitation of the structure and can be divided into galloping and interference effects to crosswind oscillation (with one degree of freedom) and flutter and divergence (with two degrees of freedom).

Galloping – wind along the hanger web

Galloping occurs on flexible structures with non-circular shaped cross-sections. Cylindrical hangers are therefore not affected, unless their cross section changes due to coating with ice.

This effect also arises when rain drops hit the hangers and generate a rivulet on the surface of the hanger. The presence of flowing water on the hanger changes its cross section and consequently the wind flow pattern. This induces a lift-force as a mechanism for vibration. The additional danger of this type of excitation is that the rivulets change their position with the oscillation, which leads to varying aerodynamic forces (VAN DE BURGH *[49]*). This phenomenon is known as *rain-wind induced vibrations*.

In GÜNTHER *[15]*, Figure 5, criteria are given whether single hangers are sensitive to rain-wind induced oscillations or not. It is more probable for larger hanger diameters and smaller eigen-frequencies. PER TVEIT confirms that for the whole hanger web it is improbable that rain-wind effects or galloping cause fatigue relevant vibrations.

Interference effects due to crosswind oscillation

Interference effects occur at closely spaced slender structures and hangers are vulnerable to such effects due to their in-line arrangement. *ENV 1991-2-4: 1995, C.3.2* provides different methods of assessment, depending on the distance between the structures, their diameters and if they are coupled or not. The distances between hangers within a web vary constantly. It is doubtful whether these calculation procedures provided by the Eurocode can be applied to network arches. In case of doubts the European standard recommends specialist advice.

Flutter and divergence

Flutter and divergence are coupled bending-torsional vibrations (SEDLACEK *[32]*). Since torsional vibrations cannot be induced in circular hangers by wind loading, these effects are not applicable. Hangers with flat plate-like cross-sections are vulnerable to such dynamic effects. In this work rectangular cross-sections for hangers are not used; thus, flutter and divergence cannot happen.

7.2.3 Conclusion

The fastening of the hangers at their intersections, which couples their deflections perpendicularly to the hanger web, is very advantageous in respect of resistance against dynamic wind excitation. Looking at the mode shapes of the hanger network in Annex C, Figure C.24, we can see that the largest oscillation amplitudes occur when the whole net moves into one direction. The amplitudes of vibrations are much smaller if each hanger is excited separately (see Figure 7.3 for an example).

Excitation of the whole net is probable under gust wind loading, but its occurrence with fatigue relevant vibrations is very doubtful. Other dynamic wind effects exciting a single hanger are not dangerous in terms of fatigue, because a response according to one of the web mode shapes is considered as very improbable.

For the determination of the aerodynamic behaviour the Eurocode refers to specialist advice. A final conclusion might only be found by wind-tunnel tests.

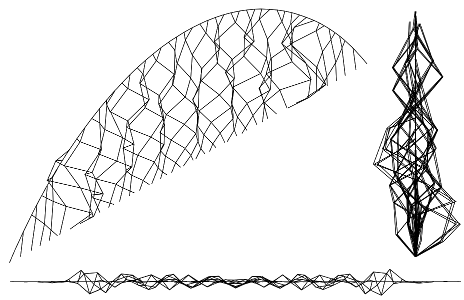

Fig. 7.3. 40th mode shape of hanger web, f = 3.24 Hz

Referring to PER TVEIT, who confirms the authors' assumption, hangers in network arches are not subjected to wind excitation in a way that would be dangerous in terms of fatigue.

For the sake of interest and in case of a wrong assumption, stress distributions in hanger connection details due to horizontal deflections are examined in Section 7.5.

7.3 Boundary conditions for hanger connection design

It is desirable to arrange each set of hangers in an individual plane. Provided that all hangers are straight, the centre distance between both hanger sets is equal to the hanger diameter. To accomplish this, the hanger connections need to be designed with an eccentricity of half the hanger diameter to the arch profile. For network arch railway bridges with spans up to about 100 metres, rolled profiles such as Universal Columns or American Wide Flange can be used for the arches. Since the bridge calculated in this work is equipped with American Wide Flange profiles, only such profiles are considered in the following investigation.

To connect hangers to the arch profile, intermediate members, such as gusset plates, are required, which constitute the actual connection. Hence, it is necessary to connect the circular hanger profile to a plate-shaped element. This will be treated separately from the connection of the plate-shape element to the arch profile. The smooth circular hangers are suitable for butt joints to the gusset plates that are equipped with a cut-out, in which the hanger is inserted and welded. Slitted hangers, in which the gusset plate is inserted and welded by means of fillet welds, as it is suggested in *DS 804 [S.8]* for rectangular hangers are not considered.

Five different types of connections were investigated, see Figure 7.4. From the results, another hanger connection was derived (Figure 7.5).

Geometric boundaries for the hanger connection design taken from the bridge that is the object of this work:

- Arch profile: American Wide Flange W 360x410x634 and W 360x410x900. The design of the hanger connections is based on W 360x410x634 representing the critical case with smaller dimensions.
- Hanger: Smooth circular bar, diameter D = 60 mm
- Material for arch profile, hanger and gusset plates: Steel grade S 460 ML

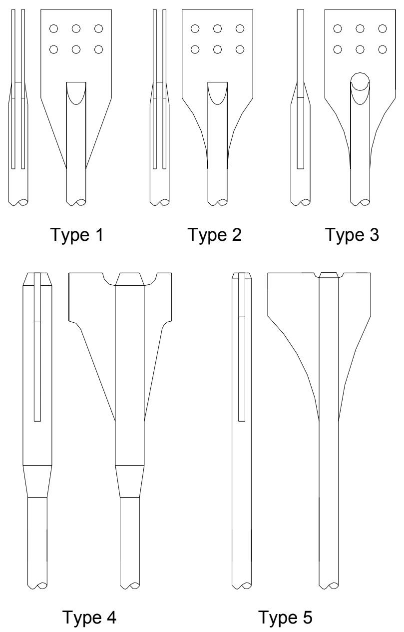

Fig. 7.4. Investigated types of hanger connections

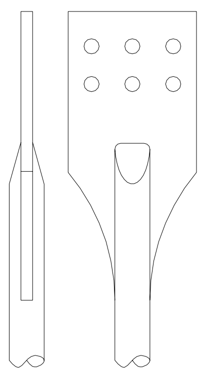

Fig. 7.5. Suggested hanger connection

7.4 Fatigue caused by axial loads

7.4.1 Fatigue assessment based on nominal stress ranges

The dynamic loading of bridges is characterised by low loads and long lives, commonly referred to as high-cycle fatigue with fatigue lives greater than 10^5 cycles. For high cycle fatigue, the nominal stress range method using SN curves is best suited, ALMAR-NÆSS *[3]*, pages 214-215. These curves (also Wöhler curves) were found by experimental fatigue tests on specimens. The fatigue strength in the form of constant stress ranges (S) is related to the number of cycles (N) until rupture, SEDLACEK *[33]*, page 4.

Eurocode 3 provides these SN curves in *ENV 1993-1-1: 1992 Figures 9.6.1, 9.6.2* and *9.6.3*, which correspond to the detail categories listed in, for example, *ENV 1993-1-1: 1992 Tables 9.8*. The reference stresses used in these curves are the nominal stresses. They are calculated with respect to net cross sections excluding all stress concentration effects. The magnitudes of the dynamic stresses are below the tensile elastic limit.

In the following, the hanger connections will be examined using the detail categories provided in the Eurocode applying the nominal stress range method (*ENV 1993-1-1: 1992 Section 9.5.2*). It should be mentioned that locations of interest at the *hanger – hanger gusset plate* joints are named (A, B …), whereas relevant locations at the *hanger gusset plate – arch profile* joint are named (I, II …).

Hanger connection type 1

This type consists of two hanger gusset plates, requiring only one gusset plate at the arch profile and therefore providing a two-shear connection. STEIMANN *[37]* found this type not to be appropriate due to the low detail category 45 (*ENV 1993-2: 1997 Table L.4/1*) at the weld connection between hanger and gusset plates (**A**). With a hanger force variation of $\Delta F_{p.1+2}$ = 440 kN and a damage equivalence factor of λ = 0.48, the hanger diameter would have to measure at least 78 mm to satisfy the fatigue check. Following the ultimate limit states, only 60 mm are required. Clearly, this particular point appears to be very critical, but, however, it can be improved by introducing a sufficiently large enough transition radius. A radius of 150 mm would make detail category 90 applicable (*ENV 1993-2: 1997 Table L.4/1*), see Figure 7.7.

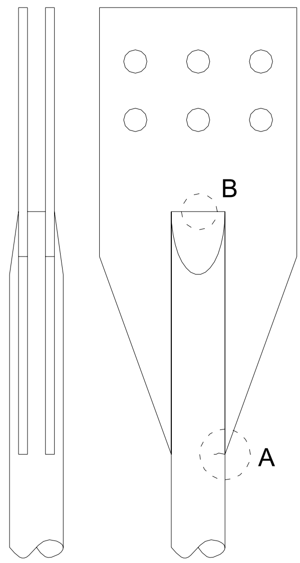

Fig. 7.6. Hanger connection type 1

Except for point (**A**), the clearance between the two gusset plates is not accessible, so that at least one butt weld can only be executed from one side. At point (**B**), this leads to detail category 36 (*ENV 1993-2: 1997 Table L.3/2*). To be able to judge this detail category, the splitting of the axial force between transverse butt weld and longitudinal butt welds needs to be determined. A splitting of the force proportional to the weld lengths and a constant stress distribution were assumed. With a total weld length of $2 \cdot 10$ mm $\cdot$ ($2 \cdot 270$ mm + 60 mm) = 12000 mm^2 and a maximum hanger force variation of ΔF_p = 440 kN, the stress variation is 36.6 N/mm^2, which is hardly greater than $\Delta\sigma_c$ = 36 N/mm^2. However, with λ = 0.48, the damage equivalent stress range becomes $\Delta\sigma_E$ = 17.6 and the fatigue check is fulfilled.

Hanger connection type 2

This connection (Figure 7.7) improves the detail category at point (**A**) from 45 to 90 by introducing a sufficiently large transition radius. The radius here of 342.5 mm is even greater than the required 150 mm in order to achieve a pleasing appearance and adopt the geometry of hanger connection type 1.

As with type 1, the hanger end is bevelled to provide a flowing transition to the gusset plate.

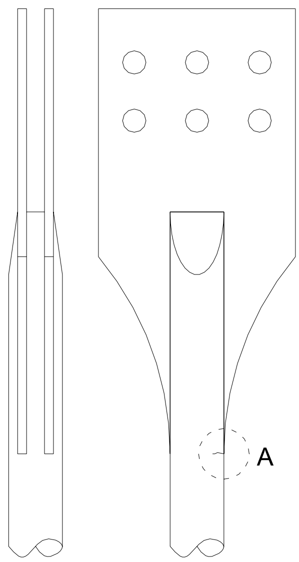

Fig. 7.7. Hanger connection type 2

Hanger connection type 3

The fact that there are two gusset plates is still regarded as disadvantageous because at least one weld can only be executed from one side. The application of a single gusset plate (Figure 7.8) improves this weak spot, but to achieve a two shear connection, two gusset plates are required at the arch profile. Here, the degradation of the fatigue strength due to an execution of the welds from one side is tolerable.

A further unfavourable point in connection with type 2 is the transverse butt weld at the end of the hanger, which is not only due to the relatively low detail category. The fabrication of this sharp 90° corner is rather inconvenient and prone to developing a crack skew into the plate. If type 2 is used, a certain sequence should be followed, in which the welds are executed. To keep residual stresses at a relatively low level, it is necessary to start with the transverse butt weld and proceed with the longitudinal welds. In any case, residual stresses should be avoided, as fatigue strength is lower for members with high residual stresses, because locations with residual stresses constitute locations of stress peaks, PETERSEN *[24]*, page 429.

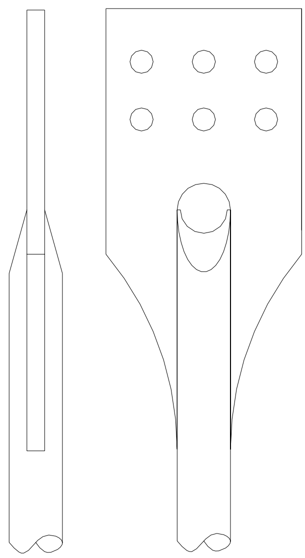

Fig. 7.8. Hanger connection type 3

In order to enhance this critical point, the hanger geometry suggested by GÜNTHER ET AL. *[15]* was adopted (Figure 7.21). It uses a hole in the plate at the end of the bevelled hanger butt end. The hole with a diameter equal to the dimension of the hanger is milled into the gusset plate and the rest of the plate where the hanger will be inserted can be cut out easily. Finally, the hanger is welded into the gusset plate and the edges and transitions are ground. The hanger is also equipped with a semi-circular cut-out. The diameter of this cut-out will be smaller than the hanger diameter, so that the ends are not pointed. The Eurocode does not provide a corresponding detail category with a respective SN curve for that detail. Therefore, the fatigue assessment based on nominal stress ranges fails here and calls for an assessment based on geometric stress ranges (Section 7.5).

Hanger connection type 4

This type of connection is derived from the German code for railway bridges *DS 804 [S.8]*, which was used in STEIMANN *[37]*. The first modification is the adjustment to a circular hanger cross section instead of a rectangular one. The main part of the connection is constituted by a widened cylindrical member, butt-welded onto the top of the hanger end (**C**). Detail category 90 (*ENV 1993-2: 1997 Table L.3/1*) is applicable.

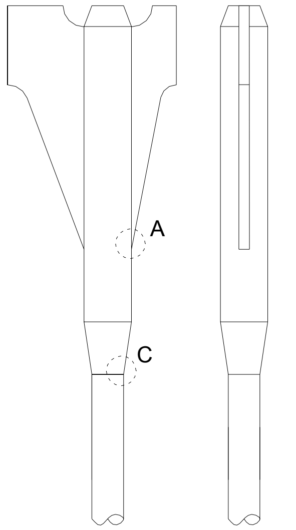

Fig. 7.9. Hanger connection type 4

The connection detail suggested in *DS 804 [S.8]* uses a slitted rectangular widened hanger end in which the gusset plate is inserted and connected by means of fillet welds. This gives detail category 80 (*ENV 1993-2: 1997 Table L.5/3*). Here, the second modification will be a full penetration butt weld between the gusset plate, which comes in two parts, and the widened hanger end. Although this leads only to detail category 45 (*ENV 1993-2: 1997 Table L.4/1*), the case is not as critical as with hanger connection 1, since the widened hanger end with its increased cross sectional area is accompanied with a lower stress level.

The nature of connection type 4 does not imply the critical point (**B**) of types 1 to 3.

Hanger connection type 5

This connection represents a further development of type 4 with the application of a sufficiently large transition radius at (**A**), as introduced with type 2. This makes the widened hanger end member redundant and the gusset plates can be directly welded to the hanger.

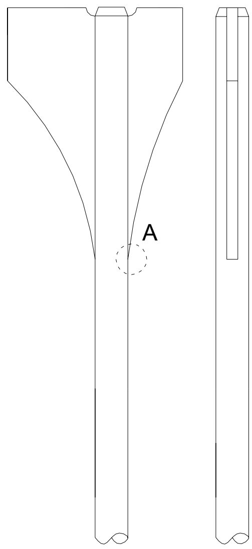

Fig. 7.10. Hanger connection type 5

Note

This fatigue assessment considers only the members constituting the actual connection. If the gusset plate is welded to the arch, the case of a crack occurring in the arch is not covered here. This check is carried out in Annex D, Section D.2.2.

7.4.2 Fatigue assessment based on geometric stress ranges

In this section geometric stress concentrations at geometric discontinuities are used for the assessment. Such stress concentrations can be obtained with the help of stress concentration factors (SCF) retrieved from diagrams for standard cases by carrying out finite element analysis or using the photoelastic method (TIMOSHENKO & GOODIER *[39],* pages 138-145). The stress concentration factor is defined as the ratio of the local stress at a relevant location to the nominal stress in the corresponding net cross section. Following Eurocode 3, the fatigue assessment based on geometric stress ranges is carried out in similar fashion to the assessment based on nominal stress ranges. The nominal stress range is adapted to the damage equivalent stress range at $2 \cdot 10^6$ cycles, which is an approved concept in engineering praxis, HARTMANN ET AL. *[16]*, page 7. The main difference is using the geometric stress range instead of the nominal stress range. Furthermore, the fatigue strength curves to be used shall be of detail categories 90, 71 or 36 (*ENV 1993-1-1: 1992 Section 9.6.3*).

It was decided to determine the stress distributions in the various hanger connection types with the help of finite element analysis in *NE/Nastran* (Annex C, Section C.1). Local stress concentration effects due to the weld geometry and discontinuities at the weld toe are to be ignored, as they are accounted for in the SN curves (*ENV 1993-1-1: 1992 Section 9.5.3 (1)*). Therefore, only the overall geometry of the hangers was modelled. The 3D modelling was carried out in *SolidWorks 3D CAD Software* (Annex C, Section C.1).

The hanger was subjected to a static tensile force of 1000 kN, which is a representative value. Constraints were applied to the contact surface around the slip-resistant high strength bolts in connection types 1 to 3. Connection type 4 and 5 were constrained at the lateral front faces of the gusset plates where it can be directly welded wither to the arch or to an end plate.

The analysis was based on linear elastic theory. The principal stresses were recorded and are given in the form of stress distribution illustrations. Where relevant, maximum or/and minimum principal stresses are considered.

Hanger connection type 1

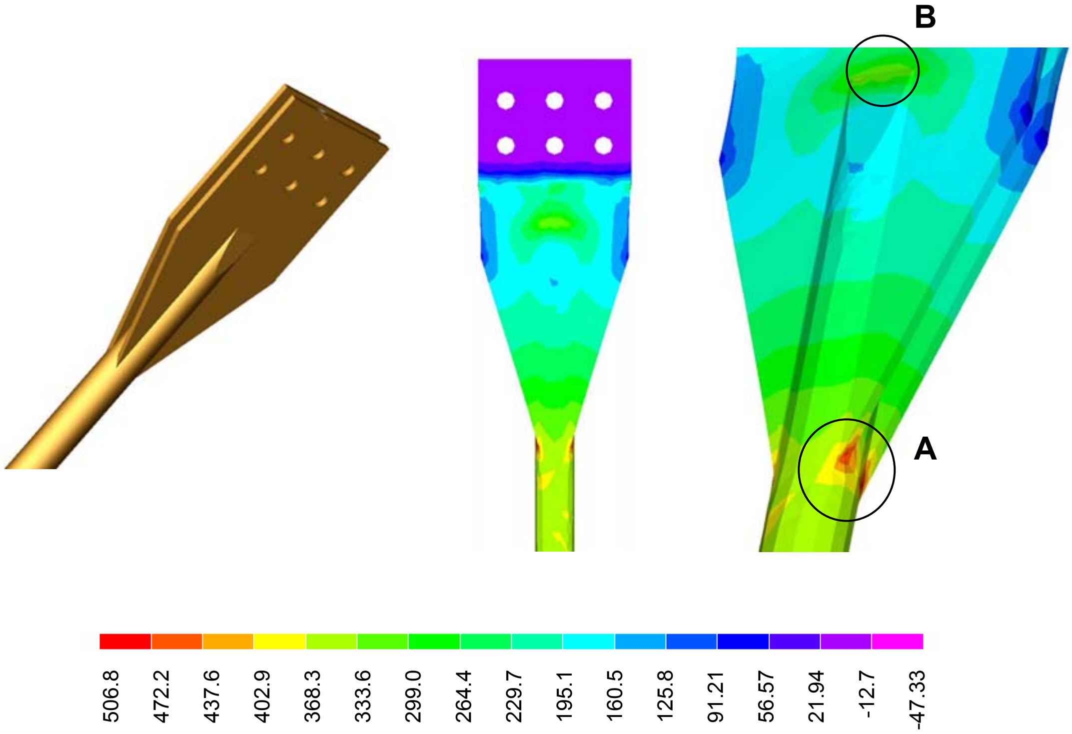

Fig. 7.11. Hanger connection type 1: Maximum principal stress [N/mm^2], deformation exaggerated

In this connection forces are almost equally distributed from the hanger into the gusset plate. This can be seen on the virtually horizontal colour gradients above the point where the free edges of the plate splay upwards. This is exactly the point with the highest stress peak of the whole hanger connection, which results from the discontinuous transition (**A**). A further stress concentration is found at the transverse joint between hanger butt end and the gusset plates (**B**).

Geometric stress concentration factors (SCF) for axial hanger force:

(**A**): 1.43 (The calculation of the stress concentration
(**B**): 1.39 factors can be found in Annex D.3.3.2)

With the help of the SCF the nominal stresses are scaled to obtain geometric stresses which are used in the assessment.

Fatigue strength curve to be used:

Eurocode 3 provides detail categories 90 and 71 for locations where the local stress concentration has negative effects on full penetration butt welds, and detail category 36 where the local stress concentration has negative effects on partial penetration butt welds and fillet welds.

(**A**): This point marks the end of the full penetration butt weld. Therefore, the SN curve for detail category 90 is taken for the assessment (*ENV 1993-1-1: 1992 Section 9.6.3 (2)*), assuming that both the weld profile and permitted weld defects acceptance criteria are satisfied.

(**B**): Here a full penetration butt weld constitutes the transverse joint between hanger butt end and gusset plate. SN curve for category 90 is taken.

The assessment shows that the stress range at (**A**) exceeds the fatigue strength at 119%, whereas the check is fulfilled with 74% at (**B**). The summary of all results is found in Figure 7.26.

Hanger connection type 2

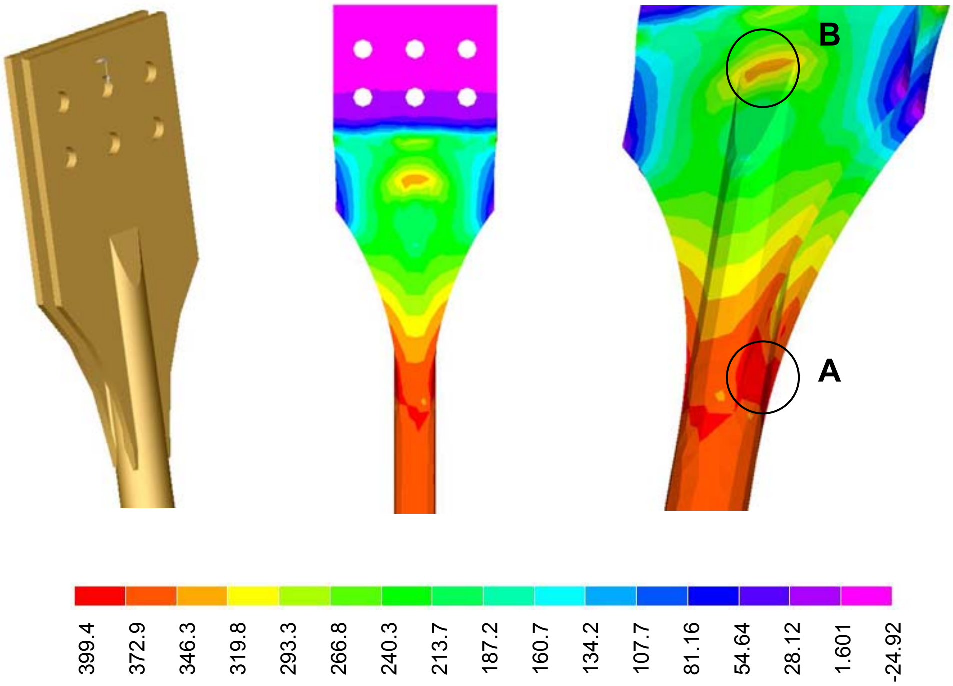

Fig. 7.12. Hanger connection type 2: Maximum principal stress [N/mm^2], deformation exaggerated

This connection type constitutes a further development of type 1. On the one hand, the stress peak at the formerly discontinuous transition between hanger and gusset plate is reduced by the introduction of a larger transition radius (**A**). On the other hand, the distribution of forces from the hanger into the plates is not as even as in type 1. The large transition radius is accompanied with a reduction of material. Consequently, forces are essentially transferred into the plate further 'upwards' or further 'inside' the plate. This can be seen on the curved colour gradients indicating higher stresses in the hanger region. That means that a larger portion of the hanger force is transferred through the butt end of the hanger, leading to higher stresses at that area (**B**), compared with hanger connection type 1. Therefore, it is suggested to increase the insertion length of the hanger into the plate in order to provide a longer longitudinal weld.

Geometric stress concentration factors (SCF) for axial hanger force:

(A): 1.13
(B): 1.47

The same SN curve as in connection type 1 is applicable.

The fatigue checks are fulfilled, at (**A**) with 94%, as well as at (**B**) with 78%.

Hanger connection type 3

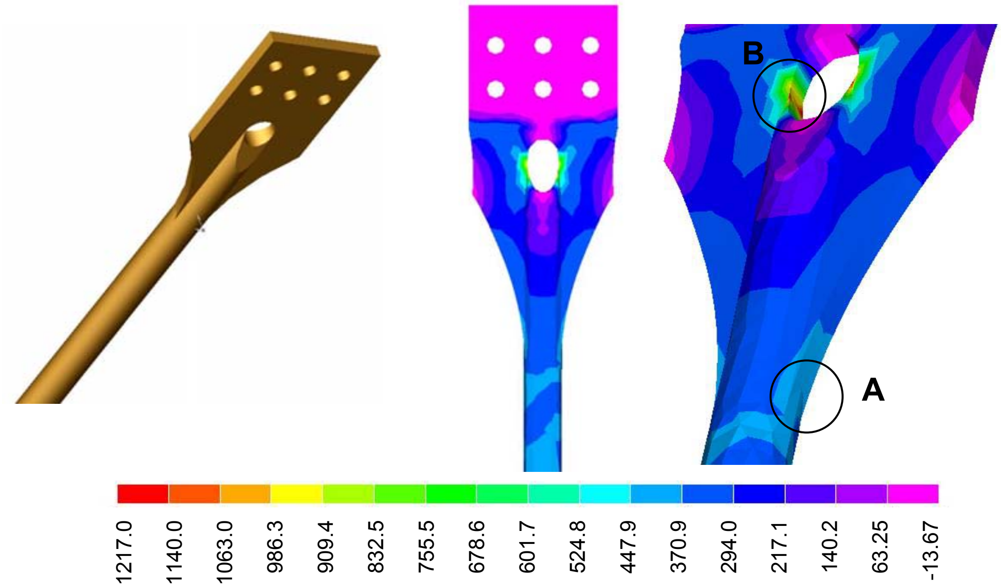

Fig. 7.13. Hanger connection type 3: Maximum principal stress [N/mm^2], deformation exaggerated

The edge of the circular cut-out at the butt end of the hanger marks the highest stress peak of this connection (**B**). However, the fact that the transverse butt weld and therefore the clashing between transverse and longitudinal butt weld is eliminated, is advantageous, as residual stresses are reduced. Still, in terms of the detail categories given in Eurocode (*ENV 1993-2: 1997 Table L*), a butt weld here would not be as harmful as with hanger connection 1 and 2, since only a single gusset plate allows the execution of the weld from both sides. At point (**A**) the transition radius is as large as in connection type 2.

Geometric stress concentration factors (SCF) for axial hanger force:

(**A**): 1.16
(**B**): 3.89

Since both stress concentrations are located at full penetration butt welds, the SN curve for detail category 90 is applicable.

The SCF at (**A**) hardly differs from the respective value in connection type 2 (SCF = 1.13). The fatigue check is here also fulfilled with 96%.

The SCF of 3.89 at the edge of the hole (**B**) appears to be rather large compared to the reference example 'hole in a plate', where the possible SCF lies between 2 and 3, GIRKMANN *[12]*. The reason for the difference is that the double symmetric plate-with-hole standard case cannot be transferred to the hanger geometry, which is only single symmetric. The continuously fixed upper end is faced by the concentrated force transmission by the hanger on the other side of the hole. Moreover, the bevelled butt end of the hanger incorporates a discontinuity in cross section, which also contributes to the higher stress concentration factor.

Fatigue strength curve to be used:

At (**B**) the circular cut-out represents a milled edge making detail category 125 applicable, GÜNTHER ET AL. *[15]*. However, since the longitudinal full penetration butt weld ends at the stress concentration location as well, it is sensible to reduce the detail category to 90 (*ENV 1993-1-1: 1992 Section 9.6.3 (2)*). The fatigue check is not fulfilled with 285%.

Hanger connection type 4

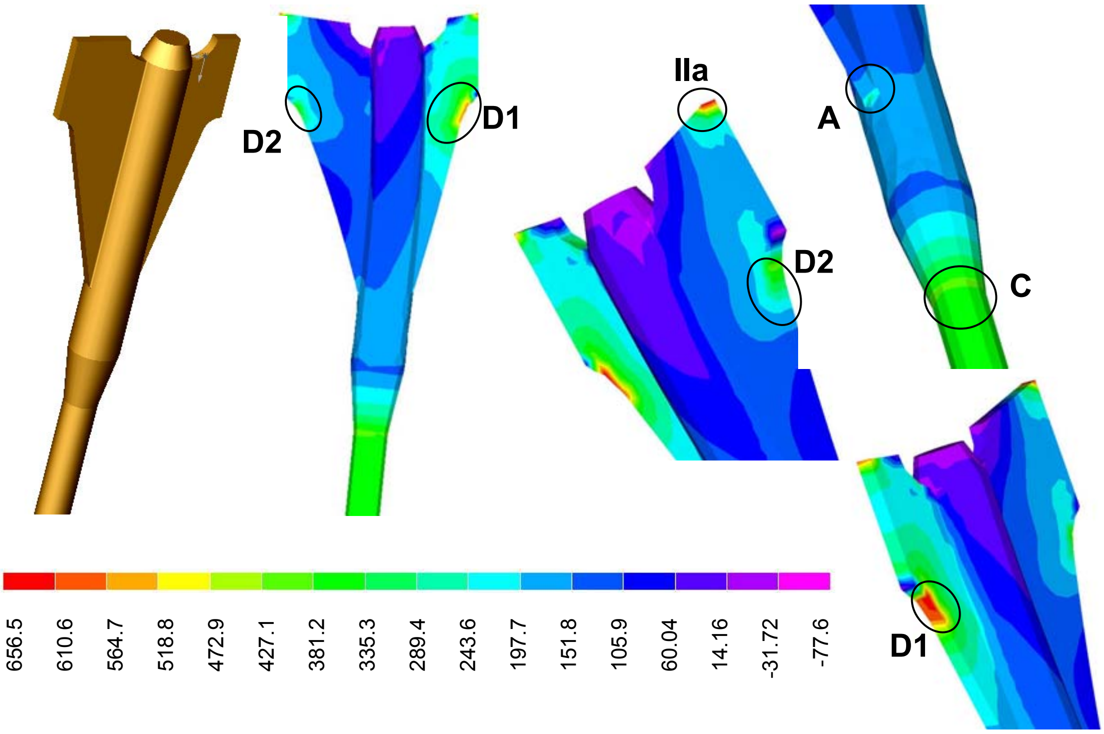

Fig. 7.14. Hanger connection type 4: Maximum principal stress [N/mm^2], deformation exaggerated

The overall body of hanger connection 4 is virtually free of stress peaks. The hanger force is continuously transferred into the widened end member and further into the gusset plates. The stress level is generally low in these areas, compared with connection types 1 to 3. A small stress concentration certainly occurs at the widening of the hanger (**C**), since an increasing cross section is also a stress concentrator, ALMAR-NÆSS, *[3]*, page 216. The butt weld splice where the widened end member is joined to the hanger should therefore be located below point (**C**) with a sufficiently large distance from that geometric discontinuity. Based on results from further investigation (Section 7.5), a distance of three times the hanger diameter is suggested (Figure 7.15).

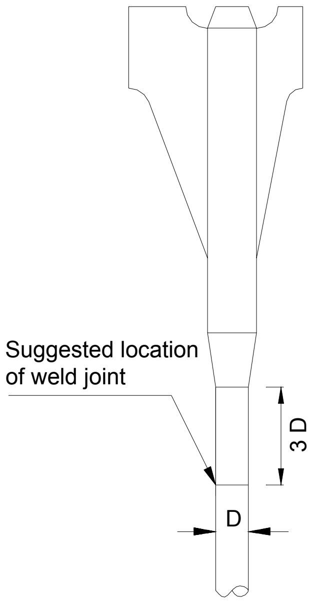

Fig. 7.15. Location of weld joint for connection type 4

Stress is also concentrated at point (**A**), which corresponds to connection type 1. However, in this case the nominal stress and therefore the geometric stress are reduced because of the widened member and are not critical.

The highest stress concentrations occur at (**D**). At these points, radii of 30 mm (**D1**) and 40 mm (**D2**) were introduced so that the lower edges of the gusset plate contact under an angle of 90° to the constraint. That allows continuous welding around the plate. The diversion of forces at the radii causes the stress concentration. At (**D1**) stresses appear to be higher, corresponding to an overall higher stress level on this side of the hanger. This is because the gusset plate on that side provides less cross sectional area.

Further stress concentrations are found at points (**IIa**) and (**IIb**), representing the corners of the continuous constraint, where the gusset plate is welded to the arch profile or an end plate. The absolute value of the minimum principal stress at point (**IIb**) appeared to be greater than the one of the maximum. The minimum principal stresses are illustrated in Figure 7.16.

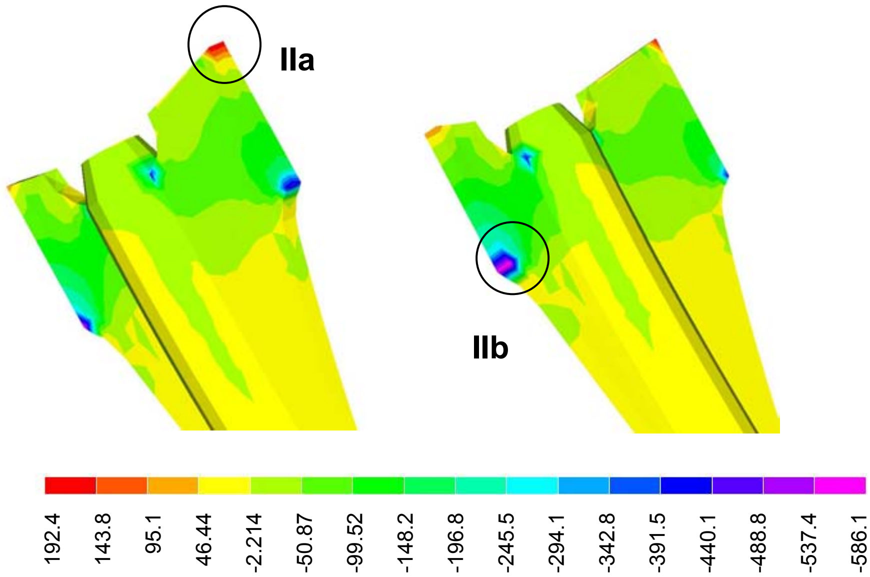

Fig. 7.16 Hanger connection type 4: Minimum principal stress [N/mm^2], deformation exaggerated

The calculation of the SCF calls for the maximum absolute value of principal stresses. Thus, the minimum principal stress is critical for point (**IIb**).

Geometric stress concentration factors (SCF) for axial hanger force:

(**C**): 1.14
(**A**): 1.81
(**D1**): 2.90
(**D2**): 3.26
(**IIa**): 4.85
(**IIb**): 2.96

Even though the absolute value of the stress concentration at (**D1**) is higher than at (**D2**), the calculation of the SCF shows inverse results. It can be seen here, that the pure value of a SCF does not give sufficient information about the actual stress. Moreover, the size of the investigated member has great influence on the nominal stress, which is the second factor besides the SCF. Taking two specimens, equal in geometry, but different in size and subjected to one and the same load, the stress concentration factor is the same for both specimens, although, the actual value of the local stress is higher at the smaller specimen (See Section 7.6).

Fatigue strength curve to be used:

(**C**): If this point is the location of the weld, detail category 90 is to be used (full penetration butt weld). But if the splice is as recommended chosen to be sufficiently distant from the widening, point (**C**) could be categorised in detail category 160 (*ENV 1993-2: 1997 Table L.1/1*). However, a reduction of the fatigue strength is necessary since (**C**) constitutes a geometric discontinuity.

(**A**): This point marks the end of the full penetration butt weld. Therefore, detail category 90 is taken for the assessment (*ENV 1993-1-1: 1992 Section 9.6.3 (2)*), assuming that both the weld profile and permitted weld defects acceptance criteria are satisfied.

(**D**): The stress concentration does not affect any weld. According to Eurocode 3, the fatigue assessment procedure using geometric stress ranges only specifies SN curves for welded connections (*ENV 1993-1-1: 1992 Section 9.6.3*). In this case, the stress concentration occurs on a gas cut edge and detail category 125 is taken (*ENV 1993-2: 1997 Table L.1/1*). A similar assumption is made in GÜNTHER ET AL. *[15]*.

(**IIa**): The ends of the constraints represent locations near fillet welds and are therefore to be classified with detail category 36 (*ENV 1993-1-1: 1992 Section 9.6.3 (2)*). This low detail category and the high stress peak will not fulfil the fatigue criteria. These points are certainly dangerous for the weld joints around the plate at that location.

The utilisation of the fatigue strength at the various points is as follows:

(**C**): 95%
(**A**): 67%
(**D1**): 111%
(**D2**): 68 %
(**IIa**): 385%
(**IIb**): 343 %

It was found that subjected to purely axial load, the whole connection experiences an inclination due to the eccentricity. The hanger is tilted and induces a bending moment around the strong axis of the hanger connection. Stresses due to the bending moment are contained in the stress distribution illustrations and therefore considered in the assessment.

Hanger connection type 5

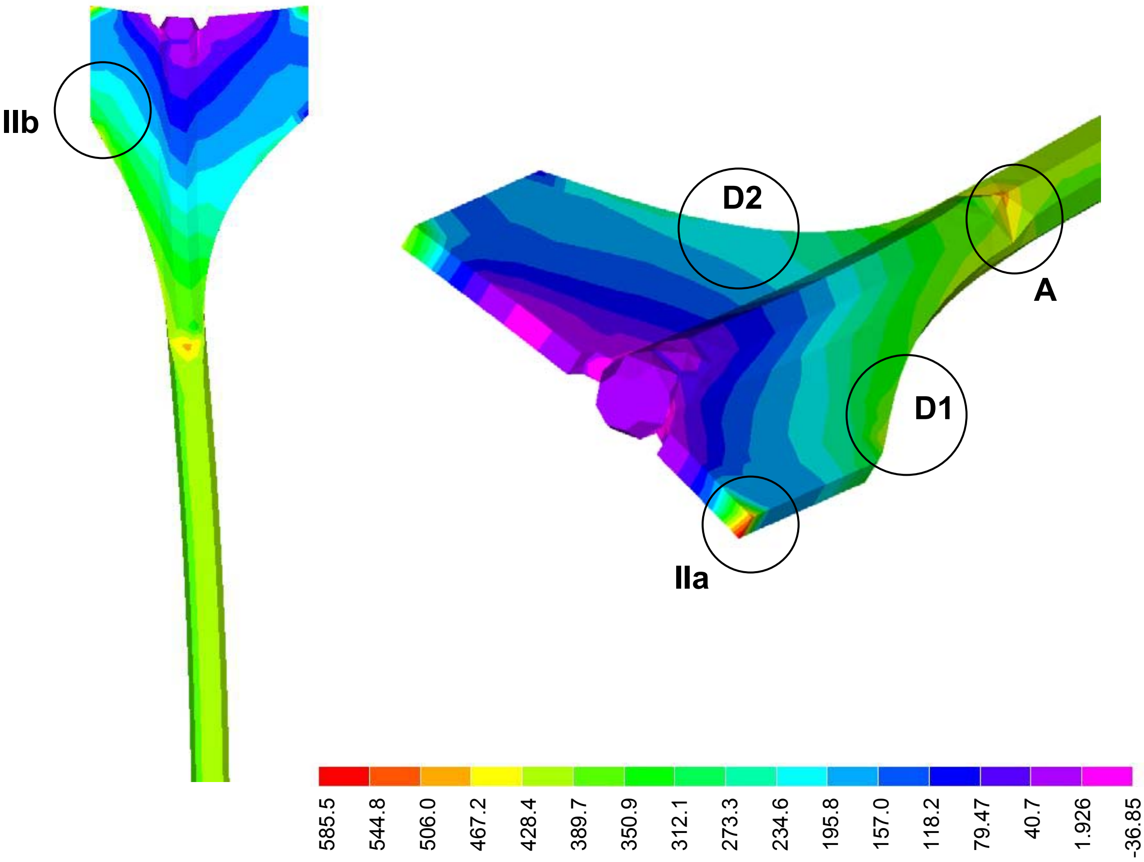

Fig. 7.17. Hanger connection type 5: Maximum principal stress [N/mm^2], deformation exaggerated

For point (**A**) the beneficial introduction of a transition radius has greater effect on the SCF than the disadvantageous elimination of the widened hanger end member of connection type 4. The SCF improved from 1.81 (type 4) to 1.27. However, the absolute stress ranges show opposite results: The geometric stress range for (**A**) in type 4 was calculated to 125.09 N/mm^2, whereas type 5 gives a value of 197.48 N/mm^2. This contradictory effect is discussed in Section 7.6.

In contrast to connection type 4, the lower edge of the gusset plate shows a larger transition radius and connects to the constraint surface with an angle smaller than 90° (**D**). The stress concentration around the circular shaped edge could therefore be decreased.

A further difference is the greater length of the constraint, which reduces the stress concentration directly at the edges of the constraint (**IIa**) and (**IIb**). See also Figure 7.18 for minimum principal stresses.

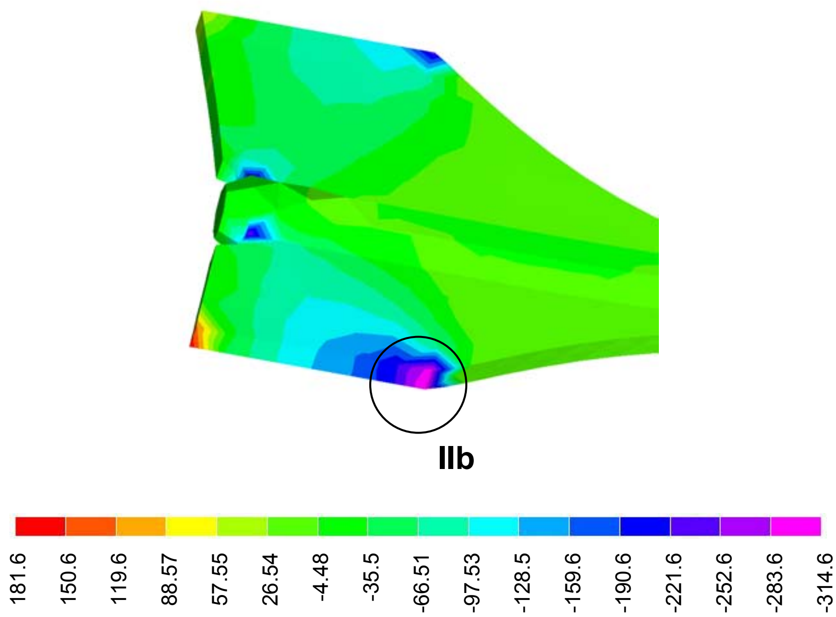

Fig. 7.18. Hanger connection type 5: Minimum principal stress [N/mm^2], deformation exaggerated

The stress concentration at (**IIa**) is greater than at (**IIb**). Since for both points the nominal stress for the fatigue check is the same, only the maximum is of interest.

Geometric stress concentration factors (SCF) for axial hanger force:

(**A**): 1.27
(**D1**): 2.10
(**D2**): 2.36
(**II**): 3.53

Fatigue strength curve to be used:

(**A**), (**D1**), (**D2**) and (**II**): See connection type 4.

The utilisation of the fatigue strength at the various points is as follows:

(**A**): 105 %
(**D1**): 56 %
(**D2**): 43 %
(**II**): 343 %

7.5 Stresses caused by horizontal deflections

According to the assumption made in Section 7.2.2, horizontal deflections of hangers occurring in network arch bridges due to wind load are not expected to cause fatigue damage in the hanger connections. Nevertheless, forces caused by railway traffic may cause fatigue critical vibrations in a horizontal direction. Therefore, it is desirable to investigate their impact. The structural analysis of the 3D bridge model showed a maximum horizontal deflection perpendicularly to the arch plane of 1.18 mm, one meter below the transition between hanger and gusset plate. This value is based on dead loads and lateral wind loads. This combination leads to maximum horizontal deflections; higher hanger forces due to additional live loads cause smaller deflections.

To obtain information about the stress behaviour in the various connection types, the 3D models were subjected to the predetermined 1.18 mm deflection causing bending about their strong axis.

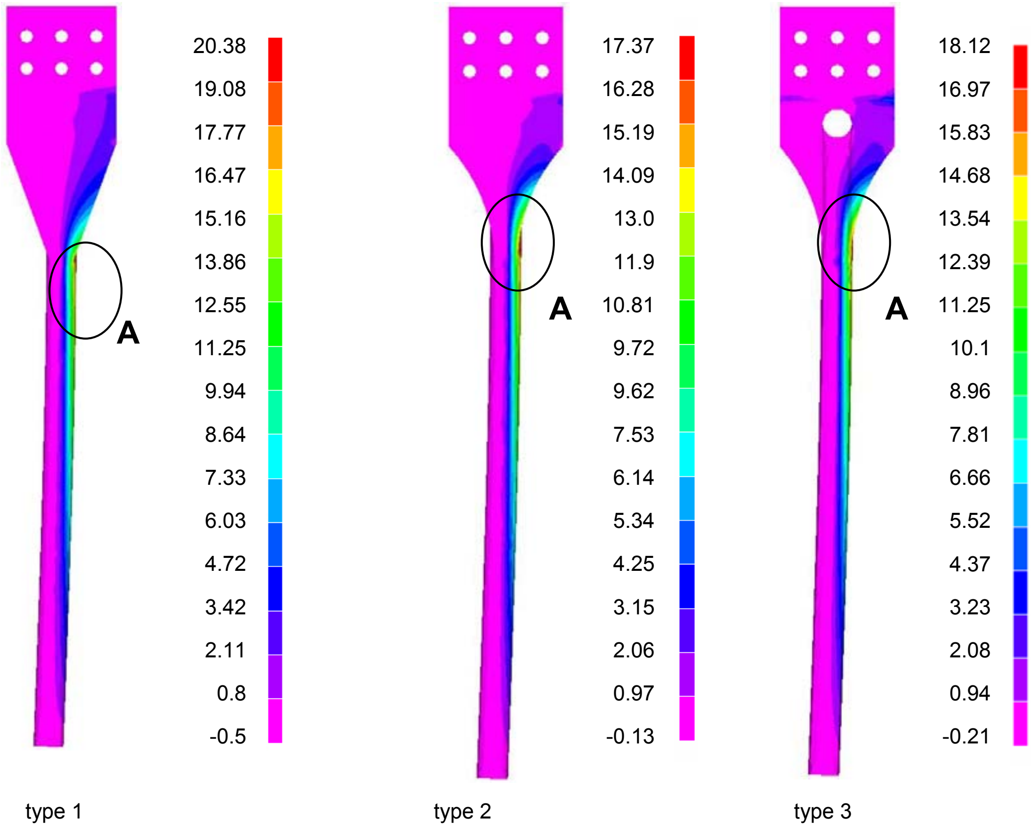

Fig. 7.19. Maximum principal stress due to horizontal deflection [N/mm^2], connection types 1, 2 and 3

An analysis of the stress distribution of connection types 1 to 3 in Figure 7.16 shows highest stress peaks at the previously introduced point (**A**). This point already marks one of the most critical stress concentrations due to axial loading (Section 7.4). Again, connection type 1 appears to be most vulnerable with a stress peak of 20.38 N/mm^2. The introduction of a transition radius (type 2) improves the weak spot, giving 17.37 N/mm^2. Connection type 3 shows a slightly worse result than type 2 because of the different number of gusset plates.

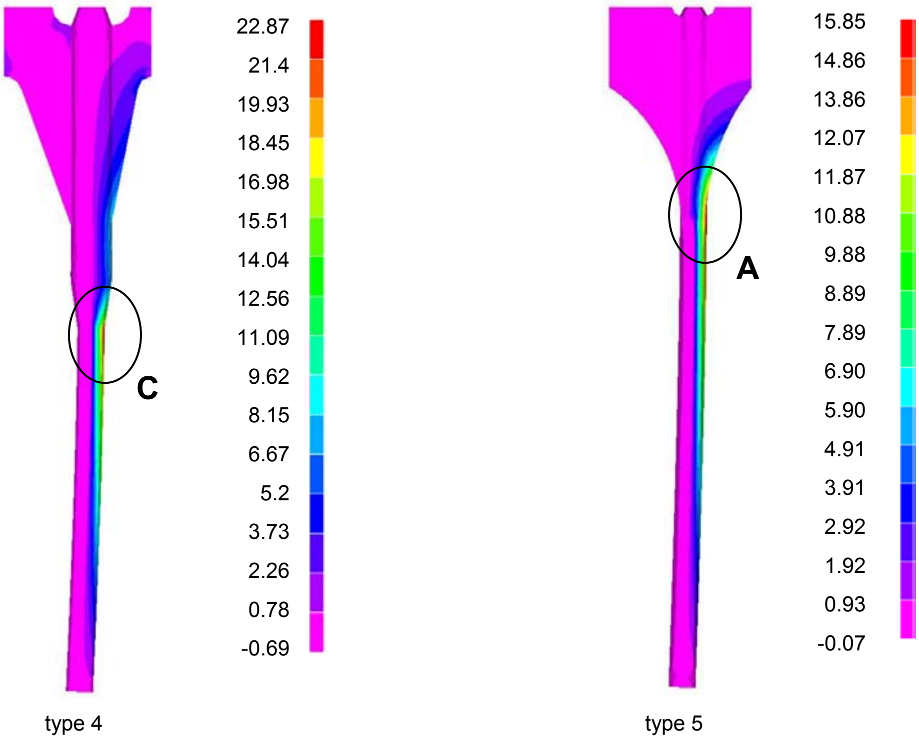

Fig. 7.20. Maximum principal stress due to horizontal deflection [N/mm^2], connection types 4 and 5

The stress peak magnitudes of connection types 4 and 5 differ significantly, which is however caused by the different geometry. Remarkable is the fact that the highest stress concentrations occur at different locations, namely (**C**) in type 4 and (**A**) in type 5. Evidently, the lower end of the widened end part constitutes a critical area and demands, as already found in Section 7.4, that the weld joint is located further below. It was found that a distance of about three times the hanger diameter is sufficient, where the stress concentration is decayed to an acceptable value (Figure 7.15).

The stress concentration at (**A**) in connection type 5 marks the lowest value of all types examined.

7.6 Evaluation

Having carried out the nominal stress range as well as the geometric stress range method using finite element analysis, the following results can be used to decide on the best hanger connection among the various types tested. Since hanger connection types 1 to 3 are of similar geometry, they will be treated separately from types 4 and 5.

Connection types 1 to 3

Advantages and disadvantages can be found in each of the types 1 to 3. The first advantage to mention is the transition radius between hanger and hanger gusset plate. The positive effect can also be found in *ENV 1993-2: 1997 Table L.4/2, detail (2)*, where fatigue strength increases with larger transition radii. Secondly, the application of only one gusset plate is beneficial, because the welds can be executed from both sides over the whole length.

In contrast, it was found that the circular cut-out at the hanger butt end (type 3) is not suitable for a hanger connection with such small dimensions as used in this work. GÜNTHER ET AL. *[15]* found the geometry shown in Figure 7.21 advantageous for bridges subjected to rain-wind induced vibrations. In that article the hanger connection was assessed for an axial force of 1311 kN.

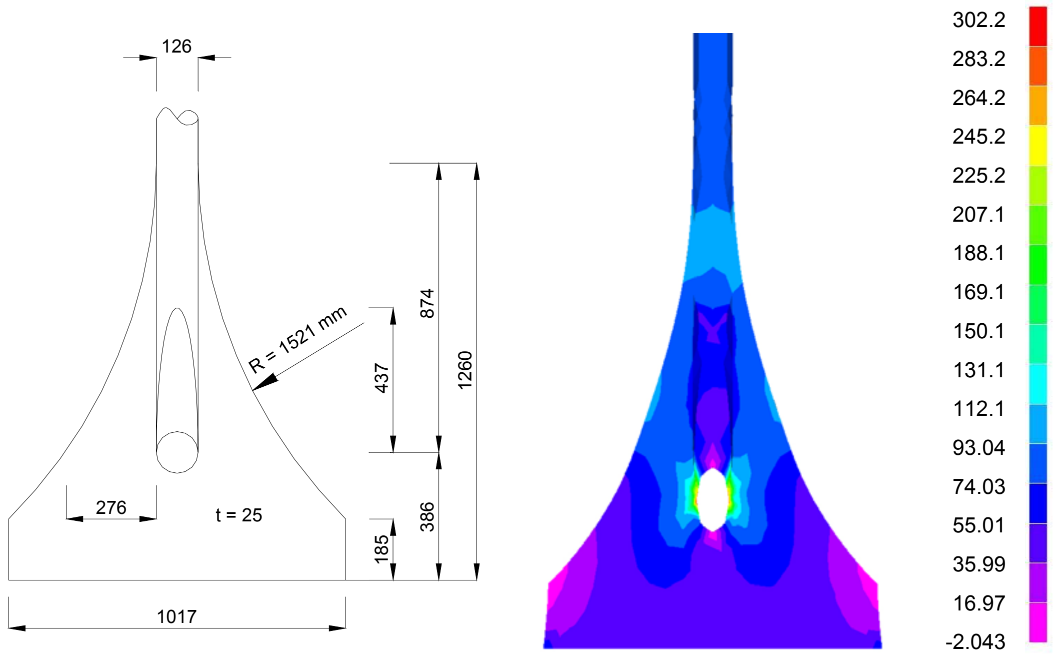

Fig. 7.21. Hanger connection suggested in GÜNTHER ET AL. *[15]*, maximum principal stress [N/mm^2], deformation exaggerated

In this connection detail, the maximum principal stresses due to an axial hanger force of 1000 kN show smaller overall stresses, as well as a smaller stress concentration around the hole compared to connection type 3. The reason for the difference is a greater cross sectional area, hence smaller nominal stresses. The connection in Figure 7.21 shows a ratio between the hole diameter and the gross cross sectional area 126 / (2·276 + 126) / = 0.19, whereas in connection type 3 this ratio is calculated to 60 / 220 = 0.27. This indicates an even smaller stress concentration factor for type 3, but the higher nominal stress has more impact and makes the connection impractical.

This proves that the SCF alone does not give enough information. The simple example of a hole in an infinitely long plate will be taken to explain the behaviour. It can be found in GIRKMANN *[12]*, page 144.

> The diameter of the hole shall be d and the width of the infinitely long plate w. Two extreme cases exist for the hole diameter. For d → w (case 1), the stress concentration factor is determined to SCF = 2, whereas for d → 0 (case 2), the factor is SCF = 3. Assuming the same uniformly distributed load p for both cases, the actual stress at the hole in case 1 will be infinitely high, due to the infinitely small net sectional area. Hence, in spite of the smaller SCF the actual stress is higher in case 1 than in case 2.

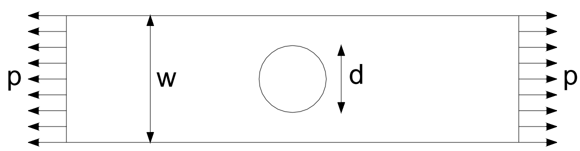

Fig. 7.22. Infinitely long plate with hole, subjected to uniformly distributed load

It is found that the application of a hole is only a feasible solution for bridges where the arch profile allows hanger connections with large dimensions. The wide acceptance and application of the feature 'hole' shows its importance and relevance. Examples can be found in Germany:

- Elbe bridge near Dömitz (semi-circular cut-out)
- Teltow-channel bridge (kidney-shaped cut-out)
- Oder-Havel-channel bridge (semi-circular cut-out)

The circular cut-out was originally adopted for connection type 3 because the sharp 90° edges as well as the transverse butt weld of the hanger end to the gusset plate constitute weak points. Firstly, the edges mark possible starting points for notches and cracks. Secondly, the existence of both transverse and longitudinal welds is a reason for additional residual stresses.

To improve the first, it is suggested to equip the corners with a small transition radius, which requires the equivalent at the hanger end. The round corner can then more easily be ground to a smooth surface (Figure 7.23). To reduce residual stresses, it is recommended to follow a certain sequence for the welding process. The transverse weld at the hanger end should be executed first, followed by the longitudinal welds. It is supposed that this method of fabrication contributes to the feasibility of this connection detail.

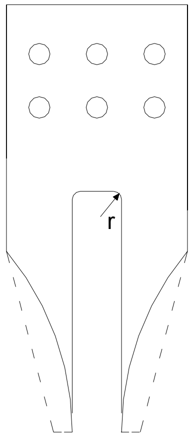

Fig. 7.23. Smooth round corner in cut-out of gusset plate

Connection types 4 and 5

Very high stress concentrations were found at points (**IIa**) and (**IIb**) in connection types 4 and 5 (Figure 7.16), and the fatigue strength using the SN curve for category 36 (fillet welds) is far too much exceeded. Using the nominal stress method, the appropriate detail category appears to be category 80 (*ENV 1993-2: 1997 Table L.5/3*), with which the fatigue check is fulfilled with 65% (**IIb**). It is therefore uncertain how to judge the FEM result.

The widened hanger end member proved to be advantageous for the assessment of location (**A**) and can generally be suggested if the connection is welded to the arch, as in STEIMANN *[37]*. It is recommended to locate the weld joint between hanger and widened hanger end at a distance of three times the diameter below the transition. In that way it does not lie in the stress concentrated range.

Suggested hanger connection

The similar overall geometry of connection types 1 to 3 recommends combining the advantageous features and abolishing the weaknesses. Figures 7.24 and 7.25 show the suggested connection detail.

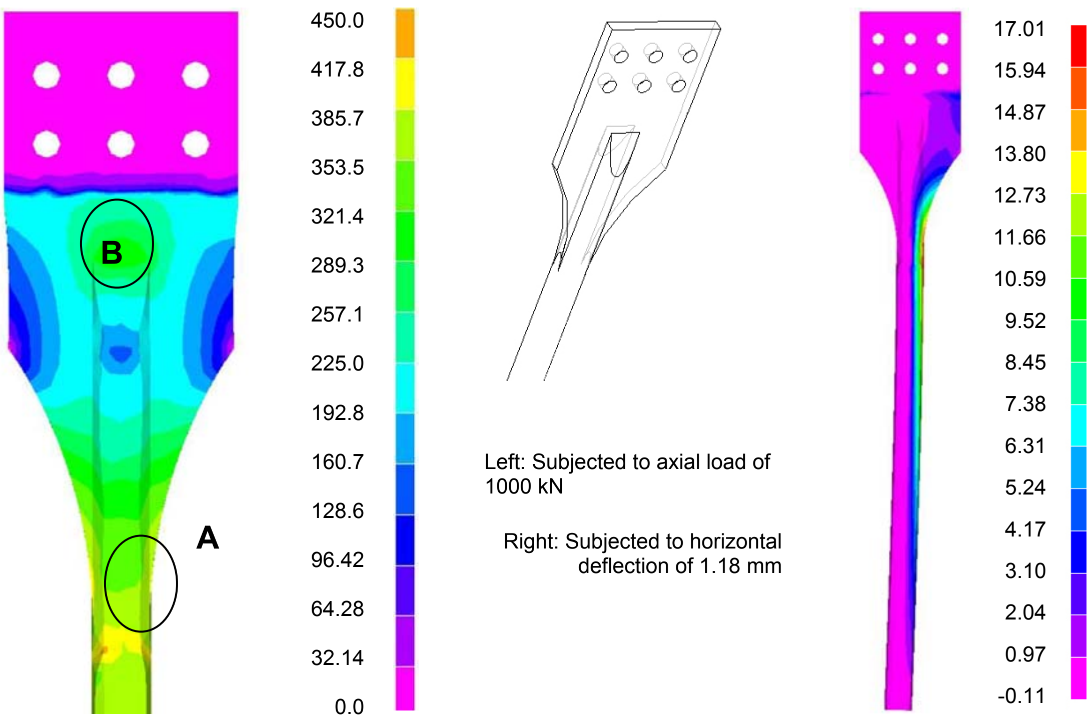

Fig. 7.24. Suggested hanger connection: Maximum principal stress [N/mm^2], deformation exaggerated

The connection detail consists of a single gusset plate, in which the hanger is inserted and joined by means of full penetration butt welds executed from both sides. The weld should be ground flush to the surface to provide smooth transitions between the adjacent members. The above suggested round corner in the gusset plate cut-out will be applied as well.

The beneficial transition radius between hanger and plate is also adopted and leads to an acceptable low stress concentration.

The suggestion of a greater insertion length (Section 7.4.2, hanger connection type 2) is adopted resulting in a smaller stress peak at (**B**) compared to connection type 2.

Geometric stress concentration factors SCF due to axial load:

(**A**): 1.14
(**B**): 1.34

The utilisation of the fatigue strength at the various points is as follows:

(**A**): 94 %
(**B**): 72 %

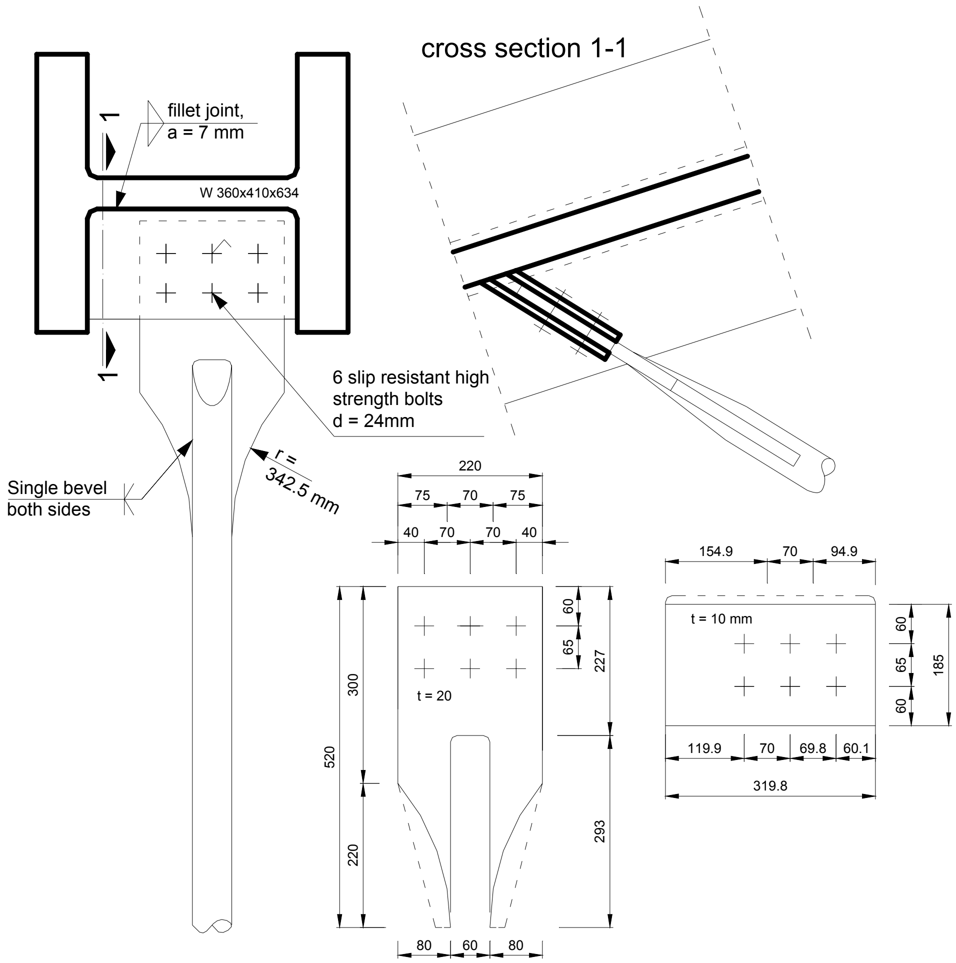

Fig. 7.25. Dimensions of suggested hanger connection

Summary

The obtained data on stress distributions in the connection details confirm certain stress concentrations at points considered as critical by detail categories in the Eurocode. These are points (**A**), (**B**) and (**C**), since they constitute geometrical discontinuities.

In contrast, the stress concentration at (**D**) had not been expected. It is questionable if the stress peak at (**D**) is relevant for fatigue or not, since no weld joint is directly affected. If the plate edge contains notches, a fatigue failure could be expected. The material should be machined after gas-cutting to reduce the danger of fatigue failure.

Comparison of results (utilisation of fatigue strength in %)			
connection type	location	method of assessment	
		nominal stress	geometric stress
1	**A**	166	119
	B	41	74
2	**A**	83	94
	B	41	78
3	**A**	83	96
	B	-	285
4	**C**	93	95
	A	74	67
	D1	-	111
	D2	-	68
	IIa	-	385
	IIb	65	343
5	**A**	83	105
	D1	-	56
	D2	-	43
	II	-	343
suggested type	**A**	83	94
	B	41	72

Fig. 7.26. Comparison between results from nominal stress and geometric stress ranges

In Figure 7.26 results from both assessment methods are compared. It can be seen that the assessment based on geometric stress ranges is beneficial for location (**A**) in connection type 1. Using the most appropriate detail category from Eurocode 3 is evidently too far on the conservative side. The actual result obtained from the FEM analysis shows a significant improvement from 166% to 119% utilisation of fatigue strength. If connection type 1 is designed with greater dimensions than in this work, it may certainly result in a feasible solution satisfying the fatigue assessment.

Comparing the results for (**A**) in types 2 and 3 leads to different conclusions. The assessment based on nominal stress ranges underestimates the stress peaks obtained from the FEM analysis. This is even more the case for location (**B**) in types 1 and 2. One explanation is that the detail categories used assume slightly different conditions and do not entirely correspond to the actual situations. For example, the chosen detail category 36 (*ENV 1993-2 Table L.3/2*) used for location (**B**) in types 1 and 2 assumes a butt splice of two plates with free edges, whereas the hanger is welded to the gusset plate on three faces. Moreover, category 36 presumes equal and constant plate thickness for both plates. The bevelled hanger end incorporates a slope and therefore a kink in the surface, which is a geometric discontinuity that increases the stress concentration.

In addition, the low category 36 results from the fact that a butt weld is carried out from one side. Using the SN curve of detail category 90 for the assessment based on geometric stress ranges does not distinguish between butt welds carried out from one side and welds carried out from two sides.

A further reason might be simplifications made for stress distributions. The stress distribution along the transverse and longitudinal butt welds in type 1 and 2 was taken as constant, which is an approximation and implies deviations from the actual distribution.

It was not possible to assess the stress concentration at the hole (**B**) in connection type 3 with the help of nominal stress ranges. Eurocode 3 does not contain any detail category which corresponds to that particular point. Even adopting the standard example 'hole in a plate' underestimates the actual conditions of the specific hanger connection detail, and the FEM analysis appeared to be essential for judging this connection.

7.7 Connection to arch profile (based on nominal stress ranges)

The connection between the circular hanger profile and the gusset plate(s) is clearly the most critical detail of the whole connection. However, it is still important to examine the fastening of the gusset plate to the arch profile.

It is advantageous to have bolted connections which can easily be fastened on site. According to Eurocode 3 for steel bridges (*ENV 1993-2: 1997 Section 6.4.3*), either fitted bolts or preloaded bolts shall be used in shear connections. Connections with fitted bolts demand higher accurateness for assembling than preloaded bolts in holes with standard clearance. The Eurocode 3 further recommends designing preloaded bolts to be non-slip at the ultimate limit states.

The geometry of the suggested hanger connections (Section 7.6) allows a bolted connection to a gusset plate which is welded between the flanges of the H-profile (Figure 7.27). This leads to detail category 112 (*ENV 1993-5: 1997 Table L.1/2*) for a double sided connection with preloaded high strength bolts (**I**).

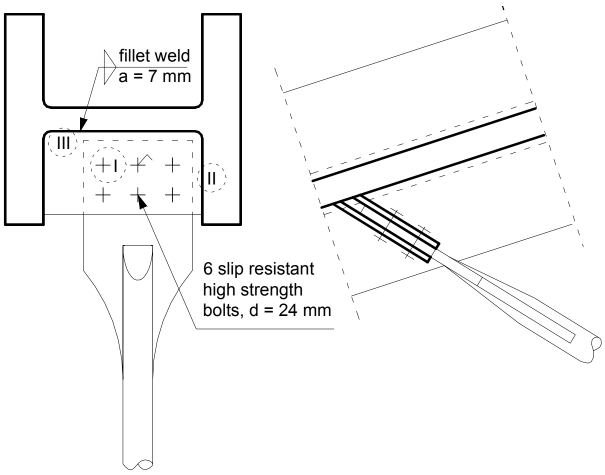

Fig.7.27. Welded connection to arch profile

The shop-welded joint between gusset plate and arch leads to two detail categories. One predicts a crack in the fillet weld (*ENV 1993-2: 1997 Table L.5/3*, detail category 80), the other predicts a crack in the arch profile (*ENV 1993-2: 1997 Table L.4.2*, detail category 80). If the arch segments are joined by means of full penetration butt welds giving detail category 90 (*ENV 1993-2: 1997 Table L.3/1*), the fillet weld at (**II**) marks the most critical point for the fatigue assessment. In cases where this would lead to the application of a larger profile, an alternative joint is proposed where the gusset plate is connected to the arch with bolts (Figure 7.28).

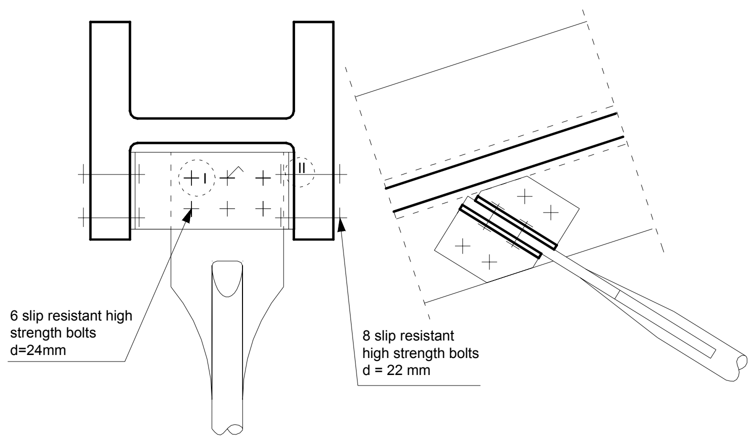

Fig.7.28. Bolted connection to arch profile

The one sided connection with preloaded high strength bolts (**II**) gives detail category 90 (*ENV 1993-2: 1997 Table L.1/2*), which is better than the welded connection. The two U-shaped plates need to fit exactly between the flanges to avoid restraining forces. Therefore, it is suggested to prefabricate this bolt connection, whereas the connection at (**I**) can be fastened on site.

Types 4 and 5 are not suitable for bolt connections such as in Figure 7.28. The continuous hanger does not allow the application of U-shaped plates between the flanges. Moreover, the two gusset plates on either side of the hanger do not provide enough space to accommodate bolts in a connection with L-profiles. Here PER TVEIT suggests bolted end plate connections which would still have to be examined (Figure 7.29).

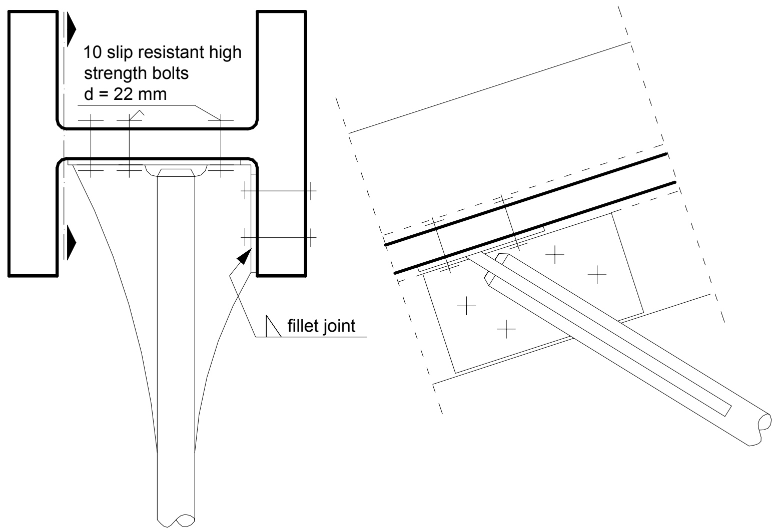

Fig.7.29. Bolted end-plate connection for connection types 4, 5

Instead of end-plate connections on either side which would have to be fitted exactly between the flanges on site, only one end-plate connects to the flange, whereas the other is bolted to the web.

The bolts in the flange end-plate connection are subjected to shear, similar to the previously discussed connections. The web end-plate connection is subjected to tension as well as shear, which is due to the inclination of the hanger. Therefore, preloaded bolts are essential here. Fitted bolts are not an option.

Due to the eccentricity of the hanger force, a torsional moment arises. This is the case for all connection types and the torsional moment can undoubtedly be taken by the arch profile. However, the geometry and the locations of fastenings of this hanger connection make it difficult to assess for and trace the transmission of the torsional moment into the profile. An assessment was not carried out. A solution might be a stiffening plate shop-welded between the top parts of the flanges to ensure that the torsional moment can be transferred into the arch profile.

7.8 Hanger connections along the tie

Different conditions are found for the hanger connections along the lower chord. Their size is not as much constricted as is the case with the connections along the arch, and significantly larger connection plates can be used (Figure 7.30). Therefore, design checks are not expected to become critical and were omitted in this work. In cases where design checks cannot be satisfied, the dimension of the connection can be increased. However, this has to account for transverse prestressing, which might intersect with the hanger connection detail. An end plate was chosen to be 410 mm long. Since the transverse prestressing thread bars are spaced with s = 270 mm, intersections are inevitable. But if either a hole is used at the end of the hanger, GÜNTHER ET AL.

[15], or as in this case the cut out is extended to the lower end of the vertical hanger gusset plate (Figure 7.30), the thread bars can go through the opening.

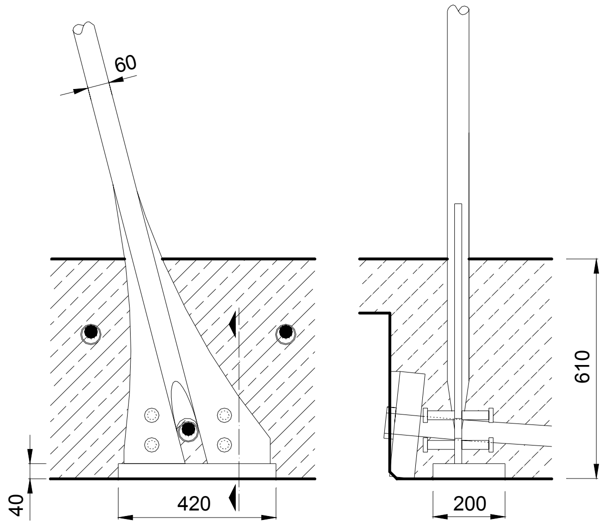

Fig.7.30. Hanger connection along the lower chord

The hanger plate is equipped with shear studs which transfer the horizontal hanger forces into the bridge deck. STEIMANN *[37]* showed that 8 shear studs with a diameter Ø22 are sufficient. Even though the bridge calculated in this work gives smaller maximum hanger forces, the hangers are more inclined than in STEIMANN *[37]* which leads to a higher horizontal component. Without a design check, it was decided to use 8 shear studs with a diameter Ø25 instead of additional studs.

It ought to be mentioned that it might be possible to reduce or even eliminate the shear studs, since hanger forces are also transferred by friction increased by prestressing.

7.9 Notes on the FEM analysis

Creating three dimensional models and determining stress results with the help of a finite element analysis programme incorporates certain aspects which have to be considered in order to be able to judge the result. The following information is supposed to give assistance and explain possible derivations from analyses carried out under different conditions.

In *NE/Nastran* (Annex C, Section C.1) the interaction between elements is based on forces exerted at the so-called grid points, where elements are connected together. The stiffness of the structure, discretised at the grid points, is generated with data on material properties and geometry. Both stiffness and forces are used to calculate displacements with which stresses and strains are generated. It was decided to use tetrahedron elements with an additional mid-node.

The mesh size of the model has significant influence on results. For each model the default mesh size suggested by *NE/Nastran* was adopted. According to ABS *[1]* it is advisable to create smooth transitions without abrupt changes in mesh sizes. The meshes did not show discontinuities in the form of abrupt changes in element size, so it was not necessary to manually remesh the model. Few warnings occurred during the analyses indicating very steep face angles exceeding 80°.

The mesh sizes varied depending on the model between 10 and 20 mm, which corresponds approximately to the thickness of the gusset plates.

The colour gradation appears to be very coarse. The different colours in the FEM result illustrations represent mean values and the given magnitudes constitute upper and lower boundaries of each colour. For the evaluation, only the mean values were considered.

Erection of the bridge using a temporary lower chord

8.1 Why a temporary lower chord

Many common arch bridges with vertical hangers possess lower steel chords consisting of transverse and longitudinal beams. Together with the arches and the hangers they form a steel skeleton strong enough to bear itself when lifted at the ends of the bridge. This gives considerable advantages for erection because the steel skeleton can be mounted accurately on side spans or construction sites besides the bridge location and then be displaced.

To exploit properly the structural behaviour of network arch bridges no permanent steel chord should be used. It is normally best to design the bridge with a concrete tie. But then the heavy self-weight impedes then a simple lift with ordinary hoisting devices.

The solution given by PER TVEIT is a temporary lower steel chord similar to the lower steel chords mentioned above. Since the temporary lower chord is only subjected to loads during erection of the bridge, it can be of a very light and efficient design. For the transversal beams the fresh concrete of the bridge deck gives maximum strains; decisive loads for the longitudinal beams are the self-weights of formwork, reinforcement and tendons. After erection the temporary lower chord is removed and can be reused, with some modifications, to erect other network arches or to serve for other structures.

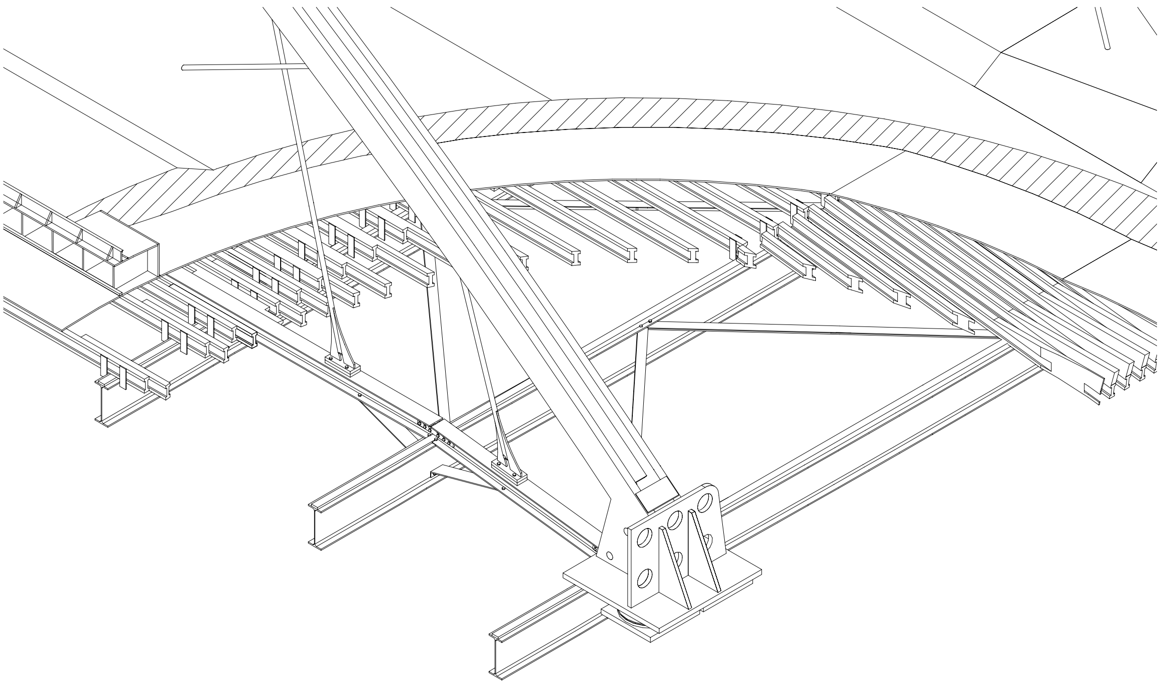

Fig. 8.1. Temporary lower chord and formwork at arch root point

For the bridge, the object of this work, a temporary lower chord was designed and assessed for all construction phases. It was refrained from listing every detail of the investigation in this section. All results are found in Annex E.

8.2 The design of the temporary lower chord and formwork

Formwork sheets

The top layer consists of 18 mm thick plywood formwork sheets, for example *Dokaplex formwork sheet, [9]*. In transverse direction six sheets with a width of 1.5 metres, two with a width of 1.25 metres and two with a width of 1 metre are needed to ensure that all edges of the formwork sheets are supported. The deflections due to fresh concrete do not exceed 0.83 mm, and therefore a virtually plane bottom surface of the bride deck can be provided.

Formwork beams

The plywood rests on longitudinal timber formwork beams with a height of 200 mm, for example *Doka formwork beam H 20 P*, *[8]*. They have a length of 4.5 metres and span 3.5 metres, which means they provide double cross section due to overlapping on a length of 1 metre at the supports. Their mid-span deflection of 4.7 mm equivalents L/750 and is tolerable in respect of a plane bottom surface, *ENV 1992-2: 1996; 4.4.3.1 (105)*.

Formwork for cantilevers

The formwork for the cantilevers consists of vertical plywood posts sawn to the required shape and horizontal formwork sheets. The vertical posts are spaced at distances of 0.5 metre. Laths are applied to ensure a transversely non-sliding constraint (Figure 8.2).

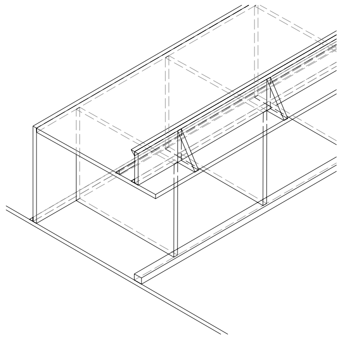
Fig. 8.2. Formwork for cantilever

Transverse steel beam

The formwork beams are supported by transverse steel beams. This is the member of the temporary lower chord subjected to largest forces, mainly bending moments. An IPEa 550 profile proved to be necessary by assessment. As part of the wind bracing it also receives axial forces. To prevent lateral torsional buckling it is restrained at the top flange by wooden cams nailed to the timber formwork beams. The structural system is a simply supported beam with a span of 10.15 metres and 1.45 metres cantilevers at both sides. The deflections of the transverse beam will be countervailed by applying a wooden camber with the shape of the deflection line on top of the steel beam. This camber accounts for deflections due to fresh concrete, maximum 54.4 mm, and ballast, sleepers and rails. Furthermore, it is used to compensate for the 20 mm difference in the height of the longitudinal steel beams and the timber formwork beams.

Diagonal members of wind bracing

Serving as diagonal members of the wind bracing three profiles L 120x10 are collocated between two transverse steel beams as shown in Figure 8.3. They are bolted to the top flange of the transverse beams.

Longitudinal steel beam

The transverse steel beams are supported by longitudinal steel beams in the arch planes. The upper flanges of the transverse beams are attached with bolts to the lower flanges of the longitudinal beam. The longitudinal beam is subjected to axial forces and bending moments during the first

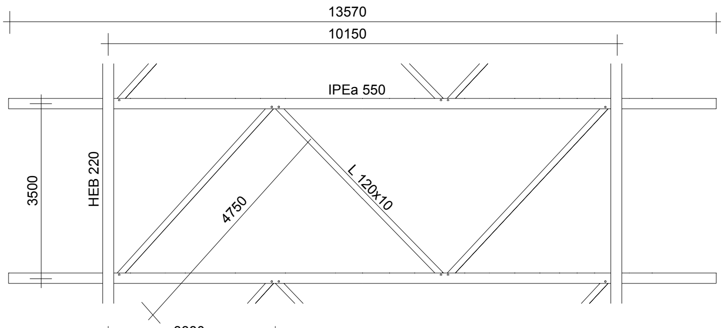

Fig. 8.3. Structural system of the temporary lower chord

construction phases. This load case is decisive for the assessment. The bending moments will increase when casting the bridge deck. Since the longitudinal beams are disconnected from the arch at this time, they will not receive axial forces and therefore additional capacity is released to bear more bending. A HEB 220 profile was found to be sufficient for the bridge calculated in this work. Eight beams with a length of 12.5 metres are needed for each side of the bridge. They are connected by butt joints with bolted cover plates.

At the lower hanger ends the longitudinal beam is connected with bolts to the end plate of the hanger connection detail. Between this plate and the top flange of the profile an 18 mm thick wooden board is placed, to ensure that the lower surface of the hanger connection plate is in one plane with the bottom surface of the bridge deck. Cut-outs are made in the formwork at these points.

8.3 Special considerations on the end of the temporary lower chord

The geometry described in Section 8.2 is appropriate for almost the whole span of the bridge. At the ends there are adaptations necessary due to the higher load of the end cross girder and the transmission of forces between the arch root point and the longitudinal temporary steel beam.

The bottom surface of the bridge deck is inclined near the end cross girder. This causes a kink in the longitudinal steel beam. The additional forces rising from this eccentricity are distributed to the nearby hangers by a truss. The web of the transverse beam at the break point forms the compression member. To obtain the desired horizontal bottom surface of the end cross girder the formwork beams receive a wooden triangular camber on their top, see Figure 8.1. The number of timber formwork beams is increased and the last transverse steel beam consists of an IPEv 550 profile to bear the higher loads.

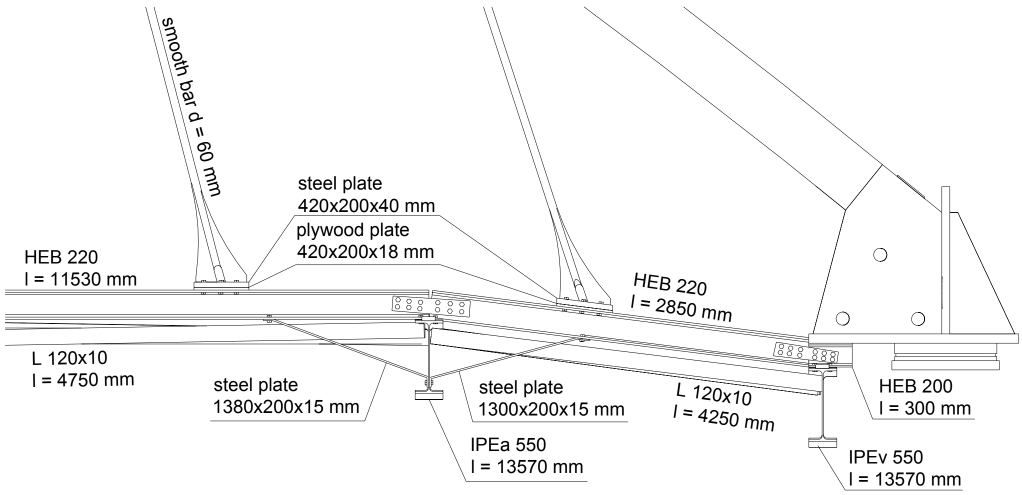

Fig. 8.4. Connection of temporary lower chord to arch root point, deflected state

8.4 Sequence of erecting the bridge

In order to explain the erection of the bridge more clearly, its construction is divided into 4 phases.

1. Mounting the steel skeleton and displacement

On already built foreshore bridges or a suitable site near the final bridge location the steel skeleton is assembled. Mounting the steel skeleton starts at one end of the span and is mainly done by one crane. The sequence should prevent erected parts from obstructing the access by the crane. Therefore, the erection method depends to some extend on the width of the place where erection is done. The stages of erection are as follows:

1a: Erecting the scaffolding on the inner sides of the planes of the arches
1b: Laying out the transverse steel beams
1c: Attaching the longitudinal beams to the transverse steel beams
1d: Connecting the diagonal wind bracing members to the transverse beams
1e: Putting the arch segments on the scaffolding
1f: Welding the arch splices and connecting the arch root point to the temporary longitudinal beams
1g: Connecting the members of the main wind bracing to the arches
1h: Connecting of the hangers first to the top and then to bottom connection details
1i: Removing of the scaffolding

The steel skeleton is now ready to be lifted at the ends of the span and transported to the final position. The total weight to be lifted is about 300 tons. Depending on the particular circumstances the appropriate method out from a great variety should be chosen. Pontoons or floating cranes are a possibility for river crossings; mobile cranes for an inland crossing.

2. Preparations for casting the bridge deck

Once the steel skeleton is in place formwork, reinforcement and the prestressing tendons can be laid out.

2a: Applying wooden parts to form the camber on top of the transverse steel beams
2b: Completing the timber formwork beams with wooden cams and putting them into place
2c: Laying out the formwork sheets
2d: Attaching the temporary railings

Steps 2b to 2d should be performed in a certain sequence. Work should start from both ends of the bridge simultaneously.

2d: Finishing the formwork under the cantilevers
2e: Putting into place the reinforcement and prestressing tendons

Due to the complicated crossing of the reinforcement and the prestressing tendons in the area of the concrete edge beam it is necessary to complete the reinforcement for the whole bridge. It can not be made separately for different construction stages. For an example of the sequence see TVEIT *[45]*, page 50.

2f: Applying formwork sheets with special cut-outs for the reinforcement between the end cross girder and the main part of the bridge deck, this also applies to the edge beams
2g: Casting of the end cross girder and first several metres of the bridge deck until the free parts of the two designated longitudinal tendons are straight across the span
2h: Curing of the concrete
2i: Partial prestressing of transverse tendons in end cross girder, three days after step 2g

At this construction state the temporary longitudinal steel beams take decisive forces.

2j: Partial prestressing of the two mentioned longitudinal tendons with 650 kN each

3. Casting the edge beams

3a: Casting one of the edge beams with a footpath beginning at mid-span and proceeding simultaneously towards both ends of the bridge

Since it is desirable to avoid hangers relaxing in fresh or semi-hardened concrete, it was examined whether starting from either both ends or mid-span gives a better result (See Annex E, Section E.8 of this work). For the bridge, the object of this work, starting from mid-span is more appropriate. It depends on the hangers' resistance to relaxation.

3b: Curing of the concrete
3c: Casting the other edge beam with a footpath beginning at mid-span and proceeding simultaneously towards both ends of the bridge
3d: Curing concrete
3e: Removal of formwork between edge beam/end cross girder and the main part of the bridge deck
3f: Partial prestressing of all longitudinal tendons with 25% of the design value, three days after step 3c, meanwhile disconnecting the temporary longitudinal steel beams from the arches

The concrete edge beam now contributes to the structural behaviour of the span.

4. Casting the rest of the bridge deck and finishing the main work

Due to the length of the bridge and the time necessary to shape the inclined upper surface properly, the casting of the deck was divided into three construction stages as shown in Figure 8.5.

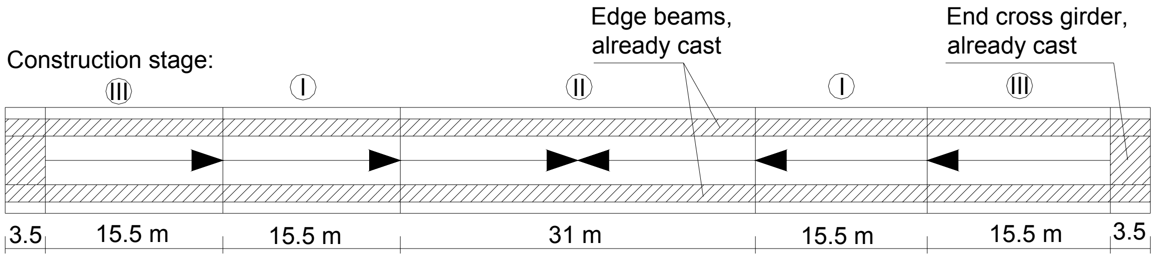

Fig. 8.5. Casting sequence of bridge deck in construction phase 4

The correct order and direction of casting were found by numerical analysis and prevent any hanger relaxing. The possibilities starting from either both ends or mid-span were also examined, but found to be inappropriate due to extensive relaxation of hangers.

4a: Casting the bridge deck in the construction stage I
4b: Casting the bridge deck in the construction stage II
4c: Casting the bridge deck in the construction stage III
4d: Removal of formwork underneath the cantilevers
4e: Full prestressing of transverse tendons in end cross girder three days after step 4c
4f: Full prestressing of all longitudinal tendons
4g: Full prestressing of the transverse tendons simultaneously at both bridge sides
4h: Attaching the railings to the cantilevers

Now the temporary lower chord can be removed and the holes of the bolted connections to the hangers filled. More details about this can be found in TVEIT *[45]*, pp. 52-55.

4i: Finishing the expansion joints at each end of the bridge
4j: Casting the space behind the anchorages of the longitudinal tendons
4k: Prestressing the transverse tendon behind the anchorages of the longitudinal tendons, three days after step 4j

Summary

The structural members of network arches are mainly subjected to axial forces. Generally, structures with this characteristic are considered as efficient.

The cross-section of the arch is designed for the axial force and the bending moments in the wind portal frame. The application of a truss with diagonal struts instead of a single bending resistant top member in the portal frame decreases the portal frame length and therefore the transverse bending moments in the arch.

After having carried out the optimisation process of the hanger arrangement the authors found their assumptions confirmed. A simple solution for an improved hanger arrangement is obtained if all hangers cross the arch at the same angle. The upper hanger nodes are equidistant. At the ends of the arch special considerations are necessary due to the disturbance range caused by the clamping. Several investigations have been carried out to determine a favourable size of the cross angle. For final conclusions these investigations have to be continued.

Common solutions for hanger connection details have to be adapted for network arches because the more slender arch profile does not provide enough space to accommodate the connection details. Especially the application of a hole at the hanger's end leads to unfavourable results due to the small gusset plate. Possibilities have been found of shaping a hanger connection detail with a satisfying resistance against fatigue strains.

At a transverse span of the bridge deck of about 10 meters concrete ties without transverse prestressing show slight economic advantages compared to those with transverse prestressing. Advantages of the prestressed alternative are less deflection, smaller depth and the possibility of avoiding cracking as a result of systematic compressive stresses.

The arch root calls for special attention while designing it. The stress range due to live load is likely to exceed the allowed limits, because of the skew weld between the arch and the end plate which takes nominal stresses and shear stresses from the large axial force in the arch. One possible solution to improve this detail is enlarging the flanges of the arch profile and transferring the forces partially to the horizontal plate above the bearings. The minimum distance of the prestressing strand anchorages and the end cross girder require an enlargement of the concrete tie at the arch root.

The drainage of the bridge also needs adapted solutions due to the extraordinarily slender lower chord. It has been shown that various possible methods exist. The feasibility of the drainage has to be considered already when designing the cross-section of the tie.

The investigation of the alternative 'stilt bearing' showed its applicability. It might be a cheaper solution where material is more expensive than labour hours. It could also lead to more economic details at the ends of the arches. Otherwise pot bearings convince with a clear transfer of forces, no restraining forces and easy handling.

The erection of a network arch can be performed using a temporary lower chord. The steel skeleton consisting of the arches, hangers, wind bracing and temporary lower chord can be lifted at the ends of the bridge and transported to the final position. Following the described sequence the longitudinal prestressing can be utilised to release the temporary longitudinal steel beams from axial forces. The casting sequence of the edge beams and the bridge deck is to determine for each project, since relaxing of hangers in fresh or semi-hardened concrete can occur. The necessary structural steel for the temporary lower chord is 15 % of the permanent structural steel.

Compared to other railway arch bridges the calculated network arch saves a significant amount of steel.

As stated in the introduction, the authors hope that more bridge engineers will consider using this type of bridge.

Criticism and proposals for future work

While working on this thesis, some investigations had to be aborted to proceed with others. Nevertheless, the authors continued thinking about the results and found mistakes and new ideas. This section is supposed to help to evaluate the results, prevent repetition of the mistakes and encourage further investigation of the ideas which seem important to the authors.

Optimisation of the hanger arrangement

According to the theory described in Section 6.6.2 an improved hanger arrangement is likely to be found by determining the line of thrust in a network arch. The authors decided on the radial arrangement because of its easy applicability. It is necessary to further investigate a favourable hanger direction especially at the arch ends. Furthermore it is desirable to determine the direction of the arch deflection relevant for the hanger forces.

The authors underestimated the influence of the stiffness ratio between arch and tie on the structural behaviour. Tests with various stiffness ratios showed significant deviations of cross angles giving small bending in the arch. An investigation of this parameter is definitely needed.

Combining the various demands of the attributes of an optimisation process requires a certain weighting. The one assumed in Section 6 is based on an equal weighting of the considered attributes. It is necessary to determine weighting factors taking into account the real ratio of the various demands in the assessment of a bridge.

Concrete tie

For the two alternatives without transverse prestressing the required number of longitudinal tendons was determined approximately. Since total costs differ only little, the price of the longitudinal tendons may influence the results of the comparison. Exact calculations of the necessary number of tendons are desirable.

"Stilt" bearing

For the assessment of the vertical bearing plate, formulas according to *Hertz pressing* were used. Considering the small cross section provided underneath the contact surfaces, these formulas give non-conservative results. Examination of more appropriate methods, maybe using finite element analysis, is desirable.

FEM-analysis of connection details

Applying finite element software requires verification with the help of a patch test. This principle was not respected. The consequences of this omission will be ascertained at this point by carrying out a patch test.

As a basis for the verification the standard example hole in a plate was chosen. The stress concentration factor in a plate around a hole with a diameter of one third of the plate width is approximately 2.5, GIRKMANN *[12]*, page 144. Further information on this standard example is given in Annex D, Section D.3.4. The following dimensions of the plate were used:

Width W = 300 mm
Thickness T = 25 mm
Length L = 1000 mm
Diameter of the hole D = 100 mm (symmetrical to the plate)

In a first test (Figure 10.1), the plate is modelled and meshed in such a way that the conditions correspond to the analyses of Section 7. The plate is constrained at the left short face and subjected to 1000 kN at the opposite face, leading to a nominal stress at the net section of σ_o = 1000 kN / (25 · 200) = 200 N/mm^2. The stress peak is found to be 441.7 N/mm^2 which gives a stress concentration factor SCF of 441.7 / 200 = 2.21.

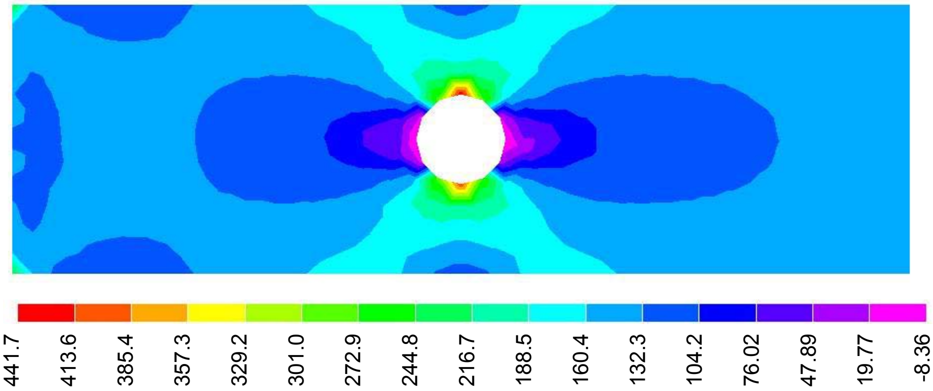

Fig. 10.1. Reference plate with hole, coarse mesh, maximum principal stress [N/mm^2]

In a second test (Figure 10.2) a finer mesh was chosen leading to a stress peak of 462.4 N/mm^2 and therefore a SCF of 462.4 / 200 = 2.31. Considering a possible range of a SCF between 2.0 and 3.0, both results appear to vary significantly from the predicted value of 2.5 in GIRKMANN *[12]*.

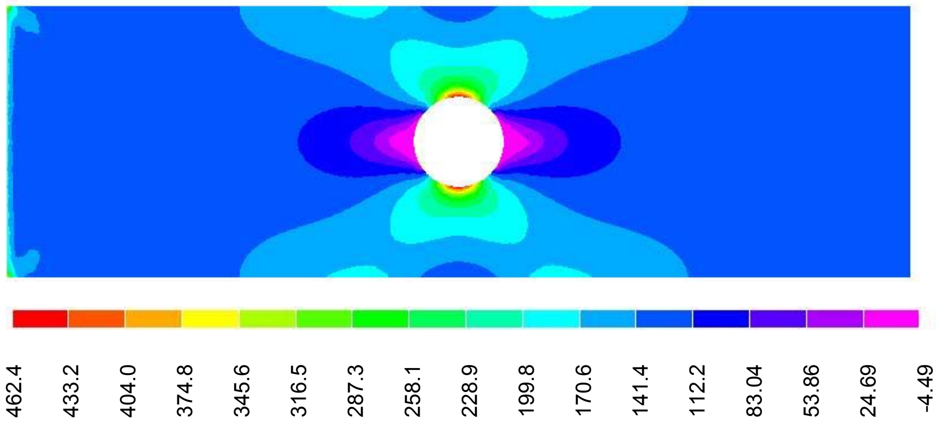

Fig. 10.2. Reference plate with hole, fine mesh, maximum principal stress [N/mm^2]

Considering the reference value, it is apparent that the analyses of the hanger connections underestimate the actual stresses. The chosen meshes appear not to be fine enough, since only the test with the refined mesh showed a tendency towards the reference result.

It is supposed that the analyses executed are still meaningful in respect of comparison between the different connection types. Locations of stress concentrations are found, but, their actual magnitudes are expected to be higher.

List of figures

Front page

“Photo composition of the bridge, the object of this work”

Section 1

-

Section 2

-

Section 3

-

Section 4

Section 5

Section 6

Section 7

Section 8

Section 9

-

Section 10

Annex A

Annex B

Annex C

Annex D

Annex E

Annex F

List of standards

[S.1]	ENV 1991-2-1: 1995	Basis of design and actions on structures – Actions on structures, Densities, self-weight and imposed loads
[S.2]	ENV 1991-2-4: 1995	Basis of design and actions on structures - Actions on structures - Wind actions
[S.3]	ENV 1991-3: 1995	Basis of design and actions on structures - Traffic loads on bridges
[S.4]	ENV 1992-1-1: 1991	Design of concrete structures – General rules and rules for buildings
[S.5]	ENV 1992-2: 1996	Design of concrete structures – Concrete Bridges
[S.6]	ENV 1993-1-1: 1992	Design of steel structures – General rules and rules for buildings
[S.7]	ENV 1993-2: 1997	Design of steel structures – Steel bridges
[S.8]	DS 804 (B6) – 09.2000	Vorschrift für Eisenbahnbrücken und sonstige Ingenieurbauwerke (VEI)

List of references

[1] ABS, American Bureau of Shipping, “Guide for the Fatigue Assessment of Offshore Structures”, Houston, Texas, USA, April 2003

[2] ACI Committee 435, “Control of Deflection in Concrete Structures”, (Appendix B of ACI 435R-95), American Concrete Institute, 2003”

[3] Almar-Næss, A. (editor), “Fatigue handbook – Offshore steel structures”, Tapir Publishers, Trondheim, Norway, 1985

[4] ARCELOR LONG COMMERCIAL S.A., “Information on American section range”, Laccolith - Cloche d'Or, Luxembourg, 2003,
http://www.europrofil.lu/Download/PDF/PV/W.pdf

[5] Becker W., ”Analogien: Bionikstrukturen (A): Wer leicht baut kann, auch schwer bauen“, Institut für Tragwerkslehre und Ingenieurholzbau, Fakultät für Architektur, TU-Wien, Austria, May 2003,
http://www.iti.tuwien.ac.at/download/files/lehre/arch/modul/TWS_BRc_Petraschka.pdf

[6] Bruger P., “Drehbare Kurzwellen-Vorhangantennen für den Einsatz bis zu sehr hohen Windgeschwindigkeiten“, Stahlbau 66, Heft 3, pp. 174-176, Ernst & Sohn – Verlag für Architektur und technische Wissenschaften GmbH, Berlin, Germany, 1997

[7] Corus Tubes Structural & Conveyance Business, “Celcius® structural hollow sections”, Corby, Northants, United Kingdom, 2003,
http://www.corustubes.com/upload/FFCF8210-4EBB-11D5-80890040CA182248/pdf/... …Hot_finished_SHS_v2.pdf

[8] Doka UK Formwork Technologies Ltd., “Doka formwork beams H 16/H 20D – List of items”, Maidstone, Kent, United Kingdom, 2003,
http://www.doka.com/imperia/md/content/doka/english/listofitems/29.pdf

[9] Doka UK Formwork Technologies Ltd., “Doka formwork sheets – List of items”, Maidstone, Kent, United Kingdom, 2003, http://www.doka.com/imperia/md/content/doka/english/listofitems/30.pdf

[10] DYWIDAG-Systems International, “DYWIDAG Bonded Post-Tensioning Systems”, Southam, Warwickshire, United Kingdom, 2003,
www.dywidag-systems.com/docs/downloads.php?topic=brochures&content=b_europe

[11] Ghali A., Favre A., Elbadry M., “Concrete Structures: Stresses and Deformations”, 3rd edition, Spon Press, London, United Kingdom, 2002

[12] Girkmann K., “Flächentragwerke – Einführung in die Elastostatik der Scheiben, Platten, Schalen und Faltwerke”, 6th edition, Springer-Verlag, Wien New York, 1978

[13] Graf W., Stransky W., ”Optimierung – Optimaler Entwurf von Tragwerken”, Lehrstuhl für Statik, Technische Universität Dresden, Germany, February 2000

[14] Graße W., “Einführung DIN-Fachbericht 101 – Lasten und Einwirkungen auf Brücken einschließlich Kombinationsregeln“, *G-M-G*-Ingenieurpartnerschaft, Dresden, Germany, 2002,
http://www.gmg-dresden.de/publikationen/FB_101.pdf

[15] Günther G. H., Hortmanns M., Schwarzkopf D., Sedlacek G., Bohmann D., “Dauerhafte Ausführung von Hängeranschlüssen an stählernen Bogenbrücken“, Stahlbau 69, Heft 11, pp.894-908, Berlin, Germany, 2000

[16] HARTMANN D., GALFFY M., WELLMANN A., "Lebensdauerorientierter Entwurf der Hängestangen bei Bogenbrücken-Modellierungen als Mehrebenenproblem", Lehrstuhl für Ingenieurinformatik im Bauwesen, Ruhr-Universität Bochum, Contribution to the International Conference on the Applications of Computer Science and Mathematics in Architecture and Civil Engineering, Weimar, Germany, 2003, http://euklid.bauing.uni-weimar.de/papers/184/M_184.pdf

[17] HERZOG M., "Stahlgewichte moderner Eisenbahn- und Straßenbrücken", Der Stahlbau 9 (1975), pp. 280-282, 1975

[18] JAY A., "Network arches – memoire en vue de l´obtention du titre d´ingenieur maitre", Høgskolen i Agder 4890, Grimstad, Norway, 1998

[19] MAURER SÖHNE & CO. KG, "Information on Maurer elastomeric deformation bearings", Munich, Germany, 2003, http://www.maurer-soehne.com/ma15/kunden/maurer/maurer.nsf/7F09

[20] MAURER SÖHNE & CO. KG, "Information on Maurer Pot bearings", Munich, Germany, 2003, http://www.maurer-soehne.com/ma15/kunden/maurer/maurer.nsf/0170

[21] MCCULLOUGH J., "Skyhook underneath – An artist tangles with structural engineering", Department of Civil Engineering, University of Strathclyde, Glasgow, Scotland, United Kingdom, 1996 http://www.strath.ac.uk/Departments/Civeng/staff/macleod/skyhook/

[22] NAKAI H., KITADA T., KUNIHIRO M., KITAZAWA M., HASINO F., "Proposition of Methods for Checking the Ultimate Strength of Arch Ribs in Steel Nielsen-Lohse Bridges", Stahlbau 64, Heft 5, pp. 129-137, Ernst & Sohn – Verlag für Architektur und technische Wissenschaften GmbH, Berlin, Germany, 1995

[23] PEIL U., TELLJOHANN G., "Dynamisches Verhalten hoher Bauwerke im böigen Wind", Stahlbau 66, Heft 3, pp. 99-109, Ernst & Sohn – Verlag für Architektur und technische Wissenschaften GmbH, Berlin, Germany, 1997

[24] PETERSEN C., "Stahlbau – Grundlagen der Berechnung und bauliche Ausbildung von Stahlbauten", Friedr. Vieweg & Sohn Verlagsgesellschaft mbH. Braunschweig, Germany, 1988

[25] PETRASCHKA K., "Brückenbau (C)", Institut für Tragwerkslehre und Ingenieurholzbau, Fakultät für Architektur, TU-Wien, Austria, March 2003, http://www.iti.tuwien.ac.at/download/files/lehre/arch/modul/TWS_BRc_Petraschka.pdf

[26] PUCHER A., "Influence lines of elastic plates", 5th revised edition, Springer-Verlag, Wien New York, Austria, 1977

[27] RÄCK M., "Entwurf einer kombinierten Strassen-Eisenbahn-Netzwerkbogenbrücke", Diploma thesis, Institut für Tragwerke und Baustoffe, Technische Universität Dresden, Grimstad, Norway, 2003

[28] RODIN S. I., "Optimisation of trusses 1 – Genetic algorithm optimization in structural mechanics", Demonstration of the software *FrameGA*, Department of material science and mechanics, Stullia, Scotland, United Kingdom, 1998 http://stullia.hypermart.net/economics/science/genetic_alg/gen_alg1.htm

[29] SCHNEIDER K.-J. (issuer), "Bautabellen für Ingenieure", 12th edition, Werner-Verlag, Düsseldorf, Germany, 1996

[30] SCHULTE H., BRUGER P., "Drehbare Kurzwellen-Vorhangantenne auf der Funksendestelle Marlow", Stahlbau 69, Heft 10, pp. 781-787, Ernst & Sohn – Verlag für Architektur und technische Wissenschaften GmbH, Berlin, Germany, 2000

[31] SCHWARZ S., "Sensitivitätsanalyse und Optimierung bei nichtlinearem Strukturverhalten", Dissertation, Bericht Nr. 34 (2001), Institut für Baustatik der Universität Stuttgart, Germany, 2001

[32] SEDLACEK G., "Praktische Anwendung der Windingenieurtechnik", Lehrstuhl für Stahlbau, Rhein.-Westf. Technische Hochschule Aachen, Germany, 2002, http://www.stb.rwth-aachen.de/lehre/umdrucke/Wind_2002.pdf

[33] SEDLACEK G., "Umdruck zur Übung Stahlbau I – Ermüdung", Lehrstuhl für Stahlbau, Rhein.-Westf. Technische Hochschule Aachen, Germany, 2002 http://www.stb.rwth-aachen.de/lehre/umdrucke/ermuedung.pdf

[34] SEIDEL C., "Grosser Beleg 2002 – Projekt Havelberg II, Entwurfsplanung für einen Ersatzneubau der Sandauer Brücke in Havelberg", unpublished student project, Institut für Tragwerke und Baustoffe, Technische Universität Dresden, Germany, 2002

[35] SELLKE F., “Brückenweb.de – Brücke Nr. 230, 230A Groβer Kolonnenweg, ” Archivnummer BAS 2002, Krefeld, Germany
http://www.brueckenweb.de/Datenbank/Suche/brueckenblatt1.php3?brueckennummer=2002

[36] SPERLING D., “Grenzzustände der Gebrauchstauglichkeit – Beschränkung von Verformungen“, Institut für Baustoffe, Massivbau und Brandschutz, Fachgebiet Massivbau, Technische Universität Braunschweig, Germany 2002/2003, http://www.ibmb.tu-bs.de/fgm/orga/script/durchbiegung.pdf

[37] STEIMANN U., “Berechnung und Konstruktion einer stählernen Eisenbahn-Stabbogenbrücke mit Netzwerkhängern“, Diploma thesis, Institut für Tragwerke und Baustoffe, Technische Universität Dresden, Grimstad, Norway, 2002

[38] TEICH S., WENDELIN S., “Vergleichsrechnung einer Netzwerkbogenbrücke unter Einsatz des Europäischen Normenkonzeptes“, Diploma thesis, Technische Universität Dresden, Institut für Tragwerke und Baustoffe, Technische Universität Dresden, Grimstad, Norway, 2001,
http://pchome.grm.hia.no/~pert/

[39] TIMOSHENKO S., GOODIER J. N., “Theory of Elasticity“, 2nd edition, McGraw-Hill, Kōgakusha, Tokyo, 1951

[40] TRINITY RIVER CORRIDOR PROJECT, “Trinity Bridges”, City of Dallas, Texas, USA,
http://www.trinityrivercorridor.org/html/trinity_bridges.html

[41] TVEIT P., “The design of network arches”, The Structural Engineer Volume 44, No 7, pp. 247 - 259, London, United Kingdom, July 1966

[42] TVEIT P., ”Report 7205 – Network arches for railway bridges“, Ren og Anvendt Mekanik, Danmarks Ingeniørakademi, Bygningsafdelingen, Aalborg, Denmark, August 1973

[43] TVEIT P., ”Considerations for Design of Network Arches”, Journal of Structural Engineering, Vol. 113, No. 10, pp. 2189-2206, © ASCE, ISSN 0733-9445/87/0010-21897 Paper No. 21892, October 1987

[44] TVEIT P., ”Wie konstruiert man die schlankste und leichteste Bogenbrücke der Welt – Ein Vortrag über Netzwerkbögen.” (”How to design the most slender and lightest arch bridge in the world. A lecture on network arches.” In German), Publication series no: 2, © Høgskolen I Agder University College, Publication series no: 2., ISSN 82-7117-301-4, Grimstad, Norway, 1996

[45] TVEIT P., “The Network Arch – An Extended Manuscript from 21 Lectures in 12 Countries”, Internet edition, Grimstad, Norway, May 2001
http://pchome.grm.hia.no/~pert/

[46] TVEIT P., “Optimal design of of Network Arches”, Contribution to the IABSE Symposium in Melbourne, Australia, September 2002

[47] TVEIT P., “Preliminary design of network arch road bridges – Examples with spans of 135 and 160 meters” , Grimstad, Norway, March 2003
http://pchome.grm.hia.no/~pert/

[48] TVEIT P., “Revision of – Erection of optimal Network Arches”, Grimstad, Norway, May 2003
http://pchome.grm.hia.no/~pert/

[49] VAN DER BURGH A.H.P., HARTONO, „Rain-wind induced vibrations of a simple oscillator”, Faculty of Information Technology and Systems, Department of Applied Mathematical Analysis, Delft University of Technology, Delft, The Netherlands, 2003,
http://ta.twi.tudelft.nl/TWA_Reports/cablis3new.pdf

[50] VERCH W., ”Umdruck zu den Vorträgen im Fach Entwurf und Gestaltung von Ingenieurbau-werken - Brückenbau”, Technische Universität Dresden, Fakultät Bauingenieurwesen, Institut für Tragwerke und Baustoffe, Dresden, Germany, October 2001,
http://www.tu-dresden.de/biwitb/mbau/download/verch_all.pdf

[51] ZALEWSKI W., ALLEN E., IANO J., “Shaping Structures: Statics CD ROM”, John Wiley & Sons, Inc., New York, USA, February 1998
http://shapingstructures.com/cdrom.html

Annexes

Photo composition of the bridge calculated in this work

Load Assumptions

A.1. Permanent actions including self-weight

1a: Profile of the arches

American wide flange beams

W 360x410x900 : $\underline{g_{1a} = 9\ kN/m}$

W 360x410x634 : $\underline{g_{1a} = 6.34\ kN/m}$

1b: hanger

smooth surface steel bars

diameter: 60 mm, ρ_{st} = 78.5kN/m^3 : $\underline{g_{1b} = 0.222\ kN/m}$

1c: lower cord slab

reinforced concrete

A = 4.96 m^2, ρ_c = 25kN/m^3 : $\underline{g_{1c} = 118.13\ kN/m}$

1d: wind bracing

CHS 219.1 x 8, *[7]* : $\underline{g_{1d} = 0.417\ kN/m}$

CHS 219.1 x 10, *[7]* : $\underline{g_{1d} = 0.515\ kN/m}$

1e: sleepers, rails and ballast

DIN-Fachbericht 101, Tabelle 1 (M.1), [14]

two tracks (v ≤ 160 km/h)

width of two tracks: 8.4 m : $\underline{g_{1e} = 105\ kN/m}$

1f: cable trough

each side:

2 x U 350 (DIN 1026)	:	= 1.212 kN/m
1 x Bl 380x5	:	= 0.15 kN/m
cables	:	= 1.138 kN/m
	:	$\underline{g_{1f} = 2.5\ kN/m}$

1g: transversal prestress

Annex B, Figure B.9

DYWIDAG threadbar 36D every 270 mm

each with : $\underline{p_{1g} = 989.1\ kN}$

1h: longitudinal prestress

Annex B, Figure B.12

6 x DYWIDAG Type 6827 each side of bridge

each with : $\underline{p_{1h} = 5467.5\ kN}$

A.2. Traffic loads

A.2.1 Actions due to railway operations

A.2.1.1 Vertical loads

21a: Load Model 71

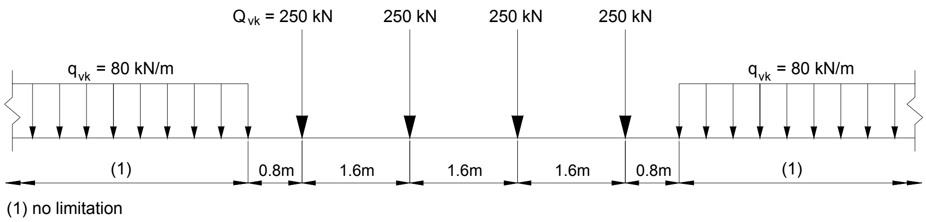

Fig. A.1. Load Model 71 and characteristic values for vertical loads, *ENV 1991-3: 1995, Fig. 6.2*

The factor α is assumed to be 1.0.

According to *ENV 1991:3 1995, 6.3.5.1 & 6.3.5.2* the wheel loads of the Load Model 71 are distributed by the rails, sleepers and the ballast in longitudinal direction to the upper surface of the concrete slab. (Figure A.2)

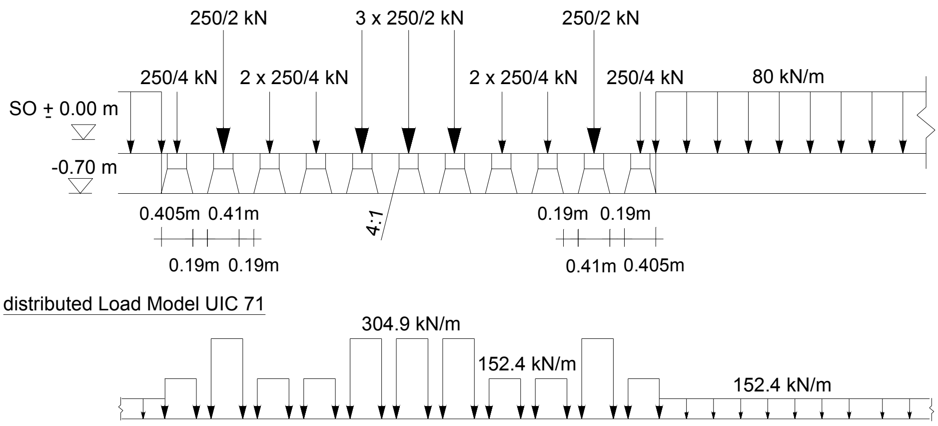

Fig. A.2. Distribution of the wheel loads of the Load Model 71 onto the upper surface of the concrete slab

According to *ENV 1991-3: 1995, 6.3.5.3* the actions are distributed transversely to a total width of 2.77 meters (width of sleepers = 2.60 m, thickness of ballast below sleepers = 0.34 m).

21b: Eccentric Load Model 71

ENV 1991-3: 1995, 6.3.1 (3)P

An eccentricity is taken into account by distributing the total axle load by the ratio 1.25:1.00 on the two wheels.

21c: Load Model "unloaded train"

ENV 1991-3: 1995, 6.3.4

<u>q_{vk} = 12.5 kN/m</u>

According to *ENV 1991-3: 1995, 6.3.5.3* the actions are distributed transversely to a total width of 2.77 meters (width of sleepers = 2.60 m, thickness of ballast below sleepers = 0.34 m).

21d: non-public footpaths

ENV 1991-3:1995, 6.3.6.1

On both sides of the bridge, 0.75 m wide $q_{fk} = 5\ kN/m^2 \cdot 0.75\ m$

$\underline{q_{fk} = 3.75\ kN/m}$

A.2.1.2 Dynamic effects

φ(φ2,φ3): dynamic factors for load cases 22a, 22b and 22c

It was taken for granted that the first natural bending frequency of the bridge loaded by permanent actions, n_0, is within the limits of *Figure 6.9* in *ENV 1991-3: 1995*. In Section C.2 the relevant mode shape was found to be the second natural mode shape of the bridge. Its eigenfrequency is:

$n_0 = 2.34\ Hz$

The criterion to fulfil is:

$94.76 \cdot L^{-0.748} > n_0 > 23.58 \cdot L^{-0.592}$; for $20m < L \leq 100m$

with L = 100m

$\underline{3.02\ Hz > 2.34\ Hz > 1.54\ Hz}$

Within the limits of n_0 there are no dynamic analysis, acceleration and fatigue check at resonance required. The dynamic effects are considered by using the dynamic factors with static analysis.

Assuming standard maintenance the factor φ_2 is chosen.

$$\varphi_2 = \frac{2.16}{\sqrt{L_\varphi} - 0.2} + 0.73$$

ENV 1991-3: 1995, 6.4.3.2 (1b)

for the arches: L_φ = half span

with $L_\varphi = 50m \rightarrow \underline{\varphi_2 = 1.044}$

ENV 1991-3: 1995, table 6.2 case 5.5

for the hangers: L_φ = half span

with $L_\varphi = 50m \rightarrow \underline{\varphi_2 = 1.044}$

In ENV 1991-3: 1995, table 6.2 case 5.6, for suspension bars in conjunction with stiffening girders a L_φ of 4 times the longitudinal spacing of the suspension bars is given. In this bridge there are no stiffening girders, but the railway traffic loads are distributed by the concrete tie. Additionally the spacing of the hangers is much smaller than it is in the bridges that the Eurocode refers to. So the dynamic effect on the hanger would be overestimated by the suggestion of Eurocode. A reasonable L_φ = half span was suggested by TVEIT.

for the concrete deck slab: L_φ = twice span of deck slab

with $L_\varphi = 19.9m \rightarrow \underline{\varphi_2 = 1.237}$

ENV 1991-3: 1995, table 6.2 case 4.3

A.2.1.3 Horizontal forces – characteristic values

21e: nosing force

ENV 1991-3: 1995, 6.5.2

Acts horizontally at the top of the rails, perpendicularly to the centre-line of the track and always combined with a vertical traffic load.

$\underline{Q_{sk} = 100\ kN}$

21e: actions due to traction and braking

ENV 1991-3: 1995, 6.5.3

These forces act at the top of the rails in longitudinal direction of the track and will be combined with the corresponding vertical loads.

Traction force: $Q_{lak} = 33\ kN/m \cdot L_{a,b}\ [m] \leq 1000\ kN$

LM 71 $L_{a,b} = 100\ m$ $Q_{lak} = 1000\ kN$

Braking force: $Q_{lbk} = 20\ kN/m \cdot L_{a,b}\ [m] \leq 6000\ kN$

LM 71 $L_{a,b} = 100\ m$ $Q_{lbk} = 2000\ kN$

Most unfavourable forces: LM 71 $\underline{Q_{la,bk,71} = 2000\ kN}$

21g combined response of structure and track to variable actions

Assuming rail expansion devices at both sides of the bridge, there are no actions due to thermal effects to be considered.

ENV 1991-3: 1995 6.5.4.3 (3)

The requirement of considering longitudinal actions occurring as a result of the vertical displacement of the bridge deck should be specified by the relevant authority. It is taken for granted that this is not demanded.

ENV 1991-3: 1995 6.5.4.5

All traction and braking forces are resisted by the fixed bearings because of the assumed rail expansion devices provided at both ends of the deck.

ENV 1991-3: 1995 6.5.4.4 (2)

$F_{bk} = Q_{la,bk}$

21h: aerodynamic effects as a result of passing trains

The area of the structure subjected to a travelling wave of alternating pressure and suction by the passing of rail traffic is very small. It is assumed that actions caused by this effect are negligible.

A.2.2 Accidental actions

22a: derailment on bridges – design situation I

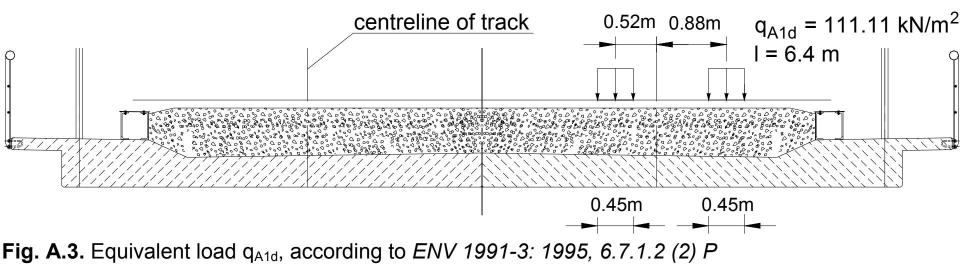

Fig. A.3. Equivalent load q_{A1d}, according to *ENV 1991-3: 1995, 6.7.1.2 (2) P*

Since, in network arch bridges, structural elements above the levels of the rails could be damaged or destroyed by collision, lateral guideways and safety catches shall be placed at a distance of 180 mm from the rail. So the lateral evasion in derailment situation is limited to this value.

DIN-Fachbericht 101, 3.4.8 [14]

22b: derailment on bridges – design situation II

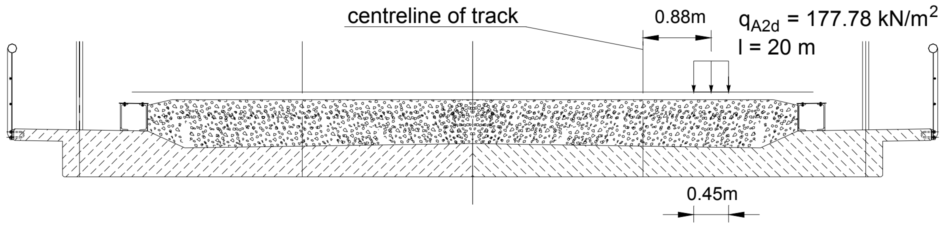

Fig. A.4. Equivalent load q_{A2d}, according to *ENV 1991-3: 1995, 6.7.1.2 (3) P*

Since, in network arch bridges, structural elements above the levels of the rails could be damaged or destroyed by collision, lateral guideways and safety catches shall be placed at a distance of 180 mm from the rail. So the lateral evasion in a derailment situation is limited to this value. *DIN-Fachbericht 101, 3.4.8 [14]*

22c: accidental action due to the severance of overhead line equipment

The catenary is connected to the lowest node of the wind bracing truss. The accidental force acts horizontally in a longitudinal direction with a design value of twice ± 20 kN. *ENV 1991-3: 1995, 6.7.2*

The most unfavourable sense of direction must be considered.

A.2.3 Assessment of traffic loads on railway bridges

The groups of loads are set up according to *ENV 1991-3: 1995, 6.8* and *DIN - Fachbericht 101, 3.4.5 [14]* separately for each factor φ_2.

gr 11: maximum vertical 1

= $1.044 \cdot (LM\ 71) + Q_{la,bk} + 0.5 \cdot Q_{sk}$ for the arches
= $1.044 \cdot (LM\ 71)$+2000kN+50kN

= $1.044 \cdot (LM\ 71) + Q_{la,bk} + 0.5 \cdot Q_{sk}$ for the hangers
= $1.044 \cdot (LM\ 71)$+2000kN+50kN

= $1.237 \cdot (LM\ 71) + Q_{la,bk} + 0.5 \cdot Q_{sk}$ for the slab
= $1.237 \cdot (LM\ 71)$+2000kN+50kN

gr 12: maximum vertical 2

= $1.044 \cdot (LM\ 71) + 0.5 \cdot Q_{la,bk} + Q_{sk}$ for the arches
= $1.044 \cdot (LM\ 71)$+1000kN+100kN

= $1.044 \cdot (LM\ 71) + 0.5 \cdot Q_{la,bk} + Q_{sk}$ for the hangers
= $1.044 \cdot (LM\ 71)$+1000kN+100kN

= $1.237 \cdot (LM\ 71) + 0.5 \cdot Q_{la,bk} + Q_{sk}$ for the slab
= $1.237 \cdot (LM\ 71)$+1000kN+100kN

gr 13: maximum longitudinal

matches gr 11

gr 14: maximum lateral

= $1.044 \cdot (LM\ 71) + Q_{sk}$ for the arches
= $1.044 \cdot (LM\ 71)$+100kN

= $1.044 \cdot (LM\ 71) + Q_{sk}$ for the hangers
= $1.044 \cdot (LM\ 71)$+100kN

= $1.237 \cdot (LM\ 71) + Q_{sk}$ for the slab
= $1.237 \cdot (LM\ 71) + 100kN$

gr 21: maxium vertical 1 (two loaded tracks)

= $\mathbf{2 \cdot (}1.044 \cdot (LM\ 71) + Q_{la,bk} + 0.5 \cdot Q_{sk}\mathbf{)}$ for the arches
= $\mathbf{2 \cdot (}1.044 \cdot (LM\ 71) + 2000kN + 50kN\mathbf{)}$

= $\mathbf{2 \cdot (}1.044 \cdot (LM\ 71) + Q_{la,bk} + 0.5 \cdot Q_{sk}\mathbf{)}$ for the hangers
= $\mathbf{2 \cdot (}1.044 \cdot (LM\ 71) + 2000kN + 50kN\mathbf{)}$

= $\mathbf{2 \cdot (}1.237 \cdot (LM\ 71) + Q_{la,bk} + 0.5 \cdot Q_{sk}\mathbf{)}$ for the slab
= $\mathbf{2 \cdot (}1.237 \cdot (LM\ 71) + 2000kN + 50kN\mathbf{)}$

gr 22: maximum vertical 2 (two loaded tracks)

= $\mathbf{2 \cdot (}1.044 \cdot (LM\ 71) + 0.5 \cdot Q_{la,bk} + Q_{sk}\mathbf{)}$ for the arches
= $\mathbf{2 \cdot (}1.044 \cdot (LM\ 71) + 1000kN + 100kN\mathbf{)}$

= $\mathbf{2 \cdot (}1.044 \cdot (LM\ 71) + 0.5 \cdot Q_{la,bk} + Q_{sk}\mathbf{)}$ for the hangers
= $\mathbf{2 \cdot (}1.044 \cdot (LM\ 71) + 1000kN + 100kN\mathbf{)}$

= $\mathbf{2 \cdot (}1.237 \cdot (LM\ 71) + 0.5 \cdot Q_{la,bk} + Q_{sk}\mathbf{)}$ for the slab
= $\mathbf{2 \cdot (}1.237 \cdot (LM\ 71) + 1000kN + 100kN\mathbf{)}$

gr 23: maximum longitudinal (two loaded tracks)

matches gr 21

gr 24: maximum lateral (two loaded tracks)

= $\mathbf{2 \cdot (}1.044 \cdot (LM\ 71) + Q_{sk}\mathbf{)}$ for the arches
= $\mathbf{2 \cdot (}1.044 \cdot (LM\ 71) + 100kN\mathbf{)}$

= $\mathbf{2 \cdot (}1.044 \cdot (LM\ 71) + Q_{sk}\mathbf{)}$ for the hangers
= $\mathbf{2 \cdot (}1.044 \cdot (LM\ 71) + 100kN\mathbf{)}$

= $\mathbf{2 \cdot (}1.237 \cdot (LM\ 71) + Q_{sk}\mathbf{)}$ for the slab
= $\mathbf{2 \cdot (}1.237 \cdot (LM\ 71) + 100kN\mathbf{)}$

A.2.4 Fatigue load models

The general design method, *ENV 1991-3: 1995 F.2*, is used for the fatigue assessment.

For steel bridges the following condition must be satisfied:

$$\gamma_{Ff} \cdot \lambda \cdot \phi_2 \cdot \Delta\sigma_{71} \leq \frac{\Delta\sigma_c}{\gamma_{Mf}}$$

The traffic loads to be considered for fatigue assessment are the following:

fatigue 1: $= \Phi_2 \cdot LM\ 71 = \underline{1.044 \cdot LM\ 71}$ for the arches

fatigue 2: $= \Phi_2 \cdot LM\ 71 = \underline{1.044 \cdot LM\ 71}$ for the hangers

fatigue 3: $= \Phi_2 \cdot LM\ 71 = \underline{1.237 \cdot LM\ 71}$ for the bridge deck

The load model has to be applied on one and/or both tracks.

A.3. Wind forces

A.3.1 Wind forces in y-direction (perpendicular to bridge centreline)

ENV 1991-2-4: 1995, 5.2

reference mean wind velocity pressure $q_{ref} = \rho/2 \cdot v^2_{ref,0}$

zone 1, altitude < 800 m $\rho = 0.625\ kg/m^3 \cdot (27.6\ m/s)^2$

$q_{ref} = 476.1\ kg/(m \cdot s^2)$

ENV 1991-2-4: 1995, Annex A.6

3a: lateral wind forces on the arches

average height: $z = 30m$

ENV 1991-2-4: 1995 10.6, 10.14

force coefficient: $c_f = c_{f,0} \cdot \psi_\lambda = 2.0 \cdot 1.0 = 2$

reference area: $A_{ref} = 0.448\ m^2/m$

exposure coefficient: $c_e(z = 30m) = 2.6$ (for terrain category III)

dynamic factor: $c_d\ (z = 30m) = 0.89$

wind force: $F_{w1} = q_{ref} \cdot c_e \cdot c_d \cdot c_f \cdot A_{ref} = 0.987\ kN/m$

attenuation of the wind force on the hind arch:

Schneider [29], 6.1.5

$\varphi = 0.1$

$a/d = 1$

$\eta = 0.85$

total lateral wind forces on the arches:

$\underline{F_w = F_{w1} + \eta \cdot F_{w1} = 1.826\ kN/m}$

3b: lateral wind forces on the hangers

ENV 1991-2-4: 1995 8.1

average height: $z = 30m$

ENV 1991-2-4: 1995 10.8.1

roughness coefficient: $c_r\ (z = 30m) = 1.013$ (for terrain category III)

topography coefficient: $c_t\ (z = 30m) = 1$ (location: valley, no funnelling effects)

mean wind velocity: $v_m\ (z = 30m) = 27.96\ m/s$

Reynolds number. $Re = \dfrac{b \cdot v_m(z = 30m)}{\nu} = 7.5 \cdot 10^4$

$c_{f,0}$ from *figure 10.8.2* in *ENV 1991-2-4: 1995*

force coefficient: $c_f = c_{f,0} \cdot \psi_\lambda = 1.2 \cdot 1.0 = 1.2$

reference area: $A_{ref} = 0.04\ m^2/m$

exposure coefficient: $c_e\ (z = 30m) = 2.6$ (for terrain category III)

dynamic factor: $c_d\ (z = 30m) = 0.89$

wind force: $F_{w1} = q_{ref} \cdot c_e \cdot c_d \cdot c_f \cdot A_{ref} = 0.053\ kN/m$

attenuation of the wind force on the hind arch:

Schneider [29], 6.1.5

$\varphi = 0.1$

$a/d = 1$

$\eta = 0.85$

total lateral wind forces on the hangers:

$\underline{F_w = F_{w1} + \eta \cdot F_{w1} = 0.098 \text{ kN/m}}$

3c: lateral wind forces on the slab

ENV 1991-2-4: 1995 10.11.2

average height: $z = 20m$

force coefficient: $c_f = c_{f,0} \cdot \psi_\lambda = 1.3 \cdot 0.95 = 1.235$ without traffic
force coefficient: $c_f = c_{f,0} \cdot \psi_\lambda = 1.75 \cdot 0.775 = 1.313$ with traffic

reference area: $A_{ref} = 1.5 \text{ m}^2/\text{m}$ without traffic
reference area: $A_{ref} = 4.9 \text{ m}^2/\text{m}$ with traffic

exposure coefficient: c_e (z = 20m) = 2.25 (for terrain category III)
dynamic factor: c_d (z = 20m) = 0.89

wind force: $F_w = q_{ref} \cdot c_e \cdot c_d \cdot c_f \cdot A_{ref} = \underline{1.43 \text{ kN/m}}$ without traffic
$F_w = q_{ref} \cdot c_e \cdot c_d \cdot c_f \cdot A_{ref} = \underline{6.134 \text{ kN/m}}$ with traffic

A.3.2 Crosswind forces in z-direction

3d: crosswind forces in z-direction

ENV 1991-2-4: 1995 10.11.3

average height: $z = 20$ m

force coefficient: $c_{f,z} = 0.15$ (d/b = 19.2)
reference area: $A_{ref} = 11.5 \text{ m}^2/\text{m}$
exposure coefficient: ce (z = 20m) = 2.25
dynamic factor: cd (z = 20m) = 0.89

wind force in z-direction: $F_{w,z} = q_{ref} \cdot c_e \cdot c_d \cdot c_{f,z} \cdot A_{ref} = \underline{1.645 \text{ kN/m}}$

A.3.3 Longitudinal wind forces in x-direction

3e: longitudinal wind forces in x-direction

ENV 1991-2-4: 1995 10.11.4

50 % of the wind forces in y-direction

total wind forces in y-direction: 585.26 kN without traffic
1055.66 kN with traffic

wind force in x-direction: $F_{w,x}$ = <u>292.63 kN</u> without traffic
<u>527.63 kN</u> with traffic

A.4. Actions due to temperature

4a: variation of the constant component of temperature

ENV 1991-2-5: 1997, 6.1.3.3

The maximum variation causes longitudinal actions due to friction in the bearings.

ENV 1991-2-5: 1997 fig. 6.1, group 3

Mounting temperature: $T_0 = 10$ °C
Minimum of constant part of temperature: $T_{e,min}(T_{min}=-24$ °C$) = -17$ °C
Maximum of constant part of temperature: $T_{e,max}(T_{max}=37$ °C$) = 40$ °C

Maximum negative variation: $\Delta T_{N,neg} = T_{e,min} - T_0 = -27$ K
Maximum positive variation: $\Delta T_{N,pos} = T_{e,max} - T_0 = 30$ K

Maximum variation: $\Delta T_{N,max} = 30$ K

Enhancement of $\Delta T_{N,max}$ for the calculation of the horizontal displacement at the bearings. *ENV 1991-2-5: 1997, 6.1.3.3 (4)P & (5)P*

$\Delta T_{N,max} = 40$ K

Maximum longitudinal displacement: $\Delta l = 10 \cdot 10^{-6}$ /K·40 K·100 m
$\Delta l = 0.04$ m

Forces due to friction in the 4 bearings: $Q_{lfk} = 4 \cdot (\mu \cdot Load_{vertical})$
$Q_{lfk} = 4 \cdot (0.05 \cdot 10000\text{kN}) =$ <u>1280 kN</u> *PTFE insert: μ in PETERSEN [21], page 1157*

4b: vertically linear variable component of temperature

The maximal negative temperature change ($\Delta T_{M,neg}$) while the upper surface is colder than the lower one causes an additional vertical displacement of the bridge. *ENV 1991-2-5: 1997, 6.1.4.1*

This effect is considered for $\Delta T_{M,neg} = 1.0 \cdot [-8\ °C] = 8\ °C$

4c: horizontally linear variable component of temperature

This effect is considered for $\Delta T = [5]°C$ *ENV 1991-2-5: 1997 6.1.4.2*

4d: differences in the constant component of temperature of different structural elements

A difference of 15 K between the slab and the arches with the hangers will be considered. *ENV 1991-2-5: 1997, 6.1.6*

A.5. Combination of actions

The combinations are to be set up using the following formulas: *ENV 1991-3: 1995 Annex G*

Ultimate limit state:

1. Transient and persistent situations

$$\sum_j \gamma_{G,j} \cdot G_{k,j} \text{"+"} \gamma_P \cdot P_k + \gamma_{Q,1} \cdot Q_{k,1} \text{"+"} \sum \gamma_{Q,i} \cdot \psi_{0,i} \cdot Q_{k,i}$$

2. Accidental situations

$$\sum_j \gamma_{GA,j} \cdot G_{k,j} \text{"+"} A_d \text{"+"} \gamma_P \cdot P_k + \psi_{1,1} \cdot Q_{k,1} \text{"+"} \sum \psi_{2,i} \cdot Q_{k,i}$$

ENV 1991-3: 1995 G2.1.2 (4)

It is assumed that the client demands the combination of LM71 with the accidental actions.

For fatigue:

1. Minimal stress variation

$$\sum_j G_{k,j} \text{"+"} \gamma_P \cdot P_k + \varphi_2 \cdot \text{LM71}$$

2. Maximum stress variation

$$\sum_j G_{k,j} \text{"+"} \gamma_P \cdot P_k + \text{twice} \cdot \varphi_2 \cdot \text{LM71}$$

Serviceability limit state:

1. Characteristic/rare load combinations

$$\sum_j G_{k,j} \text{"+"} Q_{k,1} \text{"+"} \sum \psi_{0,i} \cdot Q_{k,i}$$

2. Infrequent load combinations

$$\sum_j G_{k,j} \text{"+"} P_k + \psi'_1 \cdot Q_{k,1} \text{"+"} \sum \psi_{1,i} \cdot Q_{k,i}$$

3. Frequent load combinations

$$\sum_j G_{k,j} \text{"+"} P_k + \psi_{1,1} \cdot Q_{k,1} \text{"+"} \sum \psi_{2,i} \cdot Q_{k,i}$$

4. Quasi-permanent load combinations

$$\sum_j G_{k,j} \text{"+"} P_k + \sum \psi_{2,i} \cdot Q_{k,i}$$

The load combinations used for the calculations are shown in figures A.5 to A.8. Depending on the design checks, to obtain the most unfavourable load position, the influence lines of structural elements were analysed.

The large number of load combinations is due to the requirements of Eurocode. It is no problem, with present-day soft- and hardware, to calculate all load combinations but the analysis of the results is very time-consuming. Since for most design checks the same load combinations gave most unfavourable results, it might be allowed to limit the number to the load combinations, found to be decisive by experience.

Load combinations in ULTIMATE LIMIT STATE																			
			Persistent and transient situations												Accidental situations			Fatigue	
load comb. Number			traffic actions dominant						wind forces dominant					temp.					
Description			**1**	**2**	**3**	**4**	**5**	**6**	**7**	**8**	**9**	**10**	**11**	**12**	**13**	**14**	**15**	**16**	**17**
Selfweight	**1a**	γ	1.35	1.35	1.35	1.35	1.35	1.35	1.35	1.35	1.35	1.35	1.35	1.35	1.35	1.35	1.35	1.00	1.00
arches		Ψ	-	-	-	-	-	-	-	-	-	-	-	-	-	-	-	-	-
Hangers	**1b**	γ	1.35	1.35	1.35	1.35	1.35	1.35	1.35	1.35	1.35	1.35	1.35	1.35	1.35	1.35	1.35	1.00	1.00
hangers		Ψ	-	-	-	-	-	-	-	-	-	-	-	-	-	-	-	-	-
Bridge deck	**1c**	γ	1.35	1.35	1.35	1.35	1.35	1.35	1.35	1.35	1.35	1.35	1.35	1.35	1.35	1.35	1.35	1.00	1.00
bridge deck		Ψ	-	-	-	-	-	-	-	-	-	-	-	-	-	-	-	-	-
Wind bracing	**1d**	γ	1.35	1.35	1.35	1.35	1.35	1.35	1.35	1.35	1.35	1.35	1.35	1.35	1.35	1.35	1.35	1.00	1.00
wind bracing		Ψ	-	-	-	-	-	-	-	-	-	-	-	-	-	-	-	-	-
Ballast, rails,	**1e**	γ	1.35	1.35	1.35	1.35	1.35	1.35	1.35	1.35	1.35	1.35	1.35	1.35	1.35	1.35	1.35	1.00	1.00
sleepers		Ψ	-	-	-	-	-	-	-	-	-	-	-	-	-	-	-	-	-
Selfweight	**1f**	γ	1.35	1.35	1.35	1.35	1.35	1.35	1.35	1.35	1.35	1.35	1.35	1.35	1.35	1.35	1.35	1.00	1.00
cable trough		Ψ	-	-	-	-	-	-	-	-	-	-	-	-	-	-	-	-	-
Prestressing	**1g**	γ	1.00	1.00	1.00	1.00	1.00	1.00	1.00	1.00	1.00	1.00	1.00	1.00	1.00	1.00	1.00	1.00	1.00
trans. tendons		Ψ	-	-	-	-	-	-	-	-	-	-	-	-	-	-	-	-	-
Prestressing	**1h**	γ	1.00	1.00	1.00	1.00	1.00	1.00	1.00	1.00	1.00	1.00	1.00	1.00	1.00	1.00	1.00	1.00	1.00
long. tendons		Ψ	-	-	-	-	-	-	-	-	-	-	-	-	-	-	-	-	-
Load Model 71	**21a**	γ												1.50	1.00	1.00	1.00		
		Ψ												0.8	-	-	-		
Eccentricity	**21b**	γ	1.45	1.45	1.45	1.45	1.45	1.45	1.45	1.45	1.45	1.45		1.50	1.00	1.00	1.00	1.00	1.00
load model 71		Ψ	-	-	-	-	-	-	-	-	-	-		0.8	-	-	-	-	-
"unloaded train"	**21c**	γ											1.50						
		Ψ											1.0						
Non-public	**21d**	γ	1.50	1.50	1.50	1.50	1.50	1.50	1.50	1.50	1.50	1.50							
footpaths		Ψ	0.8	0.8	0.8	0.8	0.8	0.8	0.8	0.8	0.8	0.8							
Derailment,	**22a**	γ													1.00				
design situation I		Ψ													-				
Derailment,	**22b**	γ														1.00			
design situation II		Ψ														-			
Catenary rupture	**22c**	γ															1.00		
		Ψ															-		
Groups of loads	**gr11**	γ	1.45						1.45									1.00	
		Ψ	-						0.8									-	
	gr12	γ		1.45						1.45									
		Ψ		-						0.8									
	gr14	γ			1.45														
		Ψ			-														
	gr21	γ				1.45					1.45								1.00
		Ψ				-					0.8								-
	gr22	γ					1.45					1.45							
		Ψ					-					0.8							
	gr24	γ						1.45											
		Ψ						-											
Lateral wind on	**3a**	γ	1.50	1.50	1.50	1.50	1.50		1.50	1.50	1.50	1.50	1.50						
arches		Ψ	0.6	0.6	0.6	0.6	0.6		-	-	-	-	-						
Lateral wind on	**3b**	γ	1.50	1.50	1.50	1.50	1.50		1.50	1.50	1.50	1.50	1.50						
hangers		Ψ	0.6	0.6	0.6	0.6	0.6		-	-	-	-	-						
Lateral wind on	**3c**	γ	1.50	1.50	1.50	1.50	1.50		1.50	1.50	1.50	1.50	1.50						
bridge deck		Ψ	0.6	0.6	0.6	0.6	0.6		-	-	-	-	-						
Longitudinal wind	**3e**	γ												1.50					
		Ψ												0.6					

Fig. A.5. Load combinations for assessment in ultimate limit state, and for fatigue design checks

SERVICEABILITY LIMIT STATE - characteristic/rare load combinations														
Load comb. number			traffic actions dominant						wind forces dominant					temp.
Description			**18**	**19**	**20**	**21**	**22**	**23**	**24**	**25**	**26**	**27**	**28**	**29**
Selfweight	**1a**	γ	1.00	1.00	1.00	1.00	1.00	1.00	1.00	1.00	1.00	1.00	1.00	1.00
arches		Ψ	-	-	-	-	-	-	-	-	-	-	-	-
Hangers	**1b**	γ	1.00	1.00	1.00	1.00	1.00	1.00	1.00	1.00	1.00	1.00	1.00	1.00
hangers		Ψ	-	-	-	-	-	-	-	-	-	-	-	-
Bridge deck	**1c**	γ	1.00	1.00	1.00	1.00	1.00	1.00	1.00	1.00	1.00	1.00	1.00	1.00
bridge deck		Ψ	-	-	-	-	-	-	-	-	-	-	-	-
Wind bracing	**1d**	γ	1.00	1.00	1.00	1.00	1.00	1.00	1.00	1.00	1.00	1.00	1.00	1.00
wind bracing		Ψ	-	-	-	-	-	-	-	-	-	-	-	-
Ballast, rails,	**1e**	γ	1.00	1.00	1.00	1.00	1.00	1.00	1.00	1.00	1.00	1.00	1.00	1.00
sleepers		Ψ	-	-	-	-	-	-	-	-	-	-	-	-
Selfweight	**1f**	γ	1.00	1.00	1.00	1.00	1.00	1.00	1.00	1.00	1.00	1.00	1.00	1.00
cable trough		Ψ	-	-	-	-	-	-	-	-	-	-	-	-
Prestressing	**1g**	γ	1.00	1.00	1.00	1.00	1.00	1.00	1.00	1.00	1.00	1.00	1.00	1.00
trans. tendons		Ψ	-	-	-	-	-	-	-	-	-	-	-	-
Prestressing	**1h**	γ	1.00	1.00	1.00	1.00	1.00	1.00	1.00	1.00	1.00	1.00	1.00	1.00
long. tendons		Ψ	-	-	-	-	-	-	-	-	-	-	-	-
Load model 71	**21a**	γ												-
		Ψ												0.8
Eccentricity	**21b**	γ	1.00	1.00	1.00	1.00	1.00	1.00	-	-	-	-		-
load model 71		Ψ	-	-	-	-	-	-	0.8	0.8	0.8	0.8		0.8
"unloaded train"	**21c**	γ											1.00	
		Ψ											-	
Non-public	**21d**	γ	-	-	-	-	-	-	-	-	-	-		
footpaths		Ψ	0.8	0.8	0.8	0.8	0.8	0.8	0.8	0.8	0.8	0.8		
Groups of loads	**gr11**	γ	1.00						-					
		Ψ	-						0.8					
	gr12	γ		1.00						-				
		Ψ		-						1.0				
	gr14	γ			1.00									
		Ψ			-									
	gr21	γ				1.00					-			
		Ψ				-					0.8			
	gr22	γ					1.00					-		
		Ψ					-					1.0		
	gr24	γ						1.00						
		Ψ						-						
Lateral wind on	**3a**	γ	-	-	-	-	-		1.00	1.00	1.00	1.00	1.00	
arches		Ψ	0.6	0.6	0.6	0.6	0.6		-	-	-	-	-	
Lateral wind on	**3b**	γ	-	-	-	-	-		1.00	1.00	1.00	1.00	1.00	
hangers		Ψ	0.6	0.6	0.6	0.6	0.6		-	-	-	-	-	
Lateral wind on	**3c**	γ	-	-	-	-	-		1.00	1.00	1.00	1.00	1.00	
bridge deck		Ψ	0.6	0.6	0.6	0.6	0.6		-	-	-	-	-	
Longitudinal wind	**3e**	γ												-
		Ψ												0.6
Const. temp.	**4a**	γ	-	-	-	-	-	-	-	-	-	-	-	1.00
change		Ψ	0.6	0.6	0.6	0.6	0.6	0.6	0.6	0.6	0.6	0.6	0.6	-

Fig. A.6. Load combinations for assessment in serviceability limit state, characteristic/rare combinations

SERVICEABILITY LIMIT STATE																		
			Infrequent load combinations								frequent load combinations							
Load comb. number			traffic actions dominant				wind forces dominant			temp.	traffic actions dominant				wind forces dominant			temp.
Description			30	31	32	33	34	35	36	37	38	39	40	41	42	43	44	45
Selfweight	1a	γ	1.00	1.00	1.00	1.00	1.00	1.00	1.00	1.00	1.00	1.00	1.00	1.00	1.00	1.00	1.00	1.00
arches		Ψ	-	-	-	-	-	-	-	-	-	-	-	-	-	-	-	-
Hangers	1b	γ	1.00	1.00	1.00	1.00	1.00	1.00	1.00	1.00	1.00	1.00	1.00	1.00	1.00	1.00	1.00	1.00
hangers		Ψ	-	-	-	-	-	-	-	-	-	-	-	-	-	-	-	-
Bridge deck	1c	γ	1.00	1.00	1.00	1.00	1.00	1.00	1.00	1.00	1.00	1.00	1.00	1.00	1.00	1.00	1.00	1.00
bridge deck		Ψ	-	-	-	-	-	-	-	-	-	-	-	-	-	-	-	-
Wind bracing	1d	γ	1.00	1.00	1.00	1.00	1.00	1.00	1.00	1.00	1.00	1.00	1.00	1.00	1.00	1.00	1.00	1.00
wind bracing		Ψ	-	-	-	-	-	-	-	-	-	-	-	-	-	-	-	-
Ballast, rails,	1e	γ	1.00	1.00	1.00	1.00	1.00	1.00	1.00	1.00	1.00	1.00	1.00	1.00	1.00	1.00	1.00	1.00
sleepers		Ψ	-	-	-	-	-	-	-	-	-	-	-	-	-	-	-	-
Selfweight	1f	γ	1.00	1.00	1.00	1.00	1.00	1.00	1.00	1.00	1.00	1.00	1.00	1.00	1.00	1.00	1.00	1.00
cable trough		Ψ	-	-	-	-	-	-	-	-	-	-	-	-	-	-	-	-
Prestressing	1g	γ	1.00	1.00	1.00	1.00	1.00	1.00	1.00	1.00	1.00	1.00	1.00	1.00	1.00	1.00	1.00	1.00
trans. tendons		Ψ	-	-	-	-	-	-	-	-	-	-	-	-	-	-	-	-
Prestressing	1h	γ	1.00	1.00	1.00	1.00	1.00	1.00	1.00	1.00	1.00	1.00	1.00	1.00	1.00	1.00	1.00	1.00
long. tendons		Ψ	-	-	-	-	-	-	-	-	-	-	-	-	-	-	-	-
Load model 71	21a	γ								-								
		Ψ								0.8								
Eccentricity	21b	γ	-	-	-	-	-		-	-	-	-	-	-				
load model 71		Ψ	1.0	1.0	1.0	1.0	0.8		0.6	0.8	0.8	0.8	0.6	0.6				
Non-public	21d	γ	-	-	-	-	-	-	-									
footpaths		Ψ	0.5	0.5	0.5	0.5	0.5	0.5	0.5									
Groups of loads	gr11	γ	-				-				-							
		Ψ	1.0				0.8				0.8							
	gr14	γ		-								-						
		Ψ		1.0								0.8						
	gr21	γ			-				-				-					
		Ψ			1.0				0.6				0.6					
	gr24	γ				-								-				
		Ψ				1.0								0.6				
Lateral wind on	3a	γ	-	-	-		-	-	-		-	-	-		-	-	-	
arches		Ψ	0.5	0.5	0.5		0.6	0.6	0.6		0.0	0.0	0.0		0.5	0.5	0.5	
Lateral wind on	3b	γ	-	-	-		-	-	-		-	-	-		-	-	-	
hangers		Ψ	0.5	0.5	0.5		0.6	0.6	0.6		0.0	0.0	0.0		0.5	0.5	0.5	
Lateral wind on	3c	γ	-	-	-		-	-	-		-	-	-		-	-	-	
bridge deck		Ψ	0.5	0.5	0.5		0.6	0.6	0.6		0.0	0.0	0.0		0.5	0.5	0.5	
Longitudinal	3e	γ								-								-
wind		Ψ								0.6								0.5
Const. temp.	4a	γ	-	-	-	-	-	-	-	0.80	-	-	-	-	-	-	-	-
change		Ψ	0.6	0.6	0.6	0.6	0.6	0.6	0.6	-	0.5	0.5	0.5	0.5	0.5	0.5	0.5	0.6

Fig. A.7. Load combinations for assessment in serviceability limit state, infrequent and frequent combinations

			SERVICEABILITY LIMIT STATE				Additional load combinations	
			quasi-permanent load combinations	load combinations regarding deformations and vibrations				
Load comb. number				deck twist	rotation at the end of the deck/maximum vertical deflection	horizontal deflection of the deck	temp. effects	wind lift
Description			**46**	**47**	**48**	**49**	**50**	**51**
Selfweight	**1a**	γ	1.00	1.00	1.00	1.00	1.00	1.00
arches		Ψ	-	-	-	-	-	-
Hangers	**1b**	γ	1.00	1.00	1.00	1.00	1.00	1.00
hangers		Ψ	-	-	-	-	-	-
Bridge deck	**1c**	γ	1.00	1.00	1.00	1.00	1.00	1.00
bridge deck		Ψ	-	-	-	-	-	-
Wind bracing	**1d**	γ	1.00	1.00	1.00	1.00	1.00	1.00
wind bracing		Ψ	-	-	-	-	-	-
Ballast, rails,	**1e**	γ	1.00	1.00	1.00	1.00	1.00	1.00
sleepers		Ψ	-	-	-	-	-	-
Selfweight	**1f**	γ	1.00	1.00	1.00	1.00	1.00	1.00
cable trough		Ψ	-	-	-	-	-	-
Prestressing	**1g**	γ	1.00	1.00	1.00	1.00	1.00	1.00
trans. tendons		Ψ	-	-	-	-	-	-
Prestressing	**1h**	γ	1.00	1.00	1.00	1.00	1.00	1.00
long. tendons		Ψ	-	-	-	-	-	-
Load model 71	**21a**	γ	-	-	-	-		
		Ψ	-	1.0	1.0	1.0		
Eccentricity	**21b**	γ		-	-	-		
load model 71		Ψ		1.0	1.0	1.0		
Non-public	**21d**	γ		one side	one side			
footpaths		Ψ		0.5	0.5			
Nosing force	**21e**	γ		-	-	-		
		Ψ		0.8	0.8	0.8		
Lateral wind on	**3a**	γ		-	-	-		
arches		Ψ		0.5	0.5	0.5		
Lateral wind on	**3b**	γ		-	-	-		
hangers		Ψ		0.5	0.5	0.5		
Lateral wind on	**3c**	γ		-	-	-		
Bridge deck		Ψ		0.5	0.5	0.5		
Crosswind in	**3d**	γ						1.00
z-direction		Ψ						-
Const. temp.	**4a**	γ	-					
change		Ψ	0.5					
Vertically linear	**4b**	γ			-			
temp. change		Ψ			0.6			
Horizontally linear	**4c**	γ				-		
temp. change		Ψ				0.6		
Different temperature in different structural elements	**4d**	γ					1.00	
		Ψ					-	

Fig. A.8. Load combinations for assessment in serviceability limit state, quasi-permanent combinations, combinations regarding deformations and vibrations and additional load combinations

Preliminary design

B.1 Bridge deck

The preliminary design is be based on serviceability limit states, where category C is applicable to satisfy durability requirements (Annex D, Section D.5.2.2). Thus, the quasi-permanent combination of actions is relevant for the decompression, where no concrete tensile stresses are allowed. However, since the quasi-permanent combination does not include the Load Model 71 it is desirable to carry out the preliminary design with loads of the frequent load combination of actions applicable for the limit state of cracking. It was decided for load combination 40 with the following components and partial safety and combination factors (Annex A, Figure A.7):

ENV 1992-2: 1996
Table 4.118

- Self-weight: γ = 1.0
- Prestressing γ = 1.0
- Live load: 2 LM 71, ψ = 0.6
- Constant temperature change: ψ = 0.5

For the reason of approximation the constant temperature change is not considered.

B.1.1 Transverse direction

Statical system and loading

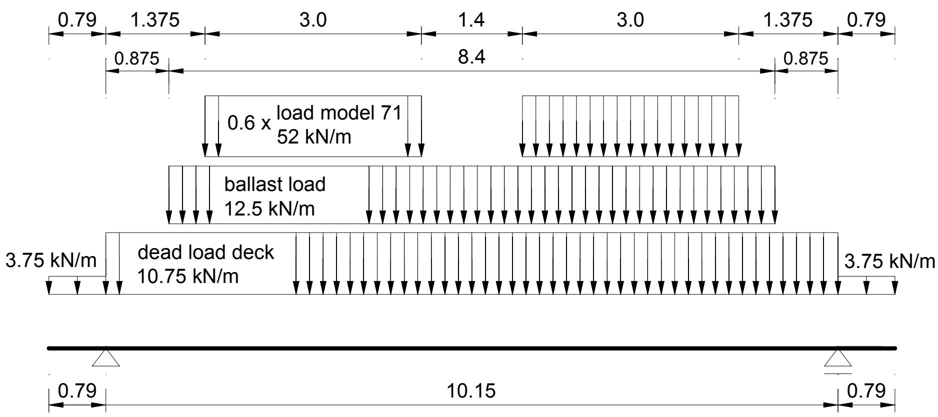

Fig. B.1: Statical system and loading in transverse direction

Internal forces and moments

For the purpose of preliminary design it is desirable to determine concrete stresses at the mid-span and at the quarter point. The respective internal forces are calculated in the following.

Dynamic factor: $\varphi_2 = 1.237$

Annex A, Section 2.1.2

1. Internal moments at $x = \frac{10.15}{4}\text{m} = 2.5375\text{m}$ (quarter point)

Bending moment due to dead load

Dead load of footpath: $3.75\frac{\text{kN}}{\text{m}^2} \cdot 0.8\text{m} = 3\frac{\text{kN}}{\text{m}}$

Dead load of deck between hangers: $10.75\frac{\text{kN}}{\text{m}^2} \cdot 10.15\text{m} = 110\frac{\text{kN}}{\text{m}}$

Reaction: $3\frac{\text{kN}}{\text{m}} + \frac{110}{2}\frac{\text{kN}}{\text{m}} = 58\frac{\text{kN}}{\text{m}}$

$$m_y = 58\frac{\text{kN}}{\text{m}} \cdot 2.5375\text{m} - 3\frac{\text{kN}}{\text{m}} \cdot \left(\frac{0.8}{2} + 2.5375\right)\text{m} - 10.75\frac{\text{kN}}{\text{m}^2} \cdot \frac{(2.5375\text{m})^2}{2}$$

$$\underline{m_y = 104\frac{\text{kNm}}{\text{m}}}$$

Bending moment due to ballast load

$$\underline{m_y = \frac{105}{2}\frac{\text{kN}}{\text{m}} \cdot 2.5375\text{m} - 12.5\frac{\text{kN}}{\text{m}^2} \cdot \frac{(2.5375\text{m} - 0.875\text{m})^2}{2} = 115.9\frac{\text{kNm}}{\text{m}}}$$

Bending moment due to LM 71

This bending moment results from the uniformly distributed load 80 kN/m. The bending moment resulting from the concentrated train load is determined below (Figure B.4, Figure B.5).

$$m_y = 0.6 \cdot 80\frac{\text{kN}}{\text{m}} \cdot 2.5375\text{m} - \frac{0.6 \cdot 80}{3}\frac{\text{kN}}{\text{m}^2} \cdot \frac{(2.5375\text{m} - 1.375\text{m})^2}{2} = 111\frac{\text{kNm}}{\text{m}}$$

$$\underline{m_y = \varphi_2 \cdot 111\frac{\text{kNm}}{\text{m}} = 137.3\frac{\text{kNm}}{\text{m}}}$$

2. Internal moments at $x = \frac{10.15}{2} m = 5.075m$ (centre point)

Bending moment due to dead load

$$m_y = 58 \frac{kN}{m} \cdot 5.075m - 3 \frac{kN}{m} \cdot \left(\frac{8}{2} + 5.075 \right) m - 10.75 \frac{kN}{m^2} \cdot \frac{(5.075m)^2}{2}$$

$$\underline{m_y = 140 \frac{kNm}{m}}$$

Bending moment due to ballast load

$$\underline{m_y = \frac{105}{2} \frac{kN}{m} \cdot 5.075m - 12.5 \frac{kN}{m^2} \cdot \frac{(5.075m - 0.875m)^2}{2} = 156.2 \frac{kNm}{m}}$$

Bending moment due to LM 71

$$m_y = 0.6 \cdot 80 \frac{kN}{m} \cdot 5.075m - 0.6 \cdot 80 \frac{kN}{m} \cdot (5.075m - 1.375m - 1.5m)$$

$$m_y = 138\, kNm/m$$

$$\underline{m_y = \varphi_2 \cdot 138 \frac{kNm}{m} = 171 \frac{kNm}{m}}$$

Distribution of concentrated train load of LM 71

For simplification in respect of the preliminary design, it is assumed that the 80 kN/m of the load model 71 are infinitely long without a gap. Hence, this load is only distributed in transverse direction. The additional 76 kN/m within the 6.4 m range are distributed in transverse as well as longitudinal direction. This 2-axial load distribution and the resulting bending moment is accounted for with the help of the influence surface charts by PUCHER *[26]*.

It was found by TEICH & WENDELIN *[38]* that for the transverse direction, results according to PUCHER *[26]* are conservative compared to results determined with a 3D model. Since the calculation of internal forces will be carried out with the help of a 3D model in SOFiSTiK, this preliminary design is on the safe side.

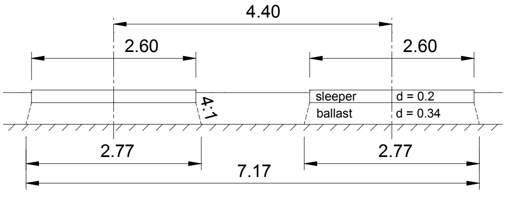

Fig. B.2. Load model 71: distribution in transverse direction, dimensions in [m]

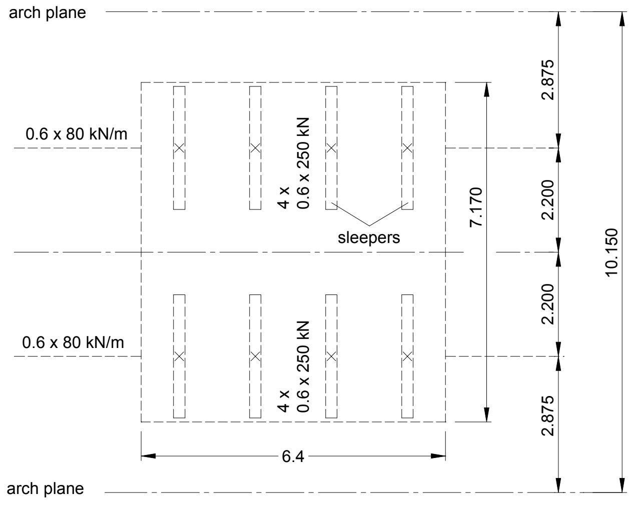

Fig. B.3. Load model 71: Distribution in plane, dimensions in [m]

The bending moments in transverse direction are calculated at the quarter point and mid-span in figures B.4 and B.5, respectively.

Quarter point: Evaluation with chart 3, PUCHER *[26]*

Loaded area	a [m]	6.4
	b [m]	7.17

Width of the deck	L [m]	10.15
Train load of LM 71	$0.6 \cdot p_{TL}$ [kN/m]	45.6
Distributed train load	p [kN/m^2] = $0.6 \cdot 2 \cdot p_{TL} / b$	12.72

Ordinates of patches on 1/4 of loaded area: h [-]				
0.5000	0.5000	0.5000	0.5200	0.5000
0.7000	0.7300	0.7500	0.8000	0.8200
1.0000	1.0000	1.0500	1.1000	1.2000
1.4500	1.4500	1.4500	1.5000	1.5000
1.7000	1.8000	1.8000	1.8000	1.8000

Sum of ordinates	Σh [-]	27.9200
Area of a single patch	A_1 [-] = $a / (10 \cdot L) \cdot b / (10 \cdot L)$	0.0045
Volume under 1/4 of loaded area	$V_{1/4}$ [-] = $A1 \cdot \Sigma h$	0.1244
Bending moment m_y [kNm/m]	m_y [kNm/m] = $4 \cdot p \cdot V_{1/4} \cdot L^2 / (8 \cdot \pi)$	25.9

Fig. B.4. Determination of bending moment at quarter point due to train load

Mid-span: Evaluation with chart 1, PUCHER *[26]*

Loaded area	a [m]	6.4
	b [m]	7.17

Width of the deck	L [m]	10.15
Train load of LM 71 per track	$0.6 \cdot p_{TL}$ [kN/m]	45.6
Distributed train load	p [kN/m^2] = $0.6 \cdot 2 \cdot p_{TL} / b$	12.72

Ordinates of patches on 1/4 of loaded area: h [-]				
1.20	1.25	1.30	1.40	1.45
1.80	1.90	2.00	2.00	1.90
2.50	2.70	2.80	2.80	2.60
2.80	2.90	3.80	3.50	3.10
6.00	5.20	4.50	3.90	3.40

Sum of ordinates	Σh [-]	68.7000
Area of a single patch	A_1 [-] = $a / (10 \cdot L) \cdot b / (10 \cdot L)$	0.0045
Volume under 1/4 of loaded area	$V_{1/4}$ [-] = $A1 \cdot \Sigma h$	0.3060
Bending moment m_y [kNm/m]	m_y [kNm/m] = $4 \cdot p \cdot V_{1/4} \cdot L^2 / (8 \cdot \pi)$	63.8

Fig. B.5. Determination of bending moment at mid-span due to train load

Materials

Concrete C80/60
ENV 1992-1-1 Table 3.1, 3.2

f_{ck} = 50 N/mm^2	Characteristic cylinder compressive strength
f_{ctm} = 4.1 N/mm^2	Mean value of the tensile strength
E_{cm} = 37000 N/mm^2	Value of the secant modulus of elasticity

Reinforcing steel S 500

f_{yk} = 500 N/mm^2	Characteristic yield strength
E_s = 200000 N/mm^2	Modulus of elasticity

DYWIDAG-SYSTEMS INTERNATIONAL [10]

Prestressing thread bars 36D	DYWIDAG Bonded Post-Tensioning Systems
$f_{p0.1k}$ = 1080 N/mm^2	Characteristic 0.1% proof-stress
f_{pk} = 1230 N/mm^2	Characteristic tensile strength
$P_y = f_{p0.1k} \cdot A_p$ = 1099 kN	Yield load
$P_u = f_{pk} \cdot A_p$ = 1252 kN	Ultimate load
A_p = 1018 mm^2	Nom. cross-sectional area
D = 36 mm	Nominal diameter
k = 0.3 °/m	Wobble factor
μ = 0.5	Friction factor
min f = 92 mm	Minimum centre distances
I.D. = 51 mm	Internal diameter of sheathing
O.D. = 57 mm	External diameter of sheathing
R_{min} = 12.1 m	Minimum radius for elastic bending

Concrete cover

Reinforcing steel: nom c = 40 mm
Prestressing thread bars: nom c = 67 mm

Annex D, Section D.5.1

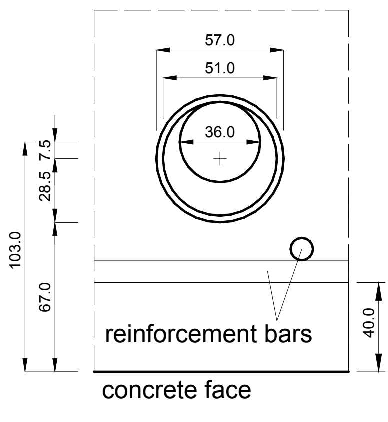

Fig. B.6. Concrete cover to thread bars, dimensions in [mm]

Prestressed concrete section properties

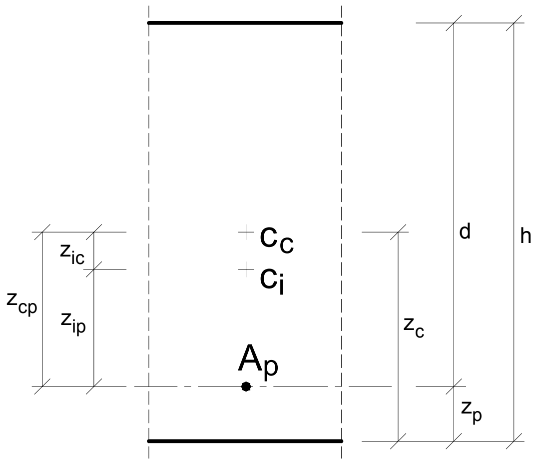

Fig. B.7. Nomenclature for prestressed concrete cross section

The relevant geometric values for calculating stresses at the top and bottom level of the prestressed concrete section as well as at the tendon level are calculated as follows:

$\alpha = E_s / E_{cm}$	(Equ. B.1)	Elastic modulus ratio
$z_c = h / 2$	(Equ. B.2)	Distance between centroid of concrete section and bottom level
$z_{cp} = z_c - z_p$	(Equ. B.3)	Distance between centroid of the concrete section and the thread bar
$z_{ic} = (\alpha - 1) \cdot A_z \cdot z_{cp} / A_i$	(Equ. B.4)	Distance between centroid of concrete section and centroid of composite section
$z_{ip} = z_{cp} - z_{ic}$	(Equ. B.5)	Distance between the thread bar and the centroid of the composite section
$I_i = I_c + (\alpha - 1) \cdot A_p \cdot z_{cp} \cdot z_{ip}$	(Equ. B.6)	Second moment of area of the composite section
$W_{it} = I_i / (z_c - z_{ci} - h)$	(Equ. B.7)	First moment of area of the composite section at top level
$W_{ib} = I_i / (z_c - z_{ci})$	(Equ. B.8)	First moment of area of the composite section at bottom level
$W_{ip} = I_i / z_{ip}$	(Equ. B.9)	First moment of area of the composite section at the prestressing level

Determination of prestressing force

ENV 1992-1-1: 1991 Section 2.5.4.2

The calculations of prestressing forces and concrete stresses were carried out by using a *Microsoft Excel* spreadsheet, Figure B.8. The formulas which were used are given and explained in the following. Reference is made by numbered equations.

The mean value of the prestressing force is given by:

$P_{m.\infty} = P_o - \Delta P_\mu - \Delta P_t(t = \infty)$ (Equ. B.10)

where:

$P_{m.\infty}$ is the mean value of the prestressing force at time $t = \infty$

P_o is the initial force at the active end of the thread bar immediately after stressing

ΔP_μ is the loss due to friction

$\Delta P_t(t = \infty)$ is the loss due to creep, shrinkage and relaxation at time $t = \infty$

Thread bars are not subjected to nut draw-in.

• Initial prestressing force

ENV 1992-1-1:1991 Section 4.2.3.5.4 (P2)

Maximum force applied to the thread bar immediately after stressing at the stressing end: $P_o \leq 0.8 \cdot A_p \cdot f_{pk}$ ($\leq 0.9 \cdot A_p \cdot f_{p0.1k}$)

ENV 1992-1-1: 1991 Section 4.2.3.5.4 (P3)

Maximum prestressing force immediately after tensioning:
$P_o \leq 0.75 \cdot A_p \cdot f_{pk}$ ($\leq 0.85 \cdot A_p \cdot f_{p0.1k}$)

• Loss of prestress

ENV 1992-1-1: 1991 Section 4.2.3.5.5

Loss of prestress in the thread bar due to friction

$$\Delta P_\mu(x) = P_o \cdot \left(1 - e^{-\mu \cdot (\Theta + k \cdot x)}\right) \qquad \text{(Equ. B.11)}$$

where:

μ is the coefficient of friction between thread bar and duct

Θ is the sum of the angular displacements over a distance x (irrespective of direction or sign)

k is an unintentional angular displacement (per unit length) related to the profile of the thread bar

x horizontal distance from stressing end

Prestressing force after the effect of friction: $P_\mu = P_o - \Delta P_\mu$ (Equ. B.12)

Loss of prestress due to nut draw-in

Thread bars are especially suitable for short tendons, because they result in very low seating loss. The threadability of the anchor nut offers the advantage of adjusting the prestress force in the tendon at any given time before grouting.

DYWIDAG-SYSTEMS INTERNATIONAL [10]

Time dependent losses due to creep, shrinkage and relaxation

$$\Delta P_t = \Delta\sigma_{p.c+s+r} \cdot A_p = \frac{\varepsilon_{s.\infty} \cdot E_s + \Delta\sigma_{pr} + \alpha \cdot \varphi(t=\infty.t_o) \cdot (\sigma_{cg} + \sigma_{cpo})}{1 + \alpha \frac{A_{p.m}}{A_c}\left(1 + \frac{A_c}{I_c} \cdot z_{cp}^2\right) \cdot (1 + 0.8 \cdot \varphi(t.t_o))} \cdot A_p \quad \text{(Equ. B.13)}$$

where:

$\Delta\sigma_{p.c+s+r}$ is the variation of stress in the thread bars due to creep, shrinkage and relaxation at location x, at time t = ∞

$\varepsilon_{S.\infty}$ is the estimated shrinkage strain at time t = ∞ taken from *ENV 1992-1-1: 1991 Table 3.4*

$\alpha = E_s / E_{cm}$ Elastic modulus ratio

$\Delta\sigma_{pr}$ is the variation of stress in the thread bar at section x due to relaxation, which is derived from *ENV 1992-1-1: 1991 Figure 4.8*, for a ratio of Initial stress/Characteristic tensile stress σ_p / f_{pk} calculated from: $\sigma_p = 0.85 \cdot \sigma_{pgo}$ (Equ. B-14)
σ_{pgo} is the initial stress in the thread bar due to prestress and permanent action with:

$$\sigma_{pgo} = \frac{P_o - \Delta P_\mu}{A_p} \quad \text{(Equ. B.15)}$$

The long term values of the relaxation losses are assumed to be three times the relaxation losses after 1000 h:
$\Delta\sigma_{pr.\infty} = 3 \cdot \Delta\sigma_{pr}$ (Equ. B-16)

ENV 1992-1-1: 1991 Section 4.2.3.4.1.

$\varphi(t = \infty, t_o)$ is the creep coefficient according to *ENV 1992-1-1: 1991 Table 3.3* with the notional size $2 \cdot A_c / u$
where:
A_c is the cross-sectional area of concrete
u is the perimeter of that area exposed to environmental conditions

σ_{cg} is the stress in the concrete adjacent to the thread bars, due to self-weight and any other permanent actions (ballast load)

$$\sigma_{cg} = \frac{m_{y.SW}}{W_p} + \frac{m_{y.B}}{W_{ip}} \quad \text{(Equ. B.17)}$$

σ_{cpo} is the initial stress in the concrete adjacent to the thread bars, due to prestress

$$\sigma_{cpo} = -\frac{\left(P_o - \Delta P_\mu\right)}{A_c \cdot f} - \frac{\left(P_o - \Delta P_\mu\right) \cdot z_{cp}}{W_p \cdot f} \quad \text{(Equ. B.18)}$$

$A_{p.m}$ is the area of the prestressing bars at the level being considered

A_c is the area of the concrete section

I_c is the second moment of area of the concrete section

z_{cp} is the distance between the centre of gravity of the concrete section and the thread bar

According to the serviceability requirement for the limit state of cracking the calculated minimum reinforcement is sufficient if the concrete stresses do not exceed the mean tensile strength, which is 4.1 N/mm^2 for C50/60 (Annex D.5, Figure D.21: Requirements). This requirement will be the basis for the preliminary design. Moreover, the concrete compressive stress shall be limited to 22.5 N/mm^2 at the time directly after prestressing (Annex D.5, Figure D.21: Requirements).

It is desired to provide a margin covering unconsidered strains such as the temperature change.

The spreadsheet in Figure B.9 provided the possibility to change the distance between the thread bars. The concrete stress at the mid-span bottom fibre appears to be decisive and a value of 0.83 N/mm^2 (tension) led to a bar distance of 270 mm.

It was necessary to split the calculation of friction losses at the quarter span, since two adjacent thread bars have different geometries (Figure B.8). Each thread bar is only stressed from one end. The dead ends lie at a higher location than the stressed ends of the neighbouring bars.

For one and the same quarter point, the thread bars stressed from the left experience different friction losses than the bar stressed from the right. Because the prestressing is calculated for one metre width, the mean value of the friction losses of two adjacent thread bars was calculated.

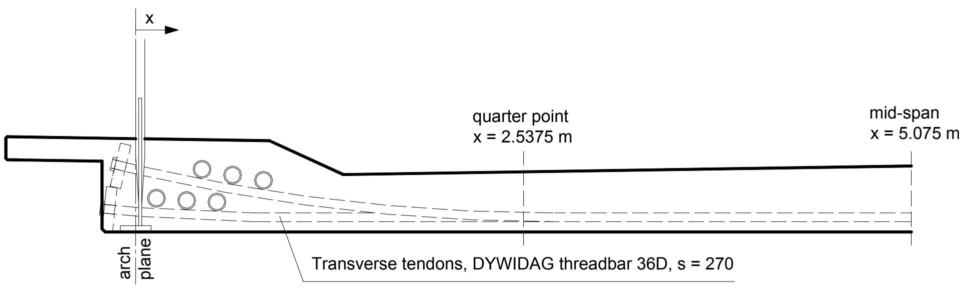

Fig. B.8. Transverse prestressing with relevant sections for preliminary design

Material properties and factors			
Compressive strength of C50/60	f_{ck} [N/mm^2]		50
Tensile strength of C50/60	f_{ctm} [N/mm^2]		4.1
Secant modulus of elasticity	E_{cm} [N/mm^2]		37000
Elastic modulus of steel	E_s [N/mm^2]		200000
Elastic modulus ratio	α	Equ. B.1	5.41
Cross-sectional area per thread ba	[cm^2]		10.18
Yield load	$f_{p0.1k} \cdot A$ [kN]		1099
Yield stress	$f_{p0.1k}$ [N/mm^2]		1080
Ultimate load	$f_{pk} \cdot A$ [kN]		1252
Ultimate stress	f_{pk} [N/mm^2]		1230
Sheathing tube inner diameter	I.D. [mm]		51
Sheathing tube outer diameter	O.D. [mm]		57
Minimum radius for elastic bending	R_{min} [m]		12.1
Wobble factor	k		0.0052
Friction factor	μ		0.5

Prestressing		
Allowable prestress force	P_0 [kN] = $0.9 \cdot f_{p0.1k} \cdot A$	989.1
	P_0 [kN] = $0.8 \cdot f_{pk} \cdot A$	1001.6
	P_0 [kN] = $0.85 \cdot f_{p0.1k} \cdot A$	934.15
	P_0 [kN] = $0.75 \cdot f_{pk} \cdot A$	939
Critical value	P_0 [kN]	934.15
Spacing of thread bars	f [m]	**0.27**
Cross-sectional area of prestressing	[m^2/m]	0.0037704

Internal moments	**coordinate x**		**2.5375**	**5.075**
Moment due to dead load	$m_{y.DL}$ [kNm/m]		104	140
Moment due to ballast	$m_{y.B}$ [kNm/m]		116	156.2
Moment due to LM 71 UDL load 80 kN/m	$m_{y.LM71.80}$ [kNm/m]		137.3	171
Moment due to concentrated train load	$m_{y.LM71.Train}$ [kNm/m]		26	64
Moment due to complete LM 71	$m_{y.LM71}$ [kNm/m]		163.3	235

Section properties				
Depth of the deck at distance x	d [m]		0.3914	0.4300
Dstance: thread bar - bottom level	z_p [m]		0.1030	0.1030
Area of concrete section	A_c [m^2/m]		0.3914	0.4300
2nd moment of area of concrete section	I_c [m^4]		0.0050	0.0066
1st m. of area at top of concrete section	W_t [m^3]		-0.0255	-0.0308
1st m. of area at bottom of concrete section	W_b [m^3]		0.0255	0.0308
1st m. of area at thread bar level	W_p [m^3]		0.0539	0.0592
Virtual area of composite section	A_i [m^2/m]		0.4080	0.4466
Dist.: centroid conc. sec. - bottom level	z_c [m]	Equ. B.2	0.1957	0.2150
Dist: centroid of conc. sec. - thread bar	z_{cp} [m]	Equ. B.3	0.0927	0.1120
Dist.: centroids conc. sec. - comp. sec.	z_{ci} [m]	Equ. B.4	0.0038	0.0042
Dist.: centroid comp. sec. - thread bar	z_{ip} [m]	Equ. B.5	0.0889	0.1078
2nd moment of area of composite section	I_i [m^4]	Equ. B.6	0.0051	0.0068
1st m. of area at top of composite section	W_{it} [m^3]	Equ. B.7	-0.0257	-0.0311
1st m. of area, bottom of composite section	W_{ib} [m^3]	Equ. B.8	0.0267	0.0324
1st m. of area, thread bar level, composite	W_{ip} [m^3]	Equ. B.9	0.0577	0.0633

Fig. B.9. Preliminary design of bridge deck in transverse direction, continued below

Friction	coordinate x:		2.5375	7.6125	5.075	5.075
Sum of angular displacements	Θ [°]		7.363	12.235	7.363	12.235
	ΔP_{μ} [kN]	Equ. B.11	63.94	111.17	69.70	105.68
Prestress loss due to friction	mean value ΔP_{μ}		87.55		87.69	
	P_{μ} [kN]	Equ. B.12	870.21	822.98	864.45	828.47
Prestressing force after friction	mean value P_{μ}		846.60		846.46	
Prestress per metre width at time t = 0	[kN/m]		3135.55		3135.04	
Thread bar stress	[N/mm^2]		831.63		831.49	
Relaxation						
Initial stress in thread bar due to P	σ_{pgo} [N/mm^2]	Equ. B.15	831.63		831.49	
	σ_p [N/mm^2]	Equ. B.14	706.89		706.77	
	σ_p / f_{pk} [%]		56.46		56.45	
ENV 1992-1-1:1991 Figure 4.8	relaxation [%]		1.50		1.50	
Relaxation loss after 1000h	$\Delta\sigma_{pr}$ [N/mm^2]		10.60		10.60	
Relaxation loss at time t=∞	$\Delta\sigma_{pr,\infty}$ [N/mm^2]	Equ. B.16	31.81		31.80	
Creep, shrinkage, relaxation losses						
Notional size [mm] = 430	$\varphi_{u,28}$ = 1.50		shrinkage coefficient $\varepsilon_{cs,u}$ = 0.00028			
Conc. stress adjacent to bars (DL)	σ_{cg} [N/mm^2]	Equ. B.17	3.94		4.83	
Initial conc. stress adjacent to bars	σ_{cpo} [N/mm^2]	Equ. B.18	-13.05		-12.84	
Prestress loss at time t=∞	ΔP_t [kN]	Equ. B.13	-138.09		-130.72	
Prestressing force after friction, relaxation, creep, shrinkage						
Prestress in thread bar at time t=∞	$P_{m,t}$ [kN]	Equ. B.10	708.50		715.74	
Prestress per [m] width at time t=∞	$P_{m,t}$ [kN/m]		2624.09		2650.90	
Thread bar stress	[N/mm^2]		695.98		703.09	
Primary strain	ε_{pm}		0.003480		0.003515	
Concrete stresses at frequent combination of actions						
At time t = 0						
Concrete stress due to prestressing						
top	[N/mm^2]		3.37		4.10	
bottom	[N/mm^2]		-19.40		-18.68	
Concrete stress due to dead load						
top	[N/mm^2]		-4.07		-4.54	
bottom	[N/mm^2]		4.07		4.54	
Sum of concrete stress						
top	[N/mm^2]		**-0.70**		**-0.44**	
bottom	[N/mm^2]		-15.32		-14.14	
At time t = ∞						
Concrete stress due to prestressing						
top	[N/mm^2]		2.82		3.47	
bottom	[N/mm^2]		-16.23		-15.80	
Concrete stress due to dead load						
top	[N/mm^2]		-8.58		-9.56	
bottom	[N/mm^2]		8.41		9.37	
Concrete stress due to load model 71						
top	[N/mm^2]		-6.35		-7.55	
bottom	[N/mm^2]		6.11		7.26	
Sum of concrete stress						
top	[N/mm^2]		-12.10		-13.63	
bottom	[N/mm^2]		**-1.72**		**0.83**	

Fig. B.9. Preliminary design of bridge deck in transverse direction

B.1.2 Longitudinal direction

The lower chord is mainly subjected to axial load. Bending moments are secondary and will therefore be neglected in the preliminary design. However, an additional prestress of 30% will be applied to compensate for the influence of bending moments.

According to TVEIT *[41]*, the axial force in the lower chord at a distance x from one support due to a uniformly distributed load is to be calculated as follows:

$$K_u = \frac{w \cdot (l - x) \cdot x}{2 \cdot h} - \frac{1}{2} \cdot l \cdot w \cdot \cot^2 v_h \qquad \text{(Equ. B.19)}$$

w	uniformly distributed load per unit length of lane
l = 100 m	length of the span
h = 17 m	rise of the arch
v_h = 60°	average angle of the hangers crossing a vertical line at a distance x from the support

The uniformly distributed load w is calculated further below.

Section properties

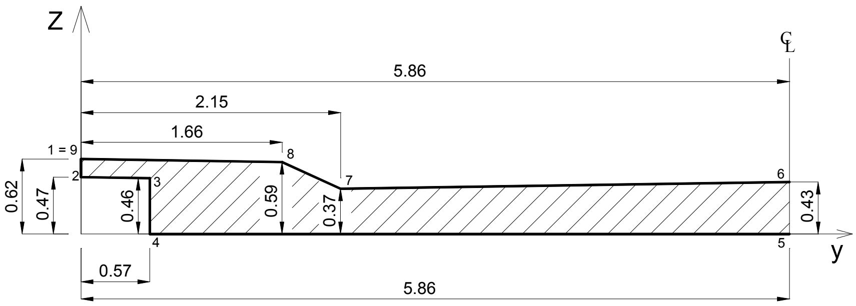

Fig. B.10. Cross section with numbered points assisting the calculation in Figure B.11

The numbering of the corner points in Figure B.10 corresponds to the first column (i) in Fig. B.11.

Calculation of cross section properties								
			A	B	C	A · C	D	E = A · (C² - D)
i	yi	zi	$y_i \cdot z_{i+1} - z_i \cdot y_{i+1}$	$y_i + y_{i+1}$	$z_i + z_{i+1}$		$z_i \cdot z_{i+1}$	
1	0	0.62	0.00	0	1.02	0	0.248	0
2	0	0.4	-0.228	0.57	0.86	-0.1961	0.184	-0.1266768
3	0.57	0.46	-0.2622	1.14	0.46	-0.1206	0	-0.05548152
4	0.57	0	0	6.43	0	0	0	0
5	5.86	0	2.5198	11.72	0.43	1.0835	0	0.46591102
6	5.86	0.43	1.2437	8.01	0.8	0.995	0.1591	0.59809533
7	2.15	0.37	0.6113	3.81	0.94	0.5746	0.2109	0.41122151
8	1.66	0.57	1.0292	1.66	1.19	1.2247	0.3534	1.09373084
9	0	0.62	0	0	1.24	0	0.3844	0
$A_c = 0.5 \cdot \Sigma A =$ 2.46					$S_y = \Sigma (A \cdot C) / 6 =$ 0.5935			
$e_b = S_y / A_c =$ 0.242					$I_y^* = 1/12 \cdot \Sigma E =$ 0.1989			
units: [m], [m²], [m⁴]					$I_y = I_y^* - A_c \cdot e_b^2 =$ 0.0555			

Fig. B.11. Calculation of section properties of one half of the bridge deck

The cross section properties calculated in Figure B.11. refer to one half of the bridge deck.

Summary of cross section areas for one half of the bridge deck:
$A_c = 2.46\ m^2$
$I_y = 0.0555\ m^4$

The tendon geometry is symmetrical to the centroid of the concrete section.

Statical system and loading

The preliminary design is to determine the required prestressing force for one edge beam. Therefore, only one half of the bridge loading is considered.

Dead load

Self-weight of prestressed concrete deck

Cross section area of one half of the concrete deck: $A = 2.46\ m^2$

$$\underline{g_{deck} = 25\frac{kN}{m^3}\cdot 2.46m^2 = 62\frac{kN}{m}}$$

Self-weight ballast, sleepers, rails

Annex A – Load Assumptions

$$\underline{g_{track} = \frac{105\,kN/m}{2} = 52.5\,kN/m}$$

Self-weight arch

For preliminary design purposes, one and the same profile will be assumed for the whole arch length.

Arch profile: American wide flange W 360 x 410 x 990
Weight: 990 kg/m
Approximate arch length: 107m

$$\underline{g_{arch} = 990\,kg/m\cdot 9.81m/s^2\cdot 107m/100m = 10.4kN/m}$$

Total dead load

$$g_k = g_{deck} + g_{track} + g_{arch}$$
$$\underline{g_k = (62 + 52.5 + 10.4)kN/m = 125\,kN/m}$$

Total dead load without ballast load

$$g_{k.no-ballast} = (62 + 10.4)kN/m = 72.4\,kN/m$$

Live load

Load model 71

Uniformly distributed load:

$q_{71.UDL} = 80\,kN/m$

Concentrated train load:

"Concentrated loads are converted into evenly distributed loads by multiplying by 2 and dividing by the length of the influence line. This is because the maximum ordinate of an influence line is usually nearly twice as big as the average ordinate", TVEIT *[47],* page 5.

$$q_{71.train} = \frac{76\,kN/m \cdot 6.4m \cdot 2}{100m} = 9.73\frac{kN}{m}$$

Total LM 71:

Multiplying by Ψ = 0.6 (frequent combination of actions)

$q_{71} = 0.6 \cdot (q_{71.UDL} + q_{71.train}) = 53.8\,kN/m$

Applying the dynamic factor:

$q_{71} = \varphi \cdot q_{71} = 1.044 \cdot 53.8 = 56.2\,kN/m$

Total

$w = g_k + q_k = (125 + 56.2)kN/m = 181.2\,kN/m$

Internal forces and moments

Axial force in lower chord due to self-weight without ballast

$$K_{u.DL} = \frac{72.4\frac{kN}{m} \cdot (100m - 50m) \cdot 50m}{2 \cdot 17m} - \frac{1}{2} \cdot 17m \cdot 72.4\frac{kN}{m} \cdot \cot^2 60° = 5118kN$$

Axial force in lower chord due to ballast load

$$K_{u.B} = \frac{52.5\frac{kN}{m} \cdot (100m - 50m) \cdot 50m}{2 \cdot 17m} - \frac{1}{2} \cdot 17m \cdot 52.5\frac{kN}{m} \cdot \cot^2 60° = 3711.5kN$$

Axial force in lower chord due to live load

$$K_{u.LL} = \frac{56.2\frac{kN}{m} \cdot (100m - 50m) \cdot 50m}{2 \cdot 17m} - \frac{1}{2} \cdot 17m \cdot 56.2\frac{kN}{m} \cdot \cot^2 60° = 3973kN$$

Axial force in lower chord due to total load

$K_u = \Sigma K_i = 12802kN$

Materials

Concrete C50/60 *ENV 1992-1-1 Table 3.1, 3.2*

$f_{ck} = 50\ N/mm^2$	Characteristic cylinder compressive strength
$f_{ctm} = 4.1\ N/mm^2$	Mean value of the tensile strength
$E_{cm} = 37000\ N/mm^2$	Value of the secant modulus of elasticity

Reinforcing steel S 500

$f_{yk} = 500\ N/mm^2$	Characteristic yield strength
$E_s = 200000\ N/mm^2$	Modulus of elasticity

Prestressing strands type 15mm (prEN 10138)	DYWIDAG Bonded Post-Tensioning Systems	*DYWIDAG-SYSTEMS INTERNATIONAL [10]*

$f_{p0.1.k} = 1500\ N/mm^2$	Yield strength
$f_{pk} = 1770\ N/mm^2$	Ultimate strength
$A_p = 150\ mm^2$	Cross-sectional area
$P_u = f_{pk} \cdot A_p = 265\ kN$	Ultimate load
$D = 15.70\ mm$	Nominal diameter
$E_s = 195000\ N/mm^2$	Modulus of elasticity
max.2.5%	Relaxation after 1000h at $0.7 \cdot P_u$

Required number of strands

The axial forces in the tie result from loads acting on the bridge deck. These loads are transferred through the hangers into the arch, resulting in a horizontal thrust which is constrained by the tie. This leads to high axial forces in the tie.

Bending moments result from local effects of loads on the bridge deck between constraints given by the hanger nodes. Furthermore, bending moments occur due to deformation of the whole bridge structure. Strains due to the axial forces are significantly higher than strains caused by the bending moments.

For the preliminary design purpose the concrete section was intended to be in compression after all prestress losses and due to axial loads, leaving a margin for the not considered but minor bending moments in the tie. With the concrete left in compression, the number of strands and tendons was determined with the help of a *Microsoft Excel* spread sheet, Figure B.12.

STEIMANN *[37]* used tendons with 27 strands making 6 tendons per edge beam necessary. It was decided to use the same tendon type:

Tendon type with 27 strands of type 15mm: Type 6827 with corrugated sheathing

DYWIDAG-SYSTEMS INTERNATIONAL [10]

I.D. = 110 mm	Internal diameter of sheathing
O.D. = 118 mm	External diameter of sheathing
Min f = 198 mm	Minimum centre distances
k = 0.3°/m	Wobble angle
μ = 0.2	Friction factor

The equations used for the preliminary design for longitudinal direction (Figure B.12) are basically the same as used for the transverse direction. Differences are explained in the following.

• Loss due to wedge draw-in

In contrast to the thread bars used in transverse direction, the prestressing of tendons in longitudinal direction experiences losses due to wedge draw-in. The slip at the stressing anchorage has to be taken to Δl_n = 2 mm, according to DYWIDAG – SYSTEMS INTERNATIONAL *[10]*. Wedge draw-in has effects within the influence length only. Since the effect of friction is largest at mid-span, this will be the decisive concrete section. The influence length of the nut draw-in does not reach the mid-span and therefore does not need to be considered. Nevertheless, the equations are given in case it is desired to determine the prestressing force at a different location.

$$\Delta P_{sl} = P_o \cdot (1 - 2 \cdot l_e \cdot \mu \cdot \gamma_1)$$ (Equ. B.20) Prestress loss due to wedge draw-in

$$l_e = \sqrt{\frac{\Delta l_n \cdot E_s \cdot A_p}{P_o \cdot \mu \cdot \gamma_1}}$$ (Equ. B.21) Influence length

Δl_n	nut draw-in in [mm]
γ_1	average angle of deflection along the influence length l_e of tendon behind the stressing end [rad/m]
μ	coefficient of friction

• Time dependent losses due to creep, shrinkage and relaxation

Creep and shrinkage coefficients

The notional size for the longitudinal direction differs from the value obtained for the transverse direction. This has influence on the creep and shrinkage coefficients, which are determined in the following.

Notional size = $\frac{2 \cdot A_c}{u}$

The perimeter of the bridge deck section was measured to u = 24.7 m

$$\frac{2 \cdot A_c}{u} = \frac{2 \cdot 2.46\text{mm}^2}{24.7\text{mm}} = 200\text{mm}$$

$\varphi(t = \infty, t_o) = 1.6$	Creep coefficient for a loading age of 28 days and 80% relative humidity *ENV 1992-1-1: 1991 Table 3.3*
$\varepsilon_{s.\infty} = -0.0003$	Shrinkage strain at time t = ∞ taken from *ENV 1992-1-1: 1991 Table 3.4*

The stress in the concrete adjacent to the tendons, due to self-weight and ballast load, is calculated on the basis of the axial force only:

$$\sigma_{cg} = \frac{K_{u.DL} + K_{u.B}}{A_c} = \frac{5118\text{kN} + 3711.5\text{kN}}{2460000\text{mm}^2} = 3.59\frac{\text{N}}{\text{mm}^2}$$ (Equ. B.22)

The initial stress in the concrete adjacent to the tendons, due to prestressing, is calculated with the following:

$$\sigma_{cpo} = -\frac{(P_o - \Delta P_\mu)}{A_c \cdot f}$$ (Equ. B.23)

Material properties			
Compressive strength of C50/60	f_{ck} [N/mm^2]		50
Tensile strength of C50/60	f_{ctm} [N/mm^2]		4.1
Secant modulus of elasticity	E_{cm} [N/mm^2]		37000
Elastic modulus of steel	E_s [N/mm^2]		195000
Elastic modulus ratio	α	Equ. B.1	5.27
Cross-sectional area per strand	[mm^2]		150
Yield strength	$f_{p0.1k}$ [N/mm^2]		1500
Ultimate strength	f_{pk} [N/mm^2]		1770
Sheathing tube inner diameter	I.D. [mm]		110
Sheathing tube outer diameter	O.D. [mm]		118
Material properties	min f [mm]		198
Wobble factor	k		0.005235988
Friction factor	μ		0.2
Nut draw-in	Δl_n [mm]		2
Number of strands per tendon	n		**27**
Number of tendons per edge beam	m		**6**
Prestressing area per tendon	A_{tendon} [mm^2]		4050

Prestressing per tendon			
Allowable prestressing force	P_0 [kN] = 0.9 · $f_{p0.1k}$		5467.5
	P_0 [kN] = 0.8 · f_{pk}		5734.8
	P_0 [kN] = 0.85 · $f_{p0.1k}$		5163.75
	P_0 [kN] = 0.75 · f_{pk}		5376.375
Critical value	P_0 [kN]		5163.75
Internal forces	**coordinate x**		**50**
Axial force due to self-weight	$K_{u.DL}$ [kN]		5118
Axial force due to ballast load	$K_{u.B}$ [kN]		3711.5
Axial force due to live load	$K_{u.LL}$ [kN]		3973
Total axial force	K_u [kN]		12802.5
Section properties			
Concrete cross section area	A_c [mm^2]		2460000
Friction			
Sum of angular displacements over dist. x	Θ [°]		20
Prestress loss due to friction	ΔP_μ [kN]	Equ. B.11	593.86
Prestressing force after friction	P_μ [kN]	Equ. B.12	4569.89
Prestress of edge beam at time t=0	P_μ [kN]		27419.36
Tendon stress	[N/mm^2]		1128.37
Wedge draw-in			
Average angle of deflection along l_e	γ_1 [rad/m]		0.017
Influence length	l_e [m]	Equ. B.21	10.08
Not applicable at mid-span	ΔP_n [kN]	Equ. B.20	0
Prestressing force after wedge draw-in	P_n [kN]		4569.89

Fig. B.12. Preliminary design of bridge deck in longitudinal direction, continued below

Relaxation			
Initial stress in thread bar due to prestress	σ_{pgo} [N/mm^2]	Equ. B.15	1128.37
	σ_p [N/mm^2]	Equ. B.14	959.11
	σ_p/f_{pk} [%]		54.19
ENV 1992-1-1:1991 Figure 4.8	relaxation [%]		1
Relaxation loss after 1000h	$\Delta\sigma_{pr}$ [N/mm^2]		9.59
Relaxation loss after 1000h	$\Delta\sigma_{pr,\infty}$ [N/mm^2]	Equ. B.16	28.77
Creep, shrinkage, relaxation losses			
Motional size [mm] = 200	σ_{cg} [N/mm^2]	Equ. B.22	3.59
Creep coefficient $\phi_{u,28}$ = 1.6	σ_{cpo} [N/mm^2]	Equ. B.23	-11.15
Shrinkage coefficient $\varepsilon_{cs,u}$ 0.0003	ΔP_{tt}	Equ. B.13	-599.67
Prestress in thread bar at time t = ∞	$P_{m,t}$ [kN]	Equ. B.10	3970.22
Prestress per edge beam at time t = ∞	$P_{m,t}$ [kN]		23821.34
P (t=0) / P (t=00)			0.87
Tendon stress	[N/mm^2]		980.30
Primary strain	ε_{pm}		0.00502719
Concrete stresses at frequent combination of actions			
At time t = 0			
Concrete stress due to prestressing	N/mm^2		-11.15
Concrete stress due to dead load	N/mm^2		2.08
Total	N/mm^2		**-9.07**
At time t = ∞			
Concrete stress due to prestressing	N/mm2		-9.68
Concrete stress due to dead load	N/mm^2		3.59
Concrete stress due to live load	N/mm^2		1.62
Total	N/mm^2		**-4.48**

Fig. B.12. Preliminary design of bridge deck in longitudinal direction

The application of 6 tendons type-6827 (DYWIDAG *[10]*) per edge beam leads to a concrete compressive stress of 4.48 N/mm^2 after all losses at mid-span (x = 50 m). The margin is to compensate for not considered bending moments.

B.2 Arch

TVEIT *[41]* provides a formula for calculating an approximate axial force in the arch. This equation will be used for the preliminary dimensioning of the arch profile. Bending moments have been omitted, as they contribute only little to the strain of the profile.

Axial force in the arch at a distance x from one support due to a uniformly distributed load:

$$K_o = \frac{1}{\cos(v_o)} \cdot \left(\frac{w \cdot (l - x) \cdot x}{2h} + \frac{1}{2} \cdot h \cdot w \cdot \cot^2 v_h \right)$$

$v_o = 0°$	slope of the arch (max. arch force expected at mid-span)
w	uniformly distributed load per unit length of lane
l = 100 m	length of the span
h = 17 m	rise of the arch
$v_h = 60°$	average angle of the hangers crossing a vertical line at mid-span

The uniformly distributed load is calculated in the following.

Loading

Loads have partly been determined in Section B.1.2 of this Annex. An additional live load on the non-public footpaths is required. The preliminary design of the arch profile will be based on the ultimate limit state. Dead loads and live loads are therefore multiplied by the partial safety factors of 1.35 and 1.5, respectively.

Dead load

Self-weight of the bridge deck, ballast, rails and sleepers:

Annex B, Section B.1.2:

$$g_k = 125\,\text{kN/m}$$

$$g_d = g_k \cdot 1.35 = 168.8\,\text{kN/m}$$

Live load

Annex B, Section B.1.2.

Annex A, Section 2.1.2

$$q_{71.UDL} = 80\,\text{kN/m}$$

$$q_{71.train} = 9.73\,\text{kN/m}$$

$\varphi_2 = 1.044$

$$q_{71.k} = \varphi_2 \cdot (q_{71.UDL} + q_{71.train}) = 1.044 \cdot (80 + 9.73)\,\text{kN/m} = 93.7\,\text{kN/m}$$

$$q_{footpath} = 5\,\text{kN/m}^2 \cdot 0.75\,\text{m} = 3.75\,\text{kN/m}$$

$$q_{71.d} = 1.5 \cdot (q_{71} + q_{footpath}) = 1.5 \cdot (93.7 + 3.75)\,\text{kN/m} = 146.2\,\text{kN/m}$$

Total

$$w = g_d + q_d = (168.8 + 146.2)\,\text{kN/m} = 315\,\text{kN/m}$$

Internal forces and moments

$$K_o = \frac{1}{\cos(v_o)} \cdot \left(\frac{w \cdot (l - x) \cdot x}{2h} + \frac{1}{2} \cdot h \cdot w \cdot \cot^2 v_h \right)$$

$$K_o = \frac{315\,\text{kN/m} \cdot (100\text{m} - 50\text{m}) \cdot 50\text{m}}{2 \cdot 17\text{m}} + \frac{1}{2} \cdot 17\text{m} \cdot 315\,\text{kN/m} \cdot \cot^2 60°$$

$$K_o = 24054\text{kN}$$

Arch profile

The bridge calculated in STEIMANN *[37]* uses an arch rise of 15 metres with otherwise similar geometric properties and loading compared to the bridge calculated in this work which has a rise of 17 metres. The higher rise leads to smaller axial forces in the arch. It has therefore been decided to use a smaller profile than that taken by STEIMANN *[37]* who uses an American Wide Flange W 360x410x990.

Chosen profile: American Wide Flange W 360x410x900 (Class 1)
Cross section area: A = 1149 cm^2
ARCELOR LONG COMMERCIAL S.A. *[4]*

ENV 1993-2: 1997
Table: 3.1a

Material: Steel S 460 ML
f_y = 430 N/mm^2

Resistance in ultimate limit state

ENV 1993-1-1: 1992
Section 5.4.4

$$N_{Sd} \leq N_{c.Rd}$$

$$N_{c.Rd} = N_{pl,Rd} = A \cdot \frac{f_y}{\gamma_{M0}} = 1149\text{cm}^2 \cdot \frac{430 \frac{N}{mm^2}}{1.1} = 44915\text{kN}$$

$$\frac{K_o}{N_{pl.Rd}} = \frac{24054\text{kN}}{44915\text{kN}} = 0.54 < 1$$

The margin in the check will compensate for bending moments as well as weakening by fastener holes which are not considered in the preliminary design.

Buckling of arch

The span and loading of the bridge calculated in this work corresponds to the conditions in STEIMANN *[37],* where buckling appeared not to be critical. It will therefore be omitted in this preliminary design.

B.3 Hangers

Loading

Dead load

Self-weight of the bridge deck, ballast, rails and sleepers:

$g_k = 125\,kN/m$

There must be a distinction made between concentrated loads and uniformly distributed loads. Even though live loads have been calculated in Section B.1 and B.2, they will be listed here again.

Live load

Load model 71

Uniformly distributed load	$q_{71.UDL} = 80\,kN/m$
Concentrated load	$Q_{71} = 76\,kN/m \cdot 6.4m = 487kN$
Live load on footpath	$q_{footpath} = 5\,kN/m^2 \cdot 0.75m = 3.75\,kN/m$

It is desirable to obtained information about hanger forces in ultimate as well as serviceability limit states. The characteristic loads are therefore multiplied with the respective partial safety factors to determine design loads. The dynamic factor will also be applied.

Dynamic factor: φ_2 = 1.044 (Annex A, Section 2.1.2)

Ultimate limit states:

$g_{d.ult} = g_k \cdot 1.35 = 125\,kN/m \cdot 1.35 = 168.75\,kN/m$

$q_{d.ult} = (q_{71.UDL} \cdot \varphi_2 + q_{footpath}) \cdot 1.5 = (80 \cdot 1.044 + 3.75)kN/m \cdot 1.5 = 130.9\,kN/m$

Total uniformly distributed load: $w_{d.ult} = g_{d.ult} + q_{d.ult} = 300\,kN/m$

$Q_{d.ult} = Q_k \cdot 1.5 \cdot \varphi_2 = 487kN \cdot 1.5 \cdot 1.044 = 762.6kN$

Serviceability limit states:

The loads for the serviceability limit states are equal to the characteristic loads, since the partial safety factors are γ = 1.0. Only the dynamic factor has to be applied.

$g_{d.ser} = g_k \cdot 1.0 = 125\,kN/m \cdot 1 = 125\,kN/m$

$q_{d.ser} = (q_{71.UDL} \cdot \varphi_2 + q_{footpath}) \cdot 1.0 = (80 \cdot 1.044 + 3.75)kN/m \cdot 1.0 = 87.27\,kN/m$

Total uniformly distributed load: $w_{d.ser} = g_{d.ser} + q_{d.ser} = 212.27\,kN/m$

$Q_{d.ser} = \varphi_2 \cdot Q_{71} = 1.044 \cdot 487kN = 508.43kN$

Internal forces and moments

Influence areas (reference bridge: Vienna 200B)

The influence areas of this bridge are calculated with the help of the influence areas of the bridge design Vienna 200B, TVEIT *[45]*. Among all network arches designed by PER TVEIT, Vienna 200B is most appropriate in respect of the ratio between dead load to live load.

Annex B, Section B.1.2

Influence areas of Vienna 200B (hangers 90-94):

Positive influence area:	$IA^{+}_{200B} = 9.56m$
Negative influence area:	$IA^{-}_{200B} = -4.20m$
Sum of influence area:	$IA_{135} = IA^{+}_{135} + IA^{-}_{135} = 5.36m$
Maximum value of influence line:	$I^{+}_{200B} = 0.38$
Minimum value of influence line:	$I^{-}_{200B} = -0.1$

The ratio between the spans of 200B and this bridge: $k = 100m/200m = 0.5$.

Hence, the influence areas of this bridge with a span of 100m:

Positive influence area:	$IA^{+}_{100} = k \cdot IA^{+}_{135} = 4.78m$
Negative influence area:	$IA^{-}_{100} = k \cdot IA^{-}_{135} = -2.10m$
Sum of influence area:	$IA_{100} = IA^{+}_{100} + IA^{-}_{100} = 2.68m$
Maximum value of influence line:	$I^{+}_{100} = 0.38$
Minimum value of influence line:	$I^{-}_{100} = -0.1$

Approximate hanger force

Ultimate limit state

$$N_{d,max} = \left(IA_{100} \cdot g_{d.ult}\right) + \left(IA^{+}_{100} \cdot q_{d.ult}\right) + \left(I^{+}_{200B} \cdot Q_{d.ult}\right)$$
$$N_{d,max} = \left(2.68m \cdot 168.75\,kN/m\right) + \left(4.78 \cdot 130.91kN/m\right) + \left(0.38 \cdot 762.6kN\right) = 1368kN$$

Serviceability limit state

$$N_{k.max} = \left(IA_{100} \cdot g_{d.ser}\right) + \left(IA^{+}_{100} \cdot q_{d.ser}\right) + \left(I^{+}_{200B} \cdot Q_{d.ser}\right)$$
$$N_{k,max} = \left(2.68m \cdot 125\,kN/m\right) + \left(4.78m \cdot 87.27\,kN/m\right) + \left(0.38 \cdot 508.43kN\right) = 945kN$$

$$N_{k.min} = \left(IA_{100} \cdot g_{d.ser}\right) - \left(IA^{-}_{100} \cdot q_{d.ser}\right) + \left(I^{-}_{200B} \cdot Q_{d.ser}\right)$$
$$N_{k,min} = \left(2.68m \cdot 125\,kN/m\right) - \left(2.10 \cdot 87.27\,kN/m\right) - \left(0.1 \cdot 508.43kN\right) = 100.89kN$$

Materials

The hangers are smooth bars of S 460 ML – steel with circular cross section. *ENV 1993-2*
f_y = 430 N/mm^2 *Table: 3.1a*

Determination of required cross-sectional area

The partial safety factor γ_{M0} is taken from *ENV 1993-2: 1997 Section 5.1.1.* *ENV 1993-1-1: 1992 Section 5.4.3*

$$N_{pl.Rd} = A \cdot \frac{f_y}{\gamma_{M0}} \quad \gamma_{M0} = 1.0$$

Minimum required area of hanger section

$$A_{min} = \frac{\gamma_{M0} \cdot N_{d.max}}{f_y} = \frac{1.0 \cdot 1368kN}{430 N/mm^2} = 3182mm^2$$

Minimum diameter of a circular hanger section:

$$D_{min} = \sqrt{\frac{4 \cdot A_{min}}{\pi}} = \sqrt{\frac{4 \cdot 3182mm^2}{\pi}} = 64mm$$

The diameter is chosen to be D = 65 mm.

FEM - Calculation

C.1 General

For the FEM-calculations two structural analysis software packages were used. Most of the investigations were performed with *SOFiSTiK AG*, Oberschleißheim-Germany*.* For the calculations of stress distribution in the hanger connection details *NE/Nastran for Windows from Norman Engineering Inc*. was used.

www.sofistik.com

www.nenastran.com

SOFiSTiK

The 3D-model used for calculations shows Figure C.1.

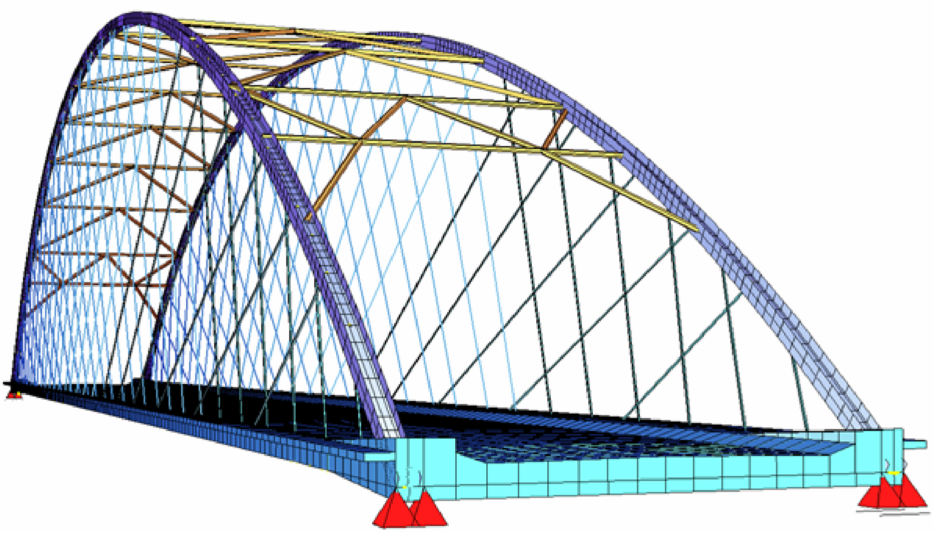

Fig. C.1. Foreshortened view of the 3D-FEM-model used for calculations

The bridge deck was modelled with plane elements. Their nodes were aligned to the bottom plane of the tie. In that way it was possible to shape the bridge deck and end cross girder like the real cross-sections by applying different thickness to the plane elements. The cantilevers were connected by couplings to the nodes of the bridge deck elements providing fixed connection to the rigid body at the reference nodes. Figure C.2 shows the partitioning of the bridge deck mesh.

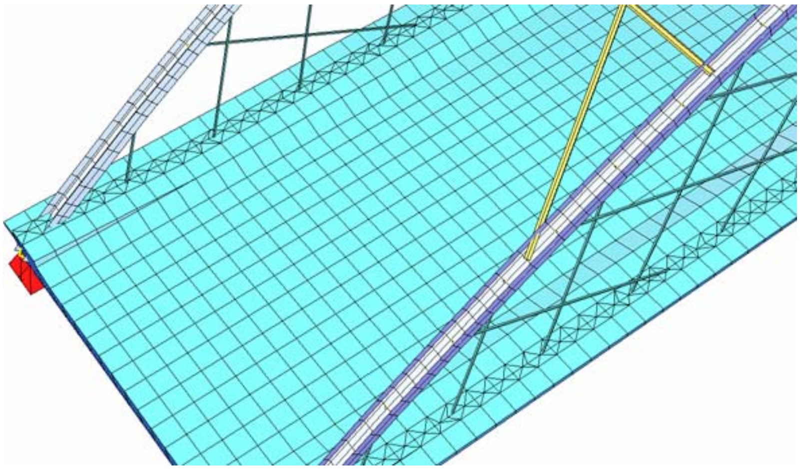

Fig. C.2. Partitioning of the mesh of the bridge deck

It was decided to connect the hanger nodes with skew triangular elements. This allowed square plane elements in the rest of the deck. Substitution of the triangular mesh by skew quadrilateral partitioning would give better results for the analysis, nevertheless. The square elements have a length of 0.6 metres.

The arches were modelled using beam elements with a length of about 0.5 metres. The truss members of the wind bracing were also beam elements with hinges at the connections to the arch. In a test without hinges bending moments of maximum 7 kNm occurred in the truss. They originate mainly in the torsional moments in the arch due to the eccentric connection of the hangers and can be ignored for the assessment.

The hangers were modelled using cable elements that only sustain tension in case of non-linear analysis. This has to be considered when calculating influence lines. Since analysis is carried out in linear fashion, hangers will take compression forces, instead of relax. This leads to increased internal forces and is therefore on the safe side. The cable elements were connected eccentrically to the arch as shown in Figure C.3. At their intersections the horizontal deflection perpendicular to the arch plane was coupled. In that way it was possible to calculate deflections and mode shapes of the hanger web.

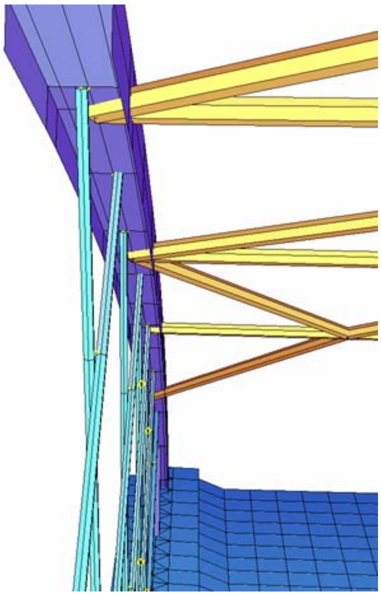

Fig. C.3. Connections and couplings of the cable elements

The SOFiSTiK module GEOS provides features to involve prestressing tendons within the plane elements. Figure C.4 shows their arrangement. It is possible to choose common tendons from reputable manufacturers. The software itself calculates the loads to apply to the structure.

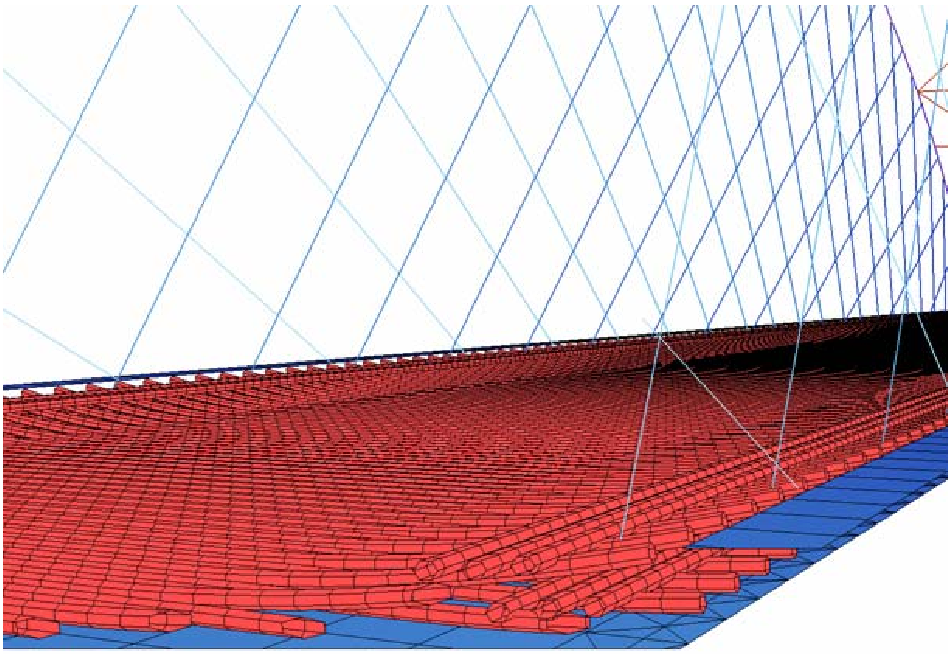

Fig. C.4. Arrangement of prestressing tendons within the plane elements of the bridge deck

Module ELSE was used for the analysis of the influence lines and module ASE for second order analysis. Figures C.5 to C.7 give the geometric properties of the final bridge design.

Geometry of hanger arrangement				
Node number	Coordinates of the hanger nodes of half span			
100+n / 200+n	low er hanger nodes		upper hanger nodes	
n	**x [m]**	**z [m]**	**x [m]**	**z [m]**
1	2.81	0	3.82	2.93
2	5.51	0	5.442	4.05
3	8.25	0	6.818	4.94
4	11.03	0	8.028	5.69
5	13.5	0	9.538	6.57
6	13.98	0	11.07	7.42
7	26.86	0	13.02	8.42
8	19.68	0	14.99	9.36
9	22.22	0	16.99	10.2
10	22.3	0	19.02	11.1
11	25.23	0	21.06	11.86
12	27.68	0	23.13	12.59
13	29.29	0	25.21	13.26
14	30.73	0	27.31	13.88
15	33.51	0	29.42	14.44
16	35.03	0	31.55	14.95
17	36.33	0	33.69	15.4
18	39.21	0	35.84	15.8
19	39.7	0	38.01	16.14
20	42.18	0	40.17	16.42
21	44.13	0	42.35	16.65
22	45.28	0	44.53	16.82
23	47.95	0	46.72	16.94
24	48.55	0	48.91	16.99

Fig. C.7. Coordinates of hanger nodes

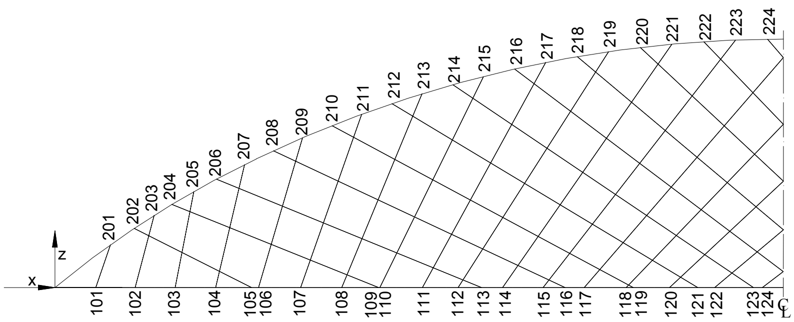

Fig. C.5. Definitions of the hanger node numbers

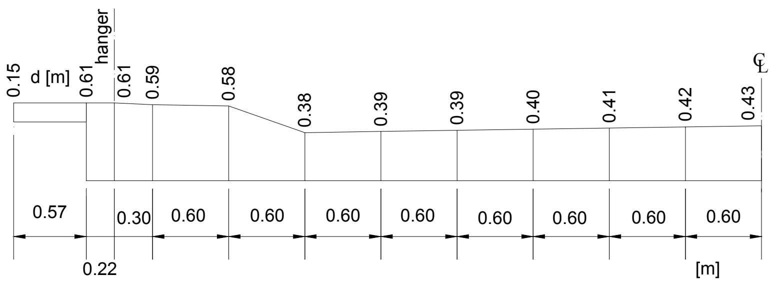

Fig. C.6. Geometry of the plane elements of the tie

NE/Nastran

The stress analysis used to evaluate the resistance against fatigue strains of the hanger connection details was performed with *NE/Nastran*. The models were shaped using *SolidWorks 3D CAD Software*. The length of the hanger extending the connection detail was chosen to be 1 metre. The default settings of *NE/Nastran's* auto-mesh feature were used for partitioning of the solid mesh, which gave element sizes between 10 and 20 mm. Figure C.8 shows an example of the meshes used. The static analysis was performed in linear fashion. Constraints and both loads, axial force and horizontal deflection, were applied to the corresponding surfaces of the 3D-model. Stress distributions and values were found by the help of the *Stress Wizard*, which is a component of *NE/Nastran*.

www.solidworks.com

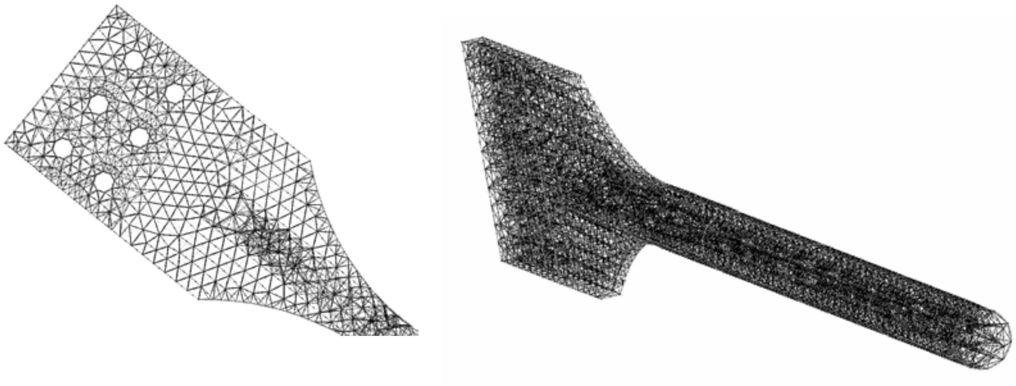

Fig. C.8. Example of solid mesh used for numeric analysis

In *NE/Nastran* the interaction between elements is based on forces exerted at the so-called mesh grid points, where elements are connected together. The stiffness of the structure, discretised at these grid points, is generated with data on material properties and geometry. Both stiffness and forces are used to calculate displacements, with which stresses and strains are generated. It was decided to use tetrahedron instead of hexahedral elements, since the additional effort required to generate high-quality hexahedral meshes cannot usually be justified by the time required to do so. However, the tetrahedron elements were equipped with additional mid-notes, leading to higher-order 10-noded elements.

C.2 Internal forces of the arch

The arches receive mainly axial compression forces and are therefore in danger of collapse due to buckling. Additionally, there are in-plane bending moments M_y due to the hanger forces and out-of-plane bending moments M_z and torsional moments M_t due to horizontal forces (like wind) on hangers and arches. Additionally the eccentricity of the hanger connections causes torsional bending. The arches will be verified using second order analysis to prove the buckling resistance.

For this purpose it is required to apply the initial bow imperfection specified in ENV 1993-1-1: 1992, 5.5.1.3 on the arch. The relevant buckling curve is the first mode shape for each axis of the arch profile. The mode shapes were determined by SOFISTIK ASE-module.

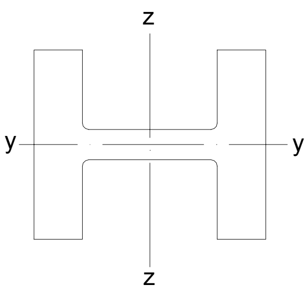

Fig. C.9. Defintion of axes in arch cross-section

C.2.1 Ultimate limit state

C.2.1.1 Collapse about the weak axis y-y

The first mode shape for in-plane arch deflection is the second mode shape of the whole bridge. But it is the symmetric vertical deflection and does not lead to any buckling. The fifth mode shape of the whole bridge (Figure C.10) represents the relevant buckling curve.

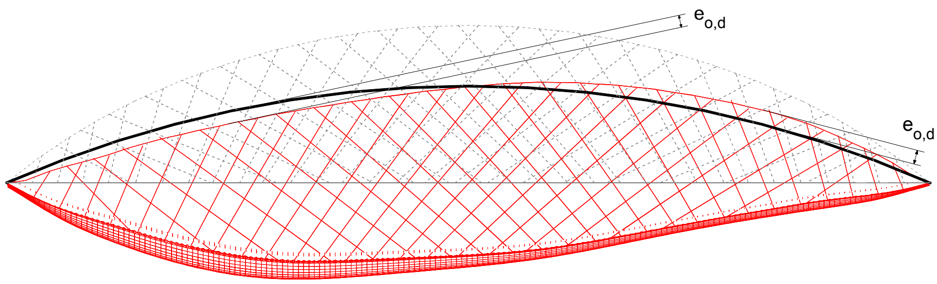

Fig. C.10. Fifth mode shape, equivalent initial bow imperfection $e_{o,d}$ *ENV 1993-1-1: 1992 Figure 5.5.1*

Eurocode ENV 1993-1-1 does not consider the special buckling behaviour of arches. Therefore, the equivalent initial bow imperfection cannot be calculated according to *ENV 1993-1-1: 1992 Figure 5.5.1*. As the German National Code, *DIN 18800,* includes clear statements about imperfections to be applied to arches, these values are used for second order analysis.

$$e_{o,d}=\frac{l}{400}=0.25\text{m}$$

DIN 18800 T.2, Abschnitt 6, Tab. 23

The determination of the critical cross-sections of the arch was performed in linear fashion. Thereto the envelopes of maximum M_y and minimum M_y were calculated (Figures C.11, C.12). The first critical cross-section is found at the top edge of the concrete tie at the clamping of the arch, where maximum M_y occurs. Further upwards the maximum and minimum values of the bending moment are distributed more or less uniformly along the arch. So it was only necessary to calculate the internal forces for the lowest butt-welded splice, since the axial force will be highest there. The influence lines of N and M_y for these two critical sections are shown in Figure C.13. The design-relevant internal forces can be found in Figure C.16.

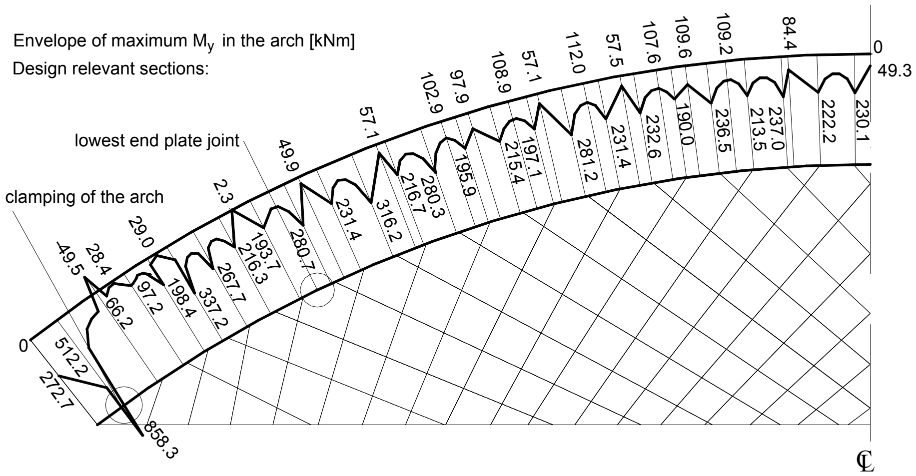

Fig. C.11. Preliminary linear calculation of bending moments M_y in the arch

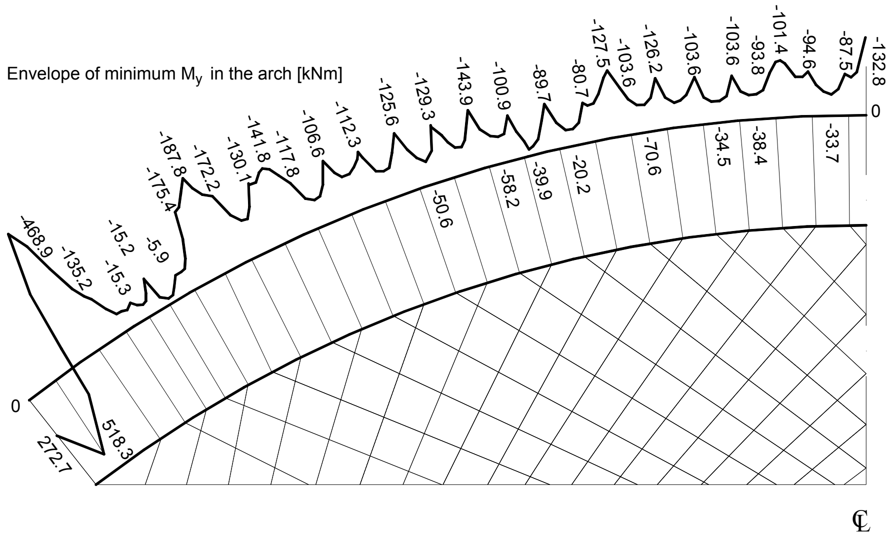

Fig. C.12. Preliminary linear calculation of bending moments M_y in the arch

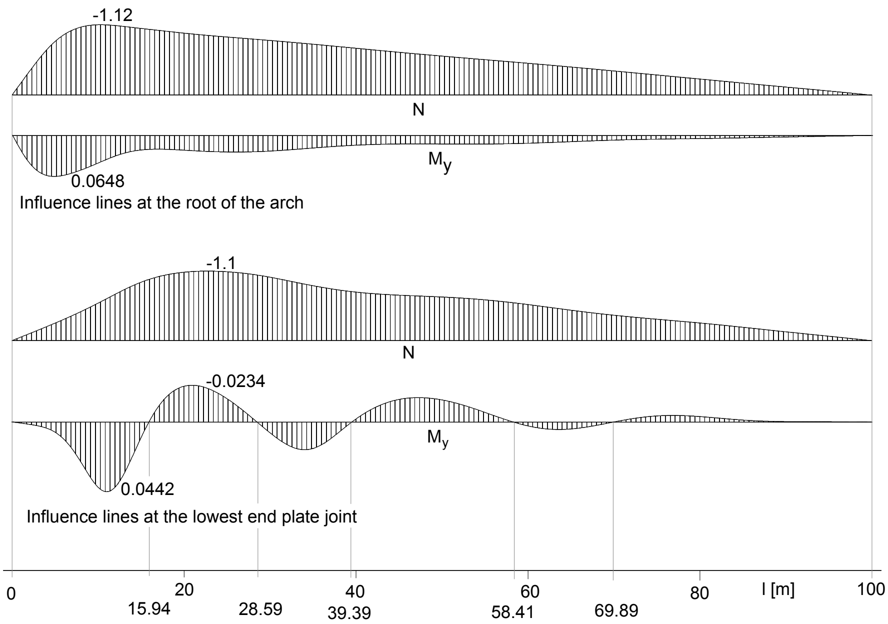

Fig. C.13. Influence lines for N and M_y at the critical sections

C.2.1.2 Collapse about the strong axis z-z

The first mode shape of the whole bridge represents the relevant buckling curve for out-of-plane buckling (Figure C.14). As in Section C.2.1.1 the equivalent initial bow imperfection is taken from *DIN 18800*.

$$e_{o,d} = \frac{l}{500} = 0.2\text{m}$$

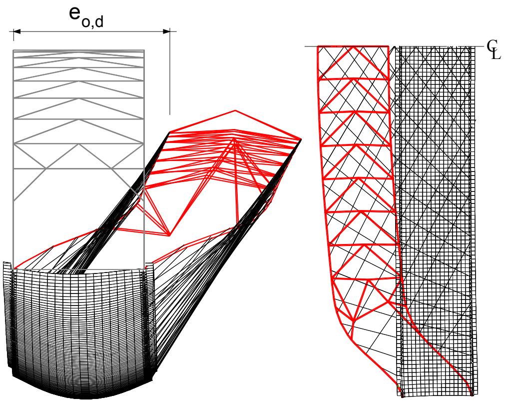

Fig. C.14. First mode shape of whole bridge

Maximum internal forces N and M_z occur at load combination 4 (Figure C.15). The design check will be performed for the section at the clamping of the arch, where the maximum bending moment and the maximum axial force are found. For all relevant forces see Figure C.16.

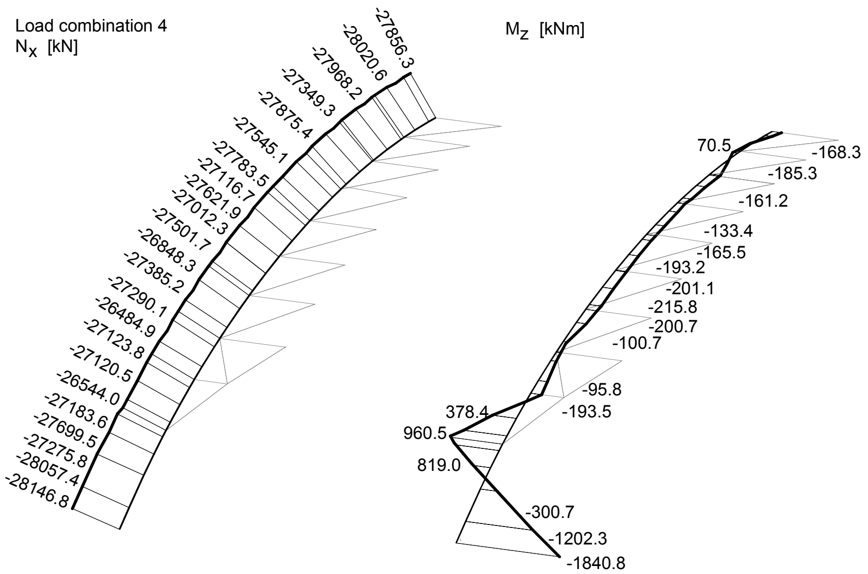

Fig. C.15. Maximum internal forces for collapse about the z-z axis of the arch (half of one arch, isometric projection)

C.2.2 Fatigue stress spectra

The cross-sections to be checked are the butt-welded splices, the connections to the wind truss beams, hanger connections and the root of the arch. For the first three locations the biggest stress range occurs at the lowest of each of these joints. The variation of internal forces due to load model 71 on one and on both of the tracks, $\Delta\sigma_1$ and $\Delta\sigma_{1+2}$, can be found in Figure C.17.

C.2.3 Serviceability limit state

The serviceability limit states to be verified by numerical assessment are limitations for stress, stress range and the maintenance of the specified clearance gauges. The maximum nominal stress $\sigma_{Ed,ser}$ and stress range $\Delta\sigma_{fre}$

to be limited occur at the root of the arch. The structural part in danger of encroaching upon the railway traffic is the lowest member of wind truss. Its horizontal and vertical deflections are Δ_x and Δ_z.

The appendant values can be found in Figure C.18.

C.2.4 Composition of the design relevant calculation results

	Ultimate limit state			
	Collapse about axis y-y			axis z-z
	Root of arch	First splice	Second splice	Root of arch
N_x [kN]	-28468.3	-27487.3	-26873.9	-28146.8
V_y [kN]	-198.3	135.4	128.7	-514.7
V_z [kN]	-511.5	-310.5	-278.3	-428.8
M_y [kNm]	1115.8	210.8	195.9	841.8
M_z [kNm]	-809.9	-100.4	-164.5	-1840.8
M_t [kNm]	-87.5	-11.3	-18.3	-114.6

Fig. C.16. Internal forces for ultimate limit state assessment

	Fatigue					
	Connection to wind truss member			Lowest hanger connection		
	Forces due to dead load	Forces due to one LM 71	Forces due to two LM 71	Forces due to dead load	Forces due to one LM 71	Forces due to two LM 71
N_x [kN]	-10362	-15810.1	-17839.9	-10618.4	-16376.9	-18526.3
V_y [kN]	-29.2	-65.2	-66.6	-24.4	-67.6	-85.5
V_z [kN]	134.7	134.9	149.9	-191.9	-259.9	-349.1
M_y [kNm]	30.8	5.10	13.2	-58.1	-59	-60.7
M_z [kNm]	86.6	202.1	209.3	-170.3	-265.9	-332.9
M_t [kNm]	-6.2	-13.3	-15.1	-10.3	-22.1	-28.9
	First splice			Root of the arch		
	Forces due to dead load	Forces due to one LM 71	Forces due to two LM 71	Forces due to dead load	Forces due to one LM 71	Forces due to two LM 71
N_x [kN]	-10331.3	-15851.7	-17912.6	-10673.8	-16441.9	-18978.8
V_y [kN]	-27.1	-28.6	-28.3	-24.4	-68.3	-86.5
V_z [kN]	89.0	28.5	30.3	105.2	75.2	97.7
M_y [kNm]	10.0	0.9	0.9	17.0	250.7	446.2
M_z [kNm]	-43.1	-39.1	-40.8	3.6	354.9	468.1
M_t [kNm]	-13.8	-12.1	-13.7	-2.9	-4.4	-6.0

Fig. C.17. Internal forces for fatigue assessment

	Serviceabiltiy limit state			
	Root of the arch		windtruss	
	Nominal stress	Variation of forces	Load combination 12	
N_x [kN]	-19245.6	5758.5	horizontal deflection	
V_y [kN]	-97.4	43.2	Δ_x	18.7 cm
V_z [kN]	102.3	68.0	vertical deflection	
M_y [kNm]	54.7	95.6	Δ_y	-4.0 cm
M_z [kNm]	479.3	0.9		
M_t [kNm]	-7.2	11.8		

Fig. C.18. Values for assessment to satisfy serviceability limits

C.3 Hanger

C.3.1 Axial forces

The labelling of the hangers is defined in Figure C.19.

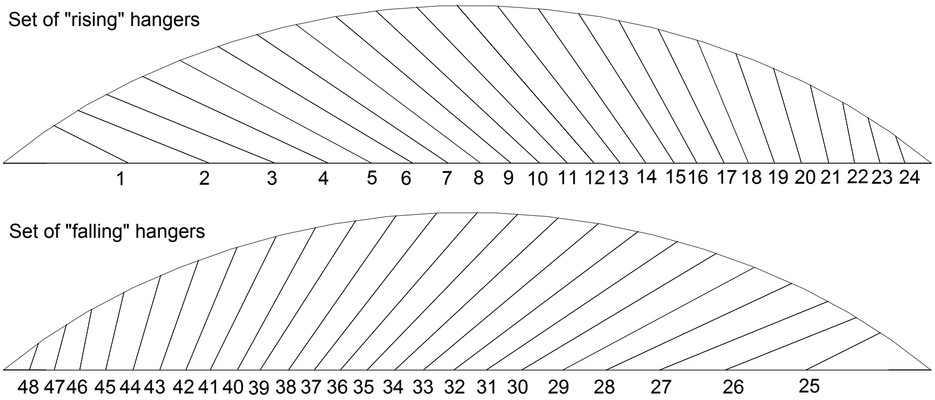

Fig. C.19. Definition of the labelling of the hangers

To obtain the maximum strains on the hangers the influence lines of all hangers were calculated and analysed by applying the load combinations for ultimate, serviceability and fatigue limit states as described in Annex A. The resulting maximum and minimum hanger forces are shown in Figure C.20.

Number of hanger, according to Figure C.19	Hanger forces [kN]							
	Ultimate limit state		Fatigue		Serviceability limit state			
					Rare / characteristic load combinations		Frequent load combinations	
	Maximum	Minimum	Δ_{1+2} N, two tracks loaded	Δ_1 N, one track loaded	Maximum	Minimum	Maximum	Minimum
1	833.16	269.12	376.03	252.51	616.34	247.81	483.11	198.25
2	1002.06	375.82	417.49	246.83	741.29	346.06	593.05	276.85
3	1016.22	364.09	434.75	268.9	751.76	335.26	595.60	274.30
4	1061.85	413.33	432.35	245.11	785.52	380.6	628.42	304.50
5	1057.03	432.28	416.5	221.28	781.96	398.05	615.56	318.44
6	1020.65	457.37	375.52	170.08	755.04	421.15	604.77	336.92
7	932.3	381.23	367.38	195.22	689.68	351.04	541.38	280.83
8	973.93	314.44	439.66	295.34	720.48	289.54	586.38	231.63
9	924.91	318.55	404.24	258.73	684.22	293.33	547.87	234.66
10	925.75	348.19	385.04	226.96	684.84	320.62	547.87	257.68
11	902.22	334.39	378.55	226.59	667.43	307.91	533.94	246.33
12	893.61	336.98	371.09	218.12	661.06	310.29	528.85	248.23
13	881.19	346.54	356.43	199.55	651.87	319.09	521.50	255.27
14	886.15	350.01	357.43	199.02	655.54	322.29	534.32	257.83
15	813.45	313.66	333.19	191.02	601.76	288.82	481.41	231.06
16	865.82	339.91	350.61	196.71	640.5	312.99	512.40	250.39
17	724.45	296.07	285.59	151.88	535.92	272.63	428.74	228.57
18	829.49	302.97	351.01	213.19	613.63	278.98	490.90	223.18
19	839.22	331.52	338.47	188.43	620.83	305.27	496.66	244.22
20	836.03	336.31	333.15	181.12	618.47	309.68	494.78	265.32
21	941.83	493.63	298.8	123.65	696.73	454.54	557.38	363.63
22	970.73	558.19	275.03	112.45	718.11	513.99	574.49	411.19
23	994.5	752.93	161.05	89.5	735.69	693.31	588.55	553.82
24	661.81	438.15	149.11	86.23	489.58	50.78	391.66	38.65

Fig. C.20. Hanger forces

In ultimate limit state hanger, number 4 receives the maximum axial forces. As an example the influence line of this hanger is presented in Figure C.21.

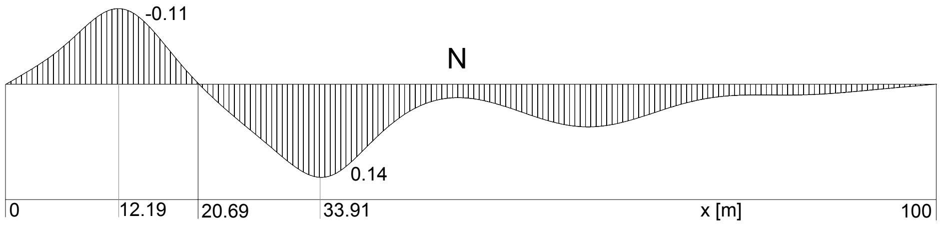

Fig. C.21. Influence line of hanger 4

C.3.2 Deflections perpendicular to the hanger axis

For the fatigue assessment of the hanger connection details, the horizontal deflection of the hangers were examined. As the lower connections of the hangers are cast in the concrete bridge deck, therefore it is assumed that horizontal movements of the hangers are not transferred to the connection, but absorbed by the concrete around it.

The upper connections consist of a steel plate that is welded to the arch perpendicularly to the plane of the hanger web, so that it can move slightly within the arch plane. Furthermore, all hangers are tied together at their crossings. Because of that it can be assumed that movements of the hangers in the plane of the arch are small and do not lead to important internal forces in the hanger connection.

Consequently the deflections of interest are perpendicular to the hanger web.

C.3.2.1 Static deflection due to wind load

To obtain a first idea of the strains caused by horizontal deflections the hanger web was loaded by the static wind forces according to Section A.3.1. Due to gusts the centre of the web was loaded with 100% and the outer parts with 60% of the full wind load, SCHULTE *[27]*. This gives larger horizontal deflections of the web centre. Since the stiffness of the hangers depends on their axial force, calculations were carried out for the fatigue load combination ‘two LM 71’ giving maximum hanger forces and without live load giving minimum hanger forces. In Figure C.22 the values of the angular rotations at the upper end of the hangers are presented.

		Minimum hanger forces		Maximum hanger forces	
Number of hanger, according to figure C.19	Hanger length until first crossing [m]	Y deflection of first crossing [mm]	Angular rotation of upper hanger end [mrad]	Y deflection of first crossing [mm]	Angular rotation of upper hanger end [mrad]
1	1.125	0.3674	1.0000	0.0942	0.2564
2	1.3349	0.5715	0.4281	0.1833	0.3207
3	1.678	0.6321	0.3767	0.1903	0.3011
4	1.6848	1.1346	0.6734	0.3399	0.2996
5	1.6808	1.3460	0.8008	0.4004	0.2975
6	1.6772	1.5034	0.8964	0.4458	0.2965
7	1.6573	1.6373	0.9879	0.4869	0.2974
8	1.6651	1.7683	1.0620	0.5313	0.3005
9	1.6477	1.8381	1.1156	0.5569	0.3030
10	1.6697	1.9184	1.1489	0.5828	0.3038
11	1.6705	1.9767	1.1833	0.5989	0.3030
12	1.667	1.9644	1.1784	0.5958	0.3033
13	1.6668	1.9644	1.1785	0.5958	0.3033
14	1.6669	1.9767	1.1859	0.5989	0.3030
15	1.6619	1.9184	1.1543	0.5828	0.3038
16	1.6671	1.8381	1.1026	0.5569	0.3030
17	1.6581	1.7683	1.0665	0.5313	0.3005
18	1.6676	1.6373	0.9818	0.4869	0.2974
19	1.6702	1.5034	0.9001	0.4458	0.2965
20	1.6722	1.3460	0.8049	0.4004	0.2975
21	1.6782	1.1346	0.6761	0.3399	0.2996
22	1.408	0.6321	0.4489	0.1903	0.3011
23	1.4466	0.5715	0.3951	0.1833	0.3207
24	3.0948	0.3674	0.1187	0.0942	0.2564

Fig. C.22. Angular rotation of upper hanger ends due to static wind loads

C.3.2.2 Deflections due to dynamic wind excitation

For dynamic investigations the mode shapes are of interest. Searching for them, the crossings of the hangers were modelled by coupling the out-of-hanger-web deflections of the nodes. The first mode shapes are shown in Figure C.24. Since the amplitudes of the oscillations are larger for less loaded hangers and since it is probable that wind excited oscillations occur for long periods of time without a train passing over the bridge, the mode shapes were calculated without live load.

mode shape number	eigen-frequency [Hz]	mode shape number	eigen-frequency [Hz]	mode shape number	eigen-frequency [Hz]
1	0.97	21	2.67	41	3.3
2	1.12	22	2.7	42	3.32
3	1.27	23	2.72	43	3.35
4	1.42	24	2.77	44	3.37
5	1.55	25	2.82	45	3.38
6	1.69	26	2.85	46	3.39
7	1.82	27	2.88	47	3.42
8	1.84	28	2.92	48	3.44
9	1.96	29	2.95	49	3.45
10	1.97	30	2.97	50	3.47
11	2.09	31	3.01	51	3.49
12	2.1	32	3.05	52	3.51
13	2.22	33	3.06	53	3.54
14	2.22	34	3.07	54	3.55
15	2.34	35	3.14	55	3.58
16	2.36	36	3.14	56	3.59
17	2.46	37	3.17	57	3.61
18	2.48	38	3.2	58	3.63
19	2.59	39	3.21	59	3.65
20	2.61	40	3.24	60	3.66
				61	3.68

Fig.23. Eigenfrequencies of the first mode shapes of the hanger web

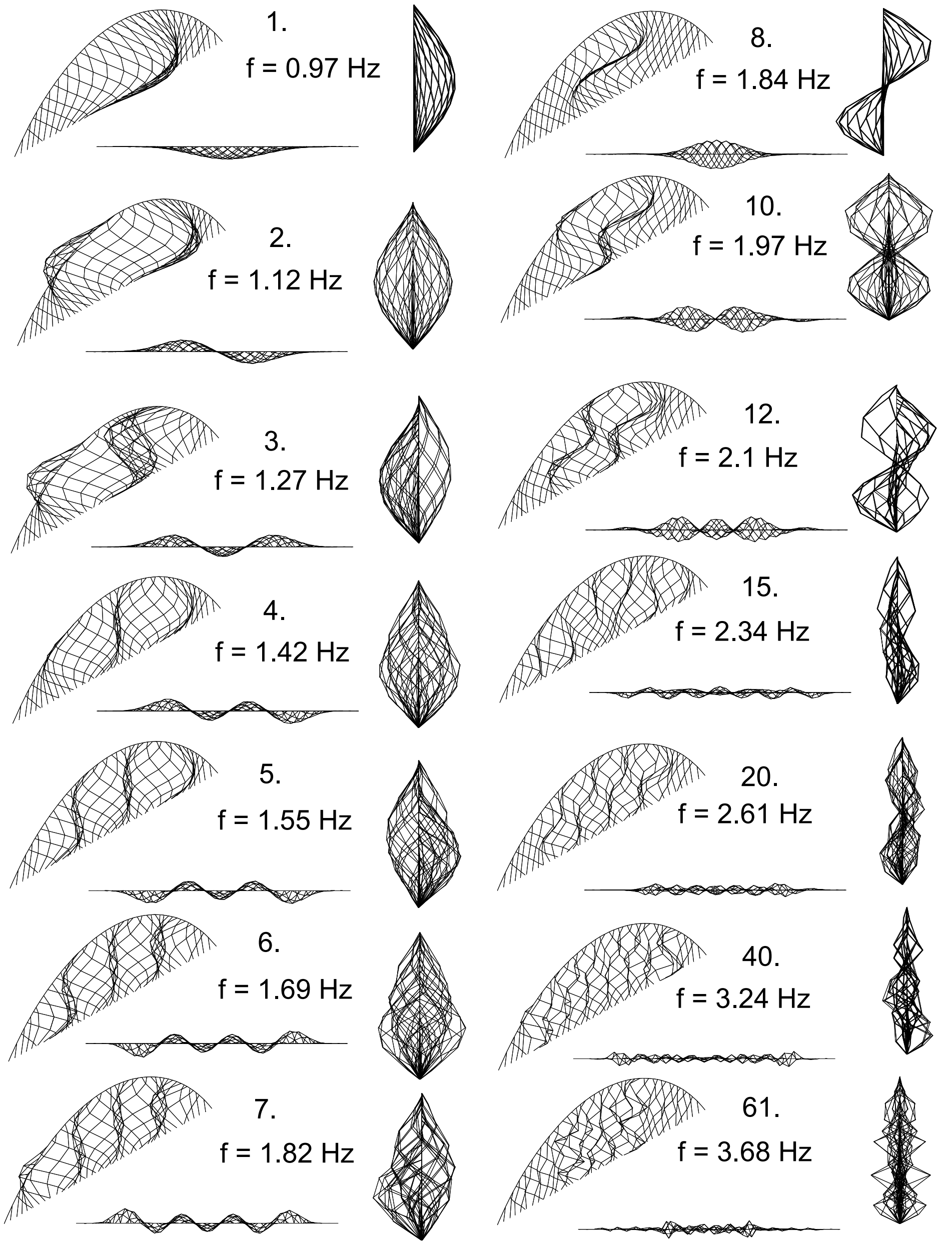

Fig. C.24. Mode shapes and eigenfrequency of the hanger web

The effects of dynamic excitation are described in Section 7.2.2. It is shown there that it is not possible to determine the dynamic behaviour of the hanger web only be means of the procedures provided by Eurocode. But it seems improbable that the web would be excited by along-wind nor crosswind. That means fatigue strains caused by wind are not existent. Nevertheless, while determining the hanger connection details in Section 7 horizontal deflections of the hangers were considered and the qualitative stress distribution caused by them will influence the decision on the shape of the connection detail.

Further investigations should be carried out with the help of wind engineers.

C.4 Internal forces in the wind bracing

The labels of the members and the nodes of the wind bracing can be seen in Figure C.25. The straight struts consisting of members 2, 3 and 16 are CHS 219.1x10. The rest are CHS 219.1x8.

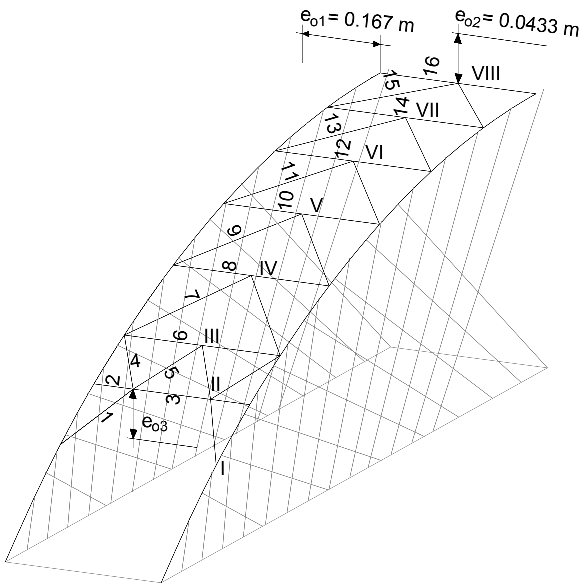

Fig. C.25. Labeling of members and nodes, initial bow imperfections

Because of the double symmetry of the truss only half of one bridge side is considered.

The wind bracing members are loaded by self-weight and restraining forces from the arch due to wind forces and buckling effects. A calculation of the secondary bending moments at the connections showed that they are negligible. According to TEICH & WENDELIN *[38]*, page 46, as forces due to vortex shedding do not influence the choice of the cross-section, they are therefore neglected.

For the analysis of the wind bracing an equivalent geometric imperfection shall be applied to the arches. For this purpose the first mode shape, shown in Figure C.14, is scaled so that its maximum deflection in the middle of the span equals the initial bow imperfection e_{o1}.

$e_{o1} = k_r\ L/500$

with $kr = \sqrt{0.2+\frac{1}{n_r}} = \sqrt{0.2+\frac{1}{2}} = 0.837$

e_{o1} = 0.837 100m/500 = <u>0.167m</u>

ENV 1993-1-1: 1992 5.2.4.4 (5.3)

As can be seen in Figure C.25, the nodes of the wind bracing lie in a cylindrical sphere between the arches. That means the members of the truss do not lie in a plane and their axial forces cause out-of-sphere movements of the nodes. This has to be impeded by the straight members (2, 3, 6, 8, 10, 12, 14, 16) which therefore receive bending moments. In case the out-of-sphere movements occur in compression members, the effect has to be treated as a stability problem. This will be performed with second order analysis. The initial bow imperfections to be applied are:

$e_{o2} = 1.33 \cdot \alpha \cdot \left(\bar{\lambda} - 0.2\right) \cdot k_\gamma \cdot \frac{W_{pl}}{A}$

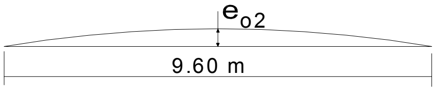

with α = 0.21 ; buckling curve "a"

$$\bar{\lambda} = \frac{\lambda}{\lambda_1} \cdot \sqrt{\beta_A} = \frac{\beta \cdot l}{i_y \cdot \pi \cdot \sqrt{\frac{E}{f_y}}} \cdot \beta_A$$

ENV 1993-1-1: 1992 5.5.1.3

with ß = 1 ; Euler case 2
l = 9.60 m

i_y = 7.4 cm
E = 210000 N/mm^2
f_y = 355 N/mm^2 ; S355
$ß_A$ = 1 ; Class 1 cross section

$$\overline{\lambda} = \frac{1 \cdot 9.6\text{m}}{7.4\text{cm} \cdot \pi \cdot \sqrt{\dfrac{210000\text{N}/\text{mm}^2}{355\text{N}/\text{mm}^2}}} \cdot 1 = 1.698$$

k_δ = 0.23 ; γ_{M1} = 1.1 & buckling curve "a"

$k_\gamma = (1\text{-}k_\delta) + 2 \cdot k_\delta \cdot \overline{\lambda} = (1\text{-}0.23) + 2 \cdot 0.23 \cdot 1.698 = 1.551$

W_{ply} = 438 cm^3
A = 65.7 cm^2

$$e_{o2} = 1.33 \cdot 0.21 \cdot (1.698 - 0.2) \cdot 1.551 \cdot \frac{438\text{cm}^3}{65.7\text{cm}^2} = \underline{4.33\text{ cm}}$$

And:

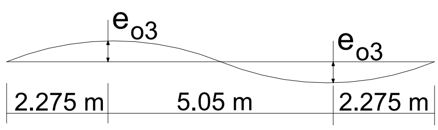

$$e_{o3} = 1.33 \cdot \alpha \cdot (\overline{\lambda} - 0.2) \cdot k_\gamma \cdot \frac{W_{pl}}{A}$$

with α = 0.21 ; buckling curve "a"

$$\overline{\lambda} = \frac{\lambda}{\lambda_1} \cdot \sqrt{\beta_A} = \frac{\beta \cdot l}{i_y \cdot \pi \cdot \sqrt{\dfrac{E}{f_y}}} \cdot \beta_A$$

with ß = 1 ; Euler case 2
l = 4.80 m
i_y = 7.4 cm
E = 210000 N/mm^2
f_y = 355 N/mm^2 ; S355
$ß_A$ = 1 ; Class 1 cross section

$$\overline{\lambda} = \frac{1 \cdot 4.8\text{m}}{7.4\text{cm} \cdot \pi \cdot \sqrt{\dfrac{210000\text{N}/\text{mm}^2}{355\text{N}/\text{mm}^2}}} \cdot 1 = 0.846$$

k_δ = 0.23 ; γ_{M1} = 1.1 & buckling curve "a"

$k_\gamma = (1\text{-}k_\delta) + 2 \cdot k_\delta \cdot \overline{\lambda} = (1\text{-}0.23) + 2 \cdot 0.23 \cdot 0.846 = 1.159$

W_{ply} = 438 cm^3
A = 65.7 cm^2

$$e_{o3} = 1.33 \cdot 0.21 \cdot (0.846 - 0.2) \cdot 1.159 \cdot \frac{438\text{cm}^3}{65.7\text{cm}^2} = \underline{1.39\text{ cm}}$$

These node deflections were applied to the 3D-FEM-model and a second order analysis was performed.

The wind bracing members are loaded by self-weight and restraining forces from the arch due to wind forces and buckling effects.

C.4.1 Ultimate limit state

The maximum and minimum axial forces of all members and the bending moments in the straight members (2, 3, 6, 8, 10, 12, 14, 16) are shown in Figure C.27.

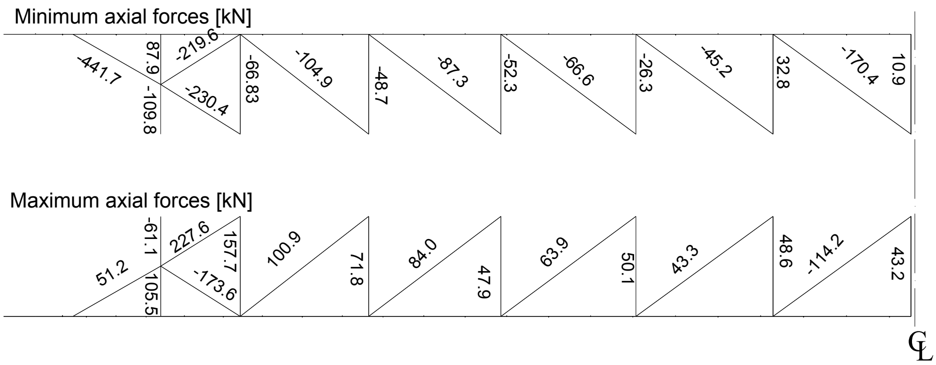

Fig. C.26. Maximum and minimum forces in the wind bracing in ultimate limit state

Internal forces in the wind bracing in ultimate limit state								
Number of member	**max N_x [kN]**	**min N_x [kN]**	**Number of node**	**max M_y [kNm]**	**min M_y [kNm]**	**max M_z [kNm]**	**min M_z [kNm]**
1	51.2	-441.7	I	-	-	-	-
2	105.5	87.9	II	-34.4	1.6	-15.9	-1.8
3	-61.1	-109.8	III	9.2	6.9	5.6	4
4	-173.6	-219.6	IV	13.2	8.8	0	0
5	227.6	-230.4	V	14.2	9.3	0	0
6	157.7	-66.8	VI	15.1	9.7	0	0
7	100.9	-104.9	VII	15.7	10.1	0	0
8	71.8	-48.7	VIII	-27.3	-2.4	0	0
9	84	-87.3					
10	47.9	-52.3					
11	63.9	-66.6					
12	50.1	-26.3					
13	43.3	-45.2					
14	48.6	32.8					
15	-114.2	-170.4					
16	43.2	10.9					

Fig. C.27. Internal forces in ultimate limit state

The critical members for compression force and buckling are number 1 and 15. Member 3 has to be designed for bending and compression force in node **II**.

C.4.2 Fatigue

The variation of the internal forces due to the fatigue load models, one and two load models 71, are shown in Figure C.28. Critical for the assessment are nodes **I** and **II**, which are connected to members 1 and 1, 2, 3, 4 and 5.

Variation of internal forces in wind bracing due to fatigue load models							
	Variation of axial force [kN]			Variation of bending moment My [kNm]		Variation of bending moment Mz [kNm]	
Number of member	one LM 71	two LM71	Number of node	one LM 71	two LM71	one LM 71	two LM71
1	120.9	174.8	I	-	-	-	-
2	15.5	26.4	II	15.4	20.3	7.4	10.3
3	30.7	47.2	III	9.2	13.4	2.3	4.5
4	14.2	19.8	IV	2.1	3.5	0	0
5	136.5	154.8	V	1.6	2.8	0	0
6	58.4	70.2	VI	1.4	2.5	0	0
7	39.8	65.3	VII	2.5	3.9	0	0
8	35.6	61.7	VIII	13.2	15.6	0	0
9	32.1	59.2					
10	28.4	54.3					
11	31.4	59.7					
12	35.6	61.2					
13	34.5	60.1					
14	6.2	8					
15	15.8	17.3					
16	9.6	14.8					

Fig. C.28. Variation of internal forces for fatigue assessment

C.4.3 Serviceability limit state

For the limitation of the nominal stress and nominal stress variation the internal forces from rare/characteristic and frequent load combinations are needed. The values are given in Figure C.29.

Internal forces in the wind bracing in serviceability limit state							
	Characteristic/rare load combinations					Frequent load combinations	
Number of member	max N_x [kN]	min N_x [kN]	Number of node	max M_y [kNm]	min M_y [kNm]	Δ N_x [kN]	Δ My [kNm]
1	-4.2	-238.5	I	-	-	139.8	-
2	83.5	56.4	II	-23.7	-2.1	21.1	16.2
3	-47.8	-75.4	III	5.1	5.2	37.8	10.7
4	-143.6	-184.3	IV	7.4	6.1	15.8	2.8
5	170.3	-172.8	V	7.9	6.5	123.8	2.2
6	112.5	-12.4	VI	8.1	6.6	56.2	2
7	75.8	-69.3	VII	8.2	7.4	52.2	3.1
8	35.8	-45.2	VIII	-21.5	-1.9	49.4	12.5
9	38.4	-41.8				47.4	
10	32.9	-38.4				43.4	
11	37.4	-47.2				47.8	
12	35.6	-12.6				48.9	
13	34.5	-32.1				48.1	
14	28.6	25.9				6.4	
15	-145.6	-140.7				13.8	
16	27.6	8.4				11.8	

Fig. C.29. Internal forces in the wind bracing in serviceability limit state

C.5 Internal forces in the bridge deck

C.5.1 Ultimate limit state

The results given in the following were obtained from analysis of the 3D bridge model in SOFiSTiK. The computation did not account for creep, shrinkage and relaxation effects; these losses were taken from the preliminary design (Annex B) and the prestressing forces in the model were reduced respectively.

The decisive forces for the bridge deck in the ultimate limit states result from load combination 4 (see Annex A.5). One load model 71 on each track is placed in the centre of the bridge giving maximum bending moments for both longitudinal and transverse directions. The maximum values do not occur at mid-span, but rather under each track (Figure C.30, Figure C.31). Moreover, the bending moments per metre width are only single-symmetric about the longitudinal bridge axis, which is due to the braking force.

The results in the following figures are only shown for the longitudinal mid-range from x = 40 m to 60 m, whereas the full width of the deck is illustrated. The included footpaths are to be neglected here, as they are treated separately.

Illustrations of membrane forces were not included, since results vary only slightly. The membrane forces occurring at locations of maximum bending moments were directly read from the software output and are given below at the appropriate position.

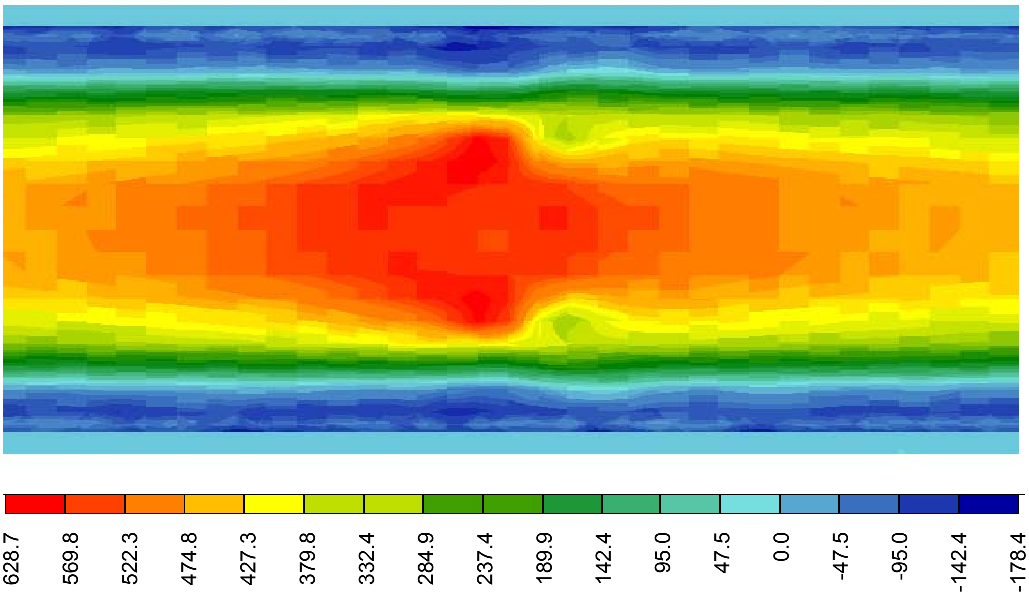

Fig. C.30. Transverse bending moments m_y, [kNm/m], x = 40…60 m

Design-relevant internal forces taken from Figure C.30 (a summary of all forces relevant for assessment can be found in Figure C.34):

Maximum bending moment:	$m_{y.max}$ = 628.7 kNm/m
	(x = 49.1 m, y = 3.28 m)
Respective axial force:	n_y = -3139 kN/m
Bending moment at smallest depth:	$m_{y.1.36}$ = 230 kNm/m (y = 1.36 m)
Respective axial force:	n_y = -3170 kN/m

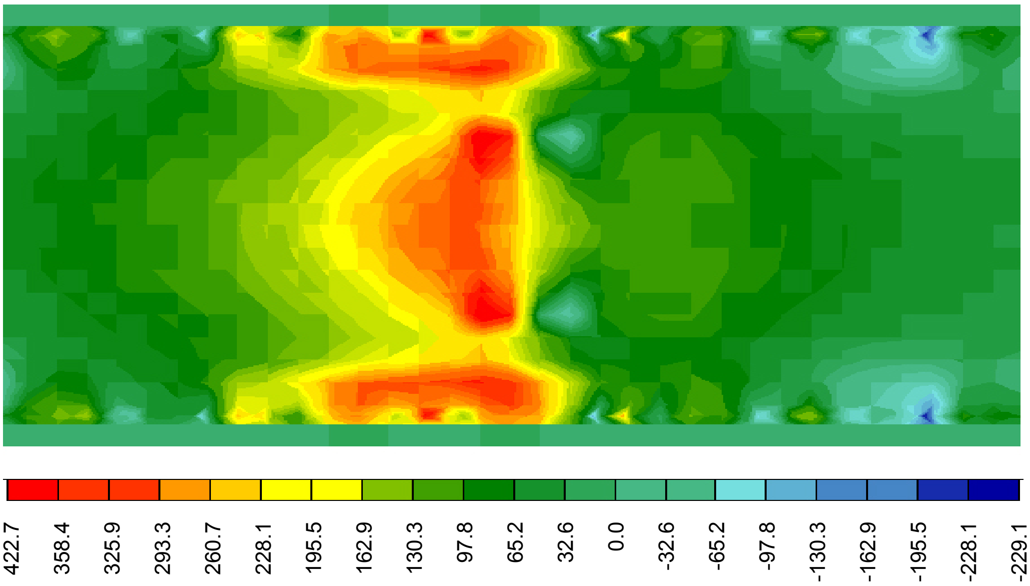

Fig. C.31. Longitudinal bending moments m_x, [kNm/m], x = 40…60 m

Design-relevant internal forces taken from Figure C.31 (a summary of all forces relevant for assessment can be found in Figure C.34):

Maximum bending moment in the slab:	$m_{x.max}$ = 422.7 kNm/m (x = 49.1 m, y = 2.69 m)
Respective axial force:	n_x = -2743 kN/m
Maximum bending moment in the edge beam:	$m_{x.max}$ = 407.9 kNm/m (x = 48.3 m)
Respective axial force:	n_x = -1691 kN/m

Figure C.32 shows the internal shear forces in transverse direction at the section where the maximum value was found. The maximum occurs at the hanger node which cannot be relevant for the shear design check. The decisive value was taken at a distance $\Delta y = 1.5 \cdot d$ (d : effective depth of the member). For punching shear, the vertical component of the maximum hanger force is critical.

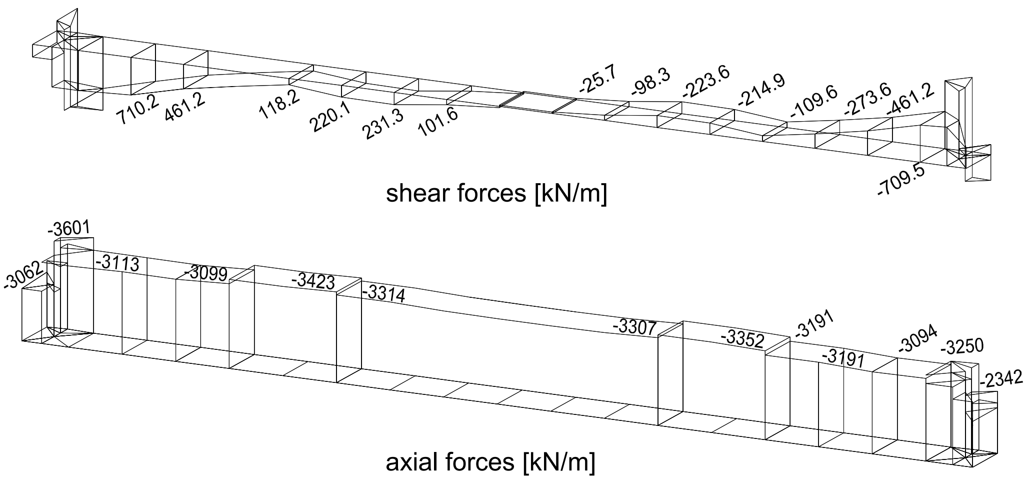

Fig. C.32. Transverse shear forces v_y and axial forces n_y [kNm/m], x = 51.5 m

Design-relevant internal forces taken from Figure C.32 (a summary of all forces relevant for assessment can be found in Figure C.34):

Critical shear force: $v_{Sd.y}$ = 710.2 kN/m
(y = 1.5 · d = 1.5 · 565 mm = 847.5 mm)
Respective axial force: n_y = -3113 kN/m

Maximum hanger force (No. 4): N_{max} = 1061.9 kN
Vertical component with α = 75.2°: $N_{max.v}$ = 1027 kN

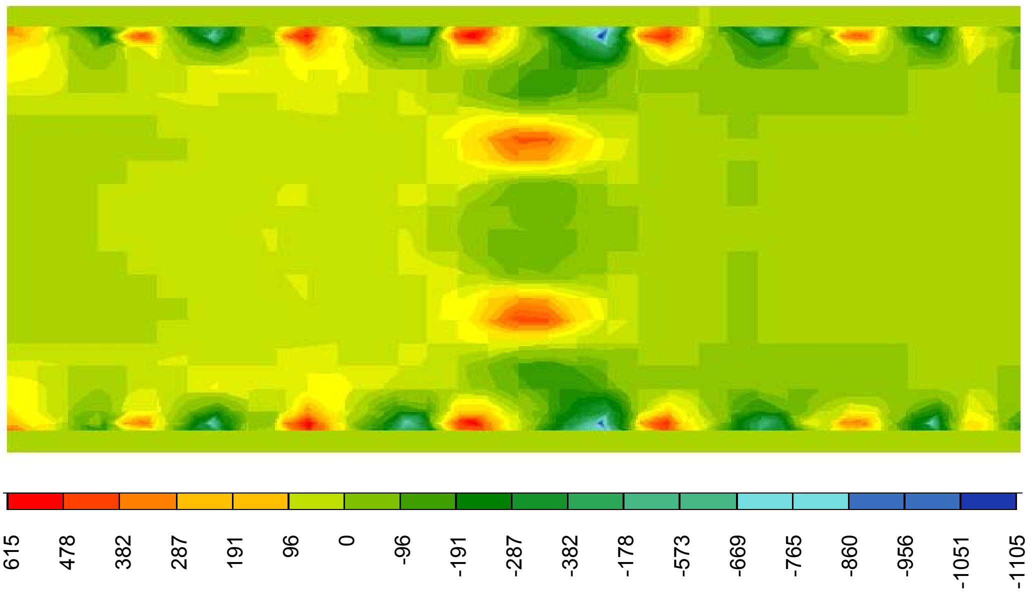

Fig. C.33. Longitudinal shear forces v_x [kNm/m], x = 40…60 m

Design-relevant internal forces taken from Figure C.33:

Critical shear force: $v_{Sd,x}$ = 615.1 kN/m (taken at a distance Δy = 1.5 · d from the maximum value)
Respective axial force: n_x = -2410 kN/m

Summary

Summary of design-relevant internal forces					
			m [kNm/m]	v [kN/m]	n [kN/m]
Bending	transverse		628.7		-3139
	longitudinal	slab	422.7		-2743
		edge beam	407.9		-1691
Shear	transverse			710.2	-3113
	longitudinal			615.1	-2410
Punching				1027 [kN]	

Fig. C.34. Summary of design-relevant internal forces for ultimate limit states

C.5.2 Serviceability limit state

In the following figures (C.35 to C.38), only the mid-range between x = 40 m and 60 m is illustrated. The footpath is not shown. It was decided not to include illustrations of all relevant stress distributions for each combination of actions. Instead, it was decided to include one representative example for each direction and location (top and bottom fibre). Figures C.35 and C.36 contain the maximum compressive stresses at the top fibre occurring in the non-frequent combination of actions. Figures C.37 and C.38 show maximum tensile stresses at the bottom fibre in the frequent combination, relevant for crack width assessment. A summary of the design relevant forces can be found in Figure C.39.

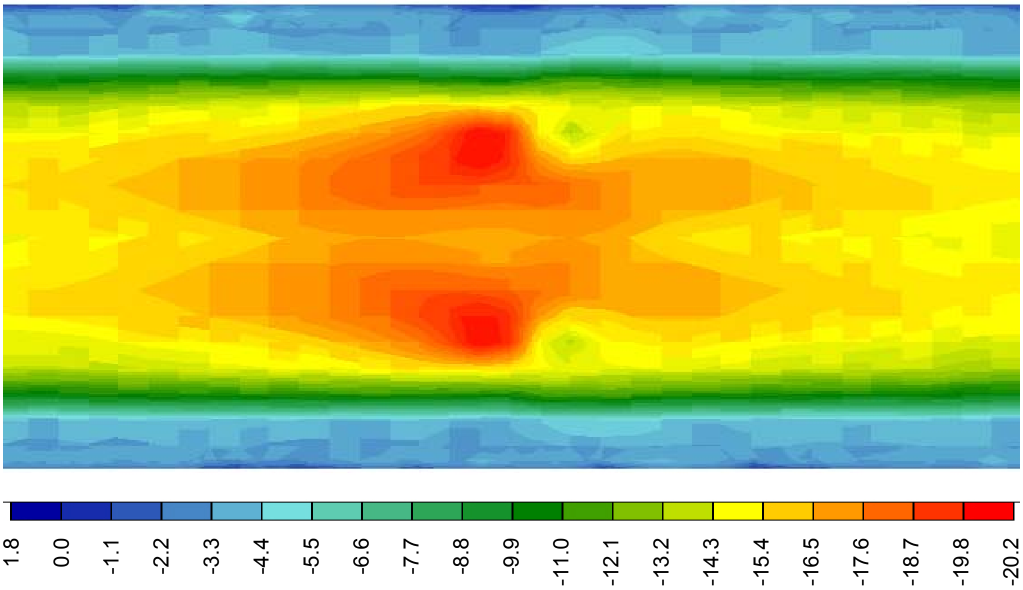

Fig. C.35. Non-frequent combination of actions: Concrete stresses $\sigma_{y.top}$ [N/mm^2], x = 40…60 m

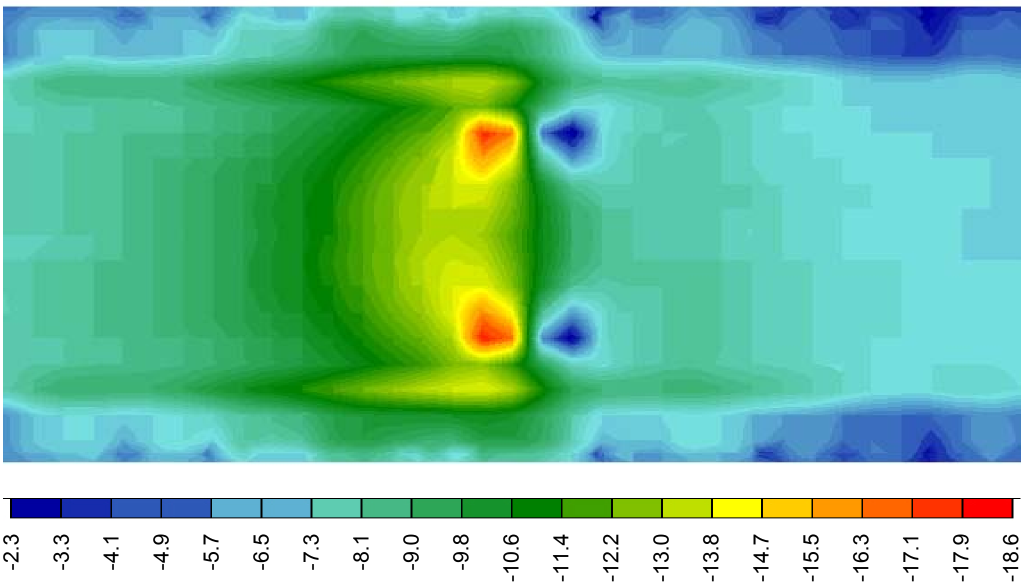

Fig. C.36. Non-frequent combination of actions: Concrete stresses $\sigma_{x.top}$ [N/mm^2], x = 40…60 m

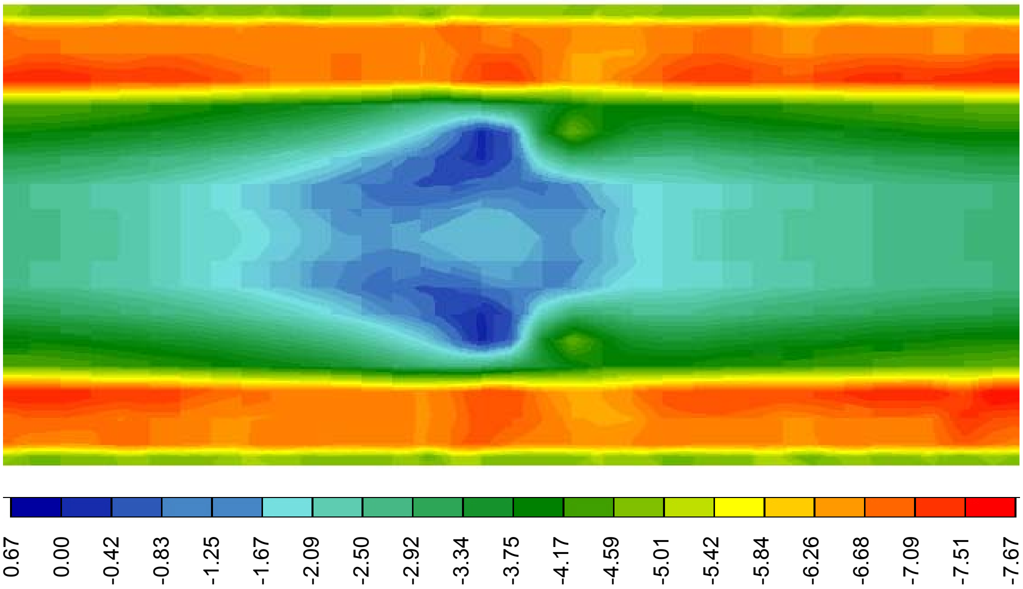

Fig. C.37. Frequent combination of actions: Concrete stresses $\sigma_{y.bottom}$ [N/mm^2], x = 40…60 m

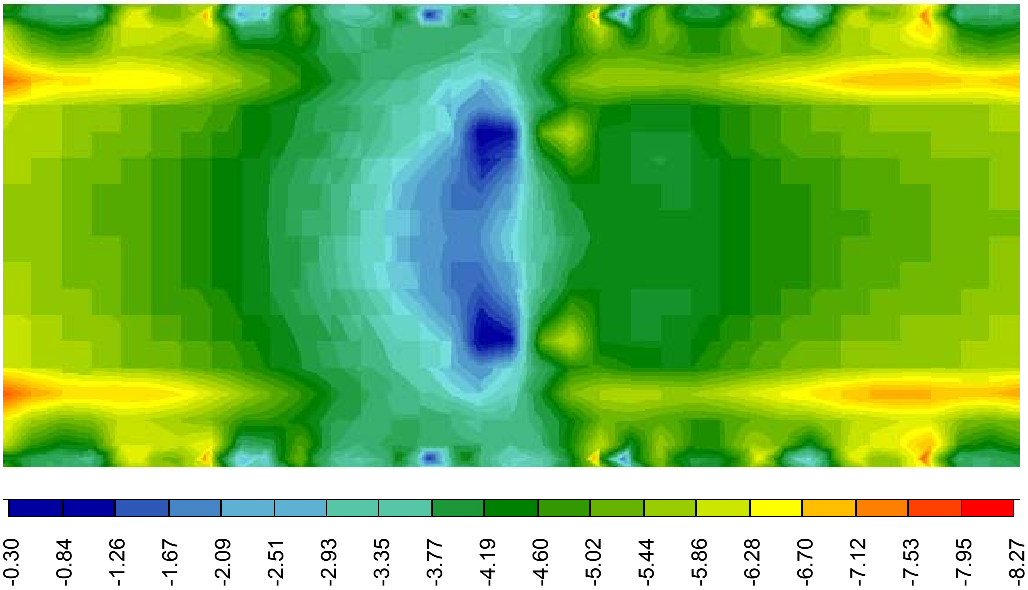

Fig. C.38. Frequent combination of actions: Concrete stresses $\sigma_{x.bottom}$ [N/mm^2], x = 40…60 m

Summary

Summary of design relevant concrete stresses					
Concrete stresses [N/mm^2]		**Longitudinal σ_x**		**Transverse σ_y**	
		min	max	min	max
Non-frequent	**Top**	**-18.6**	-1.51	**-20.2**	-2.5
	Location	deck centre	edge beam	deck centre	ede beam
	Bottom	-9.38	**4.6**	-7.13	**6.9**
	Location	deck centre	deck centre	edge beam	deck centre
Frequent	**Top**	-14.1	-3.09	-13.8	-1.25
	Location	deck centre	edge beam	deck centre	edge beam
	Bottom	-9.75	**-0.3**	-8.23	**0.67**
	Location	smallest depth	deck centre	edge beam	deck centre
Qquasi-permanent	**Top**	-12.3	-5.86	-9.38	-1.16
	Location	near diaphragm	edge beam	near diaphragm	edge beam
	Bottom	-11.4	**-3.41**	-11.8	**-4.66**
	Location	smallest depth	near diaphragm	smallest depth	edge beam
After prestressing	**Top**	**-16.5**	-3.7	**-12.3**	2
	Location	near diaphragm	near diapgragm	near diaphragm	deck centre
	Bottom	**-17.1**	-4.4	**-16.8**	-4.2
	Location	smallest depth	near diaphragm	deck centre	edge beam

Fig. C.39. Summary of design-relevant concrete stresses for serviceability limit states

C.5.3 Fatigue

The following table lists concrete stresses and shear forces necessary for the assessment of concrete in compression and shear.

Stresses and internal forces: Concrete fatigue **Frequent combination of actions**	
Compression: *ENV 1992-2: 1996 Section 4.3.7.4 (101)*	
Maximum compressive stress [N/mm²]	-14.1
Corresponding minimum [N/mm²]	-0.3
Shear: *ENV 1992-2: 1996 Section 4.3.7.4 (103)*	
Maximum shear force [kN/m]	702
Corresponding minimum [kN/m]	556
Punching: *ENV 1992-2: 1996 Section 4.3.7.4 (104)*	
Vertical component of maximum hanger force [kN]	630
Corresponding minimum [kN]	305

Fig. C.40. Stresses and internal forces for concrete fatigue assessment

In Figure C.41, stresses in the prestressing tendons are calculated based on an uncracked concrete section. Calculations were performed with the help of the known concrete stresses at the top and bottom fibre, as well as the geometric properties of the prestressed concrete section. The steel stress ranges result from different steel stresses due to different loading. For the conversion between concrete stress and steel stress, the elastic modulus ratio n = 10 was used assuming equal strains.

The assumption of an uncracked section is an approximation, especially in the case of two loaded tracks.

Steel stresses: Fatigue of prestressing steel ENV 1992-2: 1996 Section 4.3.7.5 (102) non-frequent combination of actions				
Concrete stresses [N/mm²] at centre of bridge deck	Top / Bottom	Tendon level	**Stress range**	
Dead load	-4.4	-7.5	$\Delta\sigma_{s,71} = \Delta\sigma_{1+2}$	**75**
	-8.45		$\Delta\sigma_1 = \Delta\sigma_2$	**42**
Load model 71 on one track	-9	-3.3	with	
	-1.5		$n = E_s/E_c = 10$	
Load model 71 on two tracks	-20.2	0	$h = 0.43$ m	
	6.9		$z_p = 0.103$ m	

Fig. C.41. Steel stresses for prestressing steel fatigue assessment

C.5.4 Alternatives without transverse prestressing

The existing 3D model in SOFiSTiK was changed by removing the transverse prestressing thread bars and increasing the slab thickness between the edge beams. The internal forces of the slab in transverse direction were taken directly from the software output of the new model. The internal forces in the longitudinal bridge direction were assumed unchanged.

The following tables summarise design-relevant internal forces for the two design proposals. The structural depth refers to the mid-section, where the maximum moments occur. As with the main design, decisive shear forces were taken at a distance $\Delta y = 1.5 \cdot d$ from the hanger connection.

Ultimate limit state

Alternative design proposal 1: h = 610 mm		
m_{Sdy} [kNm/m]	mid-span	1195.6
v_{Sdy} [kN/m]	at hangers	566.0
	at smallest depth	383.0
max N_{Sd} [kN]	hanger 4	1110.5

Fig. C.42. Maximum ULS internal forces, h = 610 mm

Alternative design proposal 2: h = 470 mm		
m_{Sdy} [kNm/m]	mid-span	1041.2
v_{Sdy} [kN/m]	at hangers	547.0
	at smallest depth	305.0
max N_{Sd} [kN]	hanger 4	1073.0

Fig. C.43. Maximum ULS internal forces, h = 470 mm

Serviceability limit states / Fatigue assessment

The non-frequent combination of actions is relevant for both fatigue and serviceability limit state assessments. The following tables calculate steel stresses in the reinforcement, assuming a cracked concrete section.

SCHNEIDER *[26]*, Tafel 2a, page 5.130

Calculation of steel stress in reinforcement - design proposal 1 (h = 610 mm)				
Combination: Non-frequent	**A_s [cm²/m]:** 54.54		**d [mm]:** 557.5	
	m_{Sdy} [kNm/m]	**μ_{Sd}**	**z [mm]**	**σ_s [N/mm²]**
one LM 71	598.1	0.058	535.2	204.9
two LM 71	814.1	0.079	528.5	282.4
DL only	420.6	0.041	541.3	142.5
$\Delta\sigma_{s1}$ [N/mm²]	62.4			
$\Delta\sigma_{s.71}=\Delta\sigma_{s1+2}$ [N/mm²]	140.0			

Fig. C.44. Calculation of stresses in reinforcement, structural depth h = 610 mm

Calculation of steel stress in reinforcement - design proposal 1 (h = 470mm)				
Combination: Non-frequent	**A_s [cm²/m]:** 70.12		**d [mm]:** 398	
	m_{Sdy} [kNm/m]	**μ_{Sd}**	**z [mm]**	**σ_s [N/mm²]**
one LM 71	484.0	0.093	374.9	184.1
two LM 71	700.0	0.134	363.8	274.4
DL only	306.5	0.059	382.1	114.4
$\Delta\sigma_{s1}$ [N/mm²]	69.7			
$\Delta\sigma_{s.71}=\Delta\sigma_{s1+2}$ [N/mm²]	160.0			

Fig. C.45. Calculation of stresses in reinforcement, structural depth h = 470 mm

C.6 Internal forces of the end cross girder

C.6.1 Ultimate limit state

The maximum internal forces occurring for the ultimate limit state are shown in Figure C.46.

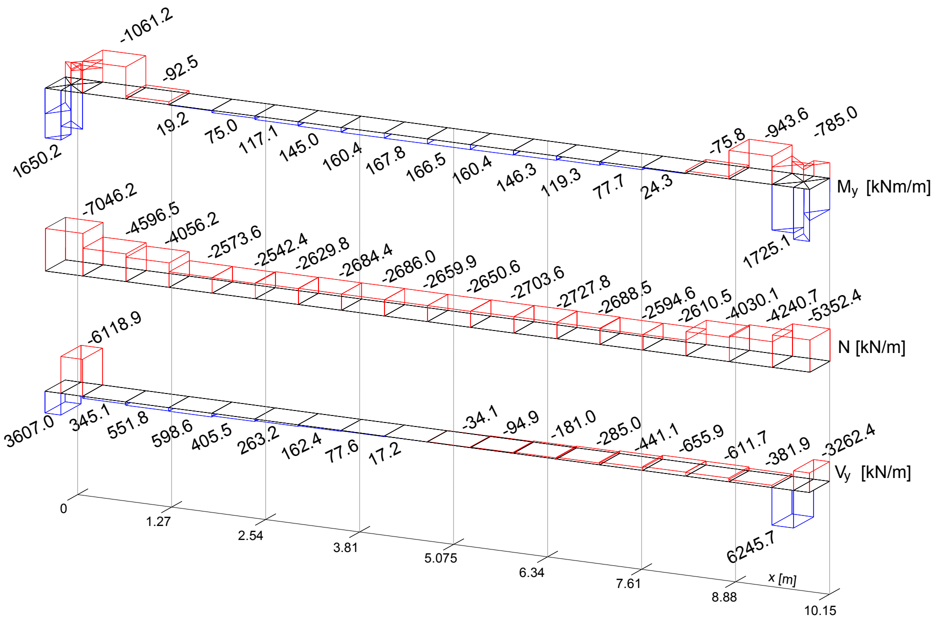

Fig. C.46. Internal forces for assessment of end cross girder in ultimate limit state

C.6.2 Serviceability limit state

The serviceability limit state to be verified by numerical assessment is limitations for stress. The critical stresses on the top and the bottom surface of the end cross girder are presented in Figure C.47.

	Non-frequent load combinations		Frequent load combinations		Quasi-permanent load combinations	
	top level	bottom level	top level	bottom level	top level	bottom level
Max stress [N/mm²]	-4.03	-2.4	-2.4	-2.84	-1.3	-5.2
Min stress [N/mm²]	-8.5	-7.9	-7.82	-9.2	-5.3	-9.6

Fig. C.47. Stresses in end cross girder in serviceability limit state, transverse direction

C.7 Actions on the bearings

Two types of bearings were examined (for details see Section 5.9):

1. Two pot bearings at each of the four supports (Figure C.48.)
2. Stilt bearing with compression support in the middle, suggestion by *P. Tveit* (Figure C.49)

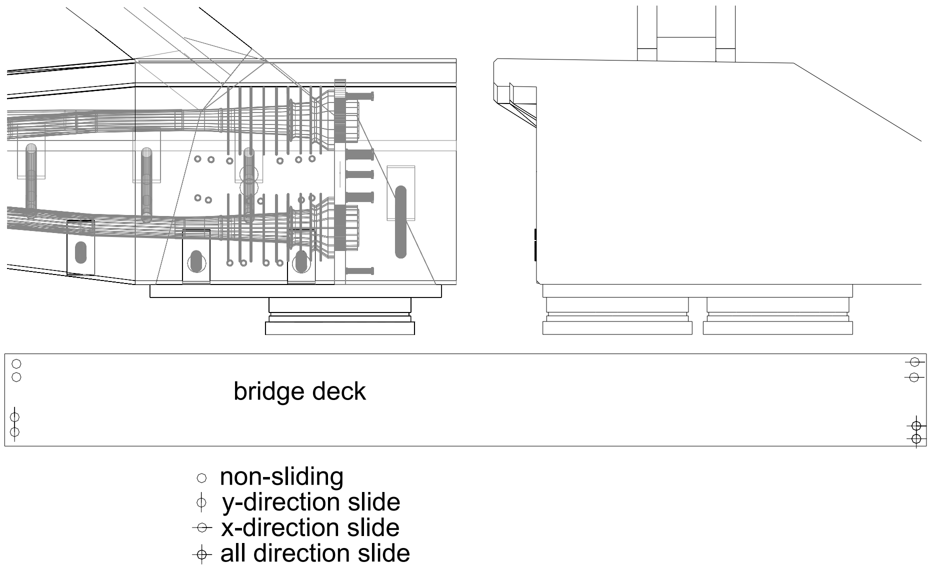

Fig. C.48. Pot bearings TF-10, TGa-10, TGe-10, MAURER SÖHNE GmbH & Co.KG *[20]*

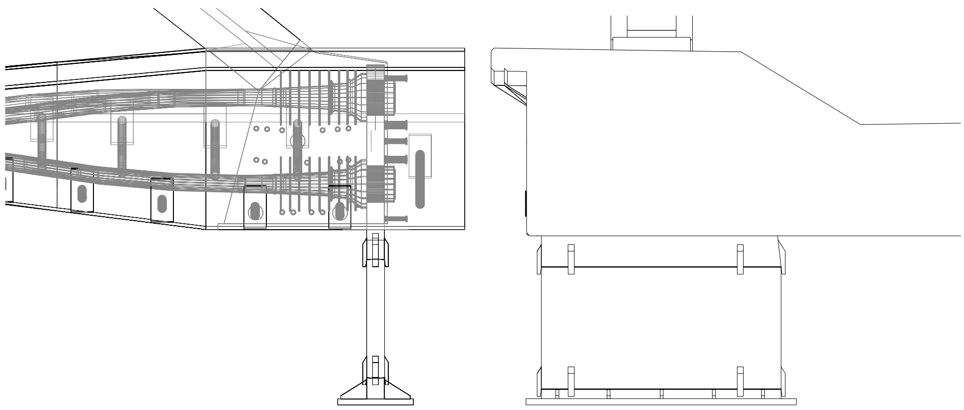

Fig. C.49. Stilt bearing, arrangement of the slide directions as in Figure C.48

The bearings had to be assessed for maximum vertical and horizontal forces, horizontal deflections and tilt/angular rotations. The minimum vertical forces do not undershoot 0 kN, and therefore there is no danger of lift-off. The internal forces were calculated in ultimate limit state.

It is unusual to have three supports at an end cross girder about 10 metres wide as in the “stilt” bearing. Therefore Figure C.50 shows the bearing forces with and without an additional compression support in the middle of the end cross girder, not only for the assessment of the bearings but also for general perceptions about a middle support.

Vertical bearing forces F_v and bending moments about the longitudinal axis of the bridge M_x in ultimate limit state											
			Pot bearings without support in the middle				Stilt-bearing with compression support in the middle				
	Load combination		F_v [kN]	M_x [kNm]	F_v [kN]	M_x [kNm]	F_v [kN]	M_x [kNm]	F_v [kN]	F_v [kN]	M_x [kNm]
		number	left		right		left		middle	right	
traffic dominant	1 LM 71 left	1	-14115	1204.46	-10791	-1004.94	-13847	430.9	-640.5	-10421	-247.58
		2	-14189	1071.7	-10801	-998.06	-13860	359.92	-560.5	-10472	-294.6
		3	-14031	1168.34	-10974	-921	-13694	471.32	-538.5	-10656	-219.28
	2 LM 71	4	-16052	2081.96	-15742	-2344.64	-15330	628.8	-1337	-15029	-941.5
		5	-16031	2004.42	-15743	-2279.42	-15365	606.02	-1225	-15087	-934.46
		6	-15848	2040.52	-15905	-2125.22	-15238	720.28	-1116	-15402	-864.12
wind dominant	1 LM 71 left	7	-13356	851.44	-10301	-877.7	-13039	216.06	-495.5	-10005	-267.34
		8	-13322	796.52	-10307	-881.06	-13044	181.16	-455.5	-10033	-292.38
	2 LM 71	9	-14806	1565.16	-14261	-1949.74	-14226	374.56	-1053	-13692	-822.76
		10	-14789	1502.86	-14262	-1897.52	-14253	356.14	-963.5	-13738	-816.8
	unloaded train	11	-9877	-92.94	-9168	-206.56	-9877	-92.94	0	-9479	-206.56

Fig. C.50. Bearing forces in ultimate limit state, wind forces from the right side, design check relevant values are framed

The idea of P.TVEIT is, as described in Section 5.9, that without live load the distance between the middle support and the bridge deck is 3 mm. The FEM-software used for the analysis does not provide such bearing conditions. Therefore the forces for the supports below the arches at a deflection of 3 mm cannot be obtained by numerical analysis. Since the analysis was performed in linear fashion, it is possible to scale the maximum values of the calculation without middle support:

Deflection due to load combination 4:	δ_1 = -7.5 mm
Deflection due to dead load:	δ_2 = 0 mm
Maximum vertical force due to dead load:	F_{v2} = -8753 kN
Maximum bending moment due to dead load:	M_{x2} = 13.85 kNm

$$F_v(\delta_1 = -3\text{ mm}) = (F_{v1} - F_{v2})\,\frac{3\text{mm}}{\delta_1 - \delta_2} + F_{v2}$$

$$F_v(\delta_1 = -3\text{ mm}) = (-15742\text{kN} + 8753\text{kN})\cdot\frac{3\text{mm}}{7{,}5\text{mm}} - 8753\text{kN} = -11548.6\text{kN}$$

$$M_x(\delta_1 = -3\text{ mm}) = M_{x1} - M_{x2}\,\frac{3\text{mm}}{\delta_1 - \delta_2} + M_{x2}$$

$$M_x(\delta_1 = -3\text{ mm}) = (-2345\text{kNm} - 13.85\text{kNm})\cdot\frac{3\text{mm}}{7{,}5\text{mm}} + 13.85\text{kNm} = -929.7\text{kNm}$$

The obtained values do not give decisive forces.

For the load combinations 1-10 the deflections of the end cross girder without the middle support are all greater than 3 mm, and so the forces after contact can be simulated by a settlement of the middle support of 3mm. This was applied while calculating the forces of the stilt bearing shown in Figure C.50.

The determination of the force acting on the middle support is difficult because in addition to the static forces it receives impulsive loads. The dynamic enlargement of this static force is 20% according to a proposal by P. TVEIT.

The maximum forces are:

1. For the pot bearings:
   F_v = -15742 kN
   F_H = 5393.4 kN
   M_x= -2344.6 kNm
2. For the stilt bearing:
   left / *right* (see Figure C.50)
   F_v = -15238 kN / -15087 kN *Section A.4*
   F_H = 4113.4 kN
   M_x = 720 kNm / 934.5 kNm
3. For the compression support:
   F_v = -1337 kN 1.2

The maximum horizontal deflections are:

1. Deflections due to changes of temperature; load case 4a
   minΔl = -0.037 m
   maxΔl = 0.04 m
2. Deflections due to creep and shrinkage

$$\varepsilon_{c,S,K} = \varepsilon_{c,S,u} + \frac{\varphi_{u,28} \cdot (\sigma_{cg} + \sigma_{cp0})}{E_c} = -0.0003 + \frac{1.6 \cdot (3.456 N/mm^2 - 11.6 N/mm^2)}{37000 N/mm^2}$$

Section B

$\varepsilon_{c,S,K} = -6.52 \cdot 10^{-4}$

$\Delta l = \varepsilon_{c,S,K} \cdot 100m = -0.065m$

3. Total

   minΔl = -0.037-0.065 m = <u>0.102 m</u>
   maxΔl = 0.04 m = 0.04 m

The maximum angular rotation is:

Θ_1 = 3.49 mrad

Assessment of the bridge

D.1 Materials, cross-sections, assessment parameters

Concrete

C50/60

Characteristic compressive strength f_{ck} = 50 N/mm^2 — *ENV 1992-1-1: 1991 Table 3.1*

Mean tensile strength f_{ctm} = 4.1 N/mm^2 — *ENV 1992-1-1: 1991 Table 3.2*

Secant elastic modulus E_{cm} = 37 kN/mm^2

Reinforcing steel — 500 S

Yield strength: f_y = 500 N/mm^2

Elastic modulus: E = 200000 N/mm^2

ENV 1992-1-1: 1991 Section 3.2
SCHNEIDER [29], page 5.26

Prestressing steel

Longitudinal prestressing — DYWIDAG Bonded Post-Tensioning System

Strand type: 15 mm according to prEN 10138
Tendon type: 6827
Steel strength: 1770/1500

DYWIDAG-SYSTEMS INTERNATIONAL [10]

Transversal prestressing — DYWIDAG Bonded Post-Tensioning

Thread bars: Type 36D
Steel strength: 1230/1080

Structural steel

Steel grade S460ML

For structural elements: Arch profile, hanger, hanger connections — *ENV 1993-2: 1997 Table 3.1a*

$t \leq$ 40mm
Yield strength: f_y = 460 N/mm^2
Ultimate tensile strength: f_u = 550 N/mm^2
Elastic modulus: E = 210000 N/mm^2

40 mm $< t \leq$ 100 mm
Yield strength: f_y = 430 N/mm^2
Ultimate tensile strength: f_u = 530 N/mm^2
Elastic modulus: E = 210000 N/mm^2

ENV 1993-2: 1997 Table 3.1b

Steel grade S355H

For structural elements: Wind bracing

t < 40 mm
Yield strength: f_y = 355 N/mm^2
Ultimate strength: f_u = 510 N/mm^2
Elastic modulus: E = 210000 N/mm^2

Arch profiles: American Wide Flange

ARCELOR LONG COMMERCIAL S.A. [4]

		W 360x410x634	W 360x410x990
A	[cm^2]	808	1262
I_z	[cm^4]	274200	450200
$W_{el,z}$	[cm^3]	11570	16960
$W_{pl,z}$	[cm^3]	14220	21620
I_y	[cm^4]	98250	15330
$W_{el,y}$	[cm^3]	4634	6938
$W_{pl.y.}$	[cm^3]	7117	10710

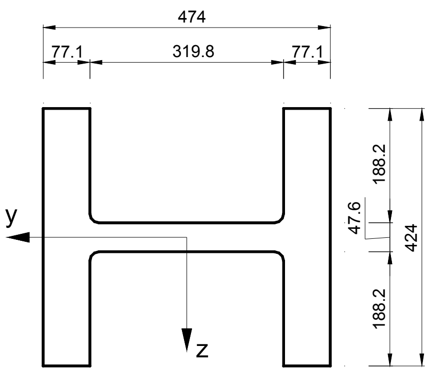

American Wide Flange
W 360 x 410 x 634

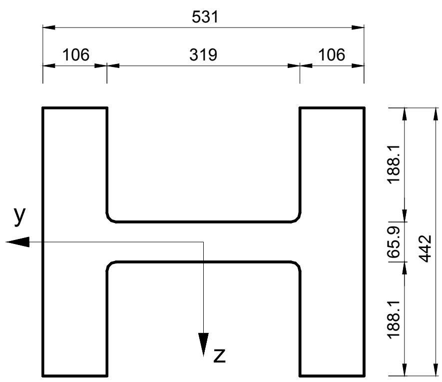

American Wide Flange
W 360 x 410 x 900

Wind bracing: Circular hollow sections

CORUS *[7]*

		CHS 219.1x8.0	CHS 219.1x10.0
A	[cm^2]	53.1	65.7
I	[cm^4]	2960	3598
W_{el}	[cm^3]	270	328
W_{pl}	[cm^3]	357	438

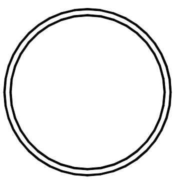

CHS 219.7 x 8

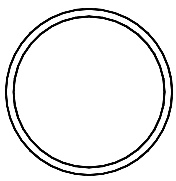

CHS 219.7 x 10

Hanger

Smooth circular steel bar, D = 60 mm

Partial safety factors

Member assessment

Ultimate limit states

γ_{M0} = 1.0
γ_{M1} = 1.1
γ_{M2} = 1.25

ENV 1993-2: 1997 Section 5.1.1

Serviceability limit states

$\gamma_{M,ser}$ = 1.25

Connection assessment

Welds

ENV 1993-2: 1997 Section 6.1

γ_{Mw} = 1.25

Bolts

γ_{Mb} = 1.25

Slip resistance, standard nominal clearance

ENV 1993-2 Section 6.4.7.1

$\gamma_{Ms,ult}$ = 1.25
$\gamma_{Ms,serv}$ = 1.1

Joints

ENV 1993-1-1: 1992 Annex K.1 (8)

γ_{Mj} = 1.1

Fatigue assessment

Structural steel elements

ENV 1993-2: 1997 Section 9.3

γ_{Ff} = 1.0
γ_{Mf} = 1.0 (for redundant structural elements: Hangers, wind bracing)
γ_{Mf} = 1.15 (for key structural elements: Arch profile)

Reinforced/prestressed concrete elements

ENV 1992-2: 1997 Section 4.3.7.2

γ_F = 1.0
γ_{Sd} = 1.0
$\gamma_{c,fat}$ = 1.5 for concrete
$\gamma_{s,fat}$ = 1.15 for reinforcement and prestressing steel

Data on fatigue assessment

The following was presumed and is applicable for all fatigue assessments in Annex D of this work.

EC Mix L = 100 m	λ_1 = 0.6	(*ENV 1993-2 Table 9.5*)
Traffic per year: 30 · 10^6 t/track	λ_2 = 1.04	(*ENV 1993-2 Table 9.6*)
Design life: 100 years	λ_3 = 1.0	(*ENV 1993-2 Table 9.7*)

n = 0.12

Data on reinforced/prestressed concrete members

ENV 1992-1-1: 1991 Table 4.1

The following was presumed and is applicable for Annex D, sections D.5, D.6.

ENV 1992-2: 1996 Table 4.118

Environmental exposure class: 2b
For decompression state and limit state of cracking: Category C

D.2 Arch

D.2.1 Ultimate limit state assessment

D.2.1.1 Collapse about weak axis y-y

Design check at the root of the arch

Values of the section vide Section D.1

1. Shear resistance

ENV 1993-1-1: 1992, 5.4.6

$V_{Sd,y}$ = -198.3 kN $\quad$ $V_{Sd,z}$ = -511.5 kN

$$V_{pl,Rd} = A_v \cdot \frac{f_y}{\sqrt{3} \cdot \gamma_{M1}}$$

A_v = A-2 b t_f+(t_w+2 r) t_f
= 1149 cm^2-2 44.2 cm 10.6 cm
+(6.59 cm+2 1.5 cm) 10.6 cm
= 313.6 cm^2

A_v = A-d t_f
= 1149 cm^2-28.9 cm 10.6 cm
= 842.7 cm^2

$$V_{pl,Rd} = 313.6cm^2 \cdot \frac{430N/mm^2}{\sqrt{3} \cdot 1.1}$$
= 7077.6 kN

$$V_{pl,Rd} = 842.7cm^2 \cdot \frac{430N/mm^2}{\sqrt{3} \cdot 1.1}$$
= 19019 kN

$\underline{|V_{Sd}| = 198.3\text{ kN} < V_{pl,Rd} = 7077.6\text{ kN}}$ $\quad$ $\underline{|V_{Sd}| = 511.5\text{ kN} < V_{pl,Rd} = 19019\text{ kN}}$

Since the design values of the shear force V_{Sd} do not exceed 50% of the design plastic shear resistance $V_{pl,Rd}$, no reduction need be made in the plastic resistance moment.

ENV 1993-1-1: 1992, 5.4.7 (2)

2. Bending and axial force

Section C.2.4, Figure C-8

N_{Sd} = -28468.3 kN
$M_{y,Sd}$ = 1115.8 kNm
$M_{z,Sd}$ = -809.9 kNm

$$N_{pl,Rd} = \frac{A \cdot f_y}{\gamma_{M1}} = \frac{1149cm^2 \cdot 430N/mm^2}{1.1} = 44915.5\text{ kN}$$

$$M_{pl,y,Rd} = \frac{W_{pl,y} \cdot f_y}{\gamma_{M1}} = \frac{10710cm3 \cdot 430N/mm2}{1.1} = 4186.6\text{ kNm}$$

ENV 1993-1-1: 1992, 5.4.4

$$M_{pl,z,Rd} = \frac{W_{pl,z} \cdot f_y}{\gamma_{M1}} = \frac{21620cm3 \cdot 430N/mm2}{1.1} = 8451.5\text{ kNm}$$

ENV 1993-1-1: 1992, 5.4.5.1

Criterion to be satisfied:

$$\frac{N_{Sd}}{N_{pl,Rd}} + \frac{M_{y,Sd}}{M_{pl,y,Rd}} + \frac{M_{z,Sd}}{M_{pl,z,Rd}} \leq 1$$

ENV 1993-1-1: 1992, 5.4.8.1 (5.36)

$$\frac{|-28468.3kN|}{44915.5kN} + \frac{1115.8kNm}{4186.6kNm} + \frac{|-809.9kNm|}{8451.5kNm} = 0.996 \leq 1$$

Design check at the first splice

Values of the section vide Section D.1

1. Shear resistance

ENV 1993-1-1: 1992, 5.4.6

$V_{Sd,y}$ = 135.4 kN $V_{Sd,z}$ = -310.5 kN

$$V_{pl,Rd} = A_v \cdot \frac{f_y}{\sqrt{3} \cdot \gamma_{M1}}$$

A_v = A-2 b t_f+(t_w+2 r) t_f
= 948.1 cm^2-2 43.2 cm 8.89 cm
+(5.56 cm+2 1.5 cm) 8.89 cm
= 256.1 cm^2

A_v = A-d t_f
= 948.1 cm^2-29.02 cm 8.89 cm
= 690.1 cm^2

$$V_{pl,Rd} = 256.1cm^2 \cdot \frac{430N/mm^2}{\sqrt{3} \cdot 1.1}$$
= 5779.9 kN

$$V_{pl,Rd} = 690.1cm^2 \cdot \frac{430N/mm^2}{\sqrt{3} \cdot 1.1}$$
= 15574.9 kN

$|V_{Sd}|$ = 135.4 kN < $V_{pl,Rd}$ = 5779.9 kN

$|V_{Sd}|$ = 310.5 kN < $V_{pl,Rd}$ = 15574.9 kN

Since the design values of the shear force V_{Sd} do not exceed 50% of the design plastic shear resistance $V_{pl,Rd}$, no reduction need be made in the plastic resistance moment.

ENV 1993-1-1: 1992, 5.4.7 (2)

2. Bending and axial force

Section C.2.4, Figure C-8

N_{Sd} = -27487.3 kN
$M_{y,Sd}$ = 210.8 kNm
$M_{z,Sd}$ = -100.4 kNm

$$N_{pl,Rd} = \frac{A_{,net} \cdot f_y}{\gamma_{M1}} = \frac{771cm^2 \cdot 430N/mm^2}{1.1} = 30139.1 \text{ kN}$$

$$M_{pl,y,Rd} = \frac{W_{pl,y,net} \cdot f_y}{\gamma_{M1}} = \frac{6908cm3 \cdot 430N/mm2}{1.1} = 2700.4 \text{ kNm}$$

ENV 1993-1-1: 1992, 5.4.4

$$M_{pl,z,Rd} = \frac{W_{pl,z,net} \cdot f_y}{\gamma_{M1}} = \frac{12138cm3 \cdot 430N/mm2}{1.1} = 4744.9 \text{ kNm}$$

ENV 1993-1-1: 1992, 5.4.5.1

Criterion to be satisfied:

$$\frac{N_{Sd}}{N_{pl,Rd}} + \frac{M_{y,Sd}}{M_{pl,y,Rd}} + \frac{M_{z,Sd}}{M_{pl,z,Rd}} \leq 1$$

$$\frac{|-27487.3kN|}{30139.1kN} + \frac{210.8kNm}{2700.4kNm} + \frac{|-100.4kNm|}{4744.9kNm} = 1.01 \leq 1.03$$

ENV 1993-1-1: 1992, 5.4.8.1 (5.36)

An overstepping of the allowed values up to 3% is tolerated.

D.2.1.2 Collapse about the strong axis z-z

Design check at the root of the arch

Values of the section vide Section D.1

1. Shear resistance

ENV 1993-1-1: 1992, 5.4.6

$V_{Sd,y}$ = -198.3 kN $V_{Sd,z}$ = -511.5 kN

$$V_{pl,Rd} = A_v \cdot \frac{f_y}{\sqrt{3} \cdot \gamma_{M1}}$$

A_v = A-2 b t_f+(t_w+2 r) t_f
= 1149 cm^2-2 44.2 cm 10.6 cm
+(6.59 cm+2 1.5 cm) 10.6 cm
= 313.6 cm^2

A_v = A-d t_f
= 1149 cm^2-28.9 cm 10.6 cm
= 842.7 cm^2

$$V_{pl,Rd} = 313.6cm^2 \cdot \frac{430N/mm^2}{\sqrt{3} \cdot 1.1}$$
= 7077.7 kN

$$V_{pl,Rd} = 842.7cm^2 \cdot \frac{430N/mm^2}{\sqrt{3} \cdot 1.1}$$
= 19019 kN

$|V_{Sd}|$= 514.7 kN < $V_{pl,Rd}$= 7077.7 kN

$|V_{Sd}|$= 428.8 kN < $V_{pl,Rd}$= 19019 kN

Since the design values of the shear force V_{Sd} do not exceed 50% of the design plastic shear resistance $V_{pl,Rd}$, no reduction need be made in the plastic resistance moment.

ENV 1993-1-1: 1992, 5.4.7 (2)

2. Bending and axial force

Section C.2.4, Figure C-8

N_{Sd} = -28146.8 kN
$M_{y,Sd}$ = 841.8 kNm
$M_{z,Sd}$ = -1840.8 kNm

$$N_{pl,Rd} = \frac{A \cdot f_y}{\gamma_{M1}} = \frac{1149cm^2 \cdot 430N/mm^2}{1.1} = 44915.5 \text{ kN}$$

$$M_{pl,y,Rd} = \frac{W_{pl,y} \cdot f_y}{\gamma_{M1}} = \frac{10710cm3 \cdot 430N/mm2}{1.1} = 4186.6 \text{ kNm}$$

ENV 1993-1-1: 1992, 5.4.4

$$M_{pl,z,Rd} = \frac{W_{pl,z} \cdot f_y}{\gamma_{M1}} = \frac{21620cm3 \cdot 430N/mm2}{1.1} = 8451.5 \text{ kNm}$$

ENV 1993-1-1: 1992, 5.4.5.1

Criterion to be satisfied:

$$\frac{N_{Sd}}{N_{pl,Rd}} + \frac{M_{y,Sd}}{M_{pl,y,Rd}} + \frac{M_{z,Sd}}{M_{pl,z,Rd}} \le 1$$

$$\frac{|-28146.8kN|}{44915.5kN} + \frac{841.8kNm}{4186.6kNm} + \frac{|-1480.8kNm|}{8451.5kNm} = 1.003 \le 1.03$$

ENV 1993-1-1: 1992, 5.4.8.1 (5.36)

An overstepping of the allowed values up to 3% is tolerated.

D.2.2 Fatigue assessment

Axial stresses

The fatigue check has to be carried out for four critical cross sections. So, first the necessary formulas are given and then the values will be presented in Figure D.1234.

$$\sigma_{p,min} = \frac{N_{min}}{A_{,net}} + \frac{M_{y,min}}{W_{el,y,net}} - \frac{M_{z,min}}{W_{el,z,net}}$$ dead load

$$\sigma_{p,max,1} = \frac{N_{max,1}}{A_{,net}} + \frac{M_{y,max,1}}{W_{el,y,net}} - \frac{M_{z,max,1}}{W_{el,z,net}}$$ dead load and one LM 71

$$\sigma_{p,max,1+2} = \frac{N_{max,1+2}}{A_{,net}} + \frac{M_{y,max,1+2}}{W_{el,y,net}} - \frac{M_{z,max,1+2}}{W_{el,z,net}}$$ dead load and two LM 71

$\Delta\sigma_1 = |\sigma_{p,max,1}-\sigma_{p,min}|$
$\Delta\sigma_{1+2} = \Delta\sigma_p = |\sigma_{p,max,1+2}-\sigma_{p,min}|$

$\Delta\sigma_{E2} = \lambda\ \varphi_2\ \Delta\sigma_p$
φ_2 is already included in the stresses due to LM 71

ENV 1993-2: 1997, Table 9.3 Table 9.6 Table 9.7

$\lambda = \lambda_1\ \lambda_2\ \lambda_3\ \lambda_4$

$\lambda_1 = 0.6$ EC Mix, L=100m
$\lambda_2 = 1.04$ Traffic per year: 30 10^6 t/track
$\lambda_3 = 1.0$ Design life: 100 years

$$\lambda_4 = \sqrt[5]{0.12 + 0.88 \cdot \left(\left(\frac{\Delta\sigma_1}{\Delta\sigma_{1+2}}\right)^5 + \left(1 - \frac{\Delta\sigma_1}{\Delta\sigma_{1+2}}\right)^5\right)}$$

ENV 1993-2: 1997, 9.5.3 (8)

$\Delta\sigma_c$ for:

ENV 1993-2: 1997

1. Connection to wind truss member $\Delta\sigma_c$ = 90 N/mm^2 *Table L.1 sheet 2*
2. Hanger connection $\Delta\sigma_c$ = 80 N/mm^2 *Table L.1 sheet 2*
3. Transverse splice between profiles $\Delta\sigma_c$ = 80 N/mm^2 *Table L.3 sheet 1*
4. Root of arch at top edge of concrete tie $\Delta\sigma_c$ = 160 N/mm^2 *Table L.1 sheet 1*

γ_{Mf} = 1.15 ; key structural element

	1.	2.	3.	4.
$\sigma_{p,min}$ [N/mm^2]	-145.99	-160.20	-138.90	-141.20
$\sigma_{p,max,1}$ [N/mm^2]	-222.40	-220.90	-208.90	-289.70
$\sigma_{p,max,1+2}$ [N/mm^2]	-250.50	-276.50	-235.80	-334.80
$\Delta\sigma_1$ [N/mm^2]	76.41	60.70	70.00	148.50
$\Delta_{\sigma 1+2}$ [N/mm^2]	104.51	116.30	96.90	193.60
λ_4	0.79	0.71	0.78	0.81
λ	0.49	0.44	0.49	0.51
$\Delta\sigma_{E2}\cdot\gamma_f$ [N/mm^2]	51.43	51.27	47.35	98.16
	$<$	$<$	$<$	$<$
$\Delta\sigma_c/\gamma_{Mf}$ [N/mm^2]	78.3	69.6	69.6	139.13

Fig. D.1. Fatigue checks for axial stresses

Shear stresses

The maximum shear forces occurring in ultimate limit state do not exceed 2.5 % (see Section D.2.1.1) of the permitted limits, so the shear stresses are considered to be not critical to fatigue strains. The fatigue check will be omitted.

Full penetration butt weld at arch root point

	Force due to dead load	Force due to LM 71	Force due to two LM 71	$\Delta F_{E2} = \Delta F_{1+2}$	ΔF_1
N_{Sd} [kN]	-11208.3	-17548	-20219	9010.7	6339.7
Vy [kN]	-20.18	-33.5	-35.8	15.62	13.32
Vz [kN]	67.3	84	139.7	72.4	16.7
M_y [kNm]	229.2	355.7	404.1	174.9	126.5
M_z [kNm]	-47	-28.7	-129.7	82.7	18.3
M_T [kNm]	3.613	-0.602	-0.803	4.416	4.215

ENV 1993-2: 1997, Section 9

$$\gamma_{Ff} \cdot \Delta\sigma_{E_2} \leq \frac{\Delta\sigma_c}{\gamma_{Mf}}$$

$$\Delta\sigma_{E_2} = \lambda \cdot \Phi_2 \cdot \Delta\sigma_p$$

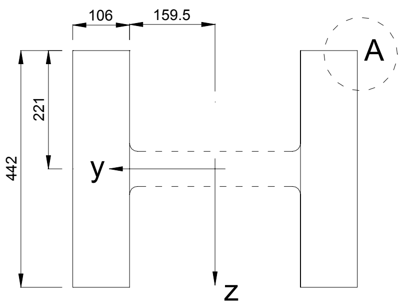

Section properties

$$A = 2 \cdot (106mm \cdot 442mm) = 93704mm^2$$

$$W_y = 2 \cdot \frac{(442mm)^2 \cdot 106mm}{6} = 6.903 \cdot 10^6 mm^3$$

$$W_z = \frac{2 \cdot \frac{(106mm)^3 \cdot 442mm}{12} + 2 \cdot 106mm \cdot 442mm \cdot \left(159.5mm + \frac{106mm}{2}\right)^2}{106mm + 159.5mm} = 1.627 \cdot 10^7 mm^3$$

The influence of the shear forces and the torsional moment will be ignored, as their contribution is very small and not decisive.

Stress variation due to two LM 71:

$$\Delta\sigma_p = \Delta\sigma_{1+2} = \frac{\Delta N_{1+2}}{A} + \frac{\Delta M_{y_{1+2}}}{W_y} + \frac{\Delta M_{z_{1+2}}}{Wz}$$

$$\Delta\sigma_p = \Delta\sigma_{1+2} = \frac{9010.7kN}{93704mm^2} + \frac{174.9kNm}{6.903 \cdot 10^6 mm^3} + \frac{82.7kNm}{1.627 \cdot 10^7 mm^3}$$

$$\Delta\sigma_p = \Delta\sigma_{1+2} = 96.16\frac{N}{mm^2} + 25.34\frac{N}{mm^2} + 5.08\frac{N}{mm^2} = 126.58\frac{N}{mm^2}$$

Stress variation due to one LM 71:

$$\Delta\sigma_1 = \frac{\Delta N_1}{A} + \frac{\Delta M_{y_1}}{W_y} + \frac{\Delta M_{z_1}}{Wz}$$

$$\Delta\sigma_1 = \frac{6340kN}{93704mm^2} + \frac{126.5kNm}{6.903 \cdot 10^6 mm^3} + \frac{18.3kNm}{1.627 \cdot 10^7 mm^3}$$

$$\Delta\sigma_1 = 67.66\frac{N}{mm^2} + 18.3\frac{N}{mm^2} + 1.12\frac{N}{mm^2} = 87.1\frac{N}{mm^2}$$

$\lambda_1 = 0.6$ EC Mix L = 100 m *ENV 1993-2: 1997*
$\lambda_2 = 1.04$ Traffic per year:30 $\cdot 10^6$ t/track *Table 9.5*
$\lambda_3 = 1.0$ Design life: 100 years *Table 9.6*
Table 9.7

$$\lambda_4 = \sqrt[5]{n + (1-n)\cdot\left(a^5 + (1-a)^5\right)}$$

n = 0.12

$$a = \frac{\Delta\sigma_1}{\Delta\sigma_{1+2}} = \frac{87.1\,N/mm^2}{126.58\,N/mm^2} = 0.688$$

$$\lambda_4 = \sqrt[5]{0.12 + [1-0.12]\cdot\left[0.688^5 + (1-0.688)^5\right]} = 0.76$$

$$\lambda = \lambda_1 \cdot \lambda_2 \cdot \lambda_3 \cdot \lambda_4 = 0.6 \cdot 1.04 \cdot 1.0 \cdot 0.76 = 0.47$$

$$\Delta\sigma_{E_2} = \lambda \cdot \Phi_2 \cdot \Delta\sigma_p$$

$$\Delta\sigma_{E_2} = 0.47 \cdot 126.58 \frac{N}{mm^2} = 59.49 \frac{N}{mm^2}$$

Detail category: 80 (ENV 1993-2:1997 Table L.3/1

$$\Delta\sigma_c = 80 \frac{N}{mm^2}$$

$\gamma_{Mf} = 1.15$ (key structural element)
$\gamma_{Ff} = 1.0$

$$1.0 \cdot 59.49 \frac{N}{mm^2} \le \frac{80\,N/mm^2}{1.15} = 69.6 \frac{N}{mm^2}$$

D.2.3 Serviceability limit state assessment

D.2.3.1 Limitation of nominal stress for characteristic/rare load combinations

The critical section is found at the root of the arch. The net cross section is used for the design check, which is on the safe side.

Axial stress

$$\sigma_{Ed,ser} = \frac{N_{ser}}{A_{,net}} + \frac{M_{y,ser}}{W_{el,y,net}} - \frac{M_{z,ser}}{W_{el,z,net}} = \frac{-21326.2kN}{1098.12cm^2} + \frac{446.2kNm}{6775cm^3} - \frac{468.1kNm}{14007cm^3}$$
$$= -161.8\ N/mm^2$$

Shear stress

$$\tau_{Ed,ser} = \frac{V_{y,ser}}{A_{vy}} = \frac{-86.5kN}{313.6cm^2}$$
$$= -2.78 N/mm^2$$

The criterion to be satisfied is:

$$\sqrt{(\sigma_{Ed,ser})^2 + 3(\tau_{Ed,ser})^2} < \frac{fy}{\gamma_{M,ser}}$$

ENV 1993-2: 1997, 4.3 (1)

$$\sqrt{(-161.8N/mm^2)^2 + 3(-2.78N/mm^2)^2} = 161.9 < 430N/mm^2 = \frac{430N/mm^2}{1.0}$$

D.2.3.2 Limitation of nominal stress range for frequent load combinations

The critical section is found at the root of the arch. The stress range will be calculated from the variation of internal forces. The net cross section is used for design check, which is on the safe side.

$$\Delta\sigma_{Ed,ser} = \frac{\Delta N_{ser}}{A_{,net}} + \frac{\Delta M_{y,ser}}{W_{el,y,net}} + \frac{\Delta M_{z,ser}}{W_{el,z,net}} = \frac{5758.5kN}{1098.12cm^2} + \frac{95.6kNm}{6775cm^3} + \frac{0.9kNm}{14007cm^3}$$

$= 66.6\ N/mm^2$

The criterion to be satisfied is:

$$\Delta\sigma_{Ed,ser} < 1.5\frac{f_y}{\gamma_{M,ser}}$$

ENV 1993-2: 1997, 4.3 (4)

$$\Delta\sigma_{Ed,ser} = 66.6N/mm^2 < 645N/mm^2 = 1.5\frac{430N/mm^2}{1.0}$$

D.2.3.3 Limits for clearance gauges

The structural part nearest to the clearance gauge is the lowest member of the wind truss. The shortest distance is 20 cm. The wind truss moves maximally 18.7 cm towards the railway traffic with a minimum upwards deflection of 4 cm in ultimate limit state. This reduces the shortest distance to 10 cm. Since the loads and the deflections are smaller for partial safety factors according to serviceability limit state, there is no danger of structural parts encroaching upon the clearance gauge.

D.3 Hanger and hanger connections

D.3.1 General

Steel strength of different members			
Member	**Criteria**	**f_y [N/mm²]**	**f_u [N/mm²]**
Hangers	40mm < t ≤ 100mm	430	530
Connection plates	t ≤ 40mm	460	550
Arch profile	40mm < t ≤ 100mm	430	530

Fig. D.2. Steel strength of different members

Design relevant internal forces (Critical: hanger No. 4)		
Ultimate limit states		
Design tensile force in the hanger	**$N_{Sd,ult}$ [kN]**	1061.9
Serviceability limit states		
Rare/characteristic combination of actions	**$N_{Sd,ser}$ [kN]**	785.5
Fatigue assessment		
Force range due to load model 71 on one track	**$\Delta N_{1,Sd}$ [kN]**	295.3
Force range due to load model 71 on two tracks	**$\Delta N_p = \Delta N_{1+2,Sd}$ [kN]**	439.7

Fig. D.3. Design-relevant hanger forces

Eccentricity of connection detail to the arch profile

The connection detail is eccentric to the arch profile, which has to be taken into account. The resulting bending moment contributes to a higher force transmitted into one flange. In the following, a factor (ψ) is calculated, which is then applied in the ultimate limit state and fatigue assessment.

Hanger type 4: Eccentricity of hanger to the arch profile: e = 3 cm
Bending moment (virtual hanger force = 1 [-]): M = 1 · 0.03 m = 0.03 m
Clearance between flanges: s = 31.98 cm
$\psi = M / s = 0.03 \text{ m} / 0.3198 \text{ m} = 0.094$

- For ultimate limit state: $N_{Sd} = 1061.9$ kN
  $N_{Sd.ecc} = N_{Sd} / 2 + N_{Sd} \cdot F = 1061.9 \text{ kN} / 2 + 1061.9 \text{ kN} \cdot 0.094 = 630.8 \text{ kN}$
- For fatigue assessment: ($\Delta N_p = 440$ kN)
  $\Delta N_{p.ecc.1} = \Delta N_p / 2 + \Delta N_p \cdot F = 440 \text{ kN} / 2 + 440 \text{ kN} \cdot 0.094 = 261 \text{ kN}$
  $\Delta N_{p.ecc.2} = 440 \text{ kN} – 261 \text{ kN} = 179 \text{ kN}$
- For determination of SCF (N = 1000 kN):
  $N_{ecc.1} = 1000 \text{ kN} / 2 + 1000 \text{ kN} \cdot 0.094 = 594 \text{ kN}$
  $N_{ecc.2} = 1000 \text{ kN} – 571 \text{ kN} = 406 \text{ kN}$

Hanger type 5: Eccentricity of hanger connection type 5: e = 2 cm
Bending moment (virtual hanger force = 1 [-]): M = 1 · 0.02 m = 0.02 m
Width of hanger gusset plate: s = 28.0 cm
$\psi = M / s = 0.02 \text{ m} / 0.28 \text{ m} = 0.0714$

- For determination of SCF (N = 1000 kN):
  $N_{ecc.1} = 1000 \text{ kN} / 2 + 1000 \text{ kN} \cdot 0.0714 = 571 \text{ kN}$
  $N_{ecc.2} = 1000 \text{ kN} – 571 \text{ kN} = 429 \text{ kN}$
- For fatigue assessment ($\Delta N_p = 440$ kN):
  $\Delta N_{p.ecc.1} = 440 \text{ kN} / 2 + 440 \text{ kN} \cdot 0.0714 = 251 \text{ kN}$
  $\Delta N_{p.ecc.2} = 440 \text{ kN} – 251 \text{ kN} = 189 \text{ kN}$

D.3.2 Ultimate and serviceability limit state assessment

D.3.2.1 Hanger

Section properties

Cross section: circular
Diameter: D = 60 mm
Cross section area: A = 2827.43 mm^2

Ultimate limit state

ENV 1993-1-1: 1992
Section 5.4.3

Criterion: $N_{Sd} < N_{t.Rd}$

Design plastic resistance

$$N_{t.Rd} = N_{pl.Rd} = \frac{A \cdot f_y}{\gamma_{M0}}$$

$$N_{pl.Rd} = \frac{2827.43\text{mm}^2 \cdot 430\,\text{N}/\text{mm}^2}{1.0} = 1215.8\text{kN}$$

$$\underline{N_{Sd} = 1061.9\text{kN} < N_{pl.Rd} = 1215.8\text{kN}}$$

Serviceability limit state

ENV 1993-2: 1997
Section 4.3

$$\sigma_{Ed.ser} < \frac{f_y}{\gamma_{M.ser}}$$

$$\sigma_{Ed.ser} = \frac{F_{ser}}{A} = \frac{785.5\text{kN}}{2827.43\text{mm}^2} = 277.82\frac{\text{N}}{\text{mm}^2}$$

$$\frac{f_y}{\gamma_{M.ser}} = \frac{430\,\text{N}/\text{mm}^2}{1.0} = 430\,\text{N}/\text{mm}^2$$

$$\underline{\sigma_{Ed.ser} = 277.82\frac{\text{N}}{\text{mm}^2} < \frac{f_y}{\gamma_{M,ser}} = 430\frac{\text{N}}{\text{mm}^2}}$$

D.3.2.2 Hanger connections

D.3.2.2.1 Connection type 1

Member assessment

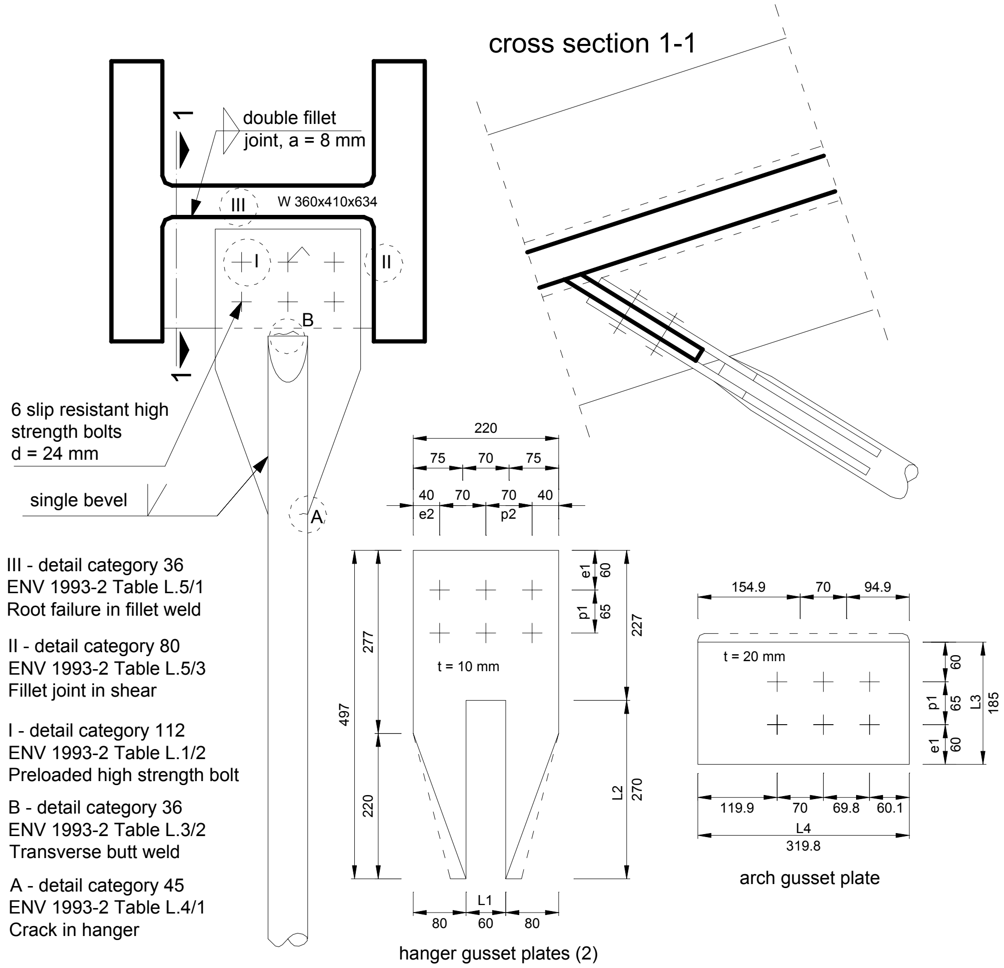

Fig. D.4. Hanger connection type 1

Hanger gusset plate

Section properties

Number of plates: $n = 2$
Width: $w = 220$ mm
Thickness: $t = 10$ mm
Total cross section area: $A = 4400\ mm^2$
Net cross section area: $A_{net} = 2840\ mm^2$ (3 holes with $d_0 = 26$ mm)

Ultimate limit state

ENV 1993-1-1: 1992
Section 5.4.3

Criterion: $N_{Sd} < N_{t.Rd}$

Design plastic resistance:

$$N_{t.Rd} = N_{pl.Rd} = \frac{A \cdot f_y}{\gamma_{M0}}$$

$$N_{pl.Rd} = \frac{4400mm^2 \cdot 460 N/mm^2}{1.0} = 2024kN$$

$$\underline{N_{Sd} = 1061.9kN < N_{t.Rd} = N_{pl.Rd} = 2024kN}$$

Design ultimate resistance of net cross-section at holes for fasteners

$$N_{t.Rd} = N_{u.Rd} = 0.9 \cdot A_{net} \cdot \frac{f_u}{\gamma_{M2}} = 0.9 \cdot 2840mm^2 \cdot \frac{550 N/mm^2}{1.25} = 1124.6kN$$

$$\underline{N_{Sd} = 1061.9kN < N_{t.Rd} = N_{u.Rd} = 1124.6kN}$$

Serviceability limit state

ENV 1993-2: 1997
Section 4.3

$$\sigma_{Ed.ser} < \frac{f_y}{\gamma_{M.ser}}$$

$$\sigma_{Ed.ser} = \frac{F_{ser}}{A_{net}} = \frac{785.5kN}{2840mm^2} = 204.6\frac{N}{mm^2}$$

$$\frac{f_y}{\gamma_{M.ser}} = \frac{430 N/mm^2}{1.0} = 430 N/mm^2$$

$$\underline{\sigma_{Ed.ser} = 204.6\frac{N}{mm^2} < \frac{f_y}{\gamma_{M.ser}} = 430\frac{N}{mm^2}}$$

Arch gusset plate

Section properties

Number of plates: $n = 1$
Shear length: $L_3 = 185$ mm
Thickness: $t = 20$ mm
Gross shear area: $A_{v.gross} = 2 \cdot 185 \text{ mm} \cdot 20 \text{ mm} = 7400 \text{ mm}^2$
Net shear area: $A_v = 5320 \text{ mm}^2$ (2 holes with $d_0 = 26$ mm)

The gusset plate is welded to the flanges as well as to the web. However, the design checks consider only the welding to the flanges.

Ultimate limit state

ENV 1993-1-1: 1992
Section 5.4.6

Criterion: $V_{Sd} < V_{pl.Rd}$

Design force: $V_{Sd} = N_{Sd} = 1061.9kN$

Design plastic shear resistance:

$$V_{pl.Rd} = \frac{A_v \cdot f_y}{\sqrt{3} \cdot \gamma_{M0}} = \frac{5320mm^2 \cdot 460 N/mm^2}{\sqrt{3} \cdot 1.0} = 1413kN$$

$$\underline{V_{Sd} = 1061.85kN < V_{pl.Rd} = 1232kN}$$

Serviceability limit state — *ENV 1993-2: 1997 Section 4.3*

$$\tau_{Ed.ser} < \frac{f_y}{\sqrt{3} \cdot \gamma_{M.ser}}$$

$$\tau_{Ed.ser} = \frac{V_{Sd}}{A_v} = \frac{785.5kN}{5320mm^2} = 147.7\frac{N}{mm^2}$$

$$\frac{f_y}{\sqrt{3} \cdot \gamma_{M.ser}} = \frac{430N/mm^2}{\sqrt{3} \cdot 1.0} = 248.6N/mm^2$$

$$\tau_{Ed.ser} = 169\frac{N}{mm^2} < \frac{f_y}{\sqrt{3} \cdot \gamma_{M.ser}} = 248.6\frac{N}{mm^2}$$

Connection assessment

Bold connection (I)

Type: Category C, slip-resistant at ultimate limit state
Preloaded high strength bolt

Properties

Bolt grade: 10.9
Yield strength: f_{yb} = 900 N/mm^2
Ultimate tensile strength: f_{ub} = 1000 N/mm^2
Bolt diameter: d = 24 mm
Hole diameter: d_o = d + 2mm = 26 mm (standard nominal clearance)
Bolt cross section area: A = 452 mm^2
Stress area: A_s = 353 mm^2
Number of bolts: n = 6

Schneider [29], Page 8.81

Geometry

Distances measured from centres of fasteners: — *ENV 1993-1-1: 1992 Section 6.5.1*

End distance in load direction: e_1
Edge distance perpendicular to load direction: e_2
Spacing between fasteners in load direction: p_1
Spacing between rows of fasteners perpendicular to load direction: p_2

Limits: — *ENV 1993-2: 1997 Section 6.3*

e_1 = 60mm ≥ min e_1 = 1.5 · d_0 = 39 mm
e_2 = 40mm ≥ min e_2 = 1.5 · d_0 = 39 mm
p_1 = 65mm ≥ min p_1 = 2.5 · d_0 = 65 mm
p_2 = 70mm ≥ min p_2 = 2.5 · d_0 = 65 mm

Maximum end and edge distances: members exposed to weather
e_1 = 60 < $e_{1.max}$ = 40 mm + 4 · t = 80 mm
(t: thickness of thinner outer connected part)

Maximum spacing in tension members
Outer row: $p_{1.0}$ = 65 mm < $p_{1.0.max}$ = 14 · t = 168 mm (200 mm)
Inner row: $p_{1.j}$ = 65 mm < $p_{1.j.max}$ = 24 · t = 336 mm (400 mm)

Criteria

ENV 1993-1-1: 1992 Table 6.5.2

$F_{v.Sd} \leq F_{s.Rd}$ slip resistance

$F_{v.Sd} \leq F_{b.Rd}$ bearing resistance

Design shear force for ultimate limit state

$$F_{v.Sd} = \frac{N_{Sd}}{n} = \frac{1061.9\text{kN}}{6} = 177\text{kN}$$

Bearing resistance

ENV 1993-1-1: 1992 Table 6.5.3

$$F_{b.Rd} = \frac{2.5 \cdot \alpha \cdot f_u \cdot d \cdot t}{\gamma_{Mb}}$$

where α is the smallest of:

$$\frac{e_1}{3 \cdot d_o} = \frac{60\text{mm}}{3 \cdot 26\text{mm}} = 0.77$$

$$\frac{p_1}{3 \cdot d_o} - \frac{1}{4} = \frac{65\text{mm}}{3 \cdot 26\text{mm}} - \frac{1}{4} = 0.58$$

$$\frac{f_{ub}}{f_u} = \frac{1000\,\text{N}/\text{mm}^2}{550\,\text{N}/\text{mm}^2} = 1.82$$

or 1

→ α = 0.58

Arch gusset plate:

$$F_{b.Rd} = \frac{2.5 \cdot 0.58 \cdot 550\,\text{N}/\text{mm}^2 \cdot 24\text{mm} \cdot 20\text{mm}}{1.25} = 306\text{kN}$$

$$\underline{F_{v.Sd} = 177\text{kN} < F_{b.Rd} = 306\text{kN}}$$

Hanger gusset plate:

$$F_{b.Rd} = \frac{2.5 \cdot 0.58 \cdot 550\,\text{N}/\text{mm}^2 \cdot 24\text{mm} \cdot 10\text{mm} \cdot 2}{1.25} = 306\text{kN}$$

$$\underline{F_{v.Sd} = 177\text{kN} < F_{b.Rd} = 306\text{kN}}$$

Slip resistance

$$F_{s.Rd} = \frac{k_s \cdot n \cdot \mu}{\gamma_{Ms}} \cdot F_{p.Cd}$$

ENV 1993-1-1 Section 6.5.8

Slip factor: μ = 0.5 *Class A surface:*
ENV 1993-2: 1997 Section 6.4.7.1 (6)
ENV 1993-1-1: 1992 Section 6.5.8.3

k_s = 1 standard nominal clearance

n = 2 number of friction interfaces

$F_{p.Cd}$ preloading force

$F_{p.Cd} = 0.7 \cdot f_{ub} \cdot A_s = 0.7 \cdot 1000\text{ N/mm}^2 \cdot 353\text{ mm}^2 = 247.1\text{ kN}$

$$F_{s.Rd} = \frac{1 \cdot 2 \cdot 0.5}{1.25} \cdot 247.1\text{kN} = 198\text{kN}$$

$$\underline{F_{v.Sd} = 177\text{kN} < F_{s.Rd} = 198\text{kN}}$$

Weld joints

Weld between hanger and hanger gusset plate

Type: Full penetration butt weld (Single bevel joint)
Thickness of gusset plates: t = 10 mm

The design resistance of a full penetration butt weld shall be taken as equal to the design resistance of the weaker of the parts joined.

ENV 1993-1-1: 1992 Section 6.6.6.1

The gusset plates have only been checked for resistance at the section weakened by the bolts. Here, the resistance of the hanger gusset plates along the weld joint and therefore the resistance of the full penetration butt welds will be checked. Only the longitudinals welds are considered for force transmission.

Ultimate limit state

ENV 1993-1-1: 1992 Section 5.4.6

Criterion: $V_{Sd} < V_{pl.Rd}$

Design force:

$$V_{Sd} = N_{Sd} = 1061.9\text{kN}$$

Shear area:

$$A_v = L_2 \cdot t \cdot 2 = 270\text{mm} \cdot 10\text{mm} \cdot 2 = 5400\text{mm}^2$$

Design plastic shear resistance:

$$V_{pl.Rd} = \frac{A_v \cdot f_y}{\sqrt{3} \cdot \gamma_{M0}} = \frac{5400\text{mm}^2 \cdot 460\,\text{N}/\text{mm}^2}{\sqrt{3} \cdot 1.0} = 1434\text{kN}$$

$$\underline{V_{Sd} = 1061.9\text{kN} < V_{pl.Rd} = 1434\text{kN}}$$

Weld between arch gusset plate and arch profile (II)

Type: Double fillet joint
Throat thickness: a = 8 mm

The gusset plate is welded to the flanges as well as to the web. However, the design check considers only the welding to the flanges.

Criterion: $F_{w.Ed} \leq F_{w.Rd}$

Section D.3.1
Figure D.3.3

Design weld force: $V_{Sd} = N_{Sd.ecc}$ = 630.8 kN

Weld length $L_w = L_3 \cdot 2 = 185\text{mm} \cdot 2 = 370\text{mm}$

Design weld force per unit length:

$$F_{w.Sd} = \frac{V_{Sd}}{L_w} = \frac{630.8\text{kN}}{370\text{mm}} = 1705\,\text{N}/\text{mm}$$

Design resistance per unit length

$$F_{w.Rd} = f_{vw.d} \cdot a$$

Design shear strength $f_{vw.d} = \dfrac{f_u/\sqrt{3}}{\beta_w \cdot \gamma_{Mw}}$

Correlation factor β_w for fillet welds ($f_u \geq 520$ N/mm^2): $\beta_w = 1.0$

ENV 1993-1-1: 1992
Section 6.6.5.3

ENV 1993-2 : 1997
Table 6.1

$$f_{vw.d} = \frac{530\,N/mm^2}{\sqrt{3}\cdot 1.0\cdot 1.25} = 244.8\frac{N}{mm^2}$$

$$F_{w.Rd} = 244.8\,N/mm \cdot 8mm = 1958\,N/mm$$

$$F_{w.Sd} = 1705\frac{N}{mm^2} < F_{w.Rd} = 1958\frac{N}{mm}$$

Alternative: Arch gusset plate bolted to the arch profile (II)

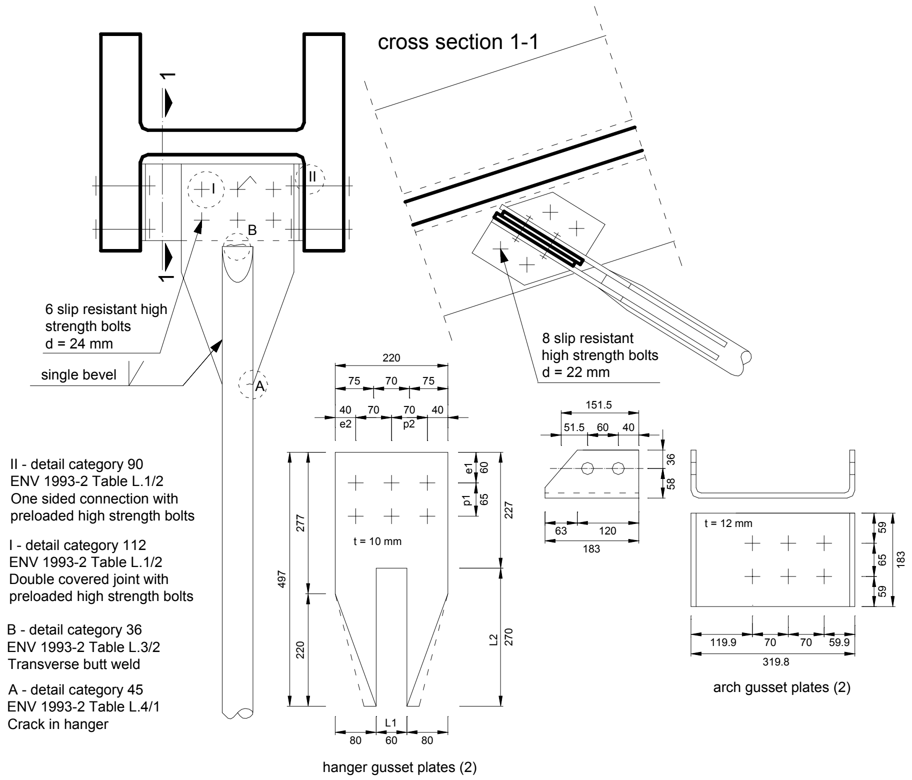

Fig. D.5. Hanger connection type 1, alternative

Type: Category C, slip-resistant at ultimate limit state
Preloaded high strength bolt

Properties

Bolt grade: 10.9
Yield strength: f_{yb} = 900 N/mm^2
Ultimate tensile strength: f_{ub} = 1000 N/mm^2
Bolt diameter: d = 22 mm
Hole diameter: d_o = d + 2mm = 24 mm (standard nominal clearance)
Bolt cross section area: A = 380 mm^2
Stress area: A_s = 303 mm^2
Number of bolts: n = 8

Geometry

Distances measured from centres of fasteners:

ENV 1993-1-1: 1992 Section 6.5.1

End distance in load direction:	e_1
Edge distance perpendicular to load direction:	e_2
Spacing between fasteners in load direction:	p_1
Spacing between rows of fasteners perpendicular to load direction:	p_2

Limits:

ENV 1993-2: 1997 Section 6.3

e_1 = 40mm ≥ min $e_1 = 1.5 \cdot d_0$ = 36 mm
e_2 = 36mm ≥ min $e_2 = 1.5 \cdot d_0$ = 36 mm
p_1 = 60mm ≥ min $p_1 = 2.5 \cdot d_0$ = 60 mm
p_2 – non-existent *Maximum distances are not critical.*

Criteria

ENV 1993-1-1: 1992 Table 6.5.2

$F_{v.Sd} \leq F_{s.Rd}$ slip resistance
$F_{v.Sd} \leq F_{b.Rd}$ bearing resistance

Section D.3.1

Design shear force for ultimate limit state: $N_{v.Sd} = N_{Sd.ecc}$ = 630.8 kN

$$F_{v.Sd} = \frac{N_{v.Sd}}{n} = \frac{630.8\text{kN}}{4} = 157.7\text{kN}$$

Bearing resistance

ENV 1993-1-1: 1992 Table 6.5.3

$$F_{b.Rd} = \frac{2.5 \cdot \alpha \cdot f_u \cdot d \cdot t}{\gamma_{Mb}}$$

where α is the smallest of:
$$\frac{e_1}{3 \cdot d_o} = \frac{40\text{mm}}{3 \cdot 24\text{mm}} = 0.56$$
$$\frac{p_1}{3 \cdot d_o} - \frac{1}{4} = \frac{60\text{mm}}{3 \cdot 24\text{mm}} - \frac{1}{4} = 0.58$$
$$\frac{f_{ub}}{f_u} = \frac{1000\,\text{N/mm}^2}{550\,\text{N/mm}^2} = 1.82$$
or 1
→ α = 0.56

$$F_{b.Rd} = \frac{2.5 \cdot 0.56 \cdot 550\,\text{N/mm}^2 \cdot 22\text{mm} \cdot 12\text{mm}}{1.25} = 162.6\text{kN}$$

$$\underline{F_{v.Sd} = 157.7\text{kN} < F_{b.Rd} = 162.6\text{kN}}$$

Slip resistance

ENV 1993-1-1: 1992 Section 6.5.8

$$F_{s.Rd} = \frac{k_s \cdot n \cdot \mu}{\gamma_{Ms}} \cdot F_{p,Cd}$$

a) ENV 1993-2: 1997 Section 6.4.7.1 (6)

b) ENV1993-1-1: 1992 Section 6.5.8.3

Slip factor: μ = 0.5 *Class A surface[a)b)]*

k_s = 1 standard nominal clearance
n = 2 number of friction interfaces
$F_{p.Cd}$ preloading force
$F_{p.Cd} = 0.7 \cdot f_{ub} \cdot A_s = 0.7 \cdot 1000\ \text{N/mm}^2 \cdot 303\ \text{mm}^2 = 212.1$ kN

$$F_{s.Rd} = \frac{1 \cdot 2 \cdot 0.5}{1.25} \cdot 212.1\text{kN} = 169.7\text{kN}$$

$$\underline{F_{v.Sd} = 157.7\text{N} < F_{s.Rd} = 169.7\text{kN}}$$

D.3.2.2.2 Connection type 2

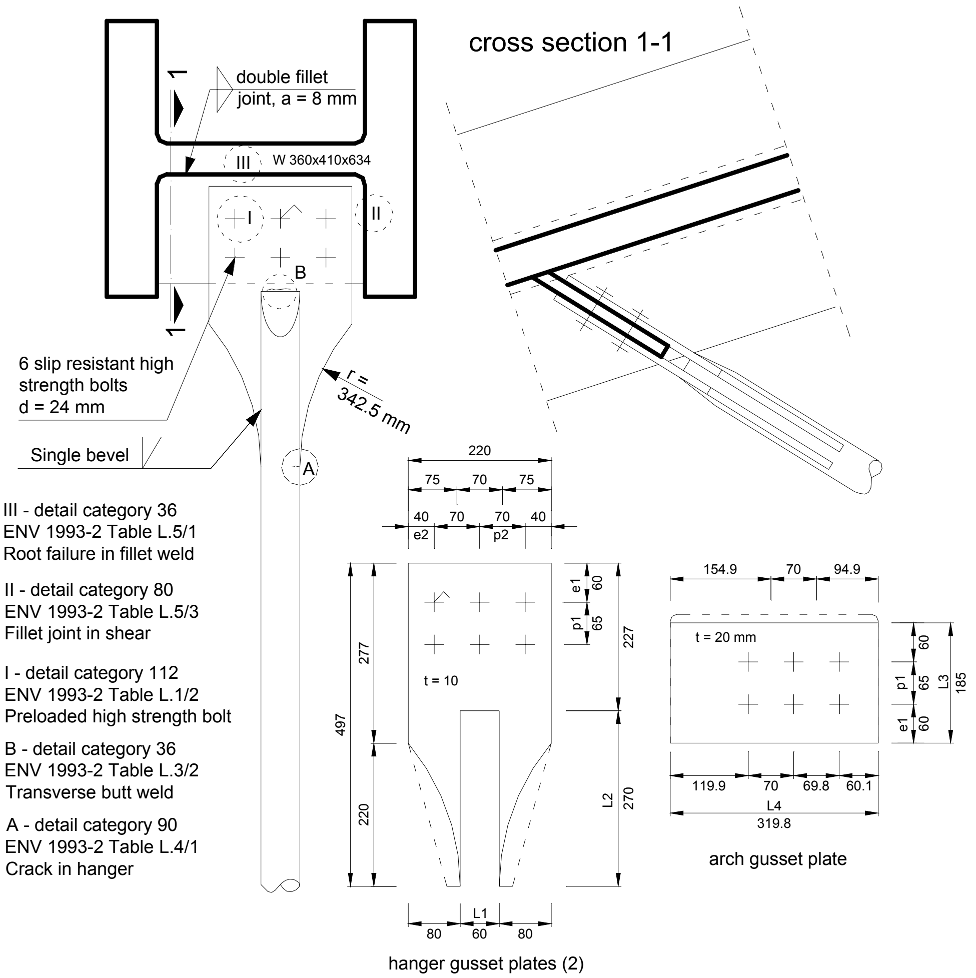

Fig. D.6. Hanger connection type 2

For member and connection design checks, please refer to connection type 1.

D.3.2.2.3 Hanger connection type 3

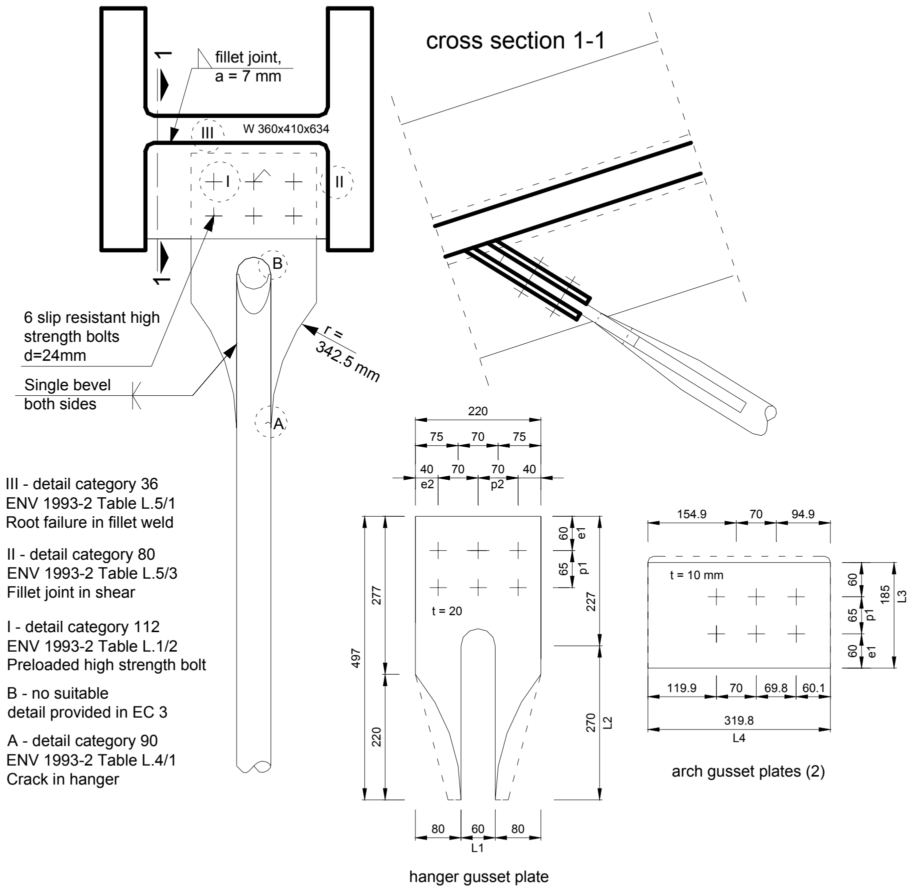

Fig. D.7. Hanger connection type 3

For member and connection design checks, please refer to connection type 2.

In contrast to hanger connection types 1 and 2, this type uses only 1 gusset plate welded to the hanger, whereas two gusset plates are welded to the arch. However, the total cross sections are equal and the design checks are therefore equivalent.

The net cross sectional area at the circular cut-out is larger than the net cross sectional area at the bolts. An additional check is therefore not required.

Weld between arch gusset plate and arch profile (II)

In contrast to connection types 1 and 2, this type uses 2 gusset plates welded to the arch profile. It is suggested using the following relation between weld leg and plate thickness: $2 \le a \le 0.7 \cdot \min(t) = 0.7 \cdot 10$ mm = 7 mm. *Schneider [29], page 8.67*

Type: Single fillet weld
Throat thickness: a = 7 mm

The gusset plate is welded to the flanges as well as the web. However, the design check considers only the welding to the flanges.

Criterion: $F_{w.Ed} \le F_{w.Rd}$

Design shear force for ultimate limit state

$N_{v.Sd} = N_{Sd.ecc} = 630.8$ kN

Section D.3.1

Weld length: $L_w = L_3 \cdot 2 = 185\text{mm} \cdot 2 = 370\text{mm}$

Figure D.3.5

Design weld force per unit length

$$F_{w.Sd} = \frac{N_{v.Sd}}{L_w} = \frac{630.8\text{kN}}{370\text{mm}} = 1705\,\text{N/mm}$$

Design resistance per unit length

$$F_{w.Rd} = f_{vw.d} \cdot a$$

Design shear strength $f_{vw.d} = \dfrac{f_u / \sqrt{3}}{\beta_w \cdot \gamma_{Mw}}$

Correlation factor β_w for fillet welds ($f_u \ge 520$ N/mm^2): $\beta_w = 1.0$

ENV 1993-1-1: 1992 Section 6.6.5.3

$$f_{vw.d} = \frac{530\,\text{N/mm}^2}{\sqrt{3} \cdot 1.0 \cdot 1.25} = 244.8\frac{\text{N}}{\text{mm}^2}$$

$$F_{w.Rd} = 244.8\,\text{N/mm} \cdot 7\text{mm} = 1713.6\,\text{N/mm}$$

ENV 1993-2: 1997 Table 6.1

$$\underline{F_{w.Sd} = 1705\frac{\text{N}}{\text{mm}^2} < F_{w.Rd} = 1713.6\frac{\text{N}}{\text{mm}}}$$

D.3.2.2.4 Hanger connection type 4

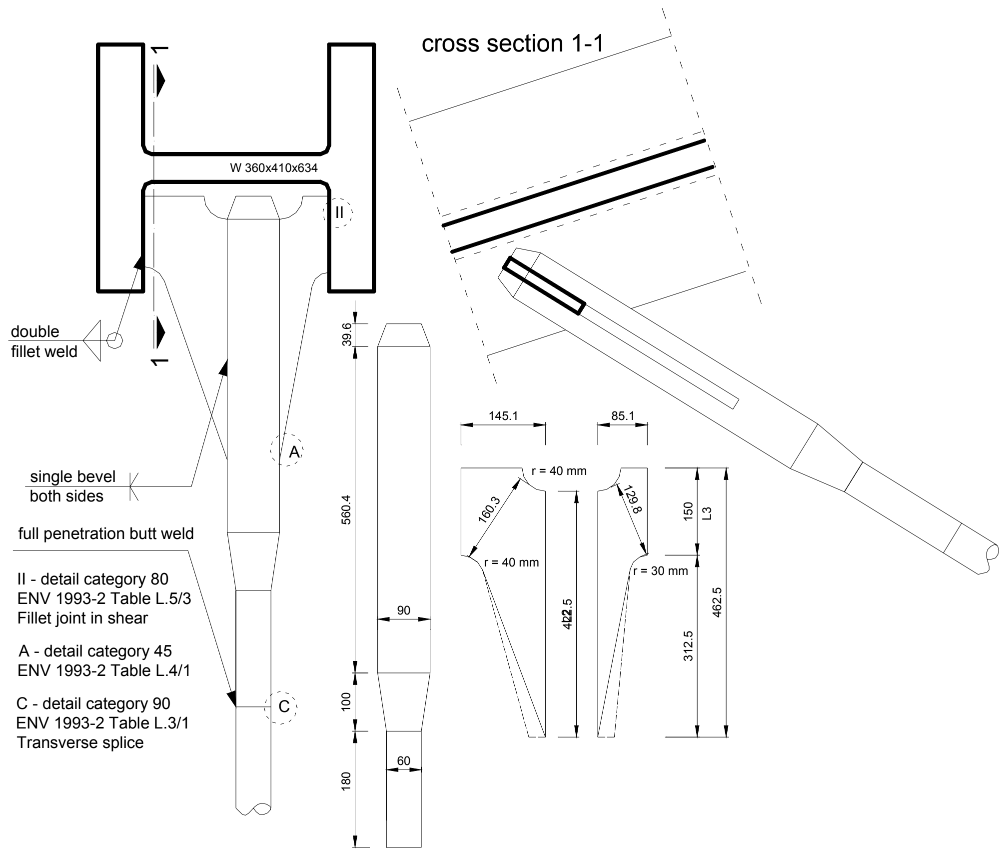

Fig. D.8. Hanger connection type 4

Gusset plate

Criterion: $V_{Sd} < V_{pl.Rd}$

Design force: $V_{Sd} = N_{Sd.ecc} = 630.8\text{kN}$ *Section D.3.1*

Shear area: A_v = 130 mm · 20 mm = 2600 mm^2

Design plastic shear resistance:

$$V_{pl.Rd} = \frac{A_v \cdot f_y}{\sqrt{3} \cdot \gamma_{M0}} = \frac{2600\text{mm}^2 \cdot 460\text{N}/\text{mm}^2}{\sqrt{3} \cdot 1.0} = 691\text{kN}$$

$$\underline{V_{Sd} = 630.8\text{kN} < V_{pl.Rd} = 691\text{kN}}$$

Weld joint to arch profile (II)

Ultimate limit state

Criterion: $F_{w.Ed} \le F_{w.Rd}$

Design weld force: $V_{Sd} = N_{Sd.ecc} = 630.8\text{kN}$ *Section D.3.1*

Weld length $L_w = L_3 \cdot 2 = 150\text{mm} \cdot 2 = 300\text{mm}$ *Figure D.3.6*

Design weld force per unit length

$$F_{w.Sd} = \frac{V_{Sd}}{L_w} = \frac{630.8kN}{300mm} = 2103\,N/mm$$

Design resistance per unit length: $F_{w.Rd} = f_{vw.d} \cdot a$

Design shear strength $f_{vw.d} = \dfrac{f_u/\sqrt{3}}{\beta_w \cdot \gamma_{Mw}}$

Correlation factor β_w for fillet welds ($f_u \geq 520$ N/mm^2): $\beta_w = 1.0$

$$f_{vw.d} = \frac{530\,N/mm^2}{\sqrt{3} \cdot 1.0 \cdot 1.25} = 244.8\frac{N}{mm^2}$$

ENV 1993-2: 1997
Table 6.1

Weld leg:

$2 \leq a \leq 0.7 \cdot \min(t) = 0.7 \cdot 20$ mm = 14 mm

chosen: 9 mm

$$F_{w.Rd} = 244.8\,N/mm \cdot 9mm = 2203\,N/mm$$

$$F_{w.Sd} = 2103\frac{N}{mm^2} < F_{w.Rd} = 2203\frac{N}{mm}$$

D.3.2.2.5 Hanger connection type 5

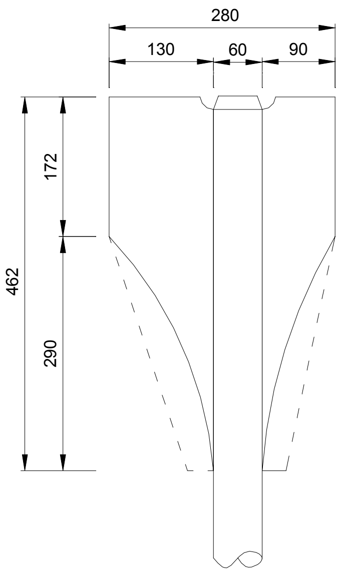

Fig. D.9. Hanger connection type 5

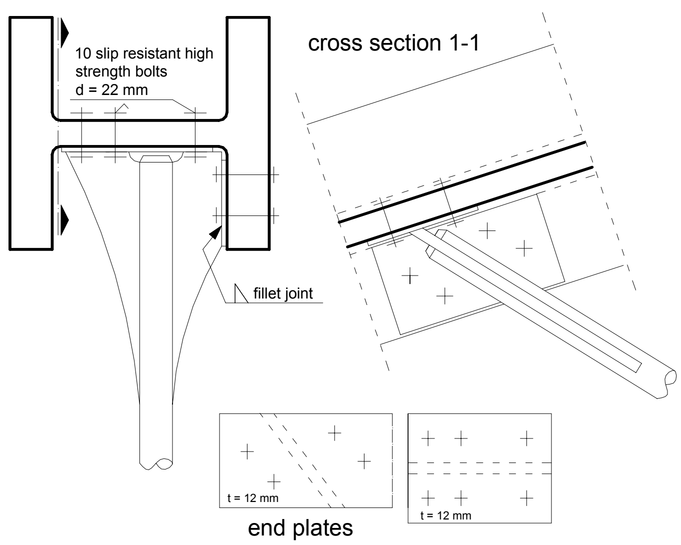

Fig. D.10. Suggested hanger connection

Figure D.9 shows connection type 5 as it was modelled in *NE/Nastran*. The geometry varies only slightly from connection type 4, so that member design checks are omitted.

The application of connection type 5 with a slightly modified geometry (Figure D.10) was suggested by PER TVEIT, Section 7.7. Member design checks were not carried out.

D.3.2.2.6 Suggested hanger connection

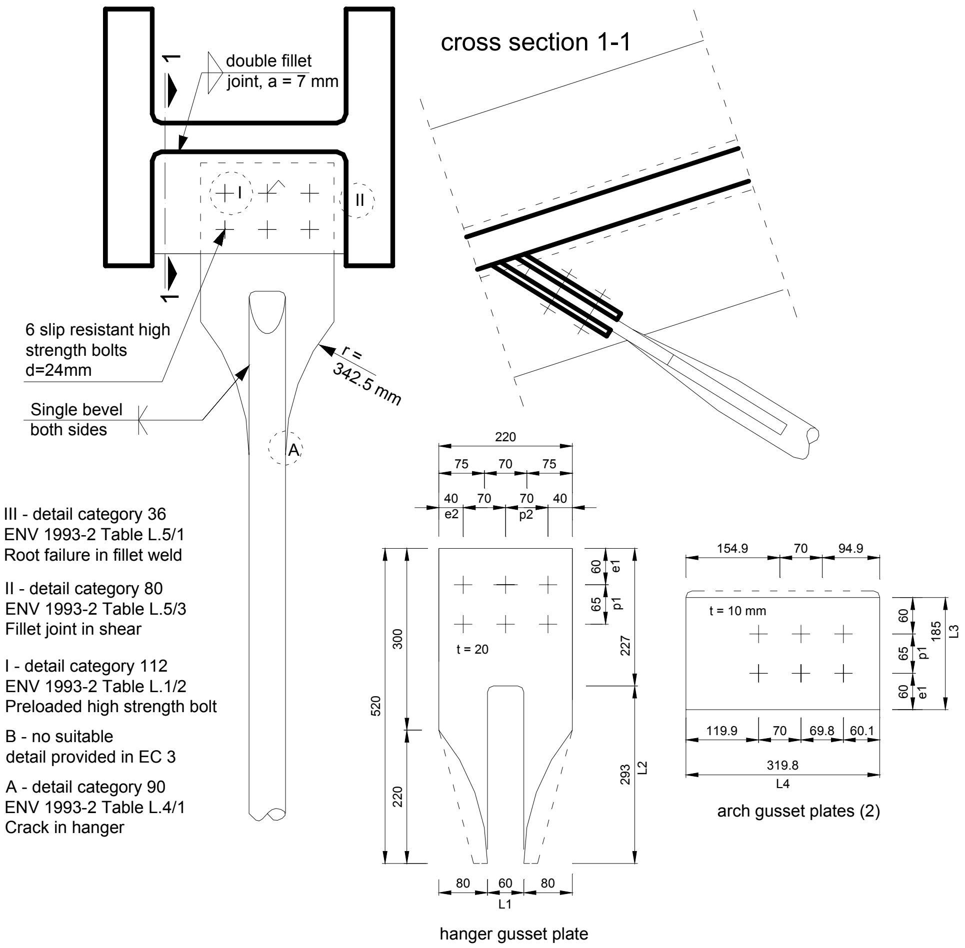

Fig. D.11. Suggested hanger connection

For member and connection assessment, refer to connection types 2 and 3.

D.3.3 Fatigue assessment

ENV 1993-2: 1997 Section 9.5

Fatigue assessment: $\gamma_{Ff} \cdot \Delta\sigma_{E_2} \le \dfrac{\Delta\sigma_c}{\gamma_{Mf}}$

$\Delta\sigma_{E_2} = \lambda \cdot \Phi_2 \cdot \Delta\sigma_p$

Damage equivalence factor $\lambda = \lambda_1 \cdot \lambda_2 \cdot \lambda_3 \cdot \lambda_4$

$\lambda_1 = 0.6$ EC Mix L = 100 m — *ENV 1993-2 Table 9.5*

$\lambda_2 = 1.04$ Traffic per year: $30 \cdot 10^6$ t/track — *ENV 1993-2 Table 9.6*

$\lambda_3 = 1.0$ Design life: 100 years — *ENV 1993-2 Table 9.7*

$\lambda_4 = 0.77$ $\dfrac{\Delta F_{p.1}}{\Delta F_{p.1+2}} = \dfrac{295.34\text{kN}}{439.7\text{kN}} = 0.67$

$\lambda_{max} = 1.4$ — *ENV 1993-2 Table 9.8*

$\underline{\lambda = 0.6 \cdot 1.04 \cdot 1.0 \cdot 0.77 = 0.48}$

ENV 1993-2 Section 9.5.3

The damage equivalent impact factor Φ_2 is already included in the design forces.

D.3.3.1 Fatigue assessment based on nominal stress ranges

D.3.3.1.1 Hanger connection type 1

ENV 1993-2: 1997 Table L.4/1

Point (A)

ENV 1993-1-1: 1992 Figure 9.6.1

Detail category: 45

$\Delta\sigma_c$ = 45 N/mm^2

Section D.3.1 Figure D.3

Design force range: ΔN_p = 439.7 kN
Cross section area of hanger: A = 2827.4 mm^2

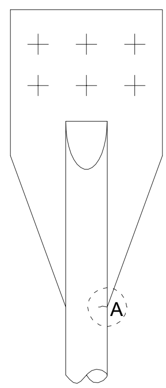

$$\Delta\sigma_p = \frac{\Delta N_p}{A} = \frac{439.7\text{kN}}{2827\text{mm}^2} = 155.5\frac{\text{N}}{\text{mm}^2}$$

$$\Delta\sigma_{E_2} = \lambda \cdot \Phi_2 \cdot \Delta\sigma_p = 0.48 \cdot 155.5\frac{\text{N}}{\text{mm}^2} = 74.65\frac{\text{N}}{\text{mm}^2}$$

$$\gamma_{Ff} \cdot \Delta\sigma_{E_2} = 1.0 \cdot 74.65\frac{\text{N}}{\text{mm}^2}$$

$$\underline{\gamma_{Ff} \cdot \Delta\sigma_{E_2} = 74.65\frac{\text{N}}{\text{mm}^2} > \frac{\Delta\sigma_c}{\gamma_{Mf}} = \frac{45}{1.0}\frac{\text{N}}{\text{mm}^2}} \text{ Check not fulfilled!}$$

Utilisation of fatigue strength: $\dfrac{74.65\,\text{N/mm}^2}{45\,\text{N/mm}^2} \cdot 100\% = 166\%$

Point (B)

Transverse butt weld made from one side only.

ENV 1993-2: 1997 Table L.3/2

Detail category: 36

$\Delta\sigma_c$ = 36 N/mm^2

Design force range: ΔN_p = 439.7 kN

Length of transverse butt weld: L_1 = 60 mm *Section D.3.1*

Length of longitudinal butt welds: L_2 = 270 mm *Figure D.3*

$$A = (L_1 + 2 \cdot L_2) \cdot t \cdot 2 = (60mm + 2 \cdot 270mm) \cdot 10mm \cdot 2 = 12000mm^2$$

$$\Delta\sigma_p = \frac{\Delta N_p}{A} = \frac{439.7kN}{12000mm^2} = 36.6\frac{N}{mm^2}$$

$$\Delta\sigma_{E_2} = \lambda \cdot \Phi_2 \cdot \Delta\sigma_p = 0.48 \cdot 36.6\frac{N}{mm^2} = 17.6\frac{N}{mm^2}$$

$$\gamma_{Ff} \cdot \Delta\sigma_{E_2} = 1.0 \cdot 14.65\frac{N}{mm^2}$$

$$\gamma_{Ff} \cdot \Delta\sigma_{E_2} = 14.65\frac{N}{mm^2} < \frac{\Delta\sigma_c}{\gamma_{Mf}} = \frac{36}{1.0}\frac{N}{mm^2}$$

Utilisation of fatigue strength: $\frac{14.65 N/mm^2}{36 N/mm^2} \cdot 100\% = 41\%$

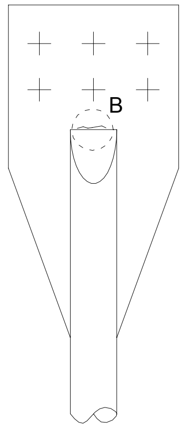

Longitudinal butt weld

The full penetration butt weld between hanger and gusset plate in shear is categorized in detail category 100 (*ENV 1993-2: 1997 Table L.5/3*). The stress distribution here can be assumed as equal to the transverse butt weld. Since this check is fulfilled, it does not need to be assessed for the longitudinal weld.

Point (I)

Double covered joint with preloaded high strength bolts. *ENV 1993-2: 1997 Table L.1/2*

Detail category 112

$\Delta\sigma_c$ = 112 N/mm^2 *ENV 1993-1-1: 1992 Figure 9.6.1*

Design force range: 439.7 kN

Hanger connection plate

$$A_{net} = (220mm - 3 \cdot 26mm) \cdot 2 \cdot 10mm = 2840mm^2$$

$$\Delta\sigma_p = \frac{\Delta N_p}{A_{net}} = \frac{439.7kN}{2840mm^2} = 154.8\frac{N}{mm^2}$$

$$\Delta\sigma_{E_2} = \lambda \cdot \Phi_2 \cdot \Delta\sigma_p = 0.48 \cdot 154.8\frac{N}{mm^2} = 74.3\frac{N}{mm^2}$$

ENV 1993-2: 1997 Section 9.4, 9.5.1

$$\gamma_{Ff} \cdot \Delta\sigma_{E_2} = 1.0 \cdot 74.3\frac{N}{mm^2}$$

$$\gamma_{Ff} \cdot \Delta\sigma_{E_2} = 74.3\frac{N}{mm^2} < \frac{\Delta\sigma_c}{\gamma_{Mf}} = \frac{112}{1.0}\frac{N}{mm^2}$$

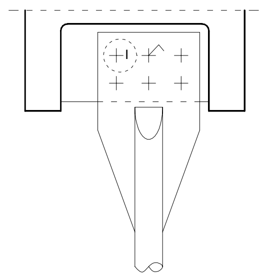

Point (II): welded

Double fillet joint

ENV 1993-2: 1997
Table L.5/3

Detail category: 80

$\Delta\sigma_c$ = 80 N/mm^2

ENV 1993-1-1: 1992
Figure 9.6.1

It is assumed that this shear loaded weld joining the gusset plate to the flanges is the main load carrying weld. For the fatigue assessment, the nominal stress range is therefore calculated with the respective weld area, neglecting the web weld.

Design force range: $\Delta N_p = \Delta N_{p.ecc}$ = 261.1 kN

Section D.3.1

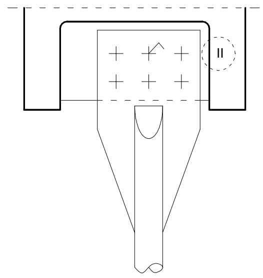

Weld length: L_3 = 185 mm
Weld leg: a = 8 mm

$$A_v = L_3 \cdot t = 185\text{mm} \cdot 8 \cdot 2\text{mm} = 2960\text{mm}^2$$

$$\Delta\tau_p = \frac{\Delta N_p}{A_v} = \frac{261.1\text{kN}}{2960\text{mm}^2} = 88.2\frac{\text{N}}{\text{mm}^2}$$

$$\Delta\tau_{E_2} = \lambda \cdot \Phi_2 \cdot \Delta\tau_p = 0.48 \cdot 88.2\frac{\text{N}}{\text{mm}^2} = 42.3\frac{\text{N}}{\text{mm}^2}$$

$$\gamma_{Ff} \cdot \Delta\tau_{E_2} = 1.0 \cdot 42.3\frac{\text{N}}{\text{mm}^2}$$

$$\gamma_{Ff} \cdot \Delta\tau_{E_2} = 42.3\frac{\text{N}}{\text{mm}^2} < \frac{\Delta\tau_c}{\gamma_{Mf}} = \frac{80\,\text{N}/\text{mm}^2}{1.0}$$

Point (III)

ENV 1993-2: 1997
Table L.5/1

Root failure in fillet joint: Detail category 36
The flange welds (**II**) are assumed to be load carrying only. An assessment of point III is therefore omitted.

Point (II): bolted

One sided connection with preloaded high strength bolts.
Detail category 90

ENV 1993-2: 1997
Table L.1/2

$\Delta\sigma_c$ = 90 N/mm^2

Design force range: $\Delta N_p = \Delta N_{p.ecc}$ = 261.1 kN

Section D.3.1

Arch connection plate:

$$A_{net} = (151.5\text{mm} - 2 \cdot 24\text{mm}) \cdot 4 \cdot 12\text{mm} = 4968\text{mm}^2$$

Figure D.3.4

$$\Delta\tau_p = \frac{\Delta N_p}{A_{net}} = \frac{261.1\text{kN}}{4968\text{mm}^2} = 53\frac{\text{N}}{\text{mm}^2}$$

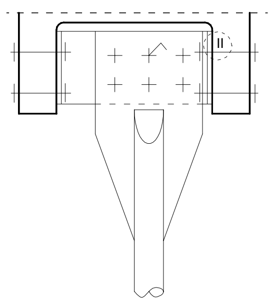

$$\tau_{E_2} = \lambda \cdot \Phi_2 \cdot \Delta\tau_p = 0.48 \cdot 53\frac{\text{N}}{\text{mm}^2} = 25\frac{\text{N}}{\text{mm}^2}$$

$$\gamma_{Ff} \cdot \Delta\tau_{E_2} = 1.0 \cdot 25\frac{\text{N}}{\text{mm}^2}$$

$$\gamma_{Ff} \cdot \Delta\tau_{E_2} = 25\frac{\text{N}}{\text{mm}^2} < \frac{\Delta\tau_c}{\gamma_{Mf}} = \frac{90}{1.0}\frac{\text{N}}{\text{mm}^2}$$

D.3.3.1.2 Hanger connection type 2

Point (A)

Detail category: 90

ENV 1993-2 : 1997
Table L.4/1

$\Delta\sigma_c$ = 90 N/mm^2

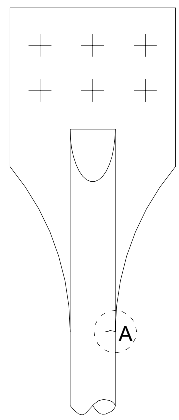

Design force range: ΔN_p = 439.7 kN
Cross section area of hanger: A = 2827.4 mm^2

$$\Delta\sigma_p = \frac{\Delta N_p}{A} = \frac{439.7kN}{2827mm^2} = 155.5\frac{N}{mm^2}$$

$$\Delta\sigma_{E_2} = \lambda \cdot \Phi_2 \cdot \Delta\sigma_p = 0.48 \cdot 155.5\frac{N}{mm^2} = 74.65\frac{N}{mm^2}$$

$$\gamma_{Ff} \cdot \Delta\sigma_{E_2} = 1.0 \cdot 74.65\frac{N}{mm^2}$$

$$\gamma_{Ff} \cdot \Delta\sigma_{E_2} = 74.65\frac{N}{mm^2} < \frac{\Delta\sigma_c}{\gamma_{Mf}} = \frac{90}{1.0}\frac{N}{mm^2}$$

Utilisation of fatigue strength: $\frac{74.65 N/mm^2}{90 N/mm^2} \cdot 100\% = 83\%$

Point (B)
See connection type 1, Section D.3.3.1.1.

D.3.3.1.3 Hanger connection type 3

Point (A)
See connection type 2

Point (B)

The detail does not correspond to any detail category given in Eurocode 3, and so the nominal stress method cannot be used here. It is necessary to obtain the local stress at the edge of the circular hole, which constitutes a stress concentration.

D.3.3.1.4 Hanger connection type 4

Point (C)

Full penetration butt joint of hanger to widened end member

ENV 1993-2: 1997
Table L.3/1

Detail category: 80

$\Delta\sigma_c$ = 112 N/mm^2

Design force range: ΔN_p = 439.7 kN
Cross section area of hanger (D = 60mm): A = 2827.4 mm^2

$$\Delta\sigma_p = \frac{\Delta N_p}{A} = \frac{439.7kN}{2827mm^2} = 155.5\frac{N}{mm^2}$$

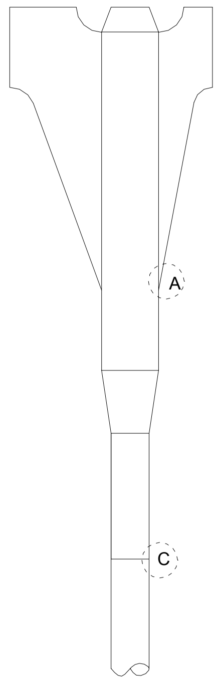

$$\Delta\sigma_{E_2} = \lambda \cdot \Phi_2 \cdot \Delta\sigma_p = 0.48 \cdot 155.5 \frac{N}{mm^2} = 74.65 \frac{N}{mm^2}$$

$$\gamma_{Ff} \cdot \Delta\sigma_{E_2} = 1.0 \cdot 74.65 \frac{N}{mm^2}$$

$$\gamma_{Ff} \cdot \Delta\sigma_{E_2} = 74.65 \frac{N}{mm^2} > \frac{\Delta\sigma_c}{\gamma_{Mf}} = \frac{80}{1.0} \frac{N}{mm^2}$$

Utilisation of fatigue strength: $\frac{74.65\,N/mm^2}{80\,N/mm^2} \cdot 100\% = 93\%$

Point (A)

Crack in hanger at joint to gusset plate
Detail category: 45

ENV 1993-2: 1997
Table L.4/1

$\Delta\sigma_c$ = 45 N/mm^2
Design force range: ΔN_p = 439.7 kN

Cross section area (D = 90 mm):

$$A = \frac{\pi}{4} \cdot (90mm)^2 = 6361.7mm^2$$

$$\Delta\sigma_p = \frac{\Delta N_p}{A} = \frac{439.7kN}{6361.7mm^2} = 69.1 \frac{N}{mm^2}$$

$$\Delta\sigma_{E_2} = \lambda \cdot \Phi_2 \cdot \Delta\sigma_p = 0.48 \cdot 69.1 \frac{N}{mm^2} = 33.2 \frac{N}{mm^2}$$

$$\gamma_{Ff} \cdot \Delta\sigma_{E_2} = 1.0 \cdot 14.65 \frac{N}{mm^2}$$

$$\gamma_{Ff} \cdot \Delta\sigma_{E_2} = 33.2 \frac{N}{mm^2} < \frac{\Delta\sigma_c}{\gamma_{Mf}} = \frac{45}{1.0} \frac{N}{mm^2}$$

Utilisation of fatigue strength: $\frac{33.2\,N/mm^2}{45\,N/mm^2} \cdot 100\% = 74\%$

Point (II)

ENV 1993-2: 1997
Table L.4/2

Longitudinal crack in the fillet weld
Detail category: 80

$\Delta\sigma_c$ = 80 N/mm^2

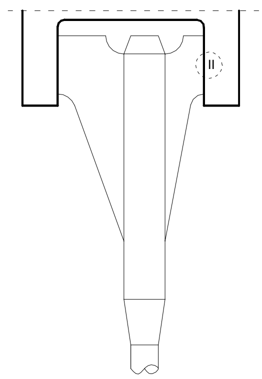

Design force range: $\Delta N_p = \Delta N_{p.ecc}$ = 261.1 kN

Cross section area: $A = 150mm \cdot 2 \cdot 8mm = 2400mm^2$

$$\Delta\sigma_p = \frac{\Delta N_p}{A} = \frac{261.1kN}{2400mm^2} = 109 \frac{N}{mm^2}$$

$$\Delta\sigma_{E_2} = \lambda \cdot \Phi_2 \cdot \Delta\sigma_p = 0.48 \cdot 109 \frac{N}{mm^2} = 52 \frac{N}{mm^2}$$

$$\gamma_{Ff} \cdot \Delta\sigma_{E_2} = 1.0 \cdot 52 \frac{N}{mm^2}$$

$$\gamma_{Ff} \cdot \Delta\sigma_{E_2} = 52 \frac{N}{mm^2} < \frac{\Delta\sigma_c}{\gamma_{Mf}} = \frac{80}{1.0} \frac{N}{mm^2}$$

Utilisation of fatigue strength: $\frac{52\,N/mm^2}{80\,N/mm^2} \cdot 100\% = 65\%$

D.3.3.1.5 Hanger connection type 5

Connection type 5 varies only slightly from type 4.
For point (**A**) see connection type 3.
For point (**II**) see connection type 4.

D.3.3.2 Fatigue assessment based on geometric stress ranges

Determination of stress concentration factors SCF

The stress concentration factors were determined by carrying out finite element analysis with *NE/Nastran*. The geometric stress magnitudes σ_{SC} were divided by the nominal stress σ_0, which is the stress calculated with the net cross section area. The numbers and results are listed in Figures D.12 and D.13.3

Determination of geometric stress concentration factors SCF					
Location		**Type 1**	**Type 2**	**Type 3**	**suggested type**
A					
Net area	A_{net} [mm²]	2827.40	2827.40	2827.40	2827.40
Nominal stress (F=1000 kN)	σ_0 [N/mm²]	353.68	353.68	353.68	353.68
Geometric stress	σ_{SC} [N/mm²]	506.80	399.40	409.40	401.75
Geometric SCF	$SCF = \sigma_{SC} / \sigma_0$	**1.43**	**1.13**	**1.16**	**1.14**
B					
Net area	A_{net} [mm²]	4400.00	4400.00	3200.00	4400.00
Nominal stress (F=1000 kN)	σ_0 [N/mm²]	227.27	227.27	312.50	227.27
Geometric stress	σ_{SC} [N/mm²]	316.30	333.05	1217.00	305.35
Geometric SCF	$SCF = \sigma_{SC} / \sigma_0$	**1.39**	**1.47**	**3.89**	**1.34**

Fig. D.12. SCF for connection types 1 to 3 and suggested type

Determination of geometric stress concentration factors SCF			
Location		**Type 4**	**Type 5**
C			
Net area	A_{net} [mm^2]	2827.43	-
Nominal stress (F=1000 kN)	σ_o [N/mm^2]	353.68	-
Geometric stress	σ_{sc} [N/mm^2]	402.00	-
Geometric SCF	SCF = σ_{SC} / σ_0	**1.14**	-
A			
Net area	A_{net} [mm^2]	6361.73	2827.43
Nominal stress (F=1000 kN)	σ_o [N/mm^2]	157.20	353.68
Geometric stress	σ_{sc} [N/mm^2]	284.00	447.80
Geometric SCF	SCF = σ_{SC} / σ_0	**1.81**	**1.27**
D1			
Net area	A_{net} [mm^2]	2620.00	3600.00
Nominal stress[1)]	σ_o [N/mm^2]	226.65	158.33
Geometric stress	σ_{sc} [N/mm^2]	656.50	331.80
Geometric SCF	SCF = σ_{SC} / σ_0	**2.90**	**2.10**
D2			
Net area	A_{net} [mm^2]	3280.00	4000.00
Nominal stress[1)]	σ_o [N/mm^2]	123.84	107.50
Geometric stress	σ_{sc} [N/mm^2]	404.15	253.95
Geometric SCF	SCF = σ_{SC} / σ_0	**3.26**	**2.36**
IIa			
Net area	A_{net} [mm^2]	3000.00	3440.00
Nominal stress[1)]	σ_o [N/mm^2]	135.40	165.70
Geometric stress	σ_{sc} [N/mm^2]	656.50	585.50
Geometric SCF	SCF = σ_{SC} / σ_0	**4.85**	**3.53**
IIb			
Net area	A_{net} [mm^2]	3000.00	3440.00
Nominal stress[1)]	σ_o [N/mm^2]	197.93	165.70
Geometric stress	σ_{sc} [N/mm^2]	586.10	314.60
Geometric SCF	SCF = σ_{SC} / σ_0	**2.96**	**1.90**

Fig. D.13. SCF for connection types 4 and 5

[1)] Nominal stress based on the following forces (due to eccentricity)
Type 4: For D1and IIb: F = 593.81 kN For D2 and IIa: F = 406.2 kN
Type 5: For D1, IIa, IIb: F = 570 kN For D2: F = 430 kN

Fatigue assessment

According to *ENV 1993-1-1: 1992 Section 9.6.3*, the fatigue strength curves for fatigue assessments based on geometric stress ranges shall be for

- full penetration butt welds: Category 90 (assumed: weld profile and permitted weld defects acceptance criteria satisfied)
- load carrying partial penetration butt welds and fillet welds: Category 36

The relevant SN curves are found in *ENV 1993-1-1: 1992 Figure 9.6.1*

The assessment is carried out in the following tables. Formulas are provided.

Fatigue assessment					
Location		Type 1	Type 2	Type 3	Suggested type
A					
Net area	A_{net} [mm^2]	2827.40	2827.40	2827.40	2827.40
Nominal stress range	$\Delta\sigma_{p.0}$ [kN] = ΔN_p / A_{net}	155.50	155.50	155.50	155.50
SCF		1.43	1.13	1.16	1.14
Geom. stress range	$\Delta\sigma_{p.SC}$ [kN] = $\Delta\sigma_p$ · SCF	222.36	175.71	180.38	177.27
$\gamma_{Ff} \cdot \Delta\sigma_{E2} = \gamma_{Ff} \cdot \lambda \cdot \Phi_2 \cdot \Delta\sigma_p$ [N/mm^2]	(T1)	**106.95**	**84.29**	**86.40**	**84.78**
		>	<	<	<
$\Delta\sigma_c$ / γ_{Mf} [N/mm^2]	(T2)	**90.00**	**90.00**	**90.00**	**90.00**
(T1) / (T2) · 100 %		119	94	96	94
B					
Net area	A_{net} [mm^2]	4400.00	4400.00	3200.00	4400.00
Nominal stress range	$\Delta\sigma_{p.0}$ [kN] = ΔN_p / A_{net}	99.92	99.92	137.39	99.92
SCF		1.39	1.47	3.89	1.34
Geom. stress range	$\Delta\sigma_{p.SC}$ [kN] = $\Delta\sigma_p$ · SCF	138.89	146.43	535.00	134.25
$\gamma_{Ff} \cdot \Delta\sigma_{E2} = \gamma_{Ff} \cdot \lambda \cdot \Phi_2 \cdot \Delta\sigma_p$ [N/mm^2]	(T1)	**66.75**	**70.29**	**256.80**	**64.44**
		<	<	>	<
$\Delta\sigma_c$ / γ_{Mf} [N/mm^2]	(T2)	**90.00**	**90.00**	**90.00**	**90.00**
(T1) / (T2) · 100 %		74	78	285	72
λ = 0.48	γ_{Ff} and γ_{Mf} = 1.0		ΔN_p [kN] = 439.66		Φ_2 incl. in ΔN_p

Fig. D.14. Fatigue assessment of connection types 1 to 3 and suggested type (geometric stress ranges)

Fatigue assessment: Connection type 4							
Location		C	A	D1	D2	IIa	IIb
Force range	ΔN_p [kN]	439.66	439.66	261.1	178.6	178.6	261.1
Net area [mm^2]	A_{net} [mm^2]	2827.43	6361.73	2620.00	3280.00	3000.00	3000.00
Nom. stress range	$\Delta\sigma_p$ [kN] = ΔN_p / A_{net}	155.50	69.11	99.66	54.45	59.53	87.03
Geometric SCF		1.14	1.81	2.90	3.26	4.85	2.96
Geom. stress range	$\Delta\sigma_{p.SC}$ [kN] = $\Delta\sigma_p$ · SCF	177.27	125.09	289.00	177.51	288.74	257.62
$\gamma_{Ff} \cdot \Delta\sigma_{E2} = \gamma_{Ff} \cdot \lambda \cdot \Phi_2 \cdot \Delta\sigma_p$ [N/mm^2]	(T1)	**85.09**	**60.04**	**138.72**	**85.21**	**138.59**	**123.66**
		<	<	>	<	>	>
$\Delta\sigma_c$ / γ_{Mf} [N/mm^2]	(T2)	**90.00**	**90.00**	**125.00**	**125.00**	**36.00**	**36.00**
(T1) / (T2) · 100%		95	67	111	68	385	343
λ = 0.48	γ_{Ff} and γ_{Mf} = 1.0						Φ_2 incl. in ΔN_p

Fig. D.15. Fatigue assessment of connection type 4 (geometric stress ranges)

Fatigue assessment: Connection type 5					
Location		A	D1	D2	II
Force range	ΔN_p [kN]	439.66	250.6	189.1	250.6
Net area [mm^2]	A_{net} [mm^2]	2827.43	3600.00	4000.00	3440.00
Nom. stress range	$\Delta\sigma_p$ [kN] = ΔN_p / A_{net}	155.50	69.61	47.28	72.85
Geometric SCF		1.27	2.10	2.36	3.53
Geom. stress range	$\Delta\sigma_{p.SC}$ [kN] = $\Delta\sigma_p$ · SCF	197.48	146.18	111.57	257.16
$\gamma_{Ff} \cdot \Delta\sigma_{E2} = \gamma_{Ff} \cdot \lambda \cdot \Phi_2 \cdot \Delta\sigma_p$ [N/mm^2]	(T1)	**94.79**	**70.17**	**53.55**	**123.44**
		>	<	<	>
$\Delta\sigma_c$ / γ_{Mf} [N/mm^2]	(T2)	**90.00**	**125.00**	**125.00**	**36.00**
(T1) / (T2) · 100%		105	56	43	343
λ = 0.48	γ_{Ff} and γ_{Mf} = 1.0				Φ_2 incl. in ΔN_p

Fig. D.16. Fatigue assessment of connection type 5 (geometric stress ranges)

D.3.4 Patch test

The following refers to Section 10 and gives additional references on the stress concentration in a plate around a hole.

The reference plate has the following dimensions:

Width W = 300 mm
Thickness T = 25 mm
Length L = 1000 mm
Diameter of the hole D = 100 mm (symmetrical to the plate)

These dimensions were used as input values in two reference calculations described in the following:

A java applet provided by David Grieve (School of Engineering, University of Plymouth)[1] gives a SCF of 2.307 at a hole in a plate with above mentioned dimensions. Regarding the used formula, reference is made to "Roark's Formulas for Stress and Strain", 6th Ed. McGraw Hill, 1989 and "Stress Concentration Factors", by R E Peterson, John Wiley and Sons, 1974.

A further source[2] provides the following formula predicting the stress concentration factor for the same problem:

$$SCF = 2 + (1 - D/W)^3 .$$

With the dimensions of the reference plate, the SCF gives

$$SCF = 2 + (1 - 100/300)^3 = 2.296 ,$$

which is virtually equal to the result given by Grieve's applet and to the result obtained with the finer mesh of the test plate. The exactness of the theoretical SCF obviously depends on the approximation of the curve between the two extremes SCF = 2.0 and SCF = 3.0. Since even the references found show different results, is it likely that further approximations exist.

[1]) *http://www.tech.plym.ac.uk/sme/desnotes/Stressc.htm*
[2]) *http://www.stacieglass.com/scf/indext.html*
(Websites accessed in July, 2003)

D.4 Wind bracing

D.4.1 Ultimate limit state assessment

Fig. C.25

Buckling resistance of member 1

Values of the cross section see Section D.1

N_{Sd} = -441.7 kN

ENV 1993-1-1: 1992, 5.5.1

The criterion to be fulfilled is: $N_{Sd} \leq N_{b,Rd}$

$$N_{b,Rd} = \chi \cdot \beta_A \cdot A \cdot \frac{f_y}{\gamma_{M1}}$$

χ depends on $\overline{\lambda}$

$$\overline{\lambda} = \frac{\lambda}{\lambda_1} \cdot \sqrt{\beta_A} = \frac{\beta \cdot l}{i_y \cdot \pi \cdot \sqrt{\frac{E}{f_y}}} \cdot \beta_A$$

with ß = 1 ; Euler case 2
l = 5.738 m
i_y = 7.47 cm
E = 210000 N/mm^2
f_y = 355 N/mm^2 ; S355
$ß_A$ = 1 ; Class 1 cross section

$$\overline{\lambda} = \frac{1 \cdot 5.738\text{m}}{7.47\text{cm} \cdot \pi \cdot \sqrt{\frac{210000\text{N/mm}^2}{355\text{N/mm}^2}}} \cdot 1 = 1.004$$

χ = 0.6656 ; buckling curve “a”
A = 53.1 cm^2
γ_{M1} = 1.1

ENV 1993-1-1: 1992 5.5.1 Table 5.5.2

$$N_{b,Rd} = 0.6656 \cdot 1 \cdot 53.1\text{cm}^2 \cdot \frac{355\text{N/mm}^2}{1.1} = 1140.6\text{kN}$$

$|N_{Sd}|$ = 441.7 kN ≤ 1140.6 kN = $N_{b,Rd}$

Fig. C.25

Buckling resistance of member 15

Values of the cross section see Section D.1

N_{Sd} = -170.4 kN

The criterion to be fulfilled is: $N_{Sd} \leq N_{b,Rd}$

$$N_{b,Rd} = \chi \cdot \beta_A \cdot A \cdot \frac{f_y}{\gamma_{M1}}$$

χ depends on $\overline{\lambda}$

$$\overline{\lambda} = \frac{\lambda}{\lambda_1} \cdot \sqrt{\beta_A} = \frac{\beta \cdot l}{i_y \cdot \pi \cdot \sqrt{\frac{E}{f_y}}} \cdot \beta_A$$

with ß = 1 ; Euler case 2
l = 7.1364 m
i_y = 7.47 cm
E = 210000 N/mm^2
f_y = 355 N/mm^2 ; S355
$ß_A$ = 1 ; Class 1 cross section

$$\overline{\lambda} = \frac{1 \cdot 7.1364\text{m}}{7.47\text{cm} \cdot \pi \cdot \sqrt{\frac{210000\text{N/mm}^2}{355\text{N/mm}^2}}} \cdot 1 = 1.249$$

χ = 0.5002 ; buckling curve “a”
A = 53.1 cm^2
γ_{M1} = 1.1

ENV 1993-1-1: 1992 5.5.1 Table 5.5.2

$$N_{b,Rd} = 0.5002 \cdot 1 \cdot 53.1\text{cm}^2 \cdot \frac{355\text{N/mm}^2}{1.1} = 870.4\text{kN}$$

$|N_{Sd}|$ = 441.7 kN ≤ 870.4 kN = $N_{b,Rd}$

Flexural buckling of member 3 after second order analysis

Fig. C.25

Values of the cross section vide Section D.1

1. Shear resistance

ENV 1993-1-1: 1992, 5.4.6

$V_{Sd,y}$ = -3.1 kN $V_{Sd,z}$ = -14.1 kN

$$V_{pl,Rd} = A_v \cdot \frac{f_y}{\sqrt{3} \cdot \gamma_{M0}}$$

$A_v = 2 \cdot A/\pi$
= 2·65.7 cm^2/π
= 41.83 cm^2

$A_v = 2 \cdot A/\pi$
= = 2·65.7 cm^2/π
= 41.83 cm^2

$$V_{pl,Rd} = 41.83\text{cm}^2 \cdot \frac{355\text{N/mm}^2}{\sqrt{3} \cdot 1.0}$$
= 857.3 kN

$$V_{pl,Rd} = 41.8\text{cm}^2 \cdot \frac{355\text{N/mm}^2}{\sqrt{3} \cdot 1.0}$$
= 857.3 kN

$|V_{Sd}|$= 3.1 kN < $V_{pl,Rd}$= 857.3 kN

$|V_{Sd}|$= 14.1 kN < $V_{pl,Rd}$= 857.3 kN

Since the design values of the shear force V_{Sd} do not exceed 50% of the design plastic shear resistance $V_{pl,Rd}$, no reduction need be made in the plastic resistance moment.

ENV 1993-1-1: 1992, 5.4.7 (2)

2. Bending and axial force

N_{Sd} = -109.8 kN
$M_{y,Sd}$ = -34.4 kNm
$M_{z,Sd}$ = -15.9 kNm

Section C.4.1, Figure C-234

$$N_{pl,Rd} = \frac{A \cdot f_y}{\gamma_{M0}} = \frac{65.7cm^2 \cdot 355N/mm^2}{1.0} = 2332.4\text{ kN}$$

ENV 1993-1-1: 1992, 5.4.4

$$M_{pl,y,Rd} = \frac{W_{pl,y} \cdot f_y}{\gamma_{M0}} = \frac{438cm3 \cdot 355N/mm2}{1.0} = 155.5\text{ kNm}$$

ENV 1993-1-1: 1992, 5.4.5.1

$$M_{pl,z,Rd} = \frac{W_{pl,z} \cdot f_y}{\gamma_{M0}} = \frac{438cm3 \cdot 355N/mm2}{1.0} = 155.5\text{ kNm}$$

Criterion to be satisfied:

ENV 1993-1-1: 1992, 5.4.8.1 (5.36)

$$\frac{N_{Sd}}{N_{pl,Rd}} + \frac{M_{y,Sd}}{M_{pl,y,Rd}} + \frac{M_{z,Sd}}{M_{pl,z,Rd}} \leq 1$$

$$\frac{|-109.8kN|}{2332.4kN} + \frac{|-34.4kNm|}{155.5kNm} + \frac{|-15.9kNm|}{155.5kNm} = 0.37 \leq 1$$

Design resistance of joint III (members 5, 6)

ENV 1993-1-1: 1992, Annex K.6

Joint III is assessed by determining the design resistance of the members 5 (Figure D.17).

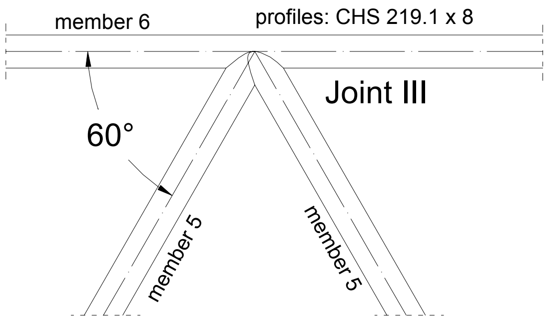

Fig. D.17. Joint III

Section properties
Elements 5, 6: CHS 219.1x8

d_i = 219.1 mm
t_i = 8 mm
A = 53.1 cm^2
W_{el} = 270 cm^3

Angles: $\Theta_1 = \Theta_2 = 60°$

Range of validity

ENV 1993-1-1: 1992 Table K.6.1

1) $0.2 \leq d_i / d_o = 1 \leq 1$
2) $5 \leq d_i / 2t_o = 13.7 \leq 25$
3) $5 \leq d_o / 2t_o = 13.7 \leq 25$
4) $5 \leq d_o / 2t_o = 13.7 \leq 20$ for X – joints
5) $\lambda_{ov} = q / p$ = 127.96 mm / 253.1 mm = 51% $\geq$ 25%
6) g = - 127.96 mm

Internal forces in the chord

$N_{Sd.6.max}$ [kN]	157.7
$N_{Sd.6.min}$ [kN]	-66
$N_{Sd.5.max}$ [kN]	227.6
$N_{Sd.5.min}$ [kN]	-230.4
$M_{y.Sd}$ [kNm]	9.2
$M_{z.Sd}$ [kNm]	5.6

Secondary moments

ENV 1993-1-1: 1992 Annex K.4 (2)

Ratio between system length and depth of the chord member:
10.15 m / 0.2191 m = 46 > 12
Ratio between system length and depth of the brace member:
5 m / 0.2191 m = 23 < 12

Secondary moments considered with 7 kNm for both directions.

σ_o is the maximum compressive stress in the chord at the joint due to axial force and bending moment.

σ_p is the value of σ_o excluding the stress due to the horizontal components of the forces in the braces at that joint

Critical: Chord in compression

$$\sigma_o = \frac{|N_{Sd}|}{A} + \frac{|M_{y,Sd}|}{W_{el}} + \frac{|M_{z,Sd}|}{W_{el}}$$

$$\sigma_o = \frac{66kN}{53.1cm^2} + \frac{(9.2+7)kNm}{270cm^3} + \frac{(5.6+7)kNm}{270cm^3} = 119.1\frac{N}{mm^2}$$

ENV 1993-1-1: 1992 Figure K.3

Conservatively and for simplification, it is assumed that: $\sigma_p = \sigma_o$
$f_{yo} = f_{yi}$ = 355 N/mm^2
$k_p = 1 - 0.3 \cdot n_p \cdot (1 + n_p)$
$n_p = \sigma_p / f_{yo}$ = 119.1 N/mm^2 / 355 N/mm^2 = 0.36 (compression)
$k_p = 1 - 0.3 \cdot 0.36 \cdot (1 + 0.36) = 0.85$

γ is the ratio of the chord diameter to twice its wall thickness

$$\gamma = \frac{d_o}{2 \cdot t_o} = \frac{219.1mm}{2 \cdot 8mm} = 13.7$$

g / t_o = -127.96 mm / 10 mm = -12.8
$k_g = 2.4$

Resistance of bracings (members 5):

$$N_{1.Rd} = \frac{f_{yo} \cdot t_o^2}{\sin\Theta_1}[1.8 + 10.2 \cdot d_1/d_o] \cdot k_p \cdot k_g \cdot \left[\frac{1.1}{\gamma_{Mj}}\right]$$

$$N_{1.Rd} = \frac{355\,N/mm^2 \cdot (8mm)^2}{\sin(60°)}[1.8 + 10.2 \cdot 1] \cdot 0.85 \cdot 2.4 \cdot \left[\frac{1.1}{1.1}\right] = 640kN$$

$$N_{2.Rd} = \frac{\sin\Theta_1}{\sin\Theta_2} \cdot N_{1,Rd} = 640kN < |N_{Sd,5,min}| = 230.4\ kN$$

Design resistance of joint I: End plate connection *Fig. C.25*

Internal forces

$N_{Sd.min}$ [kN]	51.2
$N_{Sd.max}$ [kN]	-441.7

Geometry

Angle Θ [°]	26

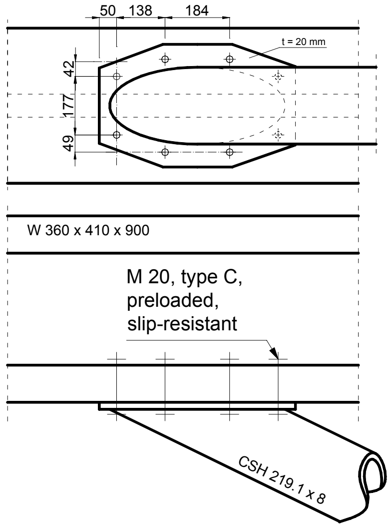

Fig. D.18. CHS end plate connection

$N_{Sd.max.\perp}$ = sin(26°) · (-441.7 kN) = -193.6 kN
$N_{Sd.min.\perp}$ = sin(26°) · 51.2 kN = 22.44 kN
$N_{Sd.max.||}$ = cos(26°) · (-441.7 kN) = 396.7 kN

Section properties

Elements 1: CHS 219.1x8
End plate: t = 20 mm
Arch profile: W 360 x 410 x 900: t_f = 106 mm

Weld design

Weld length: Conservatively and for simplification, the circular cross section is taken instead of the elliptical one.
$L_w = \pi \cdot d = \pi \cdot 219.1$ mm = 688 mm

Design force per unit length:

$$F_{w,Sd} = \frac{|N_{Sd,max}|}{L_w} = \frac{441.7\text{kN}}{688\text{mm}} = 642\,\text{N/mm}$$

Design resistance per unit length: $F_{w.Rd} = f_{vw.d} \cdot a$

Design shear strength $f_{vw.d} = \dfrac{f_u \cdot \sqrt{3}}{\beta_w \cdot \gamma_{Mw}}$

f_u nominal ultimate tensile strength of weaker part joined
f_u = 530 N/mm^2

β_w appropriate correlation factor
β_w = 0.9

$$f_{vw,d} = \frac{530\,\text{N/mm}^2}{\sqrt{3} \cdot 0.9 \cdot 1.25} = 272\,\frac{\text{N}}{\text{mm}^2}$$

Weld leg: a = 5 mm

$$F_{w.Rd} = 272\,\text{N/mm}^2 \cdot 5\text{mm} = 1360\,\text{N/mm}$$

$$\underline{F_{w.Sd} = 642\,\text{N/mm}^2 < F_{w.Rd} = 1360\,\text{N/mm}^2}$$

Bolt connection

Since the connection also takes tensile forces, the bolts must be preloaded

Preloaded, slip resistant, type C
Grade: 10.9

d = 20 mm, d_0 = 22 mm
A = 314 mm^2
Tensile stress area of bolt: A_s = 245 cm^2

Number of bolts: 8

Design shear force per bolt for the ultimate limit state:
$F_{v,Sd}$ = 396.7 kN / 8 = 49.6 kN
$F_{t,Sd}$ = 22.4 kN / 8 = 2.8 kN

Geometry

End distance in load direction:	e_1
Edge distance perpendicular to load direction:	e_2
Spacing between fasteners in load direction:	p_1
Spacing between rows of fasteners perpendicular to load direction:	p_2

e_1 = 50 mm $\geq$ min e_1 = 1.5 · d_0 = 33 mm
e_2 = 42 mm $\geq$ min e_2 = 1.5 · d_0 = 33 mm
p_1 = 184 mm $\geq$ min p_1 = 2.5 · d_0 = 55 mm
p_2 = 177 mm $\geq$ min p_2 = 2.5 · d_0 = 55 mm

Maximum end and edge distances: members exposed to weather
50 $\leq$ 40 mm + 4 · t = 120 mm (t = 20: thickness of end plate)
Maximum spacing in compression members
Outer row: $p_{1,0}$ = 177 mm $\leq$ 14 · t = 280 mm (200 mm)

Bearing resistance

$$F_{b,Rd} = \frac{2.5 \cdot \alpha \cdot f_u \cdot d \cdot t}{\gamma_{Mb}}$$

where α is the smallest of:

$$\frac{e_1}{3 \cdot d_o} = \frac{50\text{mm}}{3 \cdot 22\text{mm}} = 0.76$$

$$\frac{p_1}{3 \cdot d_o} - \frac{1}{4} = \frac{174\text{mm}}{3 \cdot 22\text{mm}} - \frac{1}{4} = 2.8$$

$$\frac{f_{ub}}{f_u} = \frac{1000\,\text{N/mm}^2}{550\,\text{N/mm}^2} = 1.82$$

$\rightarrow$ α = 0.76 < 1

ENV 1993-1-1: 1992, Table 6.5.3

$$F_{b,Rd} = \frac{2.5 \cdot 0.76 \cdot 530\,\text{N/mm}^2 \cdot 20\text{mm} \cdot 20\text{mm}}{1.25} = 322\text{kN} > F_{v.Sd} = 49.6.1\text{kN}$$

Tensile resistance

$$F_{t.Rd} = \frac{0.9 \cdot f_{ub} \cdot A_s}{\gamma_{Mb}} = \frac{0.9 \cdot 1000\,\text{N/mm}^2 \cdot 245\text{mm}^2}{1.25} = 176.4\text{kN} > F_{t.Sd} = 2.8\text{kN}$$

Combined tension and shear

ENV 1993-1-1: 1992 Section 6.5.8.4

$$F_{s.Rd} = \frac{k_s \cdot n \cdot \mu \cdot (F_{p.Cd} - 0.8 \cdot F_{t.Sd})}{\gamma_{Ms,ult}}$$

Slip factor: μ = 0.5 *Class A surface: ENV 1993-2 Section 6.4.7.1 (6)*
ENV 1993-1-1 Section 6.5.8.3

k_s = 1 standard nominal clearance
n = 1 number of friction interfaces
$F_{p,Cd}$ preloading force
$F_{p,Cd} = 0.7 \cdot f_{ub} \cdot A_s = 0.7 \cdot 1000 \text{ N/mm}^2 \cdot 245 \text{ mm}^2 = 171.5 \text{ kN}$

$$F_{s.Rd} = \frac{1 \cdot 1 \cdot 0.5 \cdot (171.5\text{N/mm}^2 - 0.8 \cdot 2.8\text{N/mm}^2)}{1.25} = 67.7\text{kN} > F_{v.Sd} = 49.6\text{kN}$$

D.4.2 Fatigue assessment

Node I

Internal forces

ΔN₁ [kN]	120.9
ΔN₁₊₂ [kN]	174.8

$A_{weld} = \pi \cdot d \cdot a = \pi \cdot 219.1 \text{ mm} \cdot 5 \text{ mm} = 3441.6 \text{ mm}^2$

$$\Delta\sigma_1 = \frac{\Delta N_1}{A} = \frac{120.9\text{kN}}{3441.6\text{mm}^2} = 35\frac{\text{N}}{\text{mm}^2} \qquad \text{one LM 71}$$

$$\Delta\sigma_{1+2} = \Delta\sigma_p = \frac{\Delta N_{1+2}}{A} = \frac{174.8\text{kN}}{3441.6\text{mm}^2} = 50.8\frac{\text{N}}{\text{mm}^2} \qquad \text{two LM 71}$$

Criterion: $\gamma_{Ff} \cdot \Delta\sigma_{E_2} \le \frac{\Delta\sigma_c}{\gamma_{Mf}}$ with $\Delta\sigma_{E_2} = \lambda \cdot \Phi_2 \cdot \Delta\sigma_p$

Damage equivalent factor $\lambda = \lambda_1 \cdot \lambda_2 \cdot \lambda_3 \cdot \lambda_4$

λ_1 = 0.6 EC Mix L = 100 m
λ_2 = 1.04 Traffic per year: $30 \cdot 10^6$ t/track
λ_3 = 1.0 Design life: 100 years

$$\lambda_4 = \sqrt[5]{0.12 + 0.88 \cdot \left(\left(\frac{\Delta\sigma_1}{\Delta\sigma_{1+2}} \right)^5 + \left(1 - \frac{\Delta\sigma_1}{\Delta\sigma_{1+2}} \right)^5 \right)} = 0.76$$

$$\lambda = 0.6 \cdot 1.04 \cdot 1.0 \cdot 0.76 = 0.47$$

$$\Delta\sigma_{E_2} = 0.47 \cdot 50.8\frac{\text{N}}{\text{mm}^2} = 23.88\frac{\text{N}}{\text{mm}^2}$$

Detail category: 40

ENV 1993-2: 1997, Table L.6 sheet 2

$$\gamma_{Ff} \cdot \Delta\sigma_{E_2} = 1.0 \cdot 23.88 \le \frac{\Delta\sigma_c}{\gamma_{Mf}} = \frac{40\text{N/mm}^2}{1.0}$$

Node II

In the sketch in Figure D.19 the critical section for the check of the fatigue resistance can be seen. In point A the hollow section of member 1 is fillet-welded to the other straight member 2-3. This is to range in detail category 71. Only the stresses in member 1 have to be checked.

ENV 1993-2: 1997, Table L.6 sheet 2

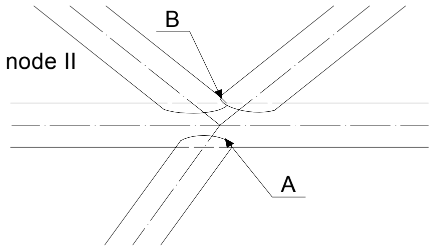

Fig. D.19. Sketch of node II

In point B the hollow sections of members 4 and 5 are fillet-welded to member 2-3 with an overlap > 30 %. Since, t_o/t_i = 1.25<1.4 according to *ENV 1993-2: 1997, Table L.7 sheet 2* this connection has to be ranged in detail category 56. The assessment has to be carried out for the members 2 and 3 as well as for members 4 and 5.

1. Node II, critical point A

$$\Delta\sigma_1 = \frac{N_{x,1}}{A} = \frac{120.9\text{kN}}{53.1\text{cm}^2} = 22.8\text{N}/\text{mm}^2 \quad \text{one LM 71}$$

$$\Delta\sigma_{1+2} = \Delta\sigma_p = \frac{N_{x,1+2}}{A} = \frac{174.8\text{kN}}{53.1\text{cm}^2} = 32.9\text{N}/\text{mm}^2 \quad \text{two LM 71}$$

$\Delta\sigma_{E2} = \lambda\ \varphi_2\ \Delta\sigma_p$

φ_2 is already included in the stresses due to LM 71

$\lambda = \lambda_1\ \lambda_2\ \lambda_3\ \lambda_4$

ENV 1993-2: 1997, 9.5.1

$\lambda_1 = 0.6$ EC Mix, L=100m

$\lambda_2 = 1.04$ Traffic per year: 30 10^6 t/track

$\lambda_3 = 1.0$ Design life: 100 years

$$\lambda_4 = \sqrt[5]{0.12 + 0.88 \cdot \left(\left(\frac{\Delta\sigma_1}{\Delta\sigma_{1+2}} \right)^5 + \left(1 - \frac{\Delta\sigma_1}{\Delta\sigma_{1+2}} \right)^5 \right)} = 0.766$$

The criterion is:

$\Delta\sigma_{E2} \le \Delta\sigma_c/\gamma_{Mf}$ with γ_{Mf} = 1.0 ; redundant structural element

$\Delta\sigma_{E2} = 0.6 \cdot 1.04 \cdot 1.0 \cdot 0.766 \cdot 32.9\text{N/mm}^2 = 15.7\text{N/mm}^2$

$\Delta\sigma_c/\gamma_{Mf} = 71\text{N/mm}^2/1.0 = 71\ \text{N/mm}^2$

$\underline{15.7\ \text{N/mm}^2 < 71\ \text{N/mm}^2}$

2. Node II, critical point B, assessment of the braces, critical member number 5

$$\Delta\sigma_1 = \frac{N_{x,1}}{A} = \frac{136.5\text{kN}}{53.1\text{cm}^2} = 25.7\text{N}/\text{mm}^2 \quad \text{one LM 71}$$

$$\Delta\sigma_{1+2} = \Delta\sigma_p = \frac{N_{x,1+2}}{A} = \frac{154.8\text{kN}}{53.1\text{cm}^2} = 29.2\text{N}/\text{mm}^2 \quad \text{two LM 71}$$

$\Delta\sigma_{E2} = \lambda\ \varphi_2\ \Delta\sigma_p$

φ_2 is already included in the stresses due to LM 71

$\lambda = \lambda_1\ \lambda_2\ \lambda_3\ \lambda_4$

$\lambda_1 = 0.6$ EC Mix, L=100m

$\lambda_2 = 1.04$ Traffic per year: 30 10^6 t/track

$\lambda_3 = 1.0$ Design life: 100 years

$$\lambda_4 = \sqrt[5]{0.12 + 0.88 \cdot \left(\left(\frac{\Delta\sigma_1}{\Delta\sigma_{1+2}} \right)^5 + \left(1 - \frac{\Delta\sigma_1}{\Delta\sigma_{1+2}} \right)^5 \right)} = 0.898$$

The criterion is:

$\Delta\sigma_{E2} \leq \Delta\sigma_c/\gamma_{Mf}$ with $\gamma_{Mf} = 1.0$; redundant structural element

ENV 1993-2: 1997, 9.5.1

$\Delta\sigma_{E2} = 0.6 \cdot 1.04 \cdot 1.0 \cdot 0.898 \cdot 29.2\text{N/mm}^2 = 16.4\text{N/mm}^2$

$\Delta\sigma_c/\gamma_{Mf} = 56\text{N/mm}^2/1.0 = 56\ \text{N/mm}^2$

$\underline{16.4\ \text{N/mm}^2 < 56\ \text{N/mm}^2}$

2. Node II, critical point B, assessment of the chord, critical members 2-3

$$\Delta\sigma_1 = \frac{N_{x,1}}{A} + \frac{M_{y,1}}{W_{el,y}} + \frac{M_{z,1}}{W_{el,z}} = \frac{30.7\text{kN}}{65.7\text{cm}^2} + \frac{15.4\text{kNm}}{328\text{cm}^3} + \frac{7.4\text{kNm}}{328\text{cm}^3} = 74.2\text{N}/\text{mm}^2$$

one LM 71

$$\Delta\sigma_{1+2} = \frac{N_{x,1}}{A} + \frac{M_{y,1}}{W_{el,y}} + \frac{M_{z,1}}{W_{el,z}} = \frac{47.2\text{kN}}{65.7\text{cm}^2} + \frac{20.3\text{kNm}}{328\text{cm}^3} + \frac{10.3\text{kNm}}{328\text{cm}^3} = 100.5\text{N}/\text{mm}^2$$

two LM 71

$\Delta\sigma_{E2} = \lambda\ \varphi_2\ \Delta\sigma_p$

φ_2 is already included in the stresses due to LM 71

$\lambda = \lambda_1\ \lambda_2\ \lambda_3\ \lambda_4$

$\lambda_1 = 0.6$ EC Mix, L=100m

$\lambda_2 = 1.04$ Traffic per year: 30 10^6 t/track

$\lambda_3 = 1.0$ Design life: 100 years

$$\lambda_4 = \sqrt[5]{0.12 + 0.88 \cdot \left(\left(\frac{\Delta\sigma_1}{\Delta\sigma_{1+2}} \right)^5 + \left(1 - \frac{\Delta\sigma_1}{\Delta\sigma_{1+2}} \right)^5 \right)} = 0.793$$

The criterion is:

$\Delta\sigma_{E2} \leq \Delta\sigma_c/\gamma_{Mf}$ with $\gamma_{Mf} = 1.0$; redundant structural element

ENV 1993-2: 1997, 9.5.1

$\Delta\sigma_{E2} = 0.6 \cdot 1.04 \cdot 1.0 \cdot 0.793 \cdot 100.5\text{N/mm}^2 = 49.7\text{N/mm}^2$

$\Delta\sigma_c/\gamma_{Mf} = 56\text{N/mm}^2/1.0 = 56\ \text{N/mm}^2$

$\underline{49.7\ \text{N/mm}^2 < 56\ \text{N/mm}^2}$

Shear stresses

The maximum shear forces occurring in ultimate limit state do not exceed 2 % (see Section D.4.1) of the permitted limits, so the shear stresses are considered to be not critical to fatigue strains. The fatigue check will be omitted.

D.4.3 Serviceability limit state assessment

D.4.3.1 Limitation of nominal stress for rare load combinations

ENV 1993-2: 1997, 4.3

The critical cross section is found in members 2 and 3 at node II.

Axial stress

$$\sigma_{Ed,ser} = \frac{N_{ser}}{A} + \frac{M_{y,ser}}{W_{el,y}} + \frac{M_{z,ser}}{W_{el,z}} = \frac{-75.4kN}{65.7cm^2} - \frac{23.7kNm}{328cm^3} - \frac{2.1kNm}{328cm^3}$$

$= -90.13\ N/mm^2$

Shear stress

$$\tau_{Ed,ser} = \frac{Vz}{A_{vz}} = \frac{-14.1kN}{41.8cm^2}$$

$= -3.4N/mm^2$

The criterion to be satisfied is:

$$\sqrt{(\sigma_{Ed,ser})^2 + 3(\tau_{Ed,ser})^2} < \frac{fy}{\gamma_{M,ser}}$$

$$\sqrt{(-90.13N/mm^2)^2 + 3(-3.4N/mm^2)^2} = 90.3 < 355N/mm^2 = \frac{355N/mm^2}{1.0}$$

D.4.3.2 Limitation of nominal stress range for frequent load combination

ENV 1993-2: 1997, 4.3 (4)

The critical cross section is found in member 1. The stress range will be calculated from the variation of internal forces.

$$\Delta\sigma_{Ed,ser} = \frac{\Delta N_{ser}}{A} = \frac{139.8kN}{53.1cm^2} = 26.6N/mm^2$$

The criterion to be satisfied is:

$$\Delta\sigma_{Ed,ser} < 1.5\frac{f_y}{\gamma_{M,ser}}$$

$$\Delta\sigma_{Ed,ser} = 26.6N/mm^2 < 532.5N/mm^2 = 1.5\frac{355N/mm^2}{1.0}$$

D.5 The bridge deck

D.5.1 Concrete cover

Exposure class

The railway bridge is assumed to be exposed to a humid environment with frost. The non-public footpath will not be subjected to de-icing agent.

Exposure class: 2b

ENV 1992-1-1: 1991 Table 4.1

Minimum concrete cover

• Requirements for minimum cover to prestressing sheets:

- 50 mm [a)]
- 35 mm with a reduction of 5 mm for concrete strength class C50/60 [b)]
- Equal to the diameter of the duct [b)]:

D = 57 mm for transverse prestressing
D = 118 mm for longitudinal prestressing

ENV 1992-2: 1996 Section 4.1.3.3 [a)]

ENV 1992-1-1: 1991 Section 4.1.3.3 [b)]

Critical values: Transversal prestressing: min c = 57 mm
Longitudinal prestressing: min c = 118 mm

• Requirements for minimum cover to reinforcement:

- 30 mm [a)]
- 25 mm with a reduction of 5 mm for concrete strength class C50/60 [b)]

Critical value: min c = 30 mm

Nominal concrete cover

Allowance for tolerance: Δh = 10 mm

ENV 1992-1-1: 1991 Section 4.1.3.3

nom c = min c + Δh

Transversal prestressing: nom c = 67 mm
Longitudinal prestressing: nom c = 128 mm
Reinforcement: nom c = 40 mm

D.5.2 Main design – Bridge deck with transverse prestressing

D.5.2.1 Ultimate limit state

D.5.2.1.1 Bending with longitudinal force

ENV 1992-1-1: 1991 Section 4.3.1

Bridge deck in transverse direction

ENV 1992-2: 1996 Section 4.3.1

The axial compression forces are virtually evenly distributed over the bridge length, which is due to the transverse prestressing. The critical point is where the bending moment has its maximum.

x = 49.1 m
y = 3.28 m

Internal forces

$m_{Sd,y}$ [kNm/m]	628.7
$n_{Sd,y}$ [kN/m]	-3139

Geometry

z_p [mm]	103
h [mm]	403.1
d [mm]	300.1
z_{s1} [mm]	98.55

For geometry see Annex B, Figure B.7.
$z_{s1} = h / 2 - z_p$

Annex C

$f_{cd} = f_{ck} / \gamma_s = 50\ N/mm^2 / 1.15 = 33.3\ N/mm^2$

$m_{sds} = m_{Sd,x} - n_{Sd,y} \cdot z_{s1}$
$m_{sds} = 628.7$ kNm/m – (-3139 kN/m) · 0.09855 m = m_{sds} = 938 kNm/m

$$\mu_{Sds} = \frac{m_{Sds}}{b \cdot d^2 \cdot f_{cd}}$$

$$\mu_{Sds} = \frac{938\,kNm/m}{(0.3m)^2 \cdot 33.3N/mm^2} = 0.31 > 0.206 \rightarrow \text{compressive reinforcement}$$

Required re-bar diameter: Ø 20
→ d_2 = 40 mm + (20 mm) / 2 = 50 mm
d_2 / d = 50 mm / 300 mm = 0.17
ω_1 = 0.366 (ω_1 and ω_2 are interpolated for d_2 / d = 0.17)
ω_2 = 0.155

Schneider [29], pages 5.126, 5.130

$f_{pd} = 0.9 \cdot f_{pk} / \gamma_s = 0.9 \cdot 1230\ N/mm^2 / 1.15 = 962.5\ N/mm^2$

$$A_{s1} = \frac{1}{f_{pd}} \cdot (\omega_1 \cdot b \cdot d \cdot f_{cd} + N_{Sd})$$

$$A_{s1} = \frac{1}{962.5N/mm^2} \cdot (0.366 \cdot 1000m \cdot 300mm \cdot 33.3N/mm^2 - 3139 \cdot 1000N/m)$$

ENV 1992-1-1: 1991 Section 4.2.3.3.3 (6)

$$\underline{A_{s1} = 5.4cm^2/m}$$

→ Ø 10, s = 14 cm (gives A_{s1} = 5.61 cm^2/m)

$$A_{s2} = \omega_2 \cdot b \cdot d \cdot \frac{f_{cd}}{f_{yd}}$$

$$\underline{A_{s2} = \cdot 0.155 \cdot 100cm \cdot 30.01cm \cdot \frac{33.3}{435} = 35.6cm^2}$$

→ Ø 20, s = 9 cm (gives A_{s2} = 34.91 cm^2/m)
(34.91 < 35.6, but difference less than 3% permissible)

Check at smallest depth

x = 49.1 m
y = 1.36 m

Internal forces

$m_{Sd,y}$ [kNm/m]	230
$n_{Sd,y}$ [kN/m]	-3170

Geometry

z_p [mm]	134
h [mm]	374
d [mm]	240
z_{s1} [mm]	53

$f_{cd} = f_{ck} / \gamma_s = 50\ N/mm^2 / 1.15 = 33.3\ N/mm^2$

$m_{sds} = m_{Sd,x} - n_{Sd,y} \cdot z_{s1}$
m_{sds} = 230 kNm/m – (-3170 kN/m) · 0.053 m
m_{sds} = 398 kNm/m

$$\mu_{Sds} = \frac{m_{Sds}}{b \cdot d^2 \cdot f_{cd}}$$

Schneider [29], page 5.130

$$\mu_{Sds} = \frac{398\,kNm/m}{(0.24m)^2 \cdot 33.3\,N/mm^2} = 0.2$$

$\omega = 0.2327$
$f_{pd} = 0.9 \cdot f_{pk} / \gamma_s = 0.9 \cdot 1230\ N/mm^2 / 1.15 = 962.5\ N/mm^2$

ENV 1992-1-1: 1991 Section 4.2.3.3.3 (6)

$$A_s = \frac{1}{f_{pd}} \cdot (\omega \cdot b \cdot d \cdot f_{cd} + N_{Sd})$$

$$A_s = \frac{1}{962.5\,N/mm^2} \cdot \left(0.2327 \cdot 1000mm \cdot 240mm \cdot 33.3\frac{N}{mm^2} - 3170 \cdot 1000N\right)$$

$$\underline{A_s = -13.6\,cm^2/m < 0}$$

No additional reinforcement required.

Bridge deck in longitudinal direction

At the critical point, the maximum bending moment faces a moderate axial compression force.

At point (x = 50.9; y = 2.69), the axial compression force is considerably smaller, but acts together with a bending moment of $m_x \approx 0$, which is not relevant.

x = 49.1 m
y = 2.69 m

Internal forces

$m_{Sd,x}$ [kNm/m]	422.7
$n_{Sd,x}$ [kN/m]	-2743

Geometry

z_s [mm]	45
h [mm]	430
d [mm]	385
z_{s1} [mm]	170

Annex C

$f_{cd} = f_{ck} / \gamma_s = 50\ N/mm^2 / 1.15 = 33.3\ N/mm^2$

$m_{sds} = m_{Sd,x} - n_{Sd,x} \cdot z_{s1}$
$m_{sds} = 422.7\ kNm/m - (-2743\ kN/m) \cdot 0.17\ m$
$m_{sds} = 889\ kNm/m$

$$\mu_{Sds} = \frac{m_{Sds}}{b \cdot d^2 \cdot f_{cd}}$$

Schneider [29], page 5.130

$$\mu_{Sds} = \frac{889\,kNm/m}{(0.385m)^2 \cdot 33.3\,N/mm^2} = 0.18$$

$\zeta = 0.88$ $z = d \cdot \zeta = 385\ mm \cdot 0.8 = 308\ mm$
$\xi = 0.3$ $x = d \cdot \xi = 385\ mm \cdot 0.3 = 115.5\ mm$
$\varepsilon_{s1} = 0.00902$

$\varepsilon_p = \varepsilon_{pm} + \varepsilon_{s1}$

$f_{sd} = f_{yk} / \gamma_s$
$f_{sd} = 500\ N/mm^2 / 1.15 = 435\ N/mm^2$

ENV 1992-1-1: 1991 Section 4.2.2.3.2 (5)

$$A_s = \frac{1}{f_{sd}} \cdot \left(\frac{m_{Sds}}{z} + n_{Sd} \right)$$

$$A_s = \frac{1}{435\,\mathrm{N/mm^2}} \cdot \left(\frac{889\,\mathrm{kNm/m}}{308\mathrm{mm}} + (-2743\mathrm{kN/m}) \right) = 3.3\,\mathrm{cm^2/m}$$

d_s = 10 mm, s = 20 mm, A_s = 3.93 cm^2/m
Minimum reinforcement: $A_{s.min}$ = 5.24 cm^2/m > 3.93 cm^2/m

Edge beam

The critical section is located between the two hanger connections at x = 48 m and x = 48.6 m, where the bending moment is maximal and the axial compression force minimal.

x = 48.3 m

Internal forces

$m_{Sd,x}$ [kNm/m]	407.9
$n_{Sd,x}$ [kN/m]	-1691

Geometry

z_s [mm]	45
h [mm]	610
d [mm]	565
z_{s1} [mm]	260

Annex C

$f_{cd} = f_{ck} / \gamma_s$ = 50 N/mm^2 / 1.15 = 33.3 N/mm^2

$m_{sds} = m_{Sd,x} - n_{Sd,x} \cdot z_{s1}$
m_{sds} = 407.9 kNm/m – (-1691 kN/m) · 0.26 m
m_{sds} = 847.6 kNm/m

$$\mu_{Sds} = \frac{m_{Sds}}{b \cdot d^2 \cdot f_{cd}}$$

Schneider [29], page 5.130

$$\mu_{Sds} = \frac{847.6\,\mathrm{kNm/m}}{(0.565\mathrm{m})^2 \cdot 33.3\,\mathrm{N/mm^2}} = 0.08$$

ζ = 0.95   z = d · ζ = 565 mm · 0.95 = 537 mm
ξ = 0.13   x = d · ξ = 565 mm · 0.13 = 73 mm
ε_{s1} = 0.02

$f_{sd} = f_{yk} / \gamma_s$
f_{sd} = 500 N/mm^2 / 1.15 = 435 N/mm^2

ENV 1992-1-1: 1991 Section 4.2.2.3.2 (5)

$$A_s = \frac{1}{f_{td}} \cdot \left(\frac{m_{Sds}}{z} + n_{Sd} \right)$$

$$A_s = \frac{1}{435\,\mathrm{N/mm^2}} \cdot \left(\frac{847.6\,\mathrm{kNm/m}}{537\mathrm{mm}} + (-1691\mathrm{kN/m}) \right) = -2.6\,\frac{\mathrm{cm^2}}{\mathrm{m}} < 0$$

No additional reinforcement required.

D.5.2.1.2 Shear

ENV 1992-1-1: 1991
Section 4.3.2

Transverse direction

ENV 1992-2: 1996
Section 4.3.2

The relevant shear force is taken at a distance y = 1.5 · d = 847.5 mm from hanger 20 at x = 60.3 m.

Internal forces

$v_{Sd,y}$ [kN/m]	710.2
$n_{Sd,y}$ [kN/m]	-3113

Geometry

h [mm]	610
z_s [mm]	45
d [mm]	565

Elements not requiring design shear reinforcement: $V_{Sd} \leq V_{Rd1}$

$V_{Rd1} = [\tau_{Rd} \cdot k \cdot (1.2 + 40 \cdot \rho_1) + 0.15 \cdot \sigma_{cp}] \cdot b_w \cdot d$

$\tau_{Rd} = 0.48$ N/mm^2 Basic design shear for C50/60

$\rho_1 = A_{s1} / (b_w \cdot d) \leq 0.02$

$A_{s1} = 5.24$ cm^2/m
d = 0.565 m
$\rho_1 = (5.24$ cm^2/m) / (1 m · 0.565 m) = 0.00093

ENV 1992-1-1: 1991
Section 4.3.2.3

$\sigma_{cp} = n_{Sd} / A_c =$ 3113 kN / (610 mm · 1m) = 5.1 N/mm^2
(Compression positive)

ENV 1992-1-1: 1991
Table 4.8

k = 1.6 – d = 1.6 – 0.575 = 1.025

$$V_{Rd1} = \left[0.48\frac{N}{mm^2}\cdot 1.025\cdot\left(1.2+40\cdot 0.00093\right)+0.15\cdot 5.1\frac{N}{mm^2}\right]\frac{1}{m}\cdot 1m\cdot 0.575m$$

$V_{Rd1} = 790$ kN/m

$\underline{V_{Sd} = 710.2\,kN/m < V_{Rd1} = 790\,kN/m}$

No shear reinforcement required.

Minimum shear reinforcement:
Concrete C50/60, steel S500: $\rho_{w,min} = 0.0013$

ENV 1992-1-1: 1991
Section 5.4.2.2

$\rho_1 = A_{s1} / (b_w \cdot d) \leq 0.02$

$A_{sw} = \rho_w \cdot b_w \cdot s$

$A_{sw} = 0.0013 \cdot 100cm \cdot 100cm = 13cm^2/m$

Longitudinal direction

The relevant shear force is taken at x = 60.3 m.

Internal forces

$v_{Sd,x}$ [kN/m]	615.1
$n_{Sd,x}$ [kN/m]	-2410

Geometry

h [mm]	610
z_s [mm]	45
d [mm]	565

Elements not requiring design shear reinforcement: $V_{Sd} \leq V_{Rd1}$

$V_{Rd1} = [\tau_{Rd} \cdot k \cdot (1.2 + 40 \cdot \rho_1) + 0.15 \cdot \sigma_{cp}] \cdot b_w \cdot d$

$\tau_{Rd} = 0.48$ N/mm^2 Basic design shear for C50/60

ENV 1992-1-1: 1991
Section 4.3.2.3

$\rho_1 = A_{s1} / (b_w \cdot d) \leq 0.02$

ENV 1992-1-1: 1991
Table 4.8

$A_{s1} = 5.24$ cm^2/m
d = 0.565 m
$\rho_1 = (5.24\ \text{cm}^2/\text{m}) / (1\ \text{m} \cdot 0.565\ \text{m}) = 0.00093$

$\sigma_{cp} = N_{Sd} / A_c = 2410\ \text{kN} / (610\ \text{mm} \cdot 1\text{m}) = 3.95\ \text{N/mm}^2$
(compression positive)

k = 1.6 – d = 1.6 – 0.575 = 1.025

$$V_{Rd1} = \left[0.48 \frac{N}{mm^2} \cdot 1.025 \cdot (1.2 + 40 \cdot 0.00093) + 0.15 \cdot 3.95 \frac{N}{mm^2}\right] \frac{1}{m} \cdot 1m \cdot 0.565m$$

$V_{Rd1} = 678$ kN/m

$\underline{V_{Sd} = 615.1 kN/m < V_{Rd1} = 678 kN/m}$

No shear reinforcement required.

Minimum shear reinforcement:
Concrete C50/60, steel S500: $\rho_{w,min} = 0.0013$

$\rho_1 = A_{s1} / (b_w \cdot d) \leq 0.02$
$A_{sw} = \rho_w \cdot b_w \cdot s$

$b_w = 1.3$ m (width of edge beam)
$A_{sw} = 0.0013 \cdot 130cm \cdot 100cm = 17 cm^2/m$

The minimum shear reinforcement for both directions has not been added together.
The greater value is applied: $A_{sw} = 17$ cm^2/m
Ø 12, 4-shear stirrups, spacing s = 20 cm (gives $A_{sw} = 22.6$ cm^2/m)

D.5.2.1.3 Punching

Punching shear is checked for with the maximal hanger force 1061.85 kN, which is found in hanger number 4 with a slope of 75.2°. The vertical component of the hanger force is $N_{max} = 1027$ kN.

ENV 1992-1-1: 1991
Section 4.3.4.5.1

Internal force

N_{Sd} [kN]	1027

Geometry of bearing plate

l [mm]	420
w [mm]	150
f [mm]	120

Geometry of concrete section

h [mm]	610
z_s [mm]	45
d [mm]	565

No shear reinforcement: $v_{Sd} \leq v_{Rd1}$

Shear per unit length: $v_{Sd} = \dfrac{V_{sd} \cdot \beta}{u}$

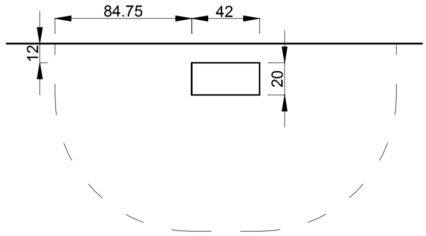

Fig. D.20. Punching shear critical perimeter

V_{Sd} total design shear force; $V_{Sd} = 1027$ kN

β coefficient taking eccentricity of loading into account; here $\beta = 1.0$

u critical perimeter; $u = 2 \cdot w + l + \pi \cdot d \cdot 1.5 + 2 \cdot f$

$$u = (2 \cdot 20 + 42 + \pi \cdot 56.5 \cdot 1.5 + 2 \cdot 12)\text{cm} = 372\text{cm}$$

$$v_{Sd} = \frac{1027\text{kN} \cdot 1.0}{3720\text{mm}} = 276\,\text{N/mm} \quad \text{(Shear per unit length)}$$

v_{Rd1} shear resistance per unit length

$v_{Rd1} = \tau_{Rd} \cdot k \cdot (1.2 + 40 \cdot \rho_1) \cdot d$

τ_{Rd} basic design shear strength;

$\tau_{Rd} = 0.48$ N/mm^2

k $k = 1.6 - d = 1.6 - 0.575 = 1.025$

$$\rho_1 = \sqrt{\rho_{1x} \cdot \rho_{1y}} + \frac{\sigma_{cpo}}{f_{yd}} \leq 0.015$$

σ_{cpo} concrete stress due to initial prestress;

transverse direction: $N_{pd.y} = 3135$ kN/m

$\sigma_{cpo.y} = 3135$ kN/m / 0.61 m = 5.1 N/mm^2

longitudinal direction: $\sigma_{cpo.x} = 11.6$ N/mm^2

average value: $\sigma_{cpo} = (5.1 + 11.6)/2$ N/mm^2 = 8.35 N/mm^2

f_{yd} design yield stress of the reinforcement;

$f_{yd} = f_y / 1.15 = 435$ N/mm^2

$A_{sx} = A_{sy} = 5.24$ cm^2/m

$\rho_{1x} = \rho_{1y} = (5.24$ cm^2/m) / (1 m $\cdot$ 0.565 m) = 0.00093

$\rho_1 = 0.00093 + 8.35$ N/mm^2 / 435 N/mm^2 = 0.02 > 0.015

$v_{Rd1} = 0.48$ N/mm^2 $\cdot$ 1.025 $\cdot$ (1.2 + 40 $\cdot$ 0.015) $\cdot$ 565 mm = 500 N/mm

$v_{Sd} = 276$ N/mm $\leq v_{Rd1} = 500$ N/mm

No punching shear reinforcement required.

D.5.2.2 Serviceability limit states

Category C is assumed for the classification of assessment conditions.

ENV 1992-2: 1996 Table 4.118

The serviceability limit state assessment is mainly based on comparison of both concrete and steel stresses with certain limits. All decisive concrete and steel stresses are listed in Annex C, Figure C.39. In Figure D.21, relevant values are compared with the serviceability limit state requirements.

State / comb.	ENV 1992-2: 1996 Section	Requirement		Stress [N/mm²] Longi-tudinal	Stress [N/mm²] Trans-verse
Time of prestressing	4.4.1.1 (102)	Max. concrete compressive stress $\leq 0.6 \cdot f_c(t)$ or $0.45 \cdot f_c(t)$ $0.45 \cdot f_c(t) = -22.5$ N/mm²		-17.1	-16.8
Decompression (quasi-permanent)	4.4.2.1 (106)	Concrete in compression		-3.41	-4.66
	4.4.1.1 (106)	Stress in tendons	1150.5 N/mm² (L)	980	-
		after losses $\leq 0.65\ f_{pk}$	800 N/mm² (T)	-	703
Non-frequent	4.4.1.1 (103)	Max. concrete compressive stress $\leq 0.6\ f_{ck} = -30$ N/mm²		-18.6	-20.2
	4.4.1.1 (105)	Limitation of tensile stress in reinforcement to $0.8 \cdot f_{yk} = 400$ N/mm²		354 [1)]	88.5 [1)]
	4.4.2.2.2 (101)	$\sigma_c \leq -1$ N/mm², otherwise minimum reinforcement		4.6 [2)]	6.9 [2)]
Crack width (frequent)	4.4.2.3 (101)	if $\sigma_c \leq f_{ctm} = 4.1$ N/mm², then min. reinf. according to (4.4.2.2.2 (101)) sufficient		-0.3	0.67

Notes:
1) The tensile stress in the reinforcement is calculated further below in the text
2) The minimum reinforcement is calculated further below in the text

Fig. D.21. Serviceability limit state assessment

Limitation of steel stress in reinforcement

The tensile stress in the reinforcement steel should be limited to $0.8 \cdot f_{yk} = 400\ \text{N/mm}^2$ for the non-frequent combination of actions. The approximate and conservative calculation was carried out with the help of the tension triangle in the uncracked stage. The concrete stresses were taken from Figure C.39, Annex C.

SCHNEIDER [29] page 5.116

In transverse direction, the prestressing steel lies within the tensile zone and is therefore additionally considered to the reinforcement. In longitudinal direction, only reinforcement lies in the tensile zone and is therefore considered exclusively.

Transverse direction

Concrete stress at top level: $\sigma_{y,top} = -20.2\ \text{N/mm}^2$
Concrete stress at bottom level: $\sigma_{y,bottom} = 6.9\ \text{N/mm}^2$

Tensile zone: $x' = \frac{0.43}{(6.9 + 20.2)} \cdot 6.9 = 0.11\text{m}$

Distance of thread bar from bottom level: z_p = 103 mm < 110 mm
→ Thread bar lies within tensile zone.

Area of prestressing steel: A_p = 37.7 cm^2/m
Area of reinforcement: A_s = 5.24 cm^2/m

Force in the tension triangle: F = 0.5 · 0.11m · 6.9 N/mm^2 = 380 kN/m

Steel stress:
σ_s = F / A_s = 380 kN/m / (5.24 +37.7) cm^2/m = 88.5 N/mm^2 < 400 N/mm^2.

Longitudinal direction

Concrete stress at top level: $\sigma_{y,top}$ = -18.6 N/mm^2
Concrete stress at bottom level: $\sigma_{y,bottom}$ = 4.6 N/mm^2

Tensile zone: $x' = \frac{0.43}{(4.6 + 18.6)} \cdot 4.6 = 0.085\text{m}$

Force in the tension triangle: F = 0.5 · 0.085m · 4.6 N/mm^2 = 195.5 kN/m
Area of reinforcement: A_s = 5.24 cm^2/m
Steel stress: σ_s = F / A_s = 185.5 kN/m / 5.24 cm^2/m = 354 N/mm^2 < 400 N/mm^2.

Minimum reinforcement – transverse direction

ENV 1992-2: 1996
Section 4.4.2.2.3

$A_s = (0.8\ k_c \cdot k \cdot f_{ctm} \cdot A_{ct}) / \sigma_s$

f_{ctm} tensile strength of the concrete: f_{ctm} = 4.1 N/mm^2

A_{ct} area of concrete within tensile zone just before cracking;
concrete stress due to prestressing:
P = 2650.9 kN (*Annex B, Figure B.9*)
$\sigma_p = P / A_c$ = - 2650.9 kN / 0.43 m^2 = - 6.16 N/mm^2
A_{ct} = 0.0859 m^2/m

σ_s maximum stress permitted in the reinforcement immediately after cracking, depending on the re-bar diameter; for a bar size of 12 mm in a prestressed concrete section: σ_s = 240 N/mm^2 (*ENV 1992-2: 1996 Table 4.120*)

k_c coefficient taking into account the nature of the stress distribution within the section immediately prior to cracking; k_c = 0.4 (conservative)

k 0.9 (interpolated value for h = 0.43 m)

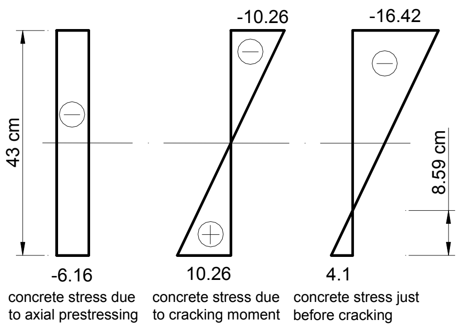

Fig. D.22. Concrete stress distribution just before cracking [N/mm^2]

A_s = (0.8 · 0.4 · 0.9 · 4.1 N/mm^2 · 859 cm^2/m) / 240 N/mm^2 = 4.3 cm^2/m
d_s = 10 mm; s = 15 cm (gives A_s = 5.24 cm^2/m)

Minimum reinforcement – longitudinal direction

Concrete slab

$A_s = (0.8\ k_c \cdot k \cdot f_{ctm} \cdot A_{ct}) / \sigma_s$

ENV 1992-2: 1996
Section 4.4.2.2.3

f_{ctm} tensile strength of the concrete: f_{ctm} = 4.1 N/mm^2.

A_{ct} area of concrete within tensile zone just before cracking;
Axial force due to prestressing: P = 2400 kN (SOFiSTiK output)
$\sigma_p = P / A_c$ = -2400 kN / 0.43 m^2 = - 5.6 N/mm^2
A_{ct} = 0.0907 m^2/m

σ_s maximum stress permitted in the reinforcement immediately after cracking, depending on the re-bar diameter; for a bar size of 12 mm in a prestressed concrete section: σ_s = 240 N/mm^2 (*ENV 1992-2: 1996 Table 4.120*)

k_c coefficient taking into account the nature of the stress distribution within the section immediately prior to cracking; k_c = 0.4 (conservative)

k 0.9 (interpolated value for h = 0.43 m)

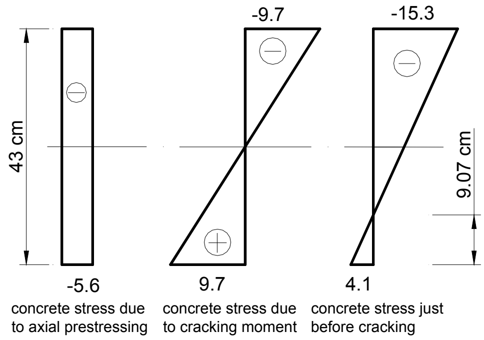

Fig. D.23. Concrete stress distribution just before cracking [N/mm^2]

A_s = (0.8 · 0.4 · 0.9 · 4.1 N/mm^2 · 907 cm^2/m) / 240 N/mm^2 = 4.5 cm^2/m
Ø 10 mm; s = 15 cm (gives A_s = 5.24 cm^2/m)

Edge beam

Axial force due to prestressing: N_p = 3000 kN (SOFiSTiK output)
Concrete stress: $\sigma_p = N_p / A_c$ = 3000 kN / 0.61 m^2 = 5 Nmm^2
Area of concrete within tensile zone just before cracking: A_{ct} = 1374 cm^2/m

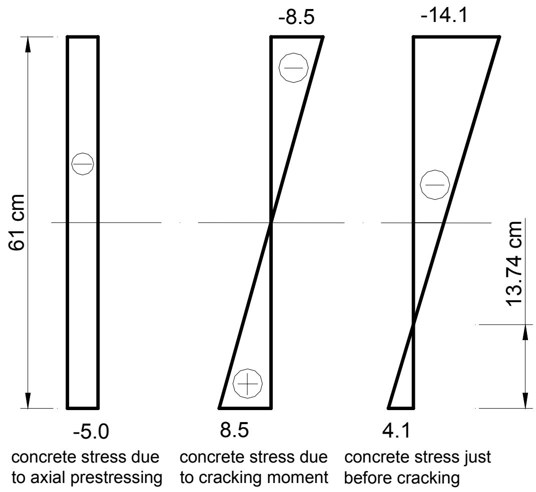

Fig. D.24. Concrete stress distribution just before cracking [N/mm^2]

k = 0.78 (interpolated value for h = 0.61 m)
A_s = (0.8 · 0.4 · 0.78 · 4.1 N/mm^2 · 1374 cm^2/m) / 240 N/mm^2 = 5.9 cm^2/m
Ø 12 mm; s = 15 cm (gives A_s = 7.54 cm^2/m)

The spacing of reinforcement steel bars shall not exceed 200 mm. This criterion is fulfilled for all reinforcement layers.

D.5.2.3 Fatigue

Relevant combination of actions: Frequent

Member in compression

If the following criterion is fulfilled, sufficient resistance against fatigue for concrete under compression is given.

ENV 1992-2: 1996 Section 4.3.7.4 (101)

$$\frac{\sigma_{c,max}}{f_{cd}} \leq 0.5 + 0.45 \cdot \frac{\sigma_{c,min}}{f_{cd}} \leq 0.9$$

$\sigma_{c.max}$ maximum compressive stress (frequent combination of actions)
$\sigma_{c.max} = -14.1\ N/mm^2$

$\sigma_{c.min}$ minimum compressive stress at the same point where $\sigma_{c.max}$ occurs
$\sigma_{c.min} = -0.3\ N/mm^2$

f_{cd} $f_{cd} = f_{ck} / \gamma_s = 50\ N/mm^2 / 1.15 = 33.3\ N/mm^2$

$$\frac{-14.1 N/mm^2}{-33.3 N/mm^2} \leq 0.5 + 0.45 \cdot \frac{-0.3 N/mm^2}{-33.3 N/mm^2} \leq 0.9$$

<u>$0.42 \leq 0.5 \leq 0.9$</u>

Member in shear

If the following criterion is fulfilled, sufficient resistance against fatigue for concrete under shear without shear reinforcement is given.

for $\left|\frac{\tau_{max}}{\tau_{Rd1}}\right| \leq 0.5 + 0.45 \cdot \left|\frac{\tau_{min}}{\tau_{Rd1}}\right| \leq 0.9 \qquad \frac{\tau_{min}}{\tau_{max}} \geq 0$

ENV 1992-2: 1996 Section 4.3.7.4 (103)

Maximum shear force (frequent combination of actions): $v_{Sd.y.max} = 702$ kN/m
Minimum shear force (frequent combination of actions): $v_{Sd,y,min} = 556$ kN/m

τ_{max} maximum shear stress under the frequent combination of actions;
$\tau_{max} = v_{Sd.y.max} / d = 702\ kN/m / 0.565\ m = 1.24\ N/mm^2$
(transverse direction)

τ_{min} minimum shear stress at the same section where τ_{max} occurs;
$\tau_{min} = v_{Sd,y,min} / d = 556\ kN/m / 0.565\ m = 0.98\ N/mm^2$

τ_{Rd1} $\tau_{Rd1} = V_{Rd1} / (1m \cdot d)$
$V_{Rd1} = 968$ kN/m (transversal direction)
$\tau_{Rd1} = 968\ kN/m / 0.565\ m = 1.71\ N/mm^2$

Section D.5.2.2.1

$$\left|\frac{1.24 N/mm^2}{1.71 N/mm^2}\right| \leq 0.5 + 0.45 \cdot \left|\frac{0.98 N/mm^2}{1.71 N/mm^2}\right| \leq 0.9$$

<u>$0.73 \leq 0.76 \leq 0.9$</u>

Punching

If the following criterion is fulfilled, sufficient resistance against fatigue for concrete subjected to punching shear is given.

$$\left|\frac{\tau_{max}}{\tau_{Rd1}}\right| \leq 0.5 + 0.45 \cdot \left|\frac{\tau_{min}}{\tau_{Rd1}}\right| \leq 0.9 \quad \text{for} \quad \frac{\tau_{min}}{\tau_{max}} \geq 0$$

ENV 1992-2: 1996
Section 4.3.7.4 (104)

$\tau = v_{Sd} / d$
$\tau_{Rd1} = v_{Rd1} / d$

$$v_{Sd} = \frac{V_{sd} \cdot \beta}{u}$$

Vertical component of maximum hanger force: $V_{Sd,max}$ = 630 kN
Vertical component of minimum hanger force: $V_{Sd,min}$ = 305 kN

β eccentricity coefficient; β = 1.0 *Section D.5.2.3*
u critical perimeter; u = 3720 mm
v_{Rd1} shear resistance per unit length; v_{Rd1} = 500 N/mm

$$v_{Sd,max} = \frac{V_{sd,max} \cdot \beta}{u} = \frac{630\text{kN} \cdot 1.0}{3720\text{mm}} = 170\frac{\text{N}}{\text{mm}} \qquad \text{(Shear per unit length)}$$

$$v_{Sd,min} = \frac{V_{sd,min} \cdot \beta}{u} = \frac{305\text{kN} \cdot 1.0}{3720\text{mm}} = 82\frac{\text{N}}{\text{mm}}$$

$\tau_{max} = v_{Sd,max} / d$ = 170 N/mm / 0.565 m = 0.3 N/mm^2
$\tau_{min} = v_{Sd,min} / d$ = 82 N/mm / 0.565 m = 0.15 N/mm^2

$\tau_{Rd1} = v_{Rd1} / d$ = 500 N/mm / 0.565 m = 0.88 N/mm^2

$$\left|\frac{0.3}{0.88}\right| \leq 0.5 + 0.45 \cdot \left|\frac{0.15}{0.88}\right| \leq 0.9$$

$\underline{0.34 \leq 0.58 \leq 0.9}$

Prestressing steel

Transverse direction

$$\gamma_F \cdot \gamma_{Sd} \cdot \Delta\sigma_{s,equ} \leq \frac{\Delta\sigma_{Rsk}\left(N^*\right)}{\gamma_{s,fat}}$$

ENV 1992-2: 1996 Section 4.3.7.2

$\gamma_F = 1.0$
$\gamma_{Sd} = 1.0$
$\gamma_{s,fat} = 1.15$

ENV 1992-2: 1996 Table 4.116

$\Delta\sigma_{Rsk}(N^*) = 120\ N/mm^2$
$N^* = 10^6$, $k_1 = 3$, $k_2 = 7$

ENV 1992: 1996 Annex A 106.3

$\Delta\sigma_{s,equ} = \lambda_s \cdot \Delta\sigma_{s,71}$

$\Delta\sigma_{s,71}$ Stress variation due to load model 71 for the non-frequent combination of actions including the dynamic factor
$\Delta\sigma_{s,71} = 75\ N/mm^2$

ENV 1992-2: 1996 Table A 106.2

$\lambda_s = \lambda_{s,1} \cdot \lambda_{s,2} \cdot \lambda_{s,3} \cdot \lambda_{s,4}$

$\lambda_{s,1}$ $\lambda_{s,1} = 0.70$

$\lambda_{s,2}$ $\lambda_{s,2} = \sqrt[k_2]{\frac{Vol}{25 \cdot 10^6}}$ Vol = $30 \cdot 10^6$ t / (track · year)

$$\lambda_{s,2} = \sqrt[7]{\frac{30 \cdot 10^6}{25 \cdot 10^6}} = 1.026$$

$\lambda_{s,3}$ $\lambda_{s,3} = \sqrt[k_2]{\frac{N_{years}}{100}}$ $N_{years} = 100$

$$\lambda_{s,3} = \sqrt[7]{\frac{100}{100}} = 1$$

$\lambda_{s,4}$ $\lambda_{s,4} = \sqrt[k_2]{n + (1-n) \cdot s_1^{k_2} + (1-n) \cdot s_2^{k_2}}$

n = 0.12 (*taken from ENV 1993-2: 1997 Section 9.5.3 (8)*)

$$s_1 = \frac{\Delta\sigma_1}{\Delta\sigma_{1+2}};\ s_2 = \frac{\Delta\sigma_2}{\Delta\sigma_{1+2}}$$

$\Delta\sigma_1$, $\Delta\sigma_2$ – Stress variation due to load model 71 on one track
$\Delta\sigma_{1+2}$ – Stress variation due to load model 71 on two tracks
$\Delta\sigma_1 = \Delta\sigma_2 = 42\ N/mm^2$
$\Delta\sigma_{1+2} = 75\ N/mm^2$

$$s_1 = s_2 = \frac{42\,N/mm^2}{75\,N/mm^2} = 0.56$$

$$\lambda_{s,4} = \sqrt[7]{0.12 + (1-0.12) \cdot 0.56^7 + (1-0.12) \cdot 0.56^7} = 0.76$$

$\lambda_s = 0.7 \cdot 1.026 \cdot 1 \cdot 0.76 = 0.55$
$\Delta\sigma_{s,equ} = \lambda_s \cdot \Delta\sigma_{s,71} = 0.55 \cdot 75\ N/mm^2 = 41.3\ N/mm^2$

$$\underline{1.0 \cdot 1.0 \cdot 50.7 \frac{N}{mm^2} = 41.3 \frac{N}{mm^2} \leq \frac{120\,N/mm^2}{1.15} = 104.3 \frac{N}{mm^2}}$$

D.5.2.4 Footpath

Structural system

Cantilever with length L = 63 cm

Geometry

Reinforcing steel: d_s = 20 mm
Concrete cover: nom c = 4 cm

Depth: h = 15 cm
Effective depth: d = 15 cm – 4 cm – 1 cm = 10 cm

Loading

Live load: $p = 5\ kN/m^2$
Dead load: $g = 25\ kN/m^3 \cdot 0.15\ m = 3.75\ kN/m^2$

$q = 1.35 \cdot g + 1.5 \cdot p = 12.56\ kN/m^2$

Internal forces

$m_{Sds} = q \cdot L^2/2 = 12.56\ kN/m^2 \cdot (0.63\ m)^2 / 2 = 2.5\ kNm/m$

$$\mu_{Sds} = \frac{m_{Sds}}{b \cdot d^2 \cdot f_{cd}}$$

$$\mu_{Sds} = \frac{2.5\,kNm/m}{(0.10m)^2 \cdot 33.3\,N/mm^2} = 0.0075 \rightarrow \text{take } \mu_{Sds.min} = 0.05$$

$\zeta = 0.966$ $z = d \cdot \zeta = 100\ mm \cdot 0.966 = 96.6\ mm$
$f_{sd} = f_{yk} / \gamma_s = 500\ N/mm^2 / 1.15 = 435\ N/mm^2$

$$A_s = \frac{1}{f_{sd}} \cdot \left(\frac{m_{Sds}}{z}\right) = \frac{1}{435\,N/mm^2} \cdot \left(\frac{2.5\,kNm/m}{96.6mm}\right) = 0.6\frac{cm^2}{m}$$

Minimum reinforcement

ENV 1992-2: 1996 Section 4.4.2.2.3

$A_s = (0.8 \cdot k_c \cdot k \cdot f_{ctm} \cdot A_{ct}) / \sigma_s$

f_{ctm} tensile strength of the concrete: $f_{ctm} = 4.1\ N/mm^2$.

A_{ct} area of concrete within tensile zone just before cracking;
$A_{ct} = 0.15 / 2\ m^2/m = 0.075\ m^2/m$.

σ_s maximum stress permitted in the reinforcement immediately after cracking, depending on the re-bar diameter;
$\sigma_s = 320\ N/mm^2$ for re-bar Ø 20 (*ENV 1992-1-1: 1991 Table 4.11*)

k_c coefficient taking into account the nature of the stress distribution within the section immediately prior to cracking;
$k_c = 0.4$

k 1.0

$A_s = (0.8 \cdot 0.4 \cdot 1.0 \cdot 4.1\ N/mm^2 \cdot 750\ cm^2/m) / 320\ N/mm^2 = 3.1\ cm^2/m$

Ø 10, s = 15 cm (gives $A_s = 5.24\ cm^2/m$)

D.5.2.5 Summary of reinforcement

Edge beam

Top: Ø 12, s = 15 cm
Bottom: Ø 12, s = 15 cm

Bridge deck: Transverse

Top: Ø 20, s = 9 cm
Bottom: Ø 10, s = 14 cm

Bridge deck: Longitudinal:

Top: Ø 10, s = 15 cm
Bottom: Ø 10, s = 15 cm

Footpath

Edge stirrups: Ø 10, s = 15 cm

Shear stirrups: Ø 12, s = 20 cm (4-shear)

Calculation of reinforcement steel weight

Geometry	[m]
Bridge length	100
Width on the top	11.85
Width on the bottom	10.59
Width of edge beam	1.3
Length of cantilever	0.6
Length of stirrup [m]	2.5
Length of cantilever strirrups	1

Fig. D.25. Geometric properties for calculation of steel weight

The calculation of the steel weight is based on the geometric properties listed in Figure D.25.

Calculation of reinforcement steel weight						
	Ø [mm]	Nom. mass [kg/m]	s [cm]	Number	Length [m]	Weight [kg]
Bridge deck: Transverse						
Top	20	2.47	9.00	1111.11	13166.67	32522
Bottom	10	0.62	14.00	714.29	7564.29	4667
Bridge deck: Longitudinal						
Top	10	0.62	15.00	74.33	7433.33	4586
Bottom	10	0.62	15.00	61.93	6193.33	3821
Edge beam						
Top	12	0.89	15.00	17.33	1733.33	1539
Bottom	12	0.89	15.00	17.33	1733.33	1539
Cantilever stirrups	10	0.62	15.00	1333.33	1333.33	823
Shear stirrups	12	0.89	20.00	2000.00	5000.00	4440
1) Additional reinforcement accounting for overlapping					**Total**	53938
of re-bars and unconsidered reinforcement					+ 15% 1)	**62028**

Fig. D.26. Calculation of steel weight

D.5.3 Alternative design proposals for bridge deck

D.5.3.1 Alternative design 1: Slab depth 610 mm

D.5.3.1.1 Ultimate limit states

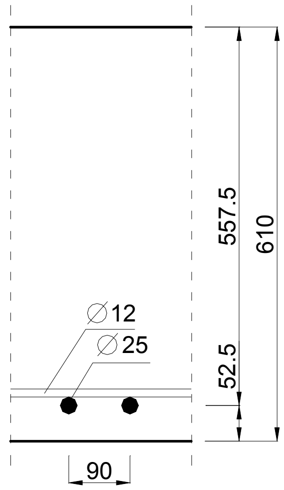

Fig. D.27. Cross section

Bending
ENV 1992-1-1 Section 4.3.1
ENV 1992-2 Section 4.3.1

The design checks are performed at mid-span, where the decisive bending moment is found.

Internal forces

$m_{Sd,y}$ [kNm/m]	1195.6

Geometry

z_s [mm]	52.5
h [mm]	610
d [mm]	557.5

$f_{cd} = f_{ck} / \gamma_s = 50 \text{ N/mm}^2 / 1.15 = 33.3 \text{ N/mm}^2$

$$\mu_{Sds} = \frac{m_{Sds}}{b \cdot d^2 \cdot f_{cd}}$$

$$\mu_{Sds} = \frac{1195.6 \text{kNm/m}}{(0.5775\text{m})^2 \cdot 33.3 \text{N/mm}^2} = 0.115$$

SCHNEIDER [29], page 5.130

$\varsigma = 0.93$ $z = d \cdot \varsigma = 557.5 \text{ mm} \cdot 0.93 = 518 \text{ mm}$

$$A_s = \frac{1}{\sigma_{Sd}} \cdot \left(\frac{m_{Sds}}{z} \right)$$

$$A_s = \frac{1}{435 \text{N/mm}^2} \cdot \left(\frac{1195.6 \text{kNm/m}}{518\text{mm}} \right) = 53 \frac{\text{cm}^2}{\text{m}}$$

Principal reinforcement:

Re-bars: Ø 25, s = 9 cm
$A_s = 54.54 \text{ cm}^2/\text{m}$

Secondary transverse reinforcement:

ENV 1992-1-1: 1991 Section 5.4.3.2.1(2)

$A_{s\perp} = A_{s\perp} / 5 = 10.9 \text{ cm}^2/\text{m}$
Re-bars: Ø 12, s = 10 cm (gives $A_{s\perp} = 11.31 \text{ cm}^2/\text{m}$)

Shear

ENV 1992-1-1 Section 4.3.2
ENV 1992-2 Section 4.3.1

Check for maximum shear force

Internal forces

$v_{Sd,y}$ [kN/m]	566

Geometry

z_s [mm]	52.5
h [mm]	610
d [mm]	557.5

Criterion for elements not requiring design shear reinforcement: $V_{Sd} \leq V_{Rd1}$

$V_{Rd1} = [\tau_{Rd} \cdot k \cdot (1.2 + 40 \cdot \rho_1) + 0.15 \cdot \sigma_{cp}] \cdot b_w \cdot d$ *ENV 1992-1-1: 1991 Section 4.3.2.3*

$\tau_{Rd} = 0.48$ N/mm^2 Basic design shear for C50/60

$\rho_1 = A_{s1} / (b_w \cdot d) \leq 0.02$ *ENV 1992-1-1: 1991 Table 4.8*

$A_{s1} = 54.54$ cm^2/m
d = 0.5575 m
$\rho_1 = (54.54\ \text{cm}^2/\text{m}) / (1\ \text{m} \cdot 0.5575\ \text{m}) = 0.01 < 0.02$

$\sigma_{cp} = 0$ N/mm^2 (No prestressing)

k = 1.6 – d = 1.6 – 0.5575 = 1.0425 > 1

$V_{Rd1} = 446.4$ kN/m

$V_{Sd} = 566\,\text{kN/m} > V_{Rd1} = 446.4\,\text{kN/m}$ Check not fulfilled!

$V_{Rd2} = 0.5 \cdot v \cdot f_{cd} \cdot b_w \cdot 0.9 \cdot d$

ENV 1992-1-1: 1991: Section 4.3.2.3 (3)

Effectiveness factor: $v = 0.7 - f_{ck} / 200 \geq 0.5$
v = 0.7 – 50 / 200 = 0.45 < 0.45
v = 0.5

$V_{Rd2} = 0.5 \cdot 0.5 \cdot 33.3\ \text{N/mm}^2 \cdot 0.9 \cdot 557.5\ \text{mm} = 4177.1$ kN/m

$V_{wd} = V_{Sd} - V_{Rd1} = 566$ kN/m – 446.4 kN/m = 120 kN/m

$$A_{sw} = \frac{V_{wd}}{0.9 \cdot d \cdot f_{ywd}}$$

ENV 1992-1-1: 1991 Section 4.3.2.4.3

$$A_{sw} = \frac{120\text{kN}}{0.9 \cdot 557.5\text{mm} \cdot 435\,\text{N/mm}^2}$$

$$A_{sw} = 5.5\,\text{cm}^2/\text{m}$$

Minimum shear reinforcement

Concrete C50/60, steel 500 S: $\rho_{w,min} = 0.0013$
$\rho_w = A_{sw} / (b_w \cdot \sin(\alpha))$
$A_{sw} = \rho_w \cdot b_w \cdot \sin(\alpha) = 0.0013 \cdot 100\ \text{cm} \cdot \sin(90)$ *ENV 1992-1-1: 1991 Section 5.4.2.2*
$A_{sw} = 13\ \text{cm}^2/\text{m} > 5.5\ \text{cm}^2/\text{m}$

The shear reinforcement for the edge beam in the longitudinal bridge direction requires a minimum of 13 cm^2/m as well and is added to the shear reinforcement in transverse direction.

ENV 1992-1-1: 1991 Section 5.4.2.2

Total required shear reinforcement: $A_{sw} = 26\ cm^2/m$

Stirrups Ø 12, s = 15 cm, four-shear (gives $A_{sw} = 30.13\ cm^2/m$)

Maximal spacing

Longitudinal spacing

$V_{Sd} = 566$ kN/m < 1/5 V_{Rd2} = 4177.1 kN/m / 5 = 835 kN/m
→ $s_{max} = 0.8 \cdot d = 0.8 \cdot 557.5$ mm = 446 mm (300 mm)
s = 150 mm < 300 mm

Transverse spacing

s_{max} = d = 557.5 mm (800 mm) not critical

Check for shear force at smallest depth

Internal forces

$v_{Sd,y}$ [kN/m]	383

Geometry

z_s [mm]	52.5
h [mm]	554
d [mm]	501.5

Criterion for elements not requiring design shear reinforcement: $V_{Sd} \leq V_{Rd1}$

ENV 1992-1-1: 1991 Section 4.3.2.3

$V_{Rd1} = [\tau_{Rd} \cdot k \cdot (1.2 + 40 \cdot \rho_1) + 0.15 \cdot \sigma_{cp}] \cdot b_w \cdot d$

$\tau_{Rd} = 0.48\ N/mm^2$ Basic design shear for C50/60

ENV 1992-1-1: 1991 Table 4.8

$\rho_1 = A_{s1} / (b_w \cdot d) \leq 0.02$

$A_{s1} = 54.54\ cm^2/m$
d = 0.5015 m
$\rho_1 = (54.54\ cm^2/m) / (1\ m \cdot 0.5575\ m) = 0.01 < 0.02$

$\sigma_{cp} = 0\ N/mm^2$

k = 1.6 – d = 1.6 – 0.5015 = 1.1 > 1

$$V_{Rd1} = \left[0.48 \frac{N}{mm^2} \cdot 1.1 \cdot (1.2 + 40 \cdot 0.01)\right] \frac{1}{m} \cdot 1m \cdot 0.5015m$$

V_{Rd1} = 423.7 kN/m

$\underline{V_{Sd} = 383\,kN/m < V_{Rd1} = 446.4\,kN/m}$ Check fulfilled!

No shear reinforcement required.

Punching

ENV 1992-1-1 Section 4.3.4

Hanger force

N_{Sd} [kN]	1110.5

Geometry of bearing plate

l [mm]	420
w [mm]	150
f [mm]	120

Geometry of concrete section

z_s [mm]	52.5
h [mm]	610
d [mm]	557.5

Criterion for elements not requiring shear reinforcement: $v_{Sd} \leq v_{Rd1}$

$$v_{Sd} = \frac{V_{sd} \cdot \beta}{u}$$

V_{Sd} total design shear force; V_{Sd} = 1110.5 kN

β coefficient taking eccentricity of loading into account; here β = 1.0

u critical perimeter; $u = 2 \cdot w + l + \pi \cdot d \cdot 1.5 + 2 \cdot f$

$$u = (2 \cdot 20 + 42 + \pi \cdot 55.75 \cdot 1.5 + 2 \cdot 12)\text{cm} = 3687\text{mm}$$

$$v_{Sd} = \frac{1110.5\text{kN} \cdot 1.0}{3687\text{mm}} = 301\text{N/mm} \text{ (shear per unit length)}$$

v_{Rd1} shear resistance per unit length

$v_{Rd1} = \tau_{Rd} \cdot k \cdot (1.2 + 40 \cdot \rho_1) \cdot d$

τ_{Rd} basic design shear strength;

τ_{Rd} = 0.48 N/mm^2

k $k = 1.6 – d = 1.6 – 0.5575 = 1.0425 > 1$

$$\rho_1 = \sqrt{\rho_{1x} \cdot \rho_{1y}} \leq 0.015$$

A_{sx} = 11.31 cm^2/m

ρ_{1x} = (11.31 cm^2/m) / (1 m $\cdot$ 0.5575 m) = 0.002

A_{sx} = 54.54 cm^2/m

ρ_{1y} = (54.54 cm^2/m) / (1 m $\cdot$ 0.5575 m) = 0.01

$$\rho_1 = \sqrt{0.002 \cdot 0.01} = 0.0045 < 0.015$$

v_{Rd1} = 0.48 N/mm^2 $\cdot$ 1.0425 $\cdot$ (1.2 + 40 $\cdot$ 0.0045) $\cdot$ 557.5 mm = 385 N/mm

$$\underline{v_{Sd} = 301\text{N/mm} \leq v_{Rd1} = 385\text{N/mm}}$$

No additional shear reinforcement required.

D.5.3.1.2 Serviceability limit state

Minimum reinforcement

Relevant combination of actions: Non-frequent

ENV 1992-2: 1996 Section 4.4.2.2.3

$A_s = (0.8 \cdot k_c \cdot k \cdot f_{ctm} \cdot A_{ct}) / \sigma_s$

f_{ctm} tensile strength of the concrete: $f_{ctm} = 4.1$ N/mm².

A_{ct} area of concrete within tensile zone just before cracking; $A_{ct} = 0.61\ m^2 /2 = 0.305\ m^2/m$.

σ_s maximum stress permitted in the reinforcement immediately after cracking, depending on the re-bar diameter; $\sigma_s = 200$ N/mm² (for re-bar Ø 25 *ENV 1992-1-1: 1991 Table 4.11*)

k_c coefficient taking the nature of the stress distribution within the section immediately prior to cracking into account; $k_c = 0.4$

k 0.78 (interpolated value for h = 0.61 m)

$A_s = (0.8 \cdot 0.4 \cdot 0.78 \cdot 4.1\ N/mm^2 \cdot 3050\ cm^2/m) / 200\ N/mm^2 = 15.6\ cm^2/m$

$\underline{15.6\ cm^2/m < 54.54\ cm^2/m}$

The minimum reinforcement at the bottom of the slab is already covered, but it still needs to be applied at the top.

Re-bars: Ø 14, s = 10 cm (gives $A_s = 15.39\ cm^2/m$)
$A_s = 15.39\ cm^2/m$ < required $15.6\ cm^2/m$, but the excess is less than 3% and therefore acceptable.

Limitation of steel stress

Relevant combination of actions: Non-frequent

Requirement: Steel stress to be limited to $0.8 \cdot f_y = 400$ N/mm²

$M_s = 814.1$ kNm/m

$$\mu_{Sds} = \frac{m_{Sds}}{b \cdot d^2 \cdot f_{cd}}$$

$$\mu_{Sds} = \frac{814.1 kNm/m}{(0.5775m)^2 \cdot 33.3 N/mm^2} = 0.079$$

$\zeta = 0.95$ $z = d \cdot \zeta = 557.5\ mm \cdot 0.995 = 528.5\ mm$

$A_s = 54.54\ cm^2/m$

$$\underline{\sigma_s = \frac{M_s}{z \cdot A_s} = \frac{814.1 kNm/m}{528.5mm \cdot 54.54\, cm^2/m} = 282\frac{N}{mm^2} < 400\frac{N}{mm^2}}$$

Crack width

ENV 1992-2: 1996 Table 4.121

For a steel stress of 282 N/mm² and re-bar diameter of Ø 25, a maximum re-bar spacing of 150 mm is allowed. The actual spacing measures 90 mm.

D.5.3.1.3 Fatigue

Reinforcing steel

Relevant combination of actions: Non-frequent

$$\gamma_F \cdot \gamma_{Sd} \cdot \Delta\sigma_{s,equ} \le \frac{\Delta\sigma_{Rsk}\left(N^*\right)}{\gamma_{s,fat}}$$

ENV 1992-2: 1996 Section 4.3.7.2

$\gamma_F = 1.0$
$\gamma_{Sd} = 1.0$
$\gamma_{s,fat} = 1.15$

$\Delta\sigma_{Rsk}(N^*) = 195$ N/mm^2
$N^* = 10^6$, $k_1 = 5$, $k_2 = 9$

ENV 1992-2: 1996 Table 4.116

$\Delta\sigma_{s,equ} = \lambda_s \cdot \Delta\sigma_{s,71}$

ENV 1992: 1996 Annex A 106.3

$\Delta\sigma_{s,71}$ Stress variation due to load model 71 for the non-frequent combination of actions including the dynamic factor
$\Delta\sigma_{s,71} = 140$ N/mm^2

$\lambda_s = \lambda_{s,1} \cdot \lambda_{s,2} \cdot \lambda_{s,3} \cdot \lambda_{s,4}$

ENV 1992-2: 1996 Table A 106.2

$\lambda_{s,1}$ $\lambda_{s,1} = 0.65$

$\lambda_{s,2}$ $\lambda_{s,2} = \sqrt[k_2]{\frac{Vol}{25 \cdot 10^6}}$ Vol = $30 \cdot 10^6$ t / (track · year)

$$\lambda_{s,2} = \sqrt[7]{\frac{30 \cdot 10^6}{25 \cdot 10^6}} = 1.026$$

$\lambda_{s,3}$ $\lambda_{s,3} = \sqrt[k_2]{\frac{N_{years}}{100}}$ $N_{years} = 100$

$$\lambda_{s,3} = \sqrt[7]{\frac{100}{100}} = 1$$

$\lambda_{s,4}$ $\lambda_{s,4} = \sqrt[k_2]{n + (1-n) \cdot {s_1}^{k_2} + (1-n) \cdot {s_2}^{k_2}}$

n = 0.12 (taken from *ENV 1993-2: 1997 Section 9.5.3 (8)*)

$$s_1 = \frac{\Delta\sigma_1}{\Delta\sigma_{1+2}}\ ;\ s_2 = \frac{\Delta\sigma_2}{\Delta\sigma_{1+2}}$$

$\Delta\sigma_1$, $\Delta\sigma_2$ – Stress variation due to load model 71 on one track
$\Delta\sigma_{1+2}$ – Stress variation due to load model 71 on two tracks
$\Delta\sigma_1 = \Delta\sigma_2 = 62.4$ N/mm^2
$\Delta\sigma_{1+2} = 140$ N/mm^2

$$s_1 = s_2 = \frac{61.55\,N/mm^2}{139.2\,N/mm^2} = 0.44$$

$$\lambda_{s,4} = \sqrt[7]{0.12 + (1-0.12) \cdot 0.44^7 + (1-0.12) \cdot 0.44^7} = 0.79$$

$\lambda_s = 0.65 \cdot 1.026 \cdot 1 \cdot 0.79 = 0.53$
$\Delta\sigma_{s,equ} = \lambda_s \cdot \Delta\sigma_{s,71} = 0.53 \cdot 140$ N/mm^2 = 73.8 N/mm^2

$$1.0 \cdot 1.0 \cdot 73.8 \frac{N}{mm^2} = 73.8 \frac{N}{mm^2} \le \frac{195\,N/mm^2}{1.15} = 169.6 \frac{N}{mm^2}$$

D.5.3.2 Alternative design proposal 2: Slab depth 470 mm

D.5.3.2.1 Ultimate limit state

Bending and longitudinal force
ENV 1992-1-1 Section 4.3.1
ENV 1992-2 Section 4.3.1

Internal forces

$m_{Sd,y}$ [kNm/m]	1041.2

Geometry

z_s [mm]	72
h [mm]	470
d [mm]	398

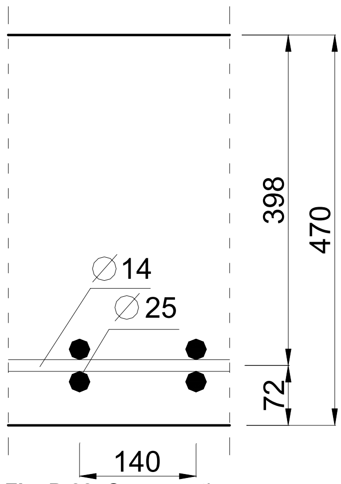

Fig. D.28. Cross section

Assumption: Re-bars Ø 25 in two layers with secondary transverse re-bars Ø 14 in-between.

$f_{cd} = f_{ck} / \gamma_s = 50\ N/mm^2 / 1.15 = 33.3\ N/mm^2$

$$\mu_{Sds} = \frac{m_{Sds}}{b \cdot d^2 \cdot f_{cd}}$$

$$\mu_{Sds} = \frac{1041.2\,kNm/m}{(0.398m)^2 \cdot 33.3\,N/mm^2} = 0.2$$

$\varsigma = 0.86$ $z = d \cdot \varsigma = 398\ mm \cdot 0.86 = 342.3\ mm$

$$A_s = \frac{1}{\sigma_{Sd}} \cdot \left(\frac{m_{Sds}}{z}\right)$$

$$A_s = \frac{1}{435\,N/mm^2} \cdot \left(\frac{1041.16\,kNm/m}{342.3mm}\right) = 70\,\frac{cm^2}{m}$$

SCHNEIDER [29], page 5.130

Principal reinforcement

Re-bars: Ø 25 in two layers, s = 14 cm (gives A_s = 70.12 cm^2/m)

Secondary transverse reinforcement:

$A_{s\perp} = A_{s\perp} / 5 = 14\ cm^2/m$
Re-bars: Ø 14, s = 10 cm (gives $A_{s\perp}$ = 15.39 cm^2/m)

ENV 1992-1-1: 1991 Section 5.4.3.2.1(2)

Shear

ENV 1992-1-1 Section 4.3.2
ENV 1992-2 Section 4.3.1

Check for maximum shear force

Internal forces

$v_{Sd,y}$ [kN/m]	547

Geometry

z_s [mm]	72
h [mm]	470
d [mm]	398

Criterion for elements not requiring design shear reinforcement: $V_{Sd} \leq V_{Rd1}$

$V_{Rd1} = [\tau_{Rd} \cdot k \cdot (1.2 + 40 \cdot \rho_1) + 0.15 \cdot \sigma_{cp}] \cdot b_w \cdot d$

$\tau_{Rd} = 0.48$ N/mm^2 Basic design shear for C50/60

$\rho_1 = A_{s1} / (b_w \cdot d) \leq 0.02$

ENV 1992-1-1: 1991
Section 4.3.2.3

$A_{s1} = 70.12$ cm^2/m
d = 0.398 m
$\rho_1 = (71.12$ cm^2/m$) / (1$ m $\cdot$ 0.398 m$) = 0.018$

ENV 1992-1-1: 1991
Table 4.8

$\sigma_{cp} = 0$ N/mm^2 (No prestressing)

k = 1.6 – d = 1.6 – 0.398 = 1.02 > 1

$$V_{Rd1} = \left[0.48\frac{N}{mm^2} \cdot 1.02 \cdot (1.2 + 40 \cdot 0.018)\right]\frac{1}{m} \cdot 1m \cdot 0.398m$$

$V_{Rd1} = 440$ kN/m

$V_{Sd} = 547\,kN/m > V_{Rd1} = 440\,kN/m$ Check not fulfilled!

$V_{Rd2} = 0.5 \cdot v \cdot f_{cd} \cdot b_w \cdot 0.9 \cdot d$

Effectiveness factor: $v = 0.7 - f_{ck} / 200 \geq 0.5$
$v = 0.7 - 50 / 200 = 0.45 < 0.45$
$v = 0.5$

$V_{Rd2} = 0.5 \cdot 0.5 \cdot 33.3$ N/mm$^2 \cdot 0.9 \cdot 398$ mm = 2982 kN/m

ENV 1992-1-1: 1991:
Section 4.3.2.3 (3)

$V_{wd} = V_{Sd} - V_{Rd1} = 547$ kN/m – 440 kN/m = 107 kN/m

$$A_{sw} = \frac{V_{wd}}{0.9 \cdot d \cdot f_{ywd}}$$

ENV 1992-1-1: 1991
Section 4.3.2.4.3

$$A_{sw} = \frac{107kN}{0.9 \cdot 398mm \cdot 435\,N/mm^2}$$

$$A_{sw} = 6.9\,cm^2/m$$

Minimum shear reinforcement

ENV 1992-1-1: 1991
Section 5.4.2.2

Concrete C50/60, steel S500: $\rho_{w,min} = 0.0013$
$\rho_w = A_{sw} / (b_w \cdot \sin(\alpha))$
$A_{sw} = \rho_w \cdot b_w \cdot \sin(\alpha) = 0.0013 \cdot 100\ cm \cdot \sin(90)$
$A_{sw} = 13\ cm^2 / m > 6.9\ cm^2/m$

The shear reinforcement for the edge beam in the longitudinal bridge direction requires a minimum of 13 cm^2/m, as well, and is added to the shear reinforcement in transverse direction.

Total shear reinforcement:

ENV 1992-1-1: 1991
Section 5.4.2.2

$A_{sw} = 26\ cm^2/m$

Stirrups Ø 12, s = 15 cm, four-shear (gives $A_{sw} = 30.13\ cm^2/m$)

Maximum spacing

Longitudinal spacing

$$V_{Sd} = 741.5\,kN/m < 2/3 \cdot V_{Rd2} = 2/3 \cdot 2982\,kN/m = 1988\,kN/m$$

$s_{max} = 0.6 \cdot d = 0.6 \cdot 398\ mm = 238.8\ mm\ (300\ mm)$
$s = 150\ mm < 238.8\ mm$

Transverse spacing

$s_{max} = d = 398\ mm\ (800\ mm)$ not critical

Check for shear force at smallest depth

Internal forces

$v_{Sd,y}$ [kN/m]	305

Geometry

z_s [mm]	72
h [mm]	414
d [mm]	342

Criterion for elements not requiring design shear reinforcement: $V_{Sd} \le V_{Rd1}$

$V_{Rd1} = [\tau_{Rd} \cdot k \cdot (1.2 + 40 \cdot \rho_1) + 0.15 \cdot \sigma_{cp}] \cdot b_w \cdot d$

ENV 1992-1-1: 1991
Section 4.3.2.3

$\tau_{Rd} = 0.48\ N/mm^2$ Basic design shear for C50/60

$\rho_1 = A_{s1} / (b_w \cdot d) \le 0.02$

ENV 1992-1-1: 1991
Table 4.8

$A_{s1} = 54.54\ cm^2/m$
$d = 0.342\ m$
$\rho_1 = (54.54\ cm^2/m) / (1\ m \cdot 0.342\ m) = 0.016 < 0.02$

$\sigma_{cp} = 0\ N/mm^2$

$k = 1.6 - d = 1.6 - 0.342 = 1.126 > 1$

$$V_{Rd1} = \left[0.48\frac{N}{mm^2} \cdot 1.26 \cdot \left(1.2 + 40 \cdot 0.016\right)\right]\frac{1}{m} \cdot 1m \cdot 0.342m$$

$V_{Rd1} = 380\ kN/m$

$\underline{V_{Sd} = 305\,kN/m < V_{Rd1} = 380\,kN/m}$ Check fulfilled!

Punching
ENV 1992-1-1: 1991 Section 4.3.4

Hanger force

N_{Sd} [kN]	1073

Geometry of bearing plate

l [mm]	420
w [mm]	150
f [mm]	120

Geometry of concrete section

z_s [mm]	72
h [mm]	470
d [mm]	398

Criterion for elements not requiring shear reinforcement: $v_{Sd} \leq v_{Rd1}$

$$v_{Sd} = \frac{V_{sd} \cdot \beta}{u}$$

V_{Sd} total design shear force; V_{Sd} = 1073 kN

β coefficient taking eccentricity of loading into account; here β = 1.0

u critical perimeter; $u = 2 \cdot w + l + \pi \cdot d \cdot 1.5 + 2 \cdot f$

$$u = (2 \cdot 20 + 42 + \pi \cdot 39.8 \cdot 1.5 + 2 \cdot 12) cm = 2936 mm$$

$$v_{Sd} = \frac{1073 kN \cdot 1.0}{2936 mm} = 365 N/mm \text{ (Shear per unit length)}$$

v_{Rd1} shear resistance per unit length

$v_{Rd1} = \tau_{Rd} \cdot k \cdot (1.2 + 40 \cdot \rho_1) \cdot d$

τ_{Rd} basic design shear strength;

$\tau_{Rd} = 0.48\ N/mm^2$

k $k = 1.6 – d = 1.6 – 0.398 = 1.2 > 1$

$$\rho_1 = \sqrt{\rho_{1x} \cdot \rho_{1y}} \leq 0.015$$

$A_{sx} = 15.39\ cm^2/m$

$\rho_{1x} = (15.39\ cm^2/m) / (1\ m \cdot 0.398\ m) = 0.0039$

$A_{sx} = 70.12\ cm^2/m$

$\rho_{1y} = (70.12\ cm^2/m) / (1\ m \cdot 0.398\ m) = 0.0176$

$$\rho_1 = \sqrt{0.0039 \cdot 0.0176} = 0.008 < 0.015$$

$v_{Rd1} = 0.48\ N/mm^2 \cdot 1.2 \cdot (1.2 + 40 \cdot 0.008) \cdot 398\ mm = 348\ N/mm$

$v_{Rd2} = 1.6 \cdot v_{Rd1} = 1.6 \cdot 348\ N/mm = 556.8\ N/mm$

$v_{Rd3} = v_{Rd1} + \Sigma A_{sw} \cdot f_{yd} \cdot \sin(\alpha) / u$

$v_{Rd3} = 348\ N/mm + (19.3\ cm^2/m \cdot 1.5 \cdot 398 mm) \cdot 435\ N/mm^2 / 2596\ mm$

$v_{Rd3} = 541\ N/mm$

$$\underline{v_{Sd} = 365 N/mm < v_{Rd3} = 541 N/mm}$$

D.5.3.2.2 Serviceability limit state

Minimum reinforcement

ENV 1992-2: 1996 Section 4.4.2.2.3

Relevant combination of actions: Non-frequent

$A_s = (0.8 \cdot k_c \cdot k \cdot f_{ctm} \cdot A_{ct}) / \sigma_s$

f_{ctm} tensile strength of the concrete: $f_{ctm} = 4.1$ N/mm^2.

A_{ct} area of concrete within tensile zone just before cracking; $A_{ct} = 0.47$ m^2/m / 2 = 0.235 m^2/m.

σ_s maximum stress permitted in the reinforcement immediately after cracking, depending on the re-bar diameter; $\sigma_s = 200$ N/mm^2 for re-bar Ø 25 (*ENV 1992-1-1: 1991 Table 4.11*)

k_c coefficient taking into account the nature of the stress distribution within the section immediately prior to cracking; $k_c = 0.4$

k 0.88 (interpolated value for h = 0.47 m)

$A_s = (0.8 \cdot 0.4 \cdot 0.88 \cdot 4.1$ N/mm$^2 \cdot 2350$ cm^2/m) / 200 N/mm^2 = 13.6 cm^2/m

13.6 cm^2/m < 70.12 cm^2/m

The minimum reinforcement at the bottom of the slab is already covered, but it still needs to be applied at the top.

Ø 14, s = 10 cm (gives A_s = 15.39 cm^2/m)

Limitation of steel stress

Relevant combination of actions: Non-frequent

Requirement: Steel stress to be limited to $0.8 \cdot f_y = 400$ N/mm^2

Steel stress to be limited to 0.8 fy = 400 (non-frequent)

M_s = 700 kNm/m

$$\mu_{Sds} = \frac{m_{Sds}}{b \cdot d^2 \cdot f_{cd}}$$

$$\mu_{Sds} = \frac{700\,\text{kNm/m}}{(0.398\text{m})^2 \cdot 33.3\,\text{N/mm}^2} = 0.134$$

$\zeta = 0.914$ $\quad z = d \cdot \zeta = 398$ mm $\cdot$ 0.935 = 363.8 mm

A_s = 70.12 cm^2/m

$$\sigma_s = \frac{M_s}{z \cdot A_s} = \frac{700\text{kNm/m}}{363.8\text{mm} \cdot 70.12\,\text{cm}^2/\text{m}} = 274\frac{\text{N}}{\text{mm}^2} < 400\frac{\text{N}}{\text{mm}^2}$$

Crack width

ENV 1992-2: 1996 Table 4.121

For a steel stress of 274 N/mm^2 and re-bar diameter of Ø 25, a maximum re-bar spacing of 150 mm is allowed. The actual spacing measures 140 mm.

D.5.3.2.3 Fatigue

The fatigue assessment is performed for the reinforcing steel. *ENV 1992-2: 1992*
Relevant combination of actions: Non-frequent *Section 4.3.7*

$$\gamma_F \cdot \gamma_{Sd} \cdot \Delta\sigma_{s,equ} \le \frac{\Delta\sigma_{Rsk}(N^*)}{\gamma_{s,fat}}$$

ENV 1992-2: 1996
Section 4.3.7.2

$\gamma_F = 1.0$
$\gamma_{Sd} = 1.0$
$\gamma_{s,fat} = 1.15$

ENV 1992-2: 1996
Table 4.116

$\Delta\sigma_{Rsk}(N^*) = 195\ N/mm^2$
$N^* = 10^6$, $k_1 = 5$, $k_2 = 9$

ENV 1992: 1996
Annex A 106.3

$\Delta\sigma_{s,equ} = \lambda_s \cdot \Delta\sigma_{s,71}$

$\Delta\sigma_{s,71}$ Stress variation due to load model 71 for the characteristic/rare combination of actions including the dynamic factor
$\Delta\sigma_{s,71} = 160.4\ N/mm^2$

$\lambda_s = \lambda_{s,1} \cdot \lambda_{s,2} \cdot \lambda_{s,3} \cdot \lambda_{s,4}$ *ENV 1992-2: 1996* *Table A 106.2*

$\lambda_{s,1}$ $\lambda_{s,1} = 0.65$

$\lambda_{s,2}$ $\lambda_{s,2} = \sqrt[k_2]{\frac{Vol}{25 \cdot 10^6}}$ $Vol = 30 \cdot 10^6$ t / (track · year)

$$\lambda_{s,2} = \sqrt[7]{\frac{30 \cdot 10^6}{25 \cdot 10^6}} = 1.026$$

$\lambda_{s,3}$ $\lambda_{s,3} = \sqrt[k_2]{\frac{N_{years}}{100}}$ $N_{years} = 100$

$$\lambda_{s,3} = \sqrt[7]{\frac{100}{100}} = 1$$

$\lambda_{s,4}$ $\lambda_{s,4} = \sqrt[k_2]{n + (1-n) \cdot s_1^{k_2} + (1-n) \cdot s_2^{k_2}}$

n = 0.12 (taken from *ENV 1993-2: 1997 Section 9.5.3 (8)*)

$$s_1 = \frac{\Delta\sigma_1}{\Delta\sigma_{1+2}};\ s_2 = \frac{\Delta\sigma_2}{\Delta\sigma_{1+2}}$$

$\Delta\sigma_1$, $\Delta\sigma_2$ – Stress variation due to load model 71 on one track
$\Delta\sigma_{1+2}$ – Stress variation due to load model 71 on two tracks

$\Delta\sigma_1 = \Delta\sigma_2 = 68.8\ N/mm^2$
$\Delta\sigma_{1+2} = 160.4\ N/mm^2$

$$s_1 = s_2 = \frac{68.8\ N/mm^2}{160.4\ N/mm^2} = 0.43$$

$$\lambda_{s,4} = \sqrt[7]{0.12 + (1-0.12) \cdot 0.43^7 + (1-0.12) \cdot 0.43^7} = 0.79$$

$\lambda_s = 0.65 \cdot 1.026 \cdot 1 \cdot 0.79 = 0.53$
$\Delta\sigma_{s,equ} = \lambda_s \cdot \Delta\sigma_{s,71} = 0.53 \cdot 160.4\ N/mm^2 = 85\ N/mm^2$

$$\underline{1.0 \cdot 1.0 \cdot 85 \frac{N}{mm^2} = 85 \frac{N}{mm^2} \le \frac{195\ N/mm^2}{1.15} = 169.6 \frac{N}{mm^2}}$$

D.5.3.3 Calculation of deflection

The deflections of concrete structures should be calculated for the quasi-permanent combination of actions taking creep, shrinkage and cracking into account, *ENV 1992-2: 1996 Section 4.4.3.1 (106).* However, the quasi-permanent combination does not include live load due to railway traffic (Annex A, Figure A.8). According to *ENV 1991-3: 1995 Section 6.8.1,* vertical deflections of railway bridges are to be calculated with one track loaded.

Therefore, the following includes permanent loads as well as live loads in the form of one load model 71. Firstly, the vertical deflections are calculated due to permanent loads with respect to creep, shrinkage and cracking. Secondly, an additional vertical deflection due to live load is determined for the cracked section.

The calculation is based on a simplified procedure. Deflections are predicted by empirical interpolation between lower (at uncracked stage) and upper bound (cracked stage). The member is assumed to have a constant section in each state, and deflections are obtained by using the moment - curvature relation (GHALI A., ET AL. *[11]*, pages 303-317).

The equations SPERLING *[36]* listed in the following were used to determine the results given in Figure D.5.10 and Figure D.5.11. Reference is made by numbered equations. The deflections calculated here are only deflections of the bridge deck slab. The total deflection of the bridge is mainly constituted by deflections of the edge beams.

The procedure is also adopted in ENV 1992-1-1: 1991 Appendix 4.

Calculation of effective elastic modulus

The effect of creep is accounted for by using an effective elastic modulus, which is a reduced elastic modulus at time t = ∞. The creep coefficient φ_∞ is taken from Annex C – Preliminary Design.

$$E_{c.eff} = \frac{E_{cm}}{1+\varphi_\infty}$$ (Equ. D.1) Effective elastic modulus

Uncracked

In the uncracked stage the bending moment acting on the member does not exceed the cracking moment. The curvature is calculated with the second moment of area of the total concrete section.

$$I^I = \frac{b \cdot h^3}{12}$$ (Equ. D.2) Second moment of area of

$$k' = \left(\frac{1}{r}\right)^I = \frac{M_{Sd}}{E_{c,eff} \cdot I^I}$$ (Equ. D.3) Curvature

Cracked

At this stage, the bending moment acting on the member exceeds the cracking moment, which means that the concrete tensile strength is exceeded. The stress distribution in the compressive zone is assumed to be linear. The flexural stiffness of the member is determined by combining the compatibility condition (Bernoulli hypothesis) and equilibrium conditions, SPERLING *[36]*, page 15.

$$\alpha_e = \frac{E_s}{E_{c,eff}}$$ (Equ. D.4) Elastic modulus ratio

$$\rho = \frac{A_s}{b \cdot d}$$ (Equ. D.5) Reinforcement

$$\frac{x}{d} = -\alpha_e \cdot \rho + \sqrt{\alpha_e \cdot \rho \cdot (2 + \alpha_e \cdot \rho)}$$ (Equ. D.6) Compression zone

$$I^{II} = \frac{b \cdot x^3}{3} + \alpha_e \cdot A_s \cdot (d - x)^2$$ (Equ. D.7) Second moment of area

$$k'' = \left(\frac{1}{r}\right)^{II} = \frac{M_{Sd}}{E_{c.eff} \cdot I^{II}}$$ (Equ. D.8) Curvature

Tension stiffening (Interpolation)

Even though the section is cracked, the concrete between cracks in the tensile zone gives contribution to the rigidity of the member. This contribution is also referred to ‘tension stiffening’. Therefore an effective or mean value of the member stiffness must be considered in the calculation of the curvature. This is done by interpolation between the lower and upper bound, i.e. interpolation between the curvatures in the uncracked and cracked stage, respectively. The interpolation coefficient is given by the cracking moment, the bending moment acting on the section and coefficients β_1 and β_2. GHALI A., ET AL. *[11]*, page 314.

β_1 accounts for the used reinforcement:

- β_1 = 1.0 for high-bond reinforcing bars
- β_1 = 0.5 for plain bars

β_2 represents the influence of the duration and repetition of loading:

- β_2 = 1.0 for short-time loading
- β_2 = 0.5 for long-time loading

$$\left(\frac{1}{r_m}\right) = \xi \cdot \left(\frac{1}{r}\right)^{II} + (1 - \xi) \cdot \left(\frac{1}{r}\right)^{I}$$ (Equ. D.9) Interpolation

$$\xi = 1 - \beta_1 \cdot \beta_2 \cdot \left(\frac{M_{cr}}{M_s}\right)^2$$ (Equ. D.10) Interpolation coefficient

$$M_{cr} = f_{ctm} \cdot W = f_{ctm} \cdot \frac{h^2 \cdot b}{6}$$ (Equ. D.11) Cracking moment

Shrinkage effect

The effect of shrinkage is accounted for by calculating curvatures in the uncracked and cracked stage and interpolating between both similarly to the procedure mentioned above. The formula corresponds to the one given in *ENV 1992-1-1: 1991 Appendix 4*.

Uncracked

$$k'_{sh} = \left(\frac{1}{r_{sh}}\right)^{I} = \frac{\varepsilon_{cs} \cdot E_s \cdot A_s \cdot z_s^{I}}{E_{c.eff} \cdot I^{I}}$$ (Equ. D.12) Curvature due to shrinkage

Cracked

$$k''_{sh} = \left(\frac{1}{r_{sh}}\right)^{II} = \frac{\varepsilon_{cs} \cdot E_s \cdot A_s \cdot z_s^{II}}{E_{c.eff} \cdot I^{II}}$$ (Equ. D.13) Curvature due to shrinkage

Interpolation

$$k_{sh} = \left(\frac{1}{r_{sh.m}}\right) = \xi \cdot \left(\frac{1}{r_{sh}}\right)^{II} + (1-\xi) \cdot \left(\frac{1}{r_{sh}}\right)^{I}$$ (Equ. D.14) Interpolation

Total curvature

The total curvature due to the applied long-term dead load and shrinkage including creep effects is determined by superposition, SPERLING *[36]*, page 21.

$$k = \frac{1}{r_{tot}} = \left(\frac{1}{r_m}\right) + \left(\frac{1}{r_{sh.m}}\right)$$ (Equ. D.15)

Deformation

The total deformation due to long-term dead loads and shrinkage is determined with the following formula:

$$\delta = k \cdot L^2 \cdot \left(\frac{1}{r}\right)$$ (Equ. D.16)

with

L	span
k	parameter of moment distribution; k = 0.104 for a uniformly distributed load acting on a simply supported beam

Deformation due to live load

The calculation due to the applied live load on the cracked reinforced concrete deck is based on the *Branson* effective moment of inertia, ACI 435 *[2]*.

$$I_e = \left(\frac{M_{cr}}{M}\right)^4 \cdot I^{I} + \left(1 - \left(\frac{M_{cr}}{M}\right)^4\right) \cdot I^{II}$$ (Equ. D.17) Effective moment of inertia

$$\varphi_m = \left(\frac{1}{r_{LL}}\right) = \frac{M}{E \cdot I_e}$$ (Equ. D.18) Mean curvature

Equation D-16 was used here with the parameter $k = \frac{3 - 4 \cdot \alpha^2}{48 \cdot (1-\alpha)}$ (Equ. D.19)

α = a / L, where *a* is the smaller distance of the single train load from the support of the simple beam, and L is the span of the bridge deck.

Alternative design proposal 1: Calculation of deflections			
Geometry			
Width [m]	b [m]	1	
Depth [m]	h [m]	0.61	
Effective depth [m]	d [m]	0.5575	
Internal forces			
Bending moment due to permament load	M [kNm/m]	303.2	
Bending moment due to live load	M [kNm/m]	541.9	
Cracking moment	M_{cr} [kNm/m]	254.27	Equ. D.11
Properties			
Reinforcement elastic modulus	E_s [N/mm^2]	200000	
Concrete elastic modulus	E_{cm} [N/mm^2]	37000	
Creep coefficient	φ_∞	1.9	
Shrinkage coefficient	$\varepsilon_{sc.\infty}$	-0.0003	
Concrete effective modulus	$E_{c.eff}$ [N/mm^2]	12758.62	Equ. D.1
Concrete tensile strength	f_{ctm} [N/mm^2]	4.1	
First moment of area	W [m^3]	0.0620	
Modulus ratio	$\alpha_e = E_s / E_{c.eff}$	15.6757	Equ. D.4
Reinforcement area	A_s [cm^2/m]	54.54	
	ρ	0.009783	Equ. D.5
	x/d	0.421299	Equ. D.6
Depth of compression zone	x	0.235	
Calculation of deflection due to permament loads and shrinkage			
Uncracked			
Second moment of area	I' [m^4]	0.018915	Equ. D.2
Curvature due to permanent loads	k'	0.001256	Equ. D.3
Curvature due to shrinkage	k'_{sh}	0.000342	Equ. D.12
Cracked			
Second moment of area	I" [m^4]	0.013218	Equ. D.7
Curvature due to permanent loads	k"	0.001798	Equ. D.8
Curvature due to shrinkage	k''_{sh}	0.000626	Equ. D.13
Interpolation			
Coefficient for high bond re-bars	β_1	1	
Coefficient for long-time loading	β_2	0.5	
Interpolation coefficient	ξ	0.6484	
Total curvature due to permanent loads	k	0.001607	Equ. D.9
Total curvature due to shrinkage	k_{sh}	0.000526	Equ. D.14
Curvature due to permanent load + shrinkage	k_{tot}	0.002134	Equ. D.15
Deflection due to permantent load + shrinkage	δ [mm]	**22.9**	Equ. D.16
Calculation of deflection due to applied live load			
Effective second moment of area	I_e [m^4]	0.013494	Equ. D.17
Curvature	k	0.001085	Equ. D.18
Parameter (single load at y = 2.875 m)	α	0.077860	Equ. D.19
Deflection due to live load	δ [mm]	7.5	
Total deflection (only concrete bridge deck)	total δ [mm]	**30.4**	

Fig. D.29. Calculation of deflection, alternative design proposal 1

Alternative design proposal 2: Calculation of deflections			
Geometry			
Width [m]	b [m]	1	
Depth [m]	h [m]	0.47	
Effective depth [m]	d [m]	0.398	
Internal forces			
Bending moment due to permament load	M [kNm/m]	286.1	
Bending moment due to live load	M [kNm/m]	541.9	
Cracking moment	M_{cr} [kNm/m]	150.95	Equ. D.11
Properties			
Reinforcement elastic modulus	E_s [N/mm^2]	200000	
Concrete elastic modulus	E_{cm} [N/mm^2]	37000	
Creep coefficient	φ_∞	1.9	
Shrinkage coefficient	$\varepsilon_{sc.\infty}$	-0.0003	
Concrete effective modulus	$E_{c.eff}$ [N/mm^2]	12758.62	Equ. D.1
Concrete tensile strength	f_{ctm} [N/mm^2]	4.1	
First moment of area	W [m^3]	0.036817	
Modulus ratio	$\alpha_e = E_s / E_{c.eff}$	15.6757	Equ. D.4
Reinforcement area	A_s [cm^2/m]	70.12	
	ρ	0.0176	Equ. D.5
	x/d	0.5167	Equ. D.6
Depth of compression zone	x	0.206	
Calculation of deflection due to permament loads and shrinkage			
Uncracked			
Second moment of area	I' [m^4]	0.008652	Equ. D.2
Curvature due to permanent loads	k'	0.002592	Equ. D.3
Curvature due to shrinkage	k'_{sh}	0.000621	Equ. D.12
Cracked			
Second moment of area	I'' [m^4]	0.006966	Equ. D.7
Curvature due to permanent loads	k''	0.003219	Equ. D.8
Curvature due to shirnkage	k''_{sh}	0.000911	Equ. D.13
Interpolation			
Coefficient for high bond re-bars	β_1	1	
Coefficient for long-time loading	β_2	0.5	
Interpolation coefficient	ξ	0.8608	
Total curvature due to permanent loads	k	0.003132	Equ. D.9
Total curvature due to shrinkage	k_{sh}	0.000870	Equ. D.14
Curvature due to permanent load + shrinkage	k_{tot}	0.004002	Equ. D.15
Deflection due to permantent load + shrinkage	δ [mm]	**42.9**	Equ. D.16
Calculation of deflection due to applied live load			
Effective second moment of area	I_e [m^4]	0.006976	Equ. D.17
Curvature	k	0.002099	Equ. D.18
Parameter (single load at y = 2.875 m)	α	0.077860	Equ. D.19
Deflection	δ [mm]	**14.5**	
Total deflection (only concrete bridge deck)	δ [mm]	**57.4**	

Fig D.30. Calculation of deflection, alternative design proposal 2

D.5.3.4 Summary of reinforcement

Neglecting end-cross girder

Alternative design proposal 1

Bridge deck: Transverse

Top:	Ø 14, s = 10 cm
Bottom:	Ø 25, s = 9 cm

Bridge deck: Longitudinal

Top:	Ø 10, s = 15 cm
Bottom:	Ø 12, s = 10 cm

Edge beam

Top:	Ø 12, s = 15 cm
Bottom:	Ø 12, s = 10 cm

Footpath:

Edge stirrups:	Ø 10, s = 15 cm

Shear stirrups: Ø 12, s = 15 cm (four-shear)

Alternative design proposal 2

Bridge deck: Transverse

Top:	Ø 14, s = 10 cm
Bottom:	Ø 25, s = 14 cm (two layers)

Bridge deck: Longitudinal

Top:	Ø 10, s = 15 cm
Bottom:	Ø 14, s = 10 cm

Edge beam

Top:	Ø 12, s = 15 cm
Bottom:	Ø 14, s = 10 cm

Footpath:

Edge stirrups:	Ø 10, s = 15 cm

Shear stirrups: Ø 12, s = 15 cm (four-shear)

Summary of reinforcement: Bridge deck

Geometry	[m]
Bridge length	100.00
Width on the top	11.85
Width on the bottom	10.59
Width of edge beam	1.30
Length of cantilever	0.60
Length of stirrup	2.50
Length of cantilever strirrups	1.00

Fig. D.31. Geometric properties for calculation of steel weight

The calculation of the steel weight is based on the geometric properties listed in Figure D.31.

Alternative design proposal 1: h = 0.61 m at mid-span						
	Ø [mm]	Nom. mass [kg/m]	s [cm]	Number	Length [m]	Weight [kg]
Bridge deck: Transverse						
Top	14	1.21	10.00	1000.00	11850.00	14339
Bottom	25	3.85	9.00	1111.11	11766.67	45302
Bridge deck: Longitudinal						
Top	10	0.62	15.00	74.33	7433.33	4586
Bottom	12	0.89	10.00	92.90	9290.00	8250
Edge beam						
Top	12	0.89	15.00	17.33	1733.33	1539
Bottom	12	0.89	10.00	26.00	2600.00	2309
Cantilever stirrups	10	0.62	15.00	1333.33	1333.33	823
Shear stirrups	12	0.89	15.00	2666.67	6666.67	5920
[1] Additional reinforcement accounting for overlapping					**Total**	83067
of re-bars and unconsidered reinforcement					+ 15% [1]	**95527**

Fig. D.32. Reinforcement steel weight of design proposal 1

Alternative design proposal 1: h = 0.47 m at mid-span						
	Ø [mm]	Nom. mass [kg/m]	s [cm]	Number	Length [m]	Weight [kg]
Bridge deck: Transverse						
Top	14	1.21	10.00	1000.00	11850.00	14339
Bottom	25	3.85	14.00 2 layers	1428.57	15128.57	58245
Bridge deck: Longitudinal						
Top	10	0.62	15.00	74.33	7433.33	4586
Bottom	14	1.21	10.00	92.90	9290.00	11241
Edge beam						
Top	12	0.89	15.00	17.33	1733.33	1539
Bottom	14	1.21	10.00	26.00	2600.00	3146
Cantilever stirrups	10	0.62	15.00	1333.33	1333.33	823
Shear stirrups	12	0.89	15.00	2666.67	6666.67	5920
[1] Additional reinforcement accounting for overlapping					**Total**	99839
of re-bars and unconsidered reinforcement					+ 15% [1]	**114814**

Fig. D.33. Reinforcement steel weight of design proposal 2

D.6 End cross girder

D.6.1 Ultimate limit state assessment

D.6.1.1 Bending and longitudinal force

The two critical points to be checked for are the middle of the end cross girder and the end above the bearings.

1. Middle of end cross girder

$x = 0$ m $\quad\quad y = 5.075$ m

Internal forces

$m_{Sd,y}$ [kNm/m]	167.8
$n_{Sd,y}$ [kN/m]	-2650.6

Geometry

z_p [mm]	103
h [mm]	780
d [mm]	677
z_{s1} [mm]	287

$f_{cd} = f_{ck} / \gamma_s = 50\ N/mm^2 / 1.15 = 33.3\ N/mm^2$

$m_{sds} = m_{Sd,y} - n_{Sd,y} \cdot z_{s1}$
$m_{sds} = 167.8\ kNm/m - (-2650.6\ kN/m) \cdot 0.287\ m$
$m_{sds} = 928.52\ kNm/m$

$$\mu_{Sds} = \frac{m_{Sds}}{b \cdot d^2 \cdot f_{cd}}$$

$$\mu_{Sds} = \frac{928.52\,kNm/m}{(0.677m)^2 \cdot 33.3\,N/mm^2} = 0.06$$

SCHNEIDER [29], page 5.126

$\mu_{Sds,lim} = 0.206$ (for concrete class > C40/50)
$\xi_{lim} = 0.35$

$\zeta = 0.96 \quad\quad z = d \cdot \zeta = 677\ mm \cdot 0.96 = 649.9\ mm$
$\xi = 0.35 \quad\quad x = d \cdot \xi = 677\ mm \cdot 0.35 = 236.95\ mm$
$\varepsilon_{s1} = 0.02$

$\varepsilon_p = \varepsilon_{pm} + \varepsilon_{s1}$
$\varepsilon_{pm} = 0.0034$ (corresponds to $P_{m,t}$ in *Annex B: Preliminary design*)
$\varepsilon_p = 0.0034 + 0.02 = 0.0234 > 0.01$

SCHNEIDER [29] page 5.128 / Tafel 1a

$f_{pd} = 0.9 \cdot f_{pk} / \gamma_s$
$f_{pd} = 0.9 \cdot 1229.86\ N/mm^2 / 1.15 = 962.5\ N/mm^2$

$$A_s = \frac{1}{f_{pd}} \cdot \left(\frac{m_{Sds}}{z} + n_{Sd}\right)$$

$$A_s = \frac{1}{962.5\,N/mm^2} \cdot \left(\frac{928.51kNm/m}{649.9mm} + (-2650.6kN/m)\right) = -12.7cm^2/m < 0$$

ENV 1992-1-1: 1991, Section 4.2.3.3.3 (6)

No additional reinforcement required.

2. End of end cross girder above bearings

X = 0 m
y = 0 m

Internal forces

$m_{Sd,y}$ [kNm/m]	-1062.1
$n_{Sd,y}$ [kN/m]	-7046.2

Geometry

z_p [mm]	625.4
h [mm]	1027.3
d [mm]	401.9
z_{s1} [mm]	-111.75

$f_{cd} = f_{ck} / \gamma_s = 50\ N/mm^2 / 1.15 = 33.3\ N/mm^2$

$m_{sds} = m_{Sd,y} - n_{Sd,y} \cdot z_{s1}$
$m_{sds} = -1026.1\ kNm/m - (-7046.2\ kN/m) \cdot (-0.11175)\ m$
$m_{sds} = -1813.5\ kNm/m$
$m_{sds} = 1813.5\ kNm/m$! For upper reinforcement !

$$\mu_{Sds} = \frac{m_{Sds}}{b \cdot d^2 \cdot f_{cd}}$$

SCHNEIDER [29], page 5.126

$$\mu_{Sds} = \frac{1813.5\,kNm/m}{(0.4019m)^2 \cdot 33.3\,N/mm^2} = 0.337$$

$\mu_{Sds,lim} = 0.206$ (for concrete class > C40/50)

$\zeta = 0.86$ $z = d \cdot \zeta = 401.9\ mm \cdot 0.86 = 345.6\ mm$
$\xi = 0.35$ $x = d \cdot \xi = 401.9\ mm \cdot 0.35 = 140.7\ mm$
$\varepsilon_{s1} = 0.0073$

$\varepsilon_p = \varepsilon_{pm} + \varepsilon_{s1}$
$\varepsilon_{pm} = 0.0033$
$\varepsilon_p = 0.0033 + 0.0073 = 0.0106 \geq 0.01$

Schneider 12 p. 5.128 Tafel 1a

$f_{pd} = 0.9 \cdot f_{pk} / \gamma_s$
$f_{pd} = 0.9 \cdot 1229.86\ N/mm^2 / 1.15 = 962.5\ N/mm^2$

$$A_s = \frac{1}{f_{pd}} \cdot \left(\frac{m_{Sds}}{z} + n_{Sd} \right)$$

ENV 1992-1-1: 1991, Section 4.2.3.3.3 (6)

$$A_s = \frac{1}{962.5\,N/mm^2} \cdot \left(\frac{1813.5\,kNm/m}{345.6mm} + (-7046.2kN/m) \right) = -18cm^2/m < 0$$

No additional reinforcement required.

D.6.1.2 Shear

The relevant shear force is taken at a distance 1360 mm from the inner bearing which is the thinnest point of the end cross girder.

Internal forces

$v_{Sd,y}$ [kN/m]	598.6
$n_{Sd,y}$ [kN/m]	-2573.6

Geometry

h [mm]	726.3
nom c [mm]	40
d [mm]	681.3

Elements not requiring design shear reinforcement

ENV 1992-1-1: 1991
Section 4.3.2.3

$V_{Sd} \leq V_{Rd1}$

$V_{Rd1} = [\tau_{Rd} \cdot k \cdot (1.2 + 40 \cdot \rho_1) + 0.15 \cdot \sigma_{cp}] \cdot b_w \cdot d$

$\tau_{Rd} = 0.48$ N/mm^2 Basic design shear for C50/60

$\rho_1 = A_{s1} / (b_w \cdot d) \leq 0.02$

$A_{s1} = 5.24$ cm^2/m minimum reinforcement
d = 0.6813 m
$\rho_1 = (5.24 \text{ cm}^2/\text{m}) / (1 \text{ m} \cdot 0.6813 \text{ m}) = 0.00077$

$\sigma_{cp} = N_{Sd} / A_c = 2573.6 \text{ kN/m} / (726.3 \text{ mm} \cdot 1\text{m}) = 3.54 \text{ N/mm}^2/\text{m}$ (compression positive)

k = 1.6 – d = 1.6 – 0.6813 = 0.9187

V_{Rd1}=[0.48N/mm^2·0.9187·(1.2 + 40·0.00077) + 0.15·3.54N/mm^2]/m·1m·0.6813m
V_{Rd1} = 731.5 kN/m

V_{Sd} = 598.6 kN/m < V_{Rd1} = 731.5 kN/m

No shear reinforcement required.

D.6.1.3 Punching at bearings

ENV 1992-1-1: 1991
Section 4.3.4

Internal force (maximal bearing forces, on the safe side)

N_{Sd} [kN]	16051.2

Geometry of bearing plate

l [mm]	1436
w [mm]	1040

Geometry of end cross girder

h [mm]	726.3
nom c [mm]	40
d [mm]	681.3

$$v_{Sd} = \frac{V_{sd} \cdot \beta}{u}$$

V_{Sd} total design shear force; V_{Sd} = 16051.2 kN

β corner column, β = 1.5

ENV 1992-1-1: 1991
Figure 4.21 (β)

u critical perimeter,

$u = w + l + \cdot\pi/2 \cdot d \cdot 1.5$

$u = 1040 \text{ mm} + 1436 \text{ mm} + \pi/2 \cdot 681.3 \text{ mm} \cdot 1.5 = 4093.06 \text{ mm}$

$$v_{Sd} = \frac{16051.2\text{kN} \cdot 1.5}{4093.06\text{mm}} = 5882.34 \,\text{N/mm}$$

v_{Rd1} shear resistance per unit length

$v_{Rd1} = \tau_{Rd} \cdot k \cdot (1.2 + 40 \cdot \rho_1) \cdot d$

τ_{Rd} basic design shear strength

$\tau_{Rd} = 0.48 \text{ N/mm}^2$

ENV 1992-1-1: 1991
Table 4.8

k $k = 1.6 – d = 1.6 – 0.6813 = 0.9137$

$$\rho_1 = \sqrt{\rho_{1x} \cdot \rho_{1y}} + \frac{\sigma_{cpo}}{f_{yd}} \leq 0.015$$

σ_{cpo} concrete stress due to initial prestress;

$\sigma_{cpo} = 5.1 \text{ N/mm}^2$

f_{yd} design yield stress of the reinforcement;

$f_{yd} = f_y / 1.15 = 435 \text{ N/mm}^2$

$A_{sx} = 5.24 \text{ cm}^2/\text{m}$ minimal reinforcement

$\rho_{1x} = (5.24 \text{ cm}^2/\text{m}) / (1 \text{ m} \cdot 0.6813 \text{ m}) = 0.00077$

$\rho_{1y} = \rho_{1x} = 0.00077$

$\rho_1 = 0.00077 + 5.1 \text{ N/mm}^2 / 435 \text{ N/mm}^2 = 0.0162 > 0.0125$

$v_{Rd1} = 0.48 \text{ N/mm}^2 \cdot 0.9137 \cdot (1.2 + 40 \cdot 0.0125) \cdot 681.3 \text{ mm} = 507.9 \text{ N/mm}$

$v_{Sd} = 5882.34 \text{ N/mm} > v_{Rd1} = 507.9 \text{ N/mm}$

Since, $v_{Sd} > v_{Rd1}$ reinforcement is required so that $v_{Sd} \leq v_{Rd3}$.

$v_{Sd} = v_{Rd3} = v_{Rd1} + A_{SW} \cdot f_{yd} \cdot \sin\alpha / u$

$\alpha = 90°$

$f_{yd} = 435 \text{ N/mm}^2$

$u = 4093.06 \text{ mm}$

$$A_{SW} = \frac{(v_{Sd} - v_{Rd1}) \cdot u}{f_{yd} \cdot \sin\alpha} = \frac{(5882.34\text{N/mm} - 537.8\text{N/mm}) \cdot 4093.06\text{mm}}{435\text{N/mm}^2 \cdot 1} = 502.89$$

Chosen reinforcement: 85 x two-shear stirrups Ø20, A = 533.8 cm²

D.6.2 Serviceability limit state assessment

For classification of assessment conditions category C is assumed.

ENV 1992-2: 1996 4.4.0.3 Tab. 4.118

D.6.2.1 Limitation of stress

1. *At time of prestressing*

Concrete compressive stress should be limited to 0.6 $f_c(t)$. Prestressing will be performed at the time when the concrete has its full compressive strength.

ENV 1992-1-1: 1991 Section 4.4.1.1 (102)

$$0.6\ f_c(t) = 0.6 \cdot f_{ck} = 0.6 \cdot 50\ N/mm^2 = 30\ N/mm^2$$

If the compressive stress in concrete does not exceed 0.45 $f_c(t)$, creep non-linearity does not need to be considered.

$$0.45\ f_c(t) = 0.45 \cdot f_{ck} = 0.45 \cdot 50\ N/mm^2 = 22.5\ N/mm^2$$

The maximum compression stress in the concrete at time of prestressing is:

$$|\sigma_c| = 17.8\ N/mm^2 < 22.5\ N/mm^2$$

2. *Non-frequent* combination of actions:

The concrete compressive stress should be limited to:

ENV 1992-2: 1991 Section 4.4.1.1 (103)

$$0.6\ f_{ck} = 0.6 \cdot 50\ N/mm^2 = 30\ N/mm^2$$

The maximum compression stress in the concrete is:

$$|\sigma_c| = 28.4\ N/mm^2 < 30\ N/mm^2$$

The tensile stress in the reinforcement steel should be limited to:

ENV 1992-2: 1991 Section 4.4.1.1 (105)

$$0.8\ f_{yk} = 0.8 \cdot 500 N/mm^2 = 400\ N/mm^2$$

The maximum tensile force in the punch reinforcement is:

$$\sigma_S = \frac{v_{Sd,ser} \cdot u}{A_S} = \frac{3921.56 N/mm \cdot 4039.6 mm}{533.8 cm^2} = 296.8 N/mm^2$$

$$\sigma_S = 296.8\ N/mm^2 < 0.8\ f_{yk} = 400\ N/mm^2$$

3. *Quasi-permanent* combination of actions:

After all losses, the stress in the transversal prestressing steel shall not exceed the elastic range and should be limited to:

ENV 1992-2: 1991 Section 4.4.1.1, (104) & (106)

$$0.65\ f_{pk} = 0.65 \cdot 1229.86\ N/mm^2 = 800\ N/mm^2$$

According to Annex B: Preliminary Design, the stress level is as follows:

$$\sigma_S = 675.6\ N/mm^2 < 800\ N/mm^2$$

D.6.2.2 Limit states of cracking

1. *Non-frequent* combination of actions:

Where the stress in concrete is greater than -1 N/mm^2, minimum reinforcement is required.

ENV 1992-2: 1996 4.4.2.2.2. (101)

The minimum compression stress in concrete is -2.4 N/mm^2 (Figure C-23). There is no minimum reinforcement required.

2. <u>*Quasi-permanent*</u> combination of actions

ENV 1992-2: 1996
4.4.2.1 (106)

No tensile stress shall be allowed.

The minimum compression stress in the concrete is -1.3 N/mm^2 (Figure C.23), and so no tensile stresses occur.

3. <u>*Frequent*</u> combination of actions

If the stresses in the concrete are limited to $\sigma_c \leq f_{ctm}$ no extra minimum reinforcement is required.

$$\sigma_c = -2.4 \text{ N/mm}^2 \leq f_{ctm} = 4.1 \text{ N/mm}^2$$

There is no minimum reinforcement required to avoid cracking in the cross girder.

The necessary minimum reinforcement is then to be calculated according to *ENV 1992-2: 1996, 4.4.2.2.3*.

In transverse direction:

$$\rho_S = \frac{0.8 \cdot k_c \cdot k \cdot f_{ctm}}{\sigma_S}$$

$k_c = 0.4$
$k = 0.664$ (h = 0.78 m)
$f_{ctm} = 4.1 \text{N/mm}^2$
$\sigma_S = 260 \text{ N/mm}^2$ (Ø 10 mm)

ENV 1992-2: 1996, Table 4.120

$$\rho_S = \frac{0.8 \cdot 0.4 \cdot 0.664 \cdot 4.1 \text{N/mm}^2}{260 \text{N/mm}^2} = 3.35 \cdot 10^{-3}$$

$A_S = \rho_S A_{ct} = 3.35\ 10^{-3}$ (0.78 m 4.1/(8.2+6.8))
$A_S = 7.1 \text{ cm}^2\text{/m}$

<u>Ø 10 s = 10 cm (A_S = 7.85 cm^2/m)</u>

In longitudinal direction (absence of prestressing):

$$\rho_S = \frac{0.8 \cdot k_c \cdot k \cdot f_{ctm}}{\sigma_S}$$

$k_c = 0.4$
$k = 0.664$ (h = 0.78 m)
$f_{ctm} = 4.1 \text{N/mm}^2$
$\sigma_S = 360 \text{ N/mm}^2$ (Ø 10 mm)

ENV 1992-2: 1996, Table 4.120

$$\rho_S = \frac{0.8 \cdot 0.4 \cdot 0.664 \cdot 4.1 \text{N/mm}^2}{360 \text{N/mm}^2} = 2.42 \cdot 10^{-3}$$

$A_S = \rho_S A_{ct} = 2.42\ 10^{-3}$ (0.78 m 4.1/(8.2+6.8))
$A_S = 5.2 \text{ cm}^2\text{/m}$

<u>Ø 10 s = 15 cm (A_S = 5.24 cm^2/m)</u>

D.7 Handrails

Loads

Horizontal load on top holm of handrail:
0.8 kN/m (γ_Q = 1.5)

ENV 1991-2-1: 1995, 6.4

Geometry

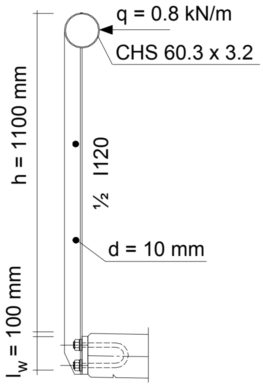

Handrail:	CHS 60.3x3.2
Intermediate holms:	Wire rope, d = 10 mm
Posts:	½ I 120
Anchorage plate:	130x200x20 [mm]
Distance of posts:	l = 3 m
Height of handrail:	h = 1.1 m
Length of welds:	l_w = 100mm
Thickness of welds:	a_w = 4mm

Material

FE 275 $f_{yd} = \frac{f_y}{\gamma_{M0}} = \frac{275N/mm^2}{1.1} = 250N/mm^2$

Bending in handrail

$M_{z,Sd} = 0.086\ q\ \gamma_Q\ l^2 = 0.086\ 0.8\ kN/m\ 1.5\ (3\ m)^2 = 0.9288\ kNm$

SCHNEIDER [29], page 4.11

The criterion to fulfil is:

$$\frac{M_{z,Sd}}{W_{el,z} \cdot f_{yd}} \leq 1$$

ENV 1993-1-1: 1992, 5.4.8.2

$$\frac{0.9288kNm}{7.78cm^3 \cdot 250N/mm^2} = 0.48 \leq 1$$

Bending in posts

$M_{y,Sd} = l\ q\ \gamma_Q\ h = 3\ m\ 0.8\ kN/m\ 1.5\ 1.1m = 3.96\ kNm$

The criterion to fulfil is:

$$\frac{M_{y,Sd}}{W_{el,y} \cdot f_{yd}} \leq 1$$

ENV 1993-1-1: 1992, 5.4.8.2

$$\frac{3.96kNm}{18.2cm^3 \cdot 250N/mm^2} = 0.87 < 1$$

Normal stress in the welds

$M_{y,Sd} = l\ q\ \gamma_Q\ h = 3\ m\ 0.8\ kN/m\ 1.5\ 1.1m = 3.96\ kNm$

The criterion to fulfil is:

$$\frac{M_{y,Sd}}{W_{el,y} \cdot f_u / \gamma_{Mw}} \leq 1$$

ENV 1993-1-1: 1992, Annex M (5)

$$\frac{3.96kNm}{13.33cm^3 \cdot 390N/mm^2 / 1.25} = 0.95 < 1$$

D.8 Drainage

In the following, the dimensions of drainage pipes are determined based on rainfall data for Dresden, Germany.

Rain discharge: $Q_r = \psi_{sm} \cdot r_{T(n)} \cdot A_E$

SCHNEIDER [29], page 13.62

A_E is the area which has to be drained. It is equal to the plane area of the bridge deck:

$$A_E = 100m \cdot 11.75m = 1175m^2 = 0.1175ha$$

$r_{T(n)}$ is the rail yield factor depending on the location (here: Dresden, Germany):

$$r_{T(n)} = r_{15(1)} = 102 \frac{l}{s \cdot ha}$$

ψ_{sm} is the discharge coefficient, which varies for different surfaces and materials. Since the bridge deck surface is partly of plain concrete (footpaths) and partly covered with ballast, the discharge coefficient of each surface has to be considered with the respective area.

For railway tracks: $\psi_{rw} = 0.4$

For concrete surfaces: $\psi_c = 0.9$

Area of railway track: $A_{rw} = 100m \cdot 8.4m = 840m^2$

Area of concrete surfaces: $A_c = 1175m^2 - 840m^2 = 335m^2$

$$\psi_{sm} = \frac{840m^2 \cdot 0.4 + 335m^2 \cdot 0.9}{1175m^2} = 0.54$$

$$\underline{Q_r = 0.54 \cdot 102 \frac{l}{s \cdot ha} \cdot 0.1175ha = 6.47 \frac{l}{s}}$$

Selected drainage pipe: Nominal diameter: DN = 250 mm

→ The critical values for slope and flow velocity in respect of sedimentation are:

v_{crit} = 0.52 m/s

I_{crit} = 1.63 $^{o}/_{oo}$

SCHNEIDER [29], page 13.70

For these critical values, the DN 250 drainage pipe with roughness coefficient k_b = 0.75 has a discharge capacity of Q = 26.3 l/s > Q_r = 6.47 l/s

SCHNEIDER [29], page 13.72

D.9 Bearings

D.9.1 Pot bearings

MAURER SÖHNE GmbH & Co. KG [20]

At each support there are two pot bearings either TF-10, TGa-10 or TGe-10 with a centre distance of a = 0.87m. Each pair shares the vertical force F_V and the bending moment about the horizontal longitudinal axis M_X. Additionally there is a bending moment due to the eccentricity of the arch centre line to the neutral axis of the two pot bearings, e = 0.062 m. The allowed vertical load for each pot bearing is 10000kN.

$$\max F_v = \frac{F_V}{2} + \frac{M_x}{a} - \frac{F_v \cdot e}{a}$$

$$= \frac{16052\text{kN}}{2} + \frac{2082\text{kNm}}{0.87\text{m}} - \frac{16052\text{kN} \cdot 0.062\text{m}}{0.87\text{m}} = 9275.2\text{kN} < 10000\text{kN}$$

The allowed horizontal loads are 10% of the vertical load limits – 1000kN. The maximum horizontal forces caused by the actions on the bridge do not exceed this limit. Therefore no additional structural elements need to be applied to bear the horizontal forces.

MAURER SÖHNE GmbH & Co. KG provides bearings with allowed horizontal eccentricities of the vertical force by shifting up to ±150 mm. The present maximal horizontal movement is 102 mm and thus below that value.

D.9.2 Stilt bearing

The fixed bearing can consist of a plate with a cylindrical upper surface, which is attached to the abutment. Its dimensions can be smaller than the dimensions in the moveable bearing. In the following only the moveable bearing is considered.

D.9.2.1 Vertical plate

Due to the bending moments in the arches and the end cross girder and the torsional moment in the edge beams, the stilt bearing receives a not uniformly distributed load. It is shown in Figure D.34.

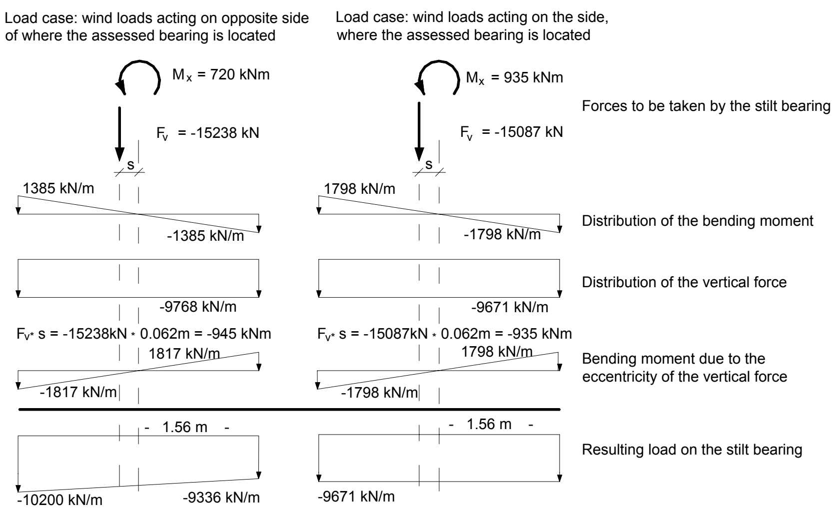

Fig. D.34. Load distribution on the stilt bearing

Due to the lack of appropriate calculation models for Hertz pressing between cylinder and plane with a linear distributed load, the maximum value was assumed to form the value of an evenly distributed dummy load. The width of the stilt bearing is b = 1.56 metres. The vertical force assumed for assessment is:

F = 10200 kN/m·1.56 m = 15912 kN

1. Hertz pressing

The vertical force is transferred through a contact surface between the vertical plates above and below and the stilt plate. Therefore, it has to be ensured that this contact surface does not exceed the area supplied by the vertical plate. The consideration of the horizontal movements to be provided has to be included into the calculation.

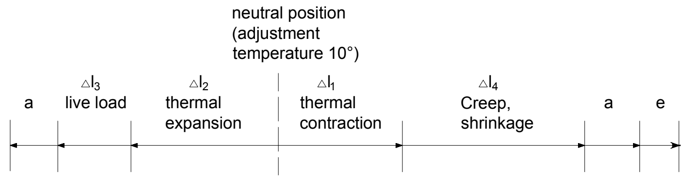

Maximum horizontal displacement:

Temperature changes:

Δl_1 = 0.037 m (towards mid-span)

Δl_2 = 0.04 m (towards abutments)

Horizontal movement of end of span due to live load after adjustment of the bearing

Δl_3 = 0.015 m (towards abutments)

Creep and shrinkage

Δl_4 = 0.065 m (towards mid-span)

Width of the contact surface:

$$2 \cdot a = 2 \cdot 1.52 \cdot \sqrt{\frac{F \cdot r}{b \cdot E}}$$

PETERSEN [24], page 1153

with F = 15912 kN
r = 0.4 m
b = 1.56 m
E = 210000 N/mm^2

$$2 \cdot a = 2 \cdot 1.52 \cdot \sqrt{\frac{15912 kN \cdot 0.4 m}{1.56 m \cdot 210000 N/mm^2}}$$

= 13.4 mm

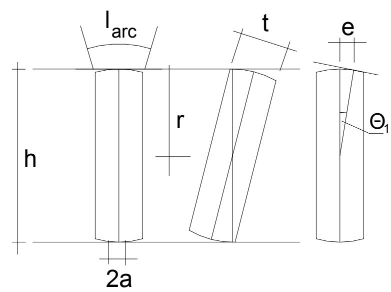

Fig. D.35. **G**eometry of the vertical plate

Eccentricity caused by angular rotation of the bridge deck:

e = r Θ_1 = 0.4 m 3.49mrad = 1.4 mm (towards mid-span)

Considering the deviation between the real load distribution underneath the contact surfaces and the calculated load according to *Hertz* an additional safety bow length is added:

l_{safe} = 10 mm

Required bow length of the cylindrical surface:

$l_{arc} \geq \Delta l_1/2 + \Delta l_2/2 + \Delta l_3/2 + \Delta l_4/2 + 2\,a + 2\,e + l_{safe}$

≥ 18.5 mm + 20 mm + 7.5 mm + 32.5 mm + 13.4 mm+ 1.4 mm + 10 mm

≥ 103.3 mm

With the thickness of the vertical plate t = 110 mm the present bow length of the cylindrical surface is:

<u>l_{arc} = 110.1 mm > 103.3 mm</u>

Furthermore the Hertz pressing has to be examined in the contact surface.
Allowed Hertz pressing:

$$\sigma_{r,d,H} = 1.77 \cdot f_u = 1.77 \cdot 550N/mm^2 = 973.5N/mm^2 \text{; S 460 ML}$$

ENV 1337-4

Present Hertz pressing:

$$\sigma_{d,H} = 0.418\sqrt{\frac{F \cdot E}{b \cdot r}} = 0.418 \cdot \sqrt{\frac{15912kN \cdot 210000N/mm^2}{1560mm \cdot 400mm}} = 967.3N/mm^2$$

PETERSEN [24], page 1153

$$\underline{\sigma_{d,H} = 967.3N/mm^2 < 973.5N/mm^2 = \sigma_{r,d,H}}$$

2. Stresses in vertical plate

l_K = 2 r = 800 mm

ENV 1993-1-1: 1992, 5.5.1.1

$$i_{min} = \sqrt{\frac{Imin}{A}} = \sqrt{\frac{\frac{b \cdot t^3}{12}}{b \cdot t}} = \sqrt{\frac{\frac{1560mm \cdot (110mm)^3}{12}}{1560mm \cdot 110mm}} = 31.75mm$$

$$\bar{\lambda} = \frac{\lambda}{\lambda_1} = \frac{\frac{l_K}{i_{min}}}{\pi\sqrt{\frac{E}{f_y}}} = \frac{\frac{800mm}{31.75mm}}{\pi\sqrt{\frac{210000N/mm^2}{430N/mm^2}}} = 0.36$$

χ = 0.88 *ENV 1993-1-1: 1992, Table 5.5.2*

$$\sigma_{S,d} = \frac{F}{b \cdot t} = \frac{15912kN}{1560mm \cdot 110mm} = 92.7N/mm^2$$

$$\sigma_{R,d} = \frac{X \cdot fy}{\gamma_{M1}} = \frac{0.88 \cdot 430N/mm^2}{1.1} = 344N/mm^2$$

$\underline{\sigma_{S,d} = 92.7 \text{ N/mm}^2 < 344 \text{ N/mm}^2 = \sigma_{R,d}}$

3. Stresses in the concrete below the load distribution plate

For the abutments concrete class C30/37 is used. The plate below the stilt bearing has a thickness of 20 mm. The pressure is distributed like in Figure D.34 with a maximum of -10200 kN/m. The allowed maximal compression stresses in the concrete is:

$$f_{cd} = \frac{f_{ck}}{\gamma_c} = \frac{30N/mm^2}{1.5} = 20N/mm^2$$

The necessary width w_c of the load distribution plate is:

$$w_c = \frac{10200kN/m}{20N/mm^2} = 510mm$$

Stiffening plates have to be arranged to support the load distribution into this horizontal plate.

MAURER SÖHNE GmbH & Co. KG [19]

D.9.2.2 Middle compression support

The additional bearing in the middle of the end cross girder receives only vertical loads. It is not subjected to horizontal forces, bending moments or horizontal deflections. The maximum static load is -1337 kN. The dynamic increase is 20 % according to a proposal of P. TVEIT. So the maximum vertical load the bearing is to assess for is:

$maxF_v$ = -1337 kN · 1.2 = 1604.4 kN

MAURER SÖHNE GmbH & Co. KG an elastomeric bearing type 1/2 – 1800 was chosen. The allowed maximal vertical load is 1800 kN and therefore above the necessary value.

MAURER SÖHNE GmbH & Co. KG [19]

The concrete pressure below the bearing is:

$$\sigma_{c,d} = \frac{\max F_v}{A_{bearing}} = \frac{1604.4\text{kN}}{0.3\text{m} \cdot 0.4\text{m}} = 13.37\text{N}/\text{mm}^2$$

$\sigma_{c,d}$ = 13.37N/mm^2 < 20 N/mm^2 = f_{cd}

D.10 Deformations

The relevant load combinations for calculating deformations are to be found in Annex A, Figure A.8. The checks for the limits of deflection and vibration shall be made with only one track loaded.

ENV 1991-3: 1995, 6.8.1 (6)P

Vertical acceleration of the deck

This check is only required for design speeds v > 220 km/h, or when the natural frequency of the bridge with a span of 100 m is above 3.02 Hz or below 1.54 Hz. The data for the bridge calculated in this work are as follows:

ENV 1991-3: 1995 G.3.1.2.1

Design speed: 160 km/h
Natural frequency: 2.34 Hz

The check is therefore not required.

Deck twist

For a design speed of 160 km/h, the maximum twist over a length of 3 m shall not exceed t = 3.0 mm.

Actual value of maximum twist: <u>t = 1.4 mm /3m < 3.0 mm/3m</u>

ENV 1991-3: 1995 G.3.1.2.2

The check is fulfilled.

Rotation at the end of the deck

For a double track bridge, the maximum transition between the deck and the embankment shall not exceed $\Theta = 3.5 \cdot 10^{-3}$ radians.

Actual value of maximum transition: <u>$\Theta = 3.48 \cdot 10^{-3}$ radians < $3.5 \cdot 10^{-3}$ radians</u>

The check is fulfilled.

ENV 1991-3: 1995 G.3.1.2.3

Horizontal deflection of the deck

For a design speed of 160 km/h, the radius of curvature shall not exceed the value of 9500 m.

Actual value of maximum horizontal deflection: δ_h = 19.6 mm
Thus, the radius of curvature measures

$$R = \frac{L^2}{8 \cdot \delta_h} = \frac{(100\text{m})^2}{8 \cdot 19.6\text{mm}} = 63776 > 9500$$

ENV 1991-3: 1995 G.3.1.2.4

The check is fulfilled.

Vertical deflection

Vertical deflection of main design

ENV 1991-3: 1995 G.3.1.3

For a comfort level “very good” of a 100 m railway bridge with one span and a design speed of 160 km/h, the maximum vertical deflection shall not exceed L/300 = 100 / 300 = 333 mm.

Actual value of maximum vertical deflection due to dead load and live load: $\underline{\delta_v = 142.4\text{mm} < 333\text{mm}}$ (Location: edge beam)

The deflection due to dead loads is usually compensated by a respective camber. Therefore, the relevant value for deflection shall be the one due to live load only:
$\underline{\delta_{LL} = 66.8\text{mm}}$

Vertical deflection of alternative design proposals

Alternative design 1:
$\underline{\delta_v = 166.8\text{mm} < 333\text{mm}}$

Alternative design 2:
$\underline{\delta_v = 185.1\text{mm} < 333\text{mm}}$

Calculation of total deflections of alternative design proposals

It is necessary to compare the deflection of the prestressed concrete bridge deck with the respective deflections of the alternative design proposals. Since the bridge is loaded asymmetrically, the edge beams experience different deflection. The higher dead load of the alternative designs lead to higher edge beam deflections, as well as to higher deflections of the concrete slab between the edge beams.

- Alternative design 1 (due to DL and LL):

  Maximum deflection of one edge beam: $\delta_{eb.1}$ = 156.7 mm
  Maximum deflection of second edge beam: $\delta_{eb.2}$ = 117.4 mm

  Relative deflection of concrete slab between edge beams:

  Due to dead load: $\delta_{slab.DL}$ = 21.5 mm
  Due to live load: $\delta_{slab,LL}$ = 7.5 mm
  Total: δ_{slab} = 29 mm

- Alternative design 2 (due to DL and LL):

  Maximum deflection of the first edge beam: $\delta_{eb.1}$ = 146.1 mm
  Maximum deflection of the second edge beam: $\delta_{eb.2}$ = 104.8 mm

  Relative deflection of concrete slab between edge beams:

  Due to dead load: $\delta_{slab.DL}$ = 42.9 mm

Due to live load: $\delta_{slab,LL}$ = 14.5 mm
Total: δ_{slab} = 57.4 mm

Location of maximum relative deflection of concrete slab

The maximum deflection of the main design with transverse prestressing occurs at one edge beam. It is very likely that the high relative deflection of the unprestressed bridge deck shifts the location of maximum total displacement to somewhere between the edge beams.

The following calculation is an approximation of the total deflection at the location where the greatest relative displacement of the bridge slab occurs.

Location of maximum relative deflection due to traffic load

The centre of one track has a distance of a = 2.850 m from the support, which is the arch plane. The span of the deck is 10.15 m and the maximum deflection is expected at a distance x from the right support (Figure D.36).

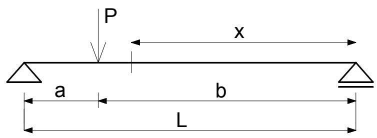

Fig. D.36. Nomenclature: Determination of location with maximum deflection

If $\alpha = a / L$, and
$\bar{\xi} = x / L$,
then the deflection line of a simple supported beam subjected to an eccentric single load P is given to:

$$\delta = \left(1 - \alpha^2 - \bar{\xi}^2\right) \cdot \alpha \cdot \bar{\xi} \cdot P \cdot L^3 / (6 \cdot EI)$$

Schneider [29], 13th edition, page 4.3

The derivation of the deflection line with α = 2.875 / 10.15 = 0.28325 leads to the location for the maximum deflection:

$\bar{\xi} = 0.554$,

hence, the x = 0.554 L = 5.623 m

Location of maximum relative deflection due to dead load

The maximum deflection due to dead load certainly occurs at the deck mid-span: x = 5.075 m

Location of maximum relative deflection due to LL and DL

The deflection due to dead load is about three times higher than to live load. The maximum deflection lies therefore closer at mid-span and the location is assumed to be at x = 5.26 m.

In the following, the deflections of the deck are calculated at x = 5.26 m, but only the components due to the edge beam displacement:

To obtain an approximate total deflection at the location, where the relative maximum deflection of the slab is largest, the following is required:

With the help of both maximum edge beam displacements, the theoretical displacement at the location x = 5.26 m neglecting the deflection of the slab can be calculated:

Alternative design 1:

$$\delta_{eb.5.623} = \frac{156.7mm - 117.4mm}{10.15m} \cdot (5.26m) + 117.4mm = 137.8mm$$

Alternative design 2:

$$\delta_{eb.5.623} = \frac{146.1mm - 104.8mm}{10.15m} \cdot (5.62m) + 104.8mm = 127.7mm$$

These values are superimposed with the in Annex D, Section D.5.3.3 calculated relative deflections of the concrete slab giving the total displacement at that location:

Alternative design 1:

$\delta_{5.623} = \delta_{eb.5.623} + \delta_{slab}$ = 137.8 mm + 29 mm = 166.8 mm

Alternative design 2:

$\delta_{5.623} = \delta_{eb.5.623} + \delta_{slab}$ = 127.7 mm + 57.4 mm = 185.1 mm

Both values are larger than the respective maximum edge beam displacements and constitute therefore the total maximum deflection of the bridge.

Annex E

Investigations on the temporary lower chord

E.1 General

The maximum deflection of the formwork should be limited to:

$$\frac{L+40}{2000} \text{ with L = span [m].}$$

ENV 1992-2: 1996, 4.4.3.1 (105)

This value can be reduced to L/300 if cracking during casting is limited. Both values were considered as limits.

Construction states are transient situation and therefore to be calculated in ultimate limit state applying the appendant partial safety factors.

Load assumptions

ENV 1991-2-1: 1995, 4.2 tab. 4.1

Self-weight:	Fresh concrete and reinforcement:	26 kN/m^3	
(γ_G = 1.35)	Plywood formwork sheet d = 18mm:	0.23 kN/m^3	*DOKA [9]*
	Timber formwork beams:	0.051 kN/m	
	Timber for transverse camber:	0.18 kN/m	*TEICH & WENDELIN [38]*
	Transverse steel beams (IPEa 550):	0.921 kN/m	
	Longitudinal steel beams (HEB 220):	0.715 kN/m	*EURONORM 19-62*

Live load: (γ_Q = 1.5)

On the cantilevers of the temporary lower chord due to casting and prestressing equipment and workers operating it: 0.5 kN/m^2

Between casting the bridge deck and transverse prestressing there is no access to the bridge deck allowed, so no further live load has to be considered.

Lateral wind on formwork: 1.43 kN/m *Section A.3.1*

E.2 Formwork sheet

Plywood formwork sheets with a thickness of 18 mm are used. The structural system is shown in Figure E.1.

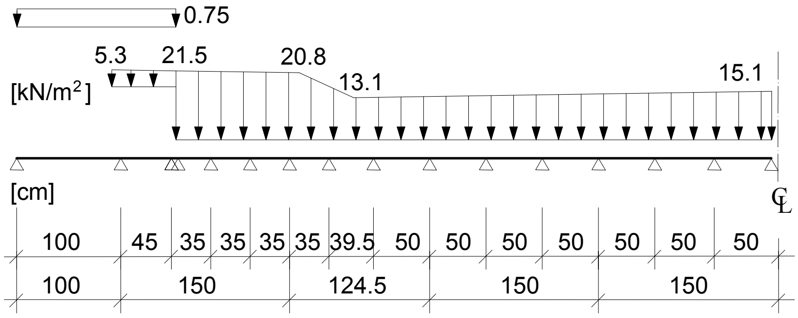

Fig. E.1. Structural system of formwork sheets, load is increased by partial safety factor

1. Underneath the cantilevers (as a simply supported beam for no live load on left side):

$L = 0.45$ m

Allowed deflection: $\delta = \dfrac{0.45\text{m} + 40}{2000} = 20.2$ mm

$\delta = 0.45\text{m}/300 = \underline{1.5 \text{ mm}}$

Present deflection:

$$\delta(6.05 \text{ kN/m}^2) = \frac{5}{384} \cdot \frac{q \cdot l^4}{EI} = \frac{5}{384} \cdot \frac{6.05\text{kN}/\text{m}^2 \cdot 0.45\text{m}^4}{8000\text{N}/\text{mm}^2 \cdot 486000\text{mm}^4/\text{m}} = 0.83 \text{ mm}$$

$\underline{0.83\text{mm} < 1.9 \text{ mm}}$

2. Underneath the edge beams (continuous beam):

$L = 0.35$ m

Allowed deflection: $\delta = \dfrac{0.35\text{m} + 40}{2000} = 20.2$ mm

$\delta = 0.35\text{m}/300 = \underline{1.2 \text{ mm}}$

Present deflection:

$$\delta(21.5 \text{ kN/m}^2) = \frac{1}{384} \cdot \frac{q \cdot l^4}{EI} = \frac{1}{384} \cdot \frac{21.5\text{kN}/\text{m}^2 \cdot 0.35\text{m}^4}{8000\text{N}/\text{mm}^2 \cdot 486000\text{mm}^4/\text{m}} = 0.2 \text{ mm}$$

$\underline{0.2 \text{ mm} < 1.5 \text{ mm}}$

3. Underneath the main bridge deck (continuous beam):

$L = 0.5$ m

Allowed deflection: $\delta = \dfrac{0.5\text{m} + 40}{2000} = 20.3$ mm

$\delta = 0.5\text{m}/300 = \underline{1.66 \text{ mm}}$

Present deflection:

$$\delta(15.1 \text{ kN/m}^2) = \frac{1}{384} \cdot \frac{q \cdot l^4}{EI} = \frac{1}{384} \cdot \frac{15.1\text{kN}/\text{m}^2 \cdot 0.5\text{m}^4}{8000\text{N}/\text{mm}^2 \cdot 486000\text{mm}^4/\text{m}} = 0.6 \text{ mm}$$

$\underline{0.6 \text{ mm} < 1.75 \text{ mm}}$

For the assessment of the plywood only allowed deflections are given by the manufacturer. They are all larger than the tolerances given by Eurocode.

E.3 Timber formwork beams

The formwork beams are collocated as shown in Figure E.2.

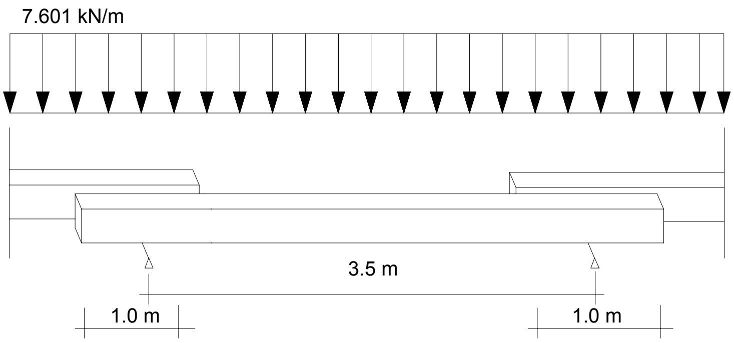

Fig. E.2. Schematic illustration of the overlapping timber formwork beams

The bridge deck is cast starting at a certain point and proceeding forward. This leads to partial loading of the continuous beam constituted by the formwork beams. Decisive bending moments are obtained as shown in Figure E.3

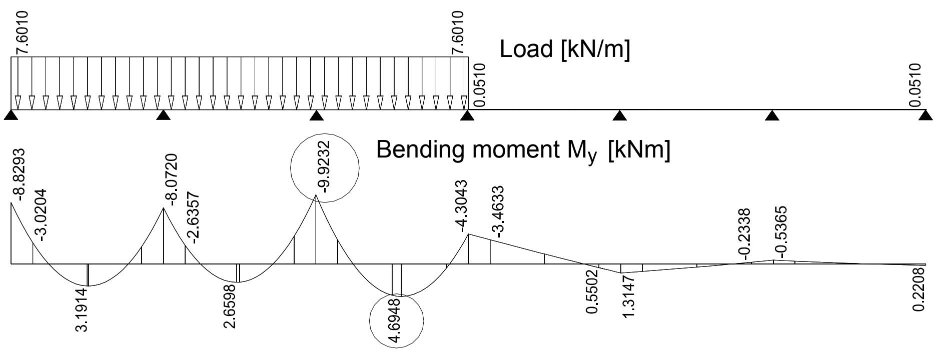

Fig. E.3. Maximum bending moments during casting

$L = 3.5$ m

Allowed deflection: $\delta = \dfrac{3.5\text{m} + 40}{2000} = 21.8$ mm

$\delta = 3.5\text{m}/300 =$ 11.7 mm

Present deflection (SOFISTIK):

$\delta(7.601$ kN/m$) =$ 4.7 mm < 10 mm

Sagging bending moment:

Allowed bending moment: M = 5.0 kNm
Present bending moment (*SOFiSTiK*):
M(7.601 kN/m) = 4.7 kNm < 5 kNm *DOKA [8]*

Hogging at the supports (double cross section):

Allowed bending moment: M = 10.0 kNm
Present bending moment (*SOFiSTiK*):
|M(7.601 kN/m)| = 9.92 kNm < 10 kNm

The formwork beams first loaded are simply supported beams. In these spans, double amount of formwork beams has to be applied.

E.4 Transverse steel beams

The transverse steel beams receive decisive loads during prestressing of the transverse tendons. Therefore they are designed only for this construction state. The contribution of the reinforced concrete cross section to the structural behaviour is not considered, so the transverse steel beams have to bear all loads.

The loads and the structural system are shown in Figure E.4.

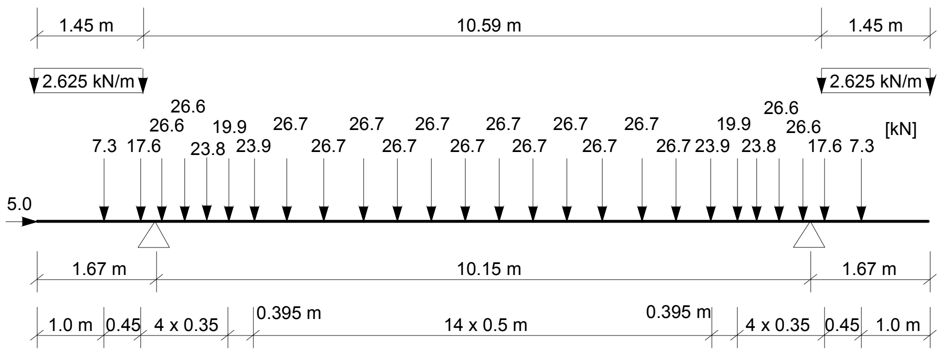

Fig. E.4. Loads and constraints of the transverse steel beam

To determine the axial forces acting in the transverse steel beam the wind loads were applied to a 3-D-model in *SOFiSTiK*. The results are shown in Figure E.5.

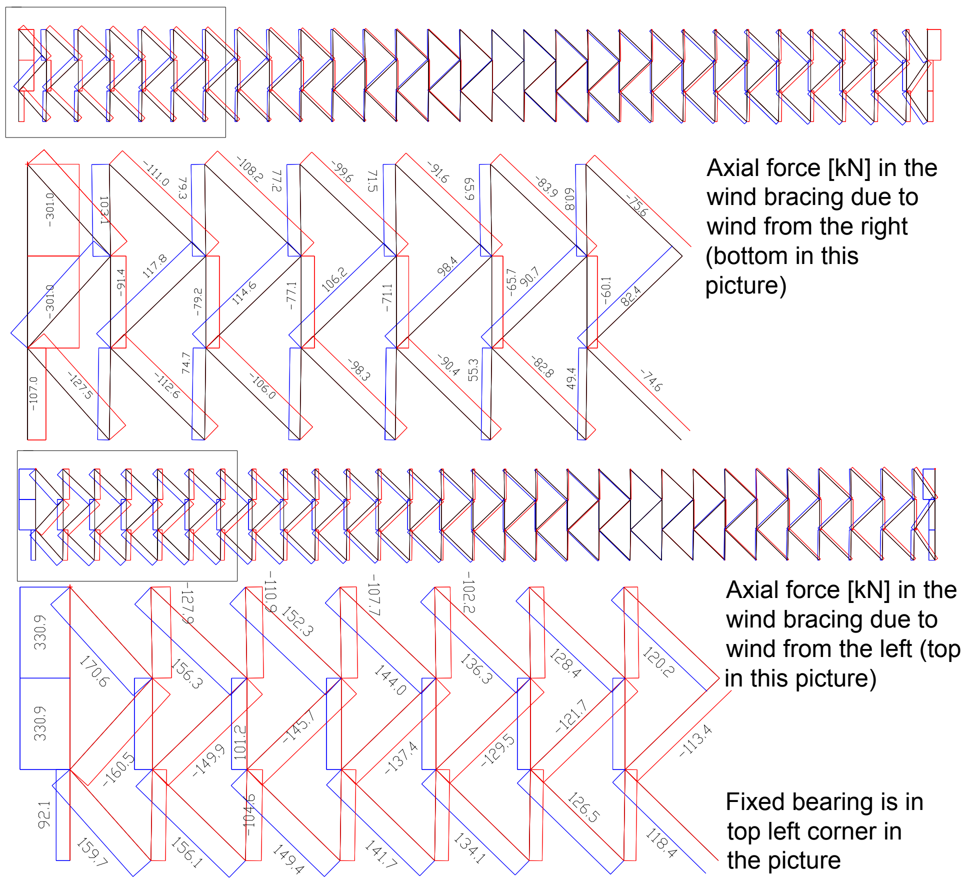

Fig. E.5. Axial forces in the wind bracing of the temporary lower chord

As shown in Figure E.5 the axial forces are far from evenly distributed along the span. The asymmetry is caused by the different bearing conditions. It is important to connect the fixed bearing with a diagonal wind bracing member. This reduces the axial forces by about 30% in the members of the first field. Since the first two transverse steel beams will consist of stronger profiles, the maximum and minimum forces are taken from the third field from the bearing.

There are two load cases to differentiate:

1. All loads:
   Maximum sagging bending moment: $M_{f,d}$ = 688.8 kNm
   $maxF_{x,d}$ = -79.2 kN

   Maximum hogging bending moment: $M_{s,d}$ = -8.8 kNm
   $maxF_{x,d}$ = -110.9 kN
   $maxV_{z,d}$ = 294.4 kN

2. All loads except live load on cantilevers:
   Maximum sagging bending moment: $M_{f,d}$ = 685.2 kNm
   $maxF_{x,d}$ = -79.2 kN

   Maximum hogging bending moment: $M_{s,d}$ = -12.4 kNm
   $maxF_{x,d}$ = -110.9 kN
   $maxV_{z,d}$ = 294.4 kN

It is not desired that the cross section of the transverse steel beams develop their plastic moment resistance. Therefore, in the following design checks it is treated as a class 3 cross section.

ENV 1993-1-1: 1992, 5.5.2 (8)

The transverse beams are restrained at the top flanges by wooden cams nailed to the timber formwork beams, which are spaced at 50 cm c/c. This can be considered as fully restrained. Therefore, the beams do not need to be checked for lateral-torsional buckling.

$M_{y,Sd} = M_{f,d}$ = 688.8 kNm
$N_{Sd} = maxF_{x,d}$ = -79.2 kN
$V_{Sd} = maxV_{z,d}$ = 294.4 kN

Cross section: IPEa 550

$A = 117\ cm^2$
$W_{el,y} = 2190\ cm^3$

$$f_{yd} = \frac{f_y}{\gamma_{M0}} = \frac{355N/mm^2}{1.1} = 322.7N/mm^2$$

ENV 1993-1-1: 1992, 5.4.8.2

Bending and axial force at mid-span, absence of shear force

The criterion to fulfil is:

$$\frac{N_{Sd}}{A \cdot f_{yd}} + \frac{M_{y,Sd}}{W_{el,y} \cdot f_{yd}} \leq 1$$

$$\frac{|-79.2kN|}{117cm^2 \cdot 322.7N/mm^2} + \frac{688.8kNm}{2190cm^3 \cdot 322.7N/mm^2} = 0.99 \leq 1$$

Shear resistance at the support *ENV 1993-1-1: 1992, 5.4.6*

$A_v = A - 2\ b\ t_f + (t_w+2r)\ t_f$
$= 117\ cm^2 - 2\ 21cm\ 1.57cm + (0.9cm + 2\ 2.4cm)\ 1.57cm$
$= 60\ cm^2$

$$V_{pl,Rd} = \frac{A_v\left(f_y/\sqrt{3}\right)}{\gamma_{M0}} = \frac{60cm^2\left(355N/mm^2/\sqrt{3}\right)}{1.1} = 1118.1kN$$

$V_{Sd} = 294.4\ kN < 1118.1\ kN = V_{pl,Rd}$

and $\frac{V_{Sd}}{V_{pl,Rd}} = \frac{294.4kN}{1118.1kN} = 0.26$

Since V_{Sd} does not exceed 50% of $V_{pl,Rd}$, no reduction needs to be made in the resistance moments. Therefore, the bending moment at mid-span is decisive. *ENV 1993-1-1: 1992, 5.4.7 (2)*

Deflections for the design of the camber

To find the shape of the bottom surface of the bridge deck, the formwork receives a camber. This camber is influenced by the deflections due to the self-weight of the concrete bridge deck and the railway equipment (ballast, sleepers and rails). The deflections due to the fresh concrete are shown in Figure E.6. The deflections due to self-weight after transverse prestressing and removal of the formwork are taken from Annex D, Section D.10.

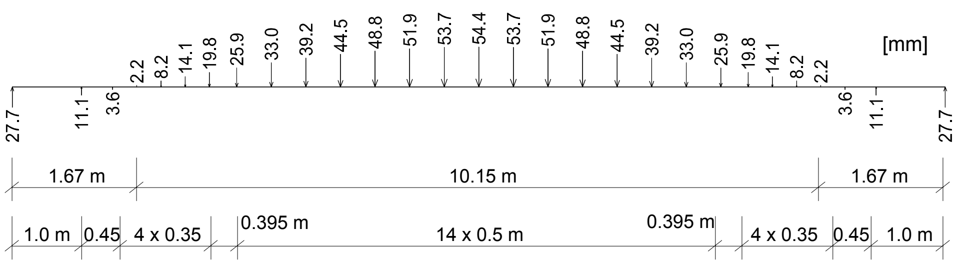

Fig. E.6. Deflections of the transverse temporary steel beam due to fresh concrete

E.5 Wind bracing members

The relevant axial force is taken from Figure E.5.

Buckling resistance of compression members *ENV1993-1-1: 1992, 5.5.1*

Geometry: l = 4.88 m

Cross section: L 120 x 10 (DIN 1028)

$A = 23.2\ cm^2$
$i_y = i_z = 3.67\ cm$
$fy = 355\ N/mm^2$ S 355

$N_{Sd} = -160.5\ kN$

The criterion to fulfil is: $N_{Sd} \leq N_{b,Rd}$

$$N_{b,Rd} = \chi \cdot \beta_A \cdot A \cdot \frac{f_y}{\gamma_{M1}}$$

χ depends on $\bar{\lambda}$

$$\bar{\lambda} = \frac{\lambda}{\lambda_1} \cdot \sqrt{\beta_A} = \frac{\beta \cdot l}{i_y \cdot \pi \cdot \sqrt{\frac{E}{f_y}}} \cdot \beta_A$$

with ß = 1 ; Euler case 2
l = 4.88 m
i_y = 3.67 cm
E = 210000 N/mm^2
f_y = 355 N/mm^2 ; S355
$ß_A$ = 1 ; Class 3 cross section

$$\bar{\lambda} = \frac{1 \cdot 4.88\text{m}}{3.67\text{cm} \cdot \pi \cdot \sqrt{\frac{210000\text{N}/\text{mm}^2}{355\text{N}/\text{mm}^2}}} \cdot 1 = 1.74$$

χ = 0.2461 ; buckling curve “c” *ENV 1993-1-1: 1992 5.5.1 Table 5.5.2*
A = 23.2 cm^2
γ_{M1} = 1.1

$$N_{b,Rd} = 0.2461 \cdot 1 \cdot 23.2\text{cm}^2 \cdot \frac{355\text{N}/\text{mm}^2}{1.1} = 184.3\text{kN}$$

$|N_{Sd}|$ = 160.5 kN ≤ 184.3 kN = $N_{b,Rd}$

E.6 Longitudinal steel beams

For the assessment of the longitudinal beams of the temporary lower chord several construction phases have to be examined to find the decisive internal forces. Only reasonable wind loads are considered. For example no casting would be performed during a storm.

E.6.1 Construction phase 1 – Mounting the steel skeleton and displacement

In this construction phase the steel skeleton is assembled and supported only at the arch root point. The formwork is still not applied.

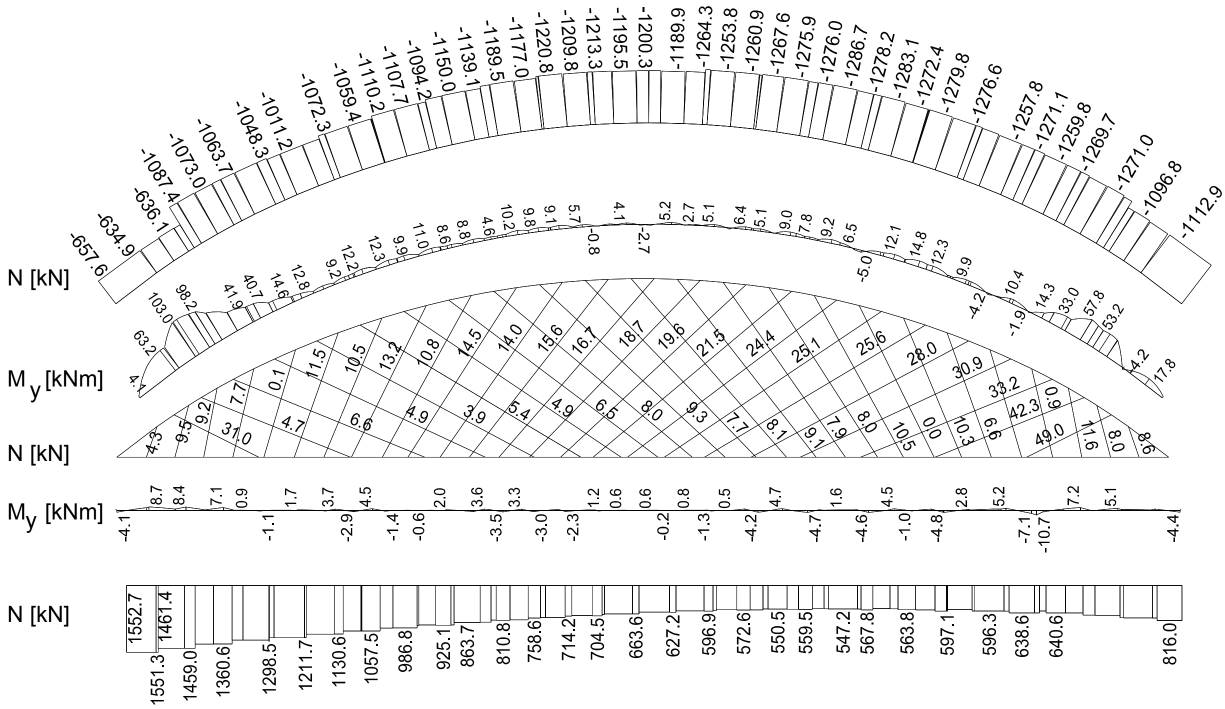

Fig. E.7. Internal forces for construction state 1, full wind load and self-weight

As can be seen in Figure E.7 bending moments in the temporary lower chord are small. Two hangers tend to relax while one is relaxed. This is not a problem, because in this construction state no casting is performed.

E.6.2 Construction phase 2 – Preparations for casting the bridge deck

After the steel skeleton has been put in place, the first approx. 3.5 meters from the ends of the bridge are cast. Then the formwork of the whole bridge is put into place starting from both ends. After that the longitudinal and transverse tendons and the reinforcement are laid out. At the point before partial prestressing of the longitudinal tendons, internal forces are calculated and shown in Figure E.8.

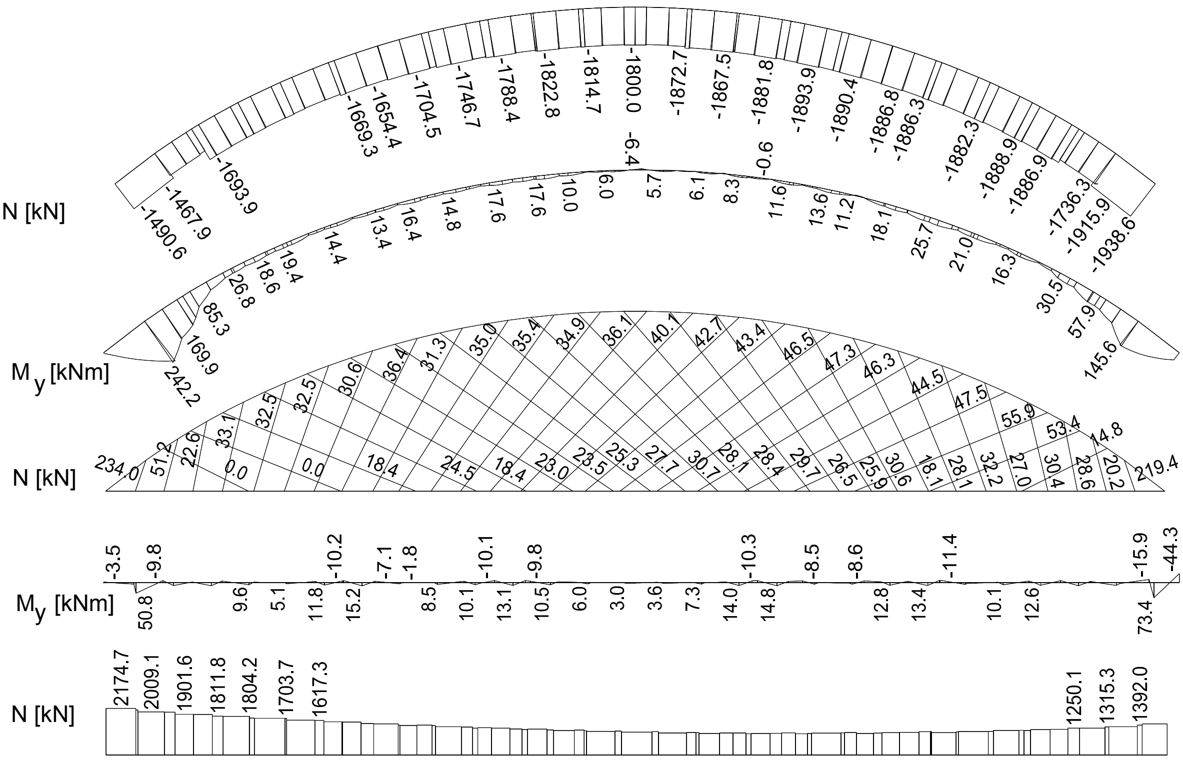

Fig. E.8. Internal forces for construction state 2, full wind load and self-weight

E.6.3 Construction phase 3 - Casting of the concrete edge beam

This phase of construction is performed in one day. It is assumed that there is no heavy wind on this day so wind loads are reduced to 25%. Two longitudinal tendons on each side are already prestressed with 650 kN each. It is possible to start casting from mid-span or from both ends. Since internal forces do not differ too much between the two methods, the decisive criterion is avoiding relaxed hangers when their bottom ends are already in concrete. If both methods show the same resistance against hanger relaxation, starting from both ends should be prioritised because the ages of the concrete of end cross girder and edge beam do not differ that much, in this case.

The two different methods were examined concerning hanger relaxation. The result is shown in Figure E.9, which extends over two pages.

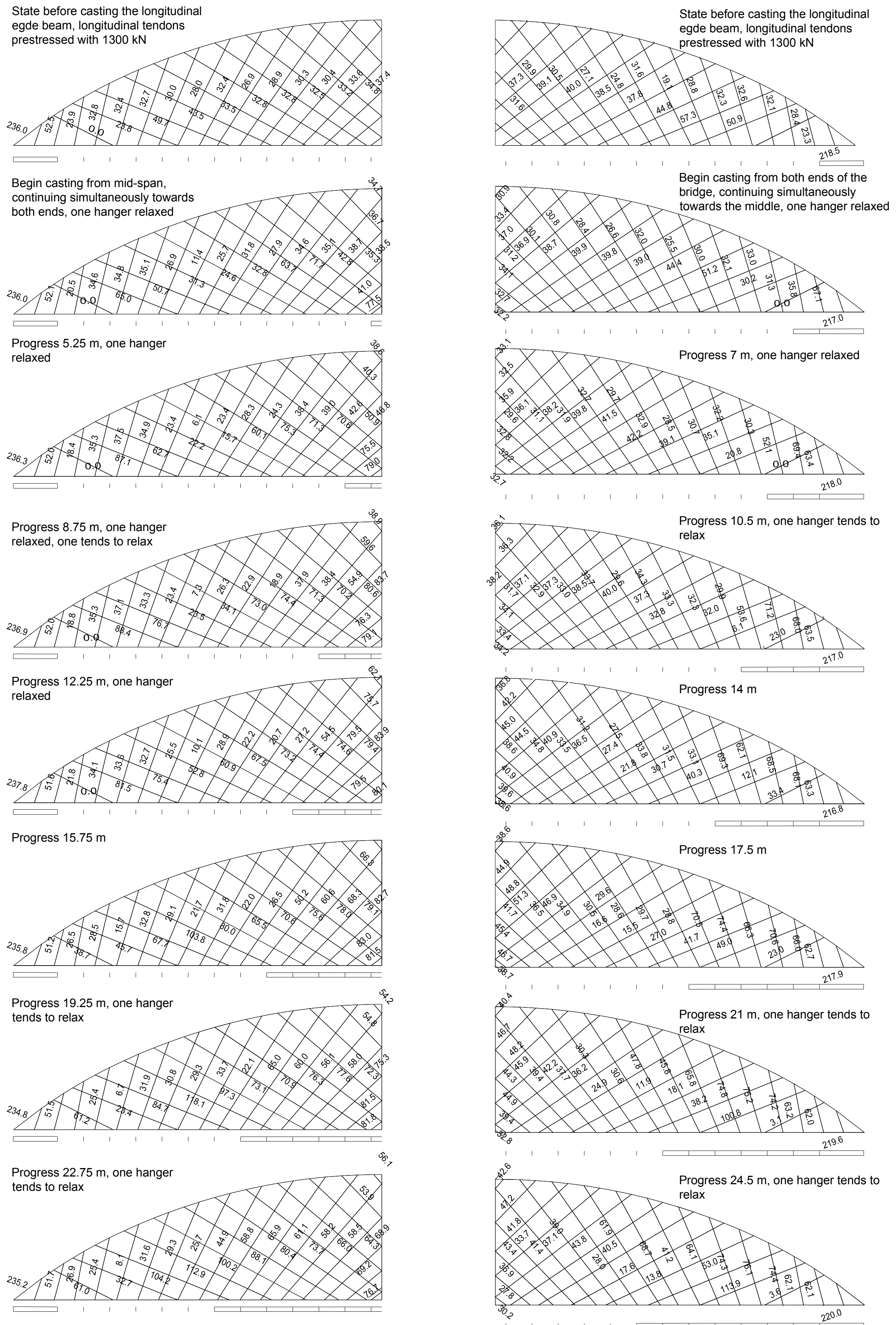

Fig. E.9. Axial forces in hangers during casting of the longitudinal concrete edge beam

Continued on next page…

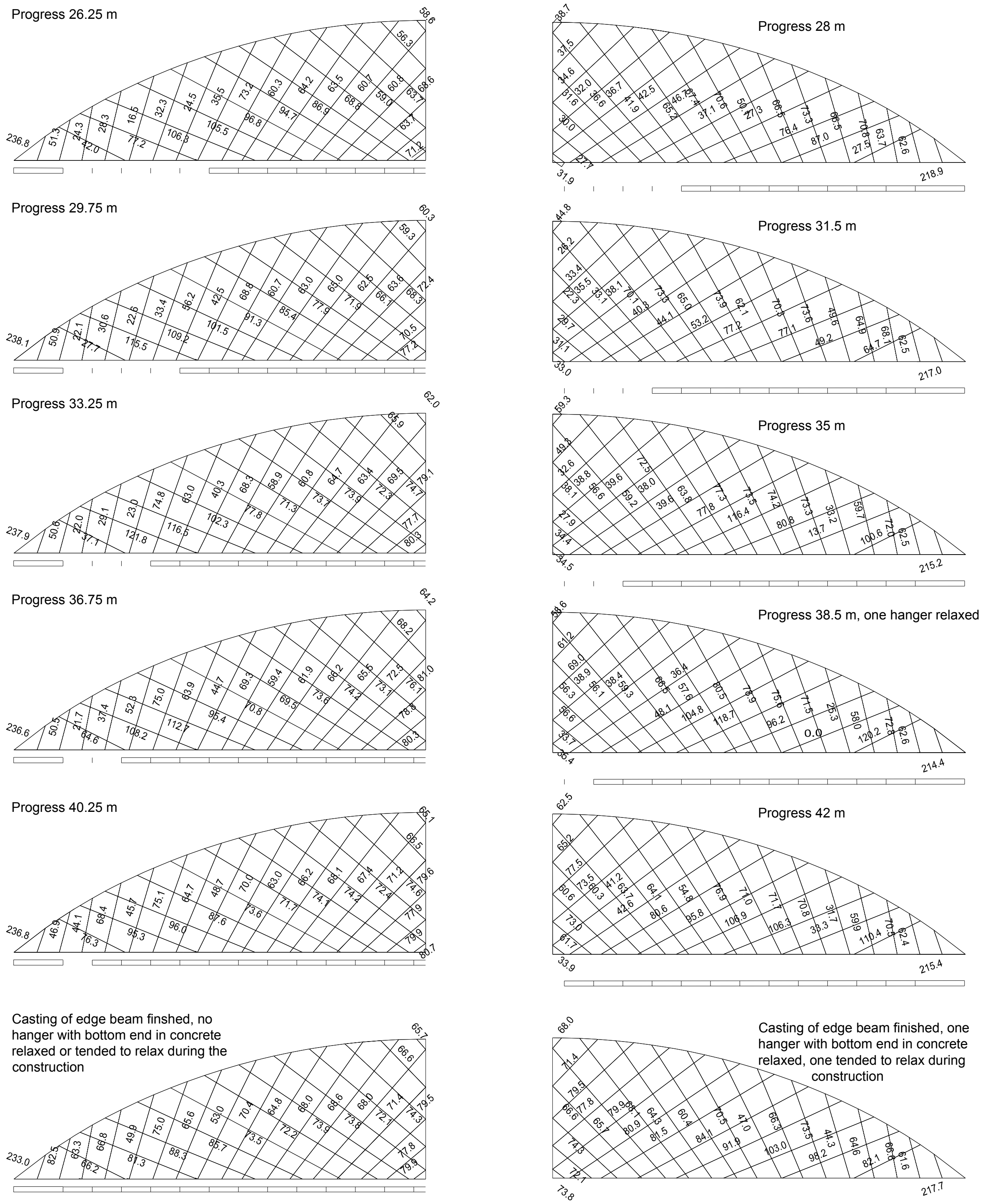

Fig. E.9. Axial forces in hangers during casting of the longitudinal concrete edge beam

The results in Figure E.9 show that starting from both ends leads to relaxed hangers when their bottom ends are already cast. Therefore it was decided to start at mid-span and then proceed simultaneously to both ends of the bridge. Since every network arch bridge will have a different geometry, hanger relaxation should be examined for every special project.

The partial longitudinal prestressing relieves the longitudinal steel beam of the temporary lower chord in such a way that the internal forces during construction and after finishing the concrete edge beam do not exceed the values of the second construction phase (before partial prestressing of longitudinal tendons). The maximum bending moment is still caused by the end cross girder (73.4 kNm). The maximum bending moment apart from this goes up to 35 kNm while the axial force is 1085 kN

E.6.4 Construction phase 4 - Casting the main part of the bridge deck

This construction phase starts after another partial prestressing of the longitudinal tendons. All of them are prestressed with 25 % of the design value. From then on the concrete edge beam contributes to the bearing of all loads which leads to small bending moments in the arch. The longitudinal beam of the temporary lower chord is then disconnected from the arch root point, that it does not receive axial forces from the arch any more. This means that the internal forces occurring in this construction phase are not decisive for the assessment of the longitudinal steel beam. Therefore, as in construction phase 3, avoiding hanger relaxation should decide the sequence of casting.

The two possibilities mentioned for construction phase 3 do not give satisfying results any more. Both lead to extensive hanger relaxation. Since the bridge deck is not cast in one day, other sequences are possible. It was decided on three construction segments and then examined in which order and direction they should be cast. Figure E.10 shows the result.

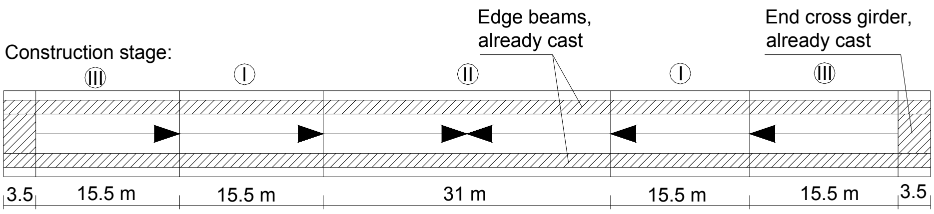

Fig. E.10. Casting sequence of bridge deck in construction phase 4

This construction method does not show any relaxed hangers at all. The maximum internal forces in the temporary longitudinal steel beam are:

M_y = 135 kNm
N_x = 0 kN
V_z = 188 kN

E.6.5 Assessment of the longitudinal steel beam

1. Construction phase 2:

Maximum sagging bending moment: $M_{f,d}$ = 73.4 kNm
$maxF_{x,d}$ = 1392 kN
Maximum hogging bending moment: $M_{s,d}$ = -44 kNm
$maxF_{x,d}$ = 1392 kN
$maxV_{z,d}$ = 106 kN

It is not desired that the cross section of the longitudinal steel beams develop their plastic moment resistance. Therefore, in the following design checks it is treated as a class 3 cross section.

$M_{y,Sd} = M_{f,d} = 73.4$ kNm
$N_{Sd} = maxF_{x,d} = 1392$ kN
$V_{Sd} = maxV_{z,d} = 106$ kN

Cross section: HEB 220

$A_{net} = 83.3\ cm^2$
$W_{el,y,net} = 694\ cm^3$

$$f_{yd} = \frac{f_y}{\gamma_{M0}} = \frac{355N/mm^2}{1.1} = 322.7N/mm^2$$

Bending and axial force at maximum sagging moment, absence of shear force *ENV 1993-1-1: 1992, 5.4.8.2*

The criterion to fulfil is:

$$\frac{N_{Sd}}{A_{net} \cdot f_{yd}} + \frac{M_{y,Sd}}{W_{el,y,net} \cdot f_{yd}} \leq 1$$

$$\frac{1392kN}{83.3cm^2 \cdot 322.7N/mm^2} + \frac{73.4kNm}{694cm^3 \cdot 322.7N/mm^2} = 0.85 \leq 1$$

Shear resistance at the support *ENV 1993-1-1: 1992, 5.4.6*

$A_v = A – 2\ b\ t_f + (t_w+2r)\ t_f$
$= 78.1\ cm^2 – 2\ 20cm\ 1.5cm + (0.9cm + 2\ 1.8cm)\ 1.5cm$
$= 24.85\ cm^2$

$$V_{pl,Rd} = \frac{A_v\left(f_y / \sqrt{3}\right)}{\gamma_{M0}} = \frac{24.85cm^2\left(355N/mm^2 / \sqrt{3}\right)}{1.1} = 463.02kN$$

$V_{Sd} = 106\ kN < 463.02\ kN = V_{pl,Rd}$

and $$\frac{V_{Sd}}{V_{pl,Rd}} = \frac{106kN}{463.02kN} = 0.23$$

Since V_{Sd} does not exceed 50% of $V_{pl,Rd}$ no reduction needs to be made in the resistance moments. Therefore the bending moment at mid-span is decisive. *ENV 1993-1-1: 1992, 5.4.7 (2)*

2. Construction phase 4:

Maximum sagging bending moment: $M_{f,d} = 135$ kNm
$maxF_{x,d} = 0$ kN
Maximum hogging bending moment: $M_{s,d} = -82.5$ kNm
$maxF_{x,d} = 0$ kN
$maxV_{z,d} = 188$ kN

$M_{y,Sd} = M_{f,d} = 135$ kNm
$N_{Sd} = \max F_{x,d} = 0$ kN
$V_{Sd} = \max V_{z,d} = 188$ kN

Cross section: HEB 220

$A_{net} = 83.3\ cm^2$
$W_{el,y,net} = 694\ cm^3$

$$f_{yd} = \frac{f_y}{\gamma_{M0}} = \frac{355N/mm^2}{1.1} = 322.7N/mm^2$$

Shear resistance at the support

ENV 1993-1-1: 1992, 5.4.6

$$A_v = A - 2\ b\ t_f + (t_w+2r)\ t_f$$
$$= 78.1\ cm^2 - 2\ 20cm\ 1.5cm + (0.9cm + 2\ 1.8cm)\ 1.5cm$$
$$= 24.85\ cm^2$$

$$V_{pl,Rd} = \frac{A_v\left(f_y / \sqrt{3}\right)}{\gamma_{M0}} = \frac{24.85cm^2\left(355N/mm^2 / \sqrt{3}\right)}{1.1} = 463.02kN$$

$V_{Sd} = 188\ kN < 463.02\ kN = V_{pl,Rd}$

and $$\frac{V_{Sd}}{V_{pl,Rd}} = \frac{188kN}{463.02kN} = 0.41$$

Since V_{Sd} does not exceed 50% of $V_{pl,Rd}$ no reduction needs to be made in the resistance moments. Therefore the bending moment at mid-span is decisive.

ENV 1993-1-1: 1992, 5.4.7 (2)

Bending and axial force at maximum sagging moment, absence of shear force

ENV 1993-1-1: 1992, 5.4.8.2

The criterion to fulfil is:

$$\frac{N_{Sd}}{A_{net} \cdot f_{yd}} + \frac{M_{y,Sd}}{W_{el,y,net} \cdot f_{yd}} \le 1$$

$$\frac{0kN}{83.3cm^2 \cdot 322.7N/mm^2} + \frac{135kNm}{694cm^3 \cdot 322.7N/mm^2} = 0.6 \le 1$$

Data from the optimisation process

F.1 Comparison of influence lines

As mentioned in Section 6.6.2 a comparison between the Åkviksound network arch TVEIT *[39]*, page 73, and a hanger arrangement according to the authors` proposal was drawn. The influence lines for bending moments in the arch and axial force in the arch and hangers served for this purpose. Many influence lines of the Åkviksound bridge were calculated by A. JAY in 1998, *[49]*. The same geometry, cross-sections and material properties as in her work were used for the authors` calculations. As a difference, a hanger arrangement with equal cross angles between the arch and the hangers was chosen. The cross angle, as defined in Section 6.6.3, was 28° which complies with the cross angle of the hangers and the axis of symmetry in the hanger arrangement of the Åkviksound network arch. It should be noted that a different cross-angle may lead to better results for the proposed arrangement.

Knowing that the 'radial' hanger arrangement is not appropriate for the arch ends where the clamping causes a disturbance range, the authors shifted the first few upper hanger nodes slightly along the arch.

In the following, the relevant data of the calculation conditions are listed:

All hangers:	Circular bars, diameter = 40 mm, E = 210,000 N/mm^2, γ = 78.5 kN/m^3
Arch profile:	UC 356x406x393, E = 210,000 N/mm^2, γ = 78.5 kN/m^3
Concrete tie:	E = 30,000 N/mm^2, γ = 30.4 kN/m^3

Span:	135 m
Arch rise:	20.25 m
Distance between arch planes:	7.55 m

The concrete tie was modelled with a thickness of 520 mm in the plane of the arch and 200 mm in the middle with a linear transition between them. The total width is 7.55 meters.

The influence lines were calculated for loads on the tie directly in the arch plane. Only one arch plane and half the tie were considered for analysis. Figures F.1 to F.5 show the comparison.

Additionally two load cases were calculated. The comparison can be seen in figures F.6 to F.9. The applied loads can be seen in those figures as well.

A composition of some relevant values is shown in Figure F.10.

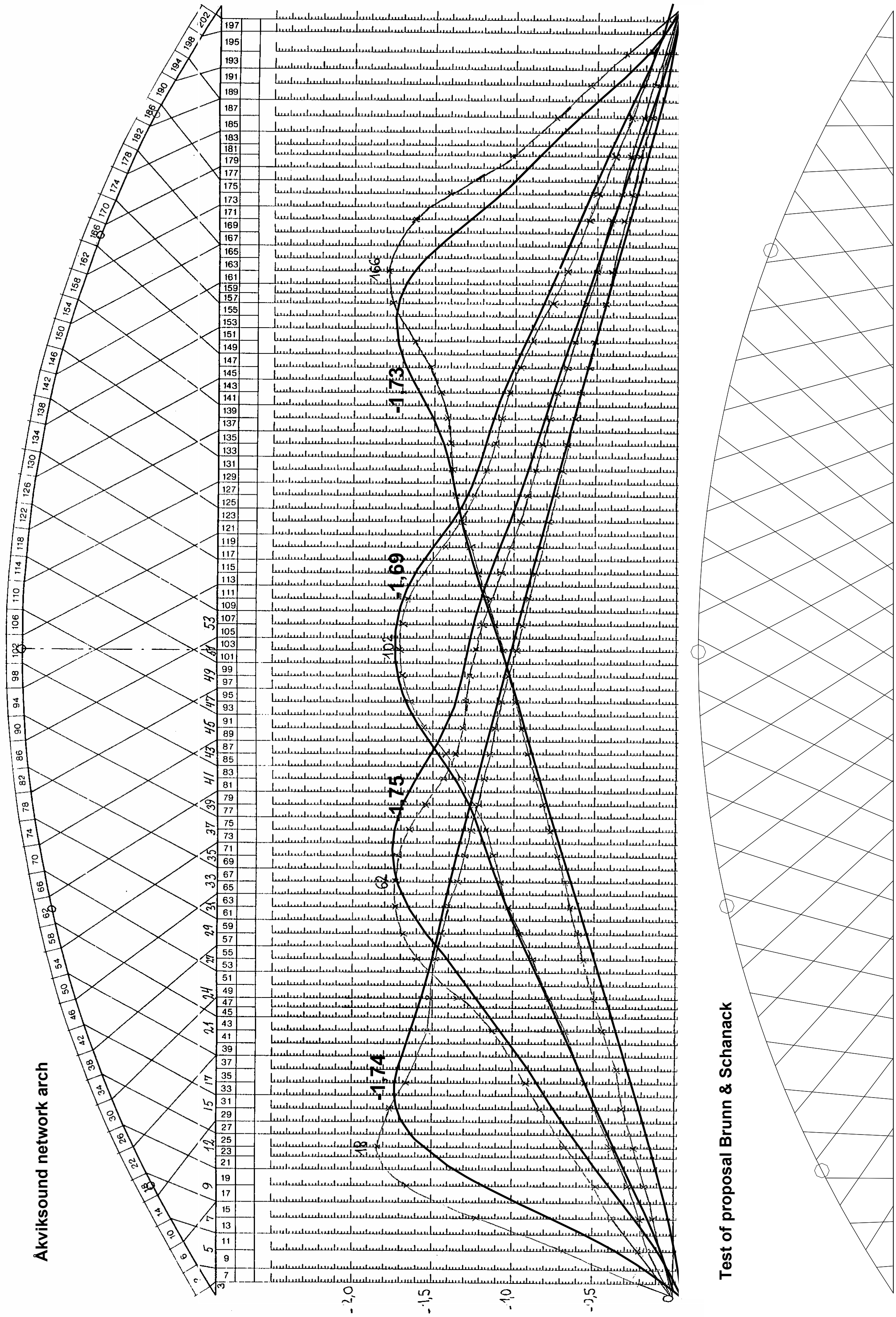

Fig. F.1. Comparison of influence lines for compression in the arch, (thin line - Åkviksound network arch / thick line - test of an arrangement according to a proposal by Brunn & Schanack)

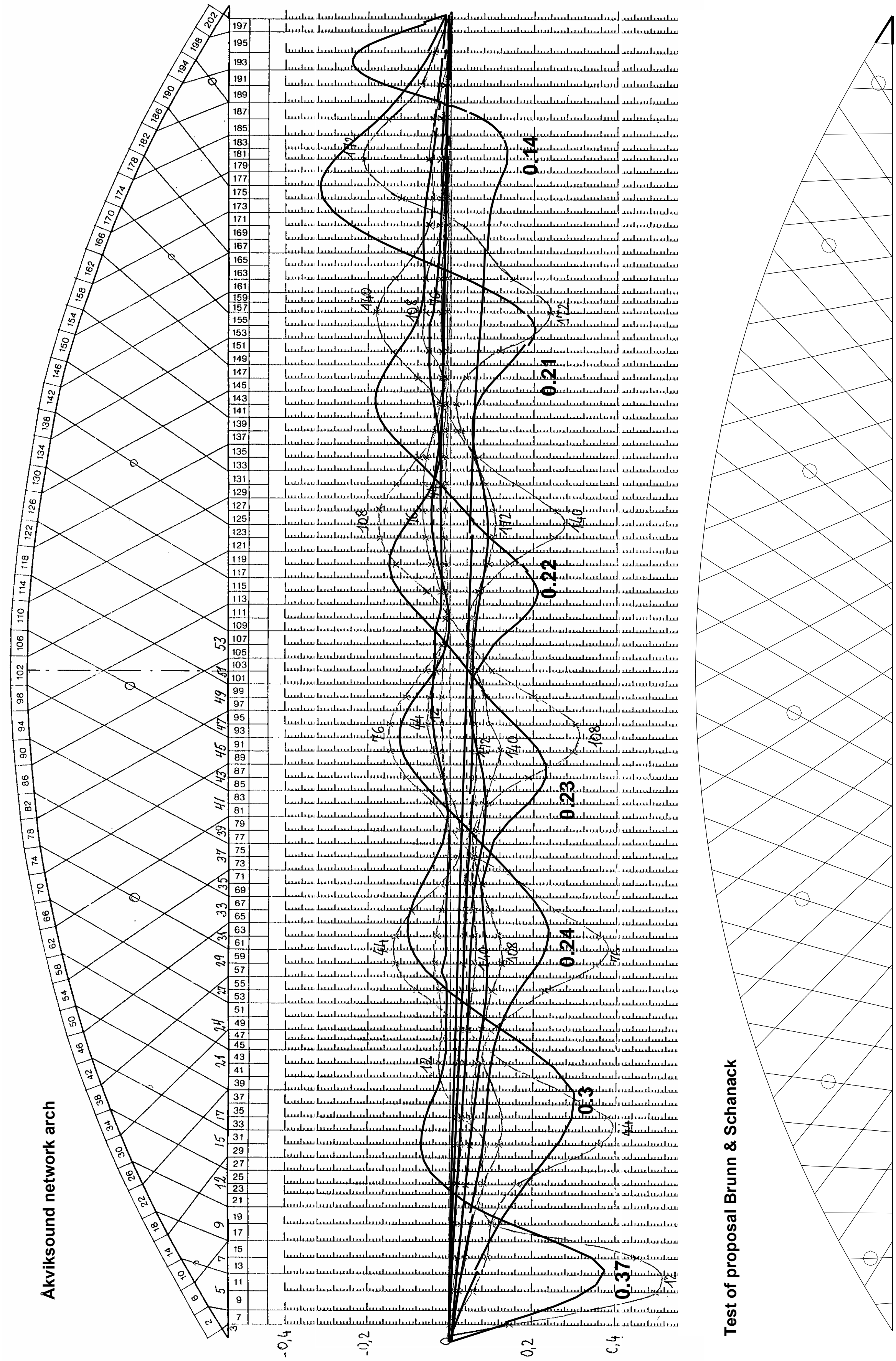

Fig. F.2. Comparison of influence lines for the force in the hangers I (thin line - Åkviksound network arch / thick line - test of an arrangement according to a proposal by Brunn & Schanack)

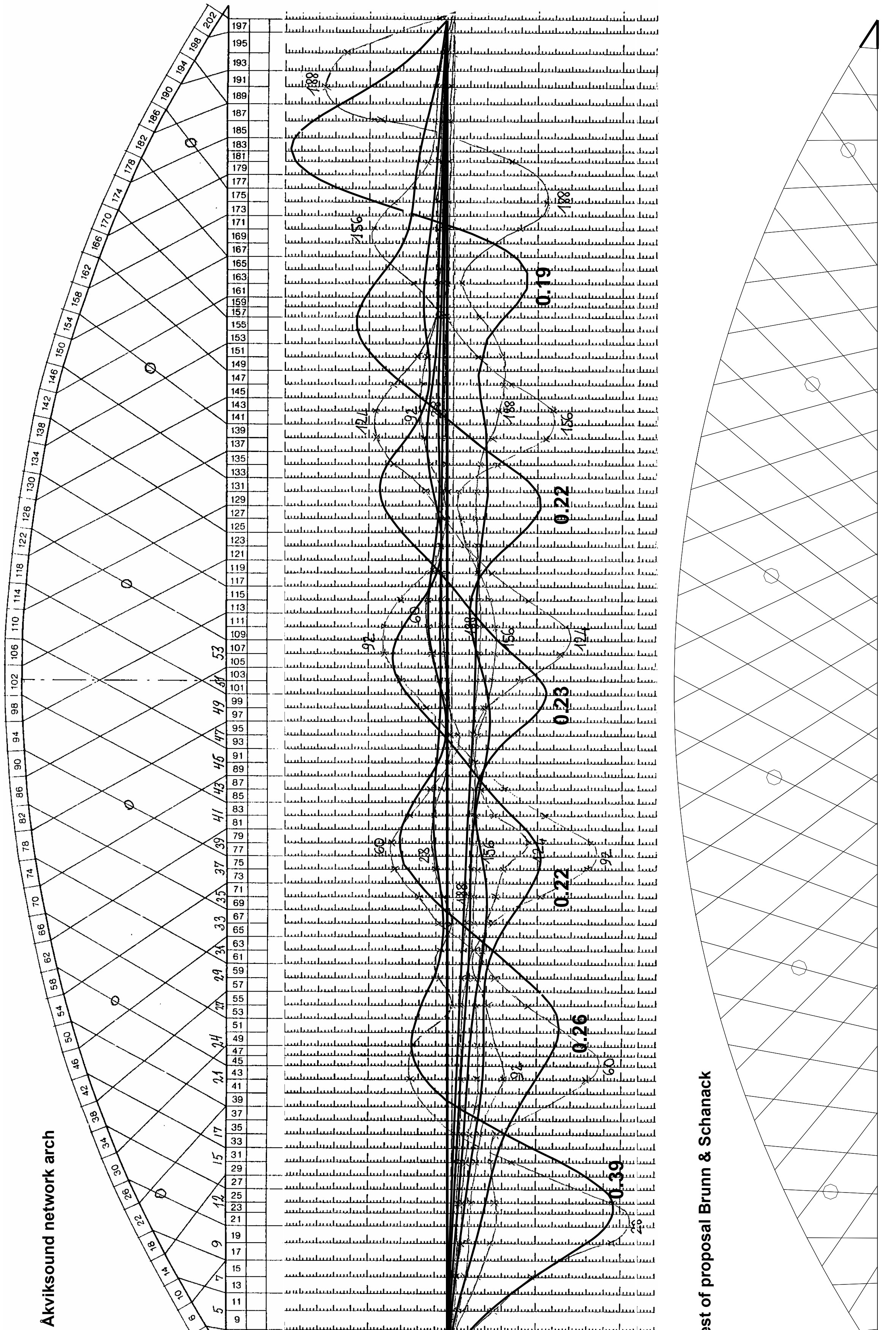

Fig. F.3. Comparison of influence lines for the force in the hangers II (thin line - Åkviksound network arch / thick line - test of an arrangement according to a proposal by Brunn & Schanack)

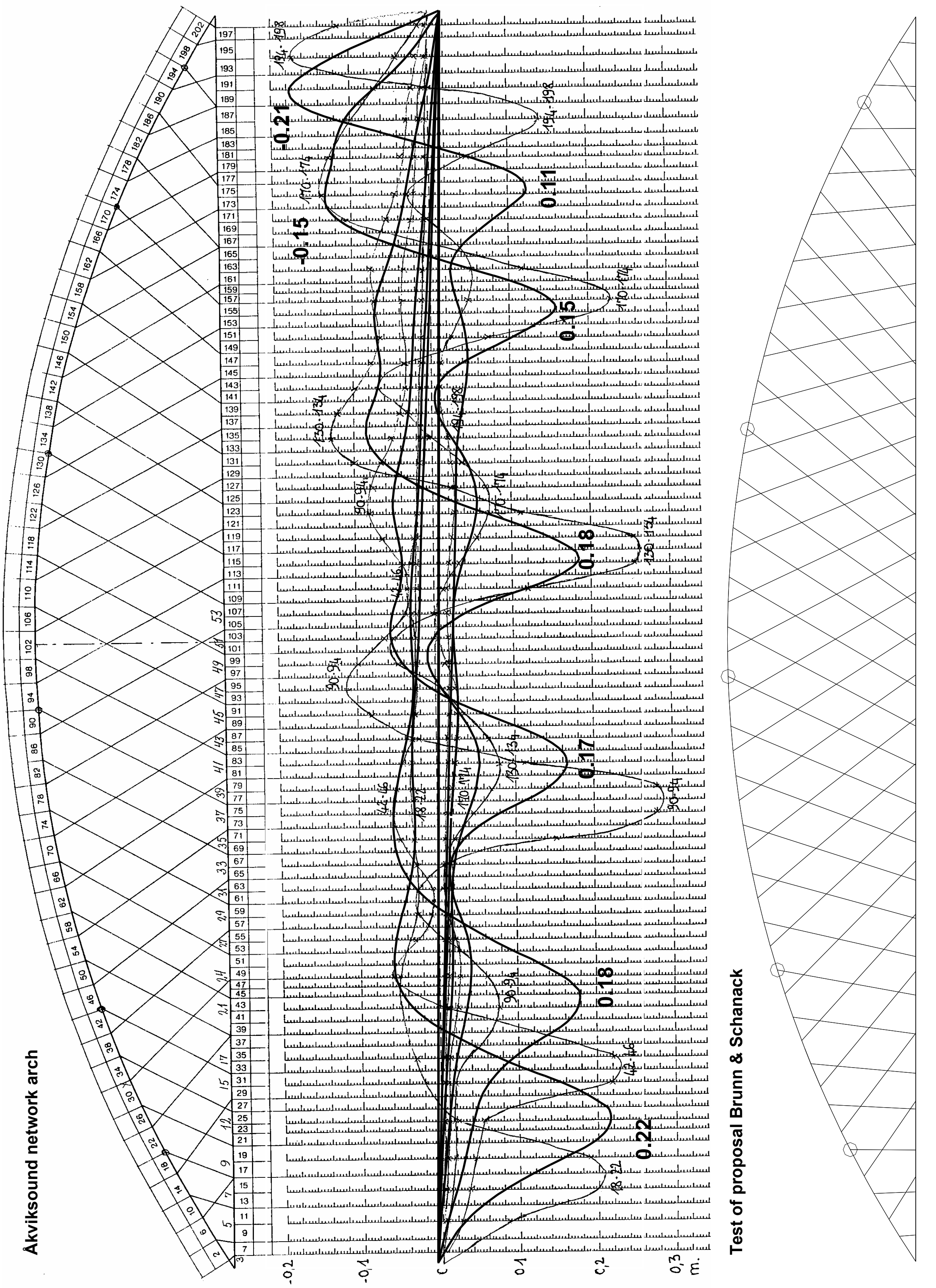

Fig. F.4. Comparison of influence lines for the bending moments in the arch I (thin line - Åkviksound network arch / thick line - test of an arrangement according to a proposal by Brunn & Schanack)

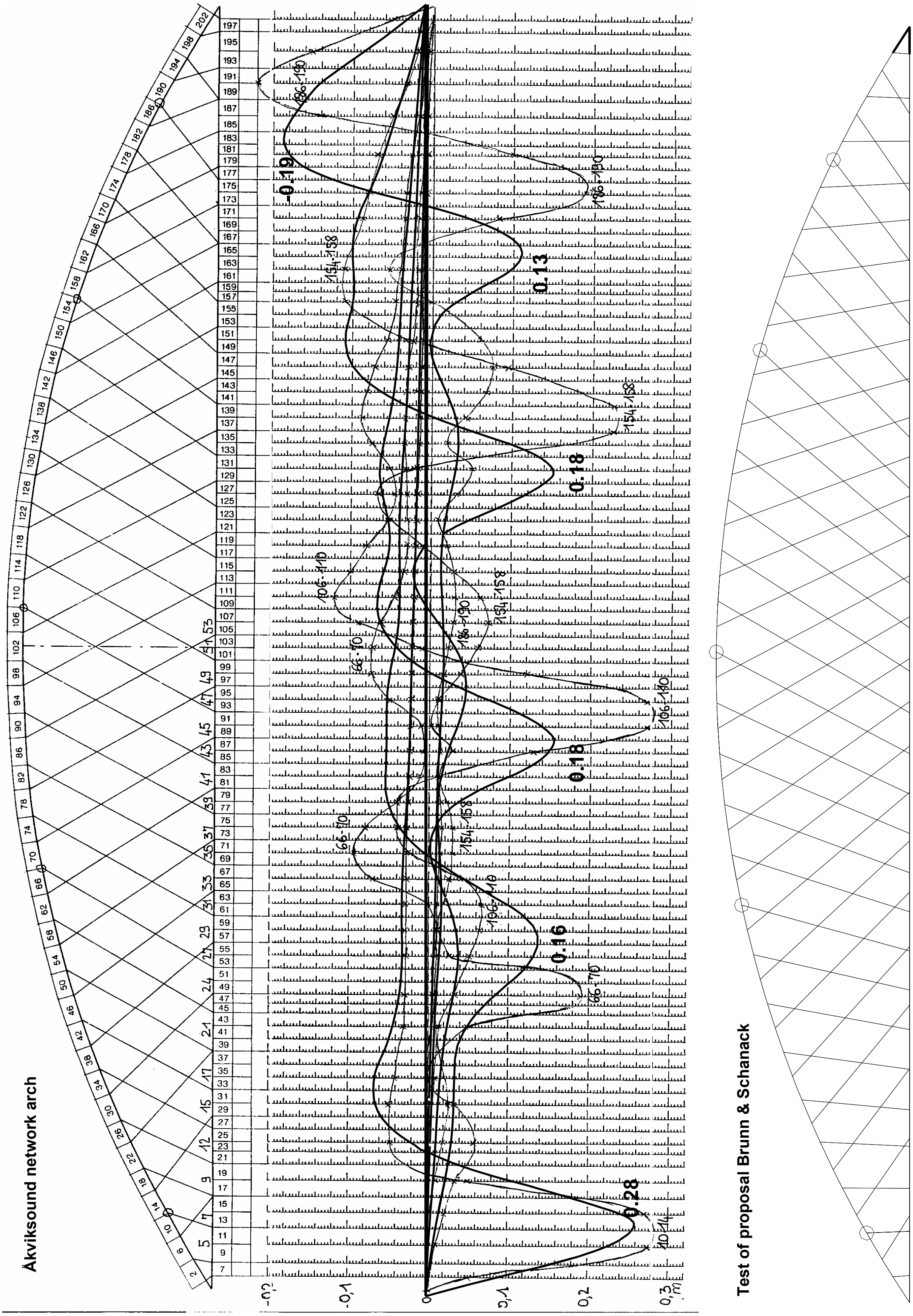

Fig. F.5. Comparison of influence lines for the bending moments in the arch II (thin line - Åkviksound network arch / thick line - test of an arrangement according to a proposal by Brunn & Schanack)

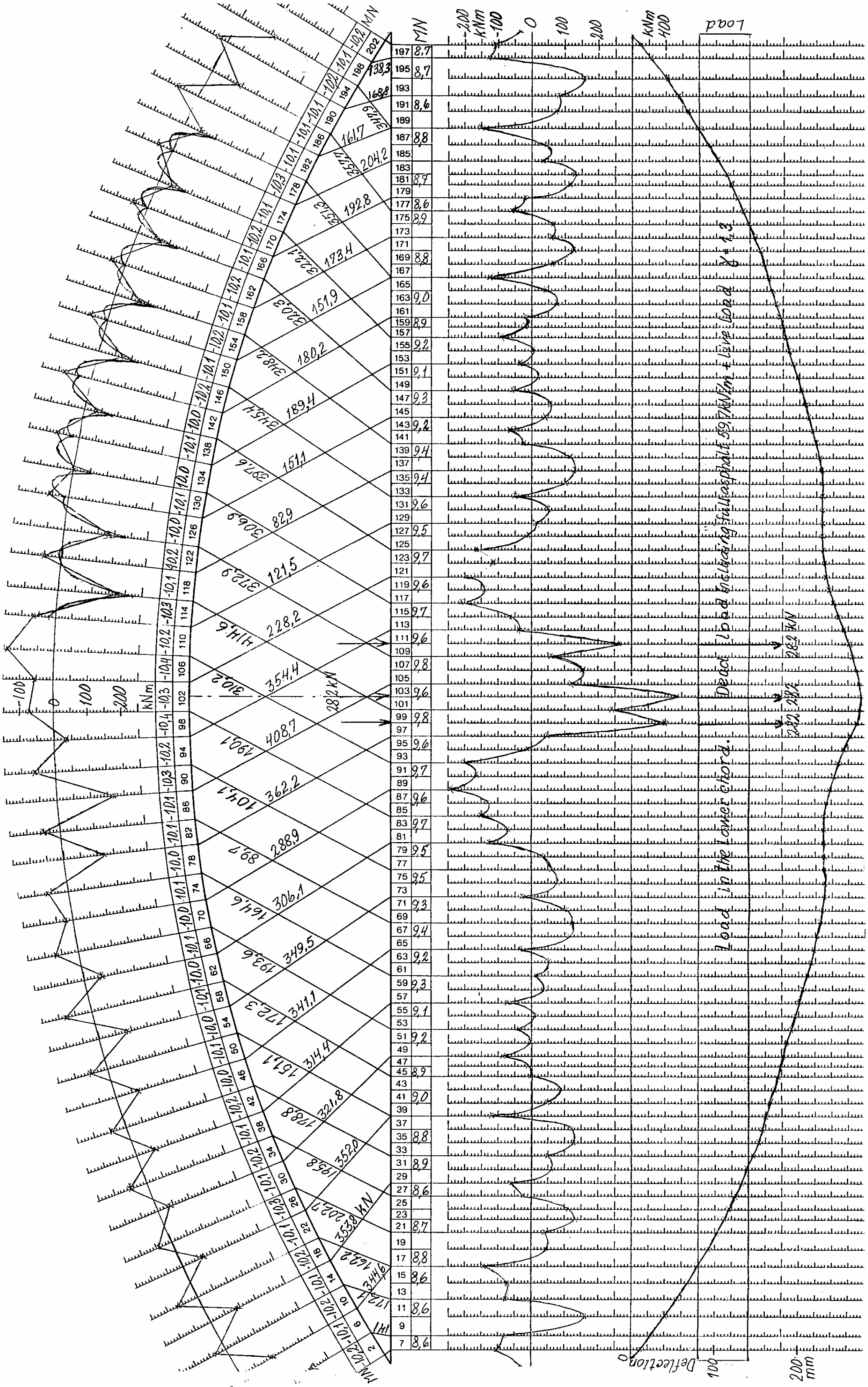

Fig. F.6. Maximum load on the Åkviksound network arch in the ultimate limit state, the wheel loads are in the middle of the span

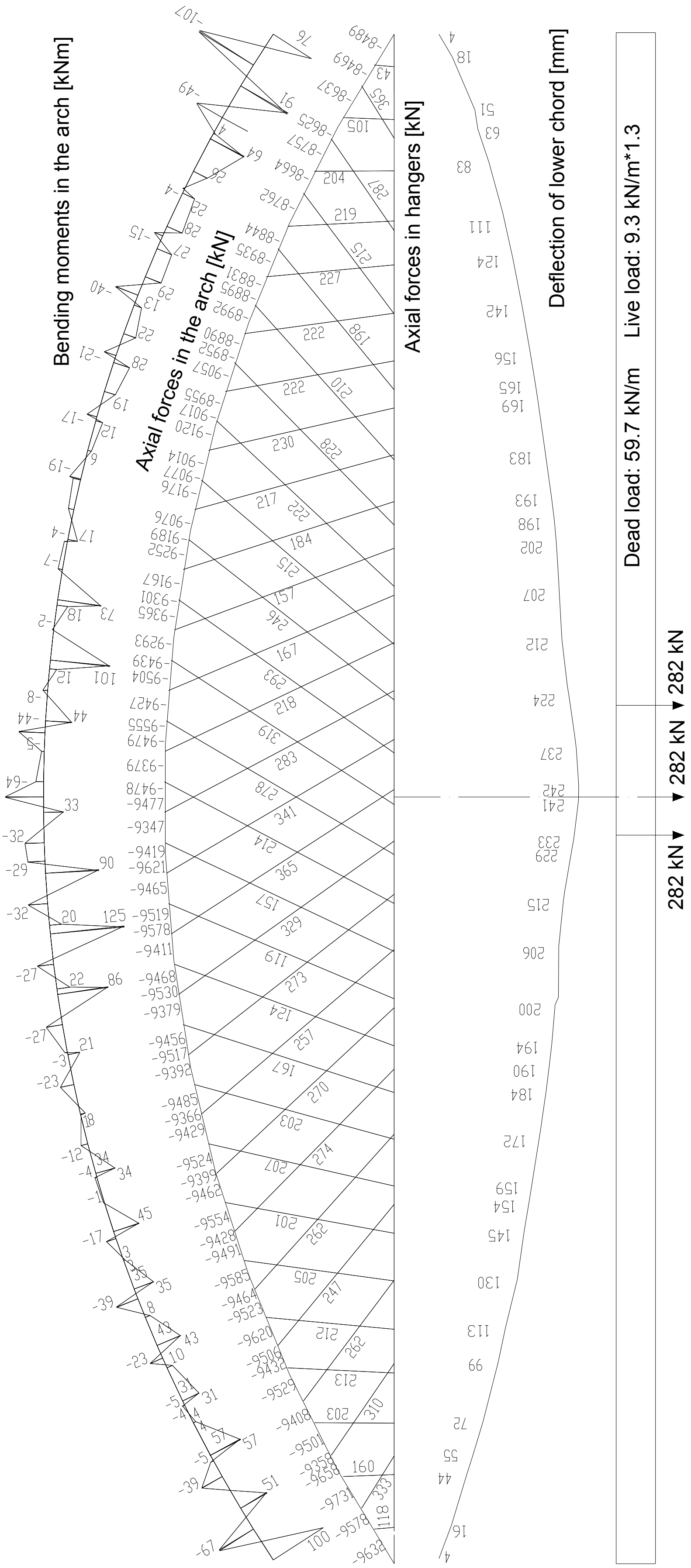

Fig. F.7. Maximum load on the bridge with a test hanger arrangement according to the proposal of Brunn & Schanack in the ultimate limit state. The wheel loads are in the middle of the span

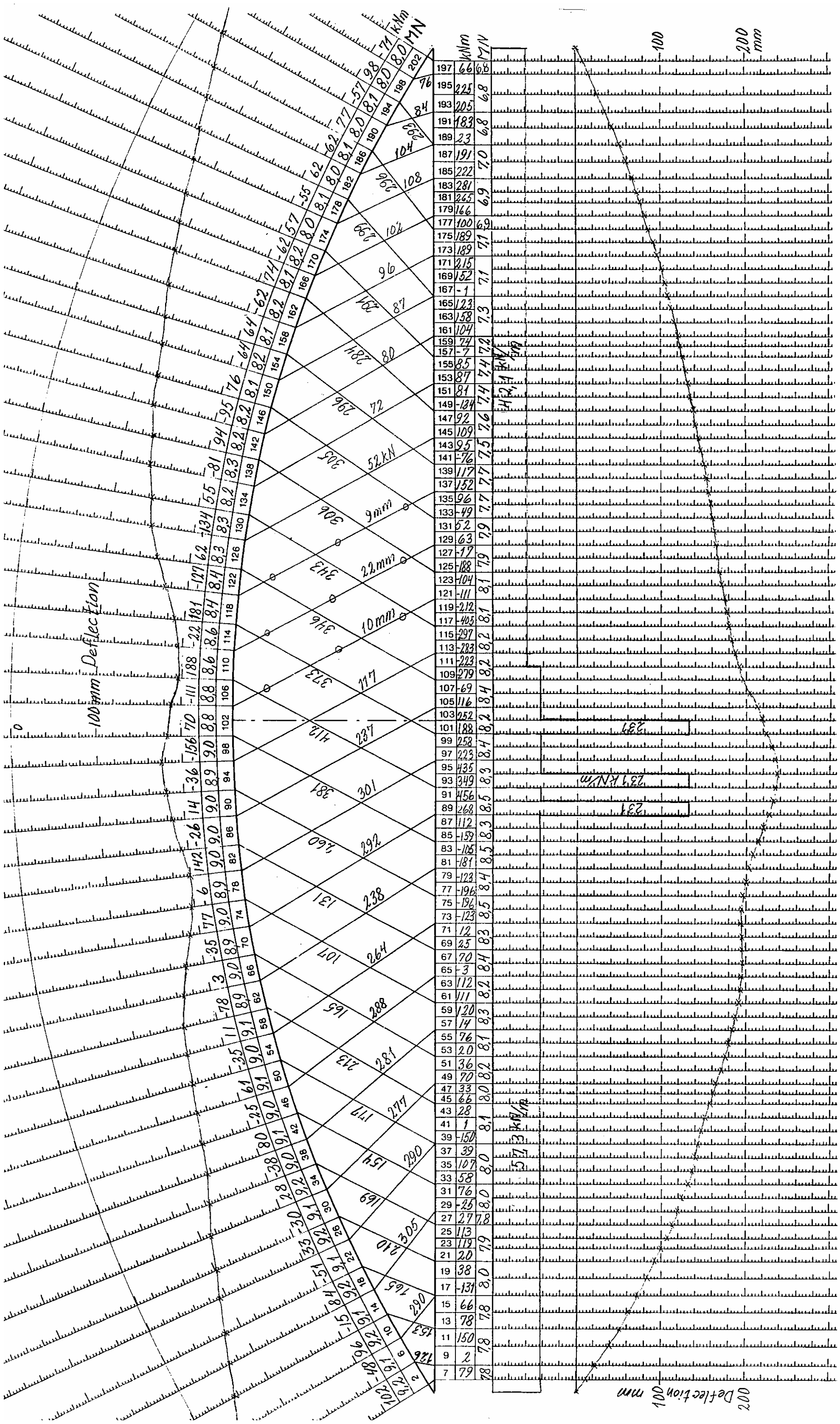

Fig. F.8. Forces due to live loads on the left 54% of the Åkviksound network arch in the ultimate limit state. Half the weight of asphalt on the whole span is assumed. Three hangers relax

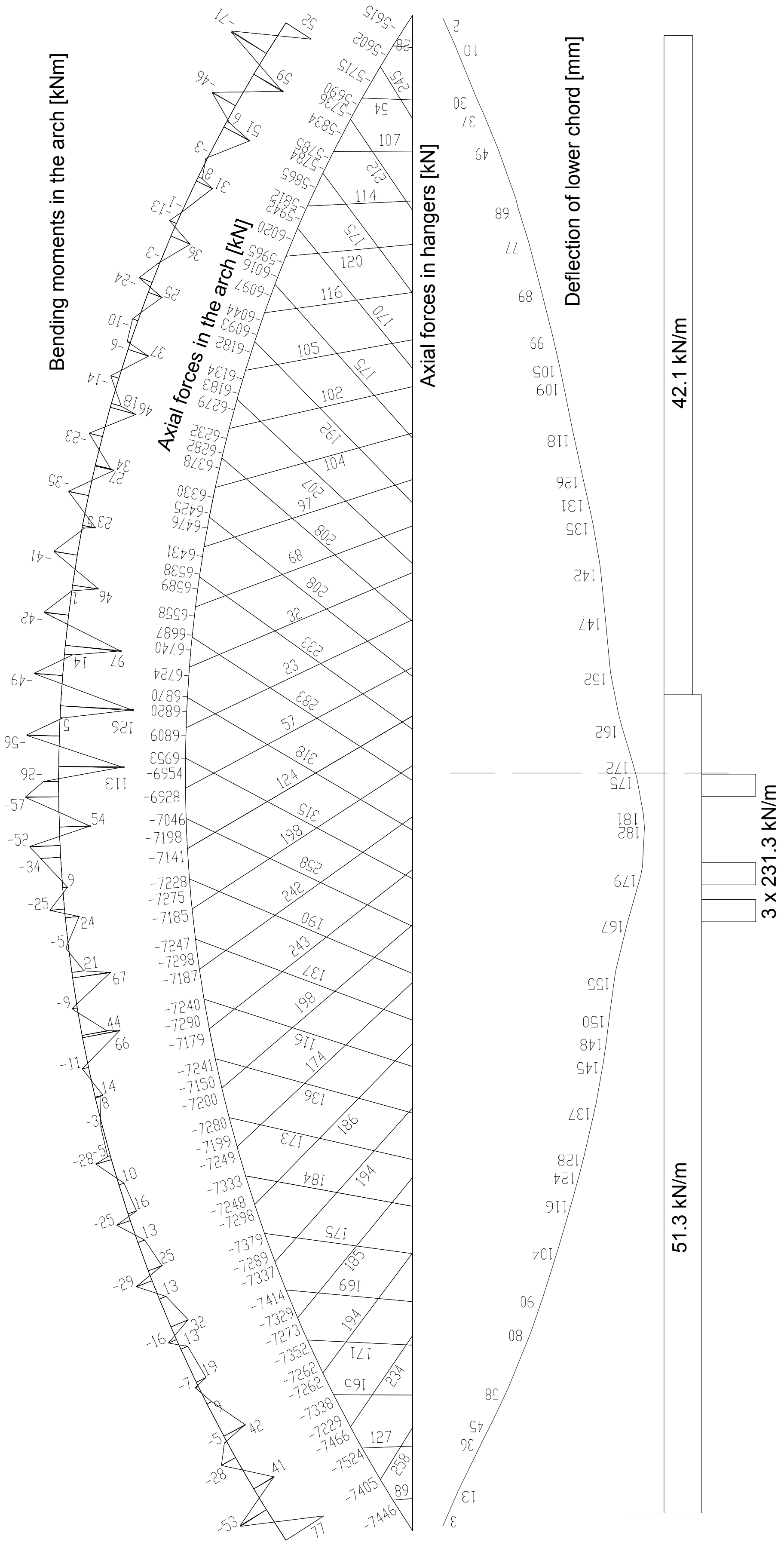

Fig. F.9. Forces due to live loads on the left 54% of the bridge with a test of the hanger arrangement proposed by Brunn & Schanack in the ultimate limit state. Half the weight of asphalt on the whole span is assumed. No hangers relax.

As can be seen in figures F.1 to F.9, the proposed hanger arrangement gives better results for all compared properties. The following table will help to estimate how much the difference is. The corresponding values of the influence lines and the maximum values from both load cases are shown.

	Åkviksound bridge	Test of proposed hanger arrangement	"Test" / "Åkviksound" [%]	average
Axial force in arch				
(Figure F.1)	-1.84	-1.74	94.57	
	-1.75	-1.75	100.00	
	-1.68	-1.69	100.60	
	-1.78	-1.73	97.19	98.09
Axial force in hangers				
(Figure F.2)	0.54	0.37	68.52	
	0.39	0.3	76.92	
	0.37	0.24	64.86	
	0.32	0.23	71.88	
	0.26	0.22	84.62	
	0.23	0.21	91.30	
(Figure F.3)	0.43	0.39	90.70	
	0.35	0.26	74.29	
	0.34	0.22	64.71	
	0.28	0.23	82.14	
	0.23	0.22	95.65	
	0.22	0.19	86.36	79.33
Bending moments in the arch				
(Figure F.4)	0.21	0.22	104.76	
	0.23	0.18	78.26	
	0.29	0.17	58.62	
	0.26	0.18	69.23	
	0.23	0.15	65.22	
	-0.21	-0.21	100.00	
(Figure F.5)	0.28	0.28	100.00	
	0.19	0.16	84.21	
	0.28	0.18	64.29	
	0.23	0.18	78.26	
	-0.22	-0.19	86.36	80.84
Load on whole span				
(Figures F.6 and F.7)				
maximum axial force in arch [MN]	-10.3	-9.7	94.17	
maximum hanger force [kN]	414.6	365	88.04	
maximum bending moment [kNm]	170	125	73.53	85.25
maximum deflection [mm]	275	242	88.00	
Load in 54% of span				
(Figures F.8 and F.9)				
maximum axial force in arch [MN]	-9.2	-7.5	81.52	
maximum hanger force [kN]	412	318	77.18	
maximum bending moment [kNm]	220	126	57.27	71.99
maximum deflection [mm]	239	182	76.15	
relaxed hangers	3	0		

Fig. F.10. Composition of some relevant values from the comparison

With the proposed hanger arrangement forces and deflections are, on an overall average, 82 % of what they are in the Åkviksound network arch. If the cross angle and the position of the first several hangers of the test hanger arrangement is optimised according to Section 6, the difference will be even bigger.

F.2 Results from the variation of the lower hanger nodes by the node distances

On the following 13 pages internal forces from the calculations explained in Section 6.5.1 are listed.

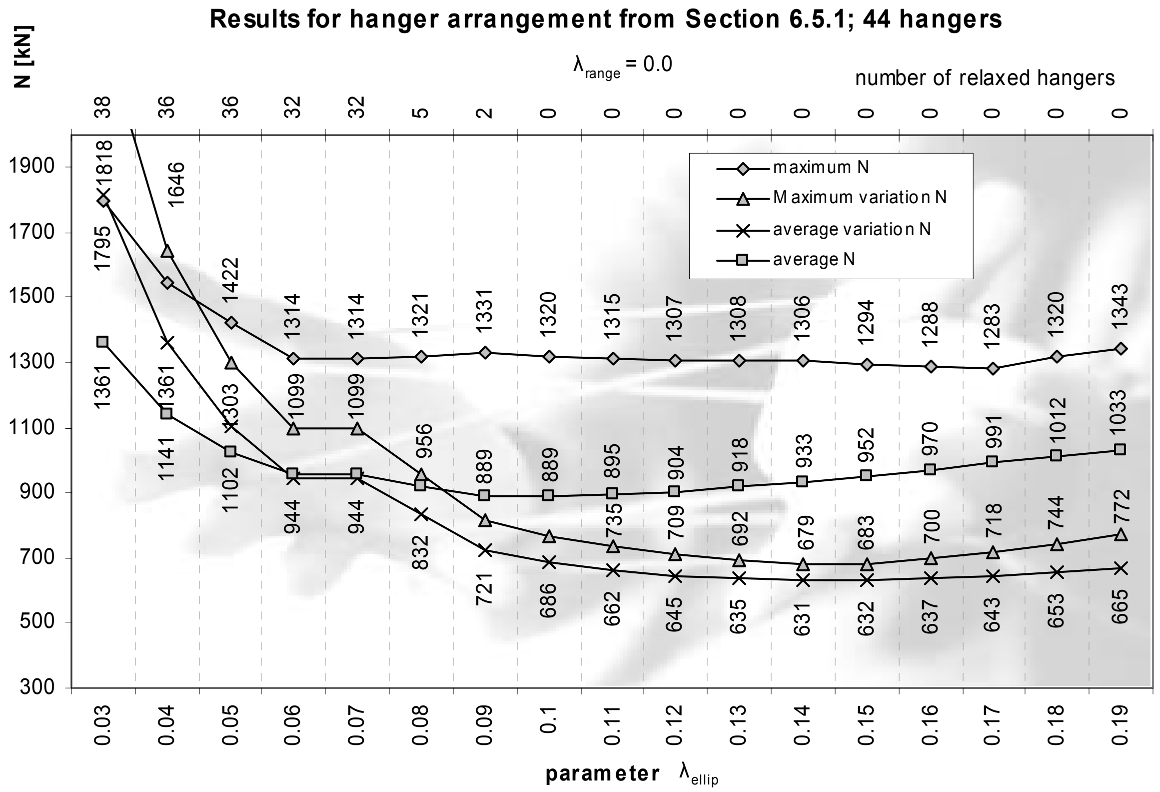

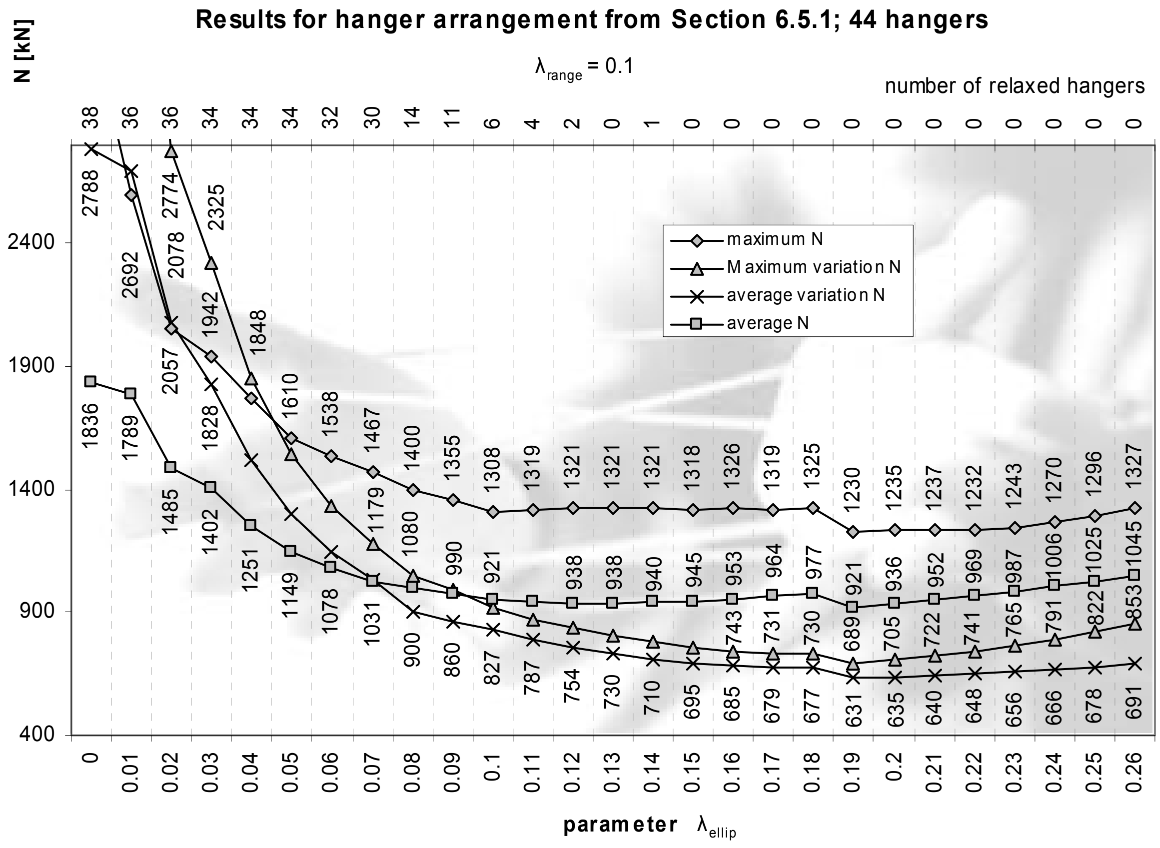

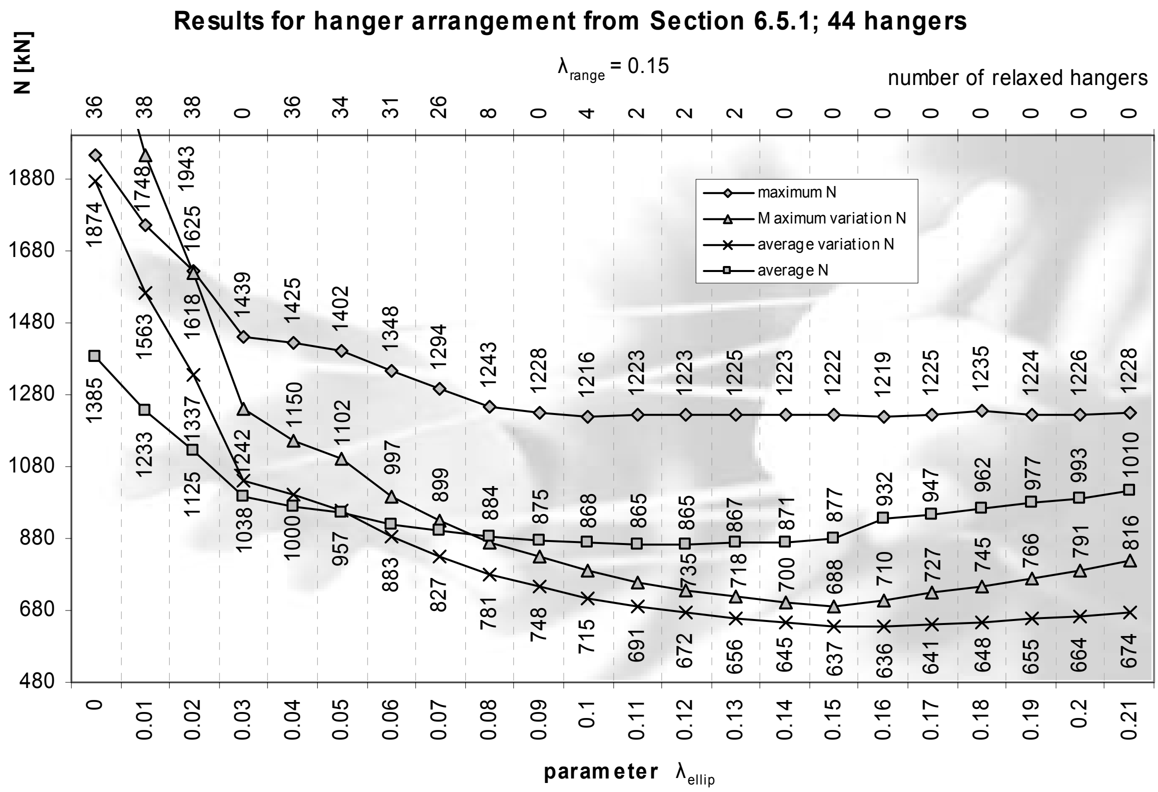
Results for hanger arrangement from Section 6.5.1; 44 hangers
λrange = 0.15
number of relaxed hangers
N [kN]
maximum N
Maximum variation N
average variation N
average N
parameter λellip

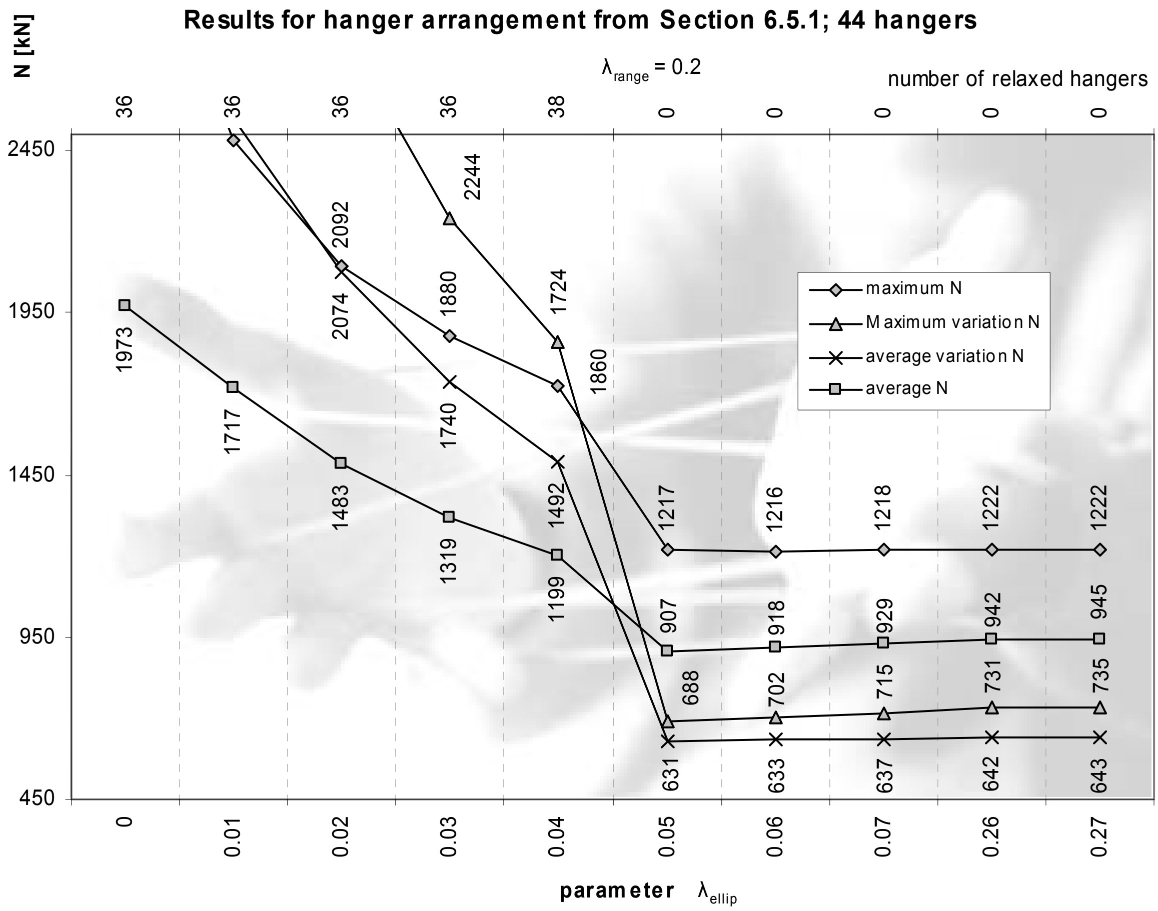
Results for hanger arrangement from Section 6.5.1; 44 hangers
λrange = 0.2
number of relaxed hangers
N [kN]
maximum N
Maximum variation N
average variation N
average N
parameter λellip

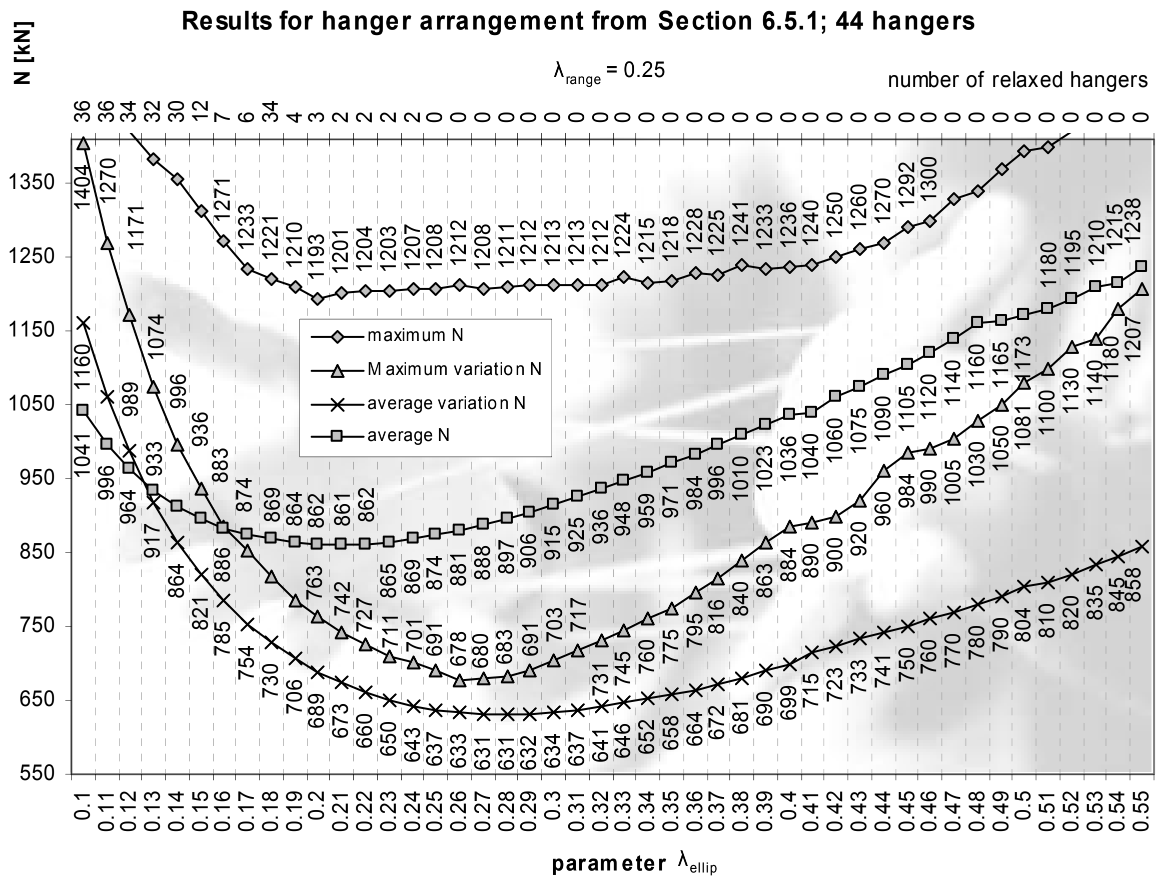
Results for hanger arrangement from Section 6.5.1; 44 hangers
λ_{range} = 0.25
number of relaxed hangers
N [kN]
maximum N
Maximum variation N
average variation N
average N
parameter λ_{ellip}

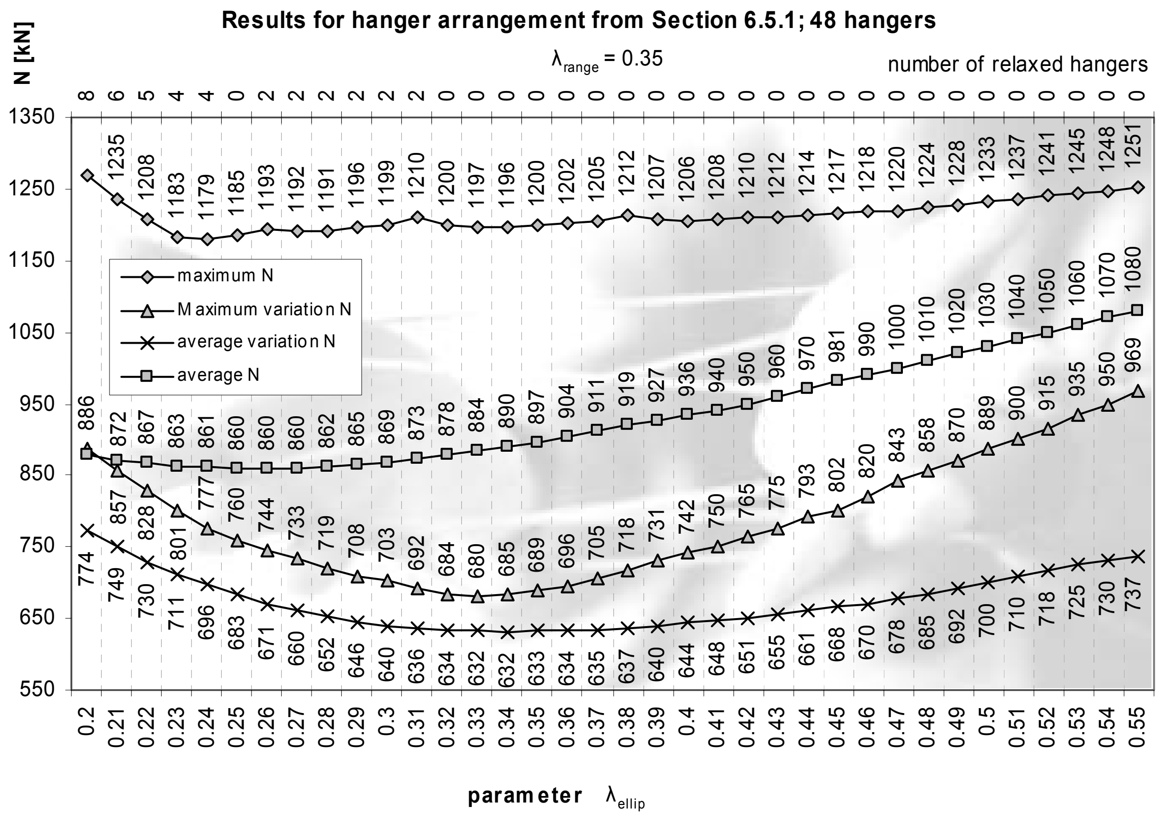
Results for hanger arrangement from Section 6.5.1; 48 hangers
λ_{range} = 0.35
number of relaxed hangers
N [kN]
maximum N
Maximum variation N
average variation N
average N
parameter λ_{ellip}

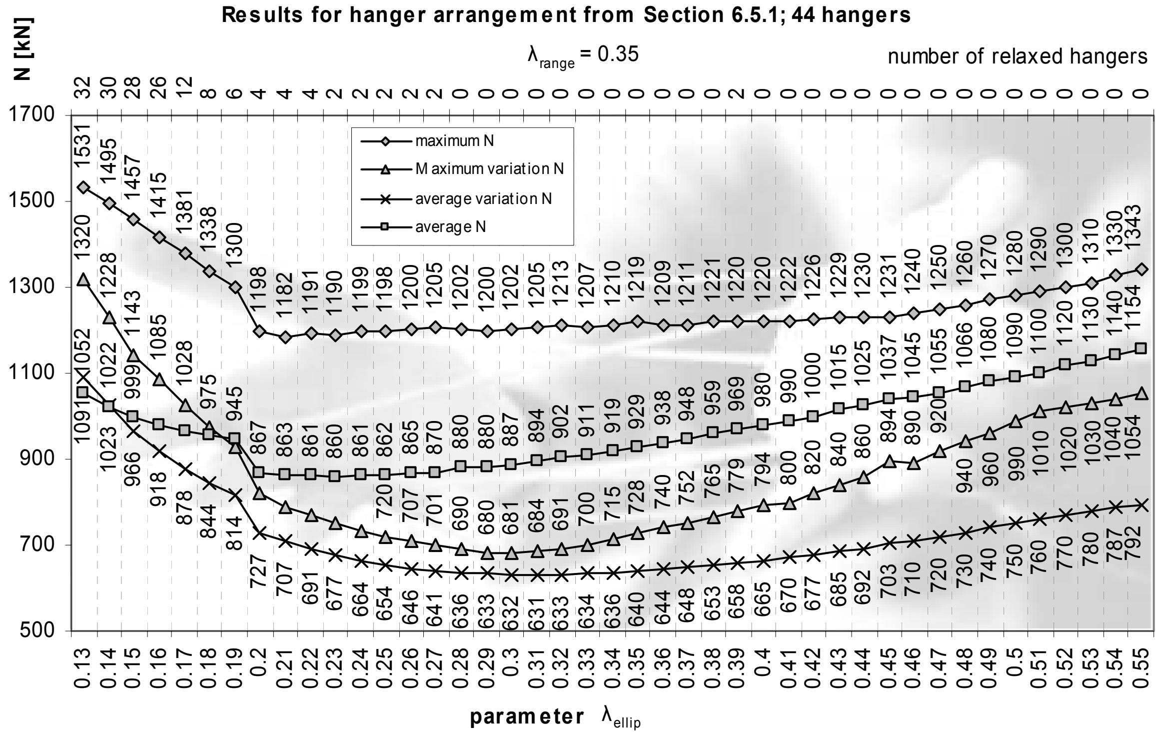
Results for hanger arrangement from Section 6.5.1; 44 hangers
λ_{range} = 0.35
number of relaxed hangers
N [kN]
maximum N
Maximum variation N
average variation N
average N
parameter λ_{ellip}

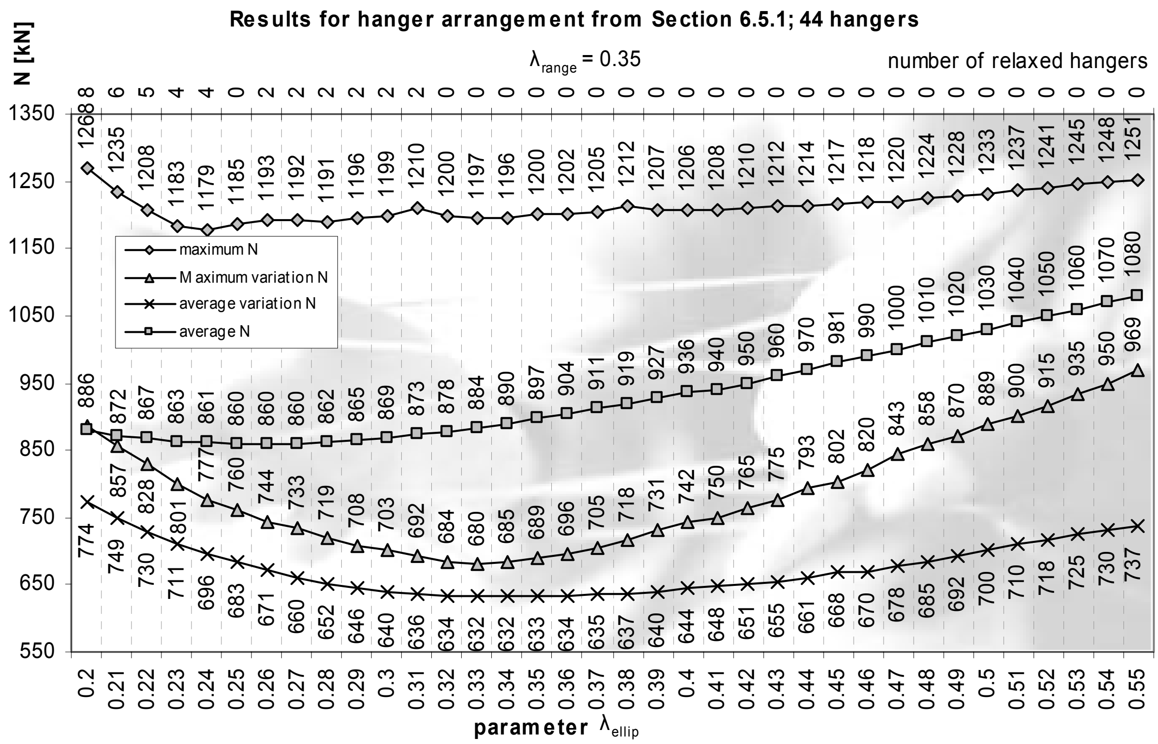
Results for hanger arrangement from Section 6.5.1; 44 hangers
λ_{range} = 0.35
number of relaxed hangers
N [kN]
maximum N
Maximum variation N
average variation N
average N
parameter λ_{ellip}

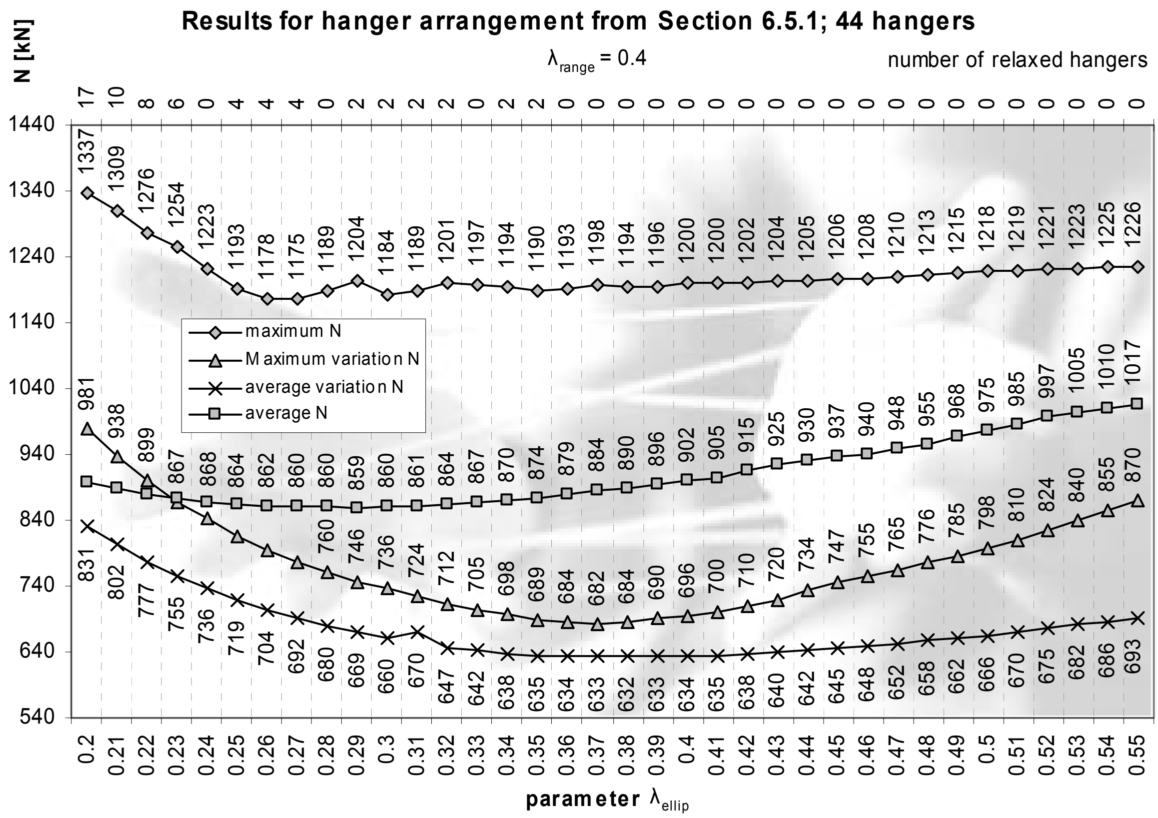
Results for hanger arrangement from Section 6.5.1; 44 hangers
λrange = 0.4
number of relaxed hangers
N [kN]
maximum N
Maximum variation N
average variation N
average N
parameter λellip

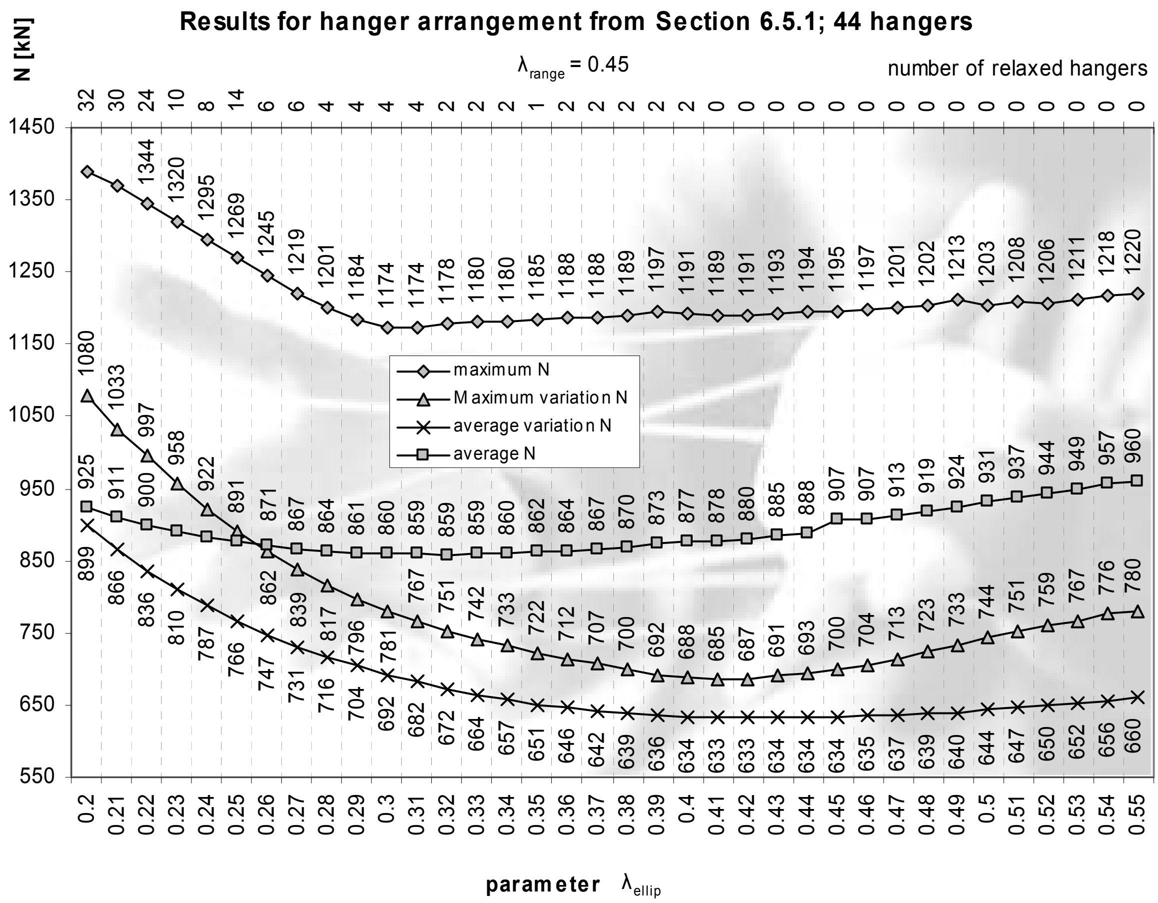
Results for hanger arrangement from Section 6.5.1; 44 hangers
λrange = 0.45
number of relaxed hangers
N [kN]
maximum N
Maximum variation N
average variation N
average N
parameter λellip

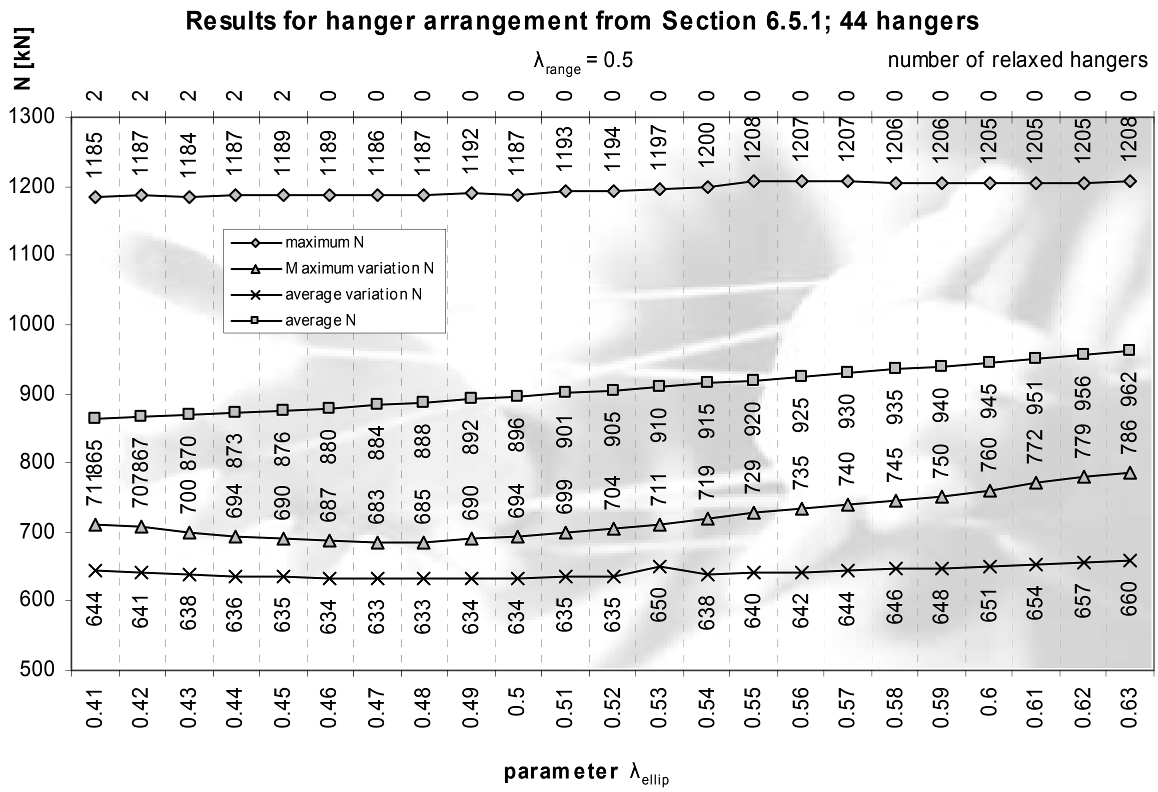
Results for hanger arrangement from Section 6.5.1; 44 hangers
λrange = 0.5
number of relaxed hangers
N [kN]
maximum N
Maximum variation N
average variation N
average N
parameter λellip

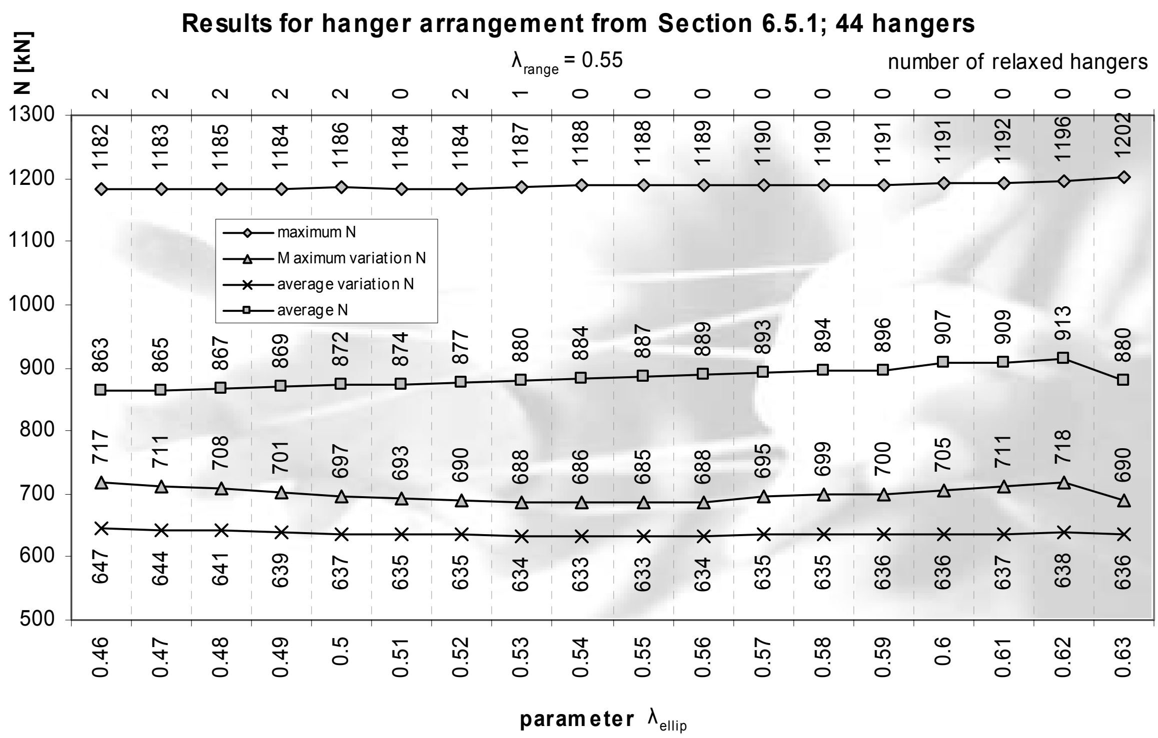
Results for hanger arrangement from Section 6.5.1; 44 hangers
λrange = 0.55
number of relaxed hangers
N [kN]
maximum N
Maximum variation N
average variation N
average N
parameter λellip

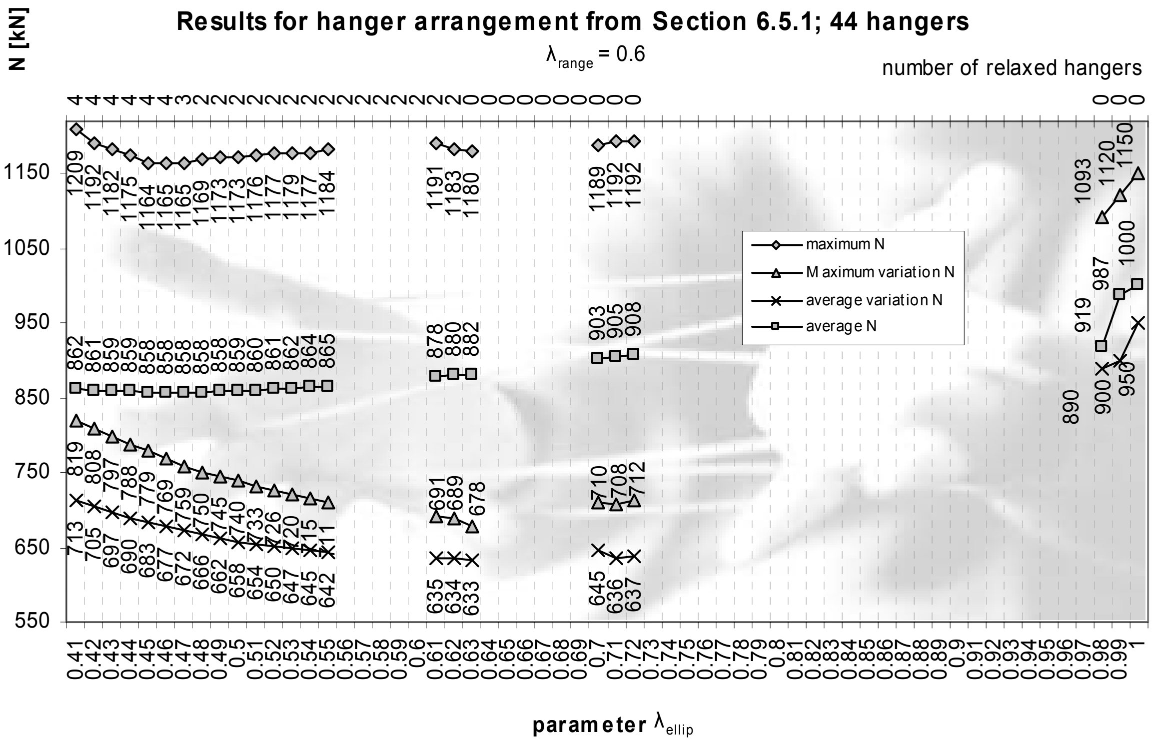
Results for hanger arrangement from Section 6.5.1; 44 hangers
λ_{range} = 0.6
number of relaxed hangers
N [kN]
maximum N
Maximum variation N
average variation N
average N
parameter λ_{ellip}

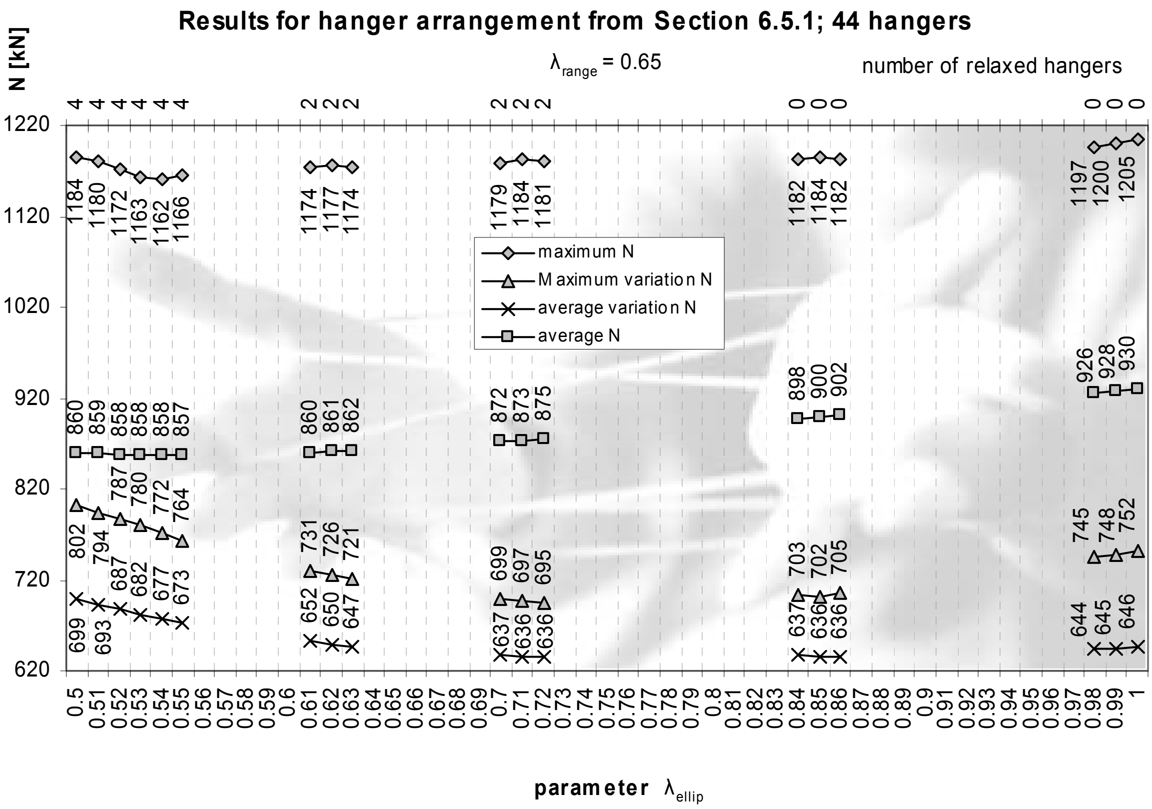
Results for hanger arrangement from Section 6.5.1; 44 hangers
λ_{range} = 0.65
number of relaxed hangers
N [kN]
maximum N
Maximum variation N
average variation N
average N
parameter λ_{ellip}

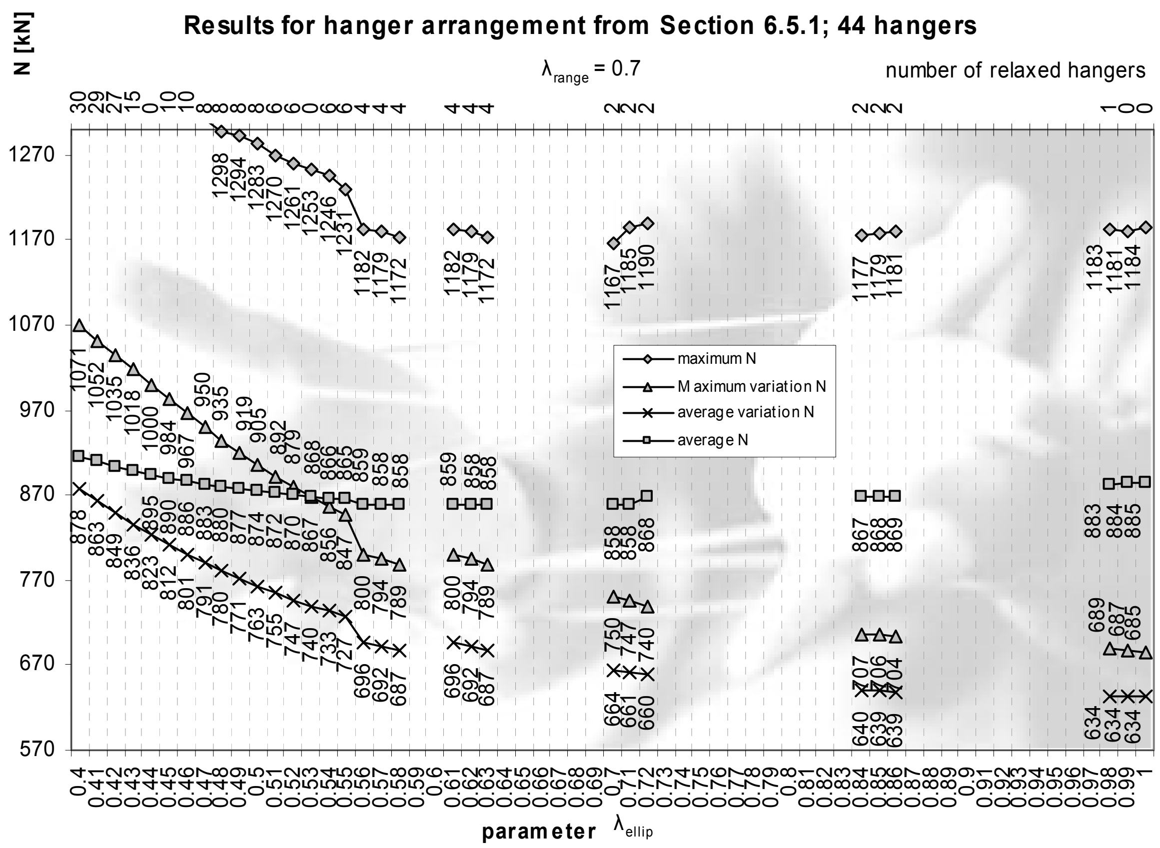
Results for hanger arrangement from Section 6.5.1; 44 hangers
λ_{range} = 0.7
number of relaxed hangers
N [kN]
maximum N
Maximum variation N
average variation N
average N
parameter λ_{ellip}

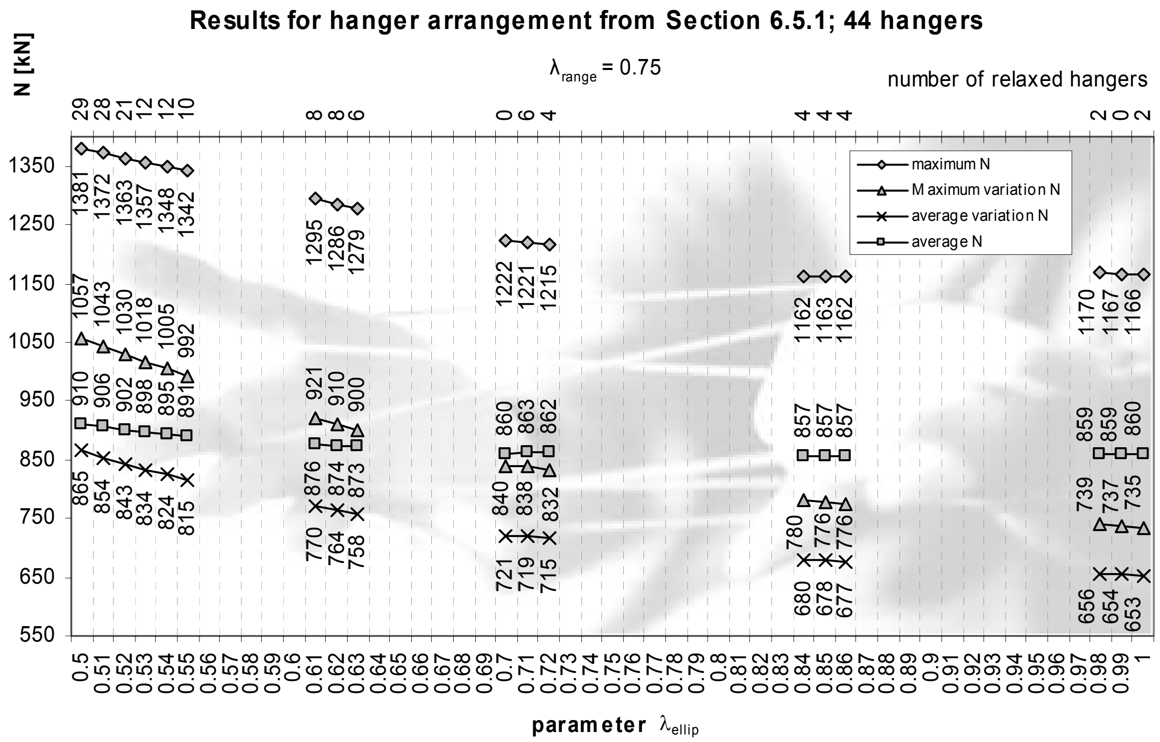
Results for hanger arrangement from Section 6.5.1; 44 hangers
λ_{range} = 0.75
number of relaxed hangers
N [kN]
maximum N
Maximum variation N
average variation N
average N
parameter λ_{ellip}

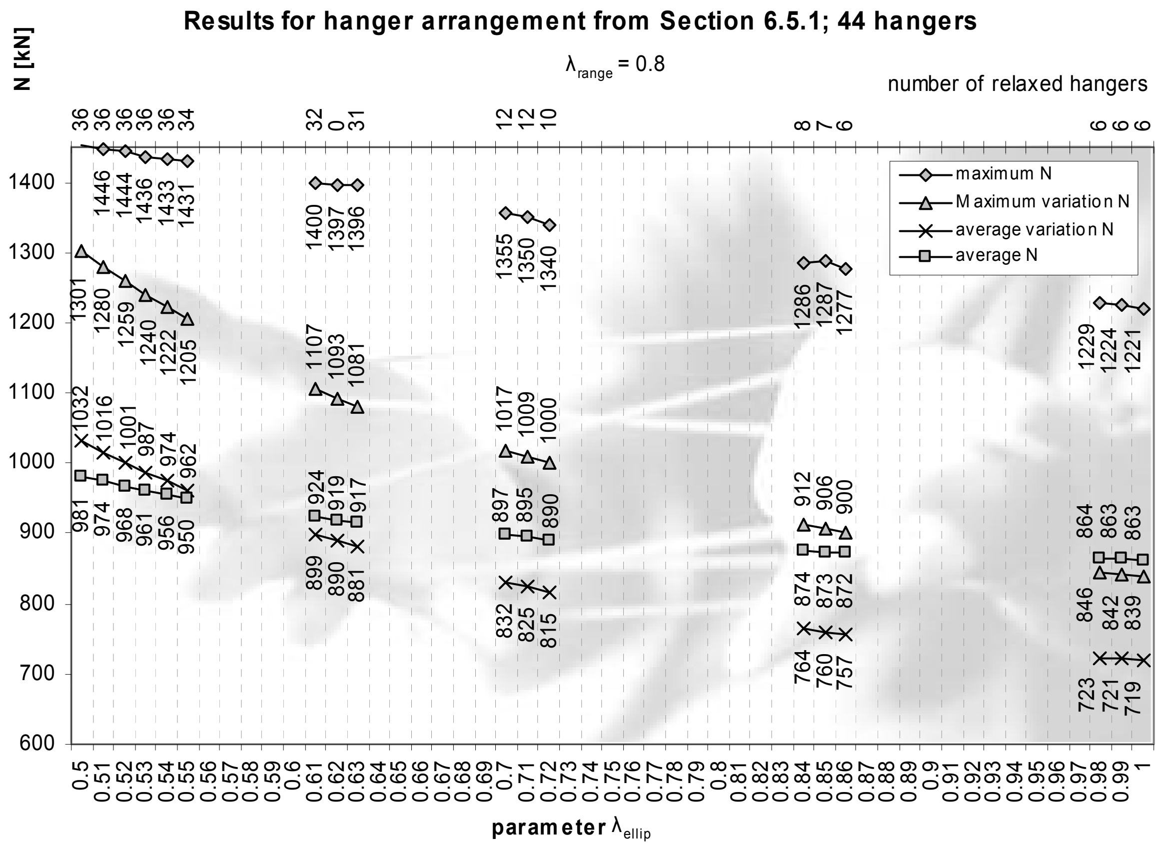
Results for hanger arrangement from Section 6.5.1; 44 hangers
λrange = 0.8
number of relaxed hangers
N [kN]
maximum N
Maximum variation N
average variation N
average N
parameter λellip

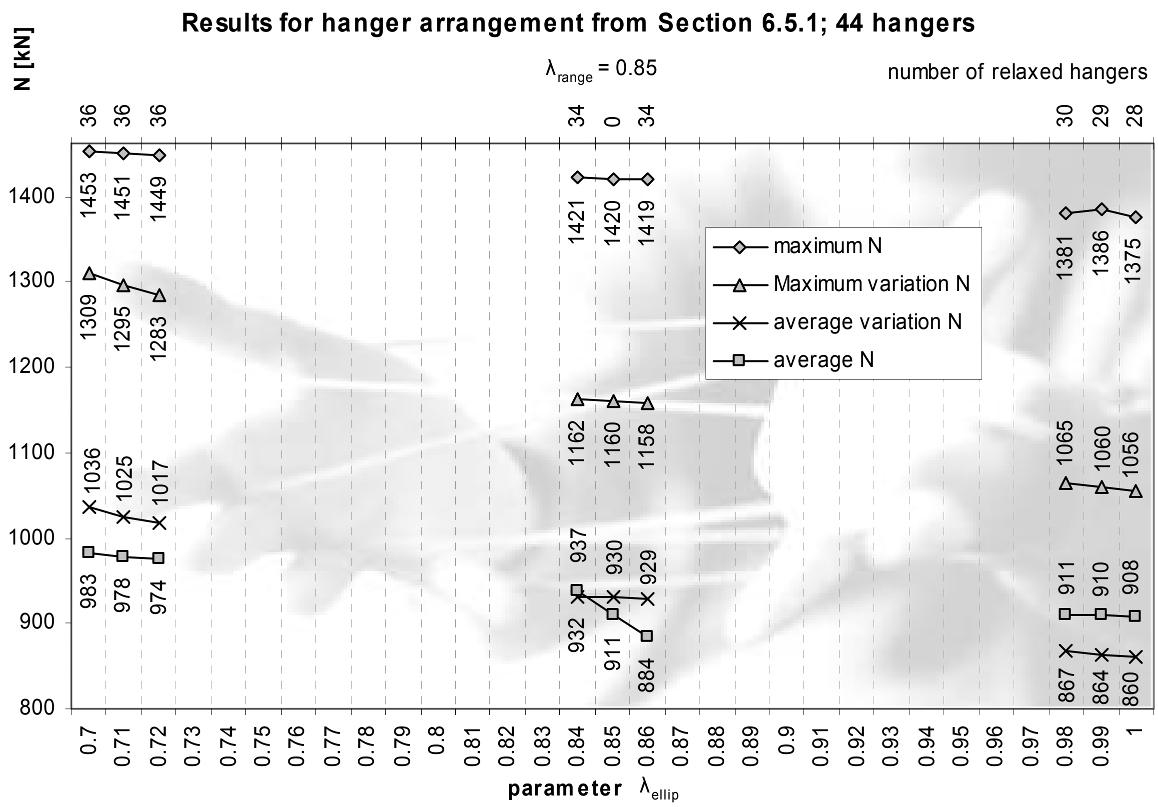
Results for hanger arrangement from Section 6.5.1; 44 hangers
λrange = 0.85
number of relaxed hangers
N [kN]
maximum N
Maximum variation N
average variation N
average N
parameter λellip

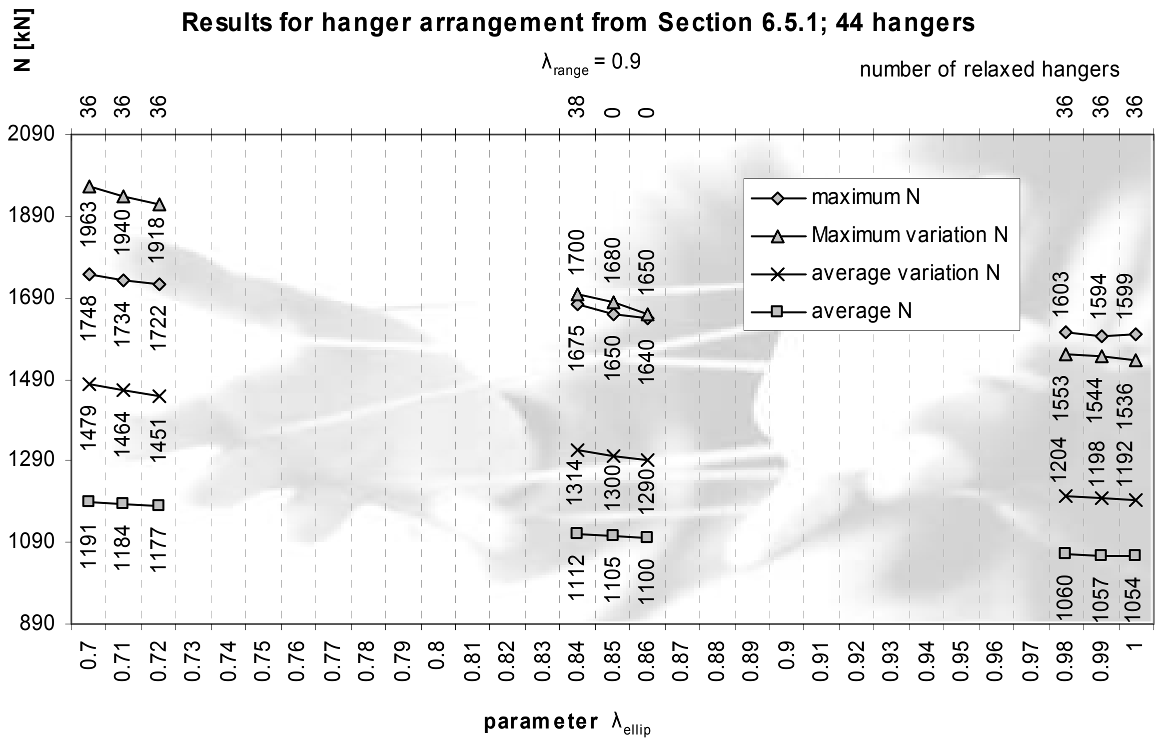
Results for hanger arrangement from Section 6.5.1; 44 hangers
λ_{range} = 0.9
number of relaxed hangers
N [kN]
maximum N
Maximum variation N
average variation N
average N
parameter λ_{ellip}

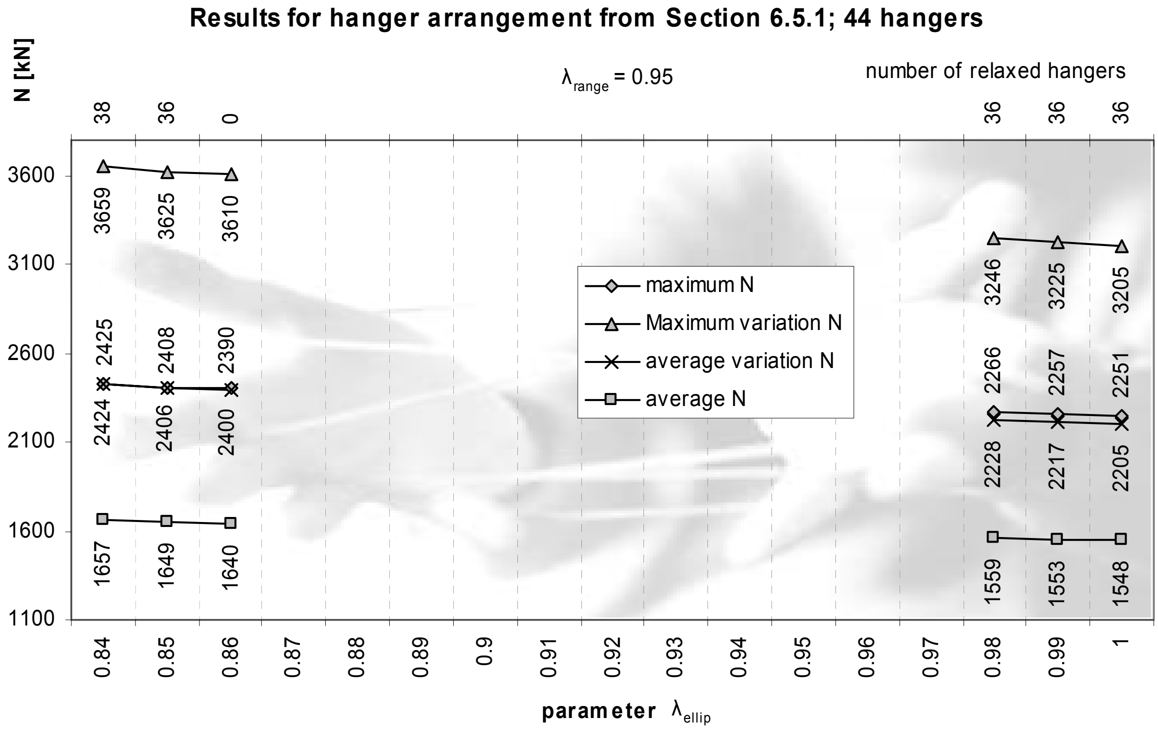
Results for hanger arrangement from Section 6.5.1; 44 hangers
λ_{range} = 0.95
number of relaxed hangers
N [kN]
maximum N
Maximum variation N
average variation N
average N
parameter λ_{ellip}

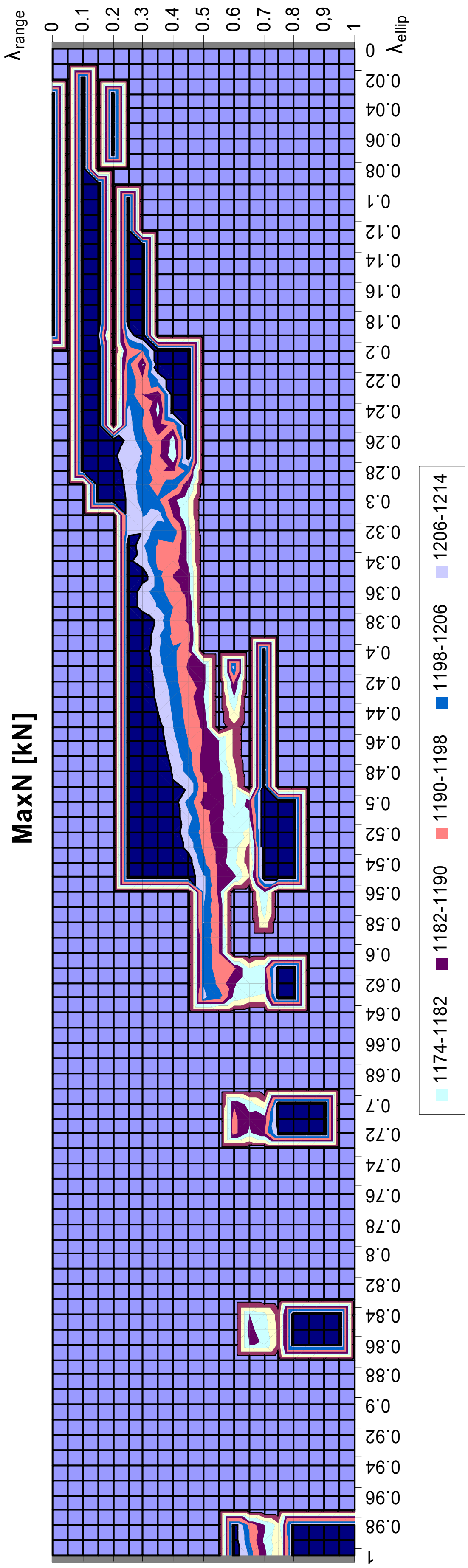
MaxN [kN]
λ_{range}
λ_{ellip}
1174-1182
1182-1190
1190-1198
1198-1206
1206-1214

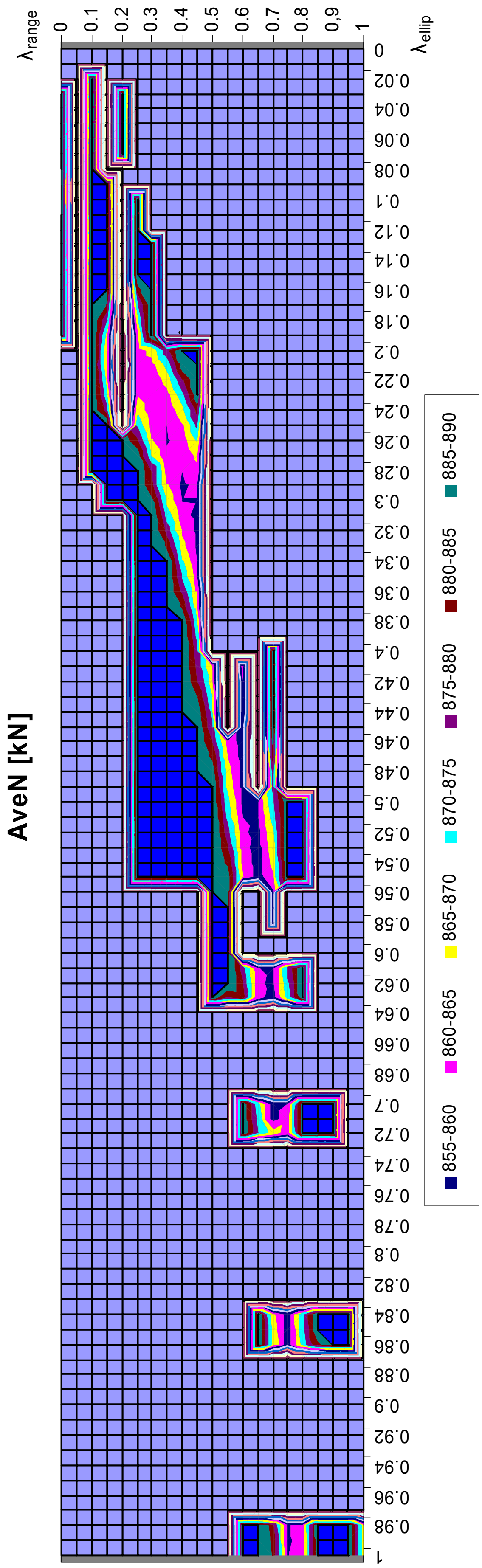
AveN [kN]
λ_{range}
λ_{ellip}
855-860
860-865
865-870
870-875
875-880
880-885
885-890

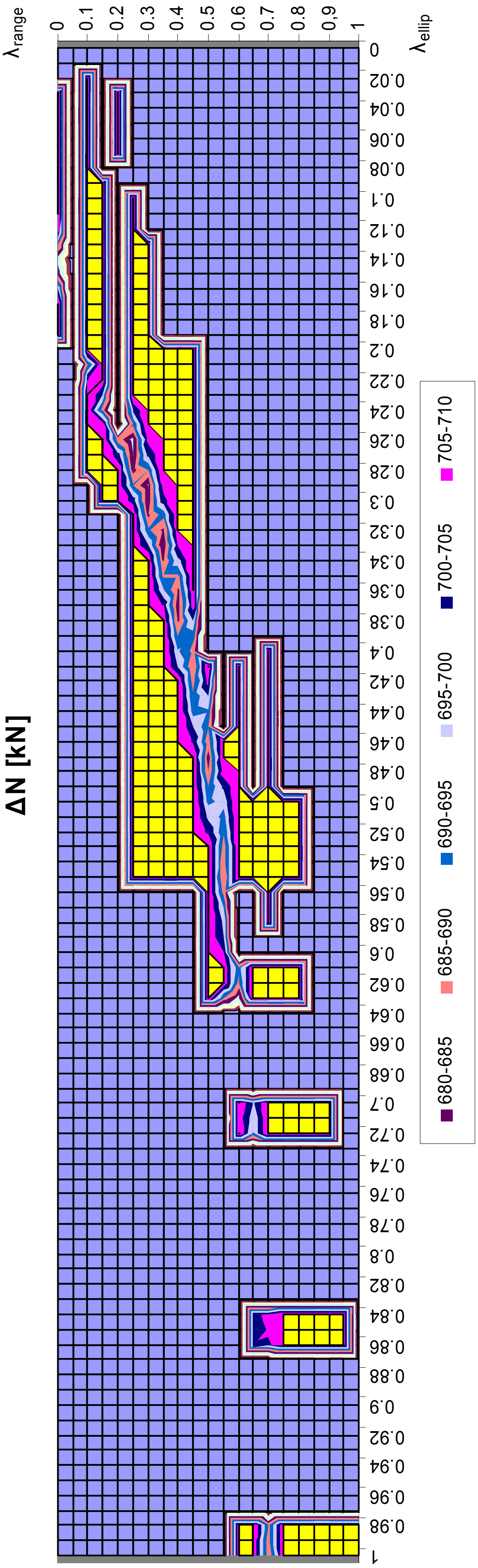
ΔN [kN]
λrange
λellip
680-685
685-690
690-695
695-700
700-705
705-710

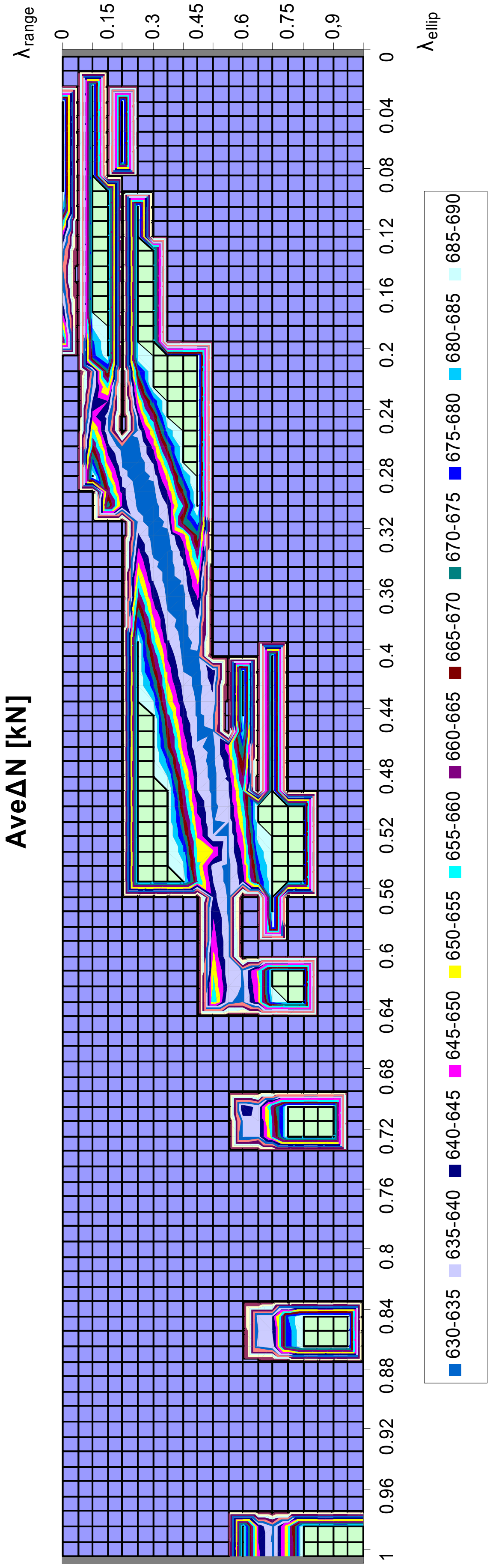
AveΔN [kN]
λrange
λellip
630-635
635-640
640-645
645-650
650-655
655-660
660-665
665-670
670-675
675-680
680-685
685-690

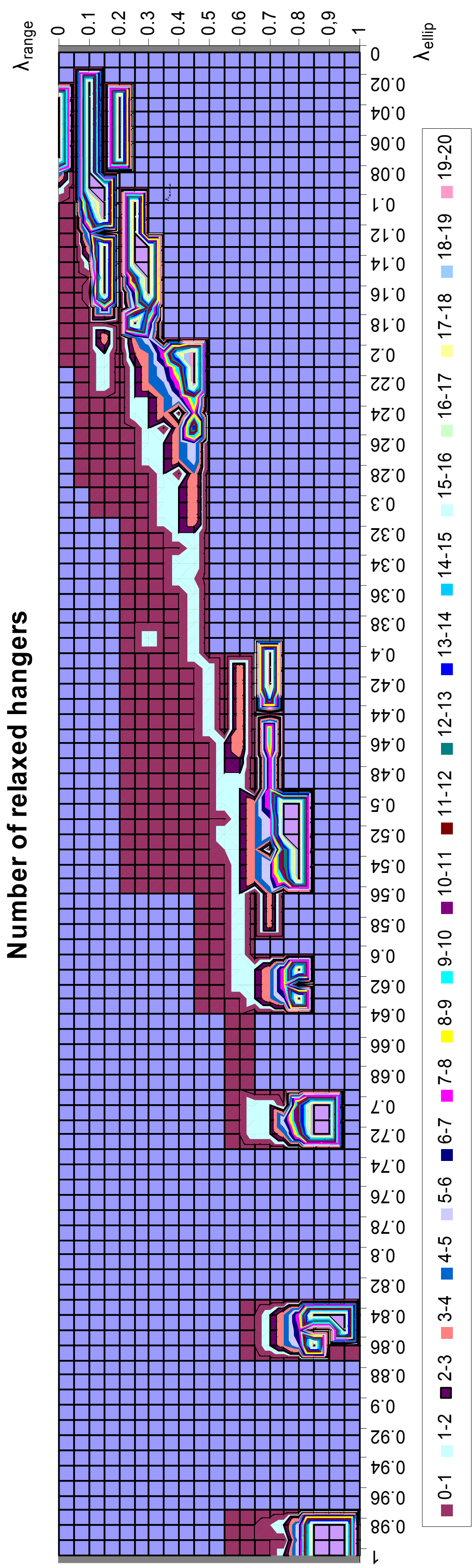
Number of relaxed hangers
λrange
0
0.1
0.2
0.3
0.4
0.5
0.6
0.7
0.8
0.9
1
λellip
0
0.02
0.04
0.06
0.08
0.1
0.12
0.14
0.16
0.18
0.2
0.22
0.24
0.26
0.28
0.3
0.32
0.34
0.36
0.38
0.4
0.42
0.44
0.46
0.48
0.5
0.52
0.54
0.56
0.58
0.6
0.62
0.64
0.66
0.68
0.7
0.72
0.74
0.76
0.78
0.8
0.82
0.84
0.86
0.88
0.9
0.92
0.94
0.96
0.98
1
0-1
1-2
2-3
3-4
4-5
5-6
6-7
7-8
8-9
9-10
10-11
11-12
12-13
13-14
14-15
15-16
16-17
17-18
18-19
19-20

F.3 Results from the variation of the lower hanger nodes by the slope of the hangers

On the following 11 pages internal forces from the calculations explained in Section 6.5.2 are listed.

Results for hanger arrangemants from Section 6.5.2, start angle 50, number of hangers 44, no variable angle change

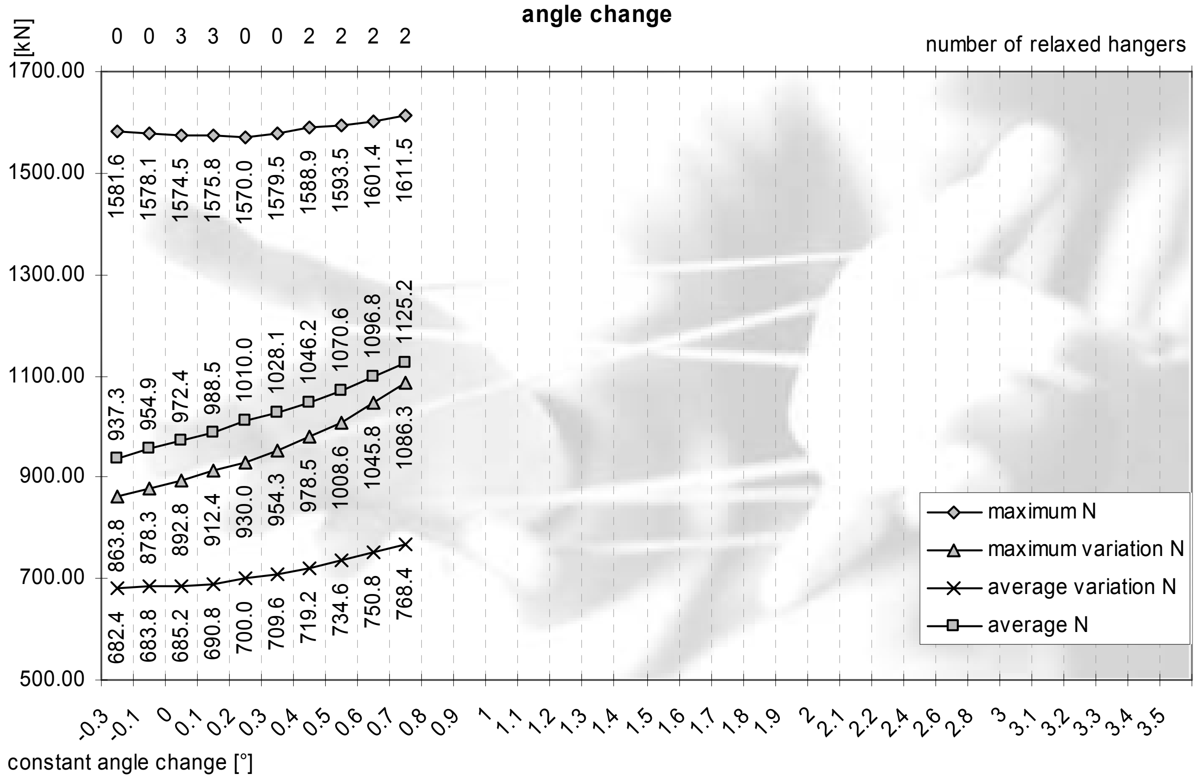

Results for hanger arrangemants from Section 6.5.2, start angle 53°, number of hangers 44, no variable angle change

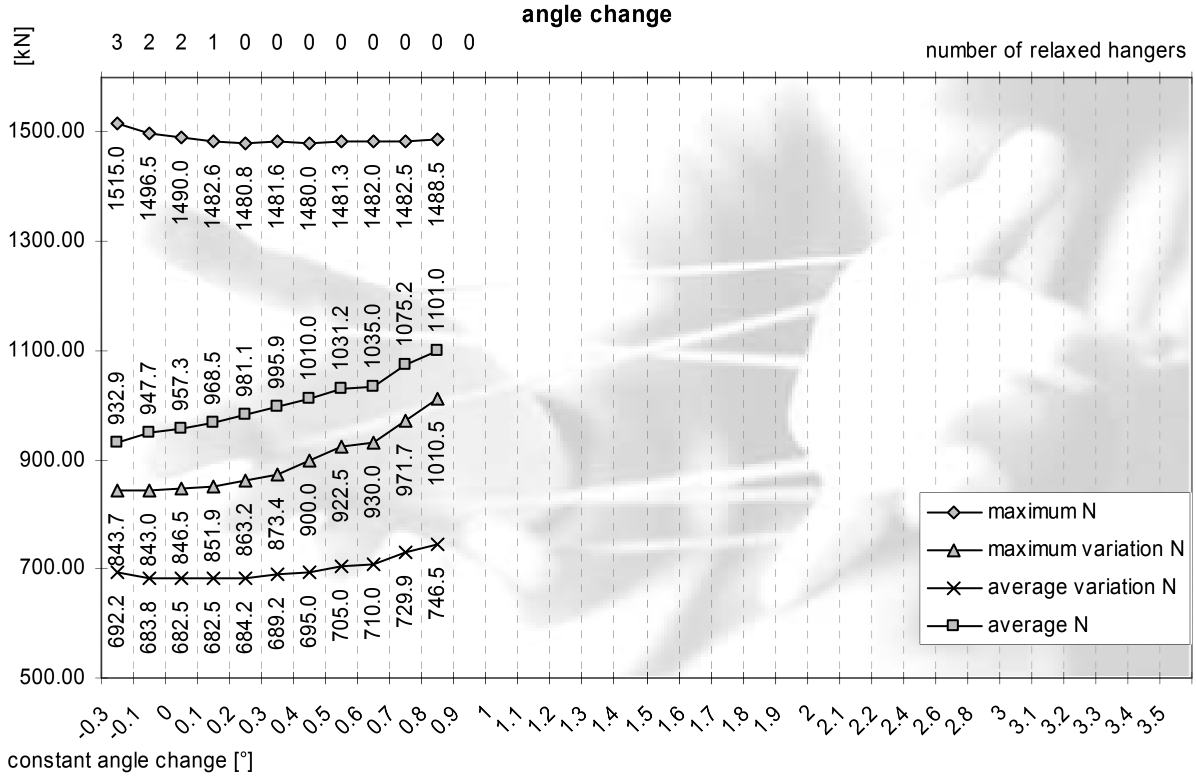

Results for hanger arrangemants from Section 6.5.2, start angle 56°, number of hangers 44, no variable angle change

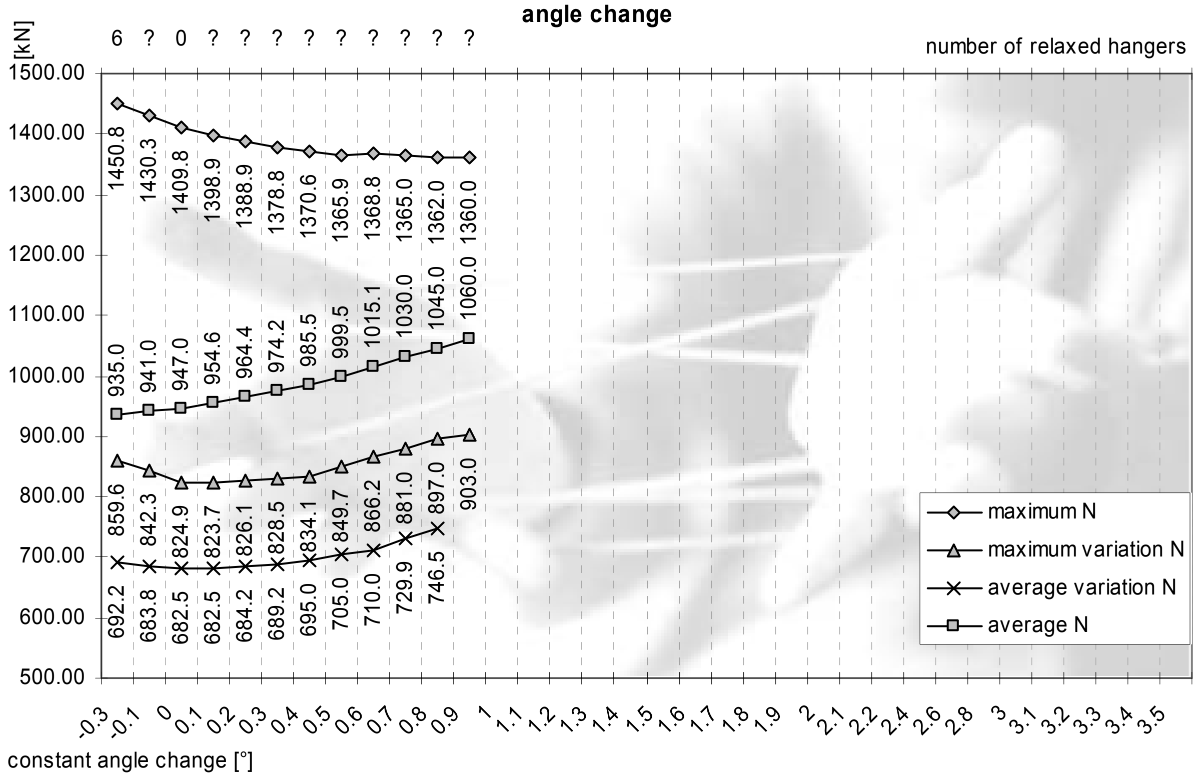

Results for hanger arrangemants from Section 6.5.2, start angle 57°, number of hangers 44, no variable angle change

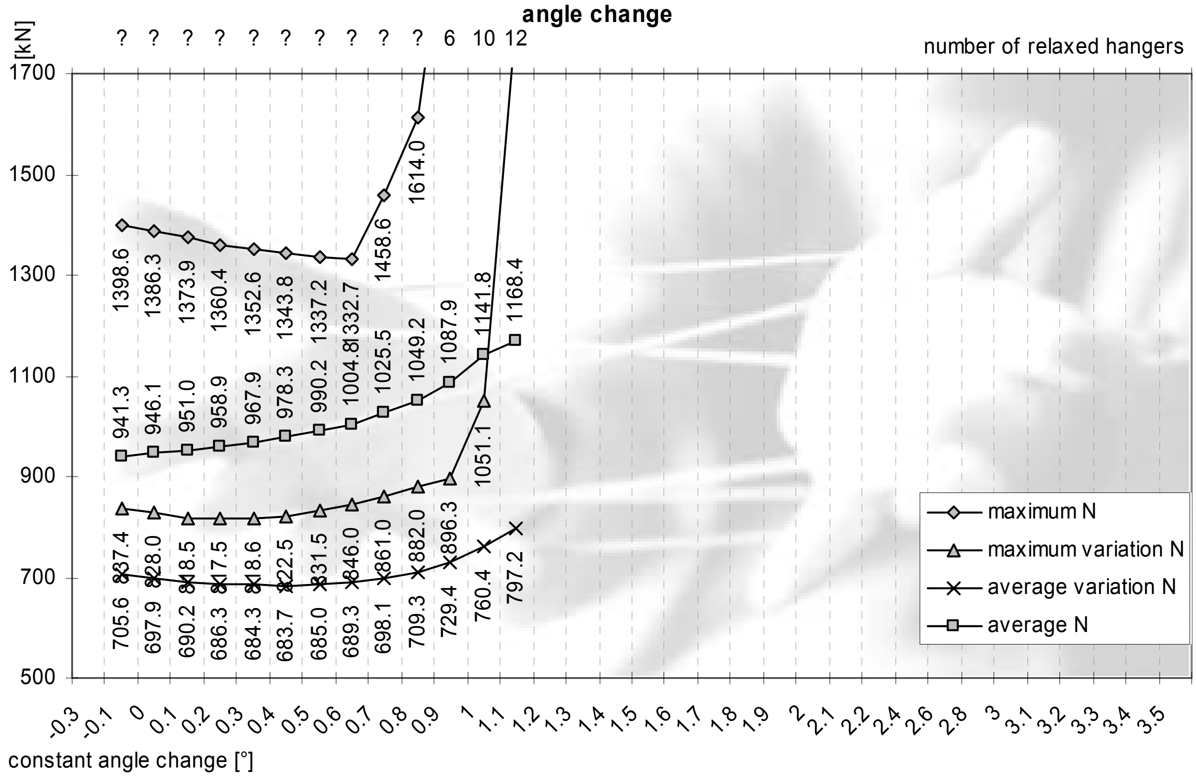

Results for hanger arrangemants from Section 6.5.2, start angle 58°, number of hangers 44, no variable angle change

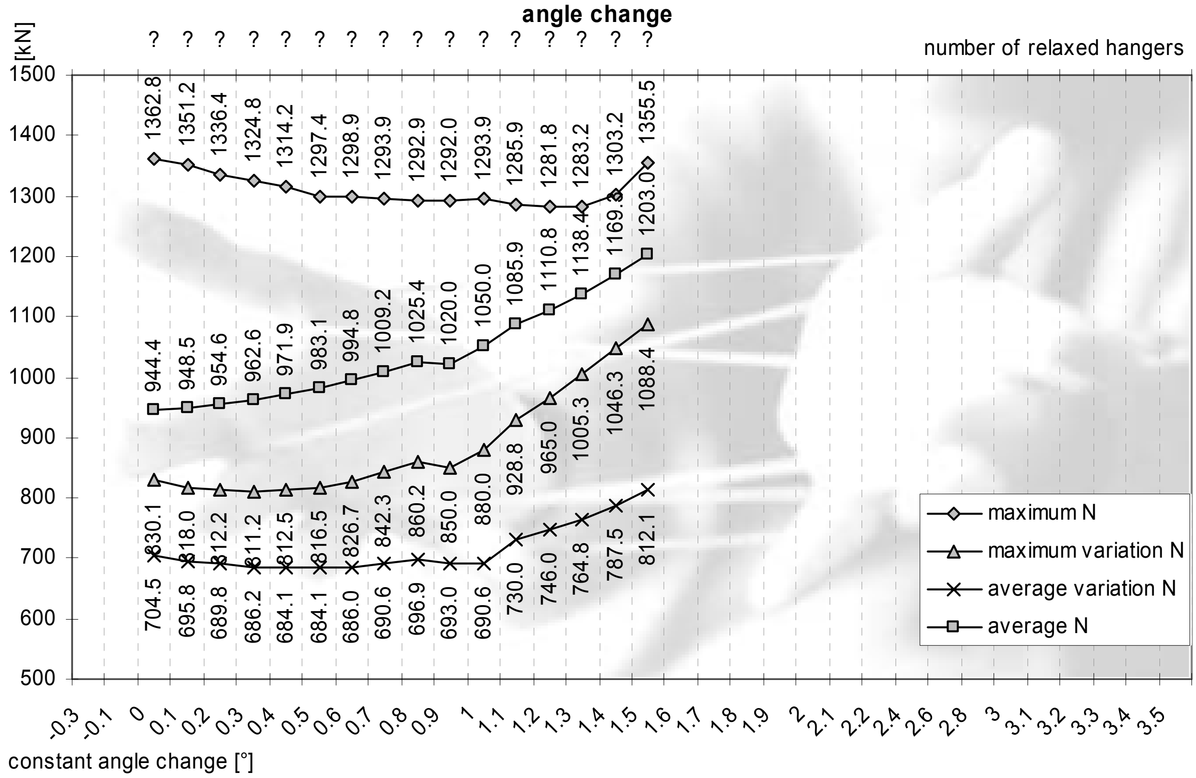

Results for hanger arrangemants from Section 6.5.2, start angle 59°, number of hangers 44, no variable angle change

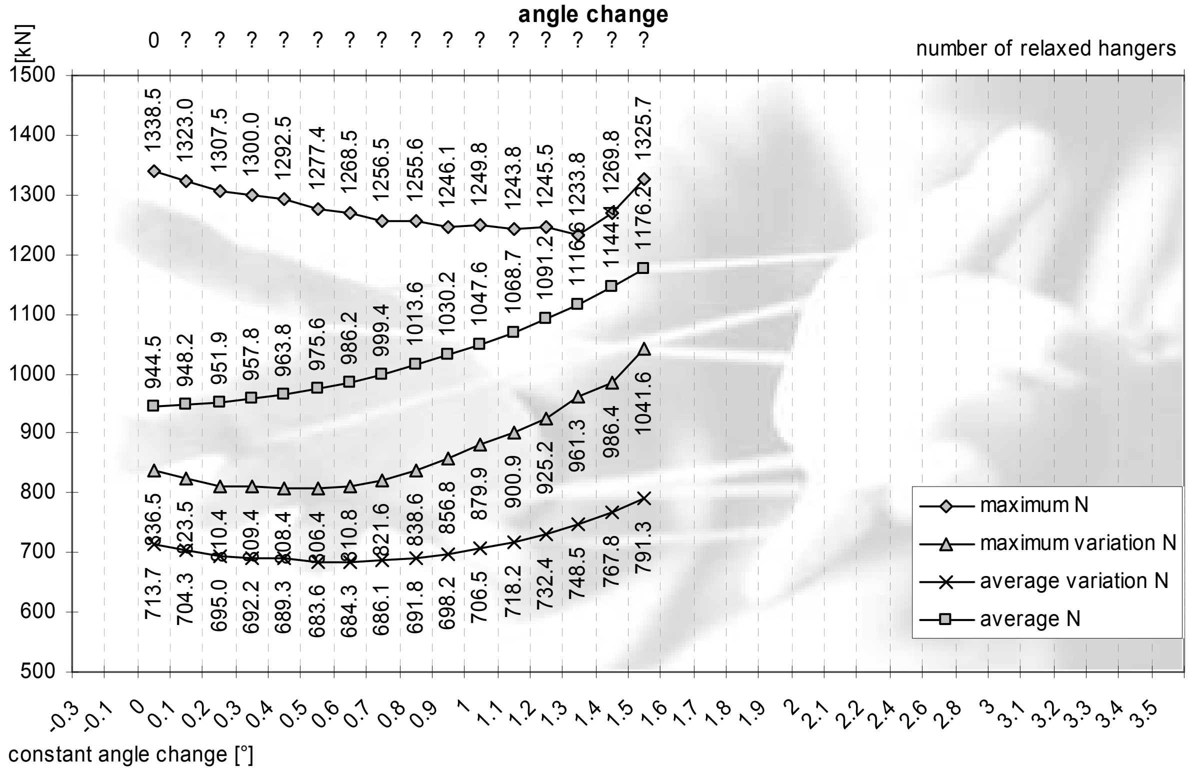

Results for hanger arrangemants from Section 6.5.2, start angle 60°, number of hangers 44, no variable angle change

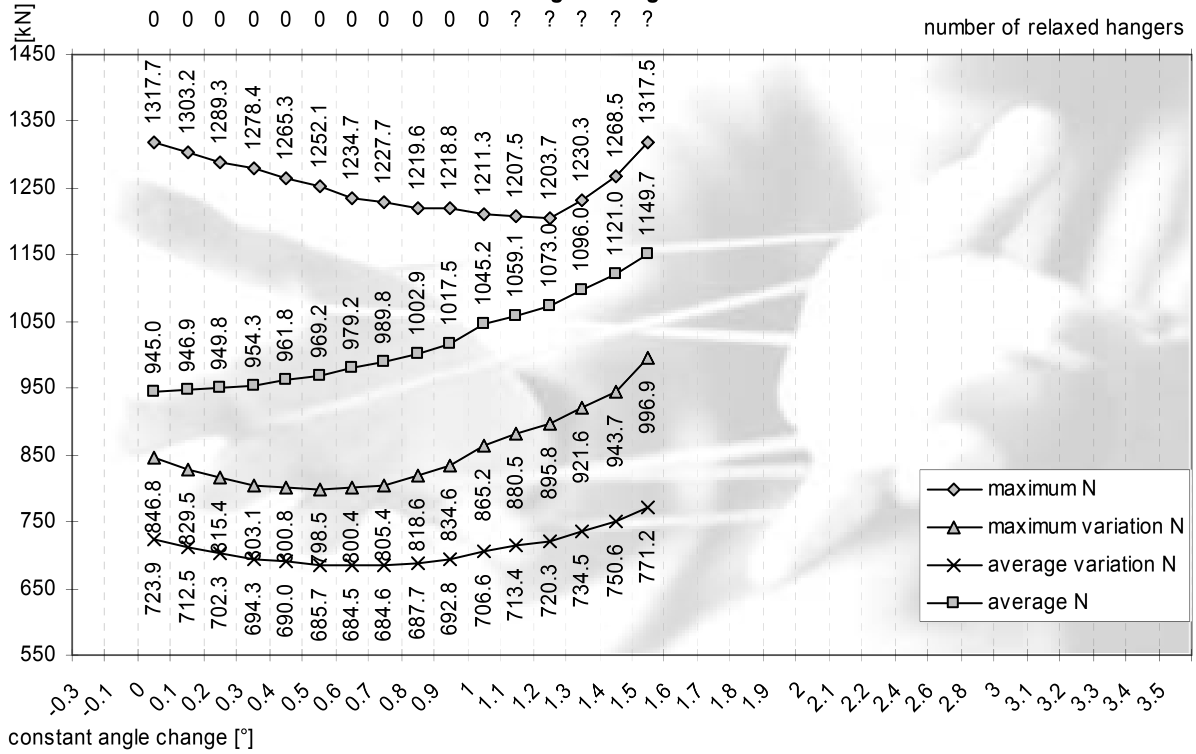

Results for hanger arrangemants from Section 6.5.2, start angle 61°, number of hangers 44, no variable angle change

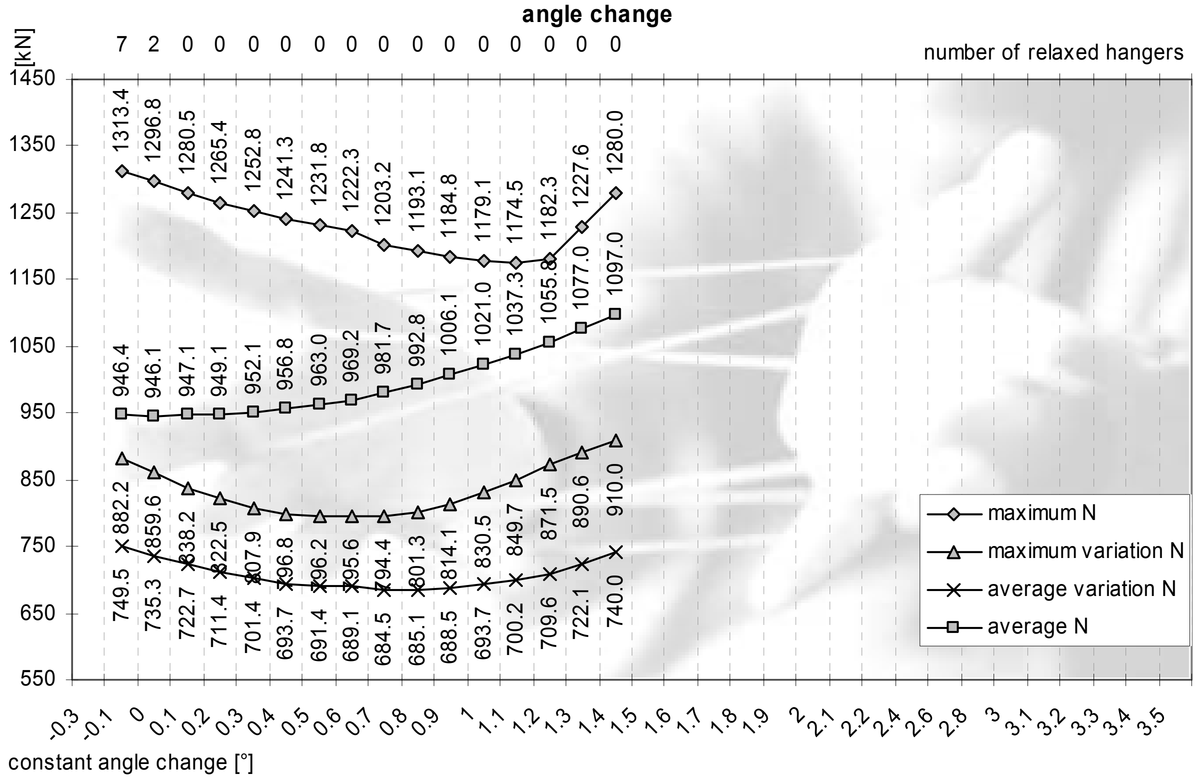

Results for hanger arrangemants from Section 6.5.2, start angle 62°, number of hangers 44, no variable angle change

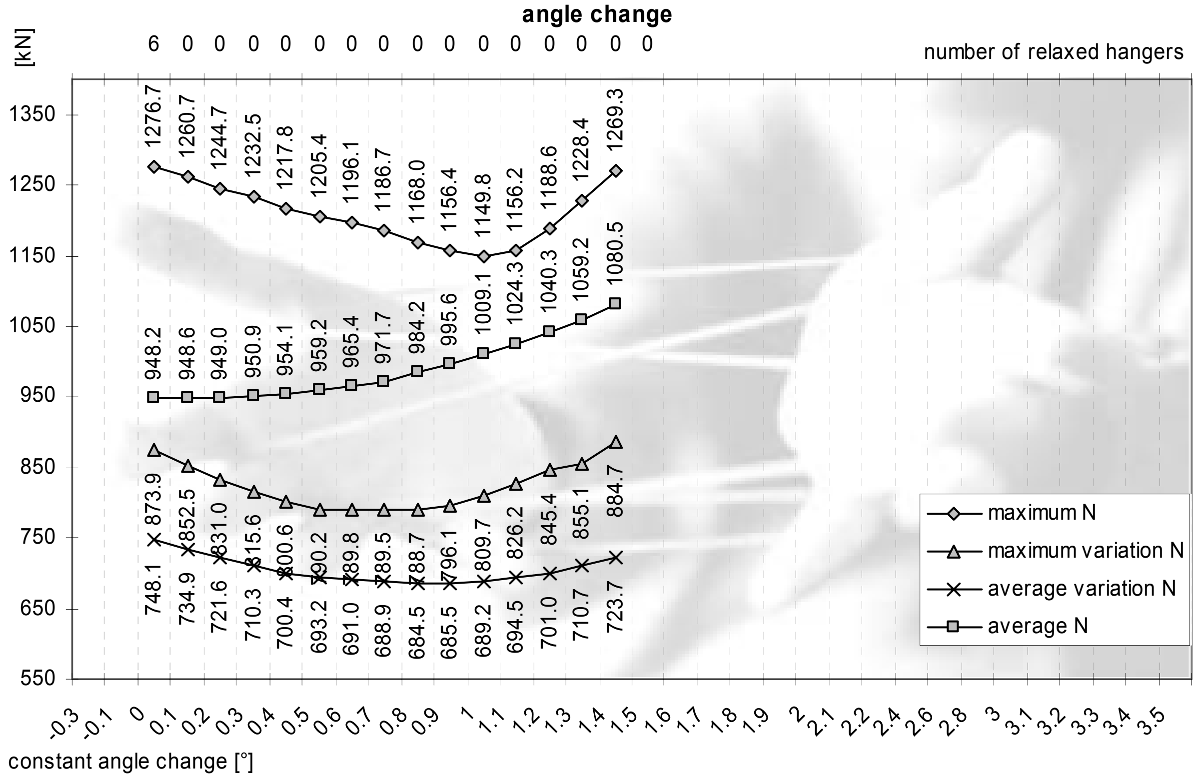

Results for hanger arrangemants from Section 6.5.2, start angle 63°, number of hangers 44, no variable angle change

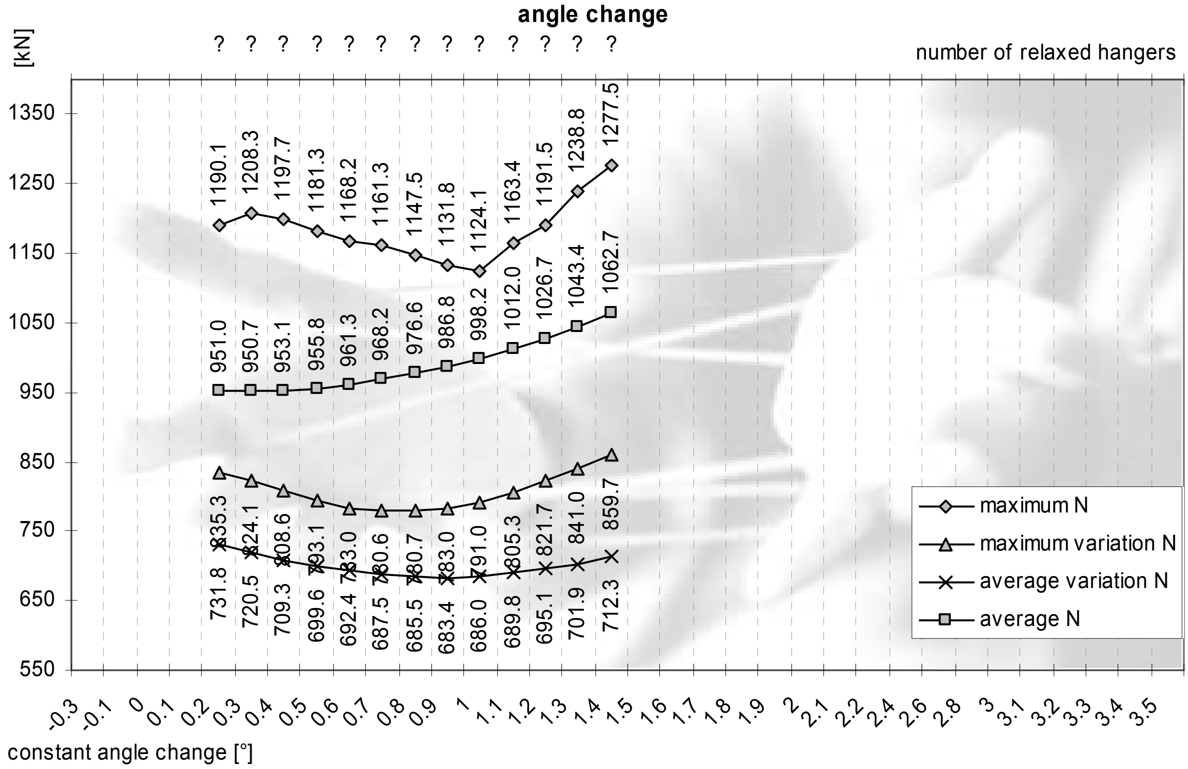

Results for hanger arrangemants from Section 6.5.2, start angle 64°, number of hangers 44, no variable angle change

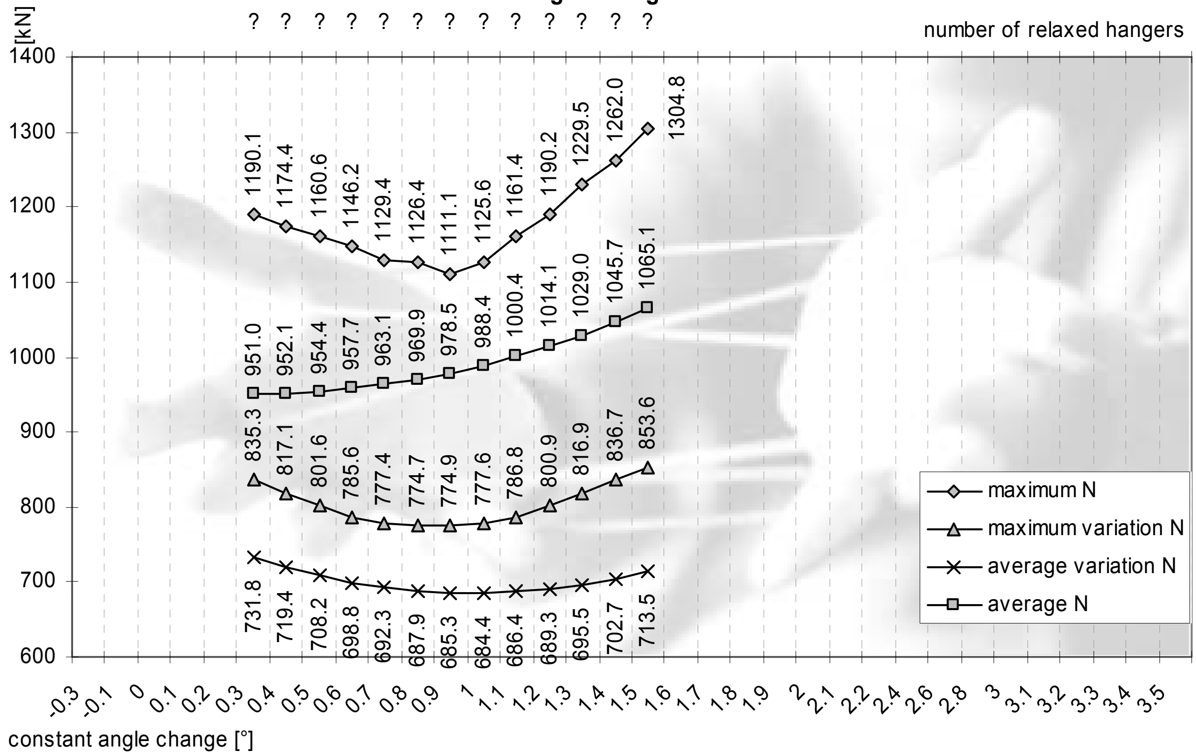

Results for hanger arrangemants from Section 6.5.2, start angle 65°, number of hangers 44, no variable angle change

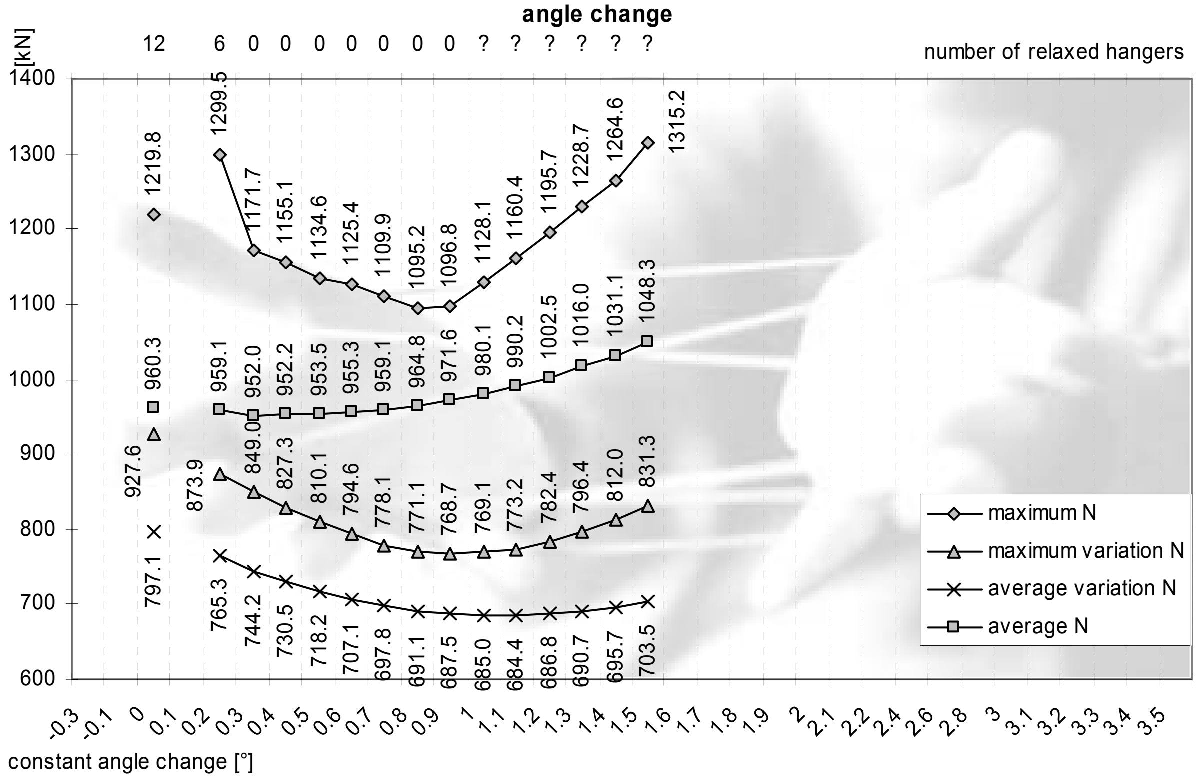

Results for hanger arrangemants from Section 6.5.2, start angle 66°, number of hangers 44, no variable angle change

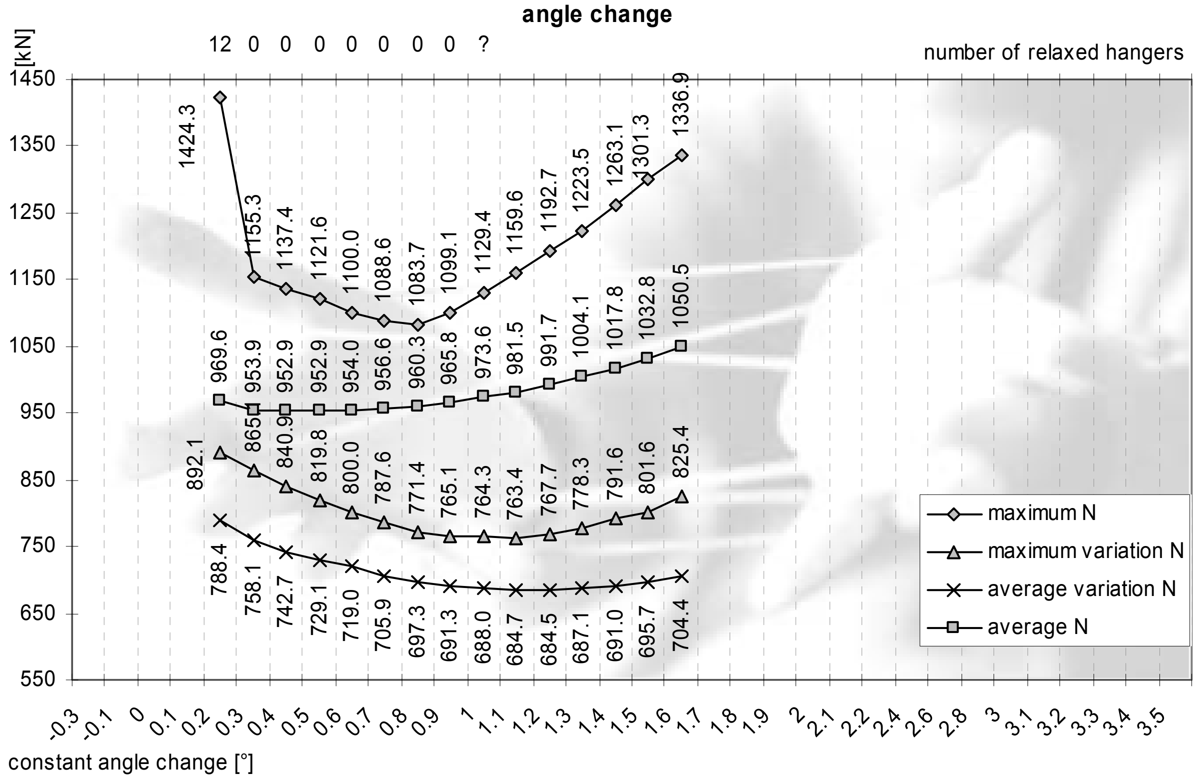

Results for hanger arrangemants from Section 6.5.2, start angle 67°, number of hangers 44, no variable angle change

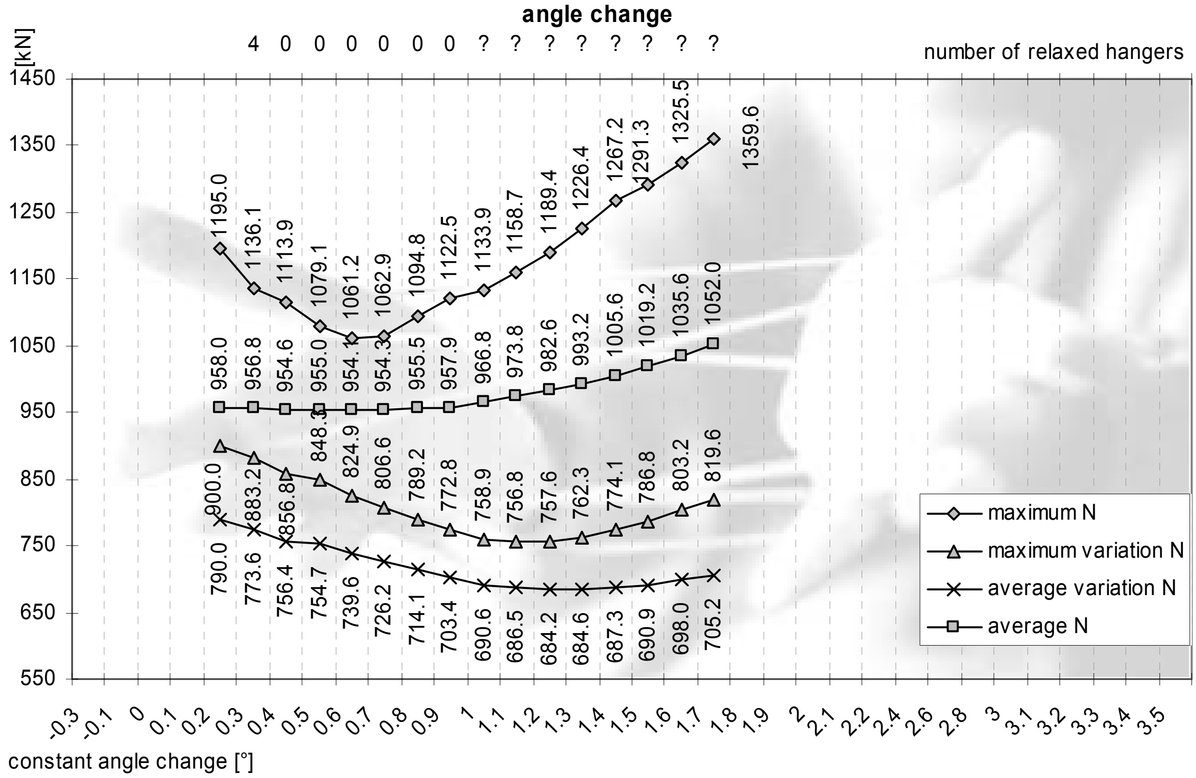

Results for hanger arrangemants from Section 6.5.2, start angle 68°, number of hangers 44, no variable angle change

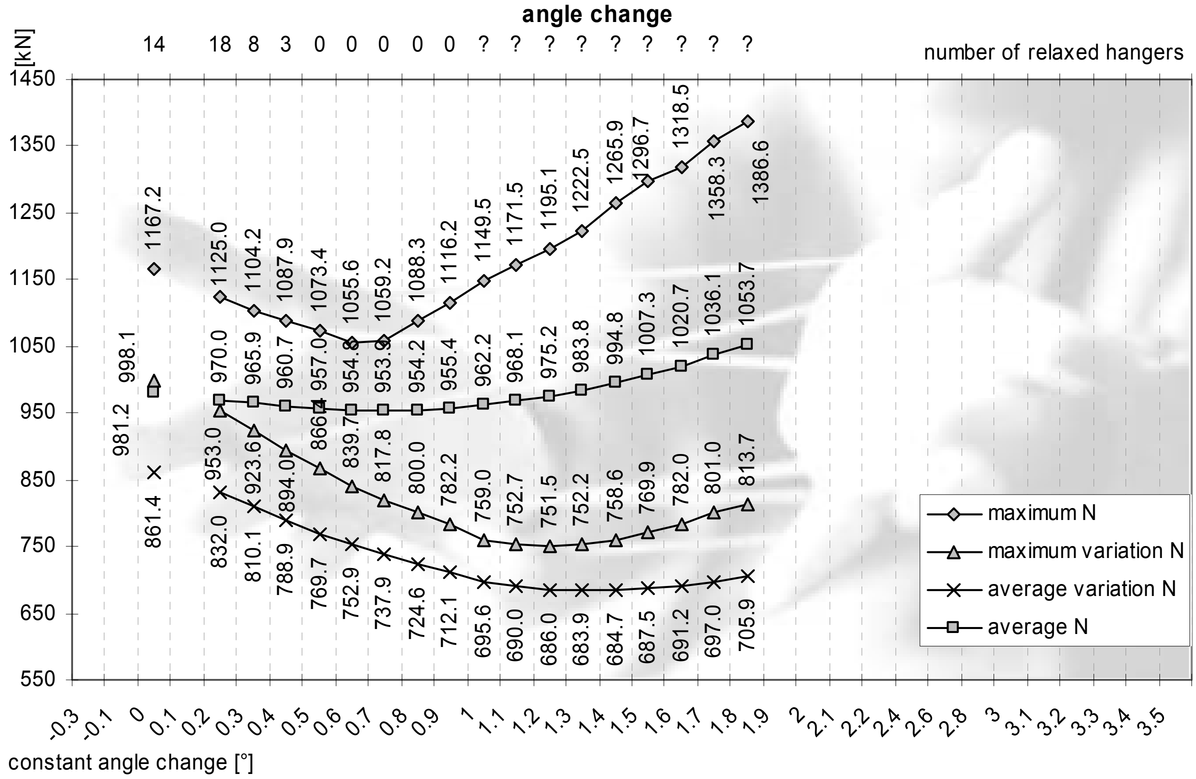

Results for hanger arrangemants from Section 6.5.2, start angle 69°, number of hangers 44, no variable angle change

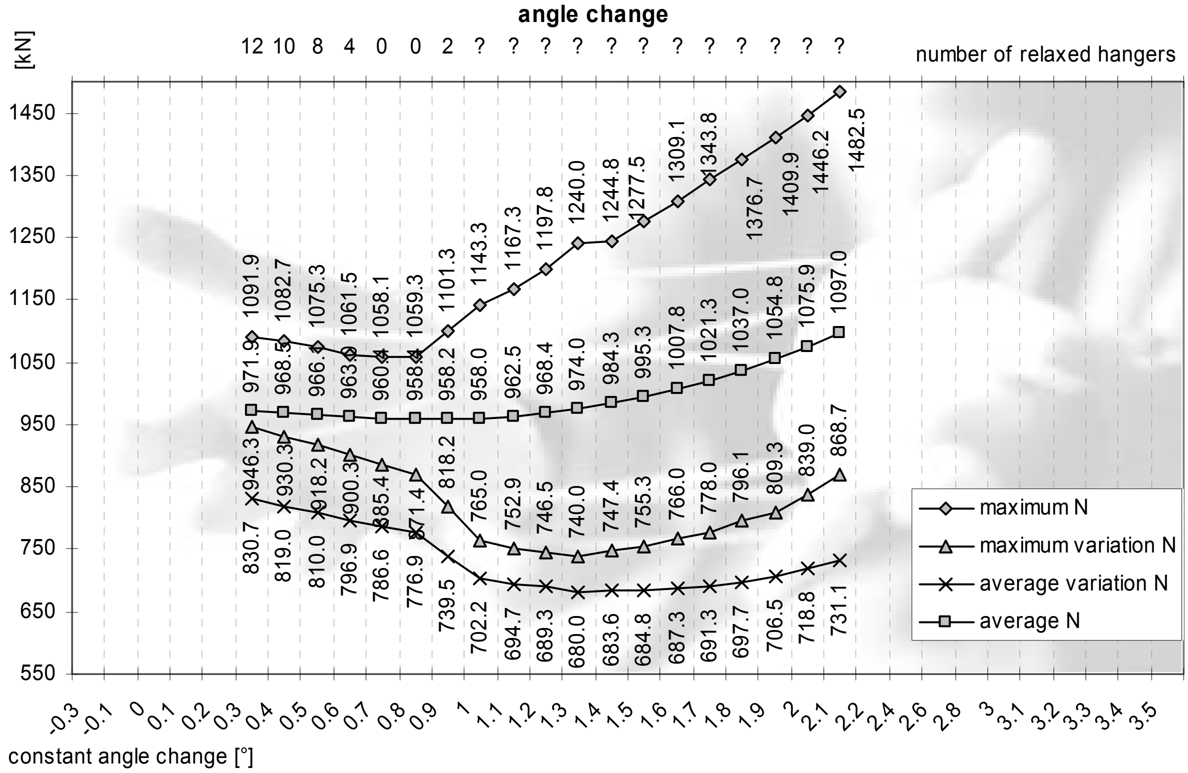

Results for hanger arrangemants from Section 6.5.2, start angle 70°, number of hangers 44, no variable angle change

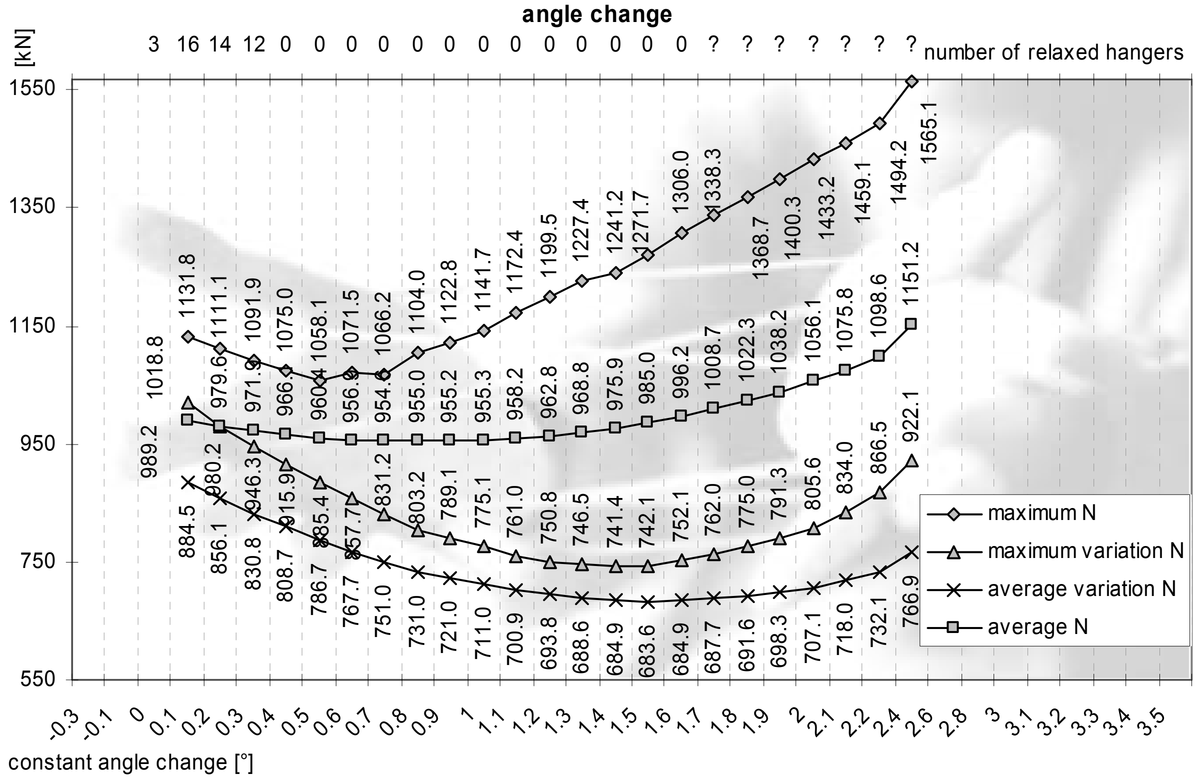

Results for hanger arrangemants from Section 6.5.2, start angle 80°, number of hangers 44, no variable angle change

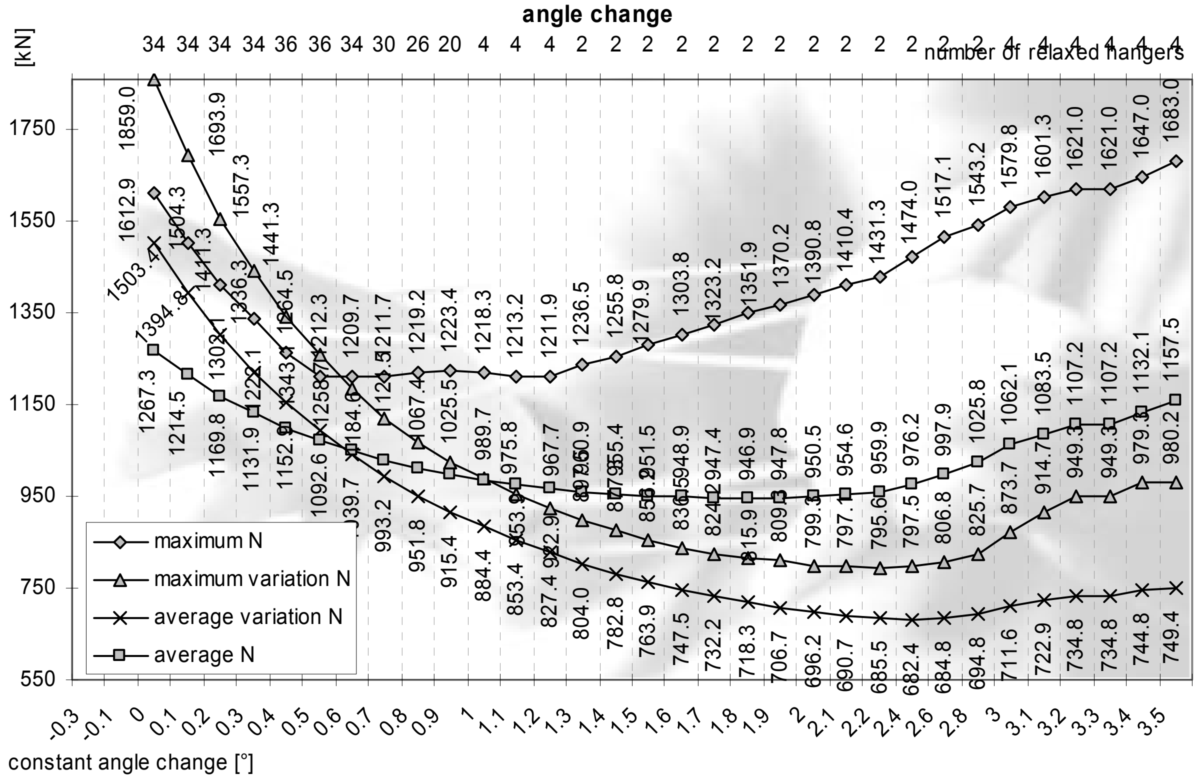

Results for hanger arrangemants from Section 6.5.2, start angle 81°, number of hangers 44, no variable angle change

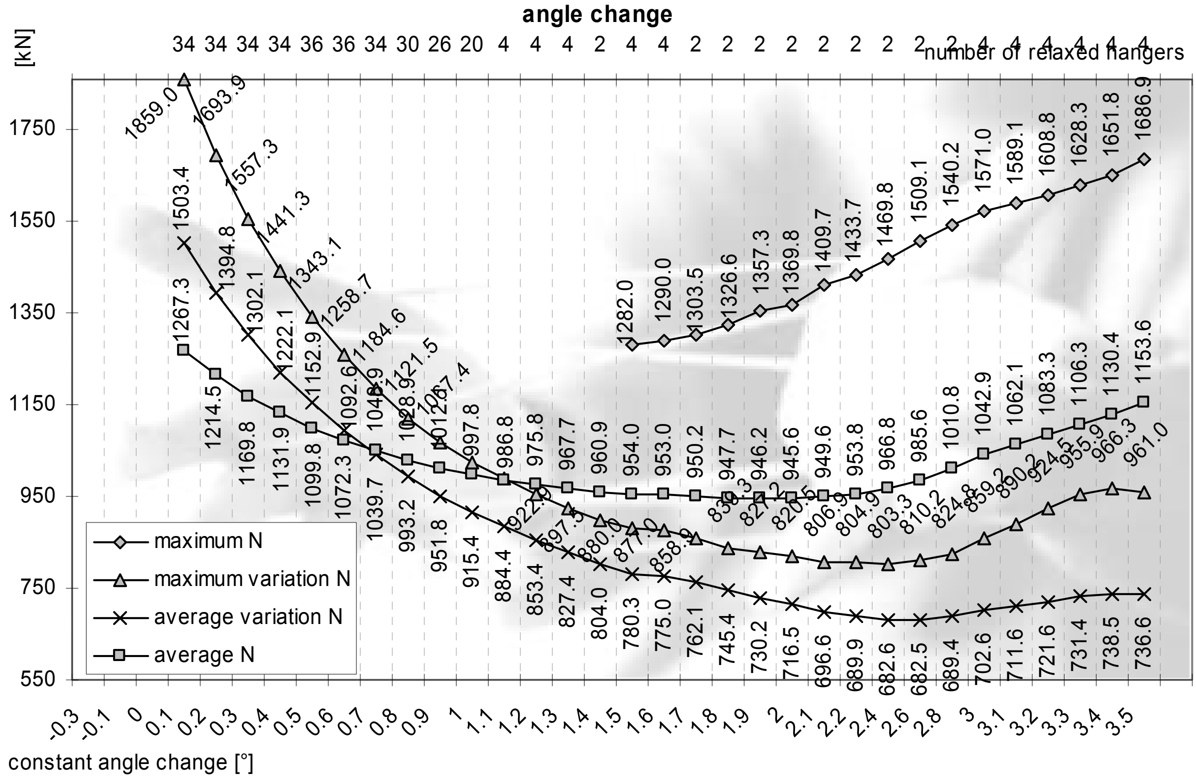

Results for hanger arrangemants from Section 6.5.2, start angle 82°, number of hangers 44, no variable angle change

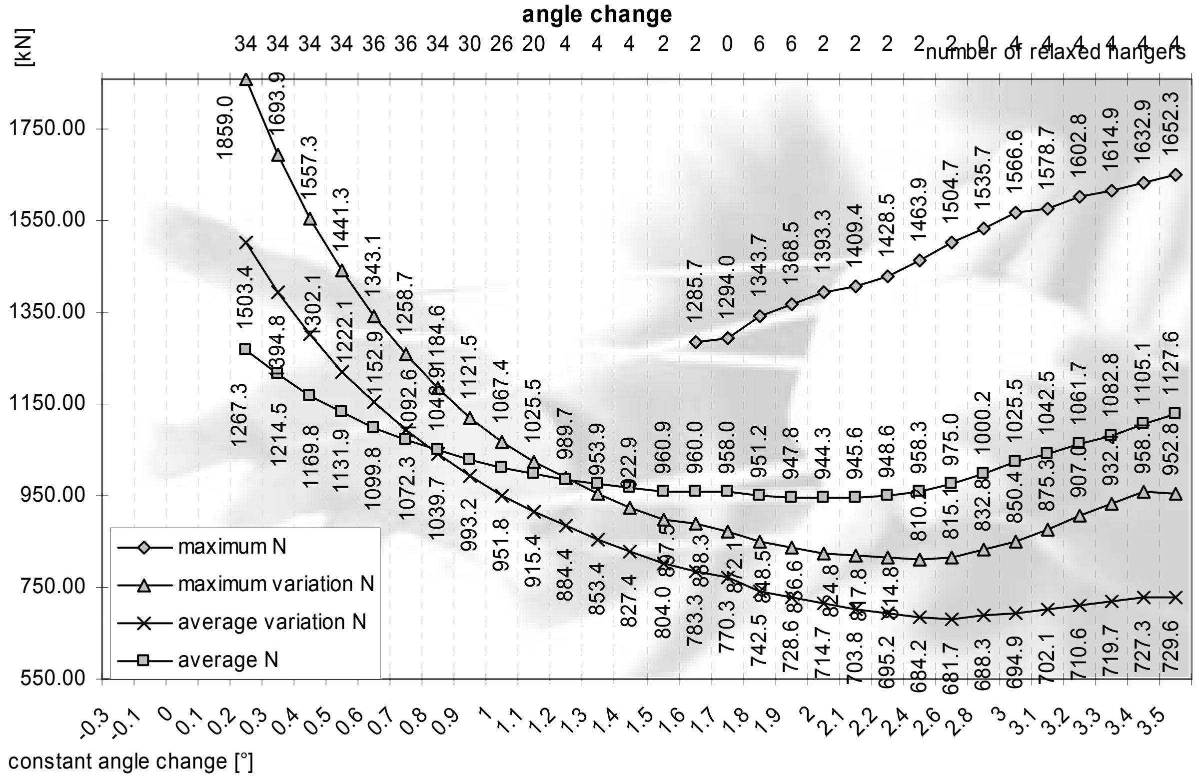

Results for hanger arrangemants from Section 6.5.2, start angle 83°, number of hangers 44, no variable angle change

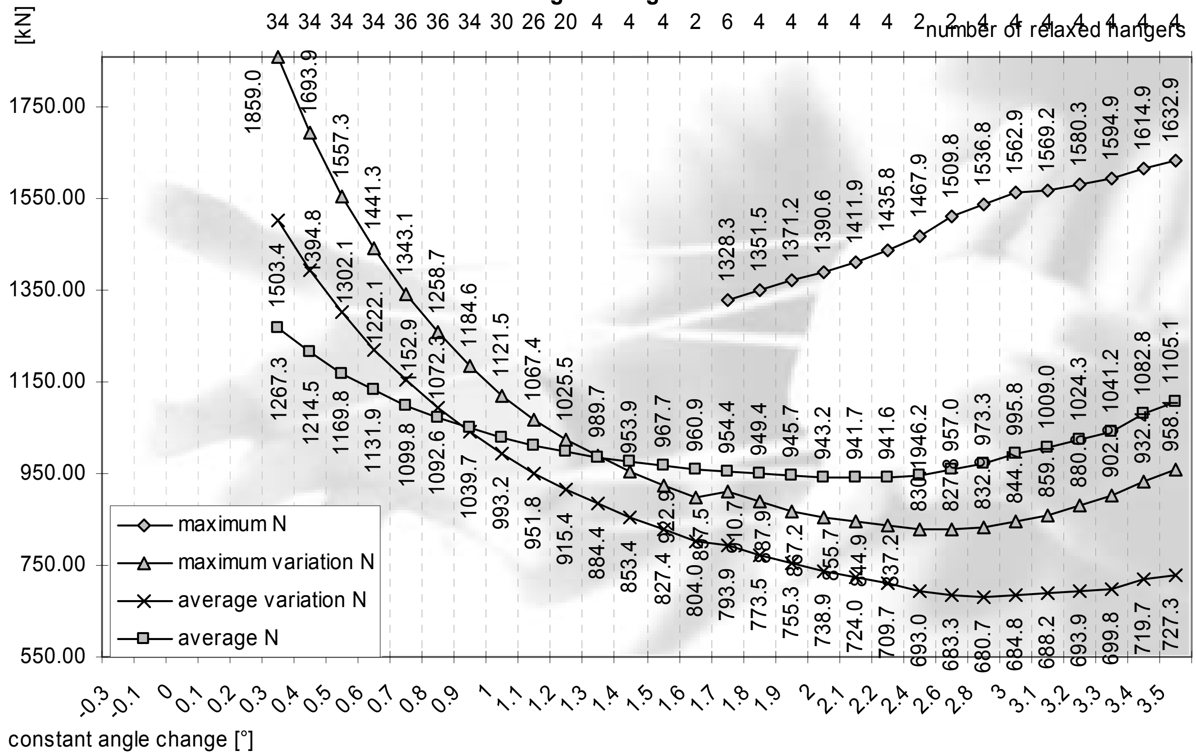

Results for hanger arrangemants from Section 6.5.2, start angle 83°, number of hangers 44, constant angle change 1°

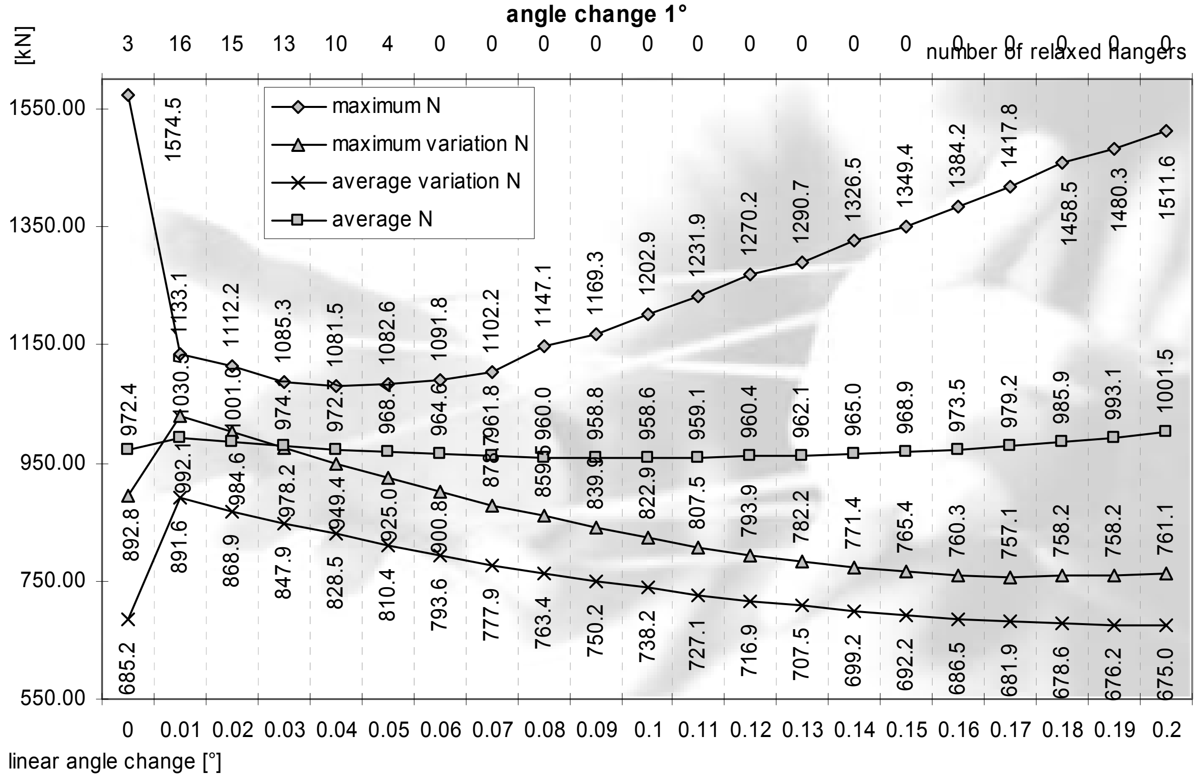

F.4 Results from variation of the lower hanger nodes using the advanced model

On the following two pages internal forces from the calculation explained Section 6.6.3 are listed.

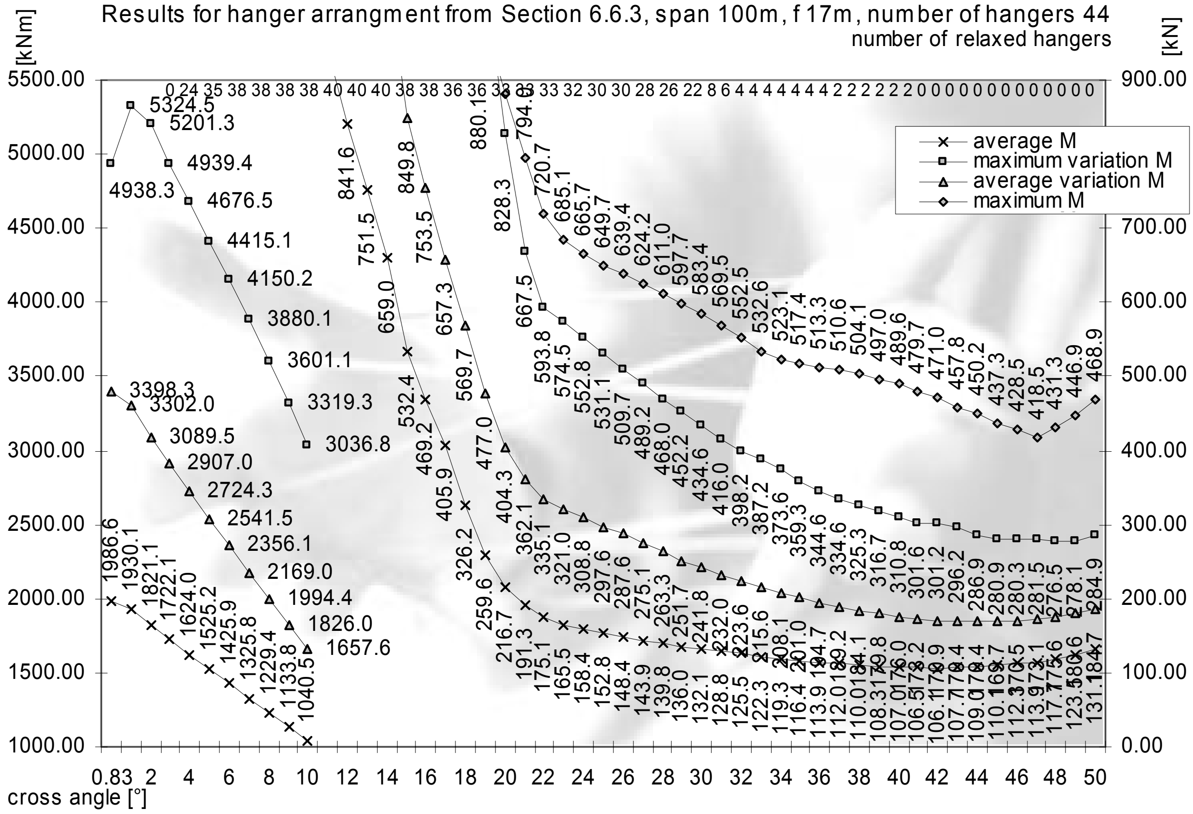

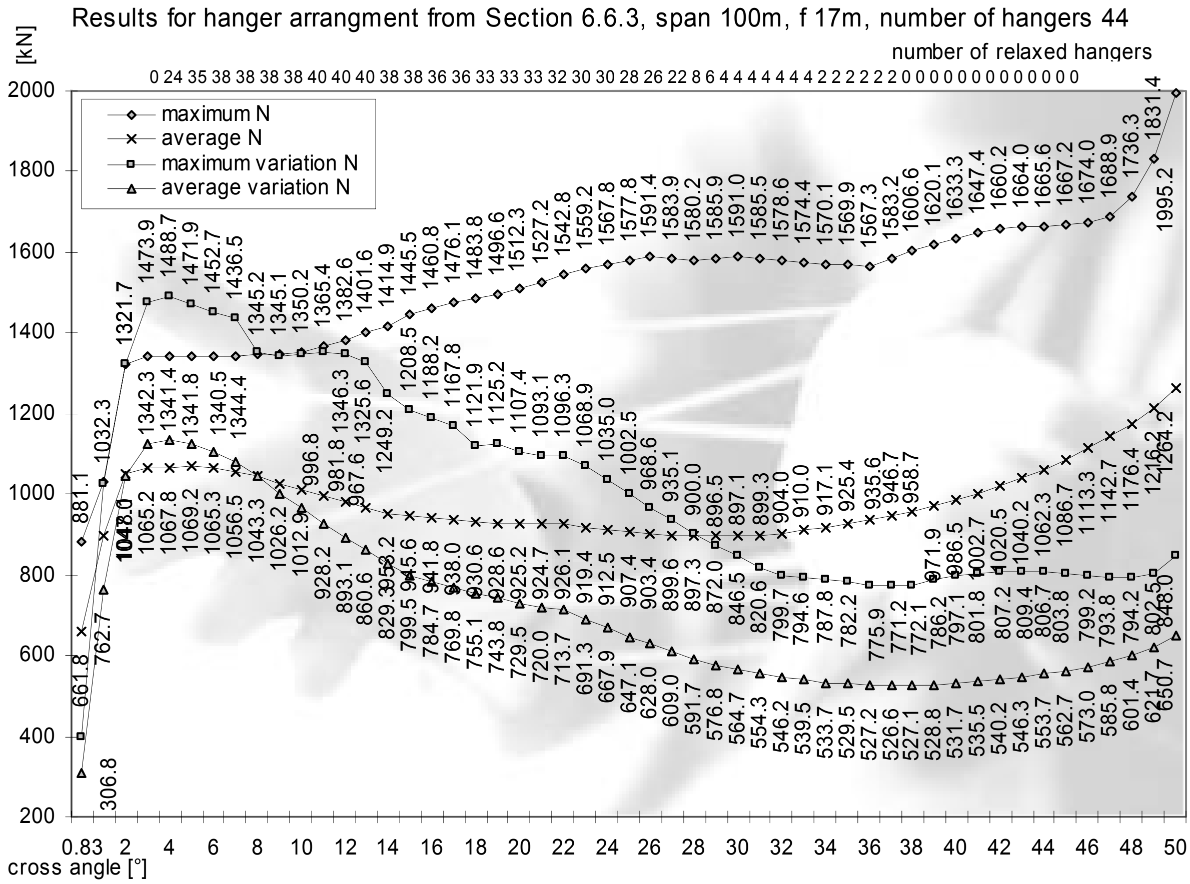

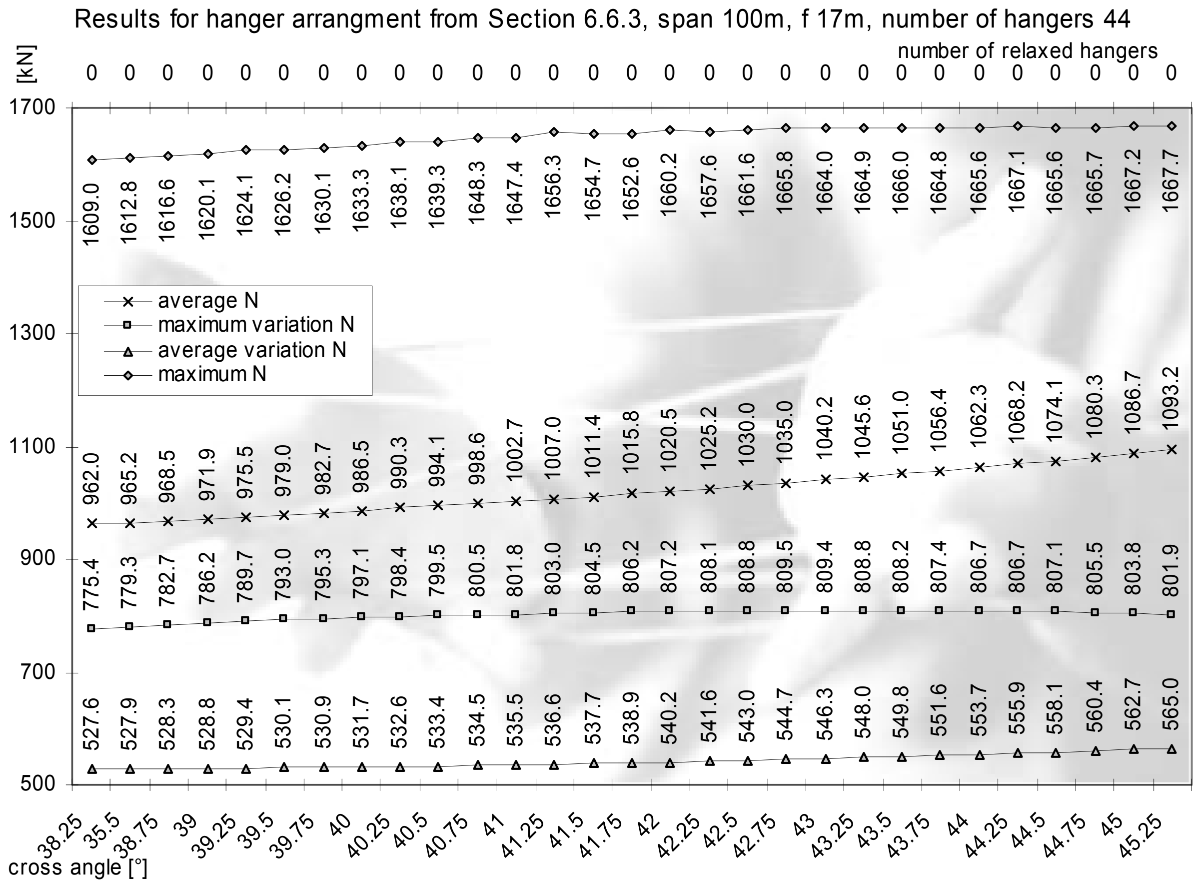
Results for hanger arrangment from Section 6.6.3, span 100m, f 17m, number of hangers 44
number of relaxed hangers
[kN]
average N
maximum variation N
average variation N
maximum N
cross angle [°]

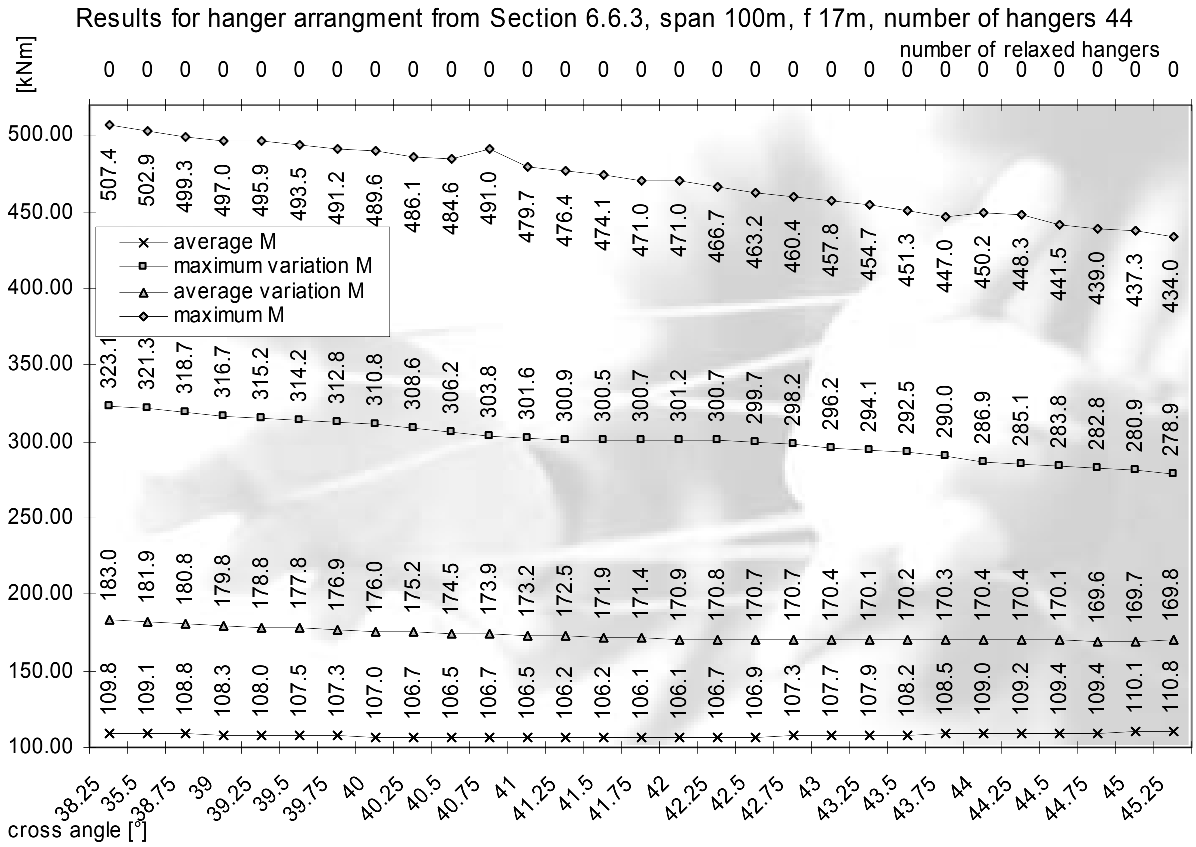
Results for hanger arrangment from Section 6.6.3, span 100m, f 17m, number of hangers 44
number of relaxed hangers
[kNm]
average M
maximum variation M
average variation M
maximum M
cross angle [°]

F.5 Results from the variation of the number of hangers and span

On the following 5 pages internal forces from the calculations explained in Section 6.7.1 are listed.

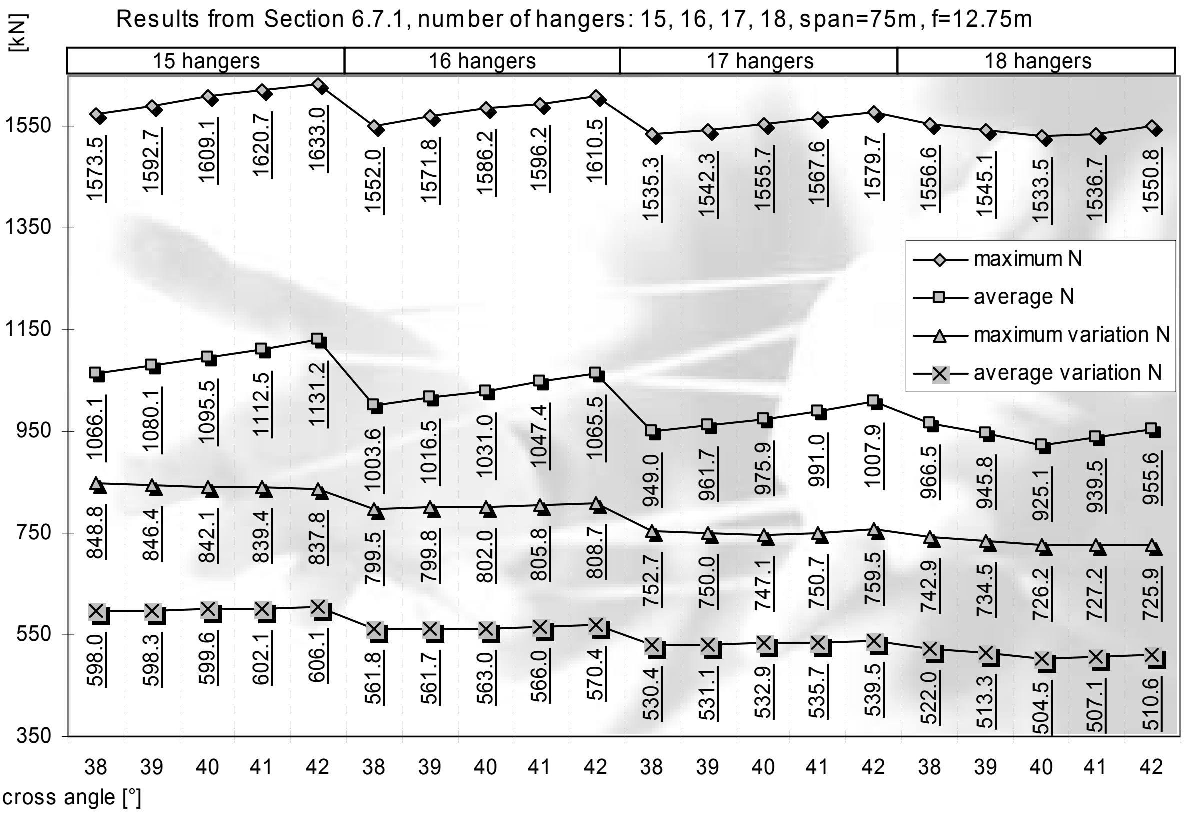

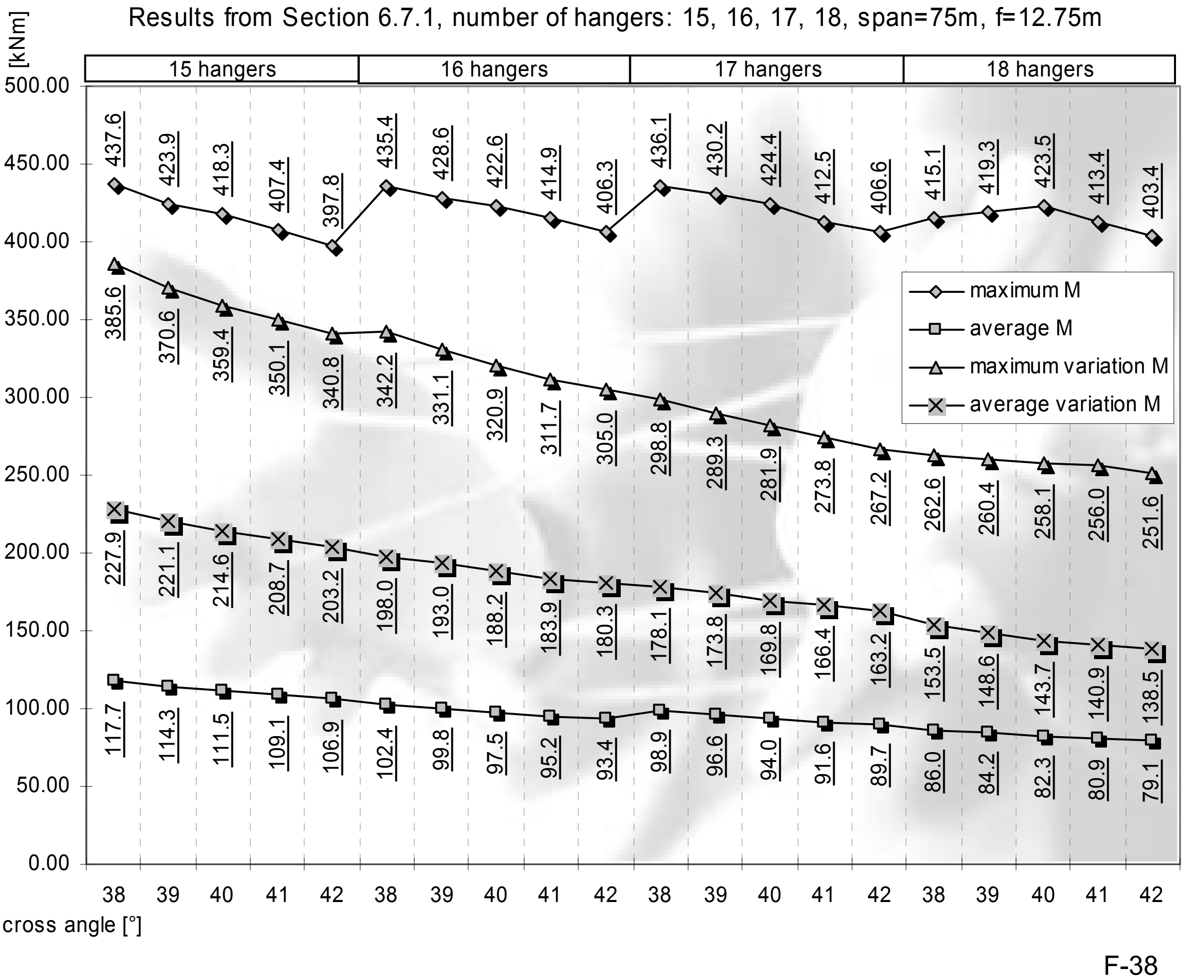

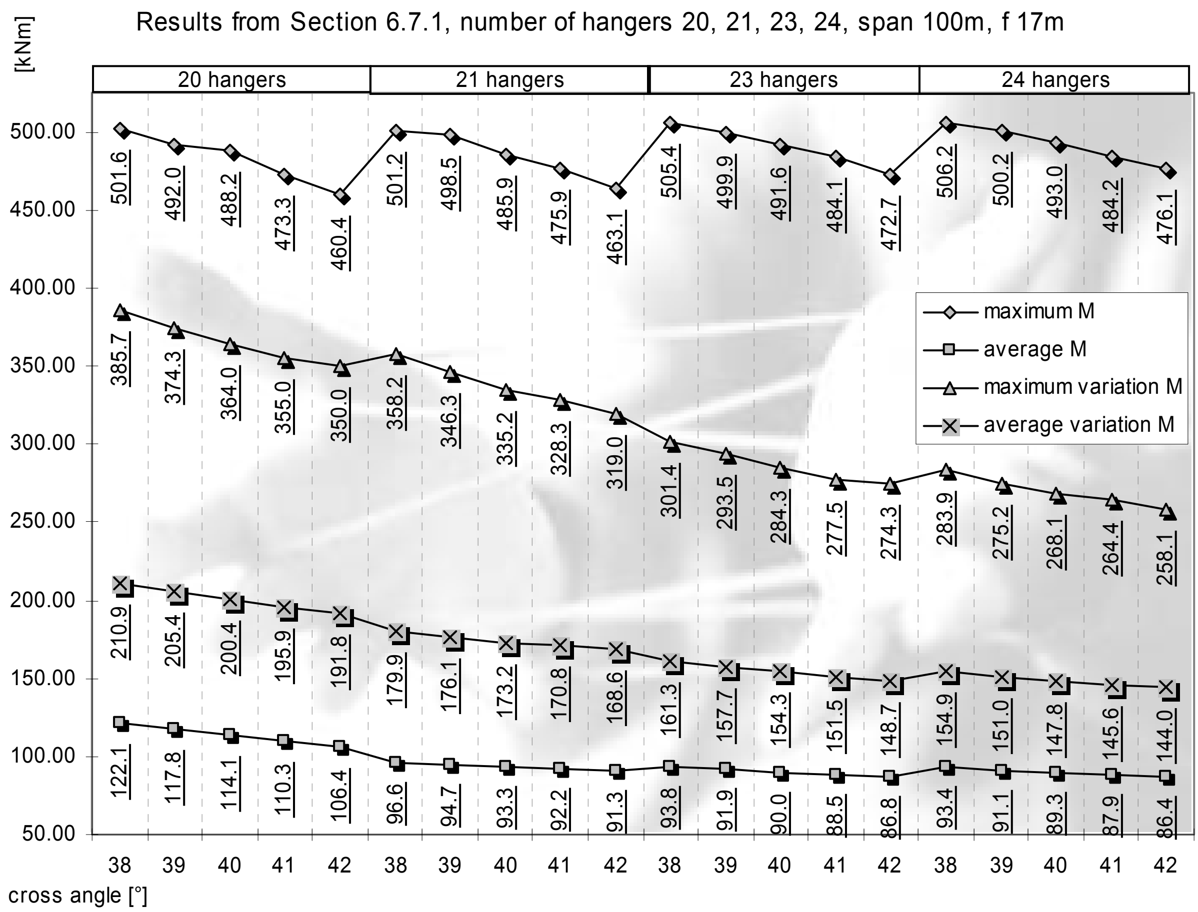
Results from Section 6.7.1, number of hangers 20, 21, 23, 24, span 100m, f 17m
[kNm]
20 hangers
21 hangers
23 hangers
24 hangers
maximum M
average M
maximum variation M
average variation M
cross angle [°]

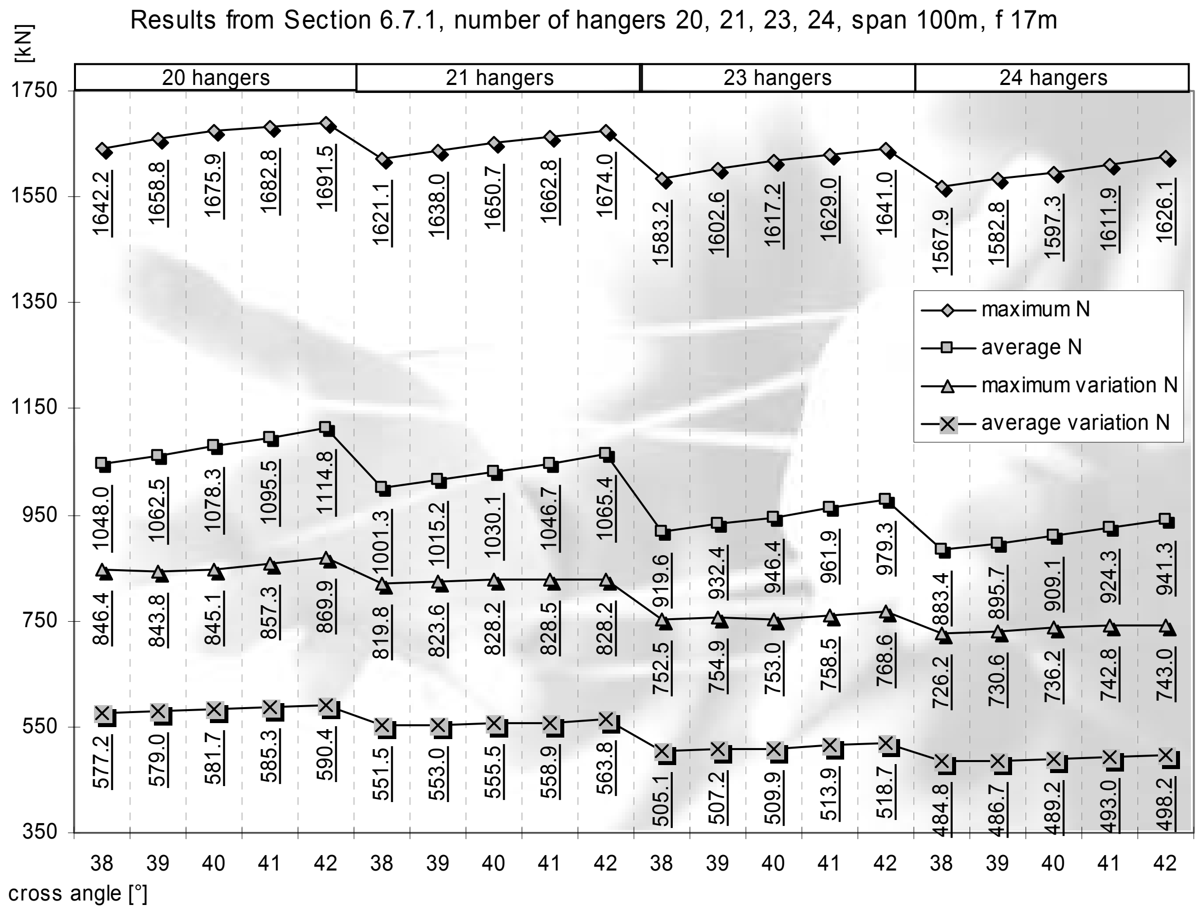
Results from Section 6.7.1, number of hangers 20, 21, 23, 24, span 100m, f 17m
[kN]
20 hangers
21 hangers
23 hangers
24 hangers
maximum N
average N
maximum variation N
average variation N
cross angle [°]

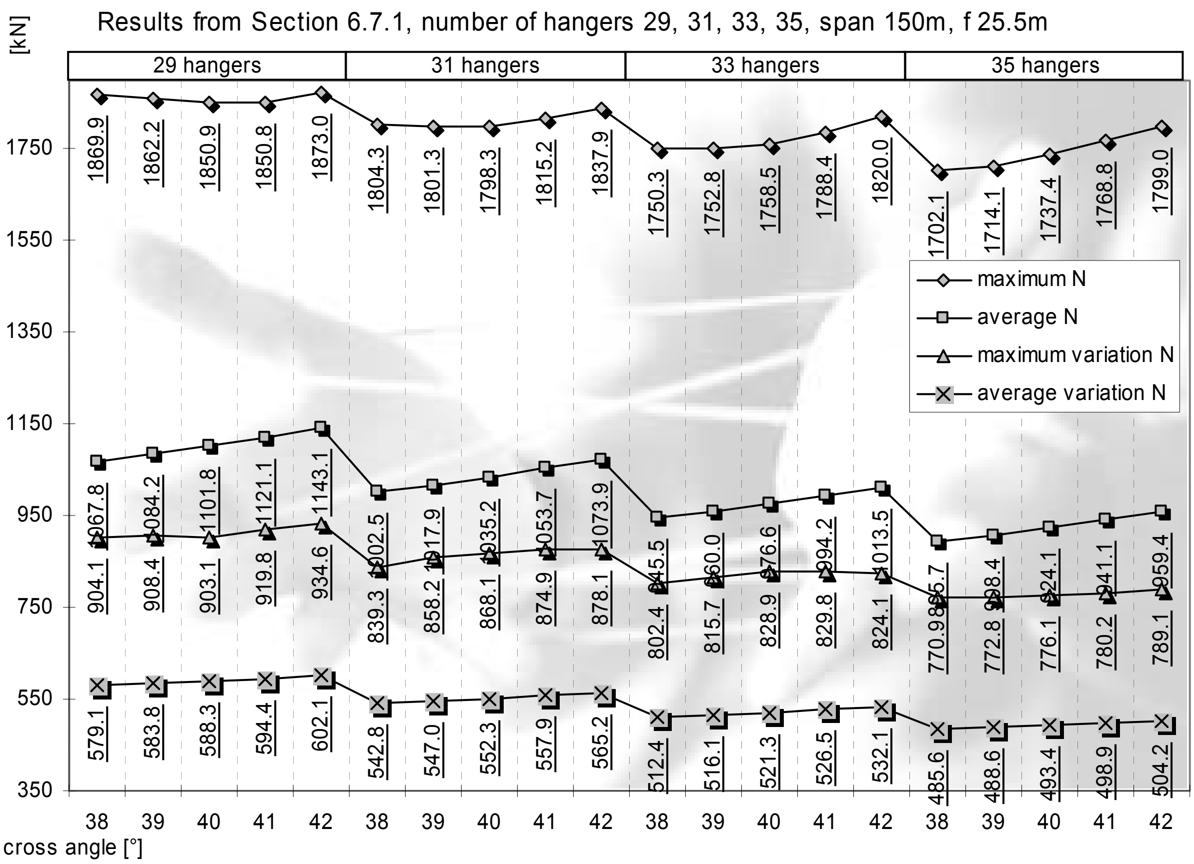
[kN]
Results from Section 6.7.1, number of hangers 29, 31, 33, 35, span 150m, f 25.5m
29 hangers
31 hangers
33 hangers
35 hangers
maximum N
average N
maximum variation N
average variation N
cross angle [°]

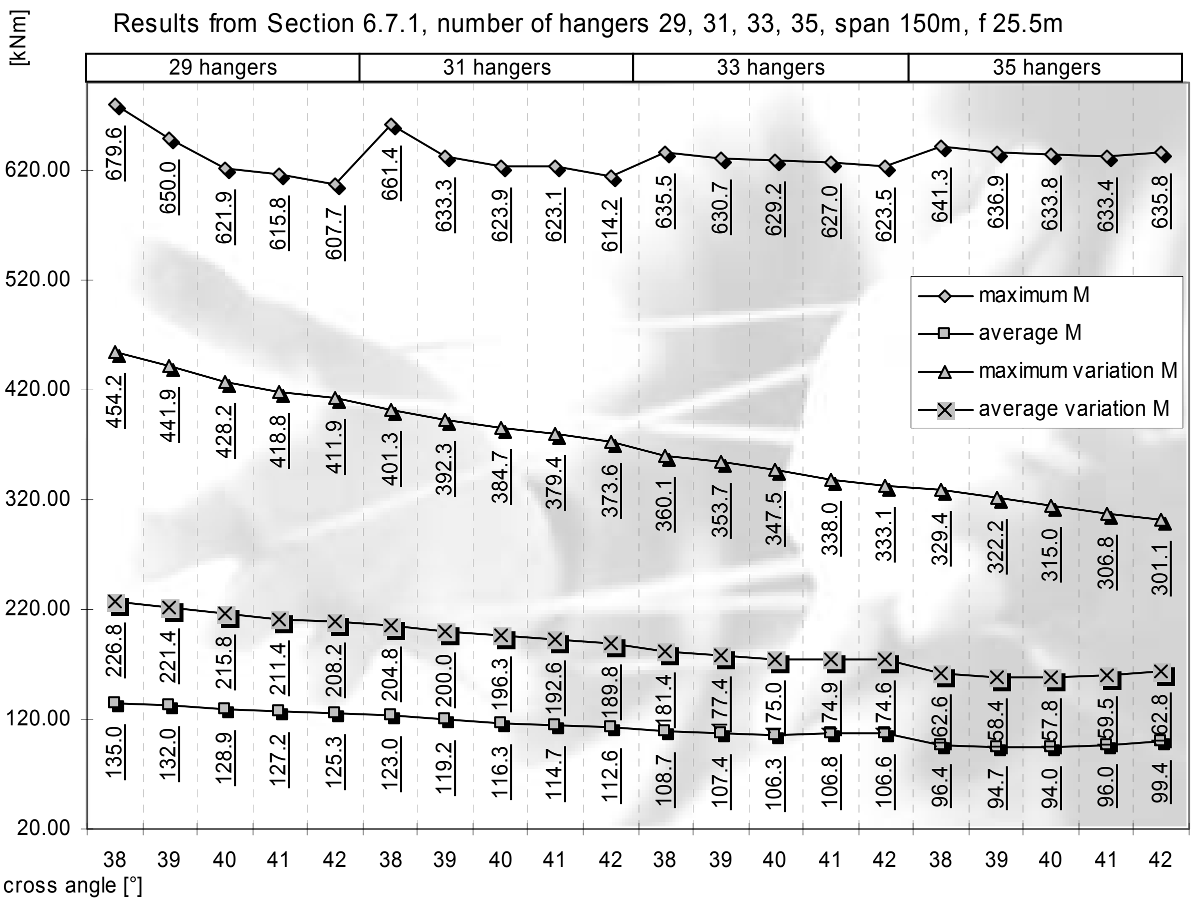
[kNm]
Results from Section 6.7.1, number of hangers 29, 31, 33, 35, span 150m, f 25.5m
29 hangers
31 hangers
33 hangers
35 hangers
maximum M
average M
maximum variation M
average variation M
cross angle [°]

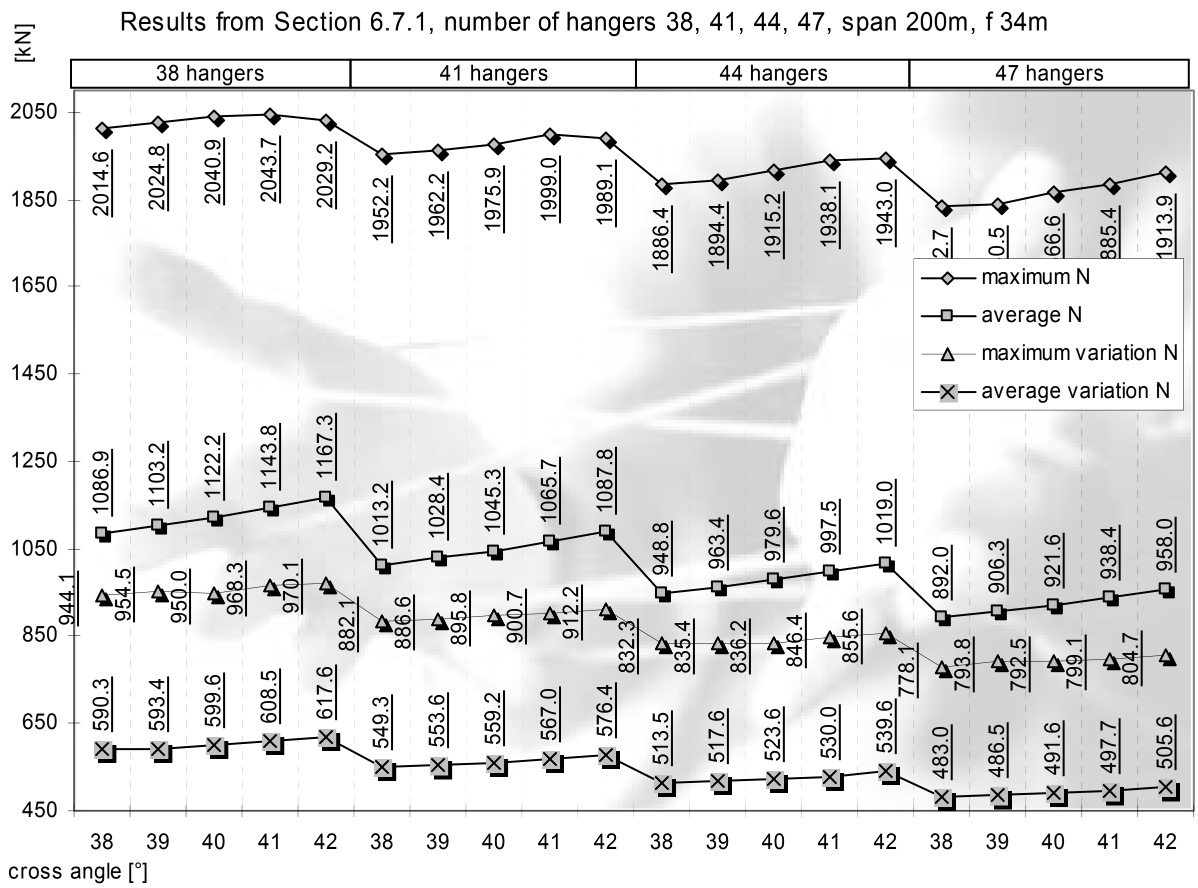
[kN]
Results from Section 6.7.1, number of hangers 38, 41, 44, 47, span 200m, f 34m
38 hangers
41 hangers
44 hangers
47 hangers
maximum N
average N
maximum variation N
average variation N
cross angle [°]

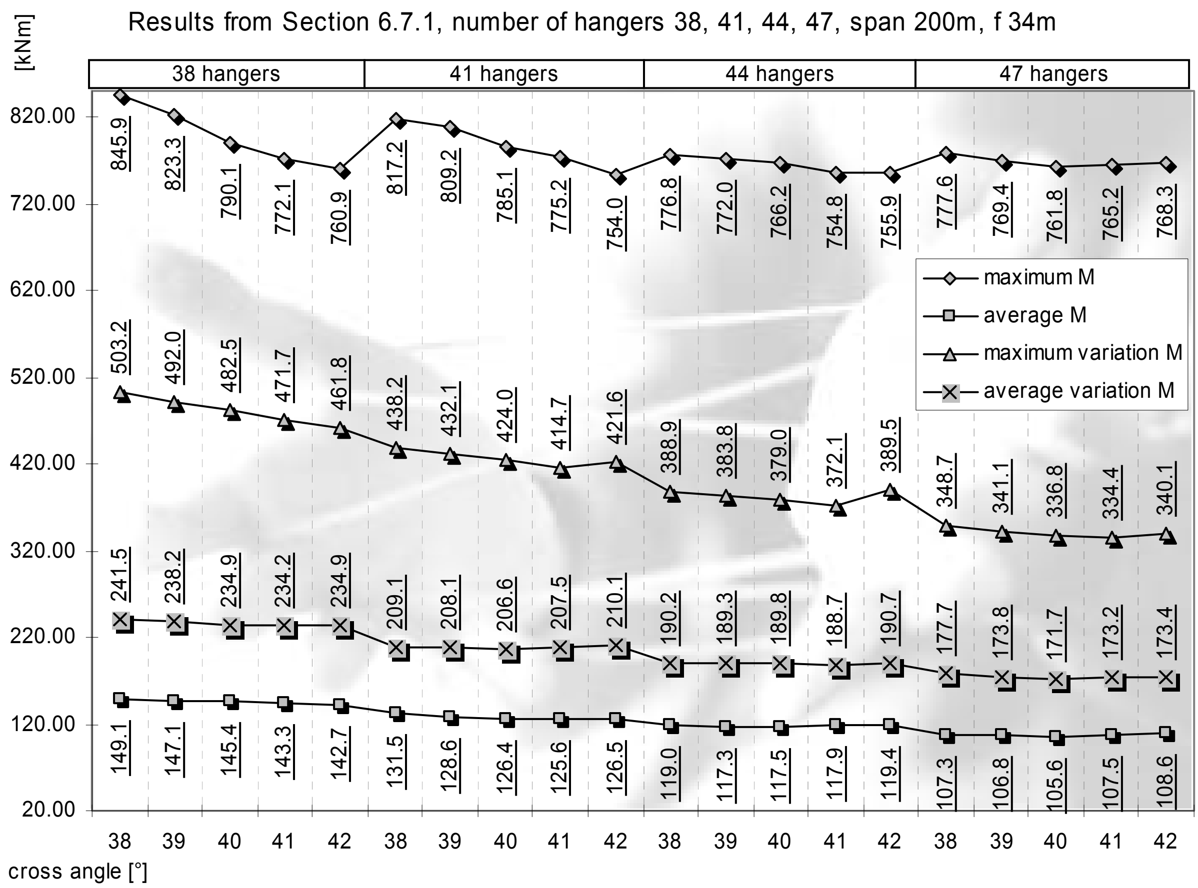
[kNm]
Results from Section 6.7.1, number of hangers 38, 41, 44, 47, span 200m, f 34m
38 hangers
41 hangers
44 hangers
47 hangers
maximum M
average M
maximum variation M
average variation M
cross angle [°]

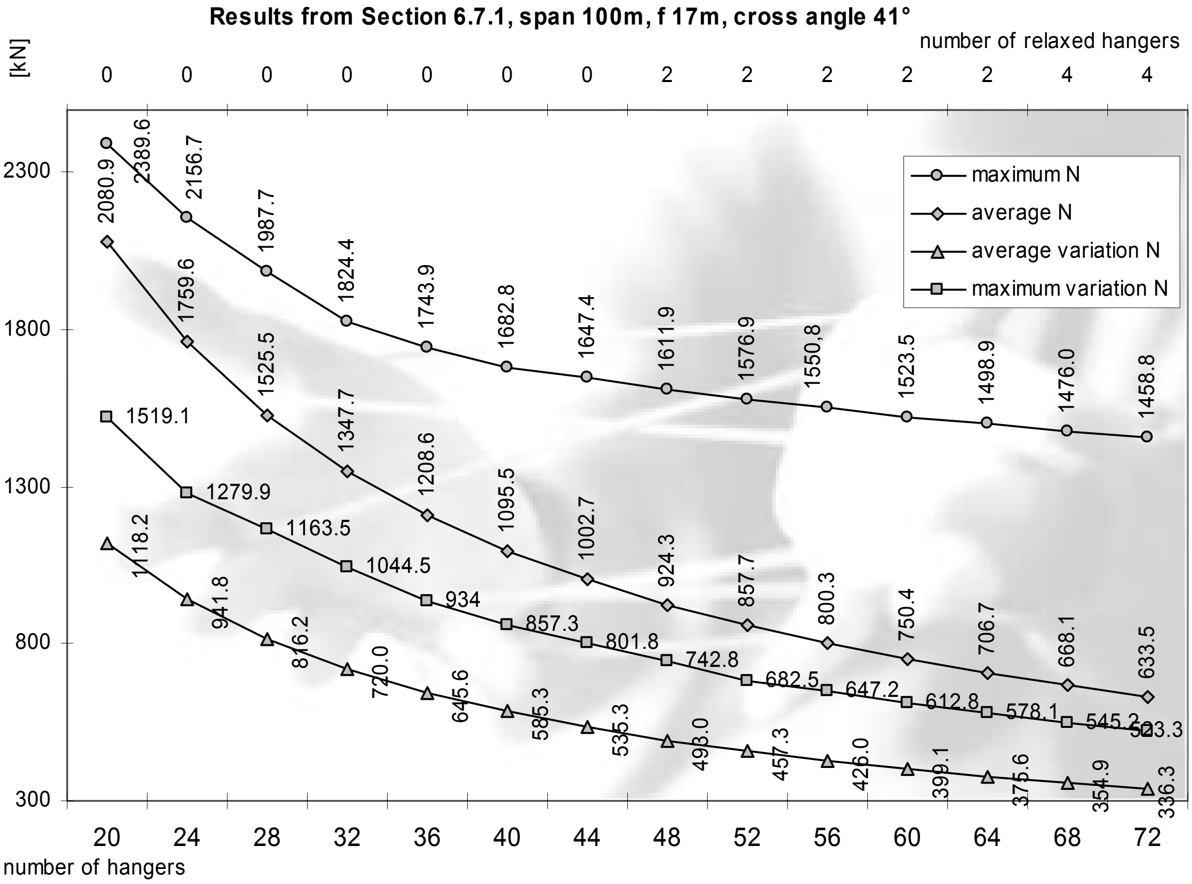
Results from Section 6.7.1, span 100m, f 17m, cross angle 41°
number of relaxed hangers
[kN]
0 0 0 0 0 0 0 2 2 2 2 2 4 4
maximum N
average N
average variation N
maximum variation N
2389.6 2156.7 1987.7 1824.4 1743.9 1682.8 1647.4 1611.9 1576.9 1550,8 1523.5 1498.9 1476.0 1458.8
2080.9 1759.6 1525.5 1347.7 1208.6 1095.5 1002.7 924.3 857.7 800.3 750.4 706.7 668.1 633.5
1519.1 1279.9 1163.5 1044.5 934 857.3 801.8 742.8 682.5 647.2 612.8 578.1 545.2 523.3
1118.2 941.8 816.2 720.0 645.6 585.3 535.3 493.0 457.3 426.0 399.1 375.6 354.9 336.3
2300
1800
1300
800
300
20 24 28 32 36 40 44 48 52 56 60 64 68 72
number of hangers

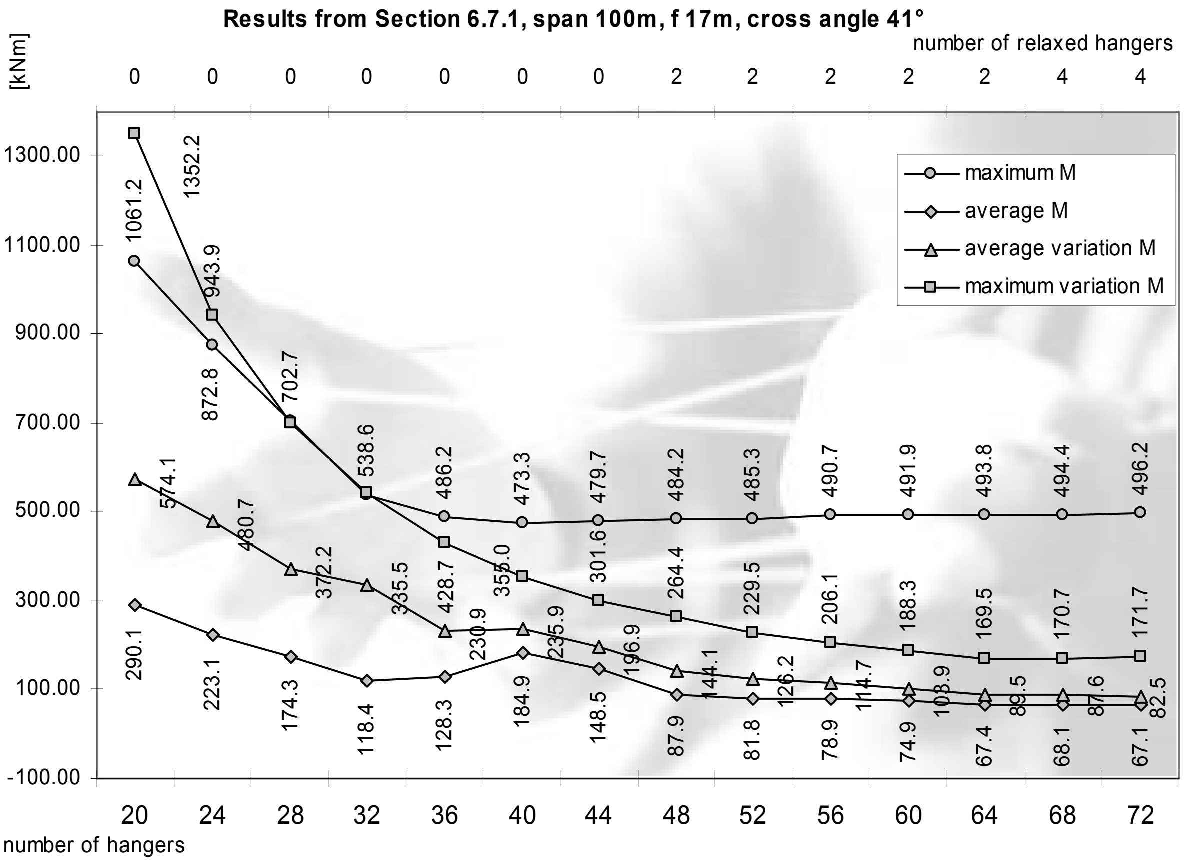
Results from Section 6.7.1, span 100m, f 17m, cross angle 41°
number of relaxed hangers
[kNm]
0 0 0 0 0 0 0 2 2 2 2 2 4 4
maximum M
average M
average variation M
maximum variation M
1061.2 872.8 702.7 538.6 486.2 473.3 479.7 484.2 485.3 490.7 491.9 493.8 494.4 496.2
1352.2 943.9 428.7 355.0 301.6 264.4 229.5 206.1 188.3 169.5 170.7 171.7
574.1 480.7 372.2 335.5 230.9 235.9 196.9 144.1 126.2 114.7 103.9 89.5 87.6 82.5
290.1 223.1 174.3 118.4 128.3 184.9 148.5 87.9 81.8 78.9 74.9 67.4 68.1 67.1
1300.00
1100.00
900.00
700.00
500.00
300.00
100.00
-100.00
20 24 28 32 36 40 44 48 52 56 60 64 68 72
number of hangers